Coastal and Sediment Dynamics in a High-energy, Rocky Environment

A thesis submitted in fulfilment of the
requirements for the Degree of

Doctor of Philosophy

in Earth Sciences

by

Peter John McComb

The University of Waikato

August 2001

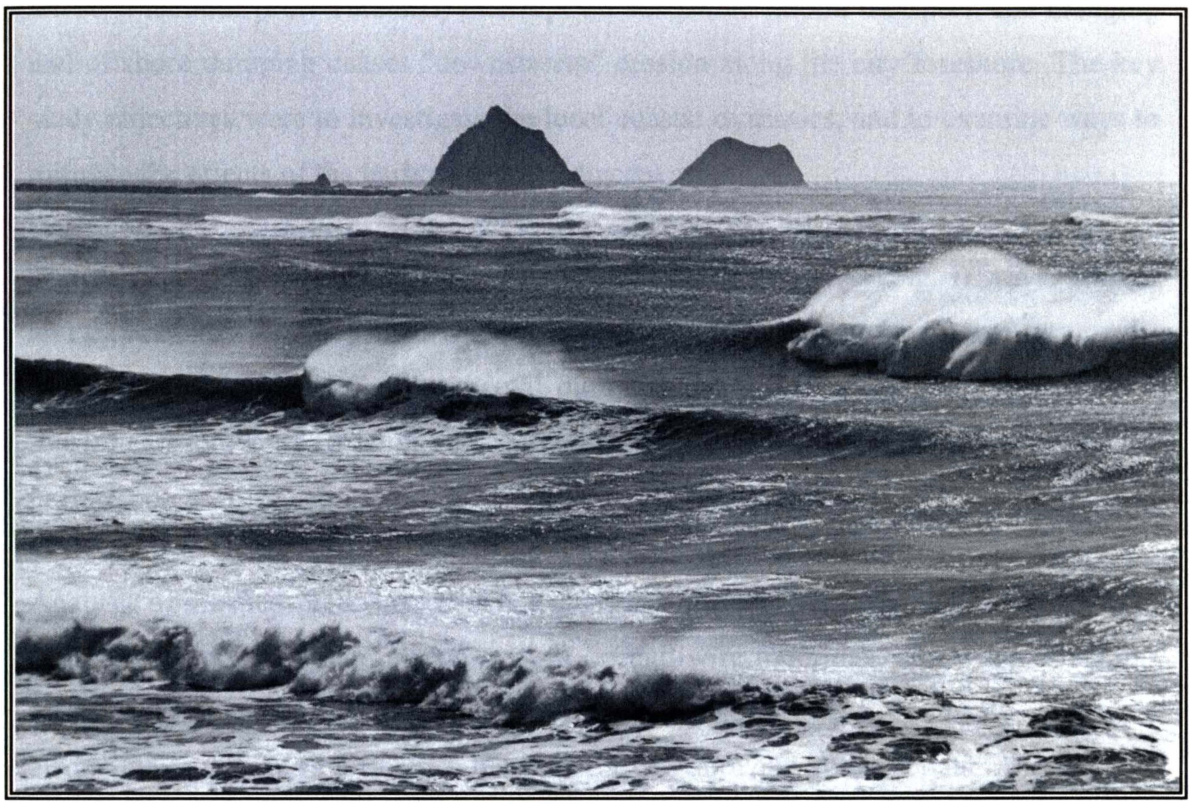

FRONTISPIECE: Looking west from Bog Works (Photo by Karen Day)

ABSTRACT

A study of the wave dynamics, hydrodynamics and sediment dynamics was conducted at an energetic open-coast site at New Plymouth, New Zealand. The location features large, shore-normal reefs of volcanic agglomerate extending from an irregular shoreline, with "black" volcanic sands intermittently overlying a rocky bed. The breakwaters of an artificial harbour (Port Taranaki) interrupt the longshore littoral transport, and dredging and offshore dumping causes "downstream" erosion along the city foreshore. The key study objectives were to investigate the local coastal dynamics, and to examine ways to mitigate the effects of the harbour on the adjacent coast.

Two large experimental field programmes were conducted involving: i) wave, current and suspended sediment measurements, ii) side-scan sonar and hydrographic survey, iii) sediment tracing, and iv) experimental dumping of 47,000 m^3 of dredged sand in a rocky nearshore zone (6-10 m depth). Sediment trap calibration experiments were also performed.

Analysis of the measured wave data has identified wave-induced motion as a significant source of velocity error in *p, u, v* meters on taut-wire moorings, and wave directions resolved from the cross-spectra of pressure and velocity have frequency dependent errors due to the phase difference between the pressure and velocity data. Accordingly, the spectra of wave direction should be resolved solely from velocity data. Calibration of sediment traps against an automated water sampler has provided the first strong evidence that traps are effective in deriving the time-averaged suspended sediment concentration SSC in a wave-dominated coastal environment. Rigid cylindrical traps of high Aspect Ratio have a 75% sampling efficiency.

Wave transformations across the complex nearshore bathymetry are dominated by seabed friction and refraction. This process was simulated using the WBEND wave refraction model, applying a constant friction coefficient for sandy beds, and a Nikuradse roughness for rocky beds. Wind vector was found to influence the spatial distribution of wave energy, with whitecapping conditions under onshore-directed

winds inducing a longshore "smoothing" in the wave energy, which appears to act in opposition to wave height reinforcement from refraction.

Sediment tracing using an artificial fluorescent material proved to be an effective method for observing the transport of littoral sediments over sandy and rocky beds, over distances of up to 5 km. The tracer exhibited a horizontal diffusivity of the order 0.1 m^2s^{-1}, of which approximately 5% was expressed in the cross-shore direction.

The time-averaged entrainment (C_o) of "black" volcanic sands under high-energy conditions may be effectively predicted using the excess non-dimensional skin friction ($\theta_{2.5}$) raised to the power of 1.5, with the mean grain size used in the sediment mobility term (Ψ) and the median grain size in the friction factor (f_w). The scale of turbulent mixing (l_s) increases linearly with elevation above the bed, with a gradient of 0.46. Suspended sediments show a systematic (and linear) reduction in mean grain size with increasing elevation above bed.

SSCs over rocky beds are supply-limited, and inversely proportional to the distance from contiguous sandy beds. Sediments are principally transported in the suspended form, and a system of irregular shore-normal reefs does not significantly obstruct the longshore flux. Rocky beds appear to be resilient to sediment inundation and the sand / rock sediment facies have remained positionally stable over 16 years. Dumping sand in a rocky reef environment does not necessarily result in adjacent beds becoming inundated with sand. In this environment, a nearshore dump mound did not migrate as a contiguous body, but slowly dispersed as suspended sediments.

Net sediment transport at New Plymouth is directed alongshore to the northeast, although the sediments respond to local and temporal perturbations, which give rise to reversing and circulating fluxes. Port Taranaki traps 174,000 m^3 of coastal sediments per year, of which 142,000 m^3 accumulates at the breakwater tip. The latter are derived from the shallow zone seaward of the breakwater wall (i.e. within ~50 m). Sediments in depths > 6 m (i.e. > 100 m from the breakwater wall) bypass the harbour and traverse the rocky reefs toward the eastern beaches. The historical offshore dumping practice

removes sediments from the nearshore littoral budget, while the orientation of the main port breakwater causes the longshore sediment flux to be directed away from the adjacent (Kawaroa) coast, further reducing the supply of littoral sediments to that region.

A new dumping ground has been identified for the breakwater-tip sediments, which is projected to retain the dredged sediments within the nearshore littoral system, feeding sand to the central and eastern city foreshore. Sedimentation of the coast immediately adjacent to the port is not expected to result from the long-term use of this ground.

ACKNOWLEDGMENTS

There are many people to thank. Firstly, my parents, Dorothy and Colin McComb, who have believed in me throughout my life, and I am grateful to them for that. Prof. Kerry Black and Mr Peter Atkinson have proved to be steadfast in providing guidance and project support over these years. Kerry has been a committed and generous supervisor, and I thank him for his time and teaching. The research funding by Westgate Transport Ltd is gratefully acknowledged. Thanks to Prof. Terry Healy for his wise council, and the input of Dr Terry Hume in planning the field experiments. Dr Richard Gorman was very helpful with data analysis, readily providing advice. Jason Sait and I spent countless hours at sea and underwater during the field experiments, and I thank him for his help and friendship. Dirk Imenga, Stephen Flint and others from the Coastal Marine Group were of invaluable assistance in the fieldwork. Westgate staff provided a supportive office environment and excellent engineering services. Bruce Gray was a magnificent boat skipper who was keen to go out in most conditions. Thanks to Captain Lim for help with collecting/processing the hydrographic data, and Nolene Brown for proof-reading. Thanks also to Bob Waugh for office accommodation in the last eight months, and Brenda Penn for focus. My two fine sons, Sam and Jake, have maintained my sense of humour, and friends and extended family have provided encouragement and assistance in many ways. Finally, I want to thank my wonderful wife, Juliet, whose enduring support and love has made this journey possible.

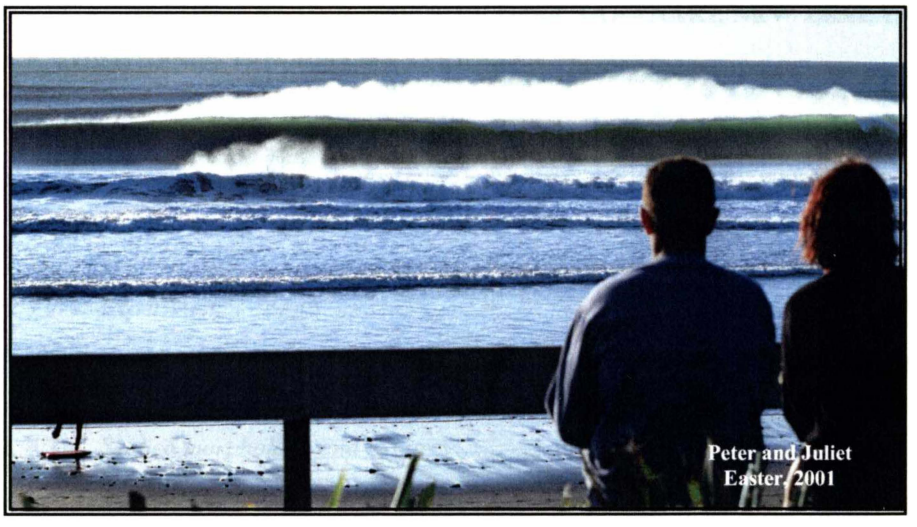

TABLE OF CONTENTS

APPENDICES

Appendix 1: A bibliography of additional work by the author, including consulting reports and additional science papers arising from the University of Waikato coastal studies at New Plymouth, as well as consulting reports that investigate the regional coastal environment.

Appendix 2: Documentation on the calibration and validation of the WBEND wave refraction model applied in the numerical studies of Black & McComb (2000) and Cole et al. (Appendix 4).

Appendix 3: An abstract on a novel procedure for using a drop video camera for high-resolution mapping of benthic habitats on shallow subtidal rocky reefs. This was delivered to the Fisheries Research Division Conference "*Direct sensing of the size and abundance of target and non-target fauna in Australian fisheries*" at Rottnest Island, Western Australia, September 2000. The abstract includes an interactive HTML CD map with linked video imagery, which is attached to the appendix. This abstract is authored by Cole, McComb and Sait.

Appendix 4: A paper that investigates the characteristic distribution of benthic habitats on a high-energy, rocky coast to establish the link between ecology and physical parameters (e.g. waves, currents, suspended sediments, surficial sediments, and subsurface light levels) at this temperate location. This paper has been prepared for submission to Liminology and Oceanography, and is authored by Cole, McComb and Black.

Appendix 5: Suspended sediment data and maps showing the tracer movements. Wave, current, wind, tide and tracer data are included on the CD.

LIST OF FIGURES

LIST OF TABLES

LIST OF SYMBOLS AND ACRONYMS

ρ	density
ω	angular frequency
ε^2	spectral width
θ	dimensionless skin-friction Shields parameter
Ψ	sediment mobility number
κ	von Karman's constant
$\theta_{2.5}$	grain-roughness dimensionless skin-friction Shields parameter
ε_s	sediment diffusivity
AR	Aspect Ratio
a_s	wave orbital radius, or wave orbital semi-excursion distance
C	concentration
CD	chart datum
C_f	seabed friction coefficient
C_o	near-bed sediment reference concentration
C_z	sediment concentration at elevation z above the seabed level
d	water depth
DGPS	a Global Positioning Satellite navigation with differential correction
D_i	inside diameter
D_o	outside diameter
f	frequency
f_d	downward flux
f_w	Swart (1974) friction factor
g	acceleration due to gravity
h	total water depth
H	wave height
$H_{1/3}$	average of the highest third of waves measured
H_s	significant wave height
k	wave number
K_h	spreading coefficient for tracer
k_s	nikuradse roughness
LAT	lowest astronomical tide
l_s	mixing length
M	mass
N_A	eddy viscosity
p	pressure

RMS	root mean squared
RSA	Rapid Sediment Analyser (fall tube)
R_t	Reynolds Number
R_v	the ratio of flow speed to particle fall velocity
S	spectral density
SIM	Spatial Integration Method
SLIMPA	Sugarloaf Islands Marine Protected Area
SSC	suspended sediment concentration
t	time
TIM	Time Integration Method
T_m	mean spectral wave period
T_p	peak spectral wave period
U	current velocity
u, v	the horizontal orthogonal components of wave orbital velocity
U_c	current velocity weighted by concentration
w	the vertical component of wave orbital velocity, or the particle settling velocity
W^*	non-dimensional w derived by normalising w to the rate of change in sealevel
z	the elevation above seabed, or above mean sea level

1 INTRODUCTION

1.1 High-energy, rocky coast dynamics

The key sediment transport processes in coastal environments are entrainment, suspension, and advection - processes that result from the interactive sum of waves, currents, seabed topography and sedimentology over the entire littoral system. These processes combine to produce a complex physical system that is characteristically variable in both time and space. Coastal regions are also proximate to high concentrations of the global urban and industrial infrastructure, which often results in added anthropogenic influences on the physical and ecological coastal environment. For example, terrigenous sediment inputs to coastal systems may be linked to fluvial and land management practices, coastal structures can alter the local sediment and hydrodynamics, and maintenance dredging of harbours and inlets for navigation can impact the nearshore littoral sediment budgets and ecological communities. Accordingly, understanding the dynamics of coastal systems has been a long-held goal of engineers and scientists - with such comprehension holding the potential for minimising negative environment effects of coastal developments, as well as optimising benefits to society.

Of the numerous coastal environments that have been classified according to morphology and climate (e.g. Komar, 1998), those that exist under high-energy wave conditions are perhaps the least understood. This may be in part due to the difficulty in collecting data in such environments (e.g. Morang *et al.*, 1997), and also to a less intensive coastal infrastructure that commonly exists there. At New Plymouth, New Zealand, on the northern Taranaki coast (Figs. 1.1 & 1.2), there is a high-energy wave climate and a variable seabed topography that features both sandy and rocky beds, with an exposed open-coast aspect. The geomorphology is dominated by laharic pyroclastic material, and the mobile sediments are "black" volcanic sands that have dense mineral constituents. The site features intensive urban and industrial development along some 7 km of irregular coastline, with an artificially constructed harbour, rock-wall coastal armouring and urbanisation of Holocene dunes. A study of the coastal and sediment

dynamics at New Plymouth represents a unique opportunity to investigate the littoral response to a wave-dominated climate over a morphologically variable seabed with a heterogeneous substrate. Furthermore, the site provides added complexity with the effects of harbour maintenance dredging on the nearshore littoral sediment budgets, and also community issues surrounding the dumping of those dredged sediments.

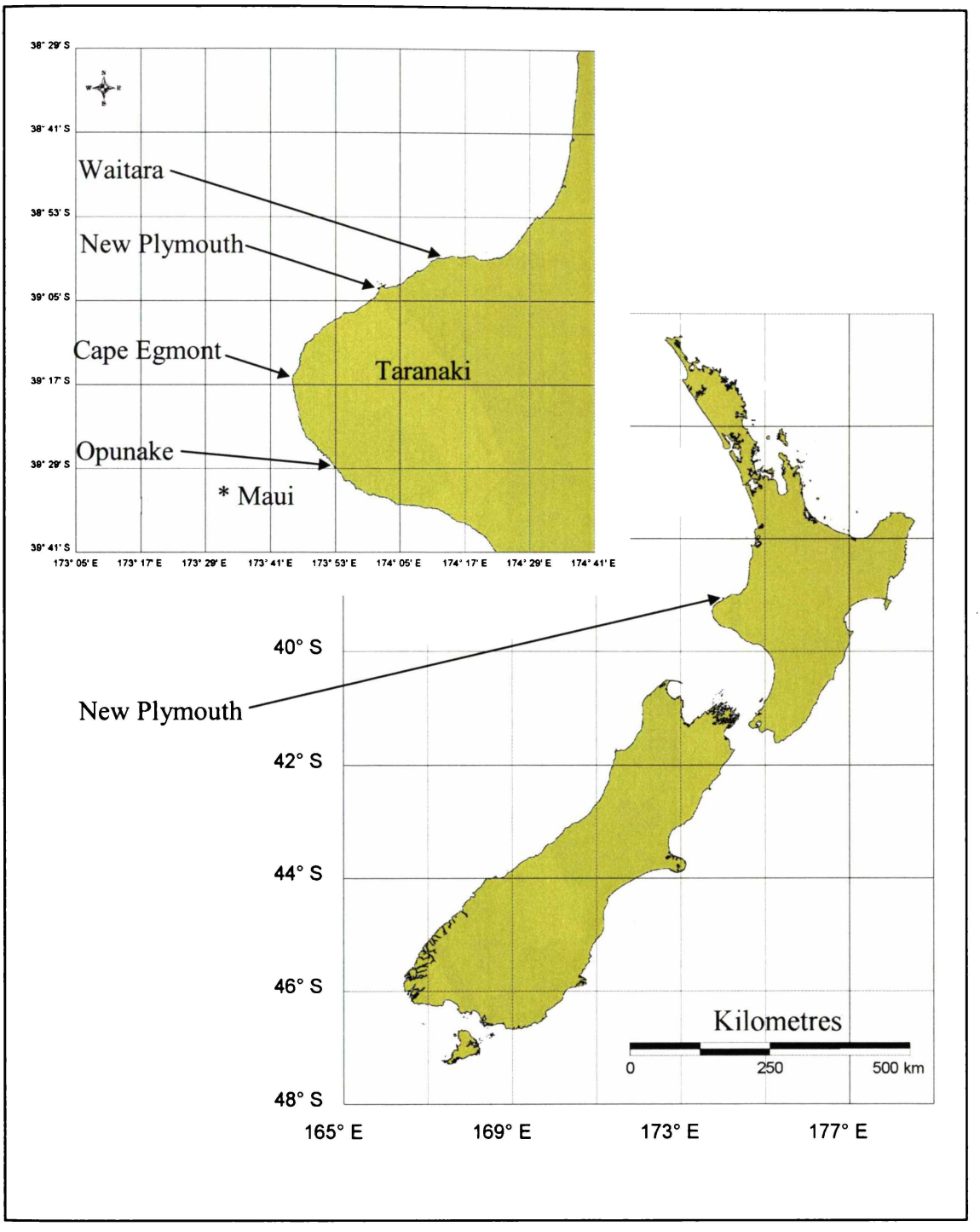

Figure 1.1: Location maps showing New Plymouth, New Zealand, and named locations within the province of Taranaki.

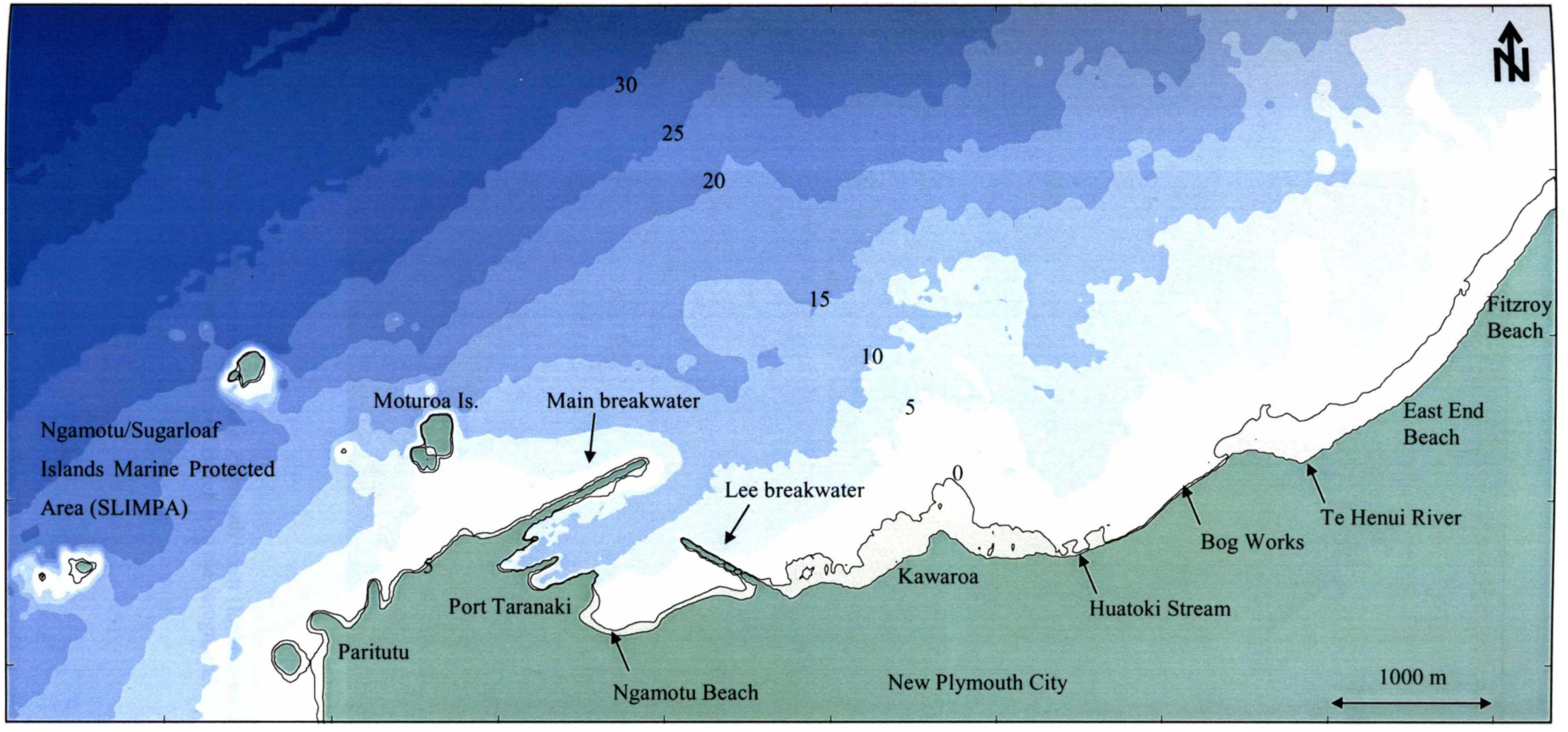

Figure 1.2: Bathymetric map (5 m isobaths) of the New Plymouth coast, showing Port Taranaki and other named features.

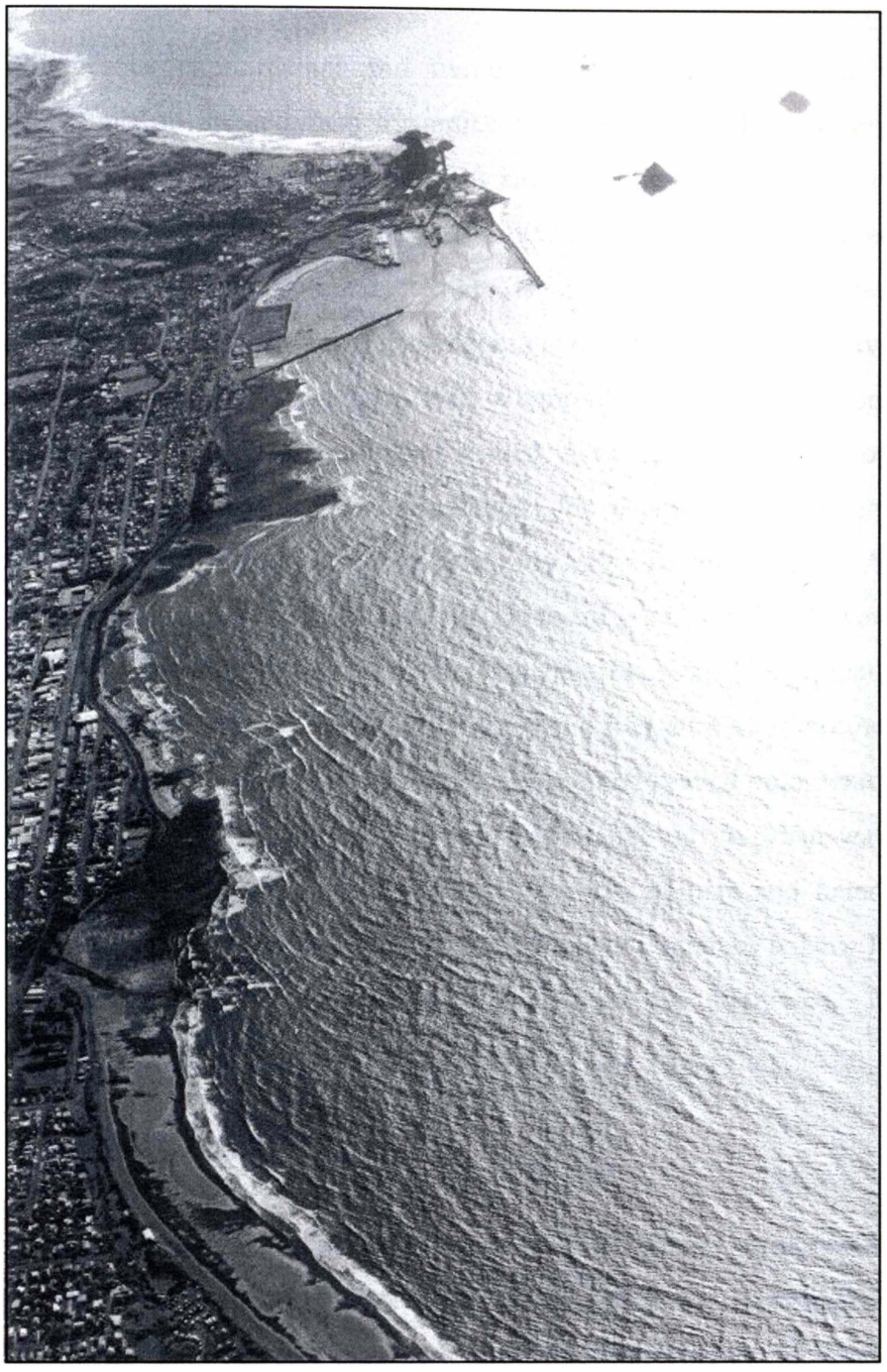

Figure 1.3: Aerial photograph of the New Plymouth coast (looking west), showing the complex patterns of wave refraction and diffraction. Fitzroy Beach is in the foreground.

1.2 Knowledge shortfalls

There are numerous experimental and numerical investigations in the scientific literature that report on the sediment dynamics of specific coastal environments. For example, Lou & Ridd (1997) used field data and numerical techniques to examine sediment dynamics in Cleveland Bay, Australia, including dispersal from a dredge-spoil ground. Similar studies were also conducted at Gisborne, New Zealand, as reported by Healy *et al.* (1998). While both those sites experience periodically high wave energy, they are characteristically different from New Plymouth, being embayed and having simple bathymetric features and an all-sand seabed. A range of large-scale open-coast sediment dynamics studies has been conducted, for example the numerous field programmes at Duck, U.S.A. (www.frf.usace.army.mil), Torrey Pines, U.S.A. (e.g. Seymour, 1986) and Terschelling, Holland (e.g. Hoekstra *et al.*, 1997). However, many of those studies have been limited to the shallow nearshore regions (i.e. typically < 10 m water depth) over uniform sandy beds. In the scientific literature there are no detailed reports of sediment dynamics for sites with the climate and seabed complexity of New Plymouth, particularly considering a broad nearshore range out to 20 m water depth. The combination of volcanic sands, a high-energy wave climate and heterogeneous substrate/bathymetry means that in examining the sediment dynamics at New Plymouth, there are fundamental knowledge shortfalls that need be addressed. These are specifically outlined as follows.

1.2.1 Coastal morphology

Large, shore-normal reefs and an irregular coastline will strongly influence the littoral sediment transport patterns (Storlazzi & Field, 2000). While the relationship between coastal morphology and sediment transport has been well studied for beaches (e.g. Komar, 1998) and indeed high-energy wave-dominated coasts (e.g. Niedoroda *et al.*, 1984; Shih & Komar, 1994), the subtidal effects in depths of up to 20 m have not. Subaqueous topographic effects are often cited as a reason for discrepancies between numerical results and nearshore sedimentary observations (e.g. Pilkey *et al.*, 1994), and the degree to which the reef structures at New Plymouth impede or modify the sediment transport cannot be inferred from other study locations. Storlazzi & Field (2000) suggest that shore-normal reefs (or ridges) can "*steer and focus currents, affect the direction of*

sediment transport, and form barriers to the alongshore transport of sediments in a manner not commonly observed along coastal plain shorelines." Wright (1987) and Cacchione & Drake (1990) consider that diabathic sediment flux under storm conditions is an important parameter in the net longshore transport along embayed rocky coasts. The New Plymouth coast is not embayed, but does have an irregular morphology, in both the subaqueous and intertidal regions.

1.2.2 Wave transformations

The topographic variability in the seabed at New Plymouth will cause the spatial distribution of wave energy to be strongly influenced by refraction (e.g Jones, 2000), as illustrated in Figure 1.3. The presence of the offshore islands and port breakwaters provide localised sheltering to the nearshore regions, and a mixed semi-diurnal tide (with a spring range of 3.1 m; Haskins, 1957) means that refractive indices are constantly varying. Similarly too for the frictional attenuation of wave energy through orbital interaction with the seabed, which is a function of both the wave characteristics and the bed roughness (Thornton & Guza, 1983; Weber, 1991). In common with other New Zealand West Coast sites, the incident wave energy spectra has a range of frequencies and directions, often occurring at the same time (Pickrill & Mitchell, 1979; Kibblewhite *et al.*, 1982). In order to quantify the nearshore sediment entrainment potentials, it is necessary to be able to numerically model the transformation of incident waves across these highly irregular reefs. While previous studies have shown good agreement between refraction model and laboratory data for irregular bathymetry (e.g. Chawla *et al.*, 1998), model validation for a site with the scale and complexity of New Plymouth is rare.

1.2.3 Sediment entrainment

Strong oscillatory near-bed motions are associated with high-energy wave conditions, especially in shallow nearshore zones. Such conditions present a rigorous test of time-averaged sediment entrainment formulae, whereby a near-bed reference concentration (C_o) is related to the grain-roughness dimensionless skin-friction Shields parameter ($\theta_{2.5}$) induced by the wave-orbital motion (e.g. Nielsen, 1992). C_o is a measure of the intensity of sediment entrainment, which is thought to have an asymptotic relationship with $\theta_{2.5}$ (e.g. Engelund & Fredsoe, 1976). This occurs because C_o will ultimately reach

a maximum value that is defined by the volume occupied by the sediment grains (approximately 0.3 vol/vol; Davies & Li, 1997). The empirically derived expression of Nielsen (1986) relates C_o to the third power of $\theta_{2.5}$, which is not asymptotic and assumes no upper limit. The Nielsen (1986) term has been widely tested in a range of time-averaged applications (e.g. Black & Rosenberg, 1991; Black, 1994; Black *et al.*, 1997; Green & Black, 1999) although it remains unknown whether the high-energy conditions at New Plymouth would exceed the useful range of this form of expression.

1.2.4 Black volcanic sands

The coastal sediments at New Plymouth contain heavy minerals, and no field data have been reported which examine the entrainment, suspension and advection of such "black" sands. Komar (1989) notes that the formation of marine placers, including "black" sands, is evidence of the selective transport through concentration by the physical coastal processes based on density and particle size. The flume studies of Li & Komar (1992) provide supportive data to that observation. While "dense" sediment particles may be related to quartz densities in terms of equivalence (e.g. settling velocity or entrainment; Komar, 1989), to date there is no field evidence that "black" sands may be similarly treated as quartz-density sands in sediment entrainment and suspension calculations. This is relevant when considering time-averaged applications, as the entrainment formulae (such as given by Nielsen, 1984) have a semi-empirical derivation.

1.2.5 Hydraulic "roughness" of the rocky reefs

A hydraulically "rough" seabed surface will have a thicker boundary layer and generate greater turbulence than a smooth bed (e.g. Nielsen, 1992), which has concomitant effects on sediment entrainment and suspension (e.g. Curray, 1965; Fredsoe & Deigaard, 1992), as well as wave friction (Nielsen, 1983). The interaction of currents (both steady and oscillatory) with elements of the bed transfers energy from the flow into turbulent motion, and this dissipation is directly related to the geometry of the bed elements (Green *et al.*, 1998). In terms of nearshore sediment dynamics, the overall effect of the hydraulic roughness of rocky reefs is unknown. Greater turbulence may influence the suspended sediment concentrations profile and flow perturbations by the

rocks may induce convective suspension (e.g. Nielsen, 1992), thereby altering the littoral flux potentials. Conversely, the roughness elements may provide quiescent zones that are conducive to the settlement of suspended particles (Green *et al.*, 1998). Gaylord (1999) and Howse (2000) have made measurements of the wave-velocity structure over rocky intertidal platforms, showing complex 3-dimensional flows that are strongly influenced by the bed geometry. Ultimately however, the effect of large areas of rocky reefs on sediment entrainment, suspension and advection is not well understood.

1.2.6 Sediment dispersal from a nearshore dredged-sand dump mound

Nearshore placement has become an accepted method of shoreline renourishment or to mitigate the effects of interruption of the littoral transport by dredged harbours and inlets (Scheffner, 1996). Dredged-sand mounds placed in wave-dominated nearshore environments typically show a shoreward migration that is ascribed to the orbital velocity asymmetry under shoaling waves (Douglass, 1995,1996). However, previously reported studies (e.g. Vera-Cruz, 1972; Schwartz & Musialowski, 1977; Jackson & Tomlinson, 1990; Uda, 1991; Andrassey, 1991; Bodge, 1994; Otay, 1995; Mesa, 1996; Foster *et. al.*, 1996, among others) have monitored mound behaviour over uniform sandy beds, and the dispersal rates and trends in a rocky reef environment have not been considered. Furthermore, the benthic ecology of shallow subaqueous reefs in temperate climates typically exhibits a higher species density and diversity than "soft" or mobile substrates (Schiel & Foster, 1986; Kingsford & Battershill, 1998). With this regard, the dispersal behaviour of a nearshore dredged-sand mound on the rocky coast at New Plymouth may cause significant ecological impacts. For example, if a mound migrates as a coherent body, then the benthic habitats in the migration pathway would become smothered by the dumped sediments.

1.2.7 Harbour sedimentation

Sedimentation at the entrance of artificially constructed harbours in wave-dominated environments is common, although the patterns and rates of accretion vary. The Port of Portland (Australia) is similar to Port Taranaki, with a near-identical breakwater system and harbour dimensions, as well as having negative downstream coastal effects from the harbour sedimentation (Cowper & Nankervis, 1997). Caldera Port (Costa Rica) also has

a breakwater that protrudes into the nearshore littoral system, although accretion within the harbour is dominated by storm events (Rodoriguez & Katoh, 1994). Unconsolidated marine sediments will find a dynamic equilibrium with the local wave and current regime (Niedoroda *et al.*, 1984), which is why regular dredging is required to maintain such harbours open to shipping. Dean (1989) discusses the use of artificial structures (such as Santa Barbara harbour, U.S.A) as sediment traps for measuring the longshore flux. He cautions that to interpret harbour trapping data in terms of the net littoral transport requires an understanding of the mechanism of accretion, as well as the adjacent littoral flow streamlines. Accordingly, obtaining this information was a key focus for the studies at New Plymouth.

1.2.8 Data collection

High-energy coastal environments present numerous challenges for data collection, particularly in temperate waters where underwater visibility is frequently poor - making SCUBA diving operations difficult. Deployment techniques needed to be refined and tested to ensure that wave and current meters would be secure under extreme wave-orbital motions, while still maintaining quality data records. The requirement to measure waves and currents at sites in water depths of 20-35 m means that influence of mooring components (e.g. taut-wires and buoyancy) on the measured data needed to be considered. Trapping methods for obtaining time-averaged suspended sediment concentrations have not been calibrated in energetic wave conditions, and it is unknown if they provide an accurate representation of the settling flux (White, 1998). Finally, sediment tracing in a predominantly rocky nearshore environment presents unique difficulties in sample collection.

1.3 Background information

The west coast of New Zealand has an exposed aspect; open to swells generated in the Tasman Sea, as well as those from the expansive Southern Ocean (Pickrill & Mitchell, 1979). Regionally, this temperate coastline receives little shelter from the mid-latitude westerly wind belt that, combined with the wave climate, results in a high-energy coastal climate.

A harbour was constructed at New Plymouth in 1881 (Fig. 1.4). Taking advantage of the Paritutu volcanic headland (Fig. 1.2), the fledgling port utilised a breakwater to provide shelter for vessels, thereby creating the only deepwater port on the West Coast of New Zealand. However, almost immediately following construction, the effects of this structure protruding into the littoral system became apparent. Sedimentation was occurring on both sides of the breakwater, and a regular dredging and offshore disposal programme was instigated to maintain an adequate navigation channel and berthage. Coincident with this sedimentation and dredging, beaches and the coastline adjacent (to the east) of the harbour were denuded of sand, and the rate of coastal erosion was observed to accelerate (Agnew, 1973).

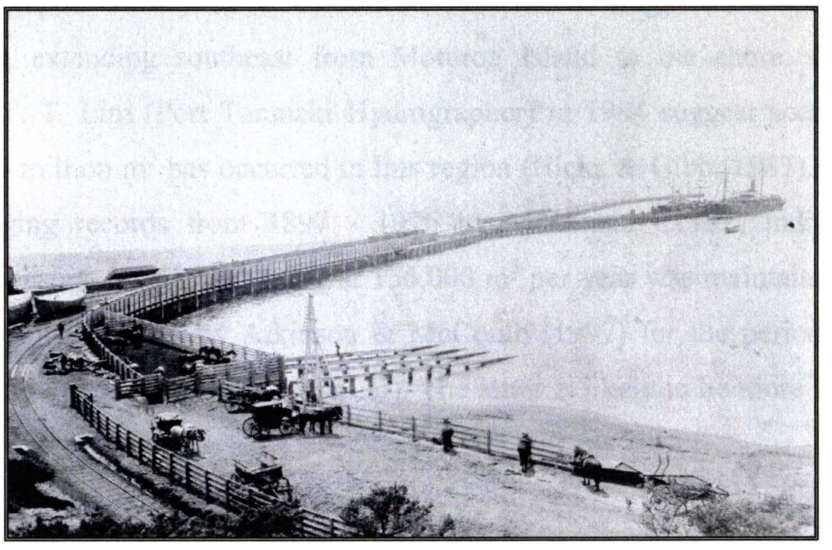

Figure 1.4: Photograph of Port Taranaki (circa 1902) showing the newly-constructed breakwater extending from the Paritutu headland.

1.3.1 Harbour sedimentation and dredging

One of the earliest investigations on reducing the sedimentation in the harbour was that conducted by Mr C. Napier Bell, whose letter to the Harbours Board was printed in the Taranaki Herald (the provincial daily newspaper) in October, 1901. In it, Bell rejects an idea to remove a section at the root the breakwater in order to allow the unimpeded northeasterly passage of sand along the coast, instead favouring continued dredging as the most appropriate course. Until 1964, the dredged sediments were dumped on a spoil ground approximately 700 m north of the harbour entrance (Fig. 1.5), after which the ground was moved further offshore to its present location. The use of the first site was discontinued after the resulting elevation of the seabed was thought to detrimentally affect wave conditions at the harbour entrance (Atkinson, *pers comm.*). The present site (Fig. 1.5) has its shoreward edge approximately 1000 m due north of the tip of the main breakwater, in water depth of 16-28 m.

The breakwater has undergone four extensions since 1889, reaching it present length of 1256 m in 1967 (Fig. 1.6). With each extension, a new sedimentary equilibrium was established for the region between the breakwater and Moturoa Island (McLennan, 1982), which has a salient morphology. This submarine tombolo was identified in a 1877 hydrographic survey by E C. Jones (Government Engineer) for the proposed harbour site, extending southeast from Moturoa Island to the shore. Comparative surveys by Y. T. Lim (Port Taranaki Hydrographer) in 1984 suggest accretion of the order 1.4-1.7 million m^3 has occurred in this region (Hicks & Gibb, 1987). An analysis of the dredging records from 1897 - 1976 by McLennan (1982) indicates that a reasonably constant level of dredging at 156,000 m^3 per year was maintained, although the more recent estimates by Atkinson & McComb (1997) for the period 1989-1996 give a higher value (~180,000 m^3 per year). The latter is likely to be more accurate due to improved survey techniques.

There exist clear patterns of sedimentation within the harbour. The main area of accretion is the breakwater tip-shoal region (Fig. 1.5), which accounts for approximately 70-75% of the harbour maintenance dredging volumes (Atkinson & McComb, 1997). Fine to medium sized sands accumulate here in a characteristic two-lobed shape, while finer material (including silts) are evenly deposited over the remaining operational area

of the harbour. Presently, the harbour is dredged biennially with a trailer suction hopper dredge to a depth of 10.5 m.

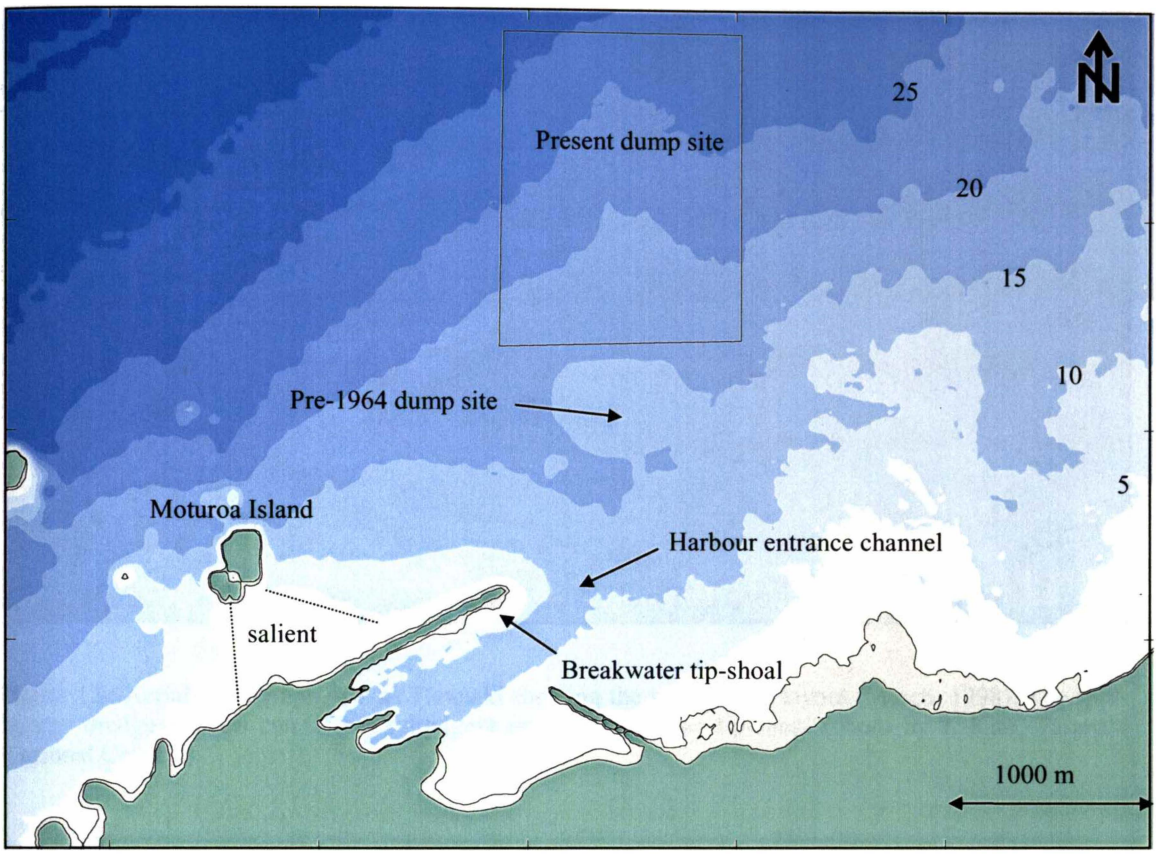

Figure 1.5: Bathymetric map of the harbour region, showing the breakwater tip-shoal, present and past dump sites for maintenance dredgings, harbour entrance channel and the salient inshore of Moturoa Island.

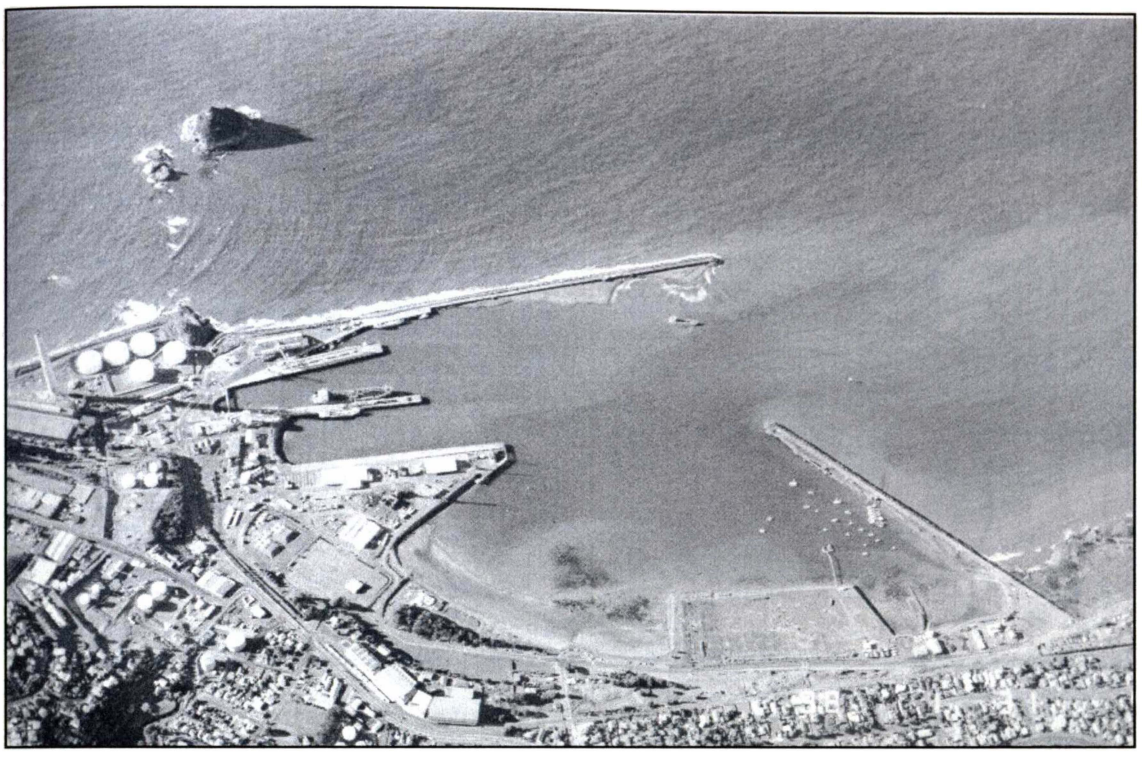

Figure 1.6: Aerial photograph of Port Taranaki showing the present-day layout (March, 1998). The split-hopper dredge *Pelican* can be seen dredging on the breakwater tip-shoal (photo by J. Kito, Taranaki Regional Council)

1.3.2 Coastal erosion and nearshore sediment budgets

Over successive years, the issue of sand depletion of the New Plymouth foreshore has galvanised the local government against the port authority, with the former strongly expressing the desire for mitigation of the downstream effects of the harbour dredging operations. Coastal rock-wall armouring of the city foreshore commenced in 1944 to halt the rapid erosion as the beaches to the east of the port were denuded of their intertidal sand deposits (e.g. Fig 1.7). From the 1970s, a series of studies were engaged to investigate foreshore erosion and beach renourishment options (i.e. Agnew, 1973; Agnew, 1976; Kirk, 1980; McLennan, 1982; Hicks & Gibb, 1987).

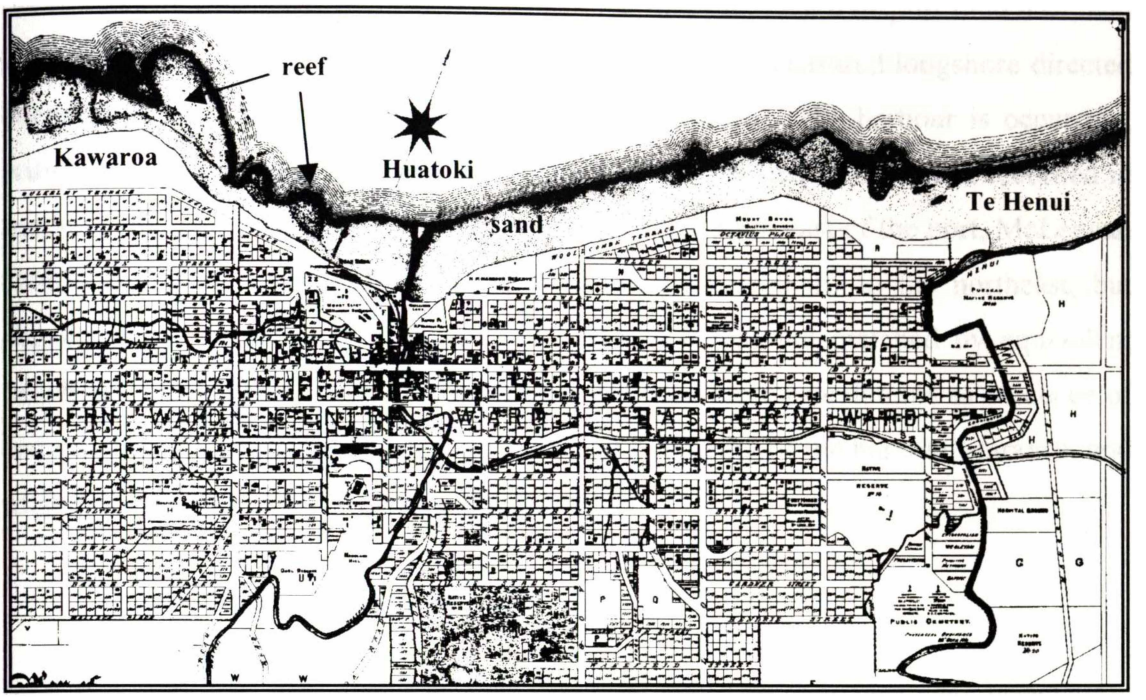

Figure 1.7: 1880 survey map of the central New Plymouth region by T. K. Skinner. The foreshore is mostly a wide sandy beach. Rocky intertidal reef platforms are evident at Kawaroa and near Te Henui as well as sandy areas on the upper shore.

While those studies did not involve detailed field experimentation, a common finding was that the net sediment transport was directed alongshore to the northeast, and the port has a significant effect on the nearshore littoral sediment budgets along the eastern city foreshore. Other factors were also identified as having negative impacts on the coast, specifically those associated with the 1908 railway re-routing which involved a major coastal re-alignment at the Huatoki rivermouth, and the re-direction of the Te Henui Stream (Fig. 1.2). The dumping of dredged sediments in the offshore spoil ground (Fig. 1.5) has been described as depleting the nearshore littoral system of sediment (e.g. Hicks & Gibb, 1987), although possible mitigation was identified through re-location of the disposal ground, or the use of an alternative method such as a pumping system to bypass sediment across the harbour entrance.

The path and flux of sediments naturally bypassing the harbour have been disputed, with McLennan (1982) concluding that the harbour totally interrupted the littoral transport at New Plymouth, while Hicks & Gibb (1987) estimate that approximately 40,000 m^3 passes across the harbour entrance annually. Hicks & Gibb (1987) also describe the effect of the main breakwater as deflecting the longshore movement of sediments out into deeper water. Sediment trapping experiments adjacent to the main

breakwater by Gorman *et al.* (1995) represent the first sediment transport field data, and showed high loads of suspended sediments. Coupled with measured longshore directed currents, their data imply that active sediment bypassing of the harbour is occurring, with bypassing fluxes of at least 10,000-20,000 m^3yr^{-1} (projected from data recorded in moderate to calm conditions). At Fitzroy Beach, some 5 km east of the port, McLennan (1982) calculated an annual longshore transport of 55,000 m^3 to the northeast, but suggested that value must be an over-estimate as it was not matched by equivalent beach erosion. Hicks & Gibb (1987), however uphold those calculations as evidence of sediment supply to the beach, both from natural bypassing of the harbour entrance, and migration from the offshore dredge spoil ground.

1.3.3 Sedimentary and coastal features

New Plymouth has an irregular coastline with an approximately east-west orientation. The Paritutu/Ngamotu volcanic extrusions dominate the western region, while the central and eastern regions contain a series of reefs and channels that extend roughly perpendicular to the shore (Fig. 1.2). At the eastern extremity of New Plymouth there is a 1.7 km long sandy beach, which exists on the western flank of the delta formed by the Waiwakaiho River (McLennan, 1982). Inter-tidal and sub-tidal structures are comprised of inter-bedded lahar deposits, often overlain by boulders, gravels and sand. The substratum lithology is classified as part of the Maitahi Formation which is a volcanic breccia containing a heterogeneous assemblage of boulders to gravels within a sandy / muddy matrix (Neall, 1994). Selective erosion of the weaker matrix has resulted in large inter-tidal platform reefs which regionally extend as sub-tidal boulder fields up to 5 km offshore (TCC, 1985). Considerable spatial variability is noted for these inter-tidal and sub-tidal features, resulting in a complex bathymetric and sedimentary environment, with both rocky and sandy substrates (Fig. 1.8). Arron & Mitchell's (1984) side-scan sonar data shows that a sandy seabed dominates the western regions, extending as far as the harbour entrance, after which the sandy bed grades into a predominantly rocky substrate. A ribbon of sand extends shore-normal across the entire nearshore zone, which has the appearance of an in-filled relict fluvial channel. With reference to Figure 1.8, Hicks & Gibb (1987) state that "*it is tempting to recognise a trail of sand patches leading from the old dumping ground northeast of the port to East End Beach*".

The mobile sands are mostly of andesitic volcanic origin (Matthews, 1977; McLennan, 1982), and there is considerable spatial variation in the median particle size, which Hicks & Gibb (1987) attribute to wave energy gradients. Regionally, they may be described as well-sorted fine sands, with solid densities that range from 2750-3730 $kg.m^{-3}$, with an average value of 2850 $kg.m^{-3}$ (Bartholomeusz, 1985). The mineral compositions remain relatively constant, with 38% (by mass) of heavy minerals (i.e. augite, opaques and horneblend) and 62% light minerals (feldspar and composites) (Bartholomeusz, 1985).

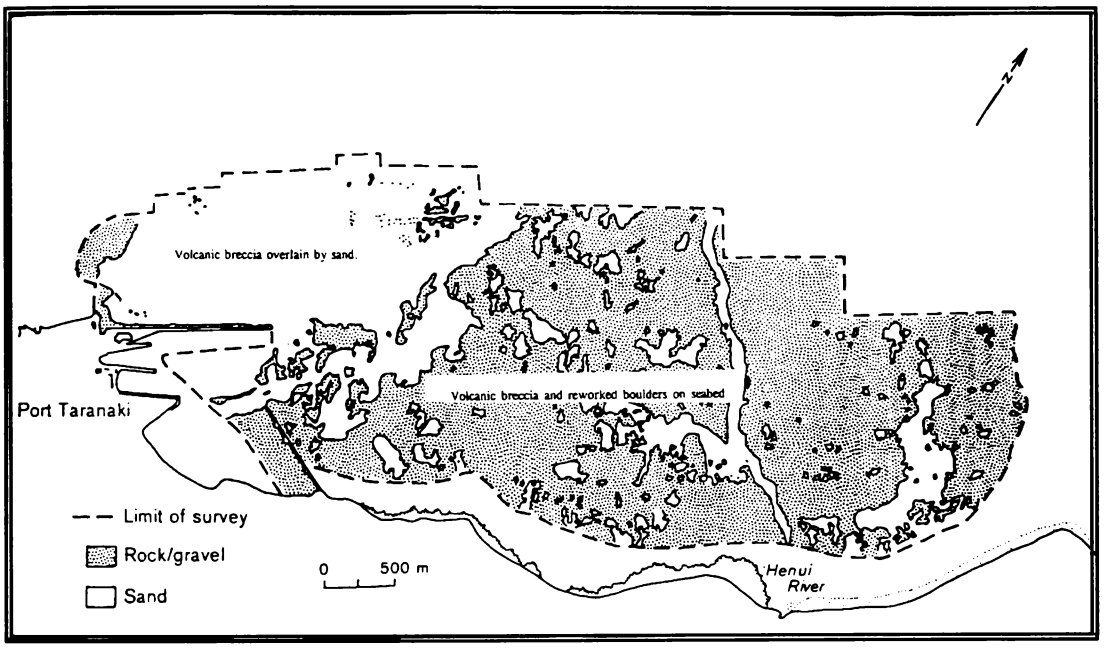

Figure 1.8: 1984 map of the sandy and rocky seabed facies at New Plymouth from the side-scan sonar survey of Aaron & Mitchell (1984).

1.3.4 Wave climate

The New Plymouth regional wave climate is considered in numerous studies (i.e. HRS, 1963; Glenn, 1972; Agnew, 1976; TCC, 1980a and b; TCC, 1981; McLennan, 1982; TCC, 1985; OSL, 1989; MOR, 1991, Gorman *et. al*, 1995), three of which (HRS, 1963; Agnew, 1976; McLennan, 1982) use data obtained from visual observations of wave height, period, and direction. Glenn (1972) reports the statistical wave climate for offshore of Port Taranaki (~ 30 m depth) generated from meteorological data. TCC (1985) reports on three months of wave data measured by a Waverider buoy moored in 20 m water depth 2.5 km offshore of the New Plymouth Airport. The general conclusion is that the North Taranaki wave climate is dominated by long-period waves approaching from the westerly quarter. MOR (1991) presents the analysis of non-directional waves from seven years of recorded data from a wave tower at the entrance to Port Taranaki. Those data show a seasonal variation in wave height (with the largest wave heights observed from May-October) and further confirmation of the wave-climate dominance by low-frequency (<0.1 Hz) components.

Wave data have been collected in the South Taranaki Maui oilfield (Fig. 1.1) over a ten-year period (September 1976-April 1987), the last year of which included directional wave information. Those data are generally representative of wave conditions along the west coast of central New Zealand with the exception of local features (Laing, 1993). Kibblewhite *et al.* (1982) have produced a wave climate based on five years (1977-81) of these data and their analysis of seasonal variations indicates a higher wave climate in the winter months. From their data for May – September, the occurrence of significant wave height in the <1, 1-2, 2-3, 3-4, 4-5, and >5 m ranges is approximately 3%, 25%, 35%, 25%, 8% and 4%, respectively. In a spectral analysis of the Maui wave data by Ewans & Kibblewhite (1992), the measurements demonstrate the importance of the south-west swell component (with a wave period of 12.4 s) arriving from distant sources in the south of the Tasman Sea and the Southern Ocean. They suggest that the westerly and south-westerly wind components also make a significant contribution to the wave climate.

1.3.5 Wind climate

The weather pattern at New Plymouth is characterised by the eastward migration of anticyclones at 5-7 day intervals, separated by low-pressure troughs. Anticyclones account for settled conditions, which occur about 25% of the time, with the rest of the weather determined by the low-pressure systems (Harris, 1990; Maunder, 1970). The path of anticyclones across New Zealand exhibits a seasonal variation, with anticyclonic influences extending further south over the summer/autumn months. Patterns are further modified in response to El Nino-Southern Oscillation (ENSO) events, whereby an El Nino event typically results in a west-southwest anomaly superimposed over the 'normal' wind conditions, causing strengthened and more frequent west-southwesterly winds. For a La Nina event the opposite is generally true, with an east-northeasterly wind field anomaly.

Winds are routinely measured at the New Plymouth Airport (14 km northeast of Port Taranaki; Fig. 1.1), and those data have been summarised by TCC (1980a, 1980b, 1981). The dominant annual wind directions are from the southeast and west (Fig. 1.9). Gorman *et al.* (1995) note that while winds at Port Taranaki are modified by topographic effects, the regional airflow is well represented by the New Plymouth Airport data.

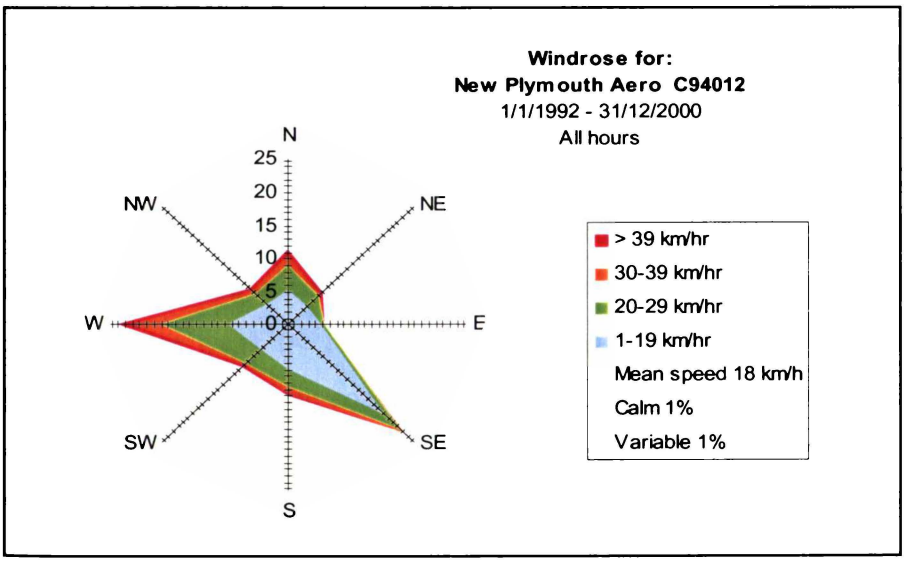

Figure 1.9: Wind rose for New Plymouth Airport (1992-2000).

1.3.6 Currents

Prior to the present study, very little data on coastal circulation patterns in the New Plymouth region was available. Measurements were made over 16 weeks (in 1992 / 1993) at 5 and 9 m depths just offshore of the New Plymouth Power Station by Black & Sokolov (1993). They found that the typical tidal currents were less than 4 cms^{-1}, representing about 4% of the total current variance. They also concluded that currents in the region generally flow along bathymetric contours and that low frequency (>0.5 cpd) variance is strongly dependent on the east-west component of wind. Field measurements by Gorman *et al.* (1995) at two sites near the harbour entrance were in concurrence with the general findings of Black & Sokolov (1993).

The broader circulation on the North Taranaki coast has been described by field investigations conducted by TCC (1981 and 1985) and OSL (1989). Data were collected primarily to assess options for marine outfalls and currents were measured at a range of North Taranaki sites and water depths (7 to 70 m). Those studies indicate that the regional circulation is primarily determined by continental shelf dynamics and local wind stresses, which concurs with the suggestions of Heath (1982) and Kibblewhite *et al.*, (1982). Currents are predominantly parabathic, and exhibit both up-coast and down-coast modes, while the net flow is predominantly down-coast. The latter suggests a base flow, most probably due to the West Auckland current (Heath, 1982). The up-coast flow is generally less persistent and is usually associated with strong west to south-westerly winds. TCC (1985) was able to relate the currents at Waitara to the wind stress, with down-coast velocities of 4.6% of the wind speed, and up-coast velocities of 2.8%. Those findings are similar to that of Kibblewhite *et al.* (1982) on the South Taranaki coast, in which the wind-forced currents had velocities of ~3% of the wind speed. Tidal currents were weak (< 10 cms^{-1}) and often masked by the wind-driven circulation. Flood tides exhibit an up-coast flow, and ebb tides have a down-coast flow.

Mid-water currents measured over a one-year period at a site north of Waitara (in 20 m water depth) show a net current vector of 5.7 cms^{-1} at a heading of 260° (TCC, 1985). Velocities were found to range from 5-30 cms^{-1}. OSL (1989) discuss the TCC data and further reports that the coastal currents are rarely likely to exceed 50 cms^{-1}. Current profiling and drogue tracking experiments by TCC (1985) indicate that current

velocities decrease with increasing depth below the water surface. While a temporal lag is evident between the surface and mid-water currents at periods of veering winds, no systematic current stratification in the water column was observed. Currents measurements made by TCC (1985) at three nearshore sites off Motunui (5 km east of Waitara, in water depths of 10-18 m) and at a single reference site off Waitara (20 m water depth) indicate a systematic reduction in velocity with increasing proximity to shore. Nearshore current directions remain congruous with the measurements made at the reference site (i.e. bimodal longshore), although a greater overall directional variability was noted. Under stormy conditions, however, the peak flows at the nearshore sites were frequently observed to exceed those measured further offshore, suggestive of strong wave-driven currents in the nearshore zones.

1.4 Mitigation studies

The Resource Management Act (1991) requires the operators of Port Taranaki (Westgate Transport Ltd) to avoid, remedy or mitigate the adverse effects of its activities. Resource consents for harbour dredging and disposal expired in 1999, and in seeking renewal, Westgate commissioned the Department of Earth Sciences, University of Waikato, to undertake coastal studies to:

- *seek the best sites for placement of the sediments dredged by the port and, once selected, to measure and predict the effects on the environment in relation to the port's regular maintenance dredging programme.*

Those studies, which commenced in 1996, were also required to address the community and cultural issues associated with dredge-spoil disposal. Specifically, the civic desire to see sandy beaches returned to parts of the foreshore needed to be balanced by the view of those who value rocky intertidal regions. Both Maori and non-Maori in the local community recognise the region immediately east of the port (i.e. the Kawaroa Reef) as a source of *kaimoana* (seafood), and did not wish to see the ecology altered. Accordingly, the constraints on site selection were to:

- Place the port's maintenance dredging sand in the littoral drift zone that is feeding the city's beaches;

- Consider independent treatment of the sand dredged from around the tip shoal and the main breakwater and the muds dredged from deeper within the port;

- Prevent any sediment flux associated with the port's dredging from damaging the local *kaimoana* beds on the intertidal and shallow subtidal Kawaroa Reef;

- Minimise re-circulation of dredged sediments back into the port, and

- Ensure that dredge-spoil disposal sites are sufficiently capable of dispersing the dumped sediments within the biennial maintenance dredging return period.

1.4.1 The author's role in the mitigation studies

The coastal studies by the Department of Earth Sciences, University of Waikato, were structured to address the port's requirements and with the intention that the research and experimental effort would additionally form the basis of the author's thesis. The author undertook the majority of the fieldwork, which involved planning and preparation for the experiments, all aspects of instrumentation, field operations (including over 500 SCUBA dives), hydrographic survey and data analysis. The information collected in the field experiments from September 1996 to June 2000 forms the substance of this thesis.

1.5 Thesis objectives

The objectives of the thesis are:

- to investigate the wave dynamics, hydrodynamics and sediment dynamics over mixed "black" sand and rock seabeds at an energetic open coast of irregular morphology, and

- to consider aspects of Port Taranaki sedimentation, dredging and dredge-spoil disposal within that environment.

1.6 Studies undertaken

Two large-scale field measurement programmes were conducted. The first was a two-month deployment of 12 wave and current meters along the New Plymouth coast, with the aim of collecting data for the calibration of a numerical wave refraction model. That model was used to identify potential nearshore dredged-sand placement sites for further study. The second was a one-year programme that involved:

- coastal hydrographic survey;
- a trial nearshore placement of 47,000 m^3 dredged sand in a specifically shaped mound;
- monthly hydrographic surveys of the trial placement and the breakwater tip shoal;
- quarterly side-scan sonar surveys;
- a two-colour artificial sediment tracer release and sampling programme, with release at the trial placement site and offshore of the main breakwater;
- a two-month measurement of suspended sediment profiles from 23 sites using sediment traps;
- a two-month deployment of 13 wave and current meters;
- a one-year deployment of directional wave and current meters inshore and offshore, and
- subtidal and intertidal monitoring of the benthic ecology.

In addition to the empirical outcomes, these data were used to calibrate/validate a suite of numerical models that were ultimately applied to the selection of future sites for the disposal of dredged sediments (under the aforementioned constraints in Section 1.2.4). The refraction modelling was undertaken as part of this thesis, while the circulation and sediment modelling was done by Black (Black and McComb, 2000). The study results are embodied in a series of five reports that cover the field measurements, numerical

studies, ecological studies, and an Assessment of Environmental Effects (AEE). These reports are listed in Appendix 1 of this thesis.

1.7 Thesis structure

The thesis is presented as a series of eight papers that have been published in or submitted to scientific journals, or presented at international conferences and published in the proceedings. These works represent various overlapping components of the coastal system at New Plymouth, and aim to address the specific knowledge shortfalls that exist for this rocky, high-energy environment. A discussion chapter links the topics together to provide an overview of the coastal and sediment dynamics, including supporting data that is not presented in the papers. The thesis structure does not adhere to the chronology in which the work was conducted, but rather seeks an order that allows the thesis objectives to be addressed in a clear and logical fashion. Each chapter was written as a stand-alone paper, which means there is some repetition in the paper introduction sections. To provide continuity, an introductory summary is presented at the start of each thesis chapter, which outlines the contextual basis for that chapter and the relationship to the overall thesis objectives. Here, a brief chapter synopsis is given.

Chapter 2 presents the methodology behind the second (and most intensive) of the field experiments. Much of the background context for the thesis is provided here, along with a summary of the main experimental techniques and some generalised field data results. This paper was delivered at the Coastal Structures '99 Conference in Santander, Spain, and has been peer-reviewed and published in the conference proceedings.

Chapter 3 is a published journal paper that evaluates the performance of a newly-developed wave/current meter (3D-ACM WAVE by Falmouth Scientific, Inc). This paper documents two methods for deriving the directional wave spectra from p, u, v meters, and identifies taut-wire mooring motion as a significant source of error in calculating directional spectra. A method for minimising this error is given, along with examples of the time-averaged directional spectra derived from coincident nearshore and offshore wave data. This paper was submitted to the IEEE Journal of Oceanic Engineering in October 1999, and a revised version was published in the April 2001 Issue.

Chapter 4 describes calibration experiments that tested the efficiency of sediment traps to measure the time-average suspended sediment concentrations under wave-dominated conditions. A variety of traps were tested to determine the most appropriate shape and dimensions for use under large waves. Following this, the efficiency of a single trap design was evaluated through comparison with an automated water sampler over a range of wave events. The findings are the first strong validation for the use of sediment traps under waves, and this paper has been submitted to Marine Geology (July, 2001).

Chapter 5 treats the shallow-water wave transformation processes at New Plymouth in a paper delivered at the Pacific Coasts and Ports 1997 Conference in Christchurch, New Zealand. This peer-reviewed work uses data from the first set of field measurements made in this project, and describes the influence of seabed friction and refraction on the nearshore distribution of wave energy. The effect of white-capping from onshore winds is also isolated and a mechanism based on reduced refraction and increased wave diffraction under onshore winds is suggested. A high-resolution numerical wave refraction model was calibrated with field data, and used to define the spatial distribution of wave energy. The results of this modelling were applied to selecting a trial site for a nearshore dredged-sand placement ground.

Chapter 6 describes the accretion of the Port Taranaki breakwater tip-shoal over a nine-month period following dredging. Monthly hydrographic surveys showing accretion rates of the order of 150,000 m^3yr^{-1} are related to the measured directional wave climate. Numerical simulations of wave refraction/diffraction were employed on three tip-shoal bathymetries to show how penetration of the refracting wave around the tip shoal drives harbour sedimentation patterns. This paper was presented at the Pacific Coasts and Ports 1999 Conference in Perth, Australia, and has been peer-reviewed and published in the conference proceedings.

Chapter 7 details the dynamics of an experimental placement of 47,000 m^3 of dredged sand in 5 - 10 m water depth. Monitoring the behaviour of the specifically shaped placement mound yields important information on how sediment is dispersed and the rates of dispersal within a predominantly rocky nearshore environment. This paper was presented at the International Coastal Symposium 2000 in Rotorua, New Zealand, and

has been peer-reviewed and accepted for publication in the Journal of Coastal Research (ICS 2000 Special Issue).

Chapter 8 presents detailed observations of littoral sediment transport from artificial sediment tracing studies. Tracers were used to investigate the sediment entrapment/bypassing of the harbour entrance, and to monitor the fate and behaviour of the sands dumped at the experimental dredge sand placement site (Chapter 7). This paper has been submitted to the Journal of Coastal Research (July, 2001), and has been accepted for publication following revision (February, 2002).

Chapter 9 establishes a methodology for predicting the suspended sediment reference concentration and profile, under energetic, wave-dominated conditions over "black" sandy beds. Using coincident data from sediment traps and bottom-mounted wave/current meters, the time-averaged near-bed reference concentration (C_o) is related to the wave-orbital induced stress on the seabed. This paper has been submitted to Marine Geology as a companion paper to Chapter 4.

Chapter 10 presents a summary and discussion that unifies the topics covered in the individual papers, and directly addresses the thesis objectives and knowledge shortfalls. Conclusions to the thesis are given in the final ***Chapter 11***.

In addition to the papers presented in the chapter format of this thesis, the author has completed and/or contributed to other related works, including papers and consulting reports. These cover a range of topics, but remain strongly linked to the central theme of the thesis. They are given in the following appendices.

Appendix 1 provides a bibliography of consulting reports and additional co-authored science papers arising from the University of Waikato coastal studies at New Plymouth, as well as consulting reports that investigate the regional coastal environment.

Appendix 2 details the calibration and validation of the WBEND wave refraction model applied in the numerical studies of Black & McComb (2000) and in the biological studies of Cole *et al.* (submitted).

Appendix 3 is an abstract on a novel procedure for using a drop-video camera for high-resolution mapping of benthic habitats on shallow subtidal rocky reefs. This was delivered to the Fisheries Research Division Conference "*Direct sensing of the size and abundance of target and non-target fauna in Australian fisheries*" at Rottnest Island, Western Australia, September 2000 (http://www.aims.gov.au/pages/research/video-sensing/papers/cole/dc/DC-START.htm). The abstract includes an interactive HTML CD map with linked video imagery, which is attached at the back of the thesis. The abstract is authored by Cole, McComb and Sait.

Appendix 4 is a paper that investigates the characteristic distribution of benthic habitats on a high-energy, rocky coast to establish the link between ecology and physical parameters (e.g. waves, currents, suspended sediments, surficial sediments, and subsurface light levels) at this temperate location. This paper has been prepared for submission to Liminology and Oceanography, and is authored by Cole, McComb and Black.

Additional data to support the thesis is provided in ***Appendix 5***. This includes suspended sediment data from the field measurement programmes and a complete set of maps showing the sediment tracer results. Time-series plots of the wave orbital velocities are included for the sediment trapping periods. A CD is also attached with the complete wave, current, wind and tide data collected in the two field measurement programmes.

1.8 Statement of authorship

The research presented in this thesis is the product of the author, and the joint authorship of the papers included herein is the result of collaboration at a collegial level. The numerical model of mooring motion (described in Chapter 3) was conceived by the author, but developed by Dr R. Gorman (National Institute of Water and Atmospheric Research) and subsequently refined with input from Dr G. Terray and Dr M. Grosenbaugh (Woods Hole Oceanographic Institute).

2 COASTAL AND SEDIMENT DYNAMICS AT PORT TARANAKI, NEW ZEALAND: A LARGE, MULTI-FACETED, FIELD EXPERIMENT

2.1 Context of the paper within the thesis

Three experimental field programmes were conducted in the course of the thesis; two that involved the large-scale deployment of oceanographic instrumentation, and one for instrument calibration. This paper reports on the second and most intensive of these programmes. The work was designed to provide the necessary data to calibrate and validate numerical models of the coastal and sediment dynamics at New Plymouth, as well as provide empirical information on sediment transport pathways, accretion within the port, and sediment dispersal from an experimental nearshore dredged-sand dump mound. Six months of planning and preparation were involved in establishing this programme, which ran for a period of 18 months from March 1998. In addition to the experimental methodology, some preliminary results are presented here, although the findings are more fully developed in subsequent chapters. This paper was presented at the Coastal Structures '99 Conference in Santander, Spain and peer-reviewed/published as:

McComb, P., Black K., Healy, T. and Atkinson, P., 1999. Coastal and sediment dynamics at Port Taranaki, New Zealand: a large, multi-faceted, field experiment. *Proceedings of Coastal Structures '99 Conference*, Santander, Spain (Vol. 2), pp. 823-832.

2.2 Abstract

A programme was implemented to seek ways to mitigate environmental impacts on the downstream coast beyond Port Taranaki, New Zealand. The port breakwaters disrupt the nearshore littoral transport system and trapped sediments are presently dredged and placed offshore at a sandy dumpsite in greater than 16 m water depth. The study region is characterised by large, distended rock reefs projecting offshore between sandy channels. Coastal sediments are of andesitic volcanic origin and net littoral transport exceeds 220,000 m^3yr^{-1}. The coast is exposed to the Tasman Sea and features a high-energy wave climate. The study examines environmental impacts and the potential to maximise environmental benefits by nearshore placement of dredged sandy sediments. Data were collected by simultaneous monitoring of physical processes over three years, including sediment dynamics and seabed character, at a range of rock reef and sandy sites along 5 km of coast adjacent to the port. The experimental design integrates a wide range of field measurement techniques. Sediment tracing, multiple simultaneous instrument deployments and a trial nearshore placement of dredged sand provide an exceptional database for future numerical model calibration/validation. The data depicts the coastal physical environment as being dominated by the wave climate and wave transformation within the reefs which side-scan sonar images show to be irregular and of variable roughness. Measurements of time-averaged suspended sediment concentrations on the reefs were large (averaging 0.052 $kg.m^{-3}$ at 0.5 m elevation) and strongly dependent on distance from sandy substrate, not on local wave conditions. However, multiple surveys over 14 years indicate that the sandy patches within and between the reefs are long-lived and remain positionally stable. Thus, while locally impacted by the port, the measurements show the system as having high suspended loads in a sand/rock region which has reached sedimentary equilibrium.

2.3 Introduction

Numerical simulation provides an effective method for resolving both the temporal and spatial variation of physical processes in complex coastal environments. However, the application of such models requires calibration and validation with appropriate field measurements, often specific to the particular study environment. This paper presents the design and implementation of a large, multi-faceted field experiment for

investigation of coastal and sediment dynamics adjacent to Port Taranaki, New Plymouth, New Zealand. After 115 years of offshore placement of dredge spoil, the cumulative effect has been advanced erosion of the downstream shoreline. Combined with other coastal works, this has resulted in placement of rock armouring along 75% of the adjacent city coastline.

A three-year programme of study was implemented to identify ways to mitigate the environmental effects of the port on the nearshore littoral transport system, and to optimise the benefits of sediment replenishment into the littoral system by informed selection of the location, shape, and elevation of a nearshore placement site.

Several potentially conflicting issues exist. The port requires a solution that is both operationally efficient and financially viable for port operations. Beyond this focus, the civic viewpoint extends toward re-establishing inter-tidal sandy beaches within the city limits and the nourishment of existing beaches. Balancing this is a concern about sediment inundation of inshore marine biota. This view is primarily voiced by local Maori who regularly harvest shellfish (*haliotis, evechinus, and turbo*) from the inter-tidal reefs. To address these issues with confidence, a comprehensive understanding of the physical processes operating in the region is needed.

Special features of the site include a heterogeneous seabed structure of mixed sand and large rocky reefs. The wave energy is high and sediments are of andesitic volcanic origin. Similar sites have rarely been studied and no large studies of the kind presented here have been attempted in similar locations. Coastal and sediment dynamics investigations, such as described by Healy *et al.* (1998) and Lou & Ridd (1997), have indicated the explicit requirement of acquiring reliable field measurements in order to adequately resolve the physical processes operating in the environment of study.

Some of the aims of the present work are similar to the aforementioned investigations, but the conditions at New Plymouth are made complex by the open coast environment, with a predominant swell approach at 45° to the shoreline, passing through a series of offshore islands. Wave conditions can vary from short-storm swell (1-4 m high and periods of 4-8 seconds) to long ground swell generated in the Southern Oceans, with inshore heights of up to 6 m and spectral peak periods of up 16-18 s. The collection of

field measurements in these conditions presents challenges when attempting nearshore deployment of field equipment at sites that are sometimes at the breakpoint of 4-6 m waves.

In this wave environment, we expected the reef and channel seabed topography to strongly influence the suspension and entrainment of littoral sediments. Spatial variability in wave energy and seabed substrate will affect the localised suspension of sediments, and the transport induced by the wave-, wind- and regional circulation systems. The open-coast nature of the study region is likely to result in highly variable circulation patterns. Furthermore, while the littoral transport of quartz sediments has been well-studied (Fredsoe & Deigaard, 1992), the behaviour of sediments containing high-density (4800 kg m^{-3}) titanomagnetite components is not as well understood.

The path and flux of sediment bypassing the harbour have been disputed. McLennan (1982) concluded that the harbour totally interrupted the littoral transport, while Hicks & Gibb (1987) estimated that approximately 40,000 m^3 passes across the harbour entrance annually. Sediment trapping experiments in the region of the breakwater tip and further offshore by Gorman *et al.* (1995) showed high suspended loads at both sites, suggesting active bypassing is occurring beyond the nearshore littoral transport zone that feeds the port's tip shoal. They measured bypassing fluxes of at least 10,000-20,000 m^3yr^{-1} from data recorded in moderate to calm conditions. Compounding the overall complexity is the effect on sand transport of numerous rocky seabeds in the study region, both at the full-reef scale and micro-scale where turbulence is induced around the individual rock elements.

In this paper, we present an overview of the circulation, which provides insight into the questions of bypassing, trapping rates and net fluxes of sediment up the coast. The study has proceeded in two stages, each with an associated data collection exercise. The first stage sought to assess the *potential* for the nearshore placement of port dredgings, and has been previously reported (McComb *et al.* 1997). A two-month field experiment provided data for the calibration of the WBEND wave refraction model (described by Black & Rosenberg, 1992b), from which the spatial distribution of wave energy within the study area was defined. Field measurements and numerical outputs clearly identified a potential nearshore placement site that was proximate to the harbour and satisfied the

criteria of navigability, capacity and potential for sediment flux. The second stage of the study focuses on optimising this nearshore region as a placement site for harbour dredge spoil and assessing the environmental impacts. This is achieved through the interpretation of field measurements in conjunction with the application of calibrated sediment transport models. The description of the field experiments associated with this second stage of the study form the basis of this paper, together with the overview summary of circulation and sediment dynamics.

2.3.1 The study site

Port Taranaki is the only deep-water harbour on the west coast of New Zealand, and is located on the northern flank of the Taranaki volcanic ring-plain (Matthews, 1977). The harbour was constructed in 1884 on a coastline which is exposed to the Tasman Sea and experiences a high-energy (1-6 m) wave climate, dominated by long-period (12-18 s) westerly quarter swell. The spring tidal range is 3.1 m.

The coastal bathymetry features a reef and channel structure comprised of volcanic breccia, intermittently overlain with boulders, gravel and sand. Andesitic volcanic islands are present adjacent to the port. Littoral sediments are predominantly of local volcanic origin, and characterised as medium-fine 'black' sands consisting of 38% heavy minerals (titanomagnetite, augite, horneblend) and 62% lighter minerals (feldspars) (Bartholomeusz, 1985). Aaron & Mitchell (1984) mapped the distribution of rocky and sandy seabed within the study area using side-scan sonar. They show a broad sandy seabed adjacent and west of the harbour, grading into a predominantly rocky bed to the east.

The port breakwaters extend some 1250 m seaward from a natural headland (Fig. 2.1) and their intrusion into the coastal littoral transport system results in the accumulation of sediments, primarily around the breakwater tip. Currently, a trailer-suction hopper dredge is used to remove approximately 180,000 m^3yr^{-1} of material, which is dumped offshore in water depths of 15–20 m (Fig. 2.1).

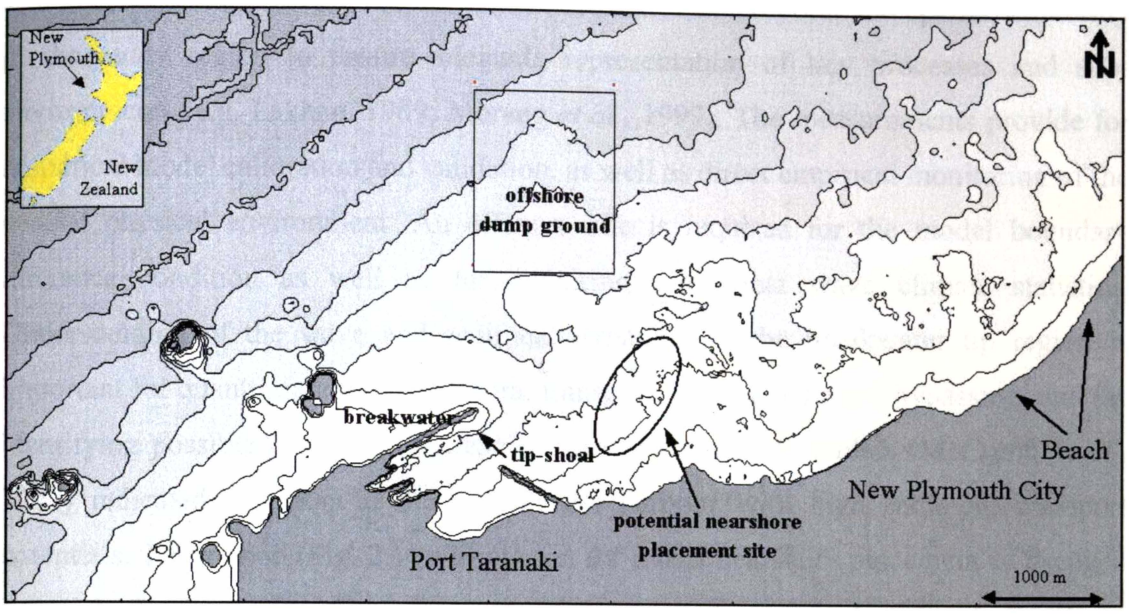

Figure 2.1: The study site showing the port, nearshore bathymetry (depths in 5 m contours), existing offshore disposal ground for port dredgings and the potential nearshore disposal site.

2.3.2 Experimental design

Key research questions that need to be addressed through interpretation of both the field data and numerical models are:

- the effects on sediment movement of the complex, sub-tidal reefs at a macro-scale;
- the importance for sediment suspension of reef roughness at a micro-scale;
- interaction and transformation of waves and currents on the reefs and the subsequent effect on sediment transport and,
- the net movement time scales and fluxes of sediment through the study region.

To address these issues, the experimental design integrates a wide range of field measurement techniques, particularly incorporating redundancy for confidence in the interpretation while also ensuring adequate data recovery in the event of instrument loss or failures in the high-energy environment.

The data acquisition programme considers the scales of temporal and spatial variability in the study region to ensure adequate representation of key processes and sub-environments (e.g. Lakhan, 1989; Morang *et al.,* 1997). The measurements provide for numerical model calibration and validation, as well as direct empirical monitoring of the coastal physical environment. An offshore site is required for the model boundary reference condition as well as for acquiring directional wave climate statistics. Understanding of the wave and sediment dynamics at the breakwater tip region is important for quantification of net littoral transport, natural sediment bypassing, and for identifying possible dredging efficiencies. Our initial model studies (McComb *et al.,* 1997) indicated a region to the east of the harbour with high sediment transport potentials. This region (Fig. 2.1) was chosen for a trial nearshore placement of dredged material. Further east, three imposing shore-normal reef and channel structures represent potential interruptions to the longshore drift connecting the port region to New Plymouth's eastern beaches. The selection of instrumentation sites within these regions needs to include all substrates. Accordingly, a one-year data collection programme was designed. The deployment plan with the following components is summarised in Figure 2.2, and the rationale is subsequently discussed.

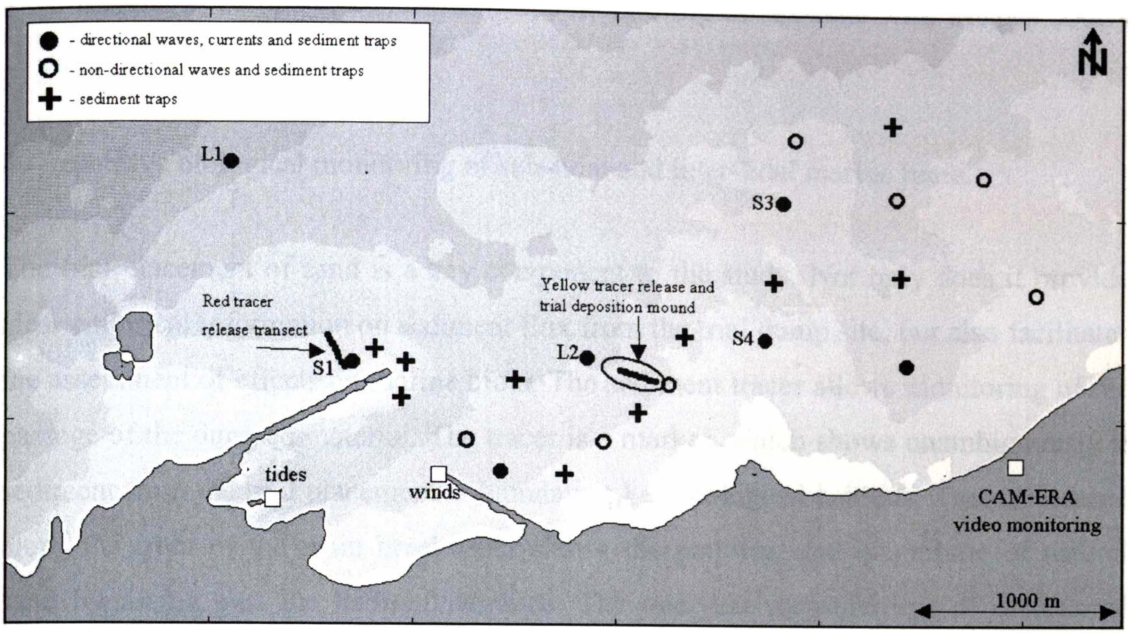

Figure 2.2: Field deployment plan including instrumentation, tracer and trial sand placement.

The key components were:

- a trial nearshore placement of dredged material;
- monthly hydrographic surveys of the trial placement and the breakwater tip shoal;
- quarterly side-scan sonar surveys;
- a two-colour artificial sediment tracer release and sampling programme, with release at the trial placement site and offshore of the main breakwater;
- a two-month measurement of suspended sediment profiles from 23 sites using sediment traps;
- a two-month deployment of 13 wave and current meters;
- a one-year deployment of directional wave and current meters inshore and offshore;
- one-year recording of tides and meteorology;

- 6-months of computer-controlled video monitoring of sea-state with images hourly and,

- repetitive biological monitoring of sub-tidal and inter-tidal marine biota.

The trial placement of sand is a key component to the study. Not only does it provide clear empirical information on sediment flux from the trial dump site, but also facilitates the assessment of effects on marine biota. The sediment tracer allows monitoring of the passage of the dumped material. The tracer is a marker, which shows unambiguously if sediment from the trial placement is inundating key biological habitats. Tracer released along the front of the main breakwater shows the pathway and magnitude of natural sand bypassing past the harbour entrance. The one-year measurement of directional waves and currents facilitates the derivation of nearshore and offshore wave climates plus physical context data to relate to measured tracer movement, trial site erosion and breakwater tip-shoal accretion. The study of biological effects is not included in this paper but is discussed by Cole *et al.* (1999).

2.4 Experimental methods

Field experiments were scheduled to commence at the conclusion of a biennial dredging campaign (March 1998). Operations at sea were conducted from a 7.5 m survey craft, equipped with DGPS for sub-metre positioning.

2.4.1 Trial nearshore placement

Some 47,000 m^3 of dredged sand was selected for the trial placement. This amount was considered to be a minimum volume for monitoring purposes, while remaining small on a regional scale, thus minimising the potential for adverse biological effects (Atkinson & McComb, 1997). Placement was effected over a 5-day period using a split-hull hopper dredge to place the sand in an elliptical mound (73 vessel loads). The target region for the placement covered an area of 11,631 m^2 in water depths prior to dumping ranging from 6-10 m (Fig. 2.2). The seabed under the mound featured regions of sandy and rocky substrate (Fig. 2.3). Monthly hydrographic surveys were conducted over the mound and adjacent seabed.

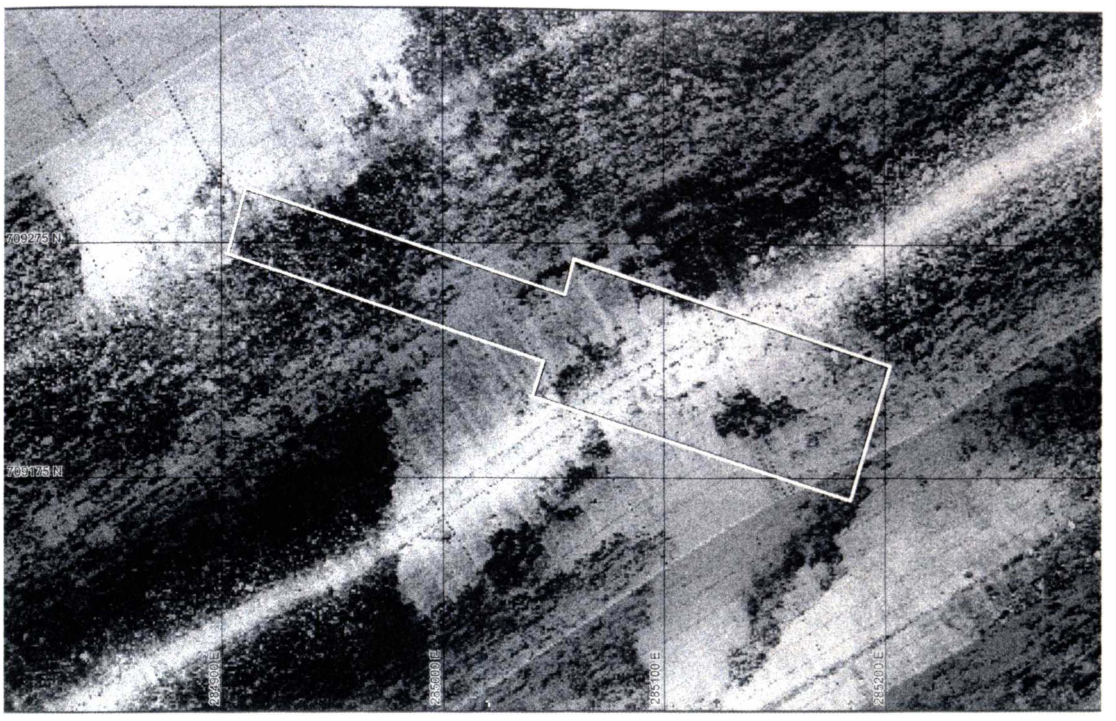

Figure 2.3: Sonograph (October, 1997) of the trial sand placement site showing the target region for sand placement.

2.4.2 Seabed morphology and features

We conducted hydrographic surveys on lines spaced 10-50 m apart to supplement existing Navy surveys, including high-resolution surveys (5 m spacing) over the trial placement site. From the cessation of dredging (March, 1998), accretion of the shoal at the tip of the breakwater (Fig. 2.1) was measured by monthly hydrographic survey for a period of one year (McComb *et al.,* 1999).

Digital side-scan sonar surveys were conducted four times. Two surveys covered the entire study region (Fig. 2.1); the first pre-trial (October 1997) and the second 15 months later. Two intermediate surveys were conducted over the nearshore placement region for monitoring sand movement. Data were processed to define the sand/rock facies and gauge the seabed roughness. The rocky substrate appears as a strongly speckled or broken signal in the sonographs while sand is seen as a uniform, brighter signal return (Fig. 2.3). Seabed sediments from 30 sites were analysed for particle size distribution and mineralogy. Fall velocity and equivalent size (Gibbs *et al.,* 1971) was obtained from the fall tube (University of Waikato Rapid Sediment Analyser), while

mineralogy was determined by X-ray diffraction, magnetic particle separation and visual microscopic inspection.

2.4.3 Sediment tracer

An artificial fluorescent material composed of a chromophore incorporated within polyamide resin (supplied by Environmental Tracing Systems Ltd, UK) was used for tracing. The tracer material was manufactured with a particle size distribution based on the equivalent settling velocity of the native sediment. Two colours were employed for the two separate release sites along 6-10 m depth transects (Fig. 2.2). A quantity of 100-kg tracer was released at each site. The material was prepared by wet mixing tracer in a 1:2 ratio with native sediment (plus anti-surfactants). For each colour, the mixture was divided into eight portions, frozen to –40 °C, and sealed in plastic sacks. After positioning along the release transect, the sacks were opened by divers. Red tracer was released from offshore of the port breakwater and yellow tracer released from the trial placement site.

Sampling for tracer commenced four days after release on March 5, 1998. A total of 11 sampling surveys were conducted over the following 308 days, resulting in 1179 samples. These seabed samples (~500 cm^3) were obtained using a van Veen grab (Fig. 2.4a) on sandy sites, and by towing a flared pipe (Fig. 2.4b) on the sand/rock substrates. The site selection as the experiment progressed was aided by preliminary analysis of sediment samples using visual inspection under UV irradiation. The sampling region boundary was adjusted to extend beyond sites where tracer was found as the monitoring progressed. A broad assessment of methods for counting tracer is the subject of a separate study (Forsyth, 2000). Ultimately, the most appropriate techniques were found to be video computer-based image analysis for automated tracer grain sizing and counting, and dissolution in acetone and hydrochloric acid for bulk fluorescence estimates in larger (30-50 g) samples (Forsyth, 2000).

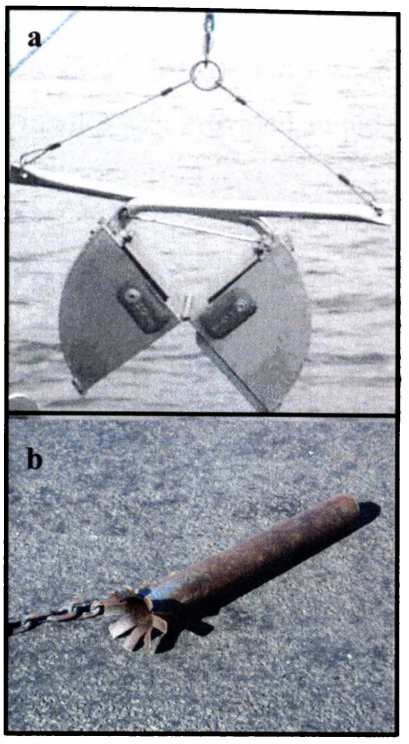

Figure 2.4: Sediment sampling devices; van Veen grab (a) and flared pipe (b)

2.4.4 Waves and currents

Waves and currents were measured using a suite of instruments, including seven directional wave/current meters and six non-directional wave meters. The location of the instrument sites was chosen to represent a range of environments along the New Plymouth coast, as well as to provide data from the proximity of the port entrance and the trial nearshore sand placement. Instruments were deployed prior to the placement of sand at the trial nearshore region. Two sites were deployed for one year (Fig. 2.2, sites L1 & L2), and the remainder for an initial intensive two-month period. Site L1 utilised a taut-wire mooring, with the instrument located in mid-water (14.9 m above the seabed in 23.4 m water depth). To facilitate monthly servicing, this mooring incorporated an in-line instrument frame. All other sites used anchored seabed frames for instrument mooring, with the current sensors positioned 1 m above the seabed. Pressure sensors for the non-directional wave meters were placed close to the bed at 0.2-0.4 m elevation. Over the intensive period, instruments were synchronised to record 2 Hz burst data for 9-18 minutes at half tidal phase intervals (373 minutes). For the subsequent 10 months using different instruments (Fig. 2.2, L1 & L2), data were collected at 5.36 Hz in 18-minute bursts at six hourly intervals. Spatial wave information was resolved from

hourly sea-state imagery obtained by a "Cam-Era" automated video station (http://www.nzniwa.com/cam-era/newplym.htm), sited on the foreshore at 65 m above sealevel (Fig. 2.2). These images also provided an aid in interpreting the oceanographic data.

2.4.5 Suspended sediments

Sediment traps at multiple levels were used to collect time-averaged suspended sediment concentration (SSC) profiles. Traps were deployed in vertical arrays, mounted on poles attached to a seabed frame (Fig. 2.5) at elevations of 0.5, 1.0, and 1.5 m. This method has been found to be effective (Flint, 1998). The traps were designed to accommodate high SS by limiting overfilling using a relatively small trap aperture (∅ = 30 mm) leading to a larger body of the trap. However, after some unexpectedly small catches were made, this aperture was enlarged (∅ = 53 mm) for the 1.5 m level traps in the latter part of the experiment. Traps were deployed at 23 sites (Fig. 2.2) over a 61-day period, and were serviced by divers on an 8–16 day cycle (dependent on weather), resulting in five sets of time-averaged SSC data.

The trapped samples were washed, wet sieved (45 μm), dried and weighed. Providing the sample was large enough, approximately 20 g of the sample was analysed by the RSA system to obtain particle size and settling velocity distributions. The masses (M) collected in the traps were converted to a downward flux (f_d) with the units $kg.m^{-2}s^{-1}$ as follows:

$$f_d = M/At \qquad \text{Eqn. 2-1}$$

where A is the area of the aperture of the trap and t is the time period of the trap sampling. The downward sediment flux was converted to a time-average suspended sediment concentration (C_{zi}) at an elevation z (elevation of the orifice for each trap) above the seabed, using the full settling velocity distribution of the trapped samples (Nishi *et al.*, 1992). Accordingly, settling velocity distributions obtained by the RSA analysis of the trap samples were then broken into bins and the concentration calculated for each bin. The distribution of the bins ranged from –3.5 to 4 phi at an interval of 0.5 phi. Concentration distributions were calculated as:

$$C_{zi} = \frac{M_i}{w_i A t} \qquad \text{Eqn. 2-2}$$

where M_i is the mass trapped, A is the area of the collection orifice of the trap, w_i is the settling velocity of the sediment particles of the i^{th} sediment fraction in the distribution. These were then summed to provide a time-averaged concentration for the whole sample as:

$$C_z = \frac{1}{t}\sum_{i=1} \frac{M_i}{w_i A} \qquad \text{Eqn. 2-3}$$

The exponential relationship of the vertical distribution of suspended sediment (Nielsen,1986) was applied to measured C_z values to obtain mixing lengths (l_s),

$$C_z = C_o\, e^{(-z/ls)} \qquad \text{Eqn. 2-4}$$

where z is the elevation of the trap and C_o is the near-bed reference concentration.

Figure 2.5: Sediment trap array on seabed frame.

2.4.6 Other physical parameters

Tide levels were recorded within the harbour and no significant tidal differences in level occur throughout the field site. Wind speed and direction were recorded at the entrance to the harbour on the exposed lee breakwater (Fig. 2.2). Sub-surface profiles of water temperature and light intensity were recorded to examine stratification and attenuation of light by fine material at one location (Fig. 2.2, L2) using four sensors vertically spaced 2 m apart on a floating mooring.

2.5 Results

2.5.1 Seabed features

A facies map produced from the November 1997 side-scan sonar survey (Fig. 2.6) shows a broad area of sand surrounding the harbour entrance and seaward. A mostly rocky bed predominates further east. The sonograph shows that bodies of sand tend to exist on the western flanks of raised bathymetric features, which is in accordance with suggestions of a net easterly sediment flux. Sand also tends to inhabit seabed depressions, as evidenced by the in-filling of a relict fluvial channel (Fig. 2.6). The positions of sand and rock patches, as determined by side-scan surveys, were found to be highly stable between our surveys. Moreover, comparison of the two recent surveys with a 1984 survey by Aaron & Mitchell (Fig. 1.8) indicated that this stability is a long-term, consistent feature of the region.

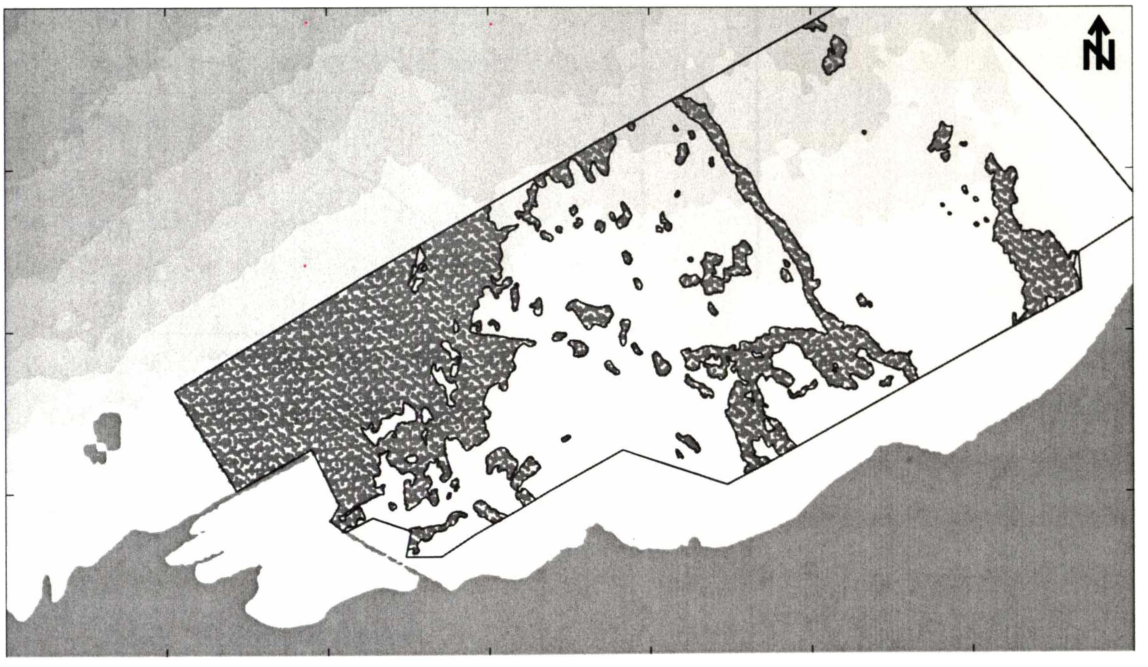

Figure 2.6: The study site showing sand (shaded) and rock (un-shaded) facies from the October 1997 side-scan survey.

2.5.2 Trial nearshore placement

Immediately following placement at the trial site by the dredge vessel, sediments were observed to disperse over a region approximately twice the size of the original target region sketched in Figure 2.3. The volumes of sand in the trial area show a steady decrease over time (Fig. 2.7), with approximately 50% of the deposited volume remaining after one year. Erosion of the mound was observed to be spatially uniform, although a slight (50-100 m) shoreward migration was noted over the first four months following placement. Side-scan images indicate that rocky areas adjacent to the mound did not become covered with sand over the monitoring period.

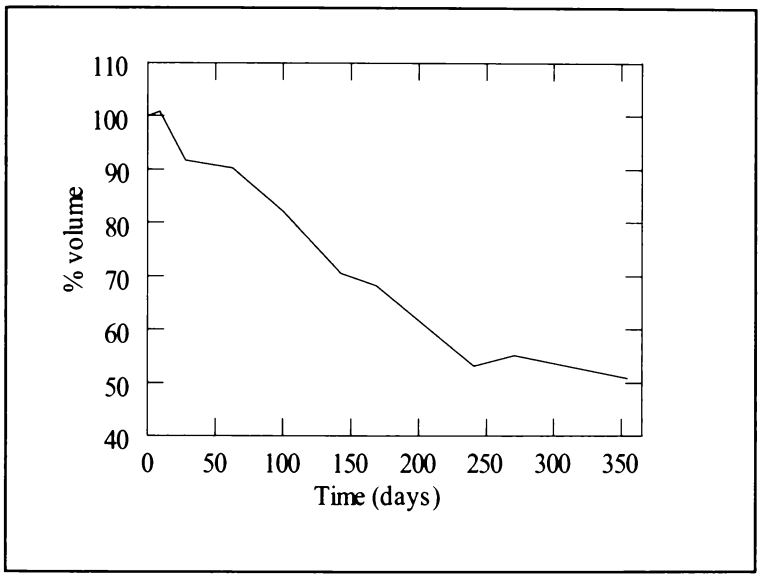

Figure 2.7: Time-series of volumes at the trial sand placement site.

2.5.3 Sediment tracer

The movement of tracer shows evidence of well-defined sediment flow streamlines (as later described in Chapter 8). Red tracer released offshore of the main breakwater (Fig. 2.2) was seen to migrate longshore to the east, but with both offshore and longshore components. The presence of red particles east of the harbour entrance confirms that the port does not trap all of the nearshore littoral sand. Similarly, yellow tracer released with the trial sand placement shows an easterly vector, with little evidence to suggest significant re-circulation of sediments back into the harbour.

2.5.4 Waves and currents

Averaged nearshore wave heights, when normalised to co-incident offshore measurements, show considerable variation across the study region. The H_s *ratio* is defined as;

$$H_s ratio = \frac{1}{N}\sum_{i-1}^{N}\left(\frac{H_s nearshore}{H_s offshore}\right) \qquad \text{Eqn. 2-5}$$

where H_s = significant wave height and N = number of observations.

H_s *ratios* from the intensive two-month period vary from 0.99 to 0.50 and show the sheltering effect of the offshore islands and port breakwaters, plus the influence of the bathymetry on wave heights (Fig. 2.8). These averaged values represent the generalised spatial variation in wave height, and we note significant influence from other factors such as tide level, wave direction, wave period, and wind vector. Wave transformations from offshore to nearshore are dominated by refraction and seabed friction (as previously noted by McComb *et al.*, 1997).

The data show a nearshore circulation system, with multiple wave and wind-driven components and influence from larger-scale regional flows. We consider results from a 13-day period, which yielded the maximum co-incidental measurements (including SSC).

Using the MATLAB routine TSERIES (Gorman, 1997) and supporting software, mean currents were extracted from the burst measurements. A weighted current was calculated using the method applied by Phillips *et al.* (1999) to indicate the direction of suspended sediment flux. With the methodology of Black & Rosenberg (1991), a near-bed reference concentration (C_o) was calculated from the measured wave orbital motions and used to define the weighted current (U_c) as;

$$U_c = \frac{\sum_{i=1}^{N} U_i C_o}{\sum_{i=1}^{N} C_o} \qquad \text{Eqn. 2-6}$$

where U_i = burst-averaged current, i is the burst number and N = number of 9-18 minute bursts.

The offshore (Fig. 2.2, L1) wave climate over this period is shown in Figure 2.9, with burst-averaged and weighted (Eqn. 2.6) currents given in Table 2.1. The direction of the weighted current, which indicates net sediment flux, is directed predominantly northeast at sites S1, S3 and S4. The weighted current at L2, however, is directed offshore to the north-north-west. This indicates a bottom current directed away from the coast, perhaps in response to local bathymetry, which exhibits a gradient in a similar direction.

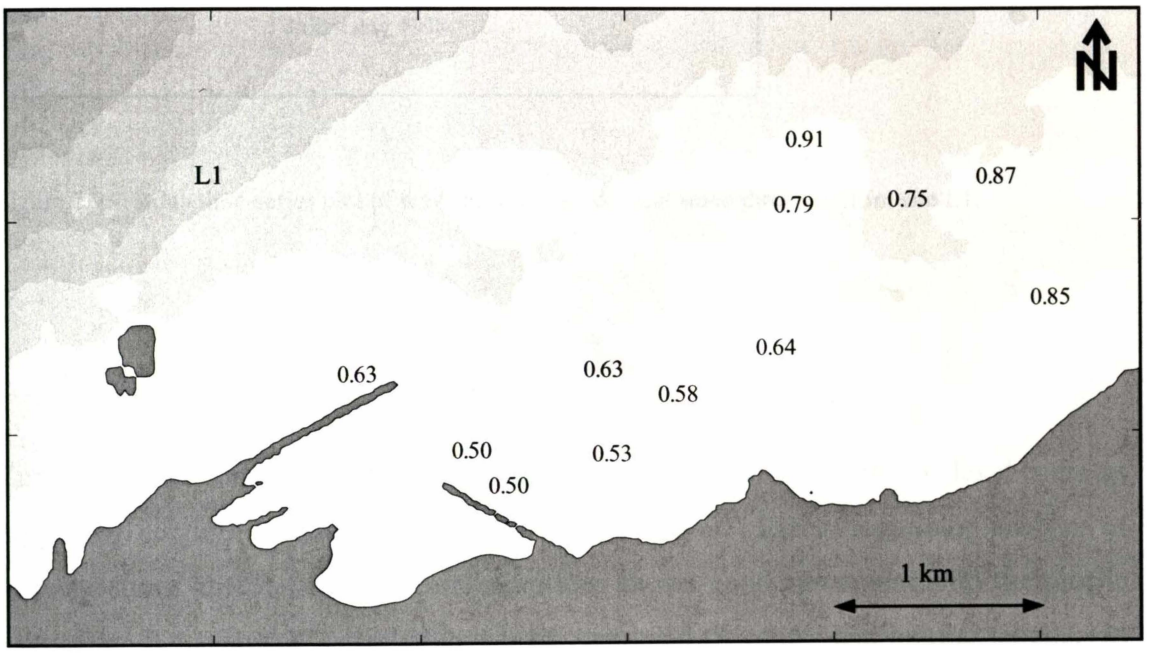

Figure 2.8: Site-averaged nearshore/offshore wave height ratios from a 2-month period.

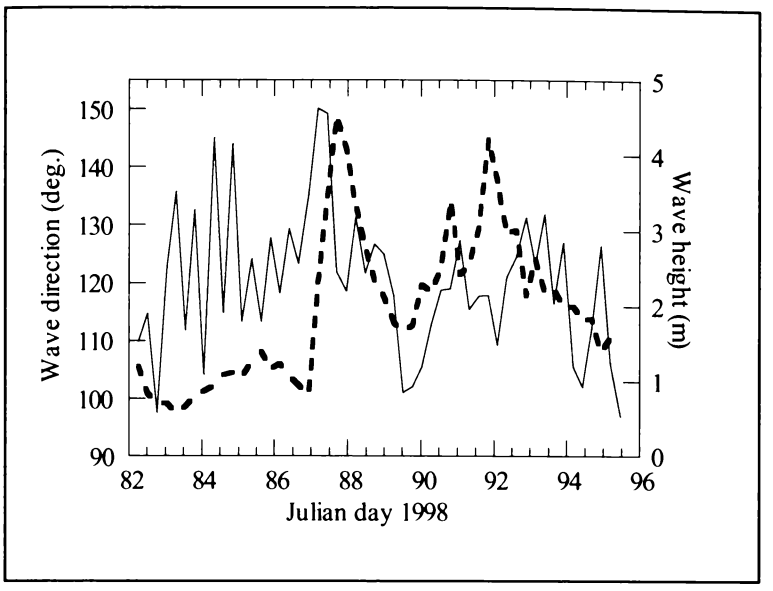

Figure 2.9: 13-day time-series plot of wave height (dashed) and wave direction from site L1.

2.5.5 Suspended sediments

Time-averaged concentrations of suspended sediment (C_z) at the 0.5 m level were as high as 0.18 kg.m^{-3} with an average value of 0.039 kg.m^{-3}. Linear regression analysis of concentrations at 0.5, 1.0 and 1.5 m elevations shows good agreement with the profile using Eqn. 2-4 (mean R^2 correlation = 0.9). Averaged C_z values and mixing lengths (l_s) obtained from the regression analysis using data from a 13-day deployment (Fig. 2.9) are given in Table 2.2.

When classified according to the seabed substrate, C_z values at 0.5 m elevation from rocky sites are markedly less than those from sandy sites. At 1.0 m elevation, however, C_z values are very similar at sandy and rocky sites. The most extreme case of isolated rocky sites, defined as being further than 300 m from a contiguous sand body, show similar patterns, although C_z at both 0.5 and 1.0 m are lower than at rocky and sandy sites. The length scales of turbulence (l_s) are greater on rocky substrates than sandy but approximately equivalent on rocky and remote rocky sites (Table 2.2). Further analysis showed that the substrate type (i.e. rocky or sandy) influences C_z values at 0.5 m

elevation more than either the wave exposure or the water depth. SSC data from each trap deployment period is tabled in Appendix 5.

Table 2.1: Mean and weighted currents from a 13-day period.

	Mean current		Weighted current	
Site	Speed (cms^{-1})	Direction (degrees)	Speed (cms^{-1})	Direction (degrees)
L2	1.7	323	3.54	340
S1	6.26	77	18.56	67
S3	4.25	52	11.54	30
S4	1.92	356	2.37	50

Table 2.2: Averaged C_z values (z = 0.5, 1.0) and mixing lengths (m) from a 13-day period, classified by substrate.

Substrate	$C_{z\ 0.5\ m}$ ($kg.m^{-3}$)	$C_{z\ 1.0\ m}$ ($kg.m^{-3}$)	l_s (m)
sandy sites	0.098	0.018	0.36
rocky sites	0.052	0.019	0.53
isolated rocky sites	0.021	0.014	0.49

2.6 Discussion

Careful planning of the deployments enabled us to meet the challenges of data collection in a high-energy nearshore coastal environment, and achieve a high-level of data recovery. The various techniques employed have yielded several lines of evidence, which give consistent results.

Empirical data from the trial nearshore placement clearly shows a sediment flux from the site. The mound was observed to erode in a spatially uniform manner with no evidence of localised scouring, and the adjacent rocky regions were not inundated with sand. This is an important observation with respect to the potential effects on the marine ecology. If the material was shown to migrate as a contiguous body, then deleterious effects on the benthic habitat along the migration path may occur. It also indicates the sediment is primarily being transported in suspension.

Measured waves and currents show considerable variability over the two-month intensive period. The range of measured events was sufficient to allow the parameterisation of the circulation patterns, based on the variables of wind, tide, and offshore waves and currents. The observed variability stems from the open-coast nature of the site and the complexity in seabed contours, and highlights the need for field measurements with adequate temporal and spatial coverage. Data from a 13-day period indicates an easterly nearshore sediment flux, in concurrence with the observed tracer movement.

The stability of sand and rock facies over time indicates a long-term seabed sedimentary equilibrium. A large contiguous region of sand (surrounding the harbour entrance) is seen to grade into reef approximately along the 10 m depth contour (Fig. 2.7). Patches of sand within the predominantly rocky region (to the east of the harbour) reflect the seabed bathymetry, in that they are associated with seabed depressions or on the western side of raised features. This possibly indicates the seabed topography influences the sediment transport, and raised features present an obstacle for sediments in transit.

Sediment trap data shows that suspended sediment is present over rocky seabeds, in quantities that are equivalent to those over sandy beds at 1.0 m elevations and above, with lesser amounts at the lower 0.5 m level. Diver observations indicate that the rocky reefs frequently have small quantities of interstitial sandy sediments. In wave-dominated environments, the sediment entrainment process is driven by wave orbital velocities, where the local substrate is the source of sediments (Antsyferov & Kos'yan 1990). Accordingly, it is likely the measured concentrations at the 0.5 m level over rocks simply reflects a limitation in the source material for sediment entrainment, relative to the sandy beds where there is no such limitation.

Nielsen (1992) discusses sediment suspension in terms of convective and diffusive mechanisms, and relates the relative dominance of these two mechanisms to the mixing length and the overall vertical scale of suspension. We consider these mechanisms with the observed equivalence of SSC at the upper (>1.0 m) elevations at sandy and rocky sites. If the calculated l_s values appropriately reflect the length scales of turbulence in the water column, then the higher l_s values obtained over rocks may indicate turbulence from the interaction of wave orbital motions with the "rough" rocky bed. This may

result in the convective suspension of material higher in the water column (compared to the relatively smooth sandy bed) and possibly account for the difference in sandy and rocky SSC profiles. Previous studies (e.g. Flint 1998, Black & Rosenberg 1991) however, indicate that mixing lengths outside of the breakpoint are typically less than 0.1 m, while the values obtained in this study are of the order generally found within the breakpoint.

Alternatively, the SSC profiles may be considered on a somewhat larger spatial scale, where the "source/sink" boundary condition (described by Black, 1994) may be applicable. The source of material collected by a given trap may not necessarily be proximate to that site. Given water depths of 4-12 m at the measurement sites, there is ample scope for sediment diffusion to upper levels. Subsequent transport of this material by the coastal circulation system may give rise to a 'background' level of suspended material, which is reflected in the time-average data. The field measurements show some confirmation of this, and we note a systematic decay in the upper level SSC with longshore (easterly) distance from large sand bodies.

An important application of the numerical modelling component of the study is the reconciliation of time-averaged SSC measurements with the burst time-series wave and current data. While the hydraulic "roughness" of the seabed will undoubtedly influence the SSC (e.g. Green *et al.,* 1998), field measurements relating turbulence to bed roughness under wave conditions are rare (Nelson, 1996). Further work will consider these observations through the incorporation of the sedimentary facies and an index of bed roughness (derived from the side-scan data) in the numerical simulations.

2.7 Conclusions

Field experiments were designed and implemented to investigate the coastal and sediment dynamics at New Plymouth, New Zealand. For a period of one year, data were collected using a wide range of measurement techniques including sediment tracing, multiple simultaneous instrument deployments, seabed surveys, and the monitoring of a trial nearshore placement of dredged sand. Results of the field data have been presented to illustrate the broad dynamics of the region.

The nearshore wave climate is dominated by refraction and seabed friction, and the open-coast nature of the site results in variable circulation patterns. Both the sediment tracer and current meter data indicate a net easterly sediment flux, and sediment bypassing of the harbour entrance is shown to occur. Erosion of sand from a nearshore placement was observed to be spatially uniform and adjacent rocky areas did not become inundated with sand. The multiple side-scan surveys indicate that the sandy patches within and between the reefs are long-lived and remain positionally stable. Measured SSC profiles are seen to be influenced by the substrate type and proximity to large sand bodies. Thus, while locally impacted by the port, the measurements show the system as having high suspended loads in a sand/rock region which has reached sedimentary equilibrium.

The results have also demonstrated the importance of considering spatial and temporal variability in field data collection to ensure adequate representation of the physical processes within the study region.

3 MEASURING DIRECTIONAL WAVE SPECTRA USING THE 3D-ACM WAVE ON FIXED AND TAUT-WIRE MOORINGS

3.1 Context of the paper within the thesis

Measuring the directional wave spectra was an important component of the field data collection, and for the second experimental programme (described in Chapter 2) two 3D-ACM WAVE meters were acquired for this purpose. As these were only recently developed instruments, it was prudent to investigate their performance in the ocean. An initial comparison between one of the 3D-ACM WAVE meters and an InterOcean S4 electromagnetic *p, u, v* meter indicated good correlation for a rigid seabed mooring system (Kun *et al.*, 1999). However, analysis of the data from a taut-wire mooring system indicated a phase difference between the measured pressure and velocity values. Subsequent investigations led to the development of this paper, which details the effect of mooring motion on wave data, and provides a method for minimising the errors in resolving the directional spectra. This paper has been peer-reviewed and published as:

McComb, P., Gorman, R., Black K. and Kun, A., 2001. Measuring directional wave spectra using the 3D-ACM WAVE on fixed and taut-wire moorings. *Journal of Oceanic Engineering*, **26** (2), 171-180.

3.2 Abstract

Field data were analysed from a simultaneous deployment of two 3D-ACM WAVE instruments; one on a fixed seabed frame in the nearshore zone, and the other further offshore on a taut-wire mooring. An inter-comparison of measurements of vertical and horizontal wave-orbital currents with pressures was used to evaluate the velocity sensor response under field conditions. Results using the fixed frame have validated the measured horizontal wave-orbital velocities, but found the vertical velocities to be less coherent with the pressure time-series. The influence of the instrument mooring system on the velocity measurements was investigated. The oscillation of the taut-wire mooring was found to influence the magnitude of the measured horizontal wave-orbital velocities and induce a phase lag between velocity and sea-surface elevation. Examination of other data from similar taut-wire moorings indicates a systematic relationship between the length of the mooring cable and the measured phase lag, consistent with the behaviour of the mooring system considered as a forced, linearly-damped oscillator. A comparison was made between the spectra of wave direction derived from both velocity and pressure data with that derived solely from velocity data. The results show a high coherence for the fixed mooring, but significant directional variability in the higher frequencies (>0.13 Hz) on the taut-wire mooring we employed, which we attribute to the mooring oscillation. The analysis further indicates that on taut-wire moorings, the spectra of wave direction should be resolved solely from velocity data. Using these findings, directional wave spectra were produced for the nearshore and offshore sites from 233 coincident events over a two-month period, and these data are presented in a time-averaged spectral format.

3.3 Introduction

Surface gravity waves in the ocean exhibit an energy spectrum distributed in both frequency and propagation direction, and the resolution of this spectrum is often an important requirement for engineering and scientific studies. Several techniques are available to collect data from which wave directional spectra may be derived. These typically involve the recording of either wave-orbital velocities, sea-surface elevations in a spatially-distributed array, or multiple degrees of freedom of motion of a wave buoy, (e.g. Paniker & Borgman, 1970; Earle & Bishop, 1984; Huang & Chen, 1998;

Dickey *et al.*, 1998; Terray *et al.*, 1999). In this study, we investigate directional wave data collection using a recently developed instrument, the 3D-ACM WAVE. This instrument combines a high-accuracy pressure sensor with acoustic velocity sensors for the recording of time-series pressure (p) and orthogonal (u, v, w) velocity.

Deriving directional wave spectra from p, u, v data involves the cross-spectral analysis of sea-surface elevations with the directional components of wave-orbital motion – and confidence in the resolved spectra is dependent on the quality of the recorded data. The use of a pressure sensor to measure the time-series of sea-surface elevations is a well-proven technique (e.g. Corson *et al.*, 1997). Similarly, the response of the acoustic velocity sensors used in the 3D-ACM WAVE has been tested in numerous tow-tank experiments (FSI, 1998), providing an effective sensor calibration under constant flow states. Such conditions do not, however, represent the non-steady 3-dimensional nature of fluid flow in the ocean. Furthermore, field data collection requires a mooring system, which may have an influence on the sensor data (e.g. Halpern & Pillsbury, 1976; Zenk *et al.*, 1980; Chhabra, 1985; Hamilton & Fowler, 1997; Hamilton et al., 1997).

The sub-surface collection of p, u, v wave data usually employs either a taut-wire mooring or a seabed frame to mount the instrument. While the latter provides a fixed platform, its use is limited to shallow waters (i.e. < 20 m) and often requires SCUBA diver intervention. The taut-wire mooring can be used over a wider depth range, allowing the instrument to be appropriately positioned within the water column for optimum data collection. This type of mooring, however, is affected by currents, and often exhibits an oscillatory motion in response to wave-orbital current (e.g. Chhabra, 1985). While discussed by Chhabra (1985), the influence of mooring motion on the measurement of wave orbital motion has not been quantified, nor has this effect been considered in resolving the directional wave spectra. Similarly, recently developed numerical models of mooring behaviour (Gobat & Grosenbaugh, 1998; Dewey, 1999) do not address mooring oscillation by wave forcing nor its effect on wave orbital measurement.

3.3.1 Experimental aims

In this study we investigate the use of the 3D-ACM WAVE in collecting data for directional wave spectra from these two types of moorings. The purpose of the study is twofold; (i) to evaluate the sensor data by inter-comparison of the measured components of wave orbital motion and pressure, and (ii) to evaluate the influence of the mooring platform on the sensor data. These findings are then applied to the derivation of directional wave spectra, defining the most appropriate methods for each of the mooring systems used.

3.3.2 The 3D-ACM WAVE

The 3D-ACM WAVE (Fig. 3.1) was developed by Falmouth Scientific Inc (FSI). Based on successful previous acoustic current meter designs (Brown, 1992), the 3D-ACM WAVE measures pressure as well as 3-dimensional (*u, v, w*) velocity at frequencies of up to 5.36 Hz. Four acoustic fingers protrude from a central support strut, with each finger containing two acoustic transceivers. Thus the current meter uses the eight acoustic transceivers to create four acoustic pathways. The flow velocity is measured by observing the phase shift of the acoustic signal along three of the four acoustic pathways (one path is contaminated by the wake of the central strut and is disregarded).

The power consumption of an instrument is a crucial factor in determining the deployment duration and frequency of data sampling. Two features of the measurement technique described above help to reduce the instrument's power consumption. First, the measurement technique uses direct acoustic paths and not reflected sound. This reduces the power dissipated into the water and thus the power required to operate the instrument. Second, the instrument measures phase shifts of the acoustic signals along the paths, not the time of travel along the individual paths. The advantage of measuring phase shift is that it can be accomplished with slower electronic circuits, which require less power to operate.

Pressure is measured using a Druck Silicon machined sensor (accuracy 0.01% FS where F.S. = 344.74 kPa). The sensor allows the derivation of sea surface elevation data at wave or tidal frequencies. Instrument orientation is resolved using a 3-axis fluxgate compass and a 2-axis electrolytic tilt sensor (measuring the instrument's angle to vertical). Thus, the instrument does not have to be mounted in a vertical position, since tilt is measured and corrected for in velocity calculations.

Data is stored on one or two PCMCIA flash memory cards, with a capacity of 32 MB per card. The use of non-volatile flash memory provides for data security in the event of accidental loss of battery power. The instrument can be used in three modes: bursting mode, vector averaging mode, and interleaved mode. In bursting mode the instrument saves every time-series data point into memory. In the vector-averaging mode, the instrument performs a vector average on the sampled data and saves these values to memory. The interleaved mode combines both the bursting and vector averaging modes.

Figure 3.1: *3D-ACM WAVE* in protective frame

3.4 Methods

3.4.1 Field data

Data were available from field experiments in New Plymouth, New Zealand. Two 3D-ACM WAVE units were deployed, along with a suite of other instruments, as part of a three-year wave and sediment dynamics study (McComb *et al.*, 1999b). The New Plymouth region is characterised by a high-energy wave climate and a complex seabed bathymetry, with nearshore wave processes dominated by refraction and seabed friction (McComb *et al.*, 1997).

The 3D-ACM WAVE instruments were simultaneously deployed at two sites (Fig. 3.2). Site L1 utilised a mid-water taut-wire mooring system in 23.4 m depth, with the velocity sensors 14.9 m above seabed. Buoyancy was provided by four VINY buoys (~120 kg resultant buoyancy; Fig. 3.3) positioned 17 m above seabed. Site L2 used a seabed frame in 9.4 m depth with the velocity sensors 1 m above a sandy seabed.

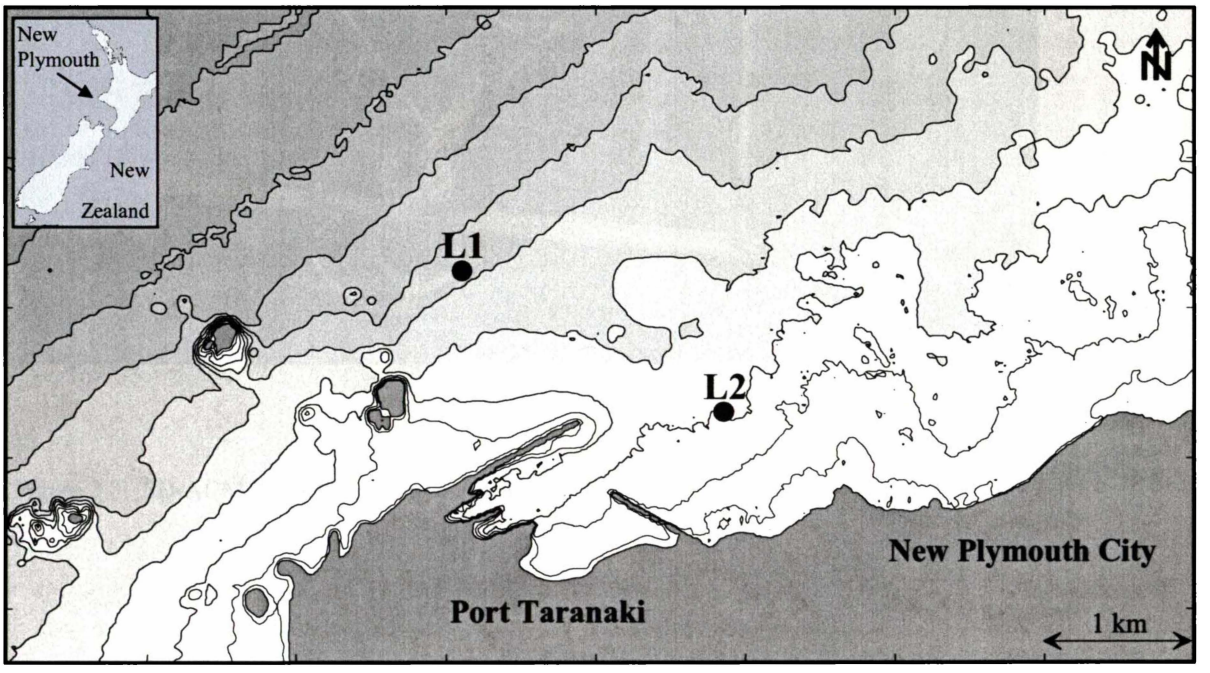

Figure 3.2: Location map of the field experiment, showing sites L1 and L2 (depths in 5 m contours)

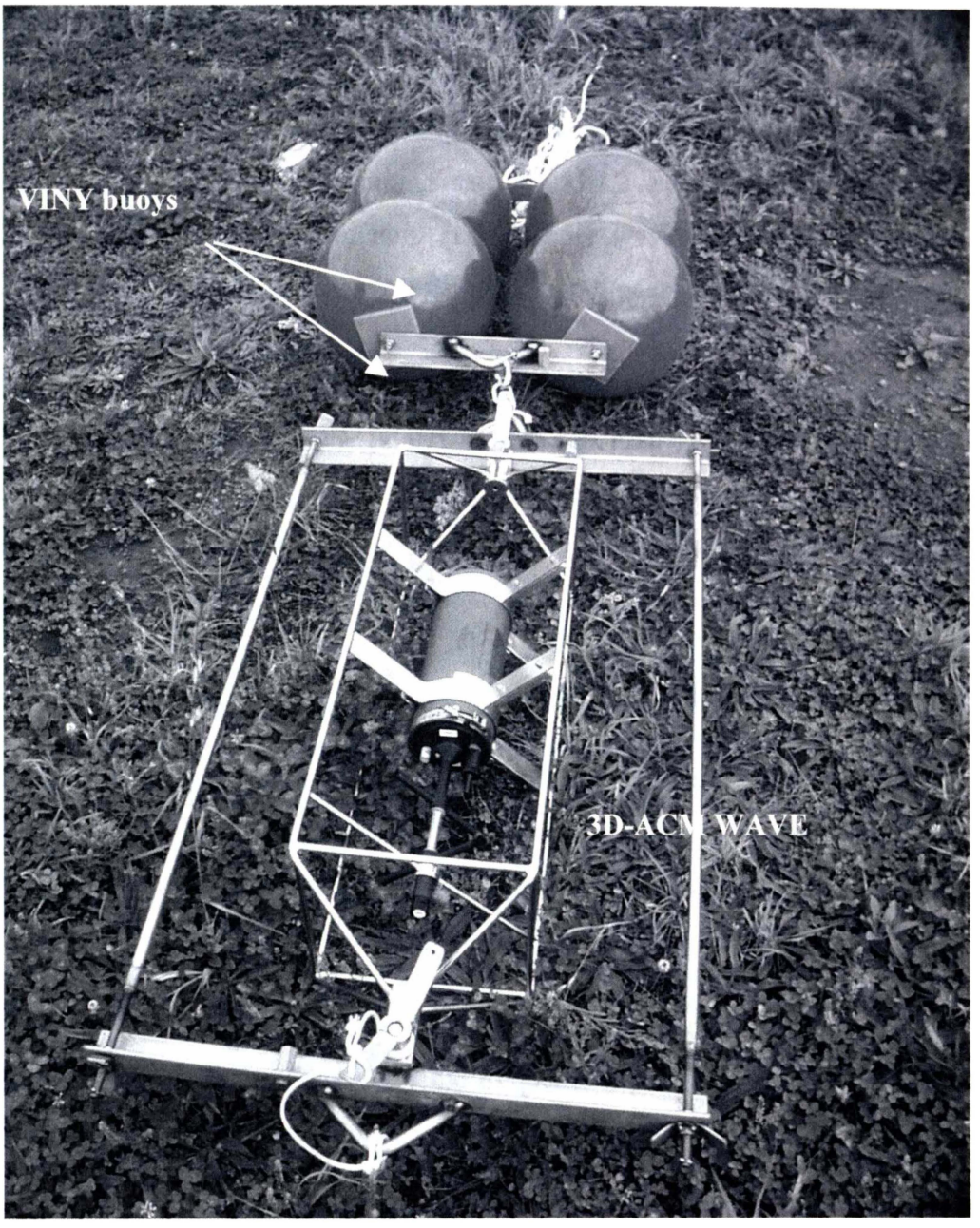

Figure 3.3: 3D-ACM WAVE mooring at site L1

The offshore site (L1) provided a reference boundary condition for directional waves and mid-water currents. The nearshore site (L2) was used for monitoring a trial nearshore disposal of harbour dredgings (measuring directional waves and near-bed wave orbital and mean currents). Sites L1 and L2 were deployed for one year (from March 1998) providing nearshore and offshore wave climate statistics as well as a comprehensive database for investigating offshore/nearshore wave response functions.

In this paper we consider data from the first two-month period of this experiment. Time-series measurements of *u, v, w* and *p* were recorded in 'burst mode sampling' of 9-minute duration at intervals of half the tidal period (373 minutes). Raw measurements were recorded at 5.36 Hz, and interpolated to 2 Hz for subsequent processing. Instrument tilt was not recorded, but was applied in the calculation of velocity.

3.4.2 Data processing

After atmospheric pressure correction, the burst time-series of pressure records were converted to sea surface elevations (z) by applying linear wave theory. This conversion involves filtering to remove frequencies above a depth-dependent cut-off,

$$f_{cut} = 0.282\sqrt{g/d}\,, \qquad \text{Eqn. 3-1}$$

(Hutt & Black, 1997) where f_{cut} is the frequency cut-off, g is gravitational acceleration and d is the instrument depth below the surface.

The surface elevation $\zeta(X,Y,t)$ in a wave field may be represented as a Fourier integral of sinusoidal wave components

$$\zeta(X,Y,t) = \int df\, d\theta\, A(f,\theta) e^{i(kX\cos\theta + kY\sin\theta - 2\pi ft)} \qquad \text{Eqn. 3-2}$$

where A is the (complex) amplitude coefficient associated with waves of frequency f, wavenumber k travelling in direction θ. As all measurements are at a single horizontal position, we may subsequently take X=Y=0, and simplify (Eqn. 3-2) to

$$\zeta(t) = \int df\; B_0(f) e^{-i2\pi ft} \qquad \text{Eqn. 3-3}$$

with B_0 the complex direction-averaged Fourier coefficient

$$B_0(f) = \int d\theta\, A(f,\theta) \qquad \text{Eqn. 3-4}$$

from which the 1-dimensional surface spectral density

$$S(f) = |B_0(f)|^2 \qquad \text{Eqn. 3-5}$$

can be found. Then in linear wave theory, the associated pressure variation at depth will be given by

$$\frac{\Delta p}{\rho g} = z(Z,t) = \int df\, B_0(f) \frac{\omega^2}{gk} \frac{\cosh[k(h+Z)]}{\sinh(kh)} e^{-i2\pi ft} \qquad \text{Eqn. 3-6}$$

where h is the total water depth, Z the vertical distance (positive upward) from the still water level, ρ the density of water, and g the gravitational acceleration. The wave number k is related to the angular frequency ω by the dispersion relation

$$\omega = 2\pi f = \sqrt{gk \tanh kh}\ . \qquad \text{Eqn. 3-7}$$

Similarly, the vertical (w) and horizontal (u,v) components of orbital velocity are

$$w(Z,t) = \int df\, B_0(f)(-i\omega) \frac{\sinh[k(h+Z)]}{\sinh(kh)} e^{-i2\pi ft} \qquad \text{Eqn. 3-8}$$

$$u(Z,t) = \int df\, B_1(f)\omega \frac{\cosh[k(h+Z)]}{\sinh(kh)} e^{-i2\pi ft} \qquad \text{Eqn. 3-9}$$

$$v(Z,t) = \int df\, B_2(f)\omega \frac{\cosh[k(h+Z)]}{\sinh(kh)} e^{-i2\pi ft} \qquad \text{Eqn. 3-10}$$

where

$$B_1(f) = \int d\theta\, A(f,\theta)\cos\theta \qquad \text{Eqn. 3-11}$$

$$B_2(f) = \int d\theta\, A(f,\theta)\sin\theta \qquad \text{Eqn. 3-12}$$

Burst measurements of w were converted to depth (z_w) at the same elevation (above seabed) as the z measurements using Eqn. 3-6, after first applying an inverse Fourier transform to Eqn. 3-8 to evaluate B_0.

For the measured data a mean velocity and direction was taken over the length of the burst. After subtracting the mean, the velocity was rotated into components of u' and v', which are respectively parallel to, and transverse to, the principal wave direction. This provides a more consistent basis for comparing velocity statistics between sites than components relative to an essentially arbitrary reference direction, such as true North, or the instrument axes. The principal wave direction was determined from the scatter of the velocity data, as the direction for which

$$\langle u'v' \rangle \equiv \frac{1}{N} \sum_{i=1}^{N} u'_i v'_i = 0 \quad , \qquad \text{Eqn. 3-13}$$

thereby minimising the variance $\langle v'^2 \rangle$ of the transverse velocities. This leaves a 180° ambiguity in the principal wave direction. For the generally swell-dominated conditions at this coastal site, this ambiguity can be simply resolved in favour of the shoreward direction.

A correlation coefficient for this regression is defined as

$$R_{uv}^2 = \frac{\langle u'^2 \rangle - \langle v'^2 \rangle}{\langle u'^2 \rangle + \langle v'^2 \rangle} \quad , \qquad \text{Eqn. 3-14}$$

using variances in the wave-aligned frame, as defined above. This definition is independent of the orientation of the original velocity coordinate frame, unlike the standard definition

$$R^2 = \frac{\langle uv \rangle^2}{\langle u^2 \rangle \langle v^2 \rangle} \qquad \text{Eqn. 3-15}$$

for linear regression.

If wave orbital motion is strongly aligned with the principal direction ($R_{uv}^2 \approx 1$) then, after resolving (u,v) to the wave-aligned axes, we can use Eqn. 3-9 and Eqn. 3-6 with $B_1(f) \approx B_0(f)$ to convert u_p to a second estimate of depth (z_u) at the same elevation as the z measurements.

In addition to the time-domain methods discussed above, spectral methods were also applied separately to deduce directional properties from the original data. Co- and cross-spectra were computed from the time-series data using the Fast Fourier Transform. This allowed the Fourier coefficients of Eqns. 3-3 to 3-12 to be evaluated as

$$\begin{aligned}
P_0 &= \mathrm{Re}(P_{zz}) = |B_0(f)|^2 = S_z(f) \\
P_1 &= (\omega/gk)^2\,\mathrm{Re}(P_{uu} + P_{vv}) = |B_1|^2 + |B_2|^2 \\
P_2 &= (\omega/gk)\mathrm{Re}(P_{zu}) = \mathrm{Re}(B_0 B_1{}^*) \\
P_3 &= (\omega/gk)\mathrm{Re}(P_{zv}) = \mathrm{Re}(B_0 B_2{}^*) \\
P_4 &= (\omega/gk)^2\,\mathrm{Re}(P_{uu} - P_{vv}) = |B_1|^2 - |B_2|^2 \\
P_5 &= 2(\omega/gk)^2\,\mathrm{Re}(P_{uv}) = 2\,\mathrm{Re}(B_1 B_2{}^*)
\end{aligned} \qquad \text{Eqn. 3-16}$$

where $P_{\sigma\tau}$ denotes the cross spectrum between variables σ and τ. P_0 is the 1-D surface spectral density derived from the pressure data. Two methods were used to calculate directional spectra. The first incorporates z, u, and v time-series data, allowing the spectra of mean direction

$$\theta_0(f) = \arctan\left(\frac{P_3}{P_2}\right) \qquad \text{Eqn. 3-17}$$

and directional spread

$$\Delta(f) = \sqrt{2 - \frac{2\sqrt{P_2^2 + P_3^2}}{P_0}} \qquad \text{Eqn. 3-18}$$

to be computed (Massel, 1996).

The second method uses only the u and v time-series data to estimate the mean direction and directional spread using

$$\hat{\theta}_0(f) = \tfrac{1}{2}\arctan\left(\frac{P_5}{P_4}\right) \qquad \text{Eqn. 3-19}$$

and

$$\hat{\Delta}(f) = \frac{1}{2}\sqrt{2 - \frac{2\sqrt{P_4^2 + P_5^2}}{P_1}}\,. \qquad \text{Eqn. 3-20}$$

The mean wave direction thus derived for each frequency has a 180° ambiguity, which is resolved in favour of the most shoreward wave direction.

The 1-D surface spectral density was also calculated from the velocity measurements using

$$S(f) \approx S_u(f) = P_1 = |B_1|^2 + |B_2|^2 \qquad \text{Eqn. 3-21}$$

Standard spectral estimates of significant wave height (H_s), mean spectral wave period (T_m) and spectral width (ε^2) (Cartwright & Longuet-Higgins, 1956) were also defined:

$$H_s = 4\sqrt{M_0}\,, \qquad \text{Eqn. 3-22}$$

$$T_m = \sqrt{M_0 / M_2}\,, \qquad \text{Eqn. 3-23}$$

$$\varepsilon^2 = 1 - \frac{M_2^{\,2}}{M_0 M_4}\,, \qquad \text{Eqn. 3-24}$$

where M_j is the jth spectral moment:

$$M_j = \int_0^\infty f^j S(f)\,df\,. \qquad \text{Eqn. 3-25}$$

The mean period as defined in Eqn. 3-23 has been found to be equivalent to the mean zero-crossing period for a Gaussian random sea (Longuet-Higgins, 1983), so provides a suitable spectral measure of period consistent with time-domain methods.

3.4.3 Data analysis

A number of events from the two-month data were selected for further study (Table 3.1), covering a range of wave heights with high (>0.7) wave direction R^2_{uv} correlation values (Eqn. 3-14). Standard linear regression analysis of the measured (z) and predicted (z_w and z_u) time-series was applied to facilitate the validation of the measured vertical (w) and horizontal (u) velocities on both mooring platforms.

The instruments were deployed in a 'fingers down' orientation, and any flow obstruction from the instrument body or mooring is likely to primarily affect the negative (downward) vertical velocities. To test this, standard deviations in the positive and negative w vectors were calculated from the burst data. This was also done for the z data (above and below the mean water level). A non-dimensional w (W*) was calculated by normalising w to the rate of change in z, and the standard deviation found for the positive and negative components of w. Instantaneous values of W* were calculated as;

$$W* = \frac{w}{dz/dt} \qquad \text{Eqn. 3-26}$$

Directional wave spectra were calculated for burst data from each site, using the methods detailed above. The results of each method were compared to consider possible influences from the mooring system on the resolved spectra.

3.5 Results

3.5.1 Sensor validation

The results of the regression analysis of the measured (z) and predicted (z_w and z_u) time-series show significant differences between the mooring platforms and between the horizontal (u) and vertical (w) velocities (Table 3.2).

Horizontal velocities

At site L2 (the seabed frame) the linear regression of z_u with z showed a high correlation (mean R^2 = 0.966) with a mean gradient of 0.950, providing a strong validation of the measured horizontal orbital motions. The regression gradients do however appear to decrease with increasing wave height.

At site L1 (the taut-wire mooring) there was a poor correlation between z_u and z (Table 3.2), and a phase lag of around 1.5 seconds was noted, with z preceding u. This lag was found to exist over the range of wave heights and periods examined (Table 3.1). After correction for the phase lag at site L1, a mean linear regression gradient of 0.563 was obtained for z_u and z, at an R^2 correlation of 0.659.

The phase of horizontal wave orbital motion should be vertically uniform with z, and it is probable that movement of the mooring system is influencing both the phase and magnitude of the measured horizontal wave orbital velocities. This is clearly illustrated in Figure 3.4, where time-series of measured and predicted horizontal velocities (i.e. values predicted from z data, and measured as u' from Eqn. 3-13) are given for event 90.28 (Table 3.1) for both sites L1 and L2. At site L2 (the fixed mooring) the measured and predicted velocities show good agreement, while at L1 the agreement is poor.

While phase lags of 1.5 seconds where observed in the L1 time-series data, this likely reflects the most energetic parts of the spectrum. At New Plymouth this is typically the lower frequencies (i.e. <0.1 Hz), and Figure 3.4 suggests that the higher frequencies exhibit a different phase response. Indeed, cross-spectral analysis of the measured and predicted velocities from site L1 indicate a phase difference of 50-60 degrees in the lower frequencies (~0.06 Hz), increasing to 80-100 degrees at the higher frequencies (0.2 Hz). This trend of increasing phase difference with increasing frequency remained consistent over the range of wave events studied. The coherence of the two velocity spectra was also similar over the wave events, with a general trend of decreasing coherence with increasing frequency. For the fixed mooring (site L2) however, coherence was high (~1) across the spectrum, and a near-zero phase difference was observed.

Vertical velocities

Values of z_w and z were poorly correlated at site L2, most probably due to the proximity of the sensors to the seabed. At 1 m elevation above bed, values of w are much less than the horizontal velocities, as w necessarily decays to zero at bed level. Turbulence is expected in this boundary region and may be manifest in the w data.

On the taut-wire mooring (site L1) where there is no such effect from the bed, z_w and z were reasonably well correlated and, although z_w values consistently under-predicted z, no trend was apparent between the gradient of the regression and the wave height. Unlike the horizontal velocities, values of z_w and z were in phase, having a mean gradient of the linear regression of 0.633 and a mean R^2 of 0.795.

When relating the change in z with w, we found there was no systematic variability between the positive and negative vertical velocities. While this does not quantify any specific effect of the instrument body on the w data, the regression analysis from site L1 nonetheless indicates that w is attenuated in some form.

3.5.2 Directional spectra

Spectral densities (S) of the sea surface elevation, derived from both the pressure (S_z) data (Eqn. 3-16) and velocity (S_u) data (Eqn. 3-21) were compared for data events where there was a high wave/current correlation (Eqn. 3-14) at both sites. We use data from Julian day 90.28 to illustrate the results, which are presented in Figure 3.5 with the S_u values normalised to S_z. At site L2, S_u agrees closely with S_z over much of the spectrum, although slightly attenuated at higher frequencies. At site L1, S_u bears little resemblance to the S_z spectrum with an apparent energy transfer from low to high frequency, which may be attributed to the effect of mooring motion on the velocity measurements. The data suggest that velocities are attenuated in the low frequency range (i.e. <0.1 Hz), but perhaps enhanced in the higher frequencies, with the highest ratio occurring around 0.17 Hz (which approximates the mean spectral wave period (Table 3.1)). This concurs with the cross-spectral analysis, with the lower coherence observed at higher frequencies (i.e. <0.1 Hz).

Accordingly, at site L2 the spectral density may be adequately derived from either velocity (Eqn. 3-21) or pressure data (Eqn. 3-16), but at site L1 the corruption in velocity data from the mooring motion negates its use in this capacity. To consider this effect on the estimation of wave direction, we compared the two methods described in Section 2.2 (i.e. using p, u, v data, and using only u, v data) to calculate the spectral distribution of wave direction and directional spread for a single event (Julian day 90.28, Table 3.1) at both sites.

The results (Fig. 3.6) show that for site L2 the mean directions derived from both methods were very similar over the frequency range 0.04 – 0.2 Hz. At site L1, however, they were similar only at frequencies up to about 0.13 Hz, after which they show significant differences. It is interesting to note that the largest deviation between the two methods occurs at a similar frequency (~0.17 Hz) to that observed in Figure 3.5 for the maximum ratio S_u / S_z for site L1.

Of the two methods used to resolve the directional components at site L1, the velocity data method (Eqns. 3-19 to 3-20) compares more favourably with the results from L2. Furthermore, the wave directions for the higher frequencies (>0.13 Hz) resolved using the pressure and velocity data (Eqns. 3-17 to 3-18) are not likely given the geographical limitations of the site (e.g. Fig. 3.2).

Table 3.1: Data events selected for study; site L1 is the taut-wire mooring, site L2 is the seabed frame.

Julian day 1998	L1 mean current		Significant wave height H_s (m)		Peak spectral period T_p (sec)		Mean spectral period T_m (sec)		Spectral width (Eqn. 3-24)		R^2_{uv} (Eqn. 3-14)	
	(ms^{-1})	dirn	L1	L2	L1	L2	L1	L2	L1	L2	L1	L2
67.23	0.042	089	1.52	1.42	10.70	10.70	6.67	6.62	0.57	0.58	0.58	0.85
69.30	0.106	354	2.4	2.31	8.03	8.03	6.05	6.66	0.41	0.42	0.69	0.80
73.45	0.133	230	2.16	1.61	6.42	6.42	6.01	5.94	0.33	0.39	0.61	0.84
87.70	0.085	241	4.52	3.13	12.84	12.84	8.18	7.75	0.61	0.55	0.65	0.83
90.28	0.110	352	2.19	1.6	16.05	12.84	6.07	6.35	0.53	0.60	0.84	0.83
90.80	0.124	293	3.4	2.97	8.02	8.02	5.84	6.19	0.41	0.36	0.79	0.73
91.32	0.080	272	2.55	1.61	9.17	9.17	7.03	6.99	0.55	0.61	0.52	0.87

Table 3.2: Standard deviations in the positive and negative vectors of w and z (above and below the mean water level). Standard deviations for W* (w normalised to the rate of change in z) for the +ve (upward) and –ve (downward) components of w. Coefficients for the linear regression analysis of the derived z_u and z_w values with measured z.

Julian Day 1998	*w* standard deviation		*z* standard deviation		W* standard Deviation		z_u - *z* regression		$z_w - z$ regression	
Site L1	+ ve	- ve-	+ ve	- ve	+ ve	- ve	gradient	R^2	gradient	R^2
67.23	4.67	5.57	0.13	0.12	13.41	211.45	* 0.650	* 0.479	0.636	0.826
69.30	8.07	7.83	0.17	0.18	24.84	31.09	* 0.571	* 0.689	0.591	0.759
73.45	6.06	6.17	0.09	0.11	19.71	18.90	* 0.566	* 0.597	0.685	0.684
87.70	12.45	15.53	0.40	0.43	9.36	8.85	* 0.412	* 0.712	0.641	0.872
90.28	7.14	7.07	0.26	0.23	9.72	7.06	* 0.658	* 0.667	0.545	0.820
90.80	11.13	13.94	0.24	0.27	9.24	16.07	* 0.553	* 0.722	0.679	0.785
91.32	8.58	9.91	0.22	0.24	13.93	18.01	* 0.530	* 0.747	0.656	0.822
Site L2										
67.23	1.94	2.02	0.12	0.12	46.25	29.87	1.048	0.968	0.813	0.177
69.30	2.97	3.93	0.18	0.19	9.24	11.58	0.996	0.967	0.966	0.324
73.45	1.93	1.80	0.09	0.09	13.18	43.03	1.047	0.943	0.561	0.073
87.70	4.58	6.46	0.36	0.27	6.24	3.82	0.819	0.976	0.485	0.089
90.28	2.51	2.60	0.19	0.14	9.42	7.49	0.937	0.963	0.681	0.105
90.80	3.93	4.48	0.23	0.22	9.18	15.82	0.852	0.973	0.397	0.042
91.32	2.22	3.22	0.16	0.16	4.94	13.02	0.949	0.972	0.615	0.138

* z_u corrected for a 1.5 second phase lag

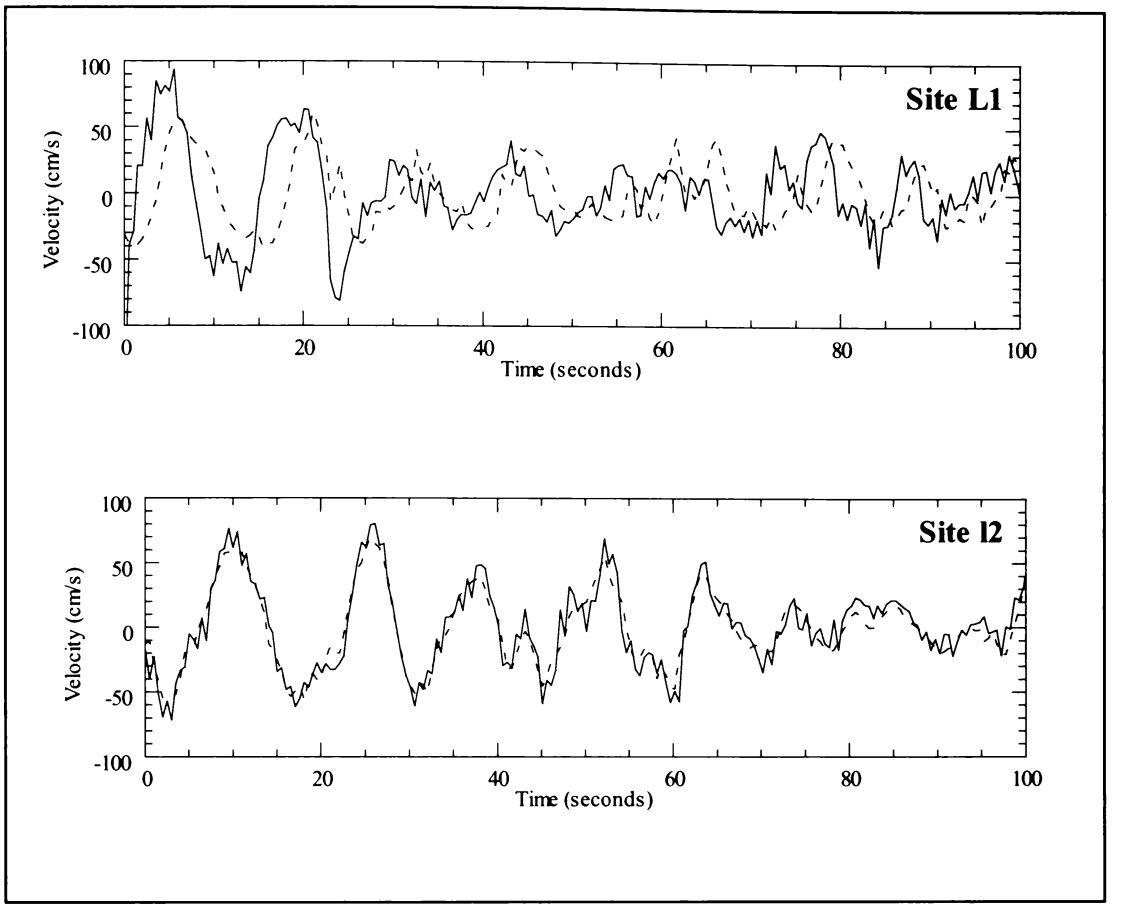

Figure 3.4: Time-series of $U_{predicted}$ (solid) and $U_{measured}$ (dashed) for sites L1 and L2 (event 90.28). $U_{predicted}$ is derived from the pressure data, while $U_{measured}$ is the velocity along the principal wave direction (from Eqn. 3-13))

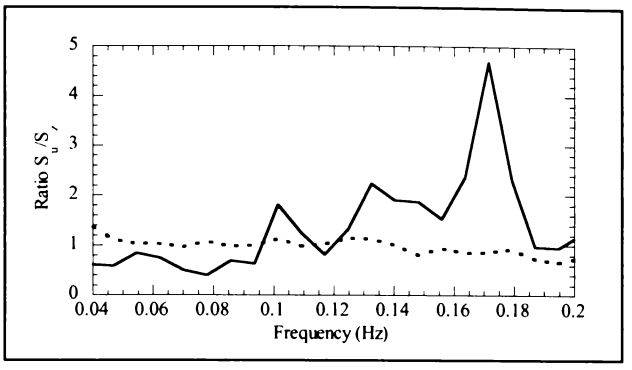

Figure 3.5: The ratio of spectral densities S_u/S_z from a single event (Julian day 90.28). Site L1 is shown as solid, site L2 is dashed

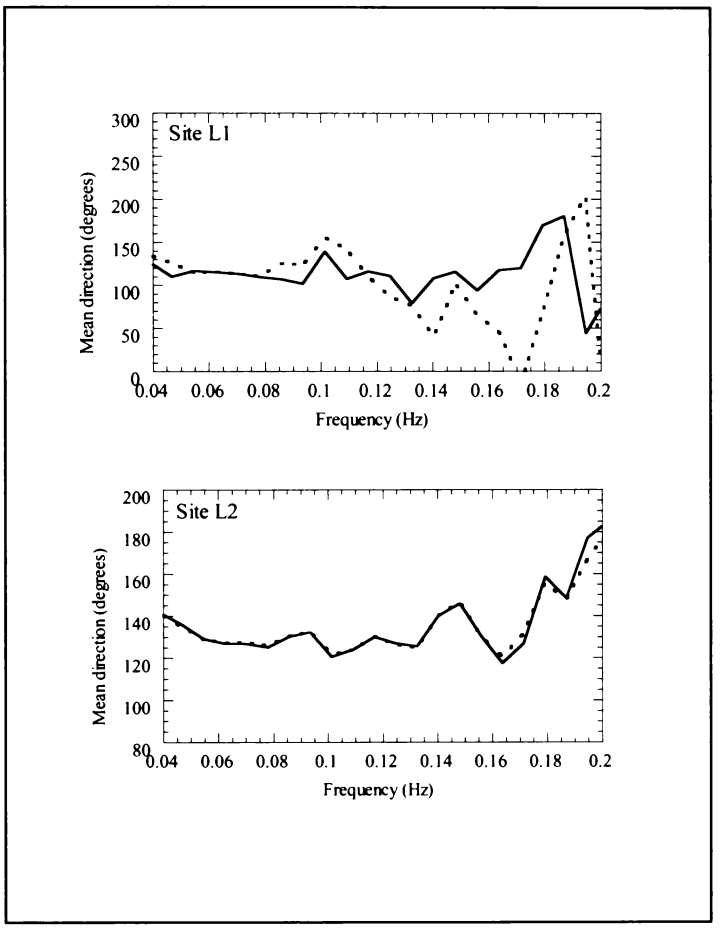

Figure 3.6: Spectral distribution of the mean wave directions from sites L1 and L2 for a single event (Julian day 90.28). Estimates derived from the pressure and velocity data are dashed, while those derived solely from velocity are solid.

3.6 Discussion

A comparison of measured velocities with predicted values (derived from pressure data using linear wave theory) has provided a validation of the sensors under field conditions. On the fixed mooring, our data show good agreement for the horizontal wave orbital velocities, but indicate that the gradients of the linear regression (between measured and predicted values) tend to decrease with increasing wave height (e.g. Fig. 3.7). Although less well correlated, the regression gradients for the phase corrected data of site L1 are similarly influenced. This may indicate either that the higher velocities associated with larger waves are less well represented in the measured data, or that errors associated with applying linear theory to real waves are amplified with increasing wave height. However, it is notable that the findings of Hutt & Black (1997) are consistent with the use of linear theory within a depth-dependent frequency band (e.g. Eqn. 3-1), providing only a 3% error for z over a 17 m depth range. Furthermore, the present case considers the relationship between the time-series of pressures and orbital velocities at the same depth, which is considered by Komar (1998) to be well represented by linear wave theory.

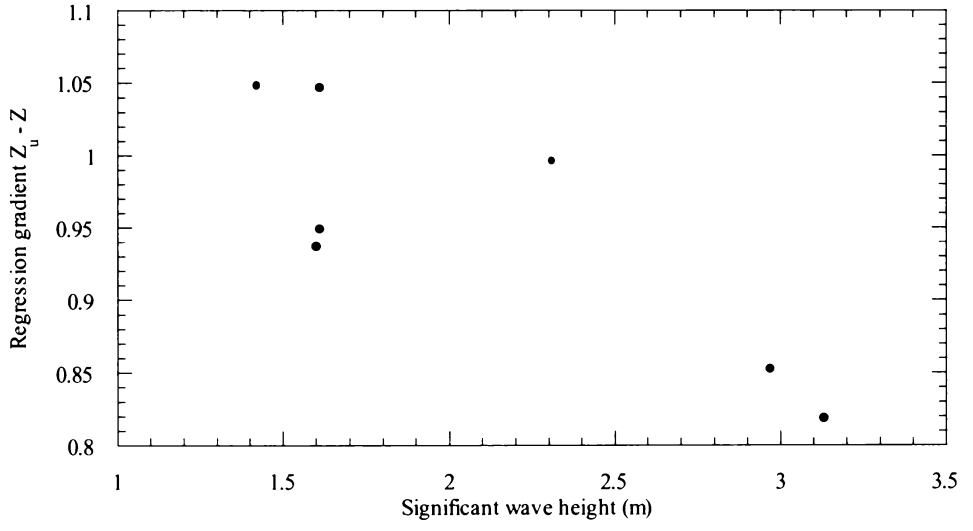

Figure 3.7: Plot of the significant wave height and the gradient of the linear regression of z_u (predicted from the measured orbital velocities) and z (derived from the pressure sensor). Data from the fixed seabed mooring site L2.

The measured vertical velocities (w) appear to be attenuated, and this may be due to flow obstruction from the instrument body or mooring components. However, the analysis did not reveal any significant differences in the velocity structure for either positive or negative vectors. The vertical data were of use in confirming the mooring motion at site L1; the time-series data show that w remained in phase with z while u did not.

Mooring motion is a well known phenomenon, yet the influence of the mooring motion on the resolution of directional wave spectra from p, u, v data is little reported. Our analysis has shown that corruption of the horizontal velocity data can lead to significant errors in the final directional wave spectra. The effect can be minimised by using the velocity only data for estimating the directional components to the spectra (Eqns. 3-18, 3-19), while deriving the spectral density from the pressure data. This is based on the assumption that the mooring motion we observed, although phase-shifting and modifying (i.e. attenuating/amplifying) the velocities relative to the surface wave motion, will not significantly affect their direction. For the case of site L1, a reasonable estimate of wave direction was attained for frequencies < 0.13 Hz, above which the directions appear erroneous. Given that the wave climate at New Plymouth is dominated by long-period (12–16 seconds) swell, the effect of mooring motion on the resolved wave direction for the peak frequencies is likely to be minimal. However, p, u, v meters are deployed on taut-wire moorings in many different coastal environments, covering a range of water depths and wave climates.

Accordingly, we considered how the mooring configuration may influence the velocity data on a taut-wire mooring. The effect of cable length on the $u - p$ phase lag may be simply illustrated. We examined data from two other experiments where p, u, v instruments had been deployed on taut-wire moorings of a similar design. Of these, DW1 was deployed off the New Plymouth coast in 1996 (McComb *et al.*, 1997), and RAGD509 (Hutt & Black, 1997) 140 km further north at Raglan. In each case, a similar buoyancy unit was used although the mooring cable length (i.e. from the seabed to the centre of the buoyancy) varied. The wave climate at Raglan is similar to New Plymouth, being dominated by long period (> 12 second) swell. The results (Fig. 3.8) show a systematic trend in the $u - p$ phase lag based on the length of the mooring cable, and

indicate that the natural resonant frequency of the mooring system is influential in the measurement of wave orbital velocities.

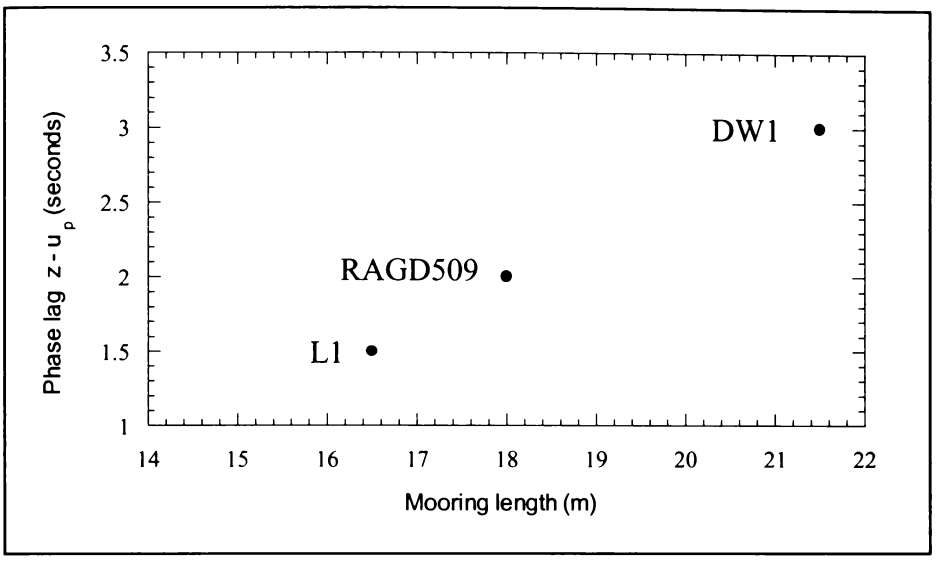

Figure 3.8: Plot of the taut-wire mooring length (m) and the phase lag (seconds) between z and u_p. Data is shown from sites L1, DW1 (New Plymouth) and RAGD509 (Raglan).

To model this motion, a taut-wire mooring subject to wave action may be treated as a forced damped oscillator. When displaced a distance x from the vertical, a horizontal restoring force will act on the instrument proportional to Tx/L, where T is the tension in the cable, and L is the cable length. The orbital velocity $U(t)$ will produce a drag force acting in the direction of the relative current $U - dx/dt$. For the sake of simplicity, we will assume linear drag, in which case the equation of motion is

$$M\frac{d^2x}{dt^2} + C\left(\frac{dx}{dt} - U(t)\right) + kx = F_{press}(t) \qquad \text{Eqn. 3-27}$$

with M the instrument mass, C a drag coefficient and the "spring constant" $k \propto T/L$. The constant of proportionality will depend on the mooring geometry, but should be of order one. $F_{press}(t)$ is the external pressure gradient force exerted on the instrument. If we imagine the water motion with and without the instrument in place, neglecting flow disturbance by the instrument, then $F_{press}(t)$ should be the same as the force driving the water volume displaced by the instrument. For periodic forcing

$$U(t) = U_0 e^{i\omega t} \qquad \text{Eqn. 3-28}$$

we can therefore compute this by putting $C = 0, k = 0$ and $M = M_{water}$ (the mass of displaced water) in Eqn. 3-26 to find

$$F_{press}(t) = i\omega M_{water} U_0 e^{i\omega t}. \qquad \text{Eqn. 3-29}$$

Returning to the case with the mooring present, the mass M should be replaced with an effective mass M_{eff} of the current meter and flotation, including buoyancy effects. This is a standard problem in dynamics (Timoshenko & Young, 1948), with a natural resonant frequency $\omega_0 = \sqrt{k/M_{eff}}$, and for which the solution has a relative velocity (as measured by the current meter).

$$U(t) - \frac{dx}{dt} = QU_0 e^{i(\omega t - \alpha)}. \qquad \text{Eqn. 3-30}$$

The attenuation factor is

$$Q = \frac{1 - \omega^2 / {\omega_0}^2 + s\omega^2 / {\omega_0}^2}{\sqrt{\left(1 - \omega^2 / {\omega_0}^2\right)^2 + \gamma^2 \omega^2 / {\omega_0}^2}} \qquad \text{Eqn. 3-31}$$

and the phase lag is

$$\alpha = \tan^{-1}\left(\frac{\gamma\omega/\omega_0}{1 - \omega^2 / {\omega_0}^2}\right), \qquad \text{Eqn. 3-32}$$

where $\gamma = \omega_0 C / k$ is a damping factor and

$$s = M_{water} / M_{eff} \qquad \text{Eqn. 3-33}$$

is a density ratio (s>1).

For low forcing frequency ($\omega/\omega_0 \approx 0$), the mooring is quasi-static, with $Q \approx 1$ and $\alpha \approx 0$ (Fig. 3.9). At resonance ($\omega/\omega_0 = 1$), the phase lag is 90° and the gain is a maximum ($Q = s/\gamma$). Above resonance, Q decreases again, and the phase lag continues to increase: in the high frequency limit the measured current becomes 180° out of phase with the true forcing velocity.

As $\omega/\omega_0 \propto \sqrt{L}$ when ω, T and M_{eff} remain fixed, we can see that the observed increase in phase lag with mooring length (Fig. 3.8) is consistent with the predicted behaviour.

For site L1, the observation of phase lags approaching 90° suggests, guided by this simple model, that the mooring system is near resonance. This is difficult to quantify without considering the broad spread of frequencies present, and the effects of a more realistic drag law.

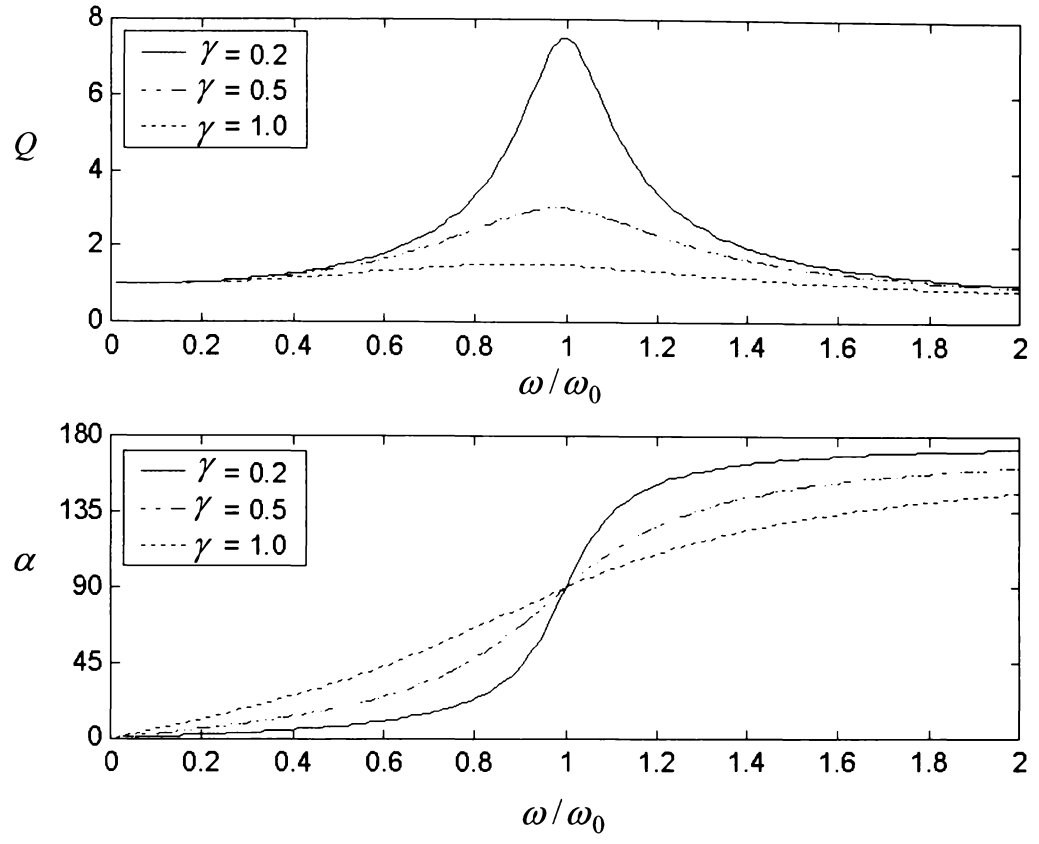

Figure 3.9: Attenuation factor Q and phase lag α for the relative current past a taut-wire mooring, treated as an ideal forced harmonic oscillator with linear damping. Solutions are shown with s = 1.5, with three values of the damping parameter γ. For $\omega/\omega_0 > 1$ the change in sign of Q in Eqn. 3-30 has been transferred to 180° shift in α.

Thus, a simple model of the mooring oscillation predicts that low frequency forcing (i.e. < 0.1 Hz) will have a minimal effect on the velocity data, and this is confirmed by the near agreement of the two methods for calculating the directional spectrum for frequencies up to ~0.13 Hz (Figs. 3.5 and 3.6). For higher frequencies, near the resonance mode of the mooring, the measured velocity signal can be amplified by mooring motion, as can be seen in Figure 3.5.

While velocities may indeed be influenced, the effect on the overall mean wave direction (as resolved by velocity only data) is likely to be minimal, as the buoy oscillation should remain aligned with the wave motion. However, directions resolved from the cross-spectra of pressure and velocity are likely to have frequency dependent errors due to the phase difference between the data.

Following on from these findings, we calculated directional spectra for each event recorded at both sites L1 and L2, over a two-month period (233 events). To illustrate these data in the form of the distribution of wave energy across frequency and direction, we present an averaged directional wave spectrum for each site (Fig. 3.10). This is an effective method of representing the entire directional wave spectra over time, as opposed to the reporting of spectral peaks and probabilities. These were compiled by averaging the spectral density, mean wave direction and directional spread from each recording event across discrete frequency bands (where the directional components were derived from velocity data). The mean direction and directional spread as derived above do not fully determine the directional distribution, but for plotting purposes the spectra were assumed to take the parametric form

$$\hat{S}(\theta,f)=P_1(f)\frac{2^{2\hat{s}-1}\Gamma^2(\hat{s}+1)}{\pi\Gamma(2\hat{s}+1)}\cos^{2\hat{s}}\left(\tfrac{1}{2}(\theta-\hat{\theta}_0(f))\right) \qquad \text{Eqn. 3-34}$$

suggested by Longuet-Higgins *et al.* (1963). Here Γ is the gamma function (Abramowitz & Stegun, 1970), and

$$\hat{s}(f)=\frac{2}{\hat{\Delta}^2(f)}-1 \qquad \text{Eqn. 3-35}$$

The respective wave climates at the nearshore (L2) and offshore (L1) sites are clearly shown on these plots. Site L1 features a broad range in wave direction with peak energy at around 0.07 Hz. We reiterate the potential uncertainty in resolved directions for frequencies >0.13 Hz, but note that at site L1 most of the energy is at frequencies less than 0.1 Hz. The spectrum from site L2 exhibits less energy with a peak around 0.08 Hz. The range in wave direction at site L2 is narrower than at L1, which results from refraction and the more sheltered position of the nearshore site.

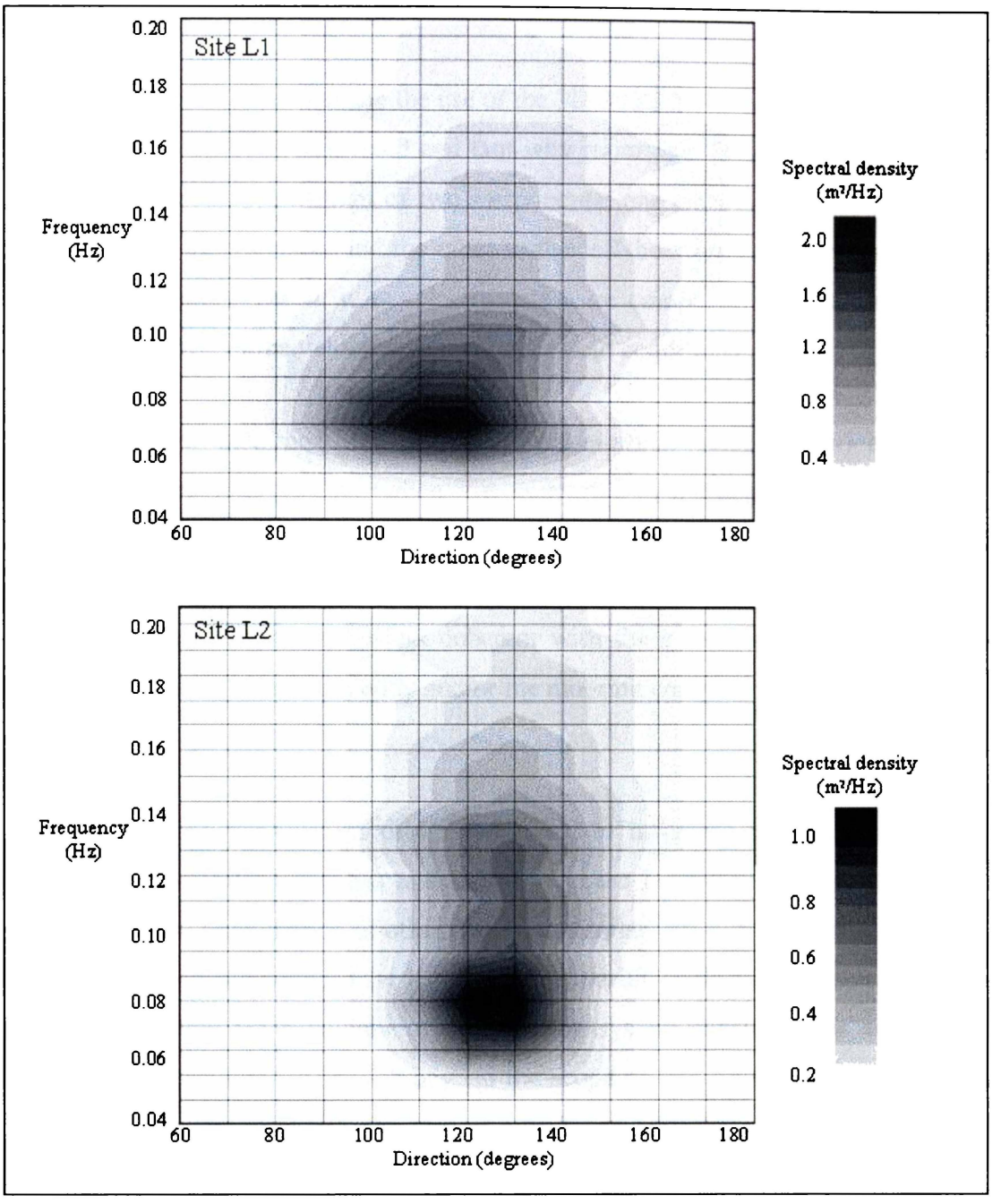

Figure 3.10: Averaged directional spectra from a two-month period (Julian days 62-124, 1998) for sites L1 and L2, New Plymouth, New Zealand

3.7 Summary

A study was conducted to evaluate the use of the 3D-ACM WAVE in collecting data for directional wave spectra from fixed and taut-wire moorings. Field data were analysed from a simultaneous deployment of two instruments; one on a nearshore fixed seabed frame (in 9.4 m water depth), and the other further offshore on a taut-wire mooring (in 23.4 m water depth). The u, v, w velocity data were compared with pressure data to provide a validation of the velocity sensors under field conditions.

The results show that measured horizontal wave-orbital velocities (u) are highly-coherent with pressure (z) data (when u is converted to z using linear wave theory) when the instrument is deployed on a fixed seabed frame, thus providing a strong validation of the velocity sensor performance. Vertical components of wave-orbital velocities (w) were found to be less coherent with the z data, possibly due to flow obstruction from the instrument body and/or the mooring components, however this was not confirmed.

The motion of the taut-wire mooring was found to influence the magnitude of the horizontal wave-orbital velocities and induce a phase lag between velocity and sea-surface elevation. Examination of other data from similar taut-wire moorings indicates a systematic relationship between the length of the mooring cable and the measured phase lag, consistent with the behaviour of the mooring system considered as an idealised forced damped oscillator. Although beyond the scope of this paper, the results suggest that an optimum taut-wire mooring design may be possible for a given wave climate, and this remains a subject of ongoing research.

A comparison was made between the spectra of wave direction derived from both velocity and pressure data with that derived solely from velocity data. The results show a high coherence for the fixed mooring, but significant directional variability in the higher frequencies (>0.13 Hz) on the taut-wire mooring. This we attribute to the phase difference between pressure and velocity on the taut-wire mooring, with the directional variability arising from the cross-spectral analysis of out-of-phase data. We conclude that for the taut-wire mooring, the spectrum of wave direction is most appropriately derived solely from the velocity data.

Directional wave spectra were produced for the nearshore and offshore sites for 233 coincident events over a two-month period, and these data have been presented in a time-averaged spectral format.

3.8 Acknowledgements

The authors thank M. Grosenbaugh (WHOI) for comments on the mooring model, and are grateful to E. Terray (WHOI) for the helpful reviews and valuable input to this work

4 MEASURING TIME-AVERAGED SUSPENDED SEDIMENT CONCENTRATIONS BY SEDIMENT TRAP AND AUTOMATED WATER SAMPLER: A COMPARATIVE STUDY UNDER WAVE-DOMINATED FLOW

4.1 Context of the paper within the thesis

This paper provides an *a posteri* calibration of the sediment traps used in the field experiments described in Chapter 2. The preliminary studies of Flint (1998) at the University of Waikato had indicated that rigid cylindrical traps were a useful method to measure the downward flux of suspended sediments. However, the experiments of Flint did not include a time-averaged application in a high-energy coastal setting. Traps were employed in the studies at New Plymouth because they allowed a large amount of data to be collected in an inexpensive manner, and it was hoped that the resultant data would provide at least a representative measure of the spatial and temporal variations in suspended sediment concentration (SSC). However, it was fortunate that the calibration experiments provided a strong validation for the use of sediment traps under waves, allowing the time-averaged SSC to be effectively derived and thereby allowing the data to be applied to other aspects of the research. The field experiments associated with this paper were conducted at New Plymouth over a 6-month period from January 2000. This paper has been submitted to Marine Geology (July, 2001) as:

McComb, P.J. and Black, K.P., (submitted). Measuring time-averaged suspended sediment concentrations by sediment trap and automated water sampler: a comparative study under wave-dominated flow.

4.2 Abstract

An experimental programme was conducted to determine the efficiency of sediment traps in a wave-dominated nearshore environment. The programme had two parts; the first tested the influence of the trap aperture size for reasonably high Aspect Ratio (*AR)* traps, and the second compared trapped samples with pumped water samples, with concurrent monitoring of waves and currents. Consistent with other studies, aperture size (and *AR*) was found to influence the trap efficiency, with an *AR* of 4.6 being too low for use in the moderately high-energy wave climate we tested. Traps with *AR*s of 7.5 and 13.3 yielded similar efficiencies - suggesting the optimum *AR* was not breached. Using a 13.3 *AR* trap, the time-averaged suspended sediment concentration (SSC) was found to be highly correlated with SSC derived from pumped water samples (R^2 = 0.986), over a wide range of SSC (0.0104-0.1418 kgm^{-3}) and wave/current conditions from six experimental deployments. From these data, the efficiency of the trap was found to be 75%, and the study has shown that sediment traps are effective tools for quantifying time-averaged SSC in wave-dominated nearshore zones - providing consistent results under a range of wave-orbital velocities.

4.3 Introduction

Sediment traps are a simple and inexpensive method of measuring the time-averaged settlement of particulate matter in the ocean. Consequently, this method has been widely applied in a range of marine environments, from the deep ocean (e.g. Honjo *et al.*, 1980) to the nearshore (e.g. Antsyferov & Kos'yan, 1990) and even the surf zone (e.g. Krause, 1987). Traps are, however, hydrodynamically intrusive devices, and considerable research has been conducted since the 1960s, investigating the most appropriate trap design for specific environments and applications to ensure biases are at least understood, and minimised where possible. Gardner (2000) provides a summary of sediment trap research, as do Bloesch & Burns (1980) and Blomquist & Håkanson (1981). It is generally held that straight-sided cylinders are the most effective trap shape (e.g. Gardner, 1980a, b).

Trapping efficiency is a measure of how well the traps represent the settlement flux, and the key parameters that influence trapping efficiency are described by Butman (1986) and Butman *et al.* (1986) as;

- The trap Aspect Ratio (AR), where

$$AR = H/D_i \qquad \text{Eqn. 4-1}$$

and H is the trap height and D_i is the inside diameter of the trap aperture.

- The trap Reynolds Number (R_t), where

$$R_t = uD_o/\upsilon \qquad \text{Eqn. 4-2}$$

and u is the velocity at the trap aperture, D_o is the outside diameter of aperture and, υ is the kinematic viscosity of the seawater.

- The ratio of flow speed to particle fall velocity (R_v), where

$$R_v = u/w \qquad \text{Eqn. 4-3}$$

and w is the settling velocity of the suspended sediment.

Sediment traps are devices that are able to sample the downward flux of suspended material, and provide a quiescent zone within the trap which allows the sediment particles to settle out, rather than become re-suspended. The AR considers the ability of the trap to retain the sediments, while R_t and R_v relate to the intrusion of the trap within the flow and the rate of settling of the suspended particles. The trapping efficiency for straight-sided cylindrical traps was shown by Butman (1986) and Butman *et al.* (1986) to decrease over a range of increasing R_t, indicating that the current velocity and/or the trap aperture size influence the overall trapping efficiency. White (1990) considers a trap aspect ratio >3 should be used in high-energy environments (where velocities exceed 0.2 ms^{-1}).

To effectively sample the downward flux of suspended particles, the trap geometry (i.e aperture size and *AR*) needs to be considered for a given velocity (u) regime. Bale (1998) notes that sediment traps cannot be considered as analogous with a rain gauge - primarily because of the effect of fluid flow on the trap. While much research has focused on trap efficiency under various flow velocities (e.g. Bale, 1998; Gust *et al.*, 1996) the performance of sediment traps in wave-dominated nearshore zones has not been addressed. This is despite the fact that a wide range of applications exist for traps in this environment (e.g. Antsyferov & Kos'yan, 1990). Under waves, the oscillating flow conditions are considerably more complex than unidirectional flow, and without empirical data it is not appropriate to merely extend the results from flow regime to another. Furthermore, in the nearshore environment, instantaneous wave-orbital velocities may be of considerable magnitude - frequently exceeding the net currents observed in previous trap studies (i.e. such as reported by Hargrave & Burns, 1979; Gardner, *et al.*, 1983; and Bale, 1998). It is also noteworthy that in a wave-dominated application, the values of R_t and R_v are constantly changing with the oscillating flows at the trap aperture. This means the Reynolds Numbers cannot be calculated for a time-averaged measurement period without making assumptions about how best to represent the distribution of wave-orbital velocities.

Unpublished work by Flint (1998) details a series of short-duration (15 minute) shallow-water experiments that tested the efficiency of straight-sided cylindrical sediment traps (*AR* 7) under waves (with peak orbital velocities of up to 0.5 ms^{-1}). By comparing trapped sediments with suspended sediments in pumped water samples, Flint estimated an average trapping efficiency of the order of 93%, although this varied from 54% to 148%. Flint (1998) concluded that traps were an effective tool for measuring the settlement of suspended sediments in the nearshore environment, but cautioned that a more rigorous calibration, under a wider range of conditions, was needed.

The present work extends that of Flint by employing a newly-developed automated water sampler to examine the effectiveness of straight-sided cylindrical sediment traps in an open-ocean experiment. Through the coincident deployment of the water sampler, sediment traps and a wave/current meter, data has been obtained to assess sediment trap efficiency under a variety of wave conditions.

4.4 Methods

Two separate experiments were conducted. The first aimed to assess the influence of the trap aperture size for reasonably high AR traps (i.e. AR >3). This is an important parameter for traps deployed in high-energy nearshore zones, as it determines the duration before the trap must be recovered (i.e. before the trap becomes "full" and the design AR range is exceeded). The second experiment involved a series of trap calibrations by comparison with an automated water sampler, with the results of the first experiment being used to specify the trap dimensions.

Field studies were conducted at New Plymouth, New Zealand (174° 11'E, 41° 03 ' S) at a site in 8 m water depth (mean sea level) on a level sandy seabed. The bed sediments are well-sorted fine sands (D_{50} = 0.22 mm) of volcanic origin.

4.4.1 Trap aperture size experiment

Three trap apertures were tested, and the dimensions are listed in Table 4.1, and illustrated in Figure 4.1. Traps were constructed from PVC pipe, and were mounted on a seabed frame so that the trap apertures were 0.55 m above bed. A spacing of 0.5 m was maintained between traps (exceeding the 3x trap diameter minimum spacing recommended by Nodder & Alexander, 1999) and the three traps were aligned parallel to the incident wave crests. Six trap deployments were conducted over February-April 2000, with trapping periods ranging from six to ten days. SCUBA divers were used for servicing. The trapped samples were wet-sieved at 45 μm, dried and weighed.

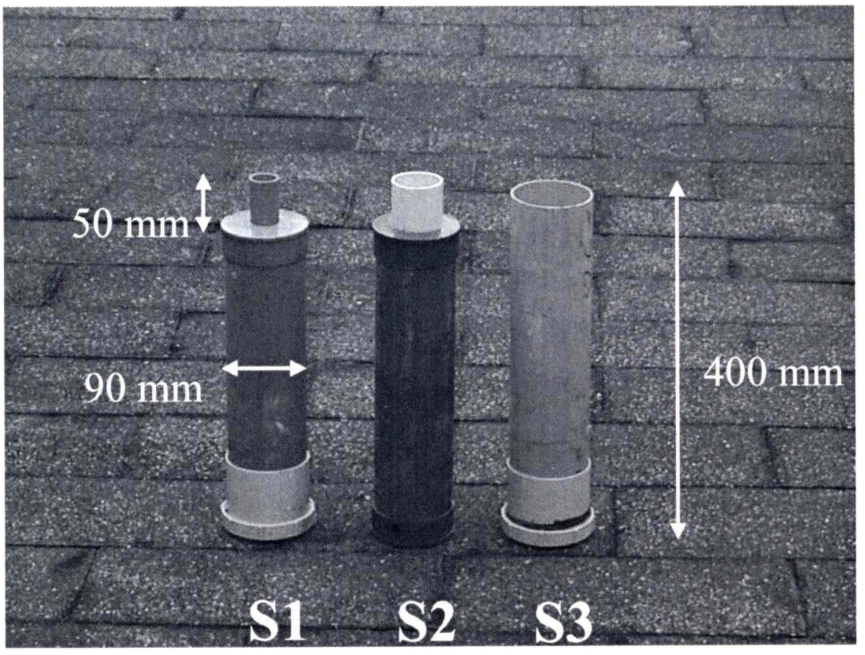

Figure 4.1 Photograph showing the dimensions of the three types of traps

Table 4.1 Dimensions of the three cylindrical trap types used in the aperture experiment. D_i and D_o refer to the inside and outside diameters of the aperture respectively. Body D_o refers to the outside diameter of the main trap body, and H is the overall trap height. These trap designs are illustrated in Fig. 4.1.

Trap Type	D_i (m)	D_o (m)	Body D_o (m)	Aperture (m^2)	H (m)	AR (H/D_i)
S1	0.030	0.033	0.090	0.00070686	0.4	13.3
S2	0.053	0.056	0.090	0.0022062	0.4	7.5
S3	0.087	0.090	0.090	0.0059447	0.4	4.6

4.4.2 Trap calibration experiment

A sturdy seabed frame was constructed to accommodate a HydroCamel (JK Instruments Ltd, New Zealand) automated water sampler as well as several of the type S1 traps (Fig. 4.2). The HydroCamel allows a user-programmed sampling regime to be conducted up to a capacity of 80 litres (20 x 4 litre sample bags), and has a flushing cycle between samples.

The inlet nozzle for the water sampler was vertically oriented (facing down) and positioned some 0.18 m from the trap aperture at the same elevation above bed level (i.e. 0.45 m). A downward orientation of the inlet tube was chosen following the work of Bosman *et al.*, (1987) and Black & Rosenberg (1984), thereby avoiding sediment settling in the tube prior to the collection periods (with an upward orientation) or over-collection due to the influence of wave-orbital velocities (for a horizontal orientation). A 3 m tube (of 7 mm internal diameter) connected the inlet nozzle to the water sampler. While several traps were set at each deployment, only the trap adjacent to the inlet nozzle was considered in the analysis. The frame was placed on the seabed for the duration of the experiment (May-July, 2000) with the HydroCamel and traps being deployed and recovered by SCUBA divers over 11 separate deployments.

The HydroCamel was set to sample approximately two litres of seawater in a 20-second period at either two or three-hourly intervals over the deployment (depending on the expected wave conditions), after which it was winched onboard the servicing boat and the sample bags retrieved. The water volume in each sample bag was measured and particulate matter extracted and aggregated using a 45 μm sieve and subsequently dried and weighed. A time-average suspended sediment concentration (SSC) was found then derived as the total (dry) mass recovered per total volume collected. Additional SSC

values (SSC_{pc}) were also derived after applying a pump correction factor of 0.8 (Bosman *et al.*, 1987), which accounts for the inertia of the suspended particles under transverse pump sampling.

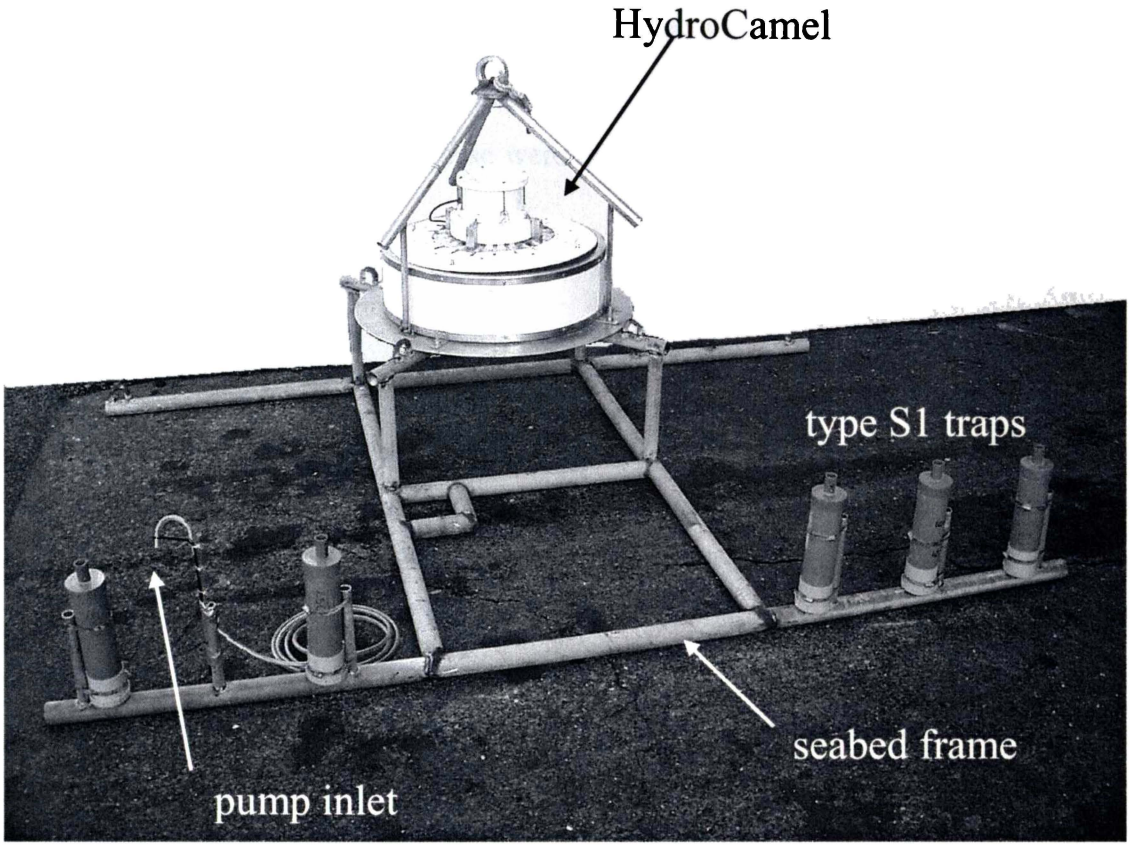

Figure 4.2 Photo of the type S1 traps and HydroCamel water sampler mounted on the seabed frame.

Trapped sediment samples were wet-sieved at 45 μm, dried and weighed. Grain size and settling velocity distributions were obtained using a 1.9 m fall-tube (RSA). In the RSA, sediment samples are released at the top of the fall-tube and a balance measures the amount of sediment settling to the bottom over time. The masses (M) collected in the traps were converted to a downward flux (f_d) with the units $kg.m^{-2}s^{-1}$ as follows:

$$f_d = M/At \qquad \text{Eqn. 4-4}$$

where A is the area of the aperture of the trap and t is the time of the sampling. The downward sediment flux was converted to a time-average suspended sediment

concentration (C) using the full settling velocity distribution of the trapped sediment (Armanini & Ruol, 1988; Nishi *et al.*, 1992). Concentration distributions were calculated as:

$$C = \frac{M_i}{w_i A \Delta t}, \qquad \text{Eqn. 4-5}$$

where M_i is the mass trapped, A is the area of the collection orifice of the trap, w_i is the settling velocity of the sediment particles of the i^{th} sediment fraction in the distribution and Δt is the deployment time. These were then summed to provide concentrations for the whole sample as:

$$C = \frac{1}{\Delta t} \sum_{i=1} \frac{M_i}{w_i A}. \qquad \text{Eqn. 4-6}$$

Waves and currents were measured with a 3D-ACM WAVE meter (e.g. McComb *et al.*, 2001). A buoyed taut-wire system was used to moor the instrument, with the velocity sensors positioned 1.7 m above the seabed. The mooring was located 10 m from the HydroCamel frame. Orthogonal velocity and pressure data were recorded at 5.36 Hz for 9 minute bursts every three hours over the deployment period. The data were used to define the directional wave climate as well as to quantify the mean (net) currents. Linear wave theory was used to transform velocity time-series from 1.7 m above bed to the 0.45 m level (same as the trap aperture), and RMS velocities were resolved (U_{RMS}) to represent the wave-orbital motions. The data processing methods we employed are fully described by McComb *et al.*, (2001).

4.5 Results

4.5.1 Trap aperture size experiment

The results of this experiment are given in Table 4.2, with the data also expressed as downward flux rates (Eqn. 4-4). By comparing the flux rates with aperture area for each deployment, systematic variations based on the trap aperture size may be noted. Figure 4.3 presents that data, showing similar f_d for all three trap types, although in the most energetic period (i.e. the sixth deployment) the type S3 trap appears to collect less material per unit area.

Table 4.2 Results of trap aperture experiment showing the masses of trapped material (>45 μm) for each trap type (e.g. Table 4.1) over the six deployments. A downward flux rate is given for each trap, where the mass trapped is normalised to the trap aperture and the deployment time (Eqn. 4-4).

Deploy	Duration (s)	Mass in Trap S1 (g)	S1 Trap f_d ($g/m^2/s$)	Mass in Trap S2 (g)	S2 Trap f_d ($g/m^2/s$)	Mass in Trap S3 (g)	S3 Trap f_d ($g/m^2/s$)
1	518400	2.114	0.0057691	10.396	0.0090899	17.852	0.0057928
2	518400	3.844	0.010490	11.830	0.010344	18.821	0.0061073
3	856800	-	-	33.410	0.017675	96.878	0.019020
4	867600	5.842	0.00952510	26.451	0.013819	39.137	0.0075882
5	536500	6.657	0.017554	-	-	35.904	0.011258
6	759600	32.3	0.060157	101.500	0.060567	172.500	0.038201

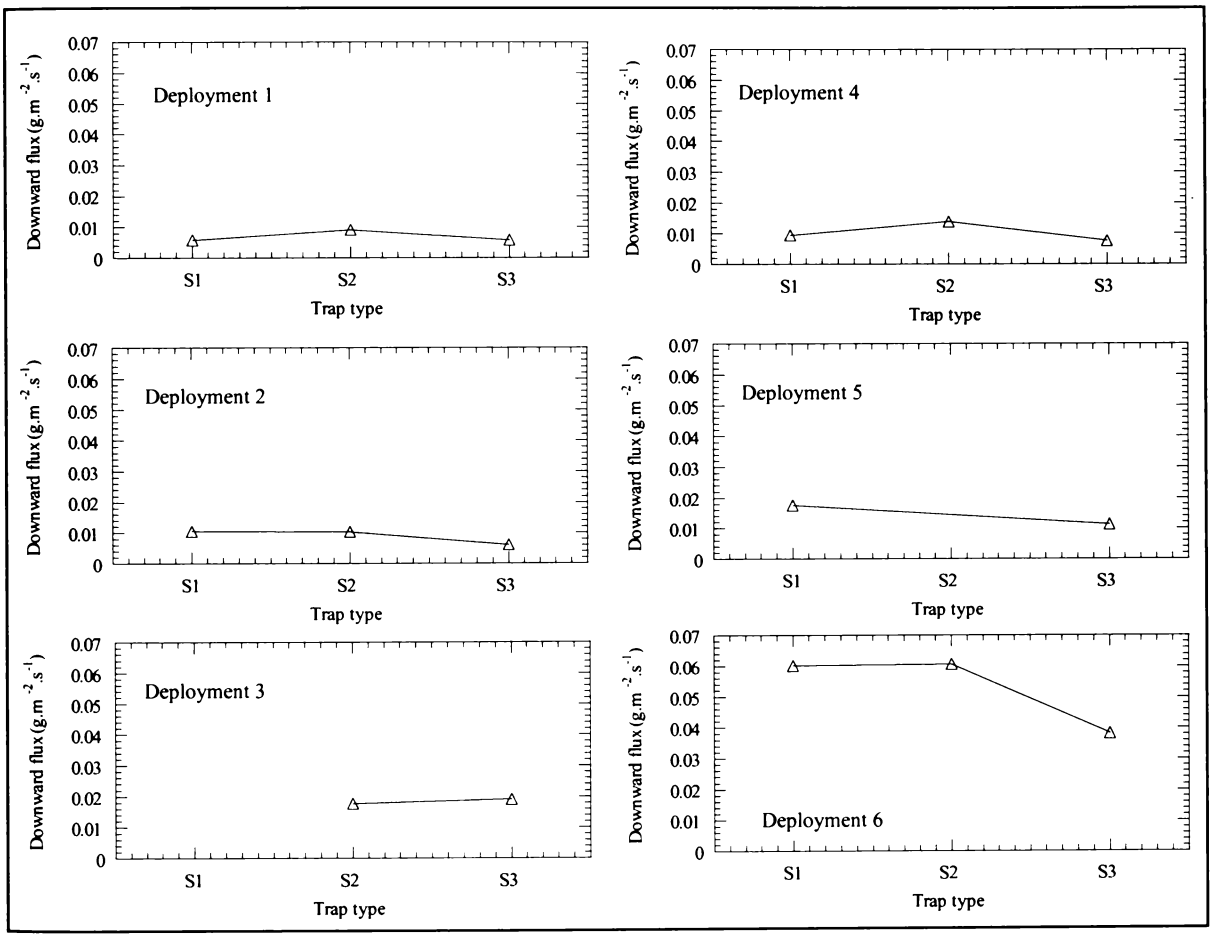

Figure 4.3 Plot showing the trap type vs downward flux rate for each of the six trap deployments. The traps types are illustrated in Figure 4.1 and detailed in Table 4.1.

4.5.2 Trap calibration experiment

Of the 11 calibration deployments (i.e. both HydroCamel and traps), six were successful in recovering both trap and water samples. The results are presented in Table 4.3, showing the mass of trapped material (>45 μm), downward flux rates (f_d), SSC derived from the trap (Eqn. 4-6) and SSC/SSC_{pc} derived from the automated water sampler. A statistical description of the wave and current conditions for each deployment are also given in Table 4.4, with the average and median significant wave heights (H_s) along with the averaged (net) currents. Wave-orbital motions at the trap aperture level are represented by U_{RMS}, which is the average of the RMS velocities within the nine-minute data bursts. The maximum U_{RMS} recorded in each deployment is also given.

SSC from the traps show very good agreement with the water sampler SSC (un-corrected for pump bias); the linear regression analysis has a high correlation (R^2 = 0.986) and indicates a trap efficiency of 93.84%. When corrected for the 0.8 pump efficiency under transverse suction, the time-averaged concentrations ranged from 0.0104-0.1418 kgm^3 over the experiment, and an averaged trap efficiency of 75.07% was obtained (Fig. 4.4). This result assumes that a linear relationship will exist over the mid-range of concentrations, as no data were obtained in this range in the experiments. In the absence of data to suggest otherwise, this assumption is consistent with the analyses of field and laboratory data by Gust *et al.* (1996).

Table 4.3 Results of calibration experiment showing the mass of trapped material (>45 μm), downward flux rates (f_d), SSC derived from the trap (Eqn. 4-6), SSC derived from the HydroCamel automated water sampler and the pump corrected values (SSC_{pc}) using the 0.8 efficiency for transverse suction (after Bosman *et al.*, 1987).

Deploy	Duration (s)	Mass trapped (kg)	Trap f_d ($kg/m^2/s$)	Trap SSC (kg/m^3)	HydroCamel SSC (kg/m^3)	HydroCamel SSC_{pc} (kg/m^3)
A	249900	0.276300	0.001564	0.107576	0.113415	0.141768
C	249300	0.049529	0.000281	0.018815	0.010200	0.012750
D	253500	0.042501	0.000237	0.016714	0.019140	0.023925
E	252000	0.017601	9.88E-05	0.009616	0.020593	0.025741
F	426300	0.023165	7.69E-05	0.005771	0.008339	0.010423
G	253500	0.260400	0.001453	0.115159	0.122572	0.153216

Table 4.4: Wave and current conditions: Mean significant wave heights (H_s) and peak spectral wave periods (T_p) are presented for each deployment, along with the mean RMS wave-orbital velocity (U_{RMS}), maximum U_{RMS} and mean net current (U_{mean}).

Deploy	Mean H_s (m)	Mean T_p (sec)	Mean U_{RMS} (cm/s)	Max. U_{RMS} (cm/s)	Mean U_{mean} (cm/s)
A	1.07	10.00	27.93	44.61	4.96
C	0.62	13.72	17.04	27.49	3.71
D	0.93	6.27	19.12	27.32	2.00
E	0.76	9.07	17.70	27.27	3.20
F	0.52	11.98	13.46	21.64	4.25
G	1.68	9.32	32.46	41.47	3.98

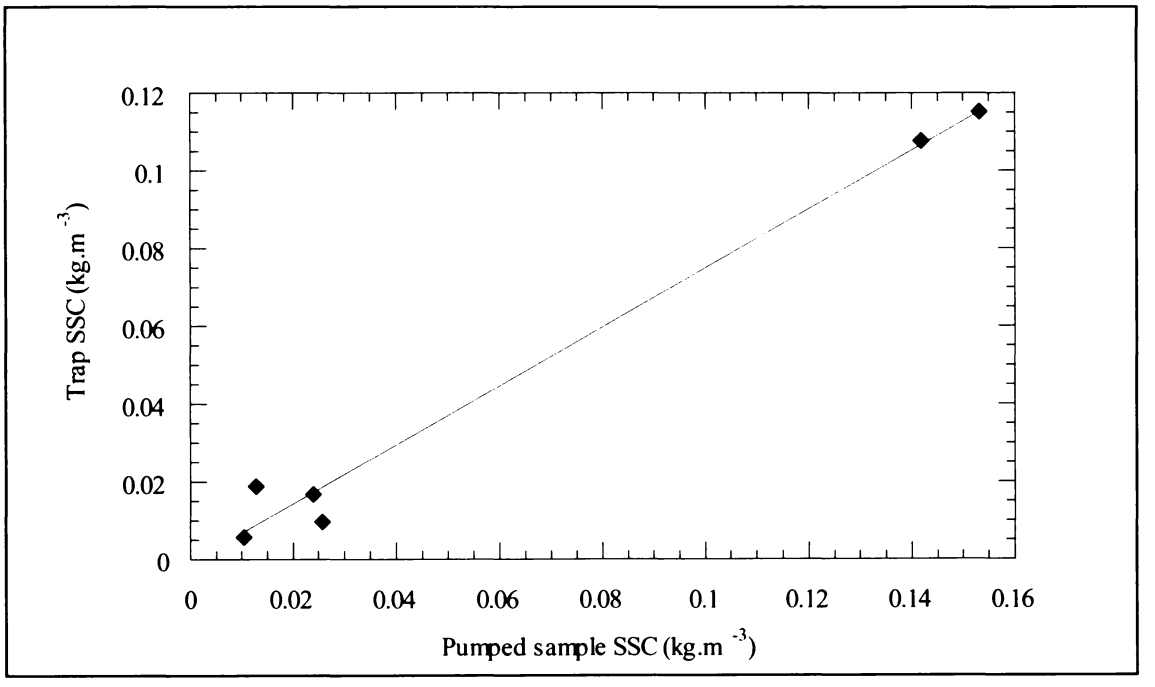

Figure 4.4 Plot of the HydroCamel SSC (corrected for the pump bias of 0.8) vs the sediment trap SSC. The linear regression of these data is highly correlated (R^2=0.98) and indicate a trap efficiency of 75.07%.

The mean (net) currents (U_{mean}) measured over the deployments ranged from 2.00-4.96 cms^{-1}, although the highest burst-average current (over the nine-minute recording period) was 10.46 cms^{-1}. Significant wave heights (H_s) were as high as 2.2 m, with the deployment-averaged values ranging from 0.52-1.68 m. Similarly, peak spectral wave periods (T_p) ranged from 4.0-18.29 s, with the deployment-averaged values ranging from 6.27-11.98 s. The deployment-averaged RMS wave-orbital velocities (U_{RMS}) at the trap level (0.45 m above seabed) were between 13.46 and 32.46 cms^{-1}, while the maximum was U_{RMS} was 44.61 cms^{-1}.

4.6 Discussion

To effectively sample f_d requires a) the entry of the particles into the receptacle, and b) containment of the particle within that receptacle. The containment of trapped material relies on the presence of a tranquil zone within the trap, allowing the sediment to settle out and not be re-suspended and circulated out of the trap (e.g. White, 1990). High *AR* (i.e. between 3-10) are widely recommended for strong or turbulent flow conditions, although the effect of the reversing wave-orbital motion on *AR* has not been reported. However, the findings of the first experiment presented here are consistent with those estimates, and indicate that an *AR* of 4.6 (trap type S3) is too low for the conditions we encountered, resulting in lesser catches per unit area under the high-energy conditions. The similar f_d values for trap types S1 and S2 (*AR* 13.2 and 7.5, respectively) indicate the effective *AR* range was not exceeded in those traps. Further, we note that traps S1 and S2 have a wide body (OD = 0.09 m; Fig. 4.1) which reduces at the aperture - thereby allowing the storage volume to be retained while the *AR* is increased.

The efficiency of a) relates to how the presence of the trap alters the local hydrodynamics, inducing vortices that may cause either under- or over-collection (e.g. Butman, 1986; and Gardner, 1980b, respectively), depending on the trap design and particle sizes. These effects have not yet been quantified under waves, although attempts have been made (e.g. Flint, 1998). The present work has employed an empirical approach to understanding trap efficiency under waves, which has been made possible with the recently developed automated water sampler.

SSCs derived from the traps were very well correlated with SSCs from the water sampler over the range of f_d measured, as well as over the varying wave and current conditions encountered through the experiment. This is an important finding as it indicates the time-averaged trap efficiency did not significantly vary over the range of flow conditions. Furthermore, the two methods (i.e. trapping and water sampling) show agreement despite the different sampling routines; with traps providing a continuous sample over the deployment, while the HydroCamel samples for only 20 seconds every 2 or 3 hours. Near the seabed, SSCs are known to exhibit changes on a wave-by-wave basis (e.g. Black & Rosenberg, 1991), although at the elevation of the trap / HydroCamel inlet (i.e. 0.45 m above bed) variation is more likely to be on an infra-gravity time-scale (e.g. Greenwood *et al.*, 1990). While such variability may be manifest in the lower SSC values, where the data show less agreement (e.g. Table 4.3), this may equally be attributed to higher experimental errors associated with the lower sample masses.

With respect to the 125% scaling of the water sampler data (to account for a pumping bias under transverse suction - Bosman *et al.*, 1987), we note that Black & Rosenberg (1994) have found similar values for pump efficiency. By comparing pumped samples with optical backscatter (OBS) data, they confirmed 0.8 is an appropriate value to apply as a transverse pumping efficiency under non-broken wave conditions.

4.7 Conclusions

A field programme was conducted to assess the efficiency of sediment traps in measuring the time-averaged downward flux of suspended material under wave-dominated conditions. Two separate experiments were conducted; the first tested the influence of the trap aperture size for reasonably high *AR* traps, and the second compared trapped samples with pumped water samples, along with monitoring of waves and currents.

The aperture size (and *AR*) was found to influence the trap efficiency, consistent with previously reported field studies. An *AR* of 4.6 would appear to be too low for use in the moderately high-energy wave climate we tested, while traps with *AR*s of 7.5 and 13.3 yielded similar efficiencies - suggesting the optimum *AR* was not breached.

A 13.3 *AR* trap was subsequently used in the second experiment. Time-averaged suspended sediment concentrations (SSC) derived from traps were found to be highly correlated with SSC derived from pumped water samples (R^2 = 0.986), over a wide range of SSC (0.0104-0.1418 kgm^{-3}) and wave/current conditions from six experimental deployments. From these data, the efficiency of the trap was found to be 75 %.

This study has shown that sediment traps are effective tools for quantifying time-averaged SSC in wave-dominated nearshore zones, and provides consistent results under a range of wave-orbital velocities.

5 HIGH-RESOLUTION WAVE TRANSFORMATIONS ON A COAST WITH COMPLEX BATHYMETRY

5.1 Context of the paper within the thesis

The initial experimental studies focused on the distribution of wave energy along the coast, as well as the general circulation patterns, with a view to identifying potential sites for nearshore dumping of dredged sands. To achieve this in a complex seabed environment at New Plymouth required numerical modelling of the wave transformations from offshore through to the surf zone. This paper reports on this exercise, which involved data collection along 5 km of the coastline, analysis of those data, and the calibration/validation of the WBEND wave refraction model. The results of this study were used in the selection of sites for further study, and in the design of the intensive field programme described in Chapter 2. The work was presented at the Pacific Coasts and Ports '97 Conference in Christchurch, New Zealand and published as:

McComb, P., Black K., Atkinson, P., Bell, R. and Healy, T., 1997. High-resolution wave transformations on a coast with complex bathymetry. *Proceedings of the 1997 Pacific Coasts and Ports Conference*, Christchurch, New Zealand (Vol. 2), pp. 995-1000.

5.2 Abstract

A wave transformation study on a coast with complex bathymetry is presented. The study involved collection of wave data from one offshore and nine inshore sites distributed longshore on the New Plymouth City coast, and the establishment of a numerical wave refraction model. Wave transformation processes are found to be dominated by seabed friction and refraction. White-capping from onshore winds is quantified in terms of wave transformations and a mechanism based on reduced refraction and increased wave diffraction is proposed. The WBEND wave refraction model was calibrated with the field data. The model was found to predict the wave height distribution in the study region and is used to produce outputs of representative wave climates.

5.3 Introduction

The New Plymouth City coast is a high-energy wave environment, exposed to waves approaching from the south-west through to the north and dominated by long period swell from the west. Bathymetric features shallower than 25 m depths are complex with reef and channel structures of inter-bedded lahar deposits predominating. The substrate is intermittently overlain with boulders, gravels and sand (Arron and Mitchell, 1984). Numerous researchers have determined that net sediment transport progresses to the north-east (e.g. McLennan, 1982). The construction of breakwaters for Port Taranaki has necessitated regular dredging of sand from the tip of the main breakwater at an average of 150,000 m^3 per year over the last 100 years (McLennan, 1982). The dredged material is currently deposited offshore in 22 m of water effectively removing it from the littoral zone. Coincidental with the breakwater construction has been an acceleration of the coastal erosion and general denudation of intertidal sand deposits along the New Plymouth City coast (Agnew, 1973). This, combined with foreshore and river-mouth realignments, has resulted in a reduced recreational amenity value of the coastline and has necessitated the construction of coastal protection structures along 73% of the city foreshore.

A study was initiated to identify potential sea dumping sites that would allow the sand from the port's maintenance dredging to return to the littoral system under natural processes, thereby maximising its beach renourishment potential. The first stage in this study is to gain an understanding of the wave dynamics which ultimately drive the sediment transport processes.

Wave transformations in shallow water over complex bathymetry will be primarily affected by the processes of refraction, diffraction, shoaling, and dissipation from both the seabed and atmospheric interfaces. Very few studies have attempted to isolate the effect of non-linear transfers of spectral energy or wave dissipation under onshore winds from intermediate to shallow depths at an open coast site.

This paper describes wave transformation processes identified on the New Plymouth City coast. Methods employed include:

- field data collection, analysis and interpretation;
- establishment of a numerical model of wave refraction;
- application of the model to define wave transformation processes and to predict seabed orbital motion for a representative wave climate.

The effect of white-capping as a dissipation function is examined by comparing events with onshore and offshore winds. The WBEND numerical refraction model is tested for resolution of complex seabed features and the use of a scheme that mimics diffraction.

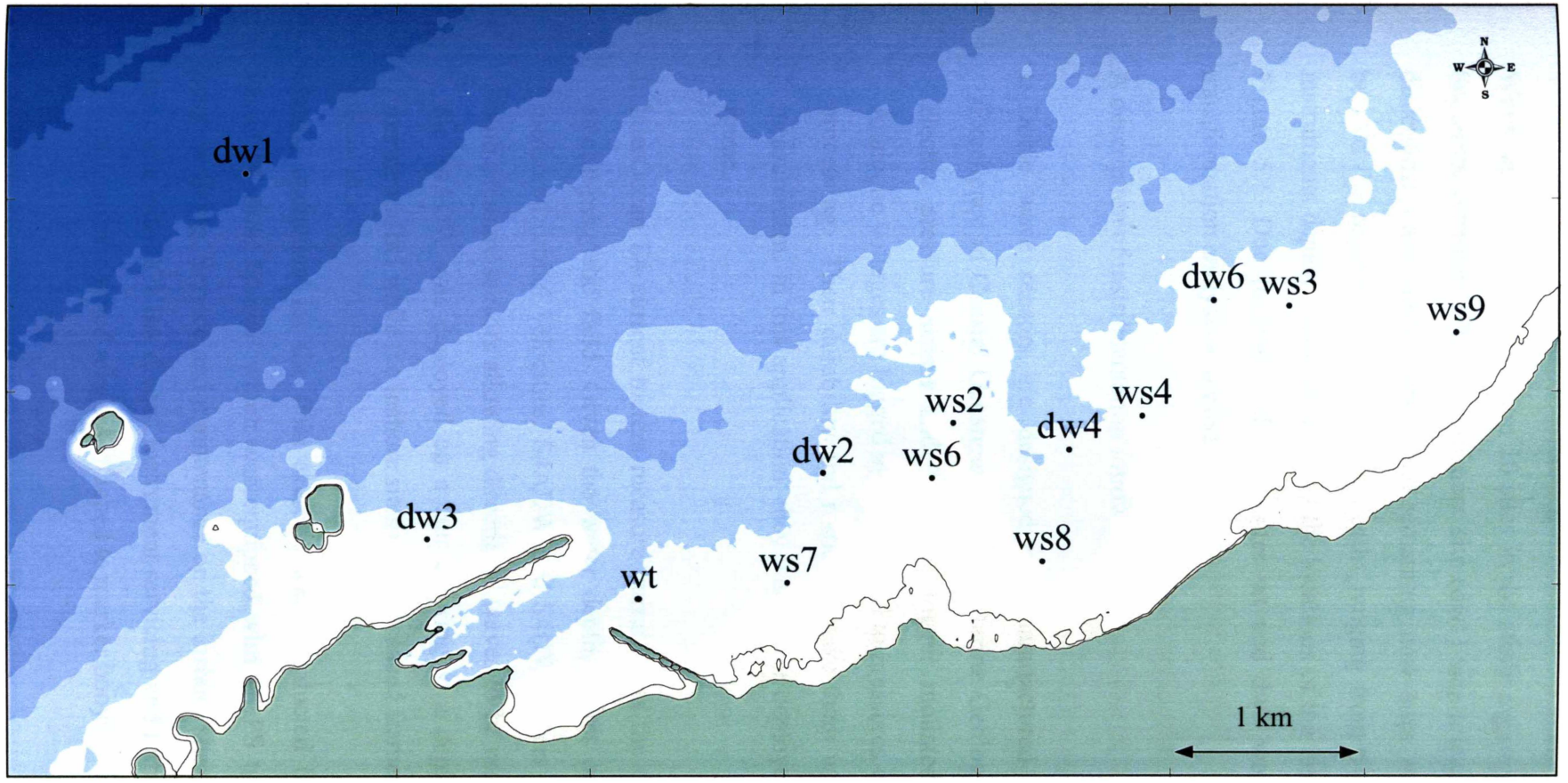

Figure 5.1. New Plymouth City Coast showing instrument locations and bathymetry in 5 m contours.

5.4 Data collection and analysis

Wave data were collected from 10 sites in the study region over a six-week period in September/October 1996. An offshore site (dw1) was selected to provide a reference directional wave energy input. The remaining nine sites were distributed longshore, beyond the regular breaker line, in depths ranging from 5-10 m. Table 5.1 lists the instruments deployed at each site and the locations of the instruments are illustrated in Figure 5.1. Due to land sheltering, sites wt and dw3 were not used in the wave transformation analysis and modelling.

A description of instrumentation follows:

1) Dobie wave sensors are designed and manufactured by the Joint Centre of Excellence in Coastal Oceanography and Marine Geology and consist of a piezo-electric pressure sensor and Tattletale logger mounted in an acrylic housing. Analogue voltages are logged and converted to pressures either internally or in post-processing. Their durability and response make them well suited to coastal wave measurement. In this application, they were diver deployed in a cradle on a seabed frame.

2) InterOcean S4 current meters measure currents via the disturbance of an induced electro-magnetic field. Given the water depth, waves may be deduced from the measured orbital velocities. S4ADW and S4DW meters are additionally equipped with pressure sensors allowing directional waves to be resolved. In this application, the S4ADW was deployed on a taut mooring at a depth to ensure clearance by marine traffic, while the inshore sites utilised seabed frames.

Marine operations for the field exercise were conducted from the Westgate survey vessel '*Kaituhi Moana*' which was equipped with DGPS to allow sub-metre surface position fixing. Service and maintenance on the inshore sites was conducted on a 7-10 day cycle with SCUBA divers. Instrument servicing and retrieval was aided by the use of 7-day galvanic timed releases attached to marker buoys.

Wave data were recorded at 2 Hz for 9 minute bursts at intervals ranging from 2 to 6 hours. Wind speed and direction were recorded by instrumentation at 14 m above MSL on the terminus of the lee breakwater. Calibration of the Dobie wave sensors was performed in a purpose-built pressure vessel, which facilitated the simultaneous calibration of up to eight Dobies and one reference instrument (Aanderaa WLR7).

All data recorded at each site were analysed using the MATLAB routine, TSERIES[1]. Conversion of pressures to wave heights utilised linear theory with a high frequency cut-off at 0.1666 Hz and a low frequency cut-off at 0.04 Hz (i.e. includes wave periods from 6-25 seconds). These filters account for the lessened resolution of higher frequency waves at the depth of the S4 at site dw1 while also eliminating the influence of surfbeat at low frequency. Spectral analysis of each event used a Hanning window over 16 bands to produce a power spectrum and spectral estimates of wave parameters. The definitions of parameters are as follows:

$H_s = 4\sqrt{m_o}$ (significant wave height)

T_p = wave period corresponding to peak energy

m_o = zeroth moment of the spectrum

Wave height and period estimates were also derived from the zero down-crossing time series. Concurrent events were extracted from the processed data set for wave transformation analysis and for calibration of the numerical wave refraction model.

[1] Gorman, R., National Institute of Water and Atmospheric Research, Hamilton, N.Z.

Table 5.1: Field deployment

Site	Instrument	Water Depth	Sensor Depth
dw1	S4 ADW	35.2 m	15.7 m
dw4	S4 DW	9.3 m	8.3 m
dw6	S4	7.1 m	6.1 m
ws2	Dobie	7.1 m	6.9 m
ws3	Dobie	6.9 m	6.7 m
ws4	Dobie	6.7 m	6.4 m
ws6	Dobie	5.5 m	5.3 m
ws7	Dobie	5.8 m	5.5 m
ws8	Dobie	6.7 m	6.5 m
ws9	Dobie	6.7 m	5.8 m

5.5 Results

The total deployment period is represented in a time series of significant wave heights (H_s), peak spectral wave periods (Tp) and the mean direction of wave advance from site dw1 (Fig. 5.2). Five storm events were recorded in which wave heights exceeded 3 m. With coincidental measurements, spatial height variability due to surf beat may introduce an analysis error, but inspection of individual time series of wave heights indicates this effect is minimal.

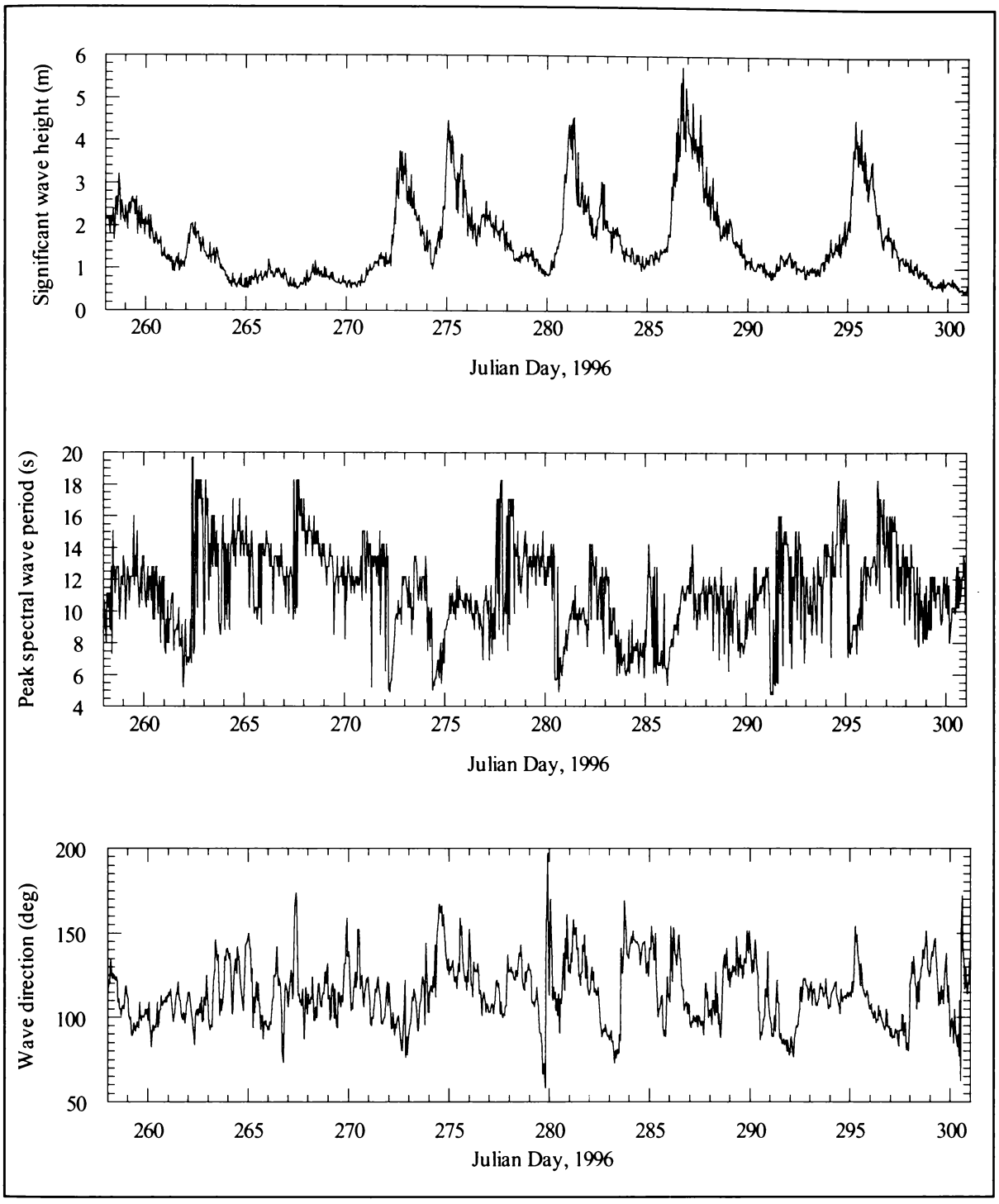

Figure 5.2: Time Series plot of the significant wave height (H_s), the peak spectral wave period (T_p) and the mean direction of wave advance measured at site dw1 from 12/09/96 to 29/10/96. These data were recorded with an InterOcean S4 ADW meter on a taut-wire mooring in 35 m water depth.

5.5.1 Monochromatic Wave Transformations

An overview of the non-breaking wave transformations in the study zone was obtained by examining the changes in the wave height and period statistics from intermediate water offshore (i.e. site dw1) to the inshore measurement sites. Ratios of inshore/offshore for H_s and T_p were produced for each site and averaged over 142 concurrent events. These averages indicate a significant spatial variation in both H_s and T_p ratios (Table 5.2). Wave transformations are further considered by examining the response of these ratios to the variables of tide, wave direction, wave height, and wave period. Zero-down crossing statistics were also obtained and the same analysis applied as for the spectrally-derived statistics. It was found that the ratio results and interpretations were unchanged.

Table 5.2: H_s and T_p Ratios

Site	H_s ratios	T_p ratios
dw4	0.79	1.14
dw6	0.76	1.03
ws2	1.00	1.10
ws3	0.77	1.04
ws4	0.88	1.03
ws6	0.79	1.12
ws7	0.77	1.03
ws8	0.68	1.08
ws9	0.63	0.99

Effects of the tide level

At sites dw4, dw6, ws2, ws3 and ws4 the H_s ratios were observed to increase on average by 0.08 at higher tides (over ~3 m tidal range). No discernible effect was noted at the remaining sites. The tide-influenced sites have a slightly more exposed aspect and are accordingly less likely to experience the refractive effects of the complex nearshore bathymetry. A tidal response is due to the frictional attenuation of the wave heights

arising from wave-orbital interaction with the bottom boundary layer. At low tide, the combined effect of wave-shoaling and the lessened depth will act to dissipate comparatively more of the wave energy approaching the inshore measurement sites (as discussed in Thornton & Guza, 1983).

The effect of tide level on T_p ratios was observed at all sites except dw4, with the mid-lower tides showing a slight shift to longer periods, reflecting increased shoaling of low frequency components and possibly an increase in attenuation of the higher frequencies in the decreased water depth. The amount of smoothing used in obtaining the spectral estimates precluded an accurate quantification of the tidal effect on T_p ratios.

Effects of the incident offshore wave direction

An effect on the H_s ratios by the offshore (dw1) wave direction was noted at all sites, with the more oblique waves generally showing lower H_s ratios. For example, at site dw4, the H_s ratio decreases by an average of 0.12 for waves with directions of advance of <100°T, compared with directions of >100°T. In the more exposed sites of ws2, ws3, ws4 the effect was only minimal. This indicates that the port headland and offshore islands have a sheltering influence on the inshore wave heights. The direction of waves was measured at two inshore sites; after travelling further through the reef system, waves at dw4 had a considerably narrower range of directions than dw6, which was more exposed and responsive to input direction.

Effects of the incident offshore wave height

The effect of offshore wave height (H_{so}) on H_s ratios was noted at all sites whereby smaller waves (<1.5 m) produced, on average, larger H_s ratios. For waves >1.5 m there was a lesser effect, which illustrates the non-linear relationship between wave height and frictional dissipation (as the frictional dissipation is proportional to H_s^3). For example, at site ws2, the H_s ratio in <1.5 m waves is approximately 20% higher than in the >1.5 m wave conditions (e.g. Fig. 5.3).

Effects of the incident offshore wave period

The incident wave period offshore (T_{po}) appears to have an effect on H_s ratios at sites dw4 and ws2, whereby longer period waves are generally associated with higher H_s ratios. This may be explained by enhanced refraction as the wave period increases. The T_p ratios are likely to be influenced by a frequency-dependent attenuation by seabed friction. Frictional dissipation depends on bottom orbital motion which is a function of wave frequency, wave height and water depth, and the effect of vertical attenuation of orbital motion becomes less pronounced as the waves enter shallow water at which stage the frequency dependence has dominance. With the exception of ws9, all sites show a spectral shift to longer periods indicating an attenuation of the higher frequencies and the deepest inshore site (dw4) exhibits the largest T_p ratio (Table 5.2).

Wave shoaling

The extent of wave shoaling at individual sites was investigated by examining the relationship between time series-derived wave heights and spectrally-derived wave heights, with the changes in H_s/depth (H_s/d). The parameter $H_{1/3}$, derived from the time series zero-down crossing analysis and representing the average of the highest third of waves measured, was compared to H_s derived from the total energy in the spectrum m_o. The slope of the linear relationship between $H_{1/3}/H_s$ and H_s/d is indicative of the extent of the non-linearity of the wave shoaling (e.g. Black & Rosenberg, 1992a). There was no significant change in the $H_{1/3}/H_s$ ratio with changes in H_s/d, indicating a minimal effect of non-linear shoaling at the measurement sites.

In summary

Taken together, this analysis of the monochromatic wave transformations suggests the nearshore coastal wave environment at New Plymouth is dominated by the processes of refraction and seabed friction.

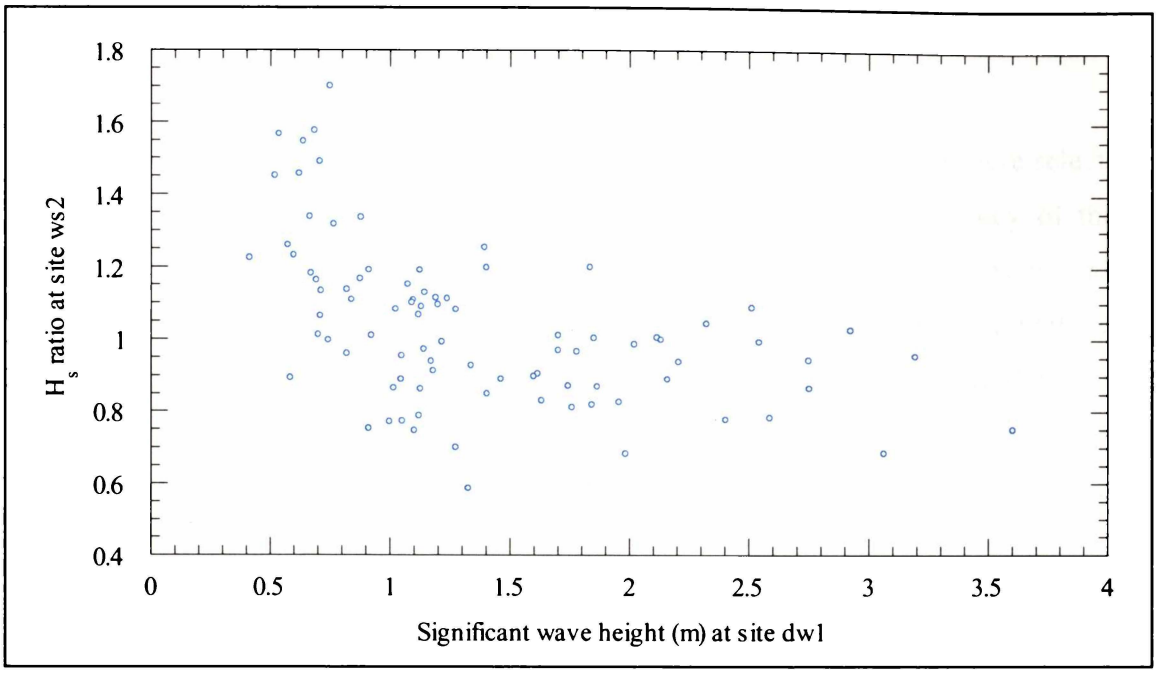

Figure 5.3 Plot of the significant wave height measured at site dw1 vs the wave height ratio at site ws2. These data were collected over the period 12/09/96 - 29/10/96.

5.5.2 Wave transformations under onshore and offshore winds

While refraction and friction are seen to dominate in the study region, the wave spectral transformations were found to be different under onshore and offshore winds. The action of a strong onshore wind is thought to be primarily dissipative, whereby the mechanism of white-capping induces a premature breaking of the waves, not primarily dependent on H/d but rather on wave steepness (H/L). Several dissipative source functions have been derived to allow inclusion of this process in numerical wave generation models (Komen *et a.l*, 1994), but the combined effect of shoaling, bed friction, refraction and white-capping remains complex.

To examine the effect of wind on the wave transformations, data were extracted that met the following criteria:

1) a directional window of 270-020°T with wind speeds >5.5 ms^{-1} was chosen for onshore wind cases. The wind speed criterion is based on a conservative estimate of initiation of whitecapping, given the elevation of the wind anemometer.

2) for offshore winds, a directional window of between 90-190°T with wind speeds of greater than 2.5 ms^{-1} was chosen.

A total of 27 cases of offshore wind and 16 cases of onshore wind events were selected. Sites dw4 and dw6 were not included as the different sampling frequency of these instruments precluded sufficient event coincidence to maintain statistical integrity of the analysis. Care was taken to ensure minimal bias in either wind category from tidal level, wave height, period or direction. Averages of H_s and T_p ratios for each wind category are presented in Table 5.3. It can be seen that at all sites the ratios of H_s are greater, and T_p are smaller for onshore wind conditions.

Table 5.3: Mean wave height and period ratios for the onshore and offshore wind casesWave height, period ratios with wind variance

Site	H_s onshore	H_s offshore	T_p onshore	T_p offshore
ws2	1.07	1.06	1.00	1.09
ws3	0.86	0.77	0.96	1.10
ws4	0.98	0.92	0.93	1.02
ws6	0.90	0.77	1.00	1.16
ws7	0.86	0.79	0.90	0.98
ws8	0.75	0.68	0.99	1.10
ws9	0.73	0.60	0.85	1.06

The sink terms in wave generation theory are S_{nl}, S_{dis} which are respectively non-linear transfers of energy between frequencies and dissipation due to white-capping or friction (Komen *et al.*, 1994). The white-capping dissipation term is given by Gunther *et al.*, (1992) as,

$$S_{dis} = \left(-\gamma_d\right)S(f) \qquad \text{Eqn. 5-1}$$

where,

$$\gamma_d = \frac{1}{2}c_{dis}\langle\omega\rangle(\langle k\rangle^2 E)^2\left(\frac{k}{\langle k\rangle} + \left(\frac{k}{\langle k\rangle}\right)^2\right) \qquad \text{Eqn. 5-2}$$

and c_{dis} =4.5 is a constant, E is the total variance, k is the wave number and $<\omega>$ and $<k>$ are mean angular frequency and mean wave number. Energy losses are proportional to spectral energy density at each frequency and the total energy in the spectrum, while increasing with wave number.

The observed T_p ratios (Table 5.3) could be interpreted as white-capping dissipation from the most energetic (peak) frequencies causing a spectral shift from the peak to higher frequencies during onshore winds, relative to the transformations of the peak wave periods under offshore winds. In order to evaluate spectral transformation, averaged spectral gain functions (G_s) were produced for each wind category between 0.063-0.156 Hz. G_s was calculated as;

$$G_i = \sum_{f=0.063}^{0.156} S_i(f) / S_o(f) \qquad \text{Eqn. 5-3}$$

at each site for each event. The overall spectral gain averaged over all events at each site is,

$$G_s = \frac{1}{N} \sum_{i=1}^{n} G_i \qquad \text{Eqn. 5-4}$$

where i is the event and N is the total number of events.

The gain functions G_s showed a similarity in shape between sites and so a single gain function G_T was then produced by averaging across all sites, in each of the two wind categories. Comparison of the two G_T (see Fig. 5.4) confirm spectral shifts in the onshore winds.

Relative to G_T values for the offshore winds, the G_T values for the onshore winds are shown to be both reduced (0.075-0.1Hz, 0.12-0.135Hz) and increased (0.1-0.12Hz, 0.135-0.16Hz). Figure 5.4 would indicate that the white-capping process causes both a dissipation of wave energy and a transfer of energy primarily from the peak to higher frequencies. However, in Table 5.3 it can be seen that the onshore H_s ratios are higher than the offshore H_s ratios, which does not suggest a dissipation process. Furthermore, the cases considered here represent fully-developed sea-states and not a fetch-limited

condition. This means that any increases in the wave height ratio under onshore winds is not likely to be due to an additional 1-2 km fetch (i.e. between the offshore and nearshore sites).

A mechanism for the observed results is proposed. The white-capping process involves both a spectral energy transfer and an increase in the local wave height variation along the crests, which leads to increased "diffraction". The shift to higher frequencies also reduces the spatial height gradients caused by refraction over the reefs. Accordingly, the spatial distribution of wave heights is smoothed under onshore winds. Higher H_s ratios noted in onshore winds are consistent with this theory, given that visual observation indicates that sites are mostly located in wave height divergence zones where refraction acts to reduce the wave height. The exception is site ws2, in a zone of height reinforcement and the height ratio at this site is correspondingly less affected (Table 5.3). A quantification of the proposed mechanism is considered beyond the scope of this paper, although the mechanism is examined in the calibration of the numerical wave refraction model.

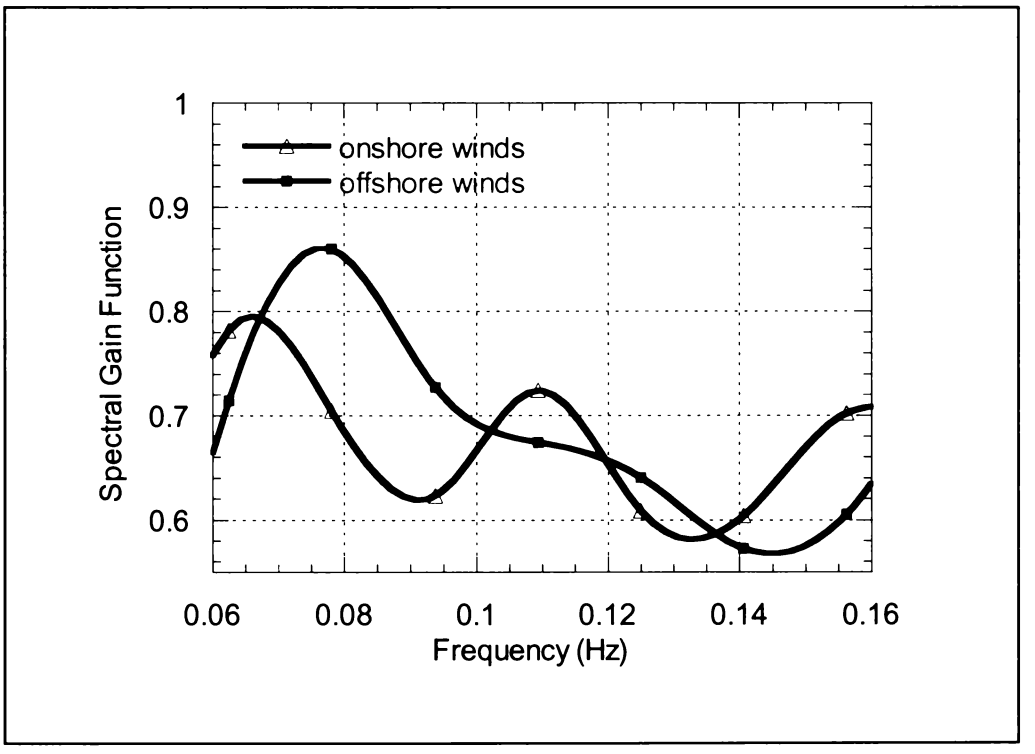

Figure 5.4: Plot of spectral gain functions for onshore and offshore wind categories

5.6 Numerical modelling

Numerical modelling of the study region utilised the WBEND wave refraction model, described by Black & Rosenberg, (1992a). WBEND is a two-dimensional wave propagation model that applies a fast, iterative, finite-difference solution of the wave action equations to solve for wave height, wave period, breakpoint location, longshore sediment transport and bed reference sediment concentration. Model equations are not presented in this paper. Diffraction is represented in the model by a smoothing factor in the form of an eddy viscosity term (N_A) that allows energy leakage to adjacent grid cells, which is similar to the effect of horizontal eddy diffusivity. Diffraction has a smoothing effect normal to the wave crests (i.e. perpendicular to the direction of wave advance) and the N_A method has been found by Black & Rosenberg, (1992b) to be an acceptable substitute for the full diffraction equations. Wave-energy dissipation by seabed friction is calculated from the maximum wave orbital velocity as a friction coefficient term (C_f) which has the same definition as that used by Thornton & Guza (1983). Both the eddy viscosity and friction coefficient terms are adjusted in the model calibration.

5.6.1 Grid Establishment

Bathymetric data was collected and collated to enable a suitable resolution of the complex seabed features in the study region. Data was interpolated onto a 25 m x 25 m grid and rotated 40 degrees anticlockwise to allow the dominant wave directions to enter the model at a minimum angle. A grid of 205 x 265 cells was produced to represent the region from Port Taranaki to the eastern extremity of Fitzroy Beach (Fig. 5.5).

5.6.2 Model Calibration

The model was calibrated for both the monochromatic and spectral wave statistics by comparing the measured and predicted wave heights at instrument sites and adjusting N_A and C_f until a minimum error was obtained. A constant C_f coefficient over the model grid was assumed. Error calculations used the formula,

$$E_r = \sum(H_p - H_m)^2 / \sum(H_m)^2 \qquad \text{Eqn. 5-5}$$

where H_p is the predicted height and H_m is the measured height. Monochromatic calibration used five events that were non-breaking at instrument sites, had calm winds, and one dominant wave direction. Spectral calibration used both an averaged spectra (42 events) and five individual events. Each frequency band is treated as a separate monochromatic wave. Events categorised by wind vector were calibrated using averaged spectra from each wind category. Calibration results are presented in Table 5.4.

Table 5.4: WBEND model calibration results

	C_f	N_A	E_r
monochromatic	0.070	0.06	0.026
spectral	0.090	0.06	0.050
offshore spectral	0.090	0.02	0.070
onshore spectral	0.105	0.06	0.050

Error values for the spectral calibration are obtained by graphical estimation to identify the minimum value, as each frequency band is treated as a monochromatic wave (with an RMS wave height) and no account is taken for the spectral transmission of energy. The obtained friction coefficients remain consistent with those of a previous investigator on a similar coast (Hutt, 1997).

Model calibration for the wind categories shows an increase of 0.015 for C_f under onshore white-capping conditions as compared to the offshore wind case. This is not an appropriate representation of white-capping dissipation (Eqn. 5.1) as this sink term is dependent on the steepness of the wave field, while C_f is dependent on maximum seabed orbital velocities, thus indicating a need for the future inclusion of a white-capping term in the model. The offshore wind conditions are seen to favour a lessened amount of diffraction (mimicked by the N_A smoothing coefficient). This is consistent with a pattern of longshore smoothing of the wave energy from localised diffraction induced by whitecapping under onshore winds.

5.6.3 Model Application

Model outputs of wave height distribution were produced for a variety of wave climates, which showed a sensitivity to both wave period and direction, and defined zones of wave height concentration. An example is given in Figure 5.5 for a 2 m wave height at 12 second period and a direction of wave advance of 110 degrees.

A directional wave probability file, obtained from 47 days measured at dw1 (Fig. 5.2), was applied to the model to produce a representation of the spatial distribution of both wave heights and seabed velocities. The resultant output for the mean seabed velocity (third moment) is presented in Figure 5.6. A detailed discussion of this figure is precluded by space restrictions and indeed the outputs are the subject of ongoing research.

5.7 Conclusions

The wave transformation processes on the New Plymouth City coast are dominated by seabed friction and refraction. The effect of onshore wind-induced white-capping on wave transformation was noted and a mechanism is proposed based on reduced refraction and increased diffraction. A high-resolution wave refraction model has been established to predict the spatial distribution of wave energy and to model the wave transformation processes in the study region. The model will be used in strategic planning for Port Taranaki and for further work in sediment transport applications.

5.8 Acknowledgements

This work was supported by a GRIF research fellowship from the Foundation for Research in Science and Technology, New Zealand.

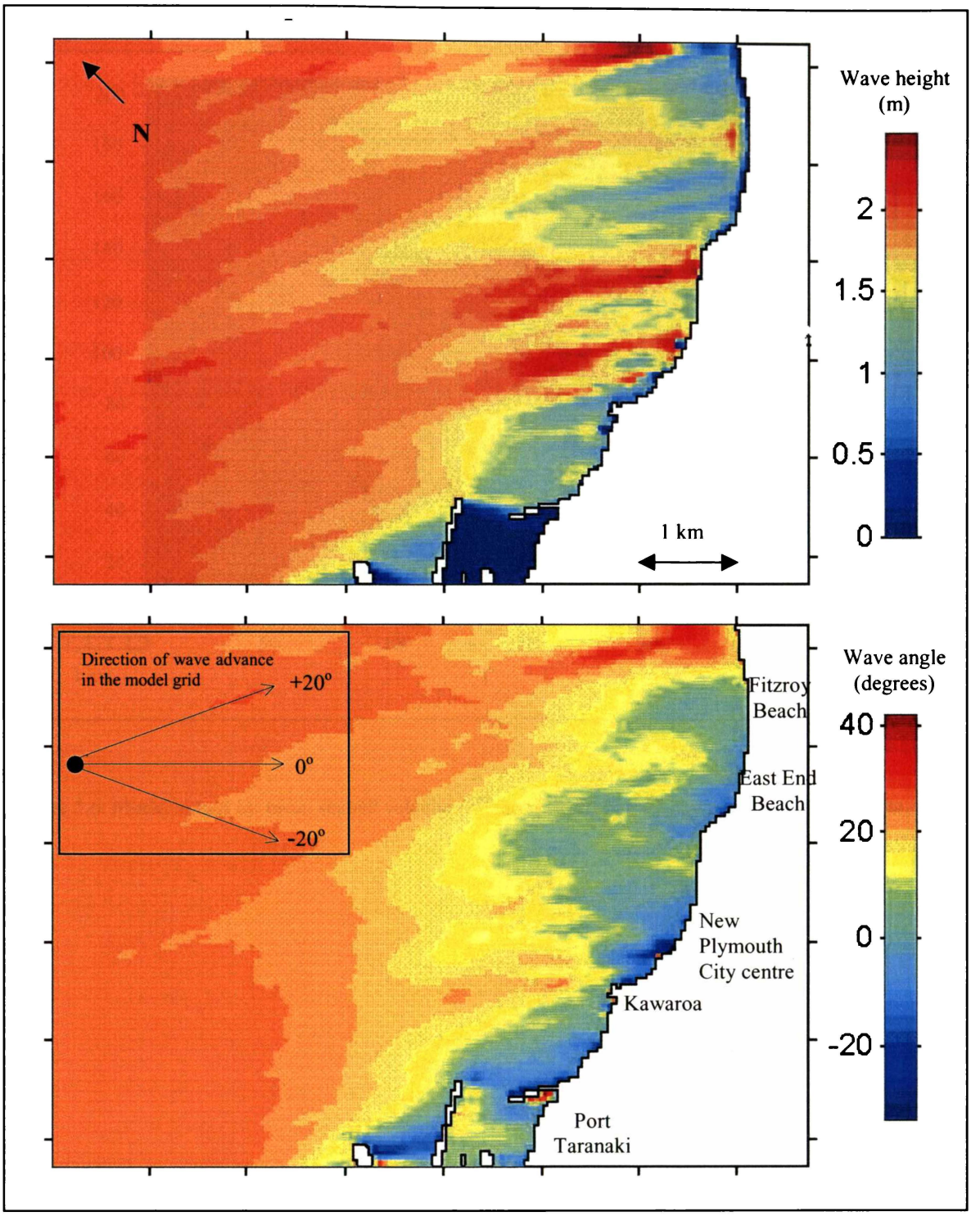

Figure 5.5: WBEND model output for a 2 m wave of 12 second period and direction (wave advance) of 110 degrees (True). Wave heights (m) are given in the upper panel, and wave angles in the lower panel. Wave angles are relative to the y axis of the model grid.

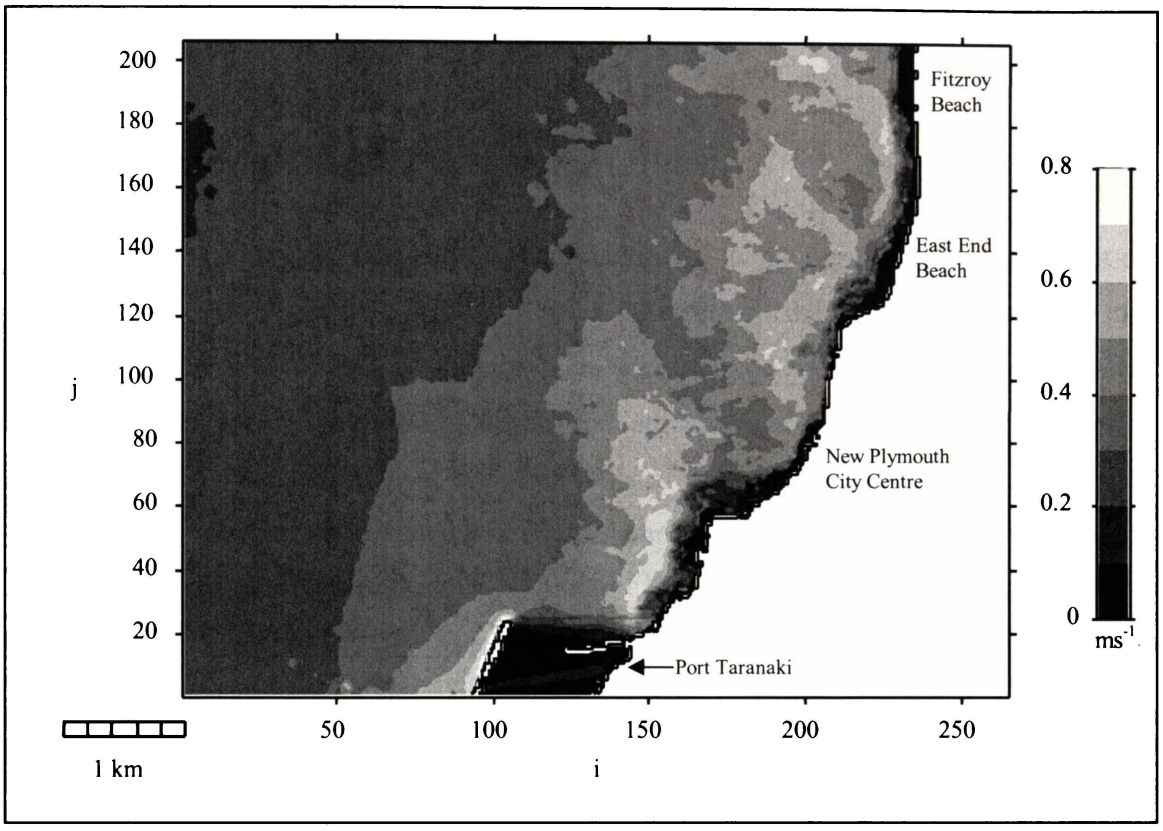

Figure 5.6: Model output for mean seabed velocity (3rd moment) from a 47-day probability wave input.

6 THE ACCRETION OF A BREAKWATER TIP-SHOAL FOLLOWING DREDGING

6.1 Context of the paper within the thesis

Sedimentation with Port Taranaki has been identified as having a significant impact on the nearshore littoral system at New Plymouth, although the processes that cause the accretion, and the conditions under which accretion occurs, have not been closely studied. This paper specifically targets the accretion at the entrance to the port, providing an understanding of the mechanism and rates of accretion. These are subsequently applied to an analysis of the impact of the harbour trapping on the nearshore sedimentary environment (Chapter 10). This paper was presented at the Pacific Coasts and Ports '99 Conference in Perth, Australia and peer-reviewed / published as:

McComb, P., Black K., Atkinson, P., Lim Y.T. and Healy, T., 1999. The accretion of a breakwater tip-shoal following dredging. *Proceedings of the 1999 Pacific Coasts and Ports Conference*, Perth, Australia (Vol. 2), pp. 420-425.

6.2 Abstract

A study of the accretion of a harbour breakwater tip-shoal is presented. The study involved repetitive hydrographic surveys over nine months following a biennial dredging campaign at Port Taranaki, New Zealand. Accretion rates are shown to be related to the measured directional wave climate. Numerical simulations of wave refraction/ diffraction, employed on three shoal bathymetries, demonstrated the influence of the penetration of the refracting wave around the tip shoal on sedimentation rates. The results indicate that consideration of the wave dynamics is important in the formulation of an efficient dredging programme.

6.3 Introduction

Port Taranaki on the west coast of New Zealand (Fig. 6.1) is exposed to the Tasman Sea and experiences a high-energy wave climate dominated by long-period westerly swell (McComb *et al.*, 1997). The coastal bathymetry features a complex reef and channel structure comprised of volcanic breccia, intermittently overlain with boulders, gravel and sand. Littoral sediments are medium "black" sands of local volcanic origin. We have estimated net longshore transport rate to be in excess of 220,000 m^3yr^{-1} to the north (unpublished results).

Current dredging practice employs a trailer-suction hopper dredge to remove some 180,000 m^3yr^{-1} from the harbour and shipping channel, with the dredging campaigns usually conducted biennially. Dredging of littoral sands from the breakwater tip shoal accounts for 75% of the total volume. An unknown volume of the littoral drift is not trapped, but passes across the shipping channel instead. The dredge cuts around the base of the tip shoal to eliminate sand from the main shipping channel and to re-establish the required depth. However, little sediment is taken from the uppermost parts of the shoal and no account is taken of local wave dynamics around the breakwater and the influence of wave penetration on tip shoal growth. Wave penetration is dependent on refraction/diffraction which, in turn, is determined by seabed bathymetry around the tip of the breakwater and input wave conditions.

The aim of this paper is to measure the shoal growth and examine whether changes to the dredging patterns could change wave penetration patterns and thereby enhance harbour sediment by-passing. Any reduction in dredging volumes has both financial and environmental benefits. This paper describes an investigation of the accretion of sand at the breakwater tip over nine months following a biennial dredging campaign. Methods employed include repetitive hydrographic survey, directional wave measurements and numerical modelling. Outcomes of the study will be used to quantify annual sediment transport rates and in the assessment of mechanical sand by-passing options.

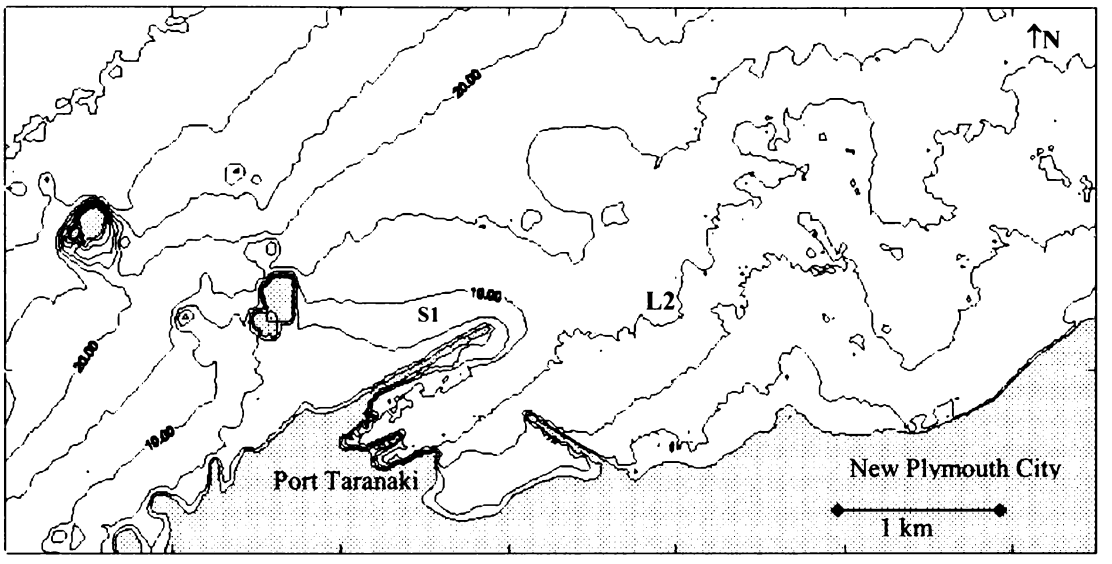

Figure 6.1: Location map of Port Taranaki and New Plymouth City (bathymetry in 5 m contours)

6.4 Data collection

Hydrographic surveys of the tip shoal area (Fig. 6.2) were conducted at approximately monthly intervals following the completion of dredging from 14/03/1998 until 2/12/1998. Data were collected with the port survey vessel, equipped with DGPS positioning and heave compensation, resulting in a vertical and horizontal accuracy of 0.05 m and 0.5 m respectively. Ten hydrographic surveys were conducted: one "pre-dredge", one "post dredge", and eight subsequent surveys over a 9-month period which are denoted as surveys "Bwt1-Bwt8".

Directional wave data were collected over the survey period using a 3D-ACM WAVE instrument (Kun *et al.*, 1999) mounted on a seabed frame in 9.4 m water at a site 1 km east of the breakwater tip (site L2, Fig. 6.1). This site showed good correlation to coincident measurements from a 61-day dataset at a site proximate to the breakwater tip (site S1, Fig. 6.1). Pressure and orthogonal velocity measurements were collected at 5.36 Hz in 18-minute bursts at 6-hourly intervals. Prior to the dredging campaign, sediments were sampled on *profiles a*, *b* and *f* along the shoal (at 6-8 m depth, Fig. 6.2) for particle size analysis.

6.5 Data analysis

An area of the tip shoal region (90,085 m^2) was defined for the study (Fig. 6.2), from which surfaces, volumes and profiles *a-f* were extracted for each survey using HYDRO software. An accuracy of 0.05 m has been defined for the survey equipment (Y.T. Lim, Port Taranaki Hydrographer, *pers comm.*), which gives rise to a volumetric accuracy of ~9,000 m^3 when comparing two surveys. Shoal growth rates were compared to directional wave statistics derived from the pressure and orthogonal current vectors measured at 1 m above the sea bed at site L2. Significant wave heights, peak spectral periods and averaged orbital velocities were extracted from the time series using the MATLAB routine, TSERIES[2]. Spectral analysis of each burst used a Hanning window over eight bands to produce a power spectrum. Surface wave parameters were obtained using linear wave theory in each frequency band of the unsmoothed spectrum to convert near-bottom to surface pressures. Definitions of parameters are: $H_s = 4\sqrt{m_o}$; where m_o is the variance of the spectrum; T_p = wave period corresponding to peak spectral energy; and T_m = mean zero-down crossing wave period. Averaged near-bed orbital motions ($U_w = 1.414\sqrt{U_{mo}}$ where U_{mo} is the variance of the orbital motion time series) were obtained directly from the measured currents.

[2] Gorman, R. National Institute of Water and Atmospheric Research, Hamilton, N.Z.

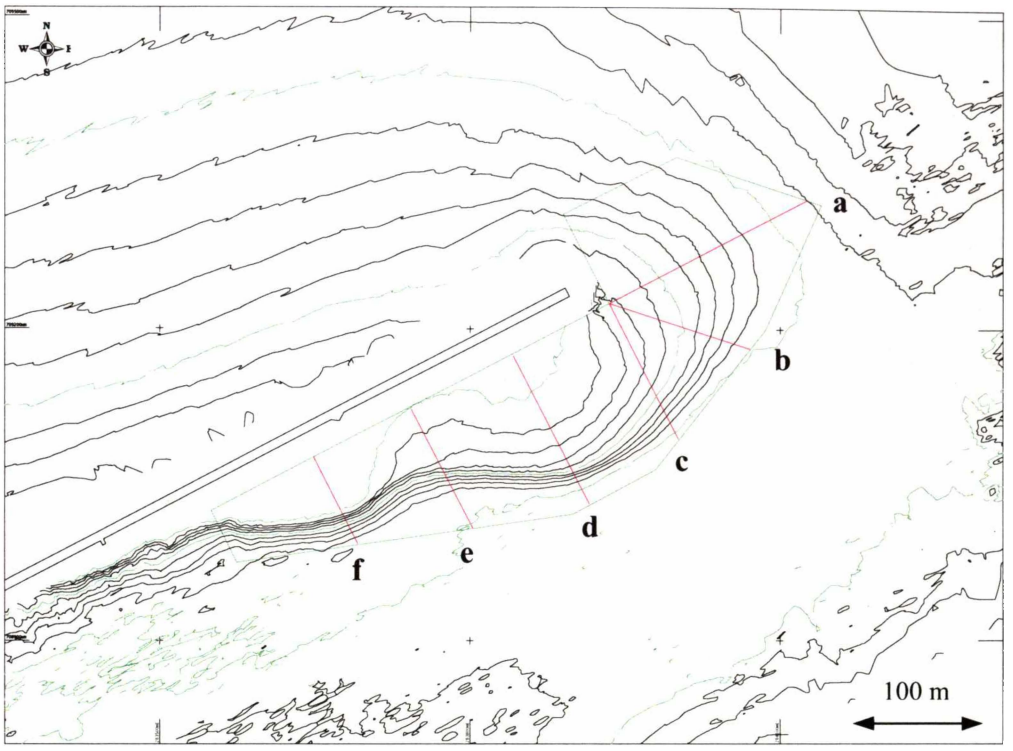

Figure 6.2 Breakwater tip-shoal with study boundary and profiles a-f. Bathymetry at 1 m contours from the "pre-dredge" survey

6.6 Results

The results of the wave and survey data analysis are summarised in Table 6.1 and discussed in the following sections. Surface contour maps were produced for each survey from which rofiles *a-f* were extracted.

6.6.1 Shoal shape and growth

The *pre-dredge* bathymetry (surveyed 21-months after the previous dredging campaign) is presented in Figure 6.2. The shoal is characterised by two well-defined lobes. There is some wave and current penetration through the breakwater wall, which could lead to transfer of sediments and possibly account for the inner lobe. However, our observations suggest this mechanism is not the primary factor.

Mean particle sizes of sediments showed a trend toward finer material further inside the breakwater (0.264 mm on *profile a*, 0.232 mm on *profile b* and 0.209 mm on *profile e*),

The flanks have increasing gradient with distance from the breakwater tip into the port. The gradient is lowest at the exposed tip (*profile a*, Fig. 6.2) and is similar to that on the offshore side of the breakwater. Shoal gradients are illustrated in Figure 6.3, with the maximum gradients seen to increase with distance along the shoal. Maximum gradients extracted from *profiles a-f* (survey Bwt8) show a progression from 0.056 (*profile a*) to 0.397 (*profile f*). The water depth at the top of the maximum gradient section of the profile decreases with distance along the shoal to 0 m at *profile f* (Fig. 6.3).

While the toe of the shoal tends to migrate furthest between *profiles a* and *b* (Fig. 6.2), maximum volumetric growth occurs along *profiles d* and *f*, which are well within the lee of the breakwater. Relative accretion rates along the shoal may be discerned from the profiles illustrated in Figure 6.4 (showing *profiles a, c, d* and *f* from the *post-dredge*, *Bwt1, Bwt4* and *Bwt7* surveys). The steep gradient on *profile f* is seen to collapse between the *"post-dredge"* and *Bwt1* surveys. It then re-established by survey *Bwt4* in response to accretion in the upper sections. Additionally, around 1.5 m of sand has been eroded from the shallow parts of *profiles a* and *c* over the study period (Fig. 6.4). Examination of bathymetric charts from previous years showed no similar pattern of erosion.

Table 6.1: Results of hydrographic survey and environmental measurements

				Hydrographic Data			Wave Data				Mean values				
Survey	Date	Time (days)	Duration (days)	Growth (m^3)	Rate ($m^3 day^{-1}$)	Volume (m^3)	# Events (events)	H_s>1m (events)	H_s>2m (events)	H_s>3m (events)	H_s (m)	T_m (sec)	T_p (sec)	Uw (cm/s)	Direction (degrees)
Bwt1	31/03/98	17	17	16700	980.1	16700	70	26	3	1	0.99	6.9	11.1	40.83	131
Bwt2	06/05/98	53	36	10300	286.1	27000	139	36	1	0	0.84	7.22	12.1	35.62	124
Bwt3	12/06/98	90	37	3100	83.8	30100	140	58	4	0	0.98	8.37	11.11	39.35	128
Bwt4	27/07/98	135	45	33400	742.1	63500	154	88	38	11	1.59	7.29	9.34	58.90	122
Bwt5	19/08/98	158	23	-60	-2.6	63400	84	36	8	2	1.05	7.68	10.46	39.74	107
Bwt6	04/09/98	173	15	7800	518.6	71200	51	19	4	1	1.08	7.69	10.1	37.26	113
Bwt7	31/10/98	232	59	24600	416.7	95800	191	103	44	9	1.39	7.17	11.13	55.05	105
Bwt8	30/11/98	263	31	3000	97.8	98700	114	14	1	0	0.61	7.8	10.72	40.62	87

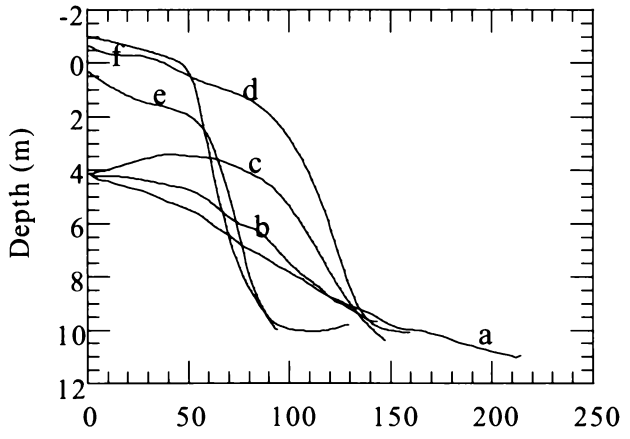

Figure 6.3: Profiles (a-f) from survey Bwt8

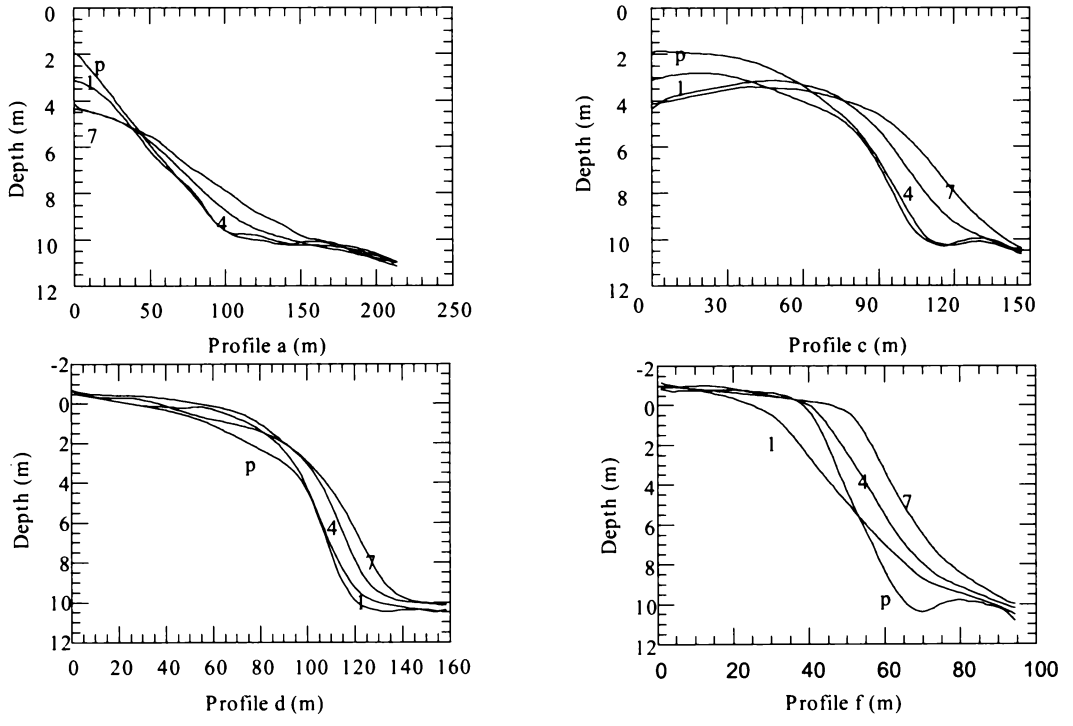

Figure 6.4: Profiles a,c,d and f from surveys "post-dredge"(p), Bwt1, Bwt4, and Bwt7.

6.6.2 Accretion rates

The volumetric growth of the tip shoal (Fig. 6.5) shows an initially rapid accretion rate immediately after dredging (*Bwt1*), followed by a variable increase over time, although the overall relationship is approximately linear (R^2 = 0.9711). It would appear that growth did not systematically slow down during the 9-month survey and suggests that equilibrium has not been reached. Linear regression of the data predicts the shoal to accrete 142,000 m^3 in one year.

6.6.3 Wave data

The wave climate over the study period was atypical in that northerly quarter sea conditions predominated and wave heights were generally less than usual (Port Taranaki Harbourmaster, *pers comm.*). The measured wave data was complete, with the exception of an 8-day period over *Bwt7*. A wave environment for each survey period is represented in Table 6.1 by time-averaged values of H_s, T_p, T_m, U_w and wave direction (advance) along with a frequency of occurrence based on wave height. The duration of the time-averaging (Table 6.1) was the full period between surveys.

6.6.4 Accretion rates and the wave climate

Accretion rates are considered with the measured wave height and direction data (Fig. 6.6). The highest accretion rate (980 m^3day^{-1}) is found after the first survey and is likely to represent a re-establishment period following dredging. Otherwise, the accretion rates are seen to respond to wave height, in that the larger wave heights are associated with higher accretion rates (Table 6.1). The accretion rates are poorly related to the median wave direction. Excluding the first data point (*Bwt1*), the gradients of the regression of height and direction against accretion rate are 0.0009 and 0.0155 with R^2=0.5428 and 0.0872 respectively. Wave orbital current intensity (Fig. 6.5) also shows a similar relationship as wave height, with a gradient of the best fit linear relationship against accretion rates of 0.0257 and R^2 = 0.404. Thus, growth rate is shown to be dependent on wave height (and orbital current intensity), as expected, with little correlation to the median wave direction.

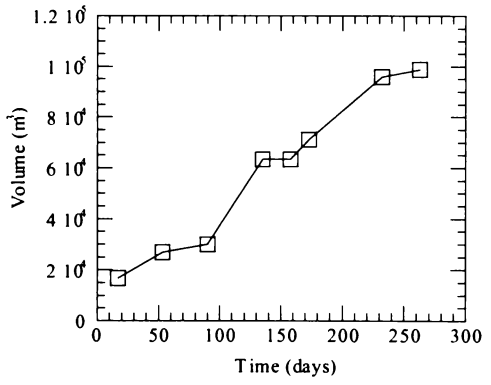

Figure 6.5: Breakwater tip shoal accretion over the study period.

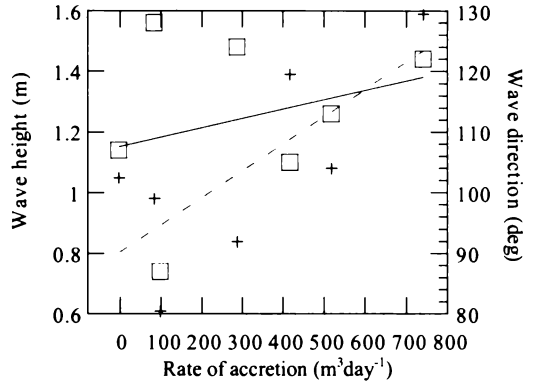

Figure 6.6: Rate of shoal accretion vs median wave height (+) and median wave direction with linear regressions (wave height is dashed).

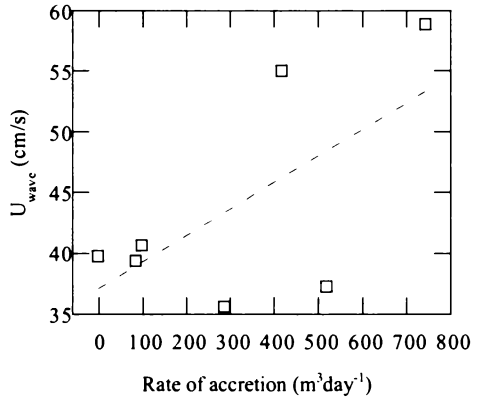

Figure 6.7: Rate of shoal accretion vs mean wave orbital velocity

6.7 Numerical modelling

Simulations of wave interactions with the breakwater-tip region employed the coupled 3-dimensional hydrodynamic and advection/diffusion model 3DD (Gorman & Black, 1997; Black, 1995).

6.7.1 Grid establishment

Bathymetry grids were assembled by interpolating data onto an 8 m x 8 m grid and rotating 46 degrees anticlockwise to align with the mean incident wave direction. A grid of 136 x 198 cells was produced to characterise the tip shoal region. A number of grids representing various shoal shapes were utilised and three are considered in this paper; *MBT2* is the "post-dredge" bathymetry, *MBT3* eliminates the shoal on the lee of the breakwater, and *MBT6* eliminates the entire exposed tip of the shoal (Fig. 6.8).

6.7.2 Model runs

The 3DD model was run with an incident wave height of 2 m, a period of 12 seconds at a tidal level of 0 m. An output of sea-levels for each case is presented in Figure 6.8. Sea-level profiles were extracted from a transect across the harbour entrance (Fig. 6.8) and are included in Figure 6.9.

The model output from the *post-dredge* configuration (*MBT2*) shows well defined peaks. The first is a refracted wave crest on the shoal (0-100 m from the start of the transect), and the second is a broader diffracted wave extending across the harbour entrance (100-400 m on the transect) (Fig. 6.9).

With the inner shoal removed, case *MBT3* shows no wave refraction in the lee of the breakwater and wave energy enters the harbour primarily through diffraction alone (Fig. 6.9). *MBT6* is intermediate with similar diffracted wave energy to the other 2 cases, but the refracted energy is less than *MBT2* (Fig. 6.9). The refracted wave height in case *MBT6* is 70% of *MBT2*.

The region between the two shoal lobes is the point at which the refracted wave crest becomes normal to the breakwater in case *MBT2* (Fig. 6.8) and represents the maximum intrusion of the refracted wave.

6.8 Discussion

The results indicate that the inner shoal acts as a sediment sink and that controlling the passage of sand into this region can be achieved by reducing wave penetration.. The profiles show a pronounced steepening with distance from the tip suggesting that sediment carried into these regions spills down the face of the shoal and is trapped. In the absence of strong tidal and other currents inside the port, the mechanism for carrying these sediments is wave stirring and wave-driven currents. A wave energy gradient is evidenced by a systematic reduction in grain size with distance from the tip.

Each of these suggests that if internal wave energy could be reduced, then the volume of sand being trapped may be minimised. The numerical model showed two distinct components of the wave energy penetration. These are a diffraction and refraction component. The model confirmed, as expected, that the diffraction component around the tip of the breakwater was mostly unaffected by the shoal bathymetry. However, the refracting component was strongly influenced. With the rounded shoal removed, the refraction component was essentially eliminated, thus reducing the total sediment transport capacity into the port. However, under the present dredging regimen, the refracting component was large and bigger than the diffracting wave (Fig. 6.9). Thus, it would appear that reductions in maintenance dredging could be achieved if the dredged locations were changed to minimise the refracting wave.

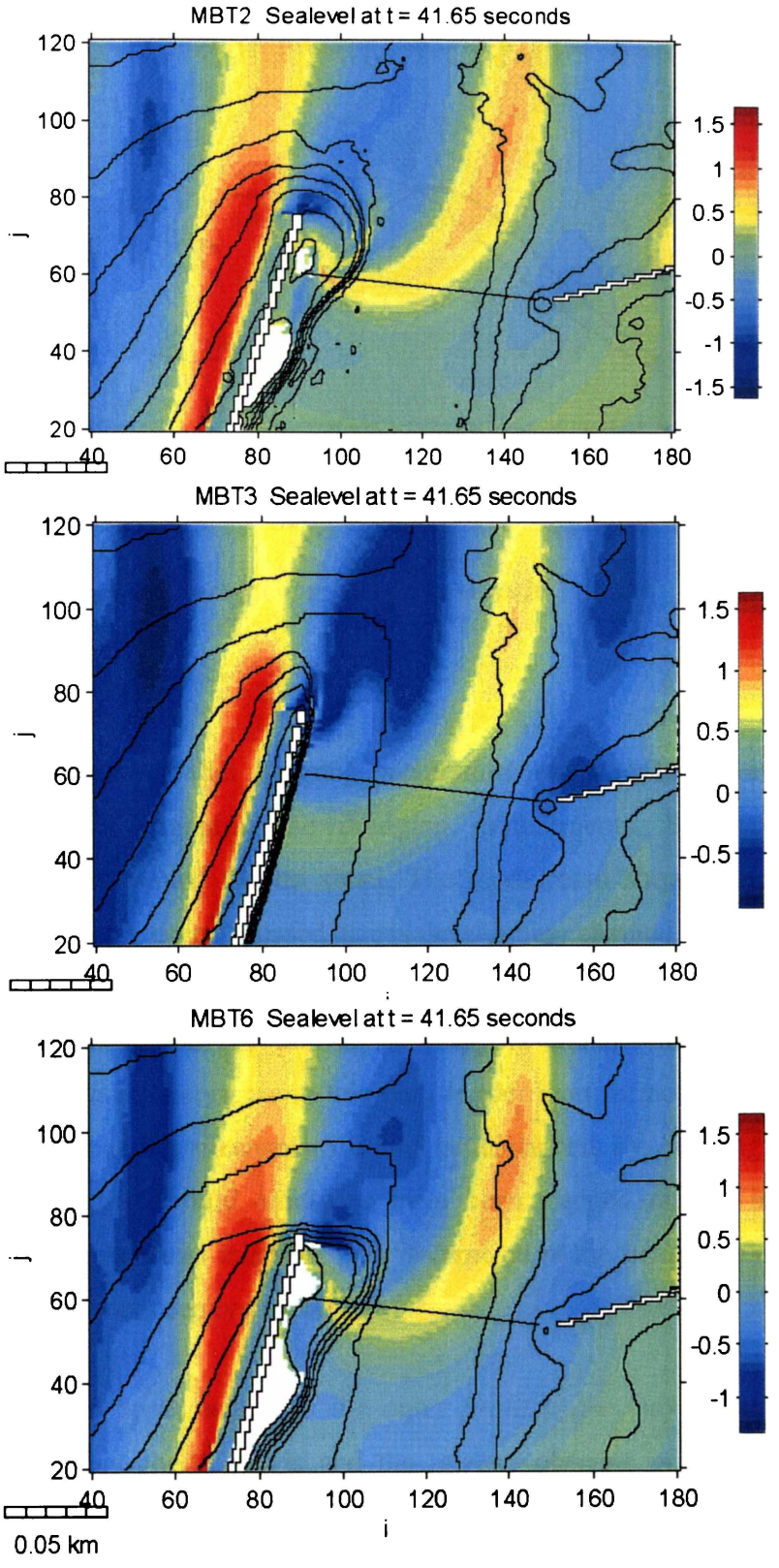

Figure 6.8: Model 3DD sea-level output (m) for grids *MBT2*, *MBT3* and *MBT6* showing depth contours (2 m)

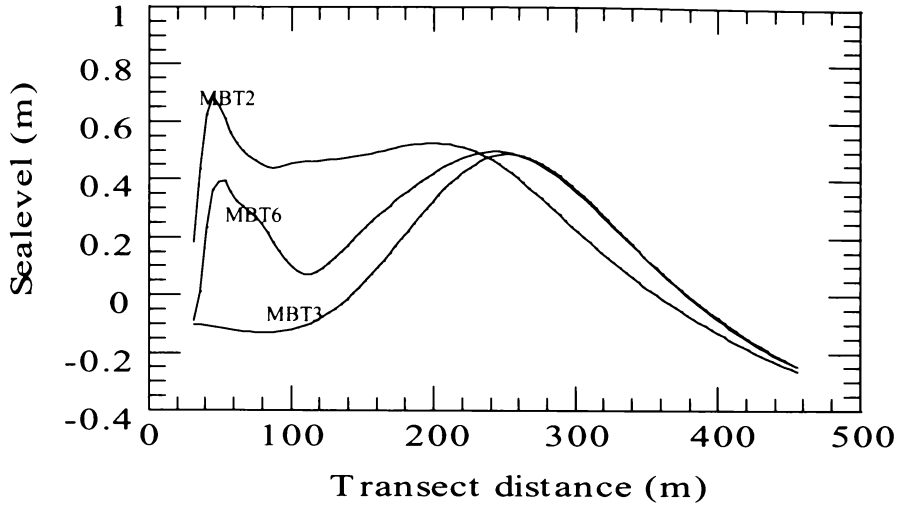

Figure 6.9: Sea-level profiles from grids *MBT2, MBT3* and *MBT6*.

It should be recognised that stopping penetration may simply move the location of deposition without changing the dredging requirements. Sediment may simply accumulate further around the tip shoal. The model also showed that, with reduced refraction, more wave energy passed across the shipping channel. Our broader studies of the region indicate that some littoral drift sediment by-passes the tip shoal and follows a route from the breakwater tip across the shipping channel to pass down-coast. By maximising the wave energy along this path (rather than refracting the waves into the harbour) the by-passing mechanism could be enhanced by carrying the component beyond the port that would otherwise have been trapped on the inner shoal. The orientation and presence of this flow path is depicted in the shoal bathymetry by the toe extending furthest between *profiles a* and *b*.

The scour on the upper levels of the outer *profiles a-c* may relate to the unusual predominance of northerly winds and the relative absence of the strong south-west swells. These swells arrive at the breakwater wall at an angle that drives a current towards the tip and brings the depositing sediment. Their absence may be reflected in the reduction of volume on the tip profiles over the study period.

The variation in steepness of the shoal with distance from the tip is notable. It would appear that the lower gradients at the end of the breakwater relate to wave exposure that tends to smooth the seabed into a more horizontal pattern. In the lee of the wall, the growth rates are fastest and steepness increases, presumably as the sand that is carried along the shallow sand bar spills off the edge. However, as sand may continue beyond the port on the exposed profiles the seabed gradient may be simply lower because of the losses which prevent the steep (accumulating) bed from forming. Thus, while growth is fastest on the inner profiles, the flux of sediment must be greatest at the tip. The dominant deposition region is from *profiles d* through *f*.

The hollow between the two lobes coincides with the location of maximum penetration of the refracted wave in the numerical model. This is confirmed by visual observations of waves refracting around the shoal. The concentration of wave energy at this point should result in increased sediment stirring and flux and thereby reduced deposition in this area.

While a considerable variability in accretion rates was observed over the study period, the overall growth showed no sign of decreasing with time. This is explained by the fact that the exposed tip has remained sub-aerial and has not formed a major blockage to the passage of sediment. Thus, accretion on the steep inner banks should proceed unabated. In addition, the shape of the exposed tip of the shoal remains ideal for enhancement of refracted wave penetration. Thus, an equilibrium reduction in accretion would not be expected with the present dredging practice until a lee inter-tidal shoal forms. In keeping with previous experience, the present study suggests that accretion is not likely to appreciably lessen over the next 12 months (prior to the next dredging campaign).

McLennan (1982) concluded from an analysis of historical harbour dredging records that the average annual volume trapped by the port was of the order 150,000 m^3 over the entire port, of which 75% is contained in the tip shoal. Our nine months of detailed records, when extrapolated, indicated trapping of 142,000 m^3 in the shoal region alone. This result, and data from the last three dredging campaigns, suggest a volume of around 180,000 $m^3 year^{-1}$ is more accurate.

One of the other issues which shoal dredging may affect is ship motion at the berths. The port periodically experiences ship motions at surface wave and infra-gravity wave frequencies. The shoal may be enhancing the passage of these waves into the port. It has been observed that ship ranging on the eastern berths is amplified on the higher tide level. This is consistent with lessened refraction on the shoal and the refracted wave crest propagating across the harbour rather than into the breakwater between the two lobes.

Only one wave direction and period was modelled and further studies of the full range of wave conditions with various dredging scenarios are needed to optimise the dredging programme. It is likely that both direction and period will have an influence, although the refraction is strongly guided by the rounded steep walls of the shoal.

6.9 Conclusions

The evolution of the Port Taranaki breakwater tip shoal is strongly dependent on wave height and only poorly on wave direction. This, and other supporting evidence, suggests that the penetration of wave energy by refraction around the tip shoal is an important factor controlling sedimentation rates in the lee of the breakwater. The primary zones of accretion are up to 400 m inside the port. By altering the shape of the shoal by dredging and encouraging waves to pass across the shipping channel rather than refracting into the port, sediment by-passing may be increased thereby reducing maintenance dredging. Numerical simulation using three different shoal configurations isolated the effect of the bathymetry on the refracting and diffracting wave components. This study has illustrated that wave dynamics should be considered in wave-dominated regions for efficient design of dredging programmes.

7 DYNAMICS OF A NEARSHORE DREDGED-SAND MOUND ON A ROCKY, HIGH-ENERGY COAST

7.1 Context of the paper within the thesis

The behaviour of dredged-sand dump mounds in nearshore coastal zones has been well reported, although no published cases have considered mound behaviour on a rocky reef seabed. This is of consequence to the studies at New Plymouth, as the manner in which the mound erodes or migrates may have significant ecological impacts on the adjacent benthic habitats. Furthermore, the rates at which a dump mound in the nearshore New Plymouth environment would erode were unknown, and the selection of a long-term nearshore dumping ground needs to ensure that the chosen site is able to disperse the dumped sediments in the period of dumping cycles. This paper reports on an experimental nearshore placement of 47,000 m^3 of sand, with a monitoring programme that specifically targets the response of the dump mound in a high-energy, rocky reef environment. The work was presented at the International Coastal Symposium 2000 Conference in Rotorua, New Zealand and has been peer-reviewed and published in the Journal of Coastal Research Special Edition (ICS 2000) as:

McComb, P.J. and Black K.P., (2001). Dynamics of a nearshore dredged-sand mound on a rocky, high-energy coast. *Journal of Coastal Research.* ICS 2000 Proceedings, 550-563.

7.2 Abstract

A placement mound of 47,000 m^3 dredged-sand was constructed at a nearshore site in water depths of 5–10 m on a predominantly rocky seabed down-drift of Port Taranaki, New Zealand. Empirical information on the manner and rate of sediment flux from the mound was gained through repetitive hydrographic and side-scan sonar surveys over an 18-month period, and directional wave/current measurements over a 12-month period. The results of the monitoring show a spatially uniform pattern of erosion from the mound, with rates of erosion that are reasonably well correlated ($R^2 = 0.42$) to the wave height (raised to the 3rd power). Measured volumes at the mound show a highly-correlated ($R^2 = 0.97$) exponential decrease with time, and after 18-months some 29% of the placed volume had been eroded. Side-scan sonar images reveal that rocky areas adjacent to the mound did not become inundated with sand, nor did the placed material migrate as a contiguous body. The data suggest that littoral transport to and from the placement region is primarily by sediment suspension, rather than bedload. An energetic wave climate was observed, with significant wave heights of up to 4.47 m and persistent long-period (12-14 second) swells. A 100° range in wave directions was recorded, although 72% of data were within a 40° directional window. Near-bed currents had a broad directional distribution and reached a maximum velocity of 29.24 cms^{-1}, with a mean value of 5.72 cms^{-1}. No direct relationship between mound erosion and the current regimen was found. The relatively slow erosion of the mound, despite high sediment entrainment potentials, is attributed to the gradual re-establishment of the pre-placement sedimentary equilibrium under a dynamic and multi-directional sediment flux. Numerical simulations of the nearshore circulation concur with measured currents and further indicate the placement region is in a zone of moderate and variable flow. This ultimately attenuates the facility of the region to disperse the placed sediments, even though prior refraction modelling had shown the site to be in a zone of relatively high wave energy.

7.3 Introduction

The environmental impacts on adjacent coastlines by harbour and inlet maintenance dredging operations are a world-wide problem and the aim of retaining trapped sediments within the nearshore littoral system has been a common objective in many

previous studies (e.g. Healy *et. al.*, 1990; Gomez-Pina & Raminez, 1994). One solution has been the use of a nearshore placement ground for dredged material– a method that relies on coastal processes to naturally disperse the placed material. The behaviour of such placement grounds has been widely reported in the literature (e.g. Vera-Cruz, 1972; Schwartz & Musialowski, 1977; Jackson & Tomlinson, 1990; Uda *et al.*, 1991; Andrassey, 1991; Bodge, 1994; Otay, 1995; Mesa, 1996; Foster *et. al.*, 1996 among others) covering a range of water depths and coastal environments. Douglass (1996) discusses many of these reports along with various models that have been developed to describe, and thus predict, the movement of material placed in a nearshore mound or berm. De Lange & Healy (1994) compare three methods for assessing mound stability (Hands & Allison, 1991 criteria; the threshold of sediment mobilisation and the sediment transport rate) with the field observations at Tauranga, New Zealand. A consistent finding in all these studies is that the dispersal of the placed material is dependent on the mobilisation of the sediment by wave-orbital motion. Furthermore, a gradual migration of the mound in the shoreward direction was observed in many of these studies – a result attributed by Douglass (1996) to the wave-orbital velocity asymmetry under finite-amplitude waves.

While providing a strong validation for the effectiveness of nearshore placements in wave-dominated environments, we note that these prior studies have been conducted in regions of relatively uniform bathymetry over mobile (i.e. sandy) substrates. In contrast, the present work describes the behaviour of a placement mound in a significantly different environment on a predominantly rocky seabed. The New Plymouth coast, New Zealand (Fig. 7.1) has an irregular bathymetry with a heterogeneous seabed substrate of sand and large rocky reefs. The littoral sediments are of andesitic volcanic origin containing dense (4680 kgm^{-3}) titano-magnetite minerals. The coast is open and exposed to the Tasman Sea, experiencing a high-energy wave climate that varies from short-storm waves (1-4 m at 4-8 s periods) to long-period (12-18 s) swell, with inshore heights of up to 6 m. The nearshore circulation is similarly variable and responds to regional flows as well as wave- and wind driven components plus a strong influence from the subtidal reefs. (McComb & Black, 2000).

The context for present study is given by McComb *et al.*, (1999b) and is briefly described herein. At Port Taranaki (Fig. 7.1), the net littoral transport is directed to the

east and some 180,000 m^3yr^{-1} of predominantly sandy sediments are dredged from within the harbour (biennially) and deposited approximately one km offshore of the harbour entrance. This procedure has been employed for the last 115 years since the establishment of the port; altering the local nearshore sedimentary regimen and contributing to the erosion of inter-tidal sand deposits along the foreshore of the City of New Plymouth. To identify ways to mitigate this effect on the nearshore littoral system, an intensive field data collection/numerical modelling exercise was implemented to assess nearshore placement options for the harbour maintenance dredgings.

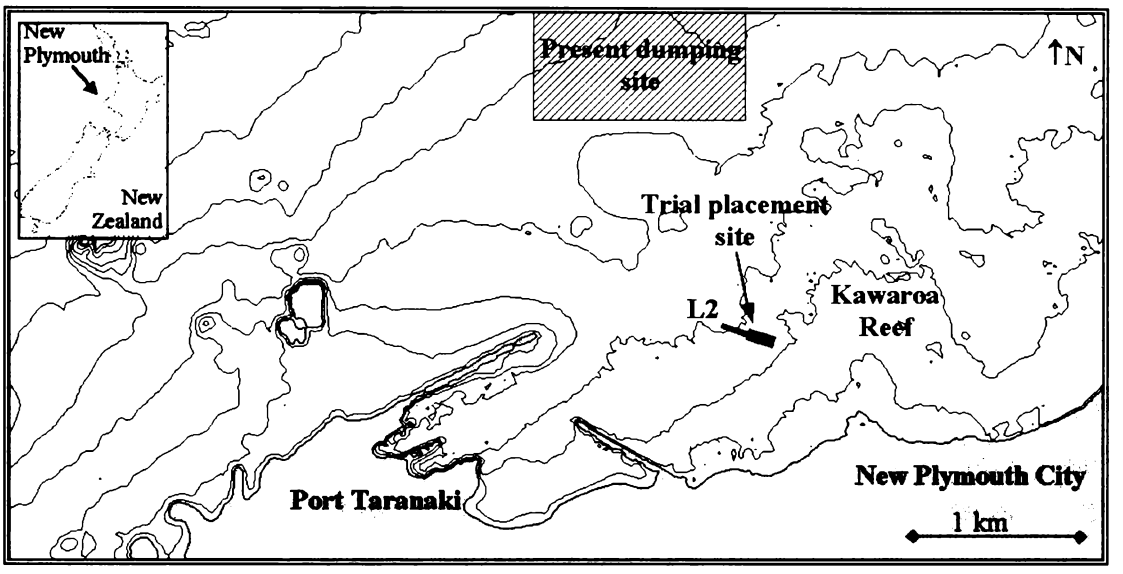

Figure 7.1: Location and bathymetric map of the study region (with depths in 5 m contours) showing the present offshore dumping site, the trial nearshore placement site and the wave/current measurement site (L2).

Intrinsic requirements for a suitable nearshore placement ground for harbour maintenance dredgings include: (1) a location within, or pathway to, the nearshore littoral system; (2) the facility to contain and disperse the required sediment quantities while minimising re-circulation back into the harbour, and (3) an acceptable level of ecological impact. The results of previous nearshore placement studies have shown the importance of waves in mobilising the placed sediments. At New Plymouth, there is ample wave energy, but the influence of a highly-variable nearshore circulation system (both spatially and temporally) on the transport of the placed material was unknown. Furthermore, the effect of the rocky seabed on the sediment flux, both at the micro-scale (i.e. turbulence around the rocks) and the macro-scale (i.e. raised bathymetric features)

was also unknown. Of paramount concern was the potential ecological impacts arising from the nearshore placement of dredged sand; much of the sub-tidal and inter-tidal regions adjacent to the harbour are rocky, and support a hardy, but reasonably diverse benthic ecology (Cole *et. al.*, 1999). While the placement of sand in this habitat will inundate the immediate placement zone, the effects on the wider region largely depend on the manner and rate of sediment transport from the site. For example, the migration of a placement mound (as observed in previous studies) will inundate rocky habitats on the pathway, but a dispersal of sediment by suspension mechanisms will have far less impact on the substrate composition in adjacent regions.

Accordingly, a controlled experimental nearshore placement of 47,000 m^3 of dredged sand was implemented to provide empirical data on the behaviour of placed material in the nearshore New Plymouth environment. This paper reports on the results of the experiment and provides an insight into the sedimentary processes occurring in this dynamic environment. The findings are also interpreted, along with numerical simulations of the nearshore circulation system, to assess the suitability of the experimental site as a long-term nearshore placement ground. Port Taranaki on the west coast of New Zealand (Fig.7.1) is exposed to the Tasman Sea and experiences a high-energy wave climate dominated by long-period westerly swell (McComb *et al.*, 1997). The coastal bathymetry features a complex reef and channel structure comprised of volcanic breccia, intermittently overlain with boulders, gravel and sand. Littoral sediments are medium "black" sands of local volcanic origin. We have estimated the net longshore transport rate to be in excess of 220,000 m^3yr^{-1} to the north (unpublished results).

7.4 Methods

7.4.1 Site selection

Initial numerical model studies and field measurements (McComb *et al.*, 1997) indicated that the western flank of the subtidal Kawaroa reef (Fig. 7.1) showed potential as a nearshore placement site. The WBEND numerical wave transformation model (Black, 1997), which predicts mean seabed wave orbital velocities, indicated a contiguous high-energy zone (Fig. 4 in McComb *et. al.*, 1997), which was subsequently

defined as the general region for the placement experiment (Atkinson & McComb, 1997). Moreover, the region is both navigable (with the presently-used dredging plant) and proximate to the harbour. A quantity of 47,500 m^3 was proposed for the experiment, which was deemed to be of sufficient size to facilitate monitoring, while remaining relatively insignificant on a regional scale, thereby minimising any potentially adverse ecological impacts.

Several factors were considered in selecting the final location and form of the placement. The material needed to be contained within a relatively contiguous mound to allow effective monitoring and a range of water depths needed to be represented. The navigational safety of the dredge vessel (with respect to rocky outcrops) also required consideration. Based on these conditions, a target region was defined for the placement (Fig. 7.2, area A). At this site the water depth ranges from 5.5 to 10 m (relative to chart datum which approximates LAT) and the seabed features both sandy and rocky substrates. The target region has an area of 11,650 m^2, is aligned along a heading of 100 degrees (True) over a length of 305 m, and is approximately centred between two slight topographical spurs (Fig. 7.2).

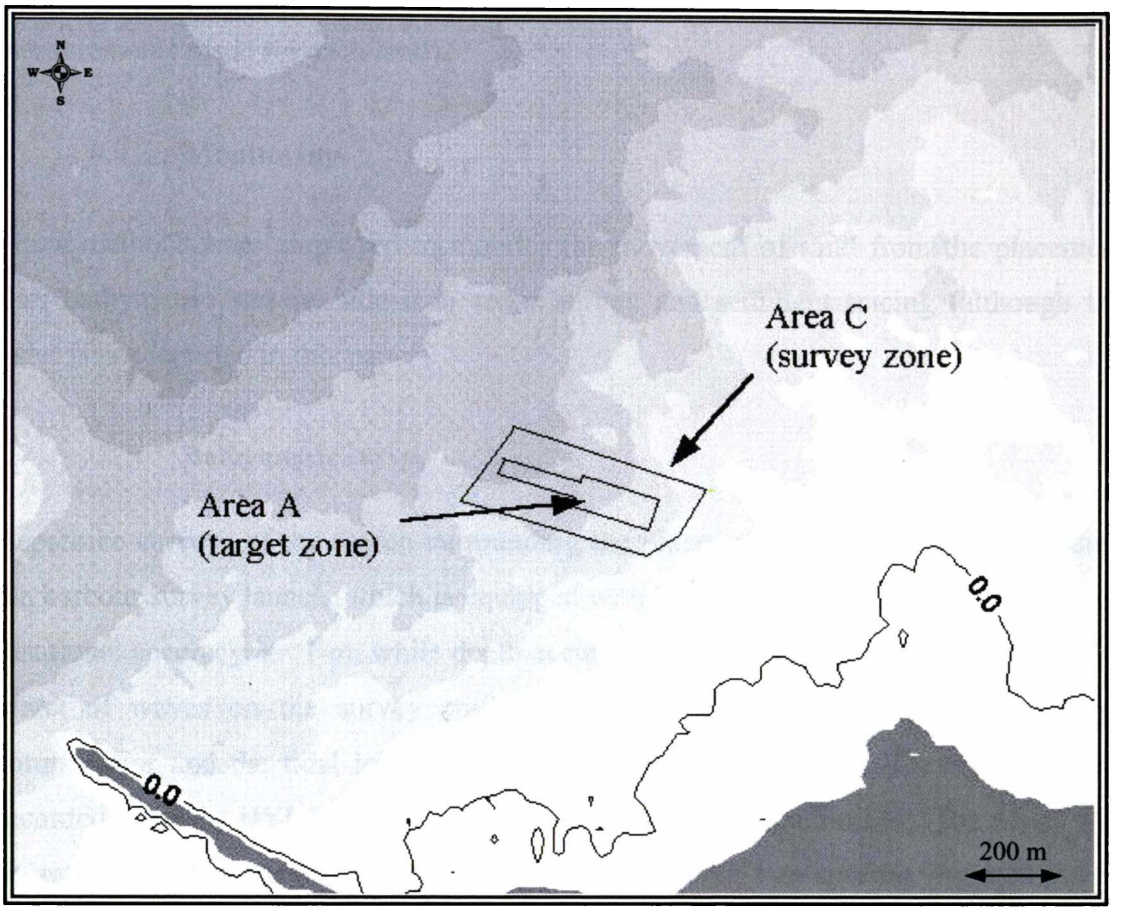

Figure 7.2: Map showing the target region for the placement operation (area A) and the wider survey region (area C).

7.4.2 Placement

The source material for the placement was limited to the Port Taranaki breakwater tip-shoal region (Fig. 7.1), where the sediments are characterised as medium-fine sands with a low silt component (McComb *et al.*, 1999). Some 75% of the port maintenance dredging quantities are sourced from this region and these sediments are considered to be of suitable quality for nearshore placement. The placement was effected using the *MV Pelican,* a split-hull trailer suction hopper dredge with ~900 m^3 hopper capacity. The vessel was equipped with DGPS positioning, and a navigational log was maintained over the duration of the sand placement. The target region (Fig. 7.2, area A) was subdivided into 15 boxes and the dredge vessel instructed to deposit a specified number of loads in each box to ensure the placement mound would be constructed to the desired

dimensions. The placement commenced with two trial loads on 25 February 1998. Over a period of calm weather from 27 February to 4 March 1998, a subsequent 71 loads were deposited on site, giving rise to a total of 46,725 m^3 (based on hopper volume measurements made for each load).

7.4.3 Monitoring

Three methods were employed to monitor the movement of sand from the placement site; bathymetric survey, side-scan sonar survey and sediment tracing (although the latter is not reported in this paper).

Bathymetric survey

Repetitive surveys of the region surrounding the placement site were conducted using the harbour survey launch, which is equipped with DGPS navigation and depth sensors. Positional accuracy is <1 m, while depth accuracy is nominally taken to be 0.05m. The effect of waves on the survey craft was accounted for using a TSS340 Heave-compensator and the tidal level from a recorder at Port Taranaki. Survey data were recorded using the HYDRO software package (Trimble Navigation Ltd). The vessel was operated at a survey speed of 4-6 kts along "run lines" of 5 m spacing, oriented at 140 degrees (True). Processing of the bathymetric data used both HYDRO and SURFER software (Golden Software Ltd), for contouring, comparisons, constructing cross-sections and volumetric calculations. A grid size of 5 x 5 m was selected and all depth measurements falling within the area of each grid block were averaged and assigned to each cell. This matrix was then used to develop surface contour maps of the survey area and relative volumes were calculated by subtracting the measured surface from the pre-placement surface. In accordance with the above estimates, an error of 0.05 m was assumed for each survey, equating to a total error of 0.10 m when two surveys were subtracted for volumetric calculations. In addition to the target zone (area A), an area of 52,127 m^2 surrounding the mound was further defined for volume calculations (Area C, Fig. 7.2).

Side-scan sonar survey

Side-scan sonar provides an efficient method of defining seabed substrate types over large areas. A Klein 595 dual frequency (100/500 kHz) digital side-scan sonar system was operated from the harbour survey launch along shore–parallel "run lines". Post-processing of the side scan data was achieved using the ISIS and DelphMap (Triton Elics 1998) software packages, following the procedures outlined by Kruger (1999). This results in a mosaic, in which data from the individual run lines are merged into a continuous coverage sonograph image. Four surveys of the placement region were conducted; the first (October 1997) provided pre-placement data; while the subsequent three surveys (March 1998, November 1998 and January 1999) provided coverage after 9, 246, and 331 days following placement, respectively.

7.4.4 Waves and currents

Directional waves and near-bed currents were recorded over a one-year period (following placement) at an adjacent site (L2, Fig. 7.1). Wave-orbital velocity and pressure data were collected in 18-minute bursts at 6-hourly intervals using a 3D-ACM WAVE meter mounted on a seabed frame (in 9.4 m water depth). Directional wave statistics and burst-averaged currents were extracted from the raw time-series using the MATLAB routine, TSERIES (Gorman, 1997). The data analysis techniques applied in deriving the directional wave spectral statistics are described by McComb *et al.* (2001).

Using the methodology of Nielsen (1984), with the U_3 definition of orbital velocities as proposed by Black & Rosenberg (1991), a time-averaged near-bed reference concentration (C_o) was calculated from each burst time-series of wave orbital motions. C_o is a widely applied parameter in sediment transport calculations; providing a measure of the sediment entrainment from the bed and thereby allowing us to relate the potential sediment entrainment (by waves) to the measured rates of erosion at the placement site. Other time-averaged entrainment equations are considered in Chapter Nine of the thesis, while here C_o is principally used to indicate the net direction of suspended sediment flux. Using the method applied by Phillips *et al.*, (1999), a weighted current (U_{Co}) was defined as;

$$U_{Co} = \frac{\sum_{i=1}^{N} U_i C_{oi}}{\sum_{i=1}^{N} C_{oi}} \qquad \text{Eqn. 7-1}$$

where U_i = burst-averaged current, i is the burst number and N = number of recording bursts. Thus for a given period, the mean flow is described by the burst-averaged currents, while the expected net direction of sediment flux derived from the weighted currents. A relative weighted current magnitude was also calculated using Eqn 7-1, where N = the total number of observations. In nearshore sediment trapping experiments at New Plymouth, Howse (2000) found that downward flux of suspended sediment was best related to the significant wave height raised to the 3rd power (H_s^3). Accordingly, similar weighted current (U_{Hs}) statistics were also derived using H_s^3 as;

$$U_{Hs} = \frac{\sum_{i=1}^{N} U_i H_s^{\,3}}{\sum_{i=1}^{N} H_s^{\,3}} \qquad \text{Eqn. 7-2}$$

7.5 Results

7.5.1 The placement mound

Hydrographic data were collected prior to the sand placement to establish the baseline bathymetry and, over 542 days following the placement, 13 subsequent surveys were conducted (Table 7.1). Immediately following the placement (POST1), the mound exhibits an elliptical form; centred about the target zone and having a maximum elevation of 2.93 m (Fig. 7.3a). The position of individual loads in relation to the target zone and the initial bathymetric survey (Fig. 7.3a) both indicate an initial dispersal of the placement material over an area approximately twice the size of the target zone; a result most probably an artefact of the placement technique rather than a natural sediment flux over the duration of the placement operation.

The initial placed volume calculated for Area C (Table 7.1) is 36,300 m^3, which is less than the value of 46,700 m^3 derived from hopper volume measurements. This difference may be attributed to several factors, including inaccuracies in the hopper volume measurements and a 'loss' of material in the interstitial rocky relief. Survey accuracy for sounding data is of the order 0.05 m. Some material may also have been ejected from the survey region during the placement operation, although the POST1 survey (Fig. 7.3) indicates these volumes are minimal.

Table 7.1:Hydrographic survey results for areas A and C.

Survey	Date	Days	Volume A (m^3)	Volume C (m^3)
PRE	15-Feb-98	-	0	0
POST1	4-Mar-98	1	18200	36300
POST9	12-Mar-98	9	18400	39000
POST28	31-Mar-98	28	16700	37800
POST63	5-May-98	63	16500	37600
POST100	11-Jun-98	100	15000	33200
POST143	24-Jul-98	143	12900	34100
POST169	19-Aug-98	169	12400	35000
POST241	31-Oct-98	241	9700	29100
POST271	30-Nov-98	271	10100	29400
POST320	19-Jan-99	320	10400	30300
POST354	22-Feb-99	354	9300	25300
POST400	9-Apr-99	400	9800	29900
POST542	28-Aug-99	542	8000	25900

Side-scan sonographs of the region prior to, and immediately after placement (Figs. 7.5 & 7.6, respectively) clearly indicate the presence of the mound. Rocky regions have a dark 'speckled' appearances while sandy seabeds show a lighter, more uniform texture. The pre-placement seabed is predominantly rocky although bodies of sand are present in the central and upper-left areas of the sonograph. Following placement, the sonograph shows a wide body of sand, both over the target zone and immediately north of it - in accordance with the first post-placement bathymetric survey (e.g. Fig. 7.3).

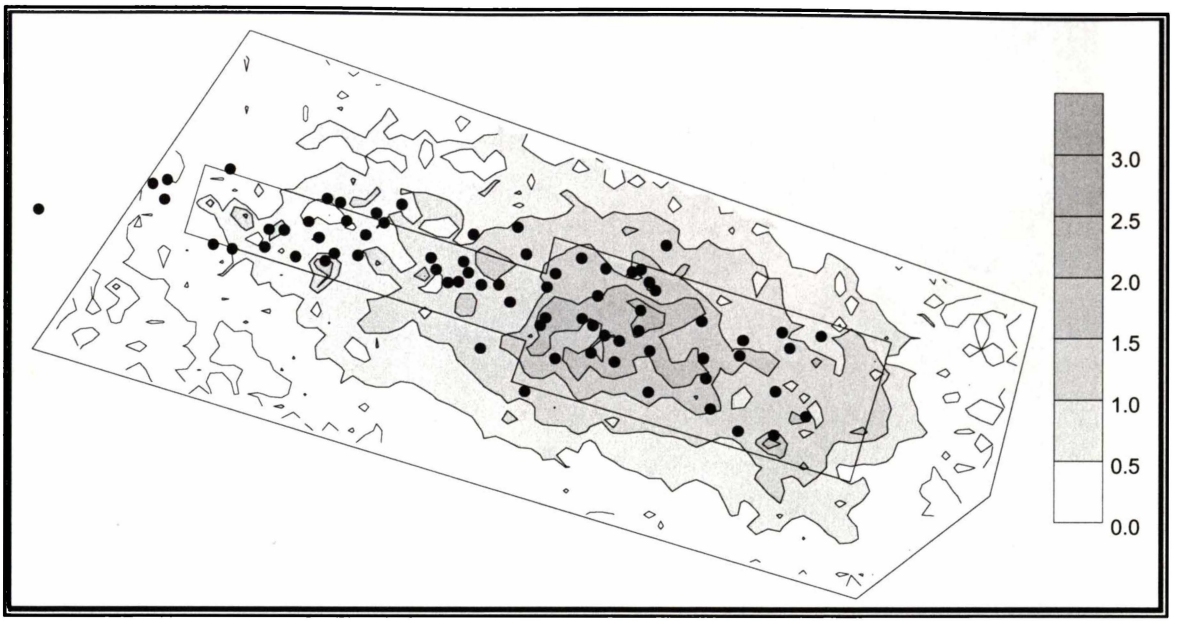

Figure 7.3: Surface difference plot (0.5 m contours) from PRE and TDG1 (immediately post placement) surveys, showing the release position of individual loads from the dredged vessel.

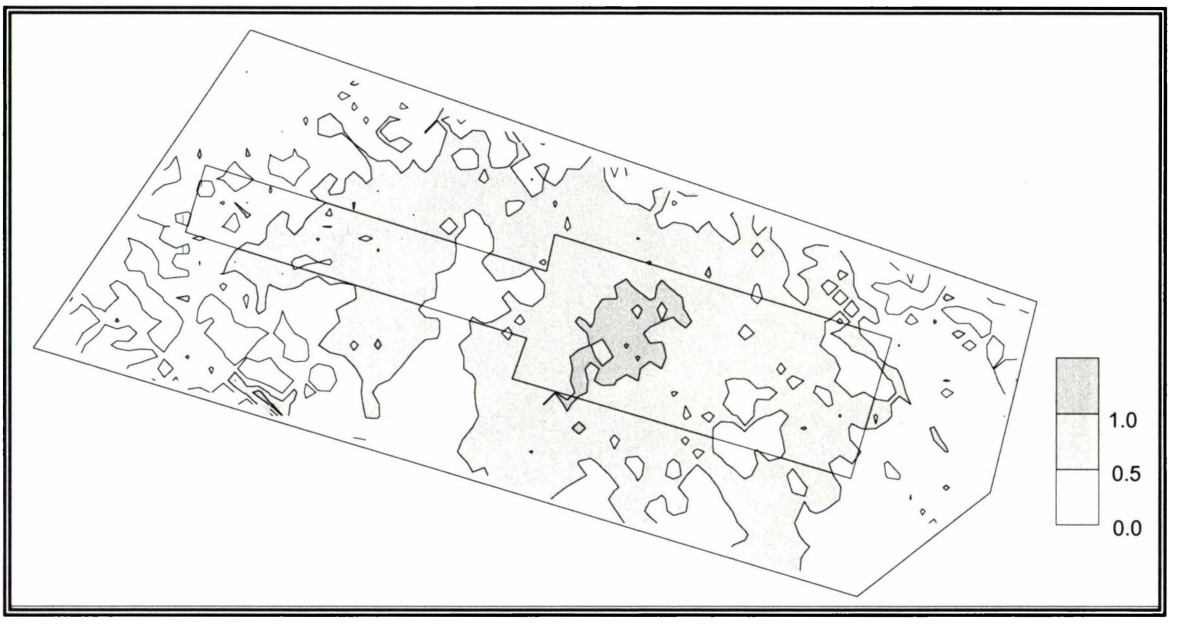

Figure 7.4. Surface difference plot (0.5 m contours) from PRE and TDG11 (354 days after placement) surveys.

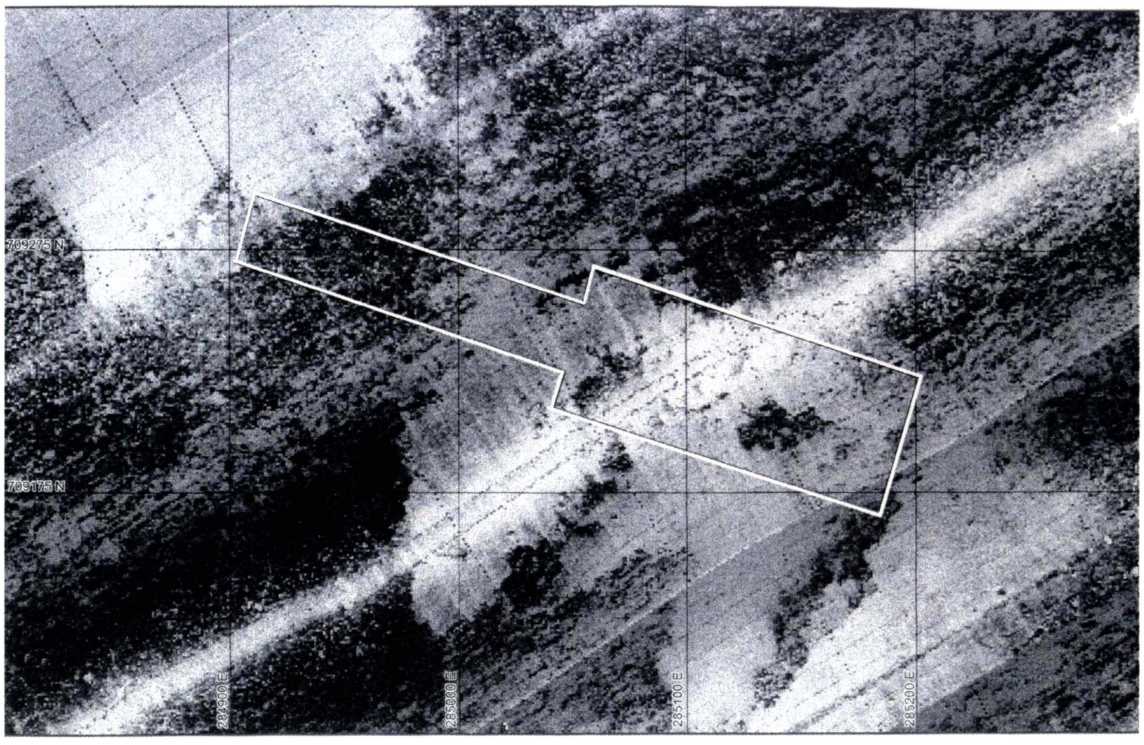

Figure 7.5: Side-scan sonar imagery (October 1997) of the placement region prior to the mound construction showing the mound target zone (area A)

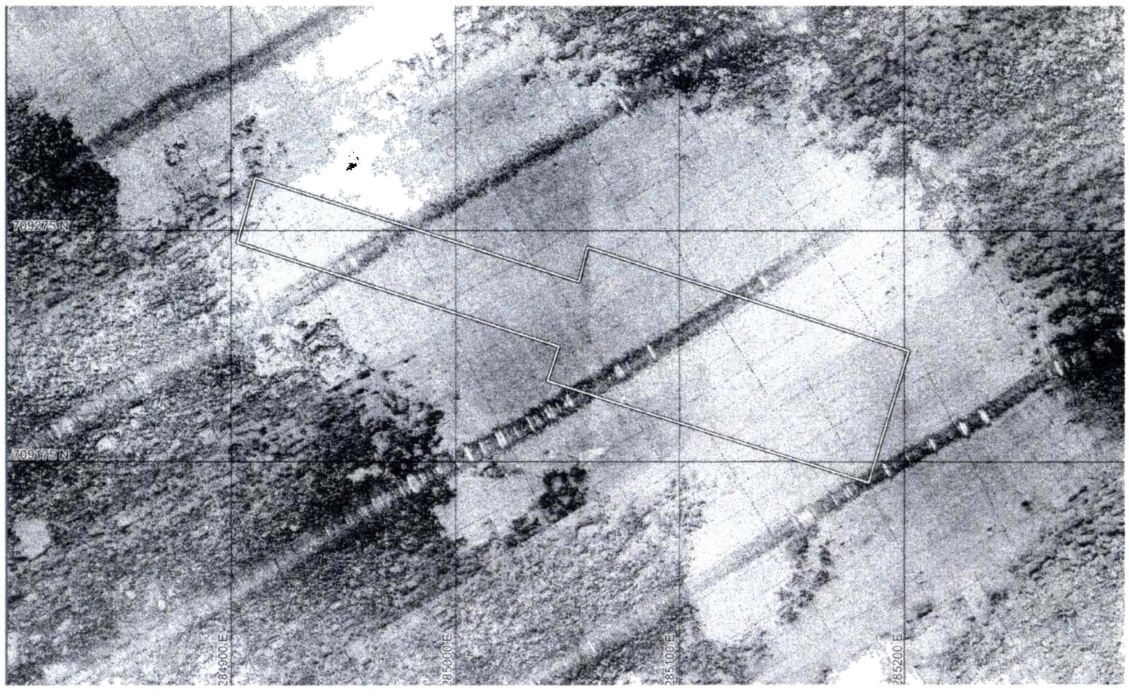

Figure 7.6: Side-scan sonar imagery (March 1998) of the placement region 9 days after mound construction.

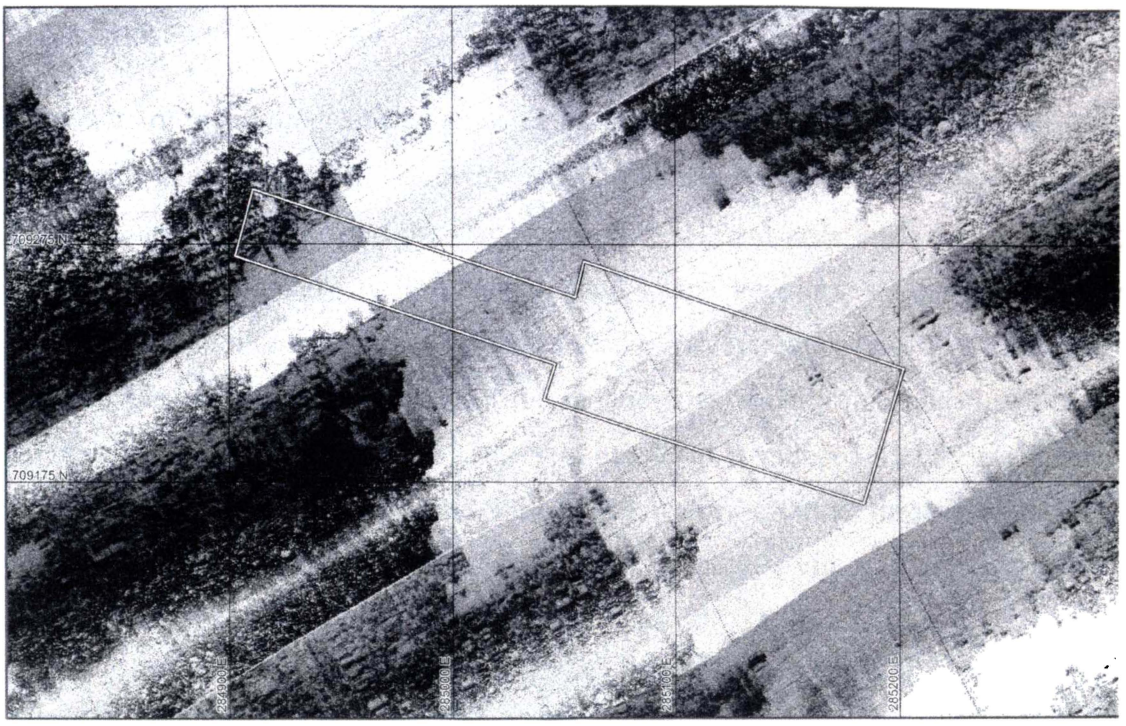

Figure 7.7 Side-scan sonar imagery (November 1998) of the placement region 246 days after mound construction.

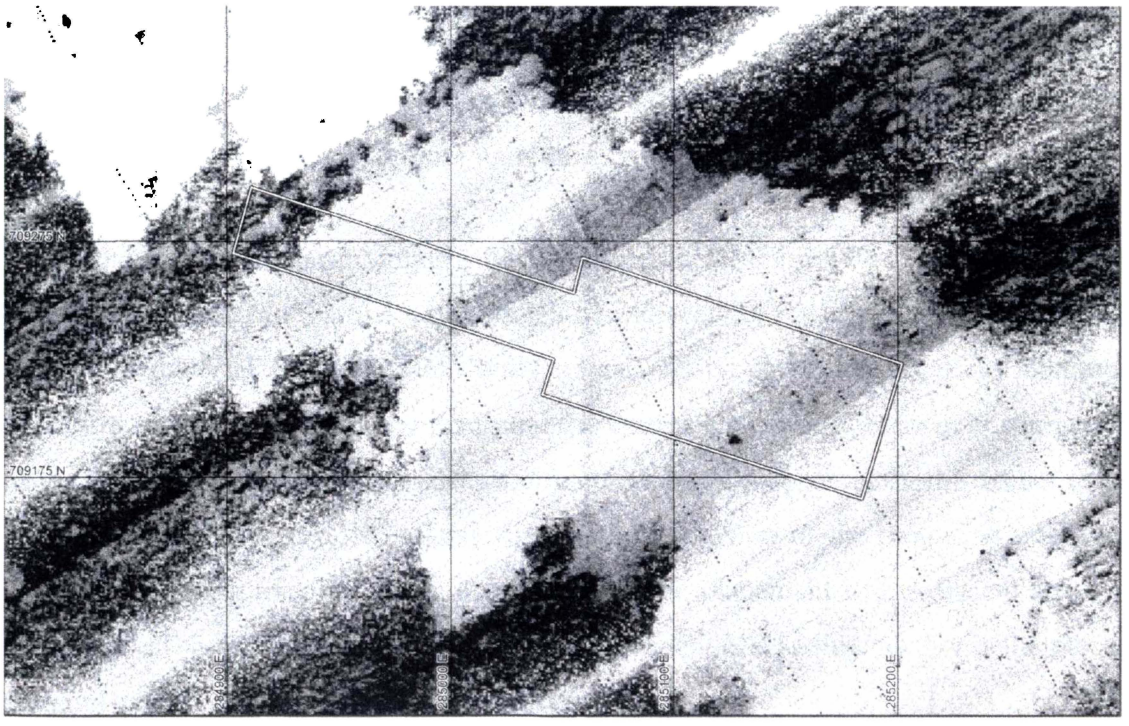

Figure 7.8: Side-scan sonar imagery (January 1999) of the placement region 331days after mound construction.

7.6 Erosion of the mound

The pattern of morphological change in the mound over time is illustrated by a series of bathymetric contour maps of the survey region, showing isobaths prior to the placement (PRE), immediately following the placement (POST1), and after one year (POST354) (Fig. 7.9). The originally well-defined mound shape becomes smoothed, although depths remain similar along the boundaries of the survey region (e.g. Fig. 7.4). After one year, the position of the centre of the mound is essentially unchanged, while the maximum elevation above the pre-placement bed level is reduced to 1.39 m. A time-series of profiles across the mound (Fig. 7.10) further clarifies these changes, and indicates a spatially-uniform pattern of erosion, although some (0.5 m) accretion is evident on the southeastern portion of area C (e.g. profile C3, Fig. 7.10).

Measured volumes in the survey area (Fig. 7.11) show a variable, but systematic decrease over time, with a volume reduction of some 29% in Area C and 56% in Area A after 542 days. Periods of accretion are evident, although the scale of variability remains within the range of measurement error. Curve-fitting of the data (Fig. 7.11) indicates the volume decrease is exponential over time, with an R^2 correlation coefficient of 0.97 for area A and 0.85 for area C. This means that as time progresses, exponentially less material is removed (eroded) from within the survey areas.

The sequence of side-scan images of the placement region (Figs. 7.5-7.8) show a remarkable stability in the rock/sand boundaries adjacent to the target zone. The gradual erosion of material from the main body of the mound is evident as rocky outcrops become more distinguished over time, and the presence of sand immediately shoreward of the target zone is a persistent feature. Erosion is equally apparent on the deeper areas of the mound. These results indicate that spatially, erosion of the mound is relatively uniform, occurring over the entire depth range at the placement site. Adjacent areas of rocky seabed show no evidence of inundation by the mobile sediments, nor is the placed material seen to migrate as a contiguous body.

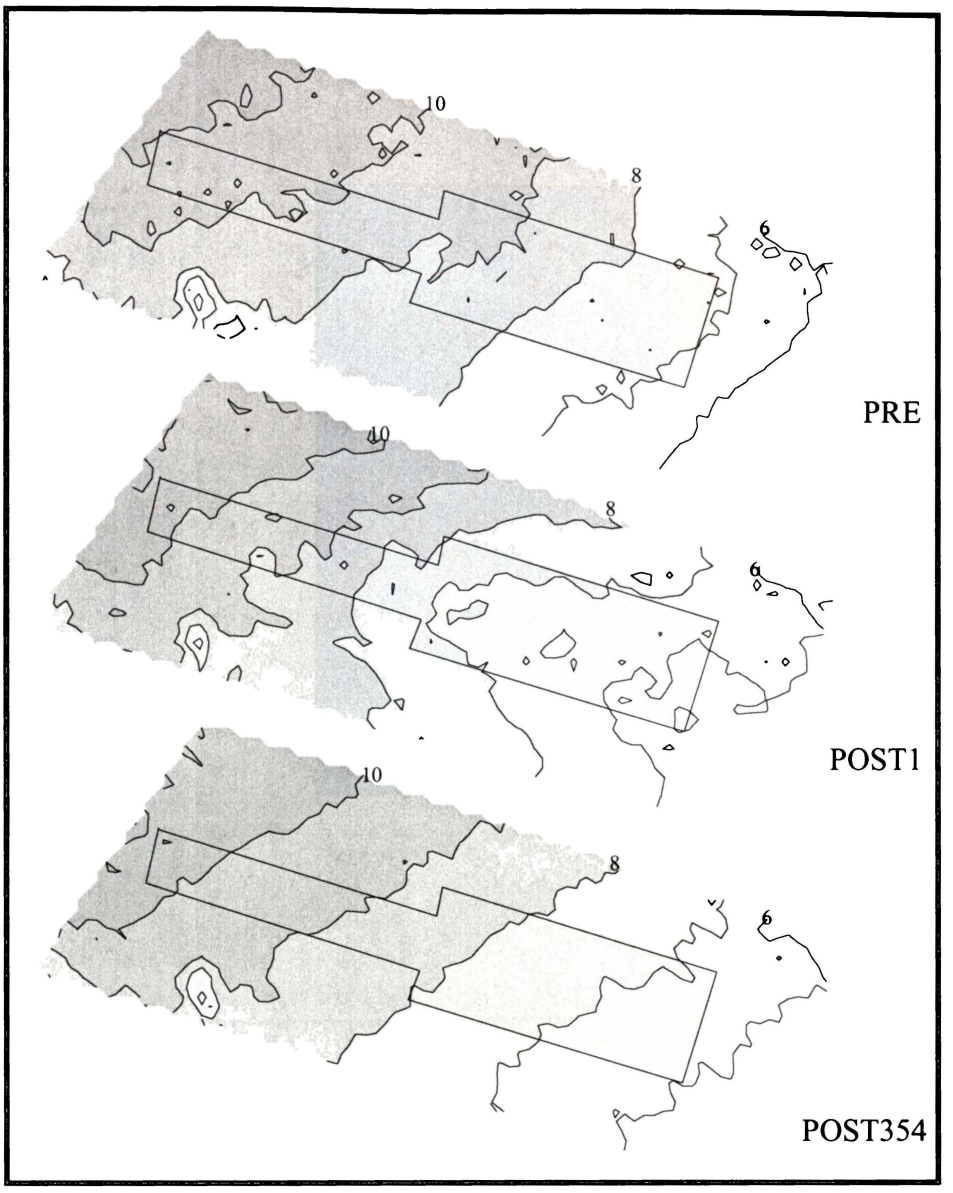

Figure 7.9: Bathymetric contour maps (1 m contours) of area C for pre-placement (PRE), immediately following placement (POST1) and 354 days following placement (POST354). The placement target region (area A) is shown on each map along with the 6, 8 and 10 m isobaths.

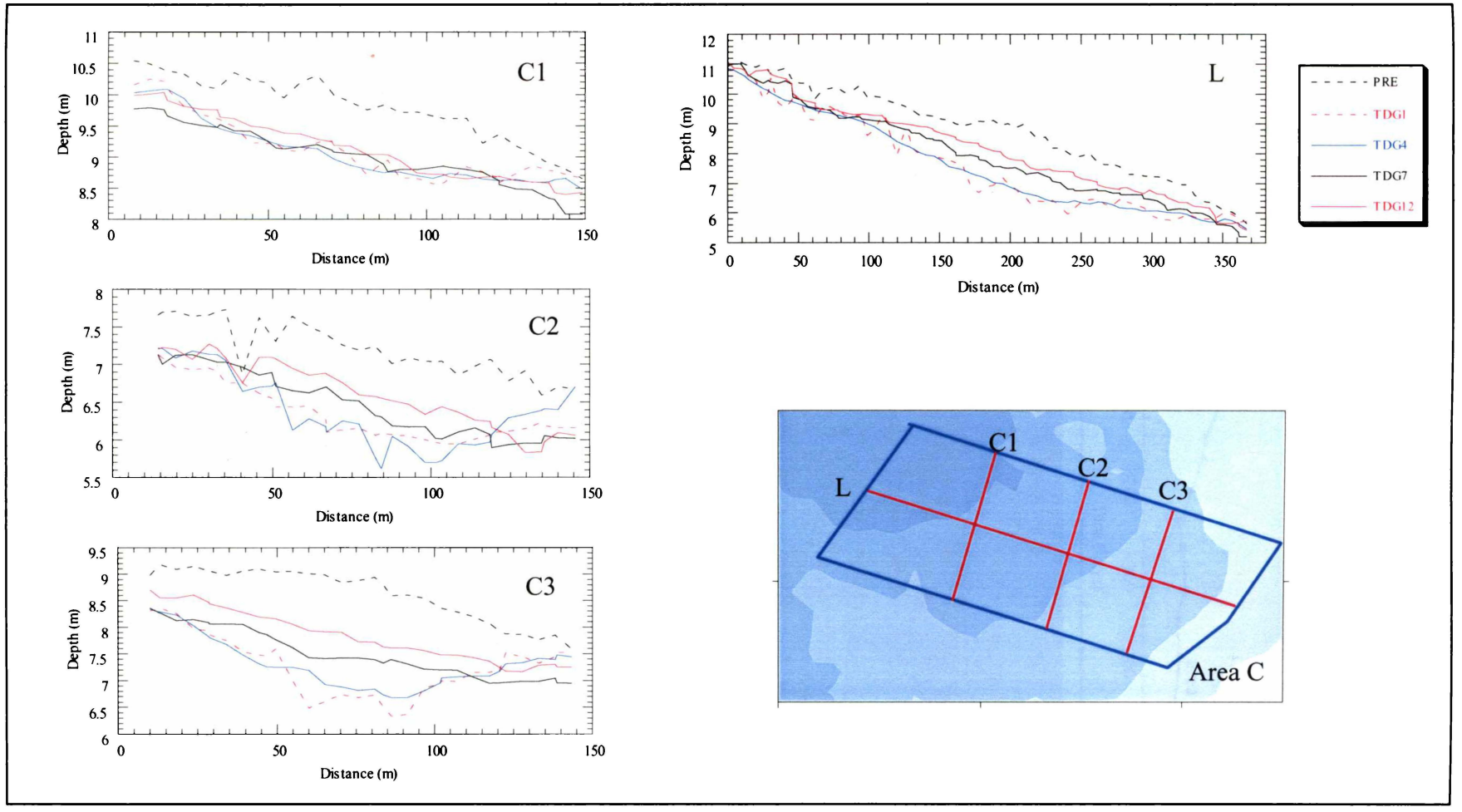

Figure 7.10: Bathymetric profiles obtained from PRE, TDG1, TDG4, TDG7 and TDG12 surveys, with the profile position s given on the inset map.

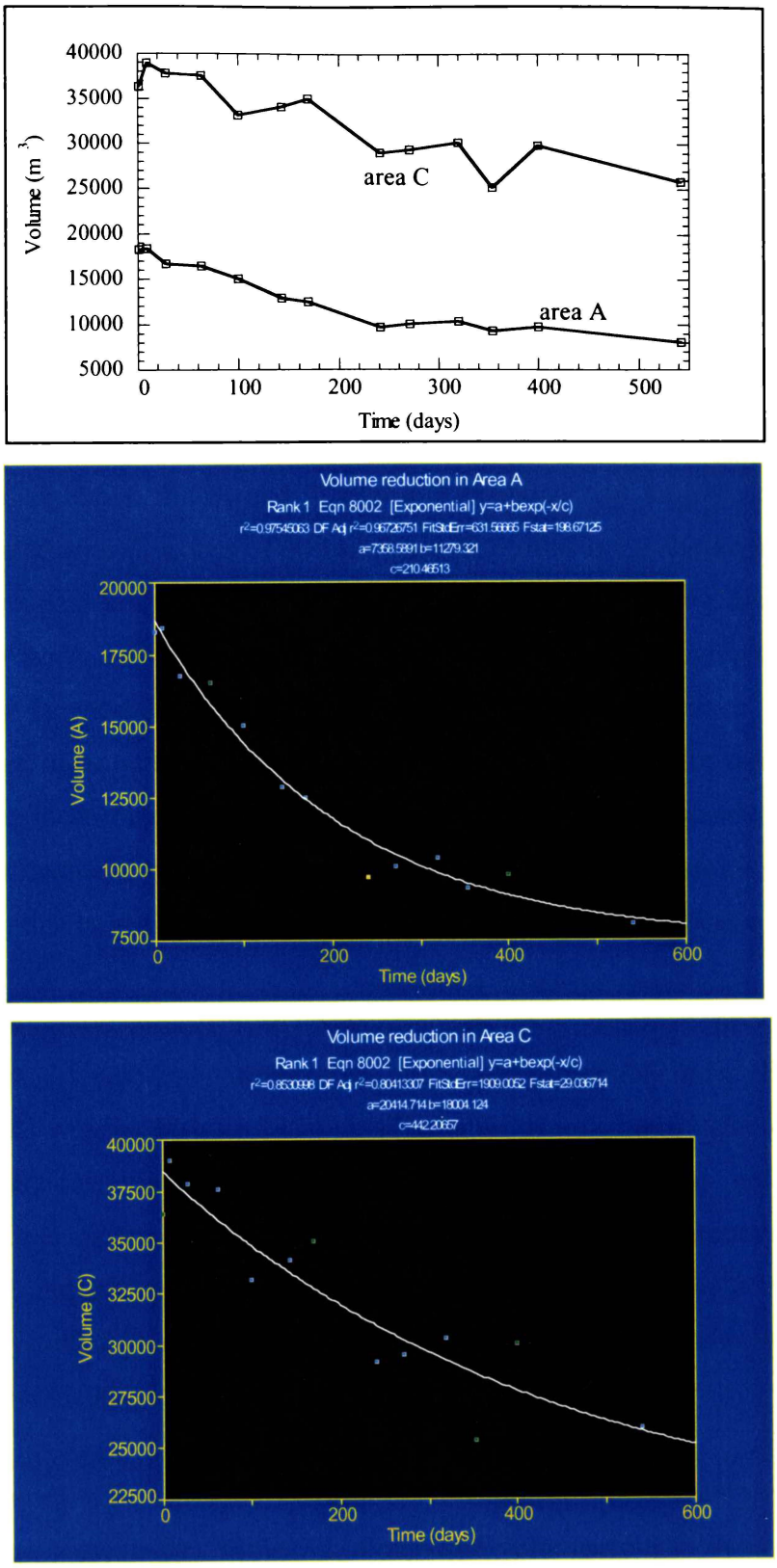

Figure 7.11: Time-series of volumes (relative to the pre-placement surface) measured in areas A and C over the 18-month monitoring period (upper panel). Curve-fitting of the data show an exponential decrease in volume over time.

7.6.1 Waves and currents

Significant wave heights (H_s), measured over one year following placement, indicate a periodically very energetic environment - three storm events were recorded where H_s exceeded 4 m (to a maximum value of 4.74 m). The percentage exceedence values for H_s were 0.32, 0.88 and 2.19 m for the 95, 50 and 5% exceedence levels, respectively. Wave spectra frequently exhibited a bimodal distribution, with both a persistent long-period swell (12-14 s periods) and locally-generated sea conditions (6-8 s periods). Peak spectral wave periods (T_p) were most commonly in the range 12–14 seconds. The joint probability distribution for H_s and T_p (Table 7.2) shows that larger wave heights are often associated with T_p values of <10 s. Wave directions at L2 show a narrower range than offshore data at New Plymouth (e.g. McComb *et al.*, 2001) due to refraction aligning the wave crests to the isobaths and a degree of topographical sheltering provided by the port headland and offshore islands. Nonetheless a 100° range in direction was measured, although 72% of these data were within a 40° directional window. The mean direction of wave advance was 116° with a standard deviation of 21°. The joint probability distribution of H_s and wave direction (from) is given in Table 7.3, showing that larger wave heights are associated with the less oblique directions (i.e. from the NW).

Measurements of near-bed currents indicate a highly variable flow. Burst-averaged current speeds were as high as 29.24 cms^{-1} with an overall mean value of 5.72 cms^{-1}. Current directions are broadly distributed, although a slight easterly (~100°) predominance is apparent – a mode also associated with higher current velocities. Data from site L2 and other sites (e.g. McComb & Black, 2000) portray a highly variable circulation system, with multiple wave- and wind-driven components as well as a strong influence from the larger-scale regional flow.

The mean values of the wave, current and C_o statistics for each survey period (POST63-POST354) are presented in Table 7.4, along with volumetric data in terms of erosion rates (in m^3day^{-1}) for areas A and C. The first two surveys (POST9 & POST28) are not included as this period may reflect an initial settlement of the placed material (Moon *et al.*, 1994). To examine the relationship between erosion rates and the sediment transport mechanisms, regression analysis was performed on the averaged data over each survey

period. Erosion rates from areas A and C were compared with all the parameters in Table 7.4 (i.e H_s, H_s^3, C_o, U, U_{Hs} and U_{Co}). The strongest correlation (R^2 = 0.50) was found using H_s^3 for area A (Fig. 7.12). Area C, however, remained poorly correlated (R^2 = 0.05). No systematic relationship between the erosion rates and the currents (weighted or unweighted) was found. The results also show that net (unweighted) currents are predominantly directed to the east, while the weighted currents (inferring the direction of sediment flux) exhibit greater variability. Furthermore, weighted current directions differ significantly with the choice of parameter used in the weighting calculation.

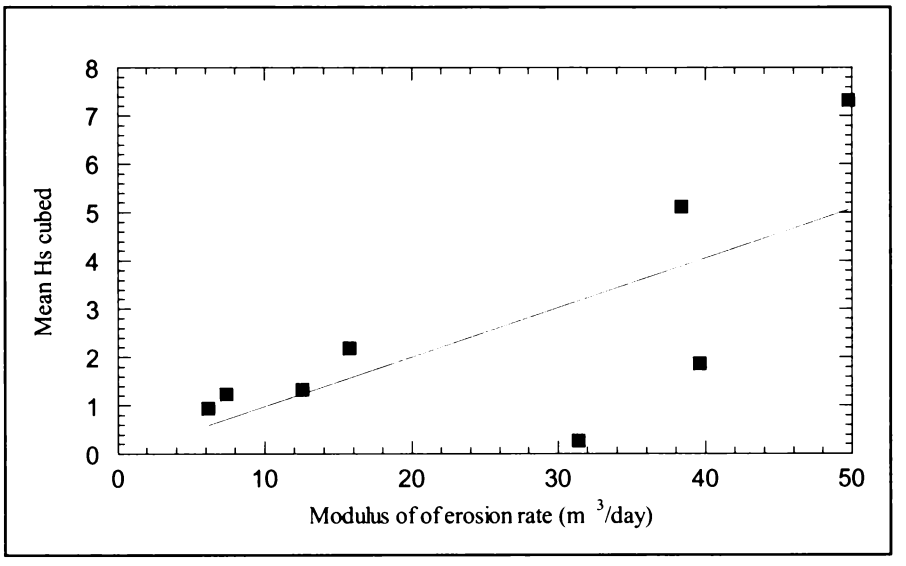

Figure 7.12: Measured erosion rates in area A (modulus) for survey periods POST63-POST354 vs the corresponding values for the mean significant wave height raised to the 3rd power (H_s^3). The linear regression of the data is reasonably well correlated (R^2 = 0.50)

Table 7.2: Joint probability distribution of significant wave heights (H_s) and peak spectral wave periods (T_p) measured over 12 months at site L2.

Wave Period (T_p)	H_s wave height (m) Site L2										
	< 0.5	0.5-1.0	1.0-1.5	1.5-2.0	2.0-2.5	2.5-3.0	3.0-3.5	3.5-4.0	4.0-4.5	4.5-5.0	SUM
3	0.15	0.51	0.15	0.07	0	0	0	0	0	0	0.88
5	1.17	5.91	2.63	0.22	0.07	0	0	0	0	0	10.00
7	0.58	2.12	3.87	2.92	1.24	0.07	0.07	00	0	0	10.88
9	1.46	5.84	4.16	4.16	1.61	0.95	0.36	0.22	0.07	0	18.83
11	2.85	5.47	2.34	0.95	1.17	0.29	0.22	0.07	0	0.07	13.43
13	6.28	12.85	4.09	1.39	0.51	0.36	0.07	0.07	0.07	0.07	25.77
15	2.34	6.42	2.12	0.22	0.15	0.07	0	0.07	0	0.07	11.46
17	0.88	4.74	1.75	0.36	0	0	0	0	0	0	7.74
19	0.22	0.51	0.22	0.07	0	0	0	0	0	0	1.02
SUM	15.91	44.38	21.31	10.36	4.74	1.75	0.73	0.44	0.15	0.22	100

Table 7.3: Joint probability distribution of significant wave heights (H_s) and mean wave direction measured over 12 months at site L2.

Wave approach	H_s wave height (m) Site L2										
	< 0.2	0.2-0.5	0.5-1.0	1.0-1.5	1.5-2.0	2.0-2.5	2.5-3.0	3.0-3.5	3.5-4.0	4.0-5.0	SUM
SSW	0	0	0.15	0	0	0	0	0	0	0	0.15
SW	0	0	0.95	0	0	0	0	0	0	0	0.95
WSW	0	0.51	3.79	0.22	0	0	0	0	0	0	4.52
W	0	1.9	10.07	5.4	0.66	0.22	0	0	0	0	18.23
WNW	0.15	6.27	16.48	9.26	3.94	1.82	0.44	0.44	0	0.07	38.88
NW	0.15	6.71	11.89	5.4	4.45	1.75	0.88	0.29	0.15	0	31.66
NNW	0	0.29	0.95	1.09	1.17	0.95	0.29	0	0.29	0.22	5.25
N	0	0.07	0	0.07	0.07	0	0	0	0.07	0	0.29
SUM	0.29	15.75	44.27	21.44	10.28	4.74	1.6	0.73	0.51	0.29	100

Table 7.4: Erosion rates for areas A and C over survey periods POST63 – POST354 and the mean values of: significant wave height (H_s); significant wave height cubed (H_s^3); near-bed sediment reference concentration (C_o); weighted currents using H_s^3 and C_o (Eqn. 7.1) and mean currents. Negative erosion rates equate to accretion.

Survey	Erosion rate area A (m^3day^{-1})	Erosion rate area C (m^3day^{-1})	Mean H_s (m)	Mean H_s^3	Mean U direction (degrees)	Mean U speed (cms^{-1})	Mean C_o (kgm^{-3})	Mean U_{Co} direction (degrees)	Mean U_{Co} speed (cms^{-1})	Mean U_{Hs} Direction (degrees)	Mean U_{Hs} speed (cms^{-1})
POST63	7.40	7.60	0.86	1.24	336	2.41	2.426	308	0.12	309	0.07
POST100	39.59	119.19	1.04	1.86	156	2.68	1.142	63	0.02	183	0.06
POST143	49.77	-21.35	1.46	7.32	116	10.42	38.856	5	5.94	246	0.93
POST169	15.73	-36.23	0.99	2.18	113	8.81	2.651	334	0.06	125	0.18
POST241	38.39	82.46	1.35	5.12	111	7.98	1.716	81	0.20	110	2.62
POST271	-12.53	-11.60	0.97	1.33	94	17.42	0.027	5	0.01	89	0.71
POST320	-6.16	-17.24	0.75	0.94	97	7.24	0.029	273	0.004	95	0.38
POST354	31.41	146.85	0.55	0.27	223	2.05	0.002	273	0.00002	246	0.01
ALL	18.82	19.26	1.03		107	5.72		7	6.67	117	3.14

7.7 Discussion

The pre-placement seabed is characterised by both sandy and rocky regions (e.g. Fig. 7.5). Multiple side-scan investigations from the present study and previous workers (Arron & Mitchell, 1984) indicate a long-term positional stability in these sedimentary facies – both around the placement region and over the wider New Plymouth coast. This is consistent with dynamic equilibrium in which the import and export sediment fluxes are balanced; a situation also maintained by the dredging/dumping procedures historically employed by the port. The side-scan data further indicates that persistent regions of sandy sediments often coincide with seabed depressions and the western flanks of raised bathymetric features. It is thus apparent that the seabed topography influences the sediment transport, and the rocky regions are not conducive to the long-term settlement of the mobile littoral sediments under the present nearshore sedimentary budgets.

Our wider studies of the New Plymouth coast have shown that the port's trapping of the nearshore littoral sediments is not total, as sand continues to pass the port and time-averaged suspended sediment concentrations remain relatively high over rocky and sandy beds alike (McComb, *et al.*, 1999b). Thus, it is likely that the rocky regions have a higher sediment flux potential than the sandy regions, thereby maintaining their rocky character. This is perhaps due to greater turbulent flow over these beds, resultant from the wave-orbital interaction with the hydrodynamically 'rough' substrate (e.g. Nelson, 1996; Green *et al.*, 1998). Our observations of the placement are consistent with this as the rock/sand boundaries have remained stable over the monitoring period, and adjacent rocky regions did not become inundated with sand – despite a net erosion of the placed material.

It is noteworthy, however, that slight accretion occurred in the southeastern portion of area C, which perhaps reflects the Douglass (1996) assertion of sediment migration due to wave-orbital velocity asymmetry – particularly in the larger wave events. The wave height/direction probability data in Table 7.3 supports this, showing that larger waves arrive from the NW quarter. However, the uniform smoothing of the mound (e.g. Figs 7.3 & 7.4), along with the side-scan sonar images, suggest that the velocity asymmetry is not the fundamental cause of erosion, but rather a sediment suspension by waves and

net transport by the (variable) coastal currents. We also note that the placement site is situated between two slight bathymetric spurs and these features may provide a degree of containment to the placed material (evidenced by the presence of some sandy beds in the region prior to the placement) and modify the direction of sediment flux.

While the sedimentary facies show long-term positional stability, a minor degree of bed level variability is likely to exist in the sandy regions. The bed level on these mobile substrates is responsive to the wave and current regimen – as observed by McComb *et al.,* (1999a) in a study of sediment accretion at the Port Taranaki breakwater tip. At the placement region, SCUBA diver observations of sessile encrusting organisms in sand/rock environments (pre-placement) indicate a variable bed level of the order 0.1 m, which may in part explain the variability in calculated volumes observed over the monitoring period. Accordingly, the placement region needs to be considered as an open system, with sediment inputs and outputs, and influenced by the larger-scale littoral flux. The data show that, while remaining similar over the long-term, erosion rates in areas A and C have considerable periodic differences (Table 7.4); rates in area A are reasonably well-correlated to the mean wave height cubed (H_s^3), while rates in area C are less well correlated. This observation may be due to area A being smaller and containing the greater elevation of placed material, thereby being more responsive to erosional events than area C. Similarly, area C is larger and more likely to be responsive to a net sediment influx.

It is also interesting to note that the most energetic survey period (POST143, Table 7.4) featured the highest measured erosion rate in area A (49.77 m^3day^{-1}), yet a net accretion was observed in area C over the same period. Somewhat conversely, the least energetic period for both waves and currents (POST354, Table 7.4) has the highest rate of erosion from area C.

The relatively slow reduction in the mound volume is surprising given the highly energetic wave climate. During storm events the calculated C_o values (at site L2) are very large, as are the instantaneous wave-orbital velocities. Thus, the potential for sediment to be entrained and transported out of the confines of the survey area is similarly large - even with residual currents as low as 0.05 ms^{-1}. The high transport potential, yet overall low mound erosion rates, may be explained by considering the

placement region as but a segment within a dynamic multi-directional littoral flux, and the observed erosion representing the gradual re-establishment of the sedimentary equilibrium to the pre-placement condition. Thus, the volumes of mobile sediments within this study zone will be influenced by the larger-scale littoral fluxes, which will ultimately control the sediment supply to this predominantly rocky nearshore region.

For mound erosion to occur, there must be an imbalance in the sedimentary equilibrium and this may be realised through an elevation of the seabed (resulting in increased wave orbital velocities at the bed), or an increased surface area for sediment suspension (i.e. placement of sediments on previously rocky beds). The influence of bed level on the near-bed wave orbital motions may be estimated using linear wave theory (Dean & Dalrymple, 1991). Considering a monochromatic wave of 2 m height and 12 second period, the erosion of the bed level from 6 to 8 m depth equates to a reduction of approximately 15% in the near-bed wave orbital velocities, thereby illustrating a clear mechanism for the heightened erosion of elevated regions of the placement mound and a general 'smoothing' of the isobaths over time. Consistent with this, the exponentially decreasing volumes in areas A and C (e.g. Fig. 7.11) suggest a systematic reduction in erosion rate with the passage of time, as the elevation of the placed material decreases.

Comparison of erosion rates in areas A and C with both the wave and current data has revealed no strong systematic trends in the magnitude or direction of the inferred sediment flux. The measurements show a highly variable current regime with only a slight easterly sediment flux mode (defined by the unweighted and H_s^3 weighted currents). Furthermore, during storm events when the sediment transport potential is high, the flows remain similarly variable. To relate the time-averaged survey data with such protean wave/current conditions is inherently difficult, and in this case it is likely the time-scale of measurement employed precludes the resolution of any trends. We further note that the wave/current records provide only a point source of data and may not necessarily represent the entire placement region - indeed the nearshore regions are approximately half the water depth of site L2.

To relate our observations of the placement within the context of the broader coastal circulation patterns, we include some results of numerical modelling investigations associated with the wider study. These investigations, reported by Black & McComb

(2000), employed a suite of models including WBEND (Black, 1997), 3DD (Black, 1995) and POL3DD (Black, 1996, Black *et. al.*, 1999), with calibration / validation from a large set of field measurements (McComb & Black, 2000). The predominant nearshore circulation patterns are presented in Figure 7.13 showing the vertically-averaged residual current vectors derived from a representative 13-day period. Currents are primarily directed to the east with strong flows associated with the breakwater tip region and the subtidal Kawaroa Reef. A weaker, less defined circulation system is evident between the port and the flanks of the Kawaroa Reef, characterised by variable currents that frequently exhibit a clockwise gyre. The nearshore placement mound is located on the edge of this system; adjacent to the strong easterly flows over the Kawaroa Reef, yet remaining within the region of weaker flow.

While our empirical observations have not identified a direct relationship between the net erosion of the placed material and the measured currents, both the current data and the model studies indicate that the placement region has a variable current regime. This reduces the capacity of the zone to disperse the placed sediments in an easterly (longshore) direction and thereby renders it unsuitable for use as a long-term placement ground.

7.8 Conclusions

An experimental placement of 47,000 m^3 of dredged sand was conducted at a predominantly rocky nearshore site in water depths of 5–10 m. Empirical observations of the behaviour of the placement mound over an 18-month period have shown a spatially uniform pattern of erosion, with rates that are related to the wave height. Within the survey area, a multi-directional dispersal of the placed sand was observed, resulting in a broad smoothing of the isobaths over time. While episodic in nature, measured volumes at the mound show a highly-correlated (R^2 = 0.97) exponential decrease with time, and after 18-months some 29% of the placed volume had been eroded. Rocky areas adjacent to the mound did not become inundated with sand, nor did the placed material migrate as a contiguous body. The data suggest that material transport to and from the placement region is primarily by sediment suspension, rather than bed-load.

While located in a high-energy wave zone, relatively slow erosion of the mound was observed. This is attributed to the gradual re-establishment of the pre-placement sedimentary equilibrium under a highly dynamic sediment flux. Currents at the placement site were highly variable with only a slight easterly (longshore) mode for the inferred direction of sediment flux. Numerical simulations of the nearshore circulation patterns indicate that the site was located within a zone of moderate currents; sheltered by the port breakwaters and influenced by the subtidal Kawaroa Reef. This, and the measured rates of erosion from the placement mound, suggest that the experimental site is unsuitable as a long-term placement ground. The study demonstrates the importance of considering both the wave energy and the nearshore circulation patterns when choosing a placement site.

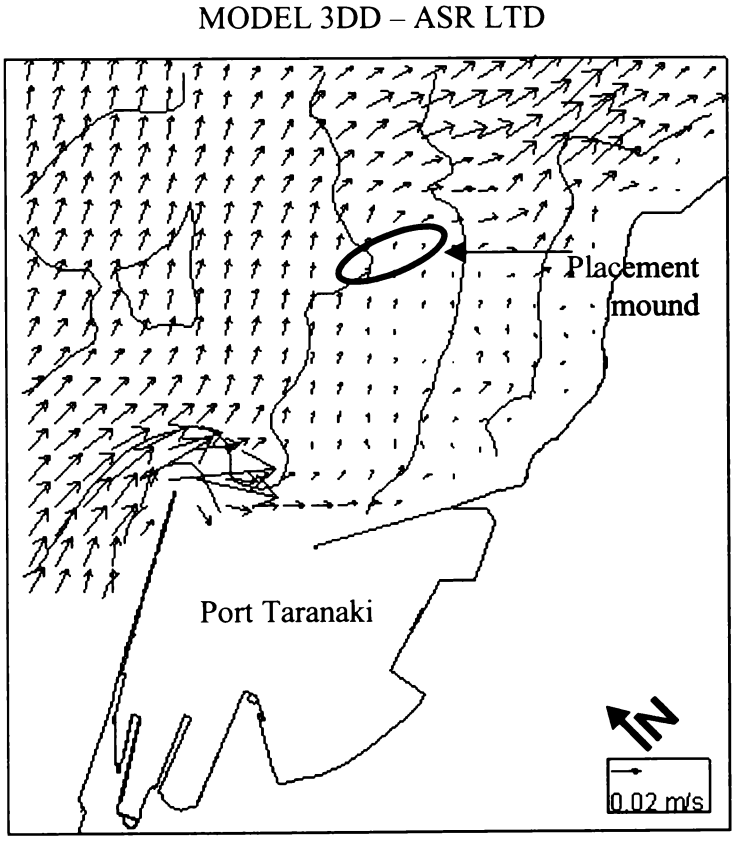

Figure 7.13: Numerical model output showing the residual current vectors in the region of the placement site. Bathymetry is shown in 5 m contours

7.9 Acknowledgements

The authors thank Mr Peter Atkinson of Westgate Port Taranaki for project support and Mr. Bruce Gray and Captain Y.T. Lim (also of Westgate) for hydrographic data collection. Mr Dirk Imenga and Mr Jens Kruger of the Department of Earth Sciences, University of Waikato, conducted the side-scan sonar survey and post-processing, respectively. Prof. Terry Healy, also of the University of Waikato, provided guidance in the design of the experiment. The assistance of Mr Jason Sait in the field data collection is warmly acknowledged.

8 DETAILED OBSERVATIONS OF LITTORAL TRANSPORT USING ARTIFICIAL SEDIMENT TRACING, WAVE AND CIRCULATION MEASUREMENTS AND NUMERICAL MODEL STUDIES IN A HIGH-ENERGY, ROCKY REEF AND BLACK SAND ENVIRONMENT

8.1 Context of the paper within the thesis

The sediment tracing studies reported in this paper provide the first direct observations of sediment movement along the New Plymouth coast. The experiment considers transport from two areas on either side of the port entrance, providing insight to harbour trapping, sediment movement from a nearshore dumpsite, and transport across rocky reefs. Tracer release and monitoring was conducted as part of the experimental programme described in Chapter 2, allowing the observations of tracer movement to be correlated with wave and current measurements. This paper was submitted to the Journal of Coastal Research (July, 2001) and has been peer-reviewed and is awaiting publication as:

McComb, P.J. and Black, K.P., (in press). Detailed observations of littoral transport using artificial sediment tracing, wave and circulation measurements and numerical model studies in a high-energy, rocky reef and black sand environment.

8.2 Abstract

On a high-energy coast, with heterogeneous nearshore bathymetry and sediment dynamics (New Plymouth, New Zealand), two colours of artificial fluorescent tracer were used to i) investigate the sediment entrapment/bypassing of a port entrance, and ii) to monitor sediment movement from an experimental nearshore dredged-sand dump mound (47,000 m^3). Two simultaneous releases (one for each colour) were made in 6 to 10 m water depths, near the port entrance and on the dump mound, 1400 m apart. The tracer was tracked over 10 months by collecting and analysing 1179 surficial sediment samples, with concomitant wave/current recording at up to 13 nearshore sites.

The results demonstrate trapping in the breakwater tip-shoal of the port, by-passing and movement through the complex nearshore reef system. The dominant transport was alongshore. Tracer released near the port entrance depicted a natural sediment "pathway" past the harbour shipping entrance and over the rocky reefs to the beaches 4.5 km away. Very little tracer was detected within the harbour, indicating that the main transport from the release depths (6-10 m) by-passed the harbour entrance and tip-shoal. The tracer shows that only sediments very close to the harbour breakwater (i.e. within 100 m) are trapped at the harbour entrance. From the dump mound, tracer was observed to migrate mostly longshore away from the port, although a minor "updrift" migration was observed.

The tracer results are in accordance with measured and numerically modelled currents, which show a dominant longshore flow away from the port and weak reversing flows in the quiescent lee of the harbour at the dump mound. The tracer data also suggest that the raised shore-normal reefs do not present a significant impediment to longshore transport, but rather that the nearshore circulation patterns are the predominant influence on the sediment transport vectors. Rates of tracer spreading were found to range from 0.095 to 0.288 m^2s^{-1}, which is consistent with a high-energy coastal environment. Diffusion and advection of suspended sediments is the primary mechanism of sediment transport, and tracer was found on beaches 4.5 km distant from the release point within 13 days of injection.

8.3 Introduction

Sediment tracing is a useful method for quantifying the magnitude and direction of littoral sediment flux. Provided the tracer material faithfully represents the native sediment characteristics (e.g. in particle size and fall velocity), tracer can provide an unambiguous marker of littoral transport through monitoring over time and space. While used in many situations, ranging from the surf zone (e.g Ciavola *et al.*, 1997), nearshore regions (e.g Foster *et al.,* 1996) or in sediment bypassing studies (e.g. Sherman *et al.*, 1990; Uda *et al.*, 1991), tracer is particularly valuable in complex environments where local dynamics may lead to strong sediment transport gradients and/or variable seabed morphologies. In these environments, integrated fluxes over the long term are difficult to measure using Eulerian techniques. Here, the tracer is able to show transport pathways that may be important, for example, to the fate of dredged sediments (e.g Marsh *et al.*, 1997). Further, when coupled with wave and current data, the tracer movements may also be related to the intensity of the wave-orbital motion (Pizzuto, 1987; Miller & Komar, 1979) and the coastal circulation and wave patterns (Cheong *et al.*, 1992, 1993).

However, as noted by Madsen (1987), there are several limitations to using sediment tracers and these are of particular relevance in a wave-dominated environment. The surficial sediment layer has a depth of vertical mixing, and over time the tracer will become distributed within that layer. This occurs through the intermittent nature of sediment suspension under waves (e.g. Hanes, 1988) and as a result of bedforms. Also, tracer dilution will occur over both time and distance from the release point. The combination of these factors may mean that a direct relationship between quantitative sediment fluxes indicated by tracer and the wave and current patterns can usually only be derived in the initial period following release. As the spatial and temporal scales increase, tracer data becomes more diffusive - portraying a time-averaged representation of the sediment movement. In this respect, Madsen (1987) describes tracers as providing important information about the gross features of the sediment transport system.

8.3.1 The present study

At New Plymouth, New Zealand (Fig. 8.1), tracing experiments were conducted to investigate littoral transport near Port Taranaki. The port breakwaters extend into the nearshore littoral zone, and a regular maintenance dredging programme is required to keep the port and shipping channel operational. For the last 100 years, the dredged harbour sediments have been dumped approximately 1 km offshore in a zone that is hydrodynamically isolated from the adjacent coastline (Black & McComb, 2000) in depths of 16-28 m. A consequence of this procedure has been the loss of beach sand along much of the foreshore of New Plymouth City (Fig. 8.1), resulting in coastal erosion.

This coast has a high-energy wave climate (McComb *et al.*, 1997; 1999b) with areas of protruding rocky reefs and intervening sand (Fig. 8.2). These combine to create complex and variable coastal dynamics. Sedimentation rates within the port are 174,000 $m^3.yr^{-1}$(McComb & Black, 2000) and the direction of net littoral drift is to the northeast (Fig. 8.1). Key aims of the tracing study reported here were to investigate the sediment entrapment/bypassing of a port entrance, and to monitor sediment movement from an experimental nearshore dredged-sand dump mound (47,000 m^3). The tracing experiments were an integral part of a wider field measurement programme using wave and current meters, sediment traps and hydrographic surveys described by McComb *et al.* (1999b). The specific aims of that work were: i) to re-introduce dredged sediments within the nearshore littoral system; ii) to prevent re-circulation of those sediments back into the harbour, and iii) to prevent the dumped sediments from inundating rocky intertidal habitats used for shellfish gathering immediately adjacent (east) of the harbour.

Submerged topographic features, such as ridges and channels, are known to influence circulation and sediment transport patterns even on sandy coasts (e.g. Slinn *et al.*, 2000), although the effect of such bed topography in a rocky environment is not well understood. Storlazzi & Field (2000) suggest that rocky, shore-normal reefs present a significant barrier to longshore sediment transport, and their morphological scale defines the spatial distribution of the nearshore sandy sediments. The latter has also been observed at New Plymouth, where sand patches are commonly found in the seabed

depressions or relict fluvial channels (McComb *et al.*, 1999b). Tait & Revenaugh (1998) report that a rocky subtidal topography may steer bottom currents, enhance turbulent shear stress at the bed, trap sediments, and fractionate sediments by grain size during transport. However, very little experimental data exists to confirm these effects, and littoral transport pathways and processes are often only inferred from the sediment characteristics (e.g. Cacchione & Drake, 1990; Tait & Revenaugh, 1998). The tracer observations reported here present a unique insight to sediment transport on predominantly rocky coasts and also the effectiveness of sediment tracing over reasonably large temporal and spatial scales within a complex environment. Tracer is also used to identify the main sediment transport pathways near the harbour entrance; clarifying the mechanisms that cause the characteristic patterns of accretion within the harbour, and illustrating the effect of a protruding breakwater on the nearshore sediment and hydrodynamics.

8.4 Tracer theory

The movement of sediment tracer is frequently described in terms of the migration of the centre of mass, and the expansion of the area occupied by the tracer. The former indicates the flux of sediment transport in response to horizontal advective forces (e.g the net currents and the wave-orbital asymmetry), while the latter reflects the spread of the tracer into the surrounding environment, which is due to horizontal diffusion and advection by currents (Miller & Komar, 1979). The Lagrangian *Spatial Integration Method* (*SIM*) (Komar & Inman, 1970; Madsen, 1987) allows the movement of the tracer centroid to be monitored in terms of the distance (Y) from the release point, given by:

$$Y = \frac{\sum_{i=1}^{N} dC}{\sum_{i=1}^{N} C}, \qquad \text{Eqn. 8-1}$$

where d = the distance from the tracer centroid, C is the measured concentration of tracer, i is the sample number and N = number of samples (assuming that N samples accounts for entire spatial distribution of tracer). The centroid velocity (U_c) is taken to represent the average particle velocity (Madsen, 1987), and is given by

$$U_C = \frac{Y_2 - Y_1}{t_2 - t_1} \qquad \text{Eqn. 8-2}$$

where (t_1 - t_2) is the time between surveys. The distance Y may also be described in terms of the orthogonal longshore and cross-shore vectors. The SIM method is best suited to environments where advection dominates over diffusion and vertical mixing (i.e. burial).

Similar to Eqn. 8-1, the spreading of the tracer may be related to the area of seabed occupied by the tracer. The relative area (A), weighted to the tracer concentration, is expressed as;

$$A = \frac{\sum_{i=1}^{N} d^2 C}{\sum_{i=1}^{N} C}, \qquad \text{Eqn. 8-3}$$

and comparison between sampling surveys will estimate the spreading of the tracer (K) as;

$$K_h = \frac{A_2 - A_1}{t_2 - t_1}, \qquad \text{Eqn. 8-4}$$

which has SI units of m^2s^{-1}. K_h is an empirical coefficient that describes the spreading of the tracer by advective and diffusive mechanisms. The accuracy with which these two methods describe the tracer behaviour is limited by the spread and density of the tracer sampling, as well as elements of the coastal morphology (e.g. coastal structures or strong sediment transport gradients). An Eulerian approach that complements the *SIM* is the *Time Integration Method* (*TIM*), whereby the tracer concentration at a given point (often "downstream" of the release) is monitored over time. A mass balance argument can be used with this method to estimate transport rates, assuming steady-state flow conditions and no loss of tracer from the system (Madsen, 1987). The initial dispersal of the tracer within the layer of mobile bed sediments (i.e. the transport thickness; White & Inman, 1989) is an important consideration for calculating sediment transport rates, and White (1998) provides a review of various methods for deriving this thickness.

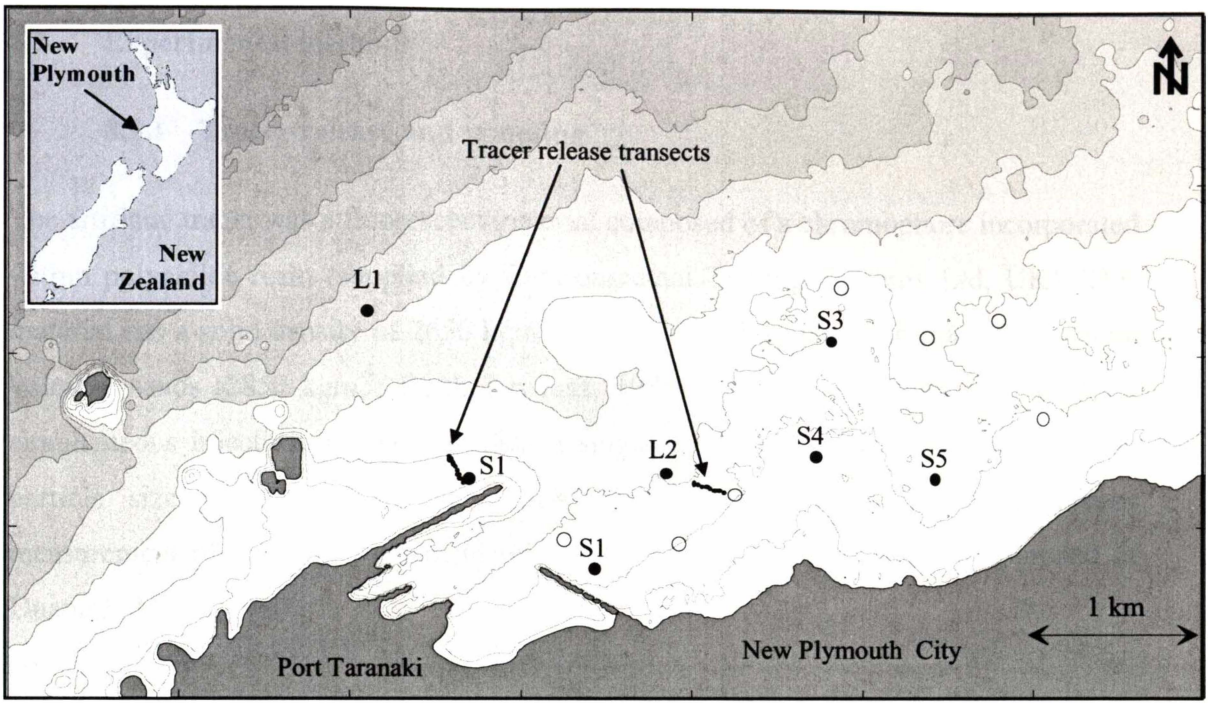

Figure 8.1: Experimental location map (5 m isobaths), showing the position of red and yellow tracer release transects, labelled directional wave/current meters (closed circles) and non-directional wave meters (open circles).

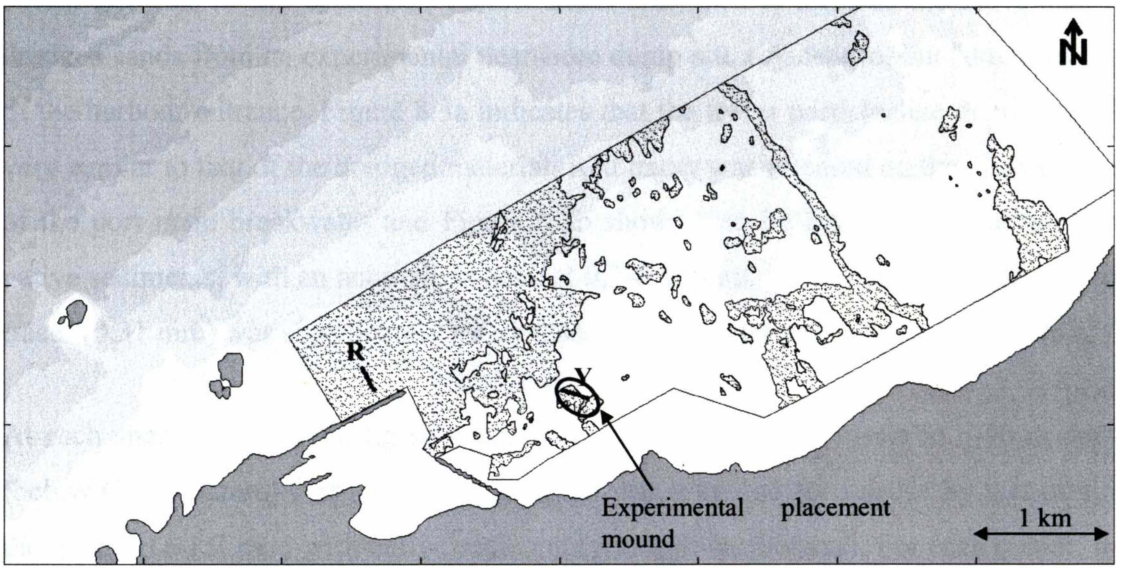

Figure 8.2: Map showing areas of sandy (shaded) and rocky (unshaded) seabed as determined by side-scan sonar. Release transects are given for the red (R) and yellow (Y) tracers, as well as the experimental nearshore placement of 47,000 m^3 dredged sand.

8.5 Experimental methods

8.5.1 Tracer release and sampling

The artificial tracer was a fluorescent material composed of a chromophore incorporated within polyamide resin (supplied by Environmental Tracing Systems Ltd, UK). This material has a solid density of 2650 kgm^{-3}, which is slightly less than that of the native volcanic sands (2850 kgm^{-3}; Bartholomeusz, 1985). Two colours were employed for simultaneous injection. Instead of using a single representative particle size, a tracer particle size range was applied which would thereby allow the simultaneous measurement of tracer movement in relation to grain size (similar to the approach of Duane & James, 1980).

The tracer was manufactured with an equivalent particle size distribution (assuming quartz spheres) based on the settling velocity of the native sediment from each release site. Figures 8.3a and 8.3b show the tracer particle size distribution for each tracer colour with the *in situ* sediment. Yellow tracer was used to monitor the movement of dredged sands from an experimental nearshore dump site adjacent to, but "downstream" of the harbour entrance. Figure 8.3a indicates that the tracer particle size distribution is very similar to that of the dredged material. Red tracer was released on the seaward side of the port main breakwater and Figure 8.3b shows it to be less representative of the native sediments, with an anomalous peak at 0.3-0.35 mm. Thus, the median size of red tracer (0.31 mm) was significantly larger than that of the native sediment (0.22 mm).

At each site, a total of 100 kg of tracer was released along a transect in 6-10 m depth (below Chart Datum) (Fig. 8.1). The material was prepared for release by wet mixing the tracer in a 1:2 ratio with native sediment (plus anti-surfactants). For each colour, the wet mixture was divided into eight portions, frozen to -40 °C, and sealed in plastic sacks. After positioning along the release transects (Fig.8.1) in holes deep enough to bring the frozen blocks level with the surrounding seabed, the sacks were opened by SCUBA divers. This burial technique provided an initial dispersal (or vertical mixing) of the tracer within the upper layer of mobile sediments.

Post-release, 1179 surficial sediment samples (~500 cm^3) were collected using a van Veen style grab (Fig. 8.4a) at sandy sites, and by towing a flared-pipe (Fig. 8.4b) over the sand/rock substrates. Low-tide beach samples were obtained by hand, and SCUBA divers were used to collect interstitial samples from areas of rocky reef. A total of 11 sampling surveys were undertaken over 308 days, and the sampling region boundary was sequentially adjusted in an attempt to extend beyond sites where tracer was found as the monitoring progressed. New site selection was aided by preliminary analysis of sediment samples using visual inspection under UV irradiation. The location of the sampling sites is shown on Figure 8.5.

8.5.2 Sample analysis

The detailed assessment of methods for detecting the artificial fluorescent tracer within the sediment samples has been the subject of a separate study by Forsyth (2000). Three analysis methods were applied to the sediment samples which were visual inspection, computer-based image analysis and spectrofluorimetry.

Visual inspection

Visual assessment of the samples was used to determine approximate tracer concentrations in order to extend the sampling region boundary as the monitoring progressed. This analysis was carried out by irradiating the samples with a broad spectrum UV lamp in a darkened room. Each sample bag (~500 cm^3) was assessed for approximately one minute by rotating and manipulating the plastic sample bag to sort through the sediment and reveal tracer grains. The number and colour of tracer grains was recorded. It should be noted that this method was not scientifically rigorous, with the analysis conducted primarily to provide feedback during the monitoring period.

Computer-based image analysis

Image analysis uses the known number of pixels in an image, within a field of view of a known size, to accurately count and measure the size of objects. Image capture and processing were accomplished using a video camera connected to a PC with specialised software. A full and detailed description of the calibration and validation procedures

undertaken during the development of the image analysis system is given by Forsyth (2000).

A small (<1 g) weighed sub-sample of sediment was fixed to adhesive tape on cards and irradiated with a broad-spectrum ultra violet (UV) light to excite the chromophore. The software counted and measured individual grains of sizes >80 μm. Three sub-samples were analysed from each sediment sample and mean values derived. This technique allowed results to be divided into specific grain size categories for each tracer colour, specifically; <120 μm, 120-200 μm, 200-300 μm and >300 μm.

Spectrofluorimetric analysis

Spectrofluorimetry was used in conjunction with the image analysis as it allowed for larger samples to be analysed (i.e. 30-50 g). Firstly, magnetic particles within the samples comprised some 70% by mass, and this fraction was removed with an isodynamic magnetic separator. This process both reduced the sample volume, and lowered the natural background luminescence. The remaining sample was then crushed in a ring-mill and washed in acetone (for one hour) to dissolve the luminophores.

A fluorimeter was used to measure the luminescence of the acetone solution, after irradiating with the known excitation frequencies for each tracer colour. The yellow and red tracer had excitation peaks of 440 nm and 627 nm, respectively. Full details of the calibration procedures employed are reported by Forsyth (2000). Forsyth also notes that the resultant luminescence is proportional to the total grain volume of tracer in the sample, not the number of individual grains.

Ultimately the two complementary techniques of video and dissolution provided a highly-sensitive detection system along with a method for enumerating the grain size fractions. Spectrofluorimetric analysis proved to be a highly sensitive method, with the ability to detect very small concentrations of tracer within a solution. Accordingly, the results provided by this method are mostly used in preference to the imaging method, although the combination of both is informative.

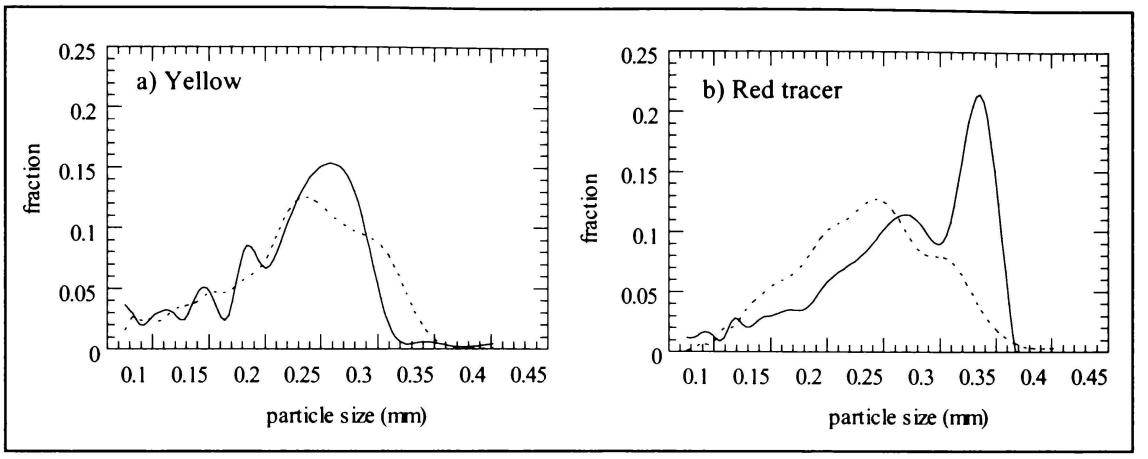

Figure 8.3: Particle size distributions for tracer (solid line) and native sediment (dashed), as determined by fall velocity analysis.

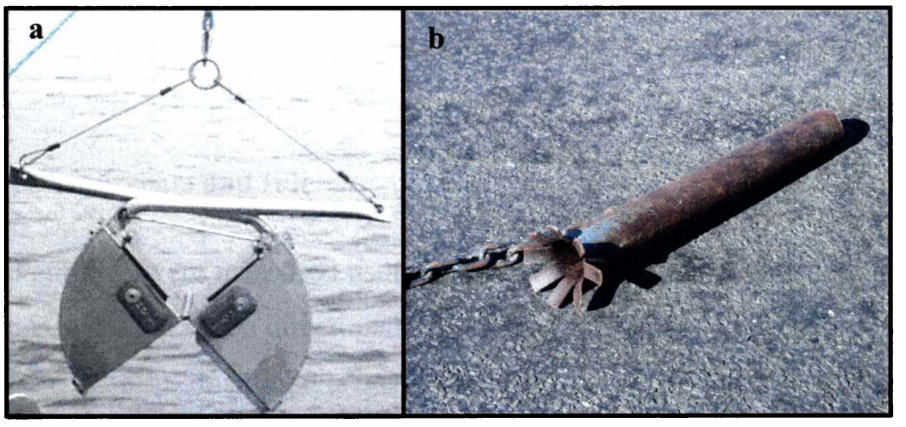

Figure 8.4: Surficial sediment sampling devices; van Veen grab (a) and flared pipe (b).

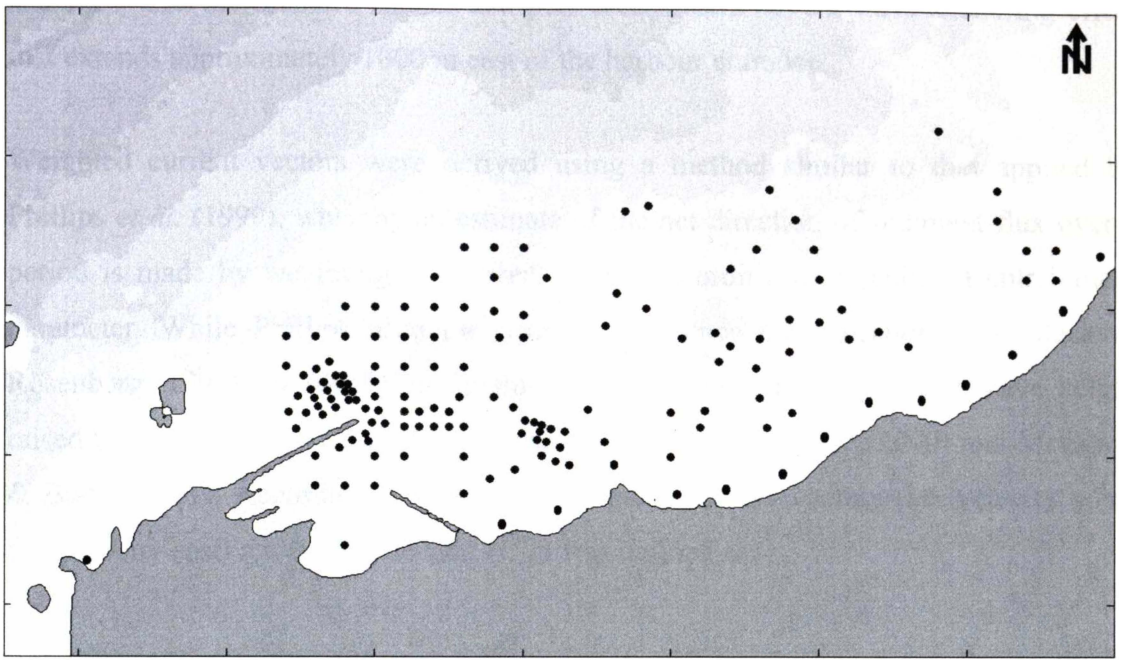

Figure 8.5: The surficial sediment sampling sites.

8.6 Waves, currents and tide

Waves and currents were measured using a suite of instruments distributed through the study region, including seven directional wave/current meters and seven non-directional wave meters (Fig. 8.1). Instruments were deployed for one year at two of the sites, and the remainder for an intensive two-month period from the tracer release time. Instruments were synchronised to record data at 2 Hz in 9-18 minute bursts every 373 minutes (i.e. half the tidal phase) in the first 2 months and subsequently at 6 hourly intervals. Further details of the full field programme are given by McComb *et al.* (1999b). Tides at New Plymouth are mixed semi-diurnal, with a spring tidal range of 3.1 m and a neap range of 1.7 m

Directional wave statistics and burst-averaged currents were extracted from the raw time-series data using the methods described by McComb *et al.* (2001). The time-series of significant wave heights measured at site L1 (Fig. 8.1) over the first 49 days following tracer release is given in Figure 8.6, showing wave heights up to 4.2 m (average 1.54 m). The spatial patterns of wave energy are illustrated by normalising the nearshore wave data with an offshore reference condition (e.g. site L1; Fig. 8.1). Mean wave height ratios and wave directions (Fig. 8.7) show higher ratios in deeper water,

and show that the offshore islands and port breakwaters have a wave-sheltering effect that extends approximately 1800 m east of the harbour entrance.

Weighted current vectors were derived using a method similar to that applied by Phillips *et al.* (1999), whereby an estimate of the net direction of sediment flux over a period is made by weighting the current vector according to a sediment entrainment parameter. While Phillips used the near-bed reference concentration (e.g. Black & Rosenberg, 1991) for weighting, in this study we apply the significant wave height raised to the 3rd power (H_s^3) following the applications of Howse (2000) and McComb & Black (2001). Accordingly, from the orthogonal current vectors (i.e. velocity north and velocity east) a weighted current (U_{Hs}) was defined as;

$$U_{Hs} = \frac{\sum_{i=1}^{N} U_i H_s^{\,3}}{\sum_{i=1}^{N} H_s^{\,3}} \qquad \text{Eqn. 8-5}$$

where U_i = burst-averaged current, i is the burst number and N = number of recording bursts.

Nearshore flows at New Plymouth have three main components; i) wind-driven, ii) wave-driven, and iii) shelf-driven currents, with the latter two being of most importance (McComb & Black, 2000). The shelf-driven currents represent the impingement of shelf flows into the nearshore zone and are strongly influenced by local bathymetric features. At New Plymouth the shelf flows are predominantly alongshore (i.e. parabathic) and exhibit approximately equal up- and down-coast occurrences. Combined with the complex nearshore bathymetry, these factors result in a highly variable, non-seasonal nearshore circulation system with frequent reversals in current directions. Weighted currents (U_{Hs}) from 6 nearshore sites shown on Figure 8.8, indicating the likely sediment vectors over the first 49 days from tracer release.

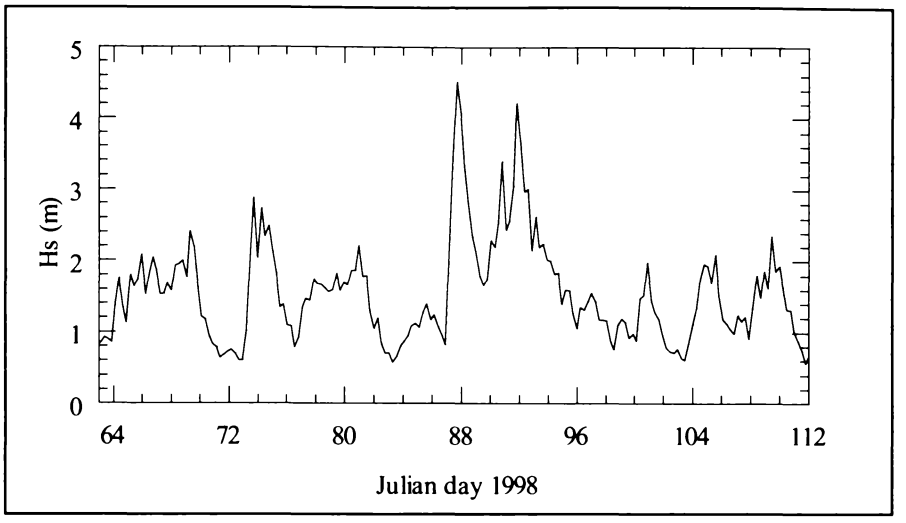

Figure 8.6: Time-series of significant wave heights (H_s) measured at the furthermost offshore wave meter (site L1; Fig. 1) over the first 49 days following tracer release

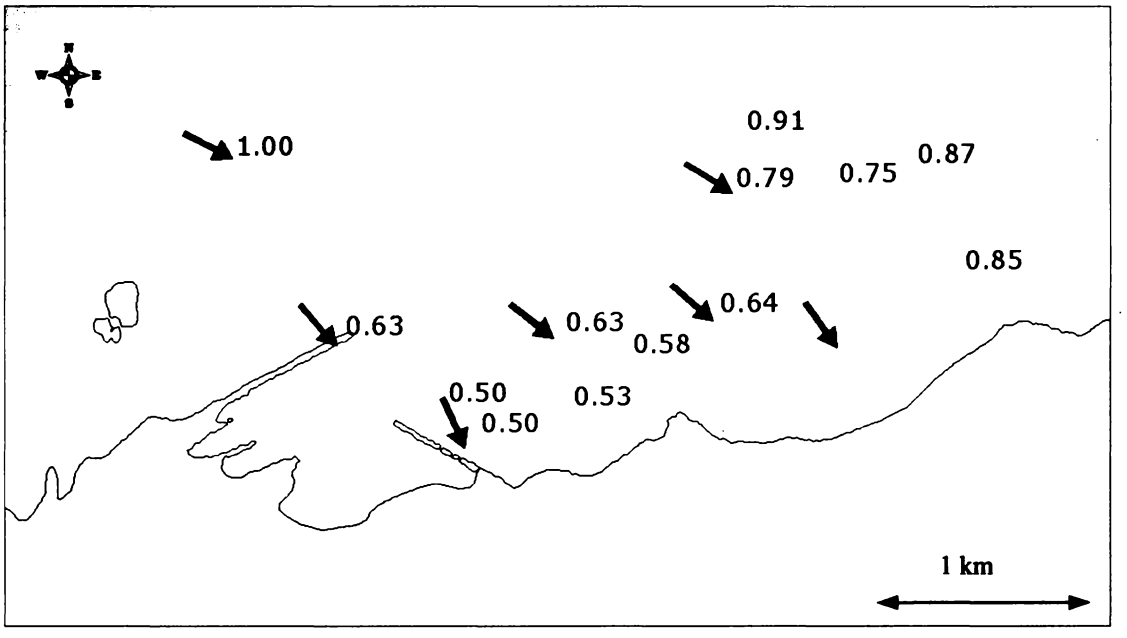

Figure 8.7: The averaged wave height ratio (nearshore/offshore), and average direction of wave advance.

Numerical models of the hydrodynamics at New Plymouth were established by Black & McComb (2000) using a suite of models including WBEND (Black & Rosenberg, 1992b), 3DD (Black, 1995) and POL3DD (Black *et. al.*, 1999), with calibration and validation from field data. In this paper, the model outputs of the circulation patterns are used to supplement the current meter data, and to show the time-averaged flows. The mean circulation patterns from a numerical simulation of an energetic 13-day period (i.e. Julian days 83 - 95, 1998; Fig. 8.6) is given in Figure 8.9.

Several flow trends are apparent from these data (Figs. 8.8 & 8.9). Firstly, strong easterly flows are common along the main port breakwater, which is likely to be feeding sediment towards the tip-shoal region of the harbour. The flow extends across the harbour entrance channel towards site S3 (Figs. 8.1 and 8.9). In the nearshore lee of the harbour, currents are much weaker (i.e. < 15 cms^{-1}) and of variable directions. The model studies of Black & McComb (2000) suggest this sheltered region often has a clockwise rotating gyre. Along the axis of the protruding shore-normal Kawaroa Reef (between sites S4 and S3), the numerical model shows a relatively strong easterly flow, compared to the flows either side of the reef. Consistent with this, the mean currents recorded at S3 and S4 (4.3 and 5.1 cms^{-1}, respectively) were higher than the adjacent sites L2 and S5 (2.7 and 1.5 cms^{-1}, respectively).

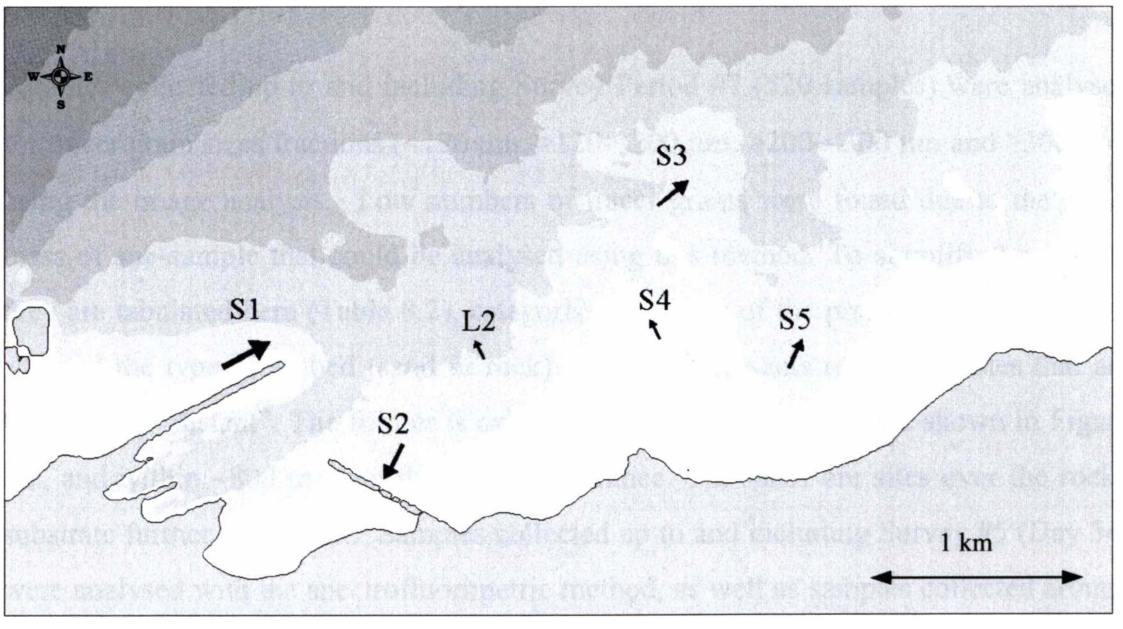

Figure 8.8: Weighted currents (from Table 8.3) presented as scaled vectors.

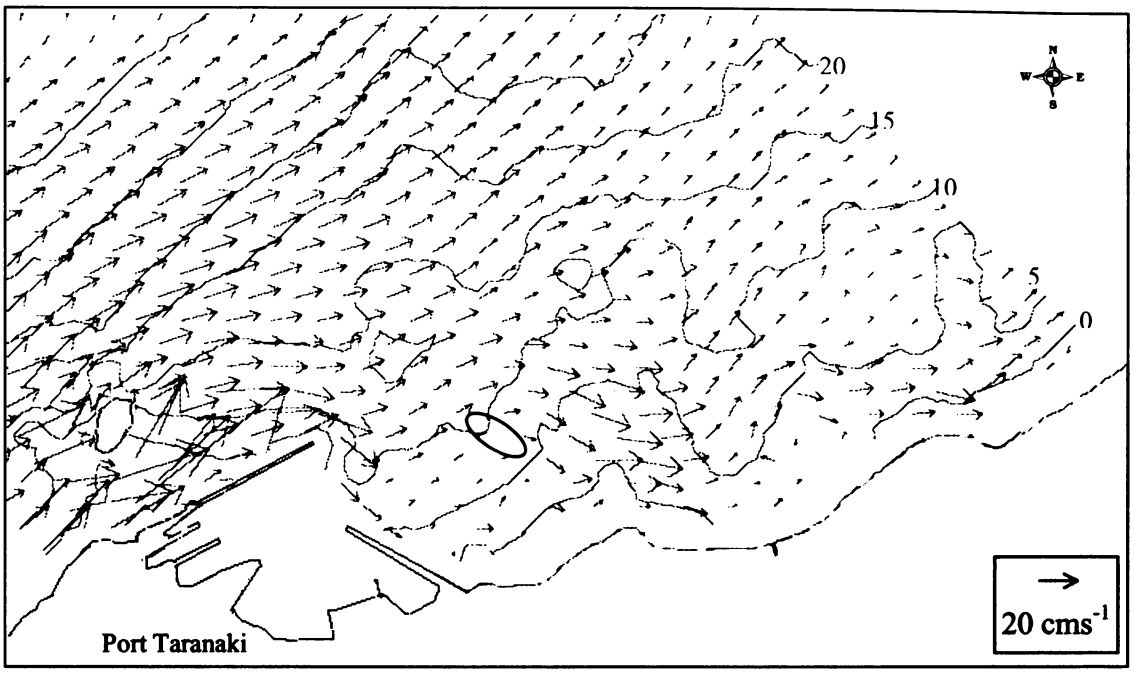

Figure 8.9: Numerical circulation model of the vertically-averaged currents from an energetic 13-day period (adapted from Black & McComb, 2000), showing Port Taranaki and the location of the dumped-sand mound (red).

8.7 Tracer movements

Surficial sampling for tracer commenced four days after the tracer release on 5 March 1998. A total of 11 sampling surveys were conducted over the following 304 days, resulting in 1179 samples from 253 sites (Fig. 8.5, Table 8.1).

Samples collected up to and including Survey Period #7 (520 samples) were analysed for tracer grain sizes fractions (<120 μm, >120-<200 μm, >200-<300 μm and >300 μm) using the image analysis. Low numbers of tracer grains were found due to the small mass of sub-sample that could be analysed using this method. To simplify the results, they are tabulated here (Table 8.2), categorised in terms of the proximity to the release site and the type of seabed (sand or rock). Table 8.2 presents results for sites that are "close" and "distant". The former is on the contiguous sandy substrate shown in Figure 8.2, and within ~800 m from the harbour entrance. The latter are sites over the rocky substrate further to the east. Samples collected up to and including Survey #5 (Day 34) were analysed with the spectrofluorimetric method, as well as samples collected around the yellow tracer release site in Survey #6 (Day 49) – a total of 315 samples.

Table 8.1: Number of samples taken on each of 11 sampling periods through the tracer experiment.

Sample Period	Date	Days Since Release	Number of Samples Obtained
1	8-3-98	4	38
2	14-3-98	11	39
3	17-3-98	13	38
4	22-3-98	18	70
5	8-4-98	34	105
6	23-4-98	49	127
7	19-5-98	75	103
8	6-7-98	124	161
9	13-8-98	161	163
10	28-9-98	207	158
11	6-1-99	308	176

Table 8.2: Total number of grains found in each of the four size fractions during each survey period (1-7). The data are grouped as "close" and "distant" to represent the proximity to the harbour entrance (i.e. within 800 m). This also approximates a morphological boundary, where the contiguous sand body near the harbour is "close", and "distant" is the heterogeneous substrate to the east (e.g. Fig. 8.2).

	Red tracer		Yellow tracer	
Survey	Grains "close"	Grains "distant"	Grains "close"	Grains "distant"
<120 μm size fraction				
1	17	1	3	
2/3	11	3	6	
4	11		4	
5			9	
6	3		18	1
7			5	1
120 - 200 μm size fraction				
1	1		3	
2/3	8		1	
4	1			
5			7	
6	1	1	4	1
7			2	1
200 - 300 μm size fraction				
1	3		3	
2/3			2	
4			1	
5			4	
6			1	1
7			6	1
>300μm size fraction				
1	2		1	
2/3				
4	2		2	
5			1	
6	2			
7			2	

8.7.1 After 13 days (Surveys #2/3)

Red tracer was found near the release site, but also in even higher concentrations on the other side of the harbour (to the east), near and inshore of the yellow release transect (Fig. 8.10). Yellow tracer was found near and shoreward of the release, as well as in significant concentrations in the red release area. Within the harbour, both red and yellow tracer were detected at one site on the inner breakwater shoal. Both red and yellow tracers were also observed in beach samples 4.5 km to the east of the harbour.

The sea conditions over this 13-day period were moderate, with offshore significant wave heights reaching 2.7 m (average of 1.49 m). Currents measured at sites S1 and S3 both show the initial three days had flows directed west, followed by a series of reversals and then a predominantly easterly flow over last four days. Mean velocities at sites S1, S3 and L2 were 6.5 cms^{-1}, 4.5 cms^{-1}, and 2.6 cm^{-1}, respectively.

8.7.2 After 18 days (Survey #4)

Survey #4 data (Fig. 8.11) show a similar pattern to that of Surveys #2/3 - an expected outcome over the reasonably calm intervening five days between surveys. The survey boundaries were extended slightly, and data further confirm an exchange between the two release sites. No tracer was observed within the harbour.

8.7.3 After 34 days (Survey #5)

Survey #5 involved 108 samples collected 34 days after release (Fig. 8.12) As with surveys 2/3 and 4, red tracer was again noted on the eastern beaches, some 4.5 km distant from the release, with several intermediate observations on that pathway. Both red and yellow tracer were detected on the beach to the west of the port headland. While no red was observed within the harbour, considerable amounts of yellow were found throughout the surveyed region, including inside the harbour on the breakwater tip-shoal.

Between Survey #4 and this survey, wave conditions were very energetic, with offshore H_s reaching 4.5 m. The predominant current vectors at sites S1 and S3 were directed to the east, and were particularly strong during the high wave events (up to 57 cms^{-1} at site

S1). Circulation patterns in the region of the yellow release site (sites L2, S2 and S4) were considerably less coherent, showing no definite vector (with the exception of S4 which exhibited strong easterly wave-driven flows). As with the previous surveys, the highest tracer concentrations for red and yellow were found adjacent to the initial release transect, which indicates the buried tracer was still releasing material.

8.7.4 Subsequent surveys (49-308 days after release)

While only the samples collected up to Survey #5 (and part of Survey #6) were analysed with the spectrofluorimetric method, all 1,179 samples from the 11 surveys were visually scrutinised under UV irradiation. Those results remain generally consistent with the quantitative methods, although they had much less sensitivity in detecting the finer particles. Nonetheless, two main migration trends emerged from these qualitative results over the surveys 6-11. Firstly, the yellow tracer was observed to move greater distances from the release site (compared to the red tracer), dispersing in an easterly longshore direction and staying mostly within the 3-8 m depth range. The red tracer also displayed a net easterly vector, but with a broader cross-shore distribution, transgressing the harbour entrance toward the yellow release site, as well as moving offshore to depths of 14 m. By the last two survey periods (207 and 308 days after release), very little tracer was observed, and only at sites relatively close (i.e. within 800 m) of the release sites for both colours. The results of visual sample inspection from Survey #9 are given in Figure 8.13, clearly showing the longshore trend after 161 days.

Table 8.3: Vector-averaged currents over the first 49 days following tracer release. Weighted currents apply the significant wave height raised to the third power (Eqn. 8-1).

Site	Speed (cms^{-1})	Direction (deg)	Weighted speed (cms^{-1})	Weighted direction (deg)
L2	5.05	106.08	0.78	334.09
S1	1.65	50.40	5.29	61.74
S2	1.43	183.58	3.24	208.63
S3	1.61	45.17	3.23	50.15
S4	0.93	334.42	0.83	331.47
S5	0.90	6.23	2.22	24.71

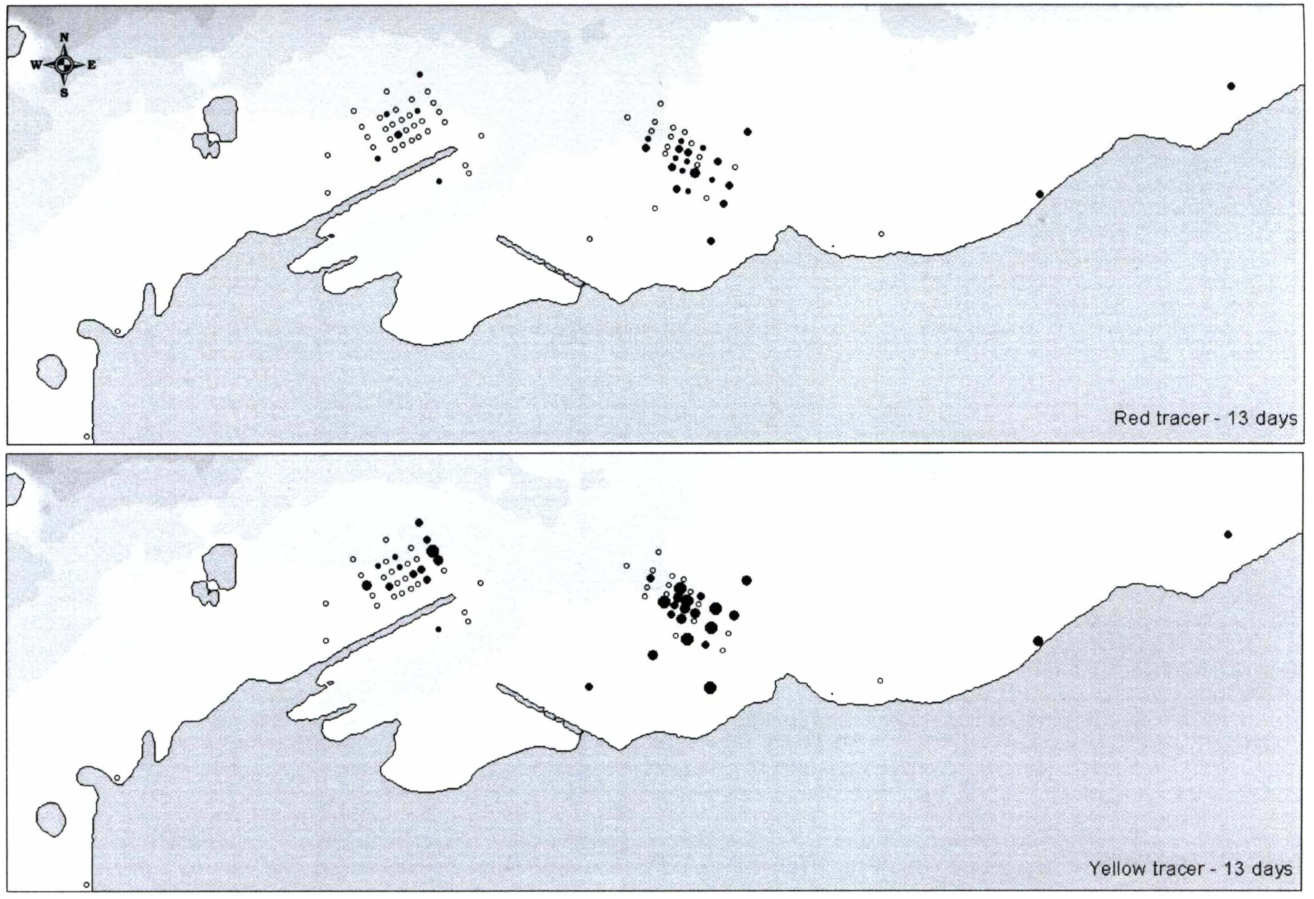

Figure 8.10: Spectrofluorimetric tracer results for samples collected 11 and 13 days after release. Closed circles are scaled to represent the square-root of the measured concentration. Open circles indicate where no tracer was found.

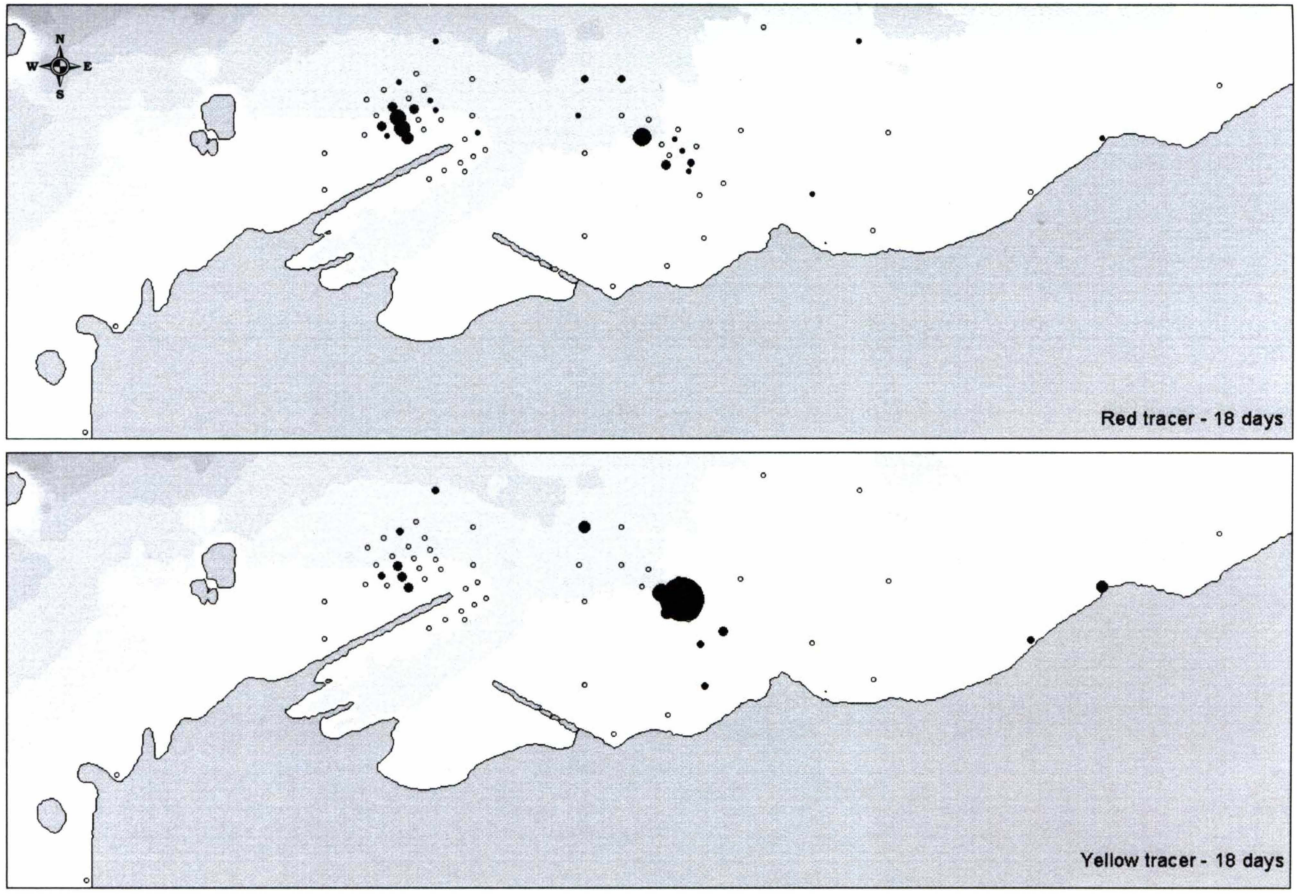

Figure 8.11: Spectrofluorimetric tracer results for samples collected 18 days after release. Closed circles are scaled to represent the square-root of the measured concentration. Open circles indicate where no tracer was found.

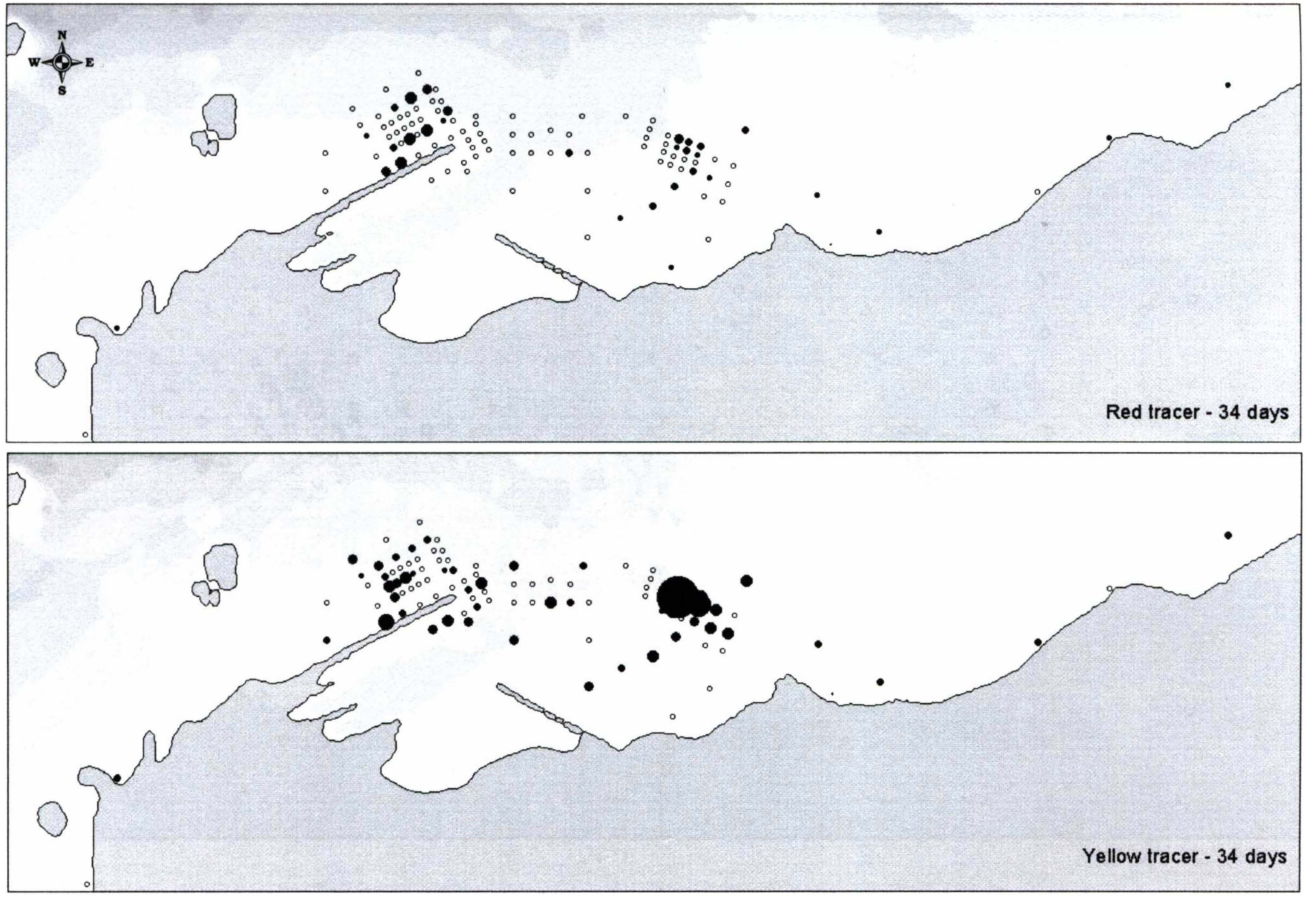

Figure 8.12: Spectrofluorimetric tracer results for samples collected 34 days after release. Closed circles are scaled to represent the square-root of the measured concentration. Open circles indicate where no tracer was found.

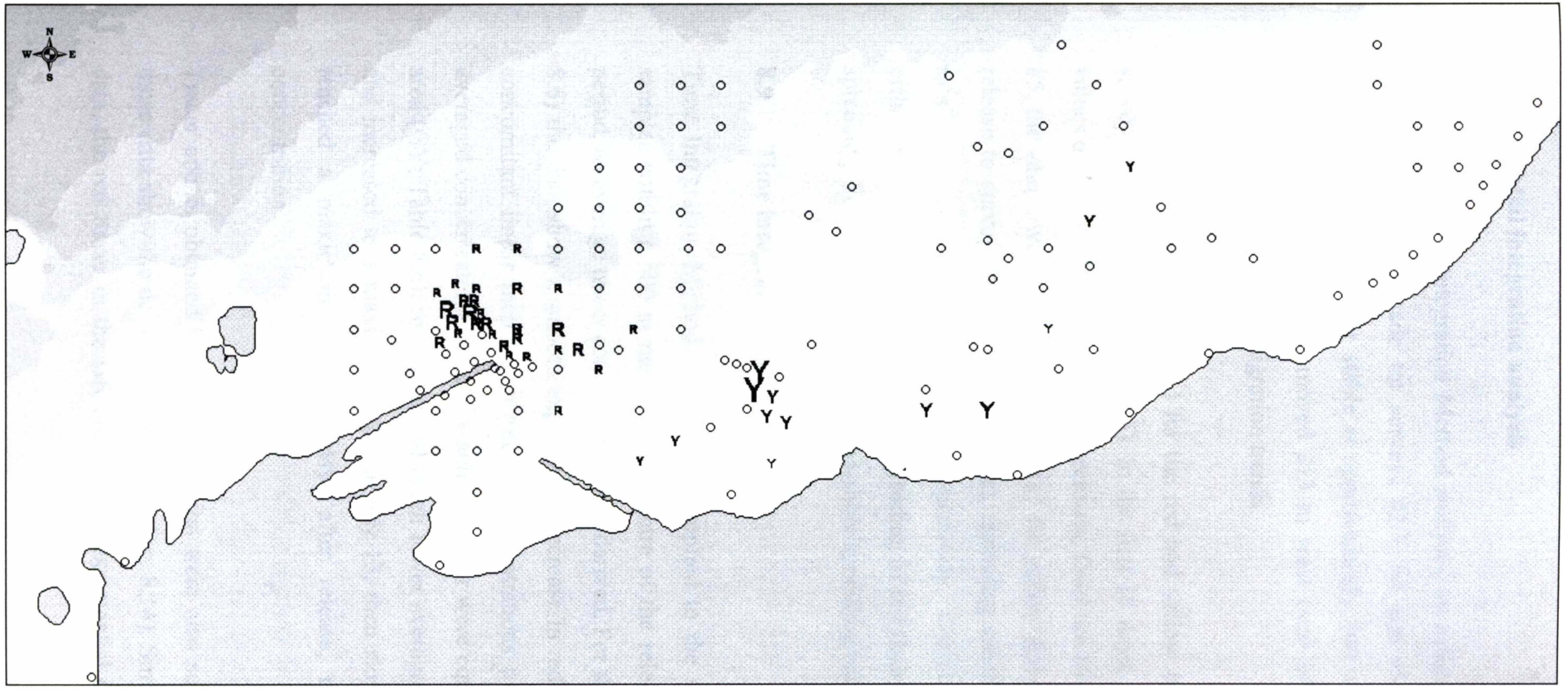

Figure 8.13: Visual observations of tracer (under UV light) for samples collected 161 days after release. Red (R) and yellow (Y) tracer data are linearly scaled to represent numbers found. Open circles indicate where no tracer was found.

8.8 Spatial integration analysis

Using the Spatial Integration Method analysis, an estimation of the migration of the centre-of-mass was made for surveys #2/3, #4 and #5 (Table 8.4). The red tracer centroid was found to be stable at approximately 500 m east of the release transect, while the yellow centroid moved 213 m west over 34 days. Both tracer centroids showed little cross-shore migration trends.

The spreading coefficient (K_h) for the red and yellow tracer was estimated from the survey #4 and #5 data (Table 8.5). In the first 18 days, yellow and red tracer had K_h values of 0.095 and 0.288 m^2s^{-1}, respectively. Over the 16 days between surveys # 4 and #5, the values were 0.129 and 0.11 m^2s^{-1} for yellow and red. For the total period from release to survey #5 (the first 34 days), spreading coefficients were 0.111 and 0.204 m^2s^{-1} for yellow and red tracer, respectively. Comparing the spreading rates in orthogonal vectors, the cross-shore spreading of red tracer was 6.22% of the longshore spreading. For the yellow tracer, cross-shore spreading was 2.82% of longshore values.

8.9 Time integration analysis

Time Integration Method analysis was applied to the spectrofluorimetric data from samples within a 500 m radius of the centre of the release transect. For each survey period, an average tracer concentration was derived. For the red release area (GR; Table 8.6) the data show a smooth exponential decrease in red tracer concentrations, with a concomitant linear increase in yellow concentrations over time. After 34 days, the averaged concentrations of yellow and red tracer were equivalent. In the yellow release area (GY; Table 8.6), red tracer had much lower averaged concentrations than yellow, and increased to a maximum value at day 13, then slowly decreased. Yellow tracer reached a maximum value 18 days after release, then gradually decreased in concentration.

Tracer counts obtained by visual detection were also subjected to *TIM* analysis, and those data show the decay over 308 days (Fig. 8.14). Similar to the spectrofluorimetric data, the red tracer in the GR area has an exponential decrease in counts over time.

However, the yellow tracer in the GY area displays a considerably different decay pattern; increasing to a maximum 75 days after release, and then slowly decreasing.

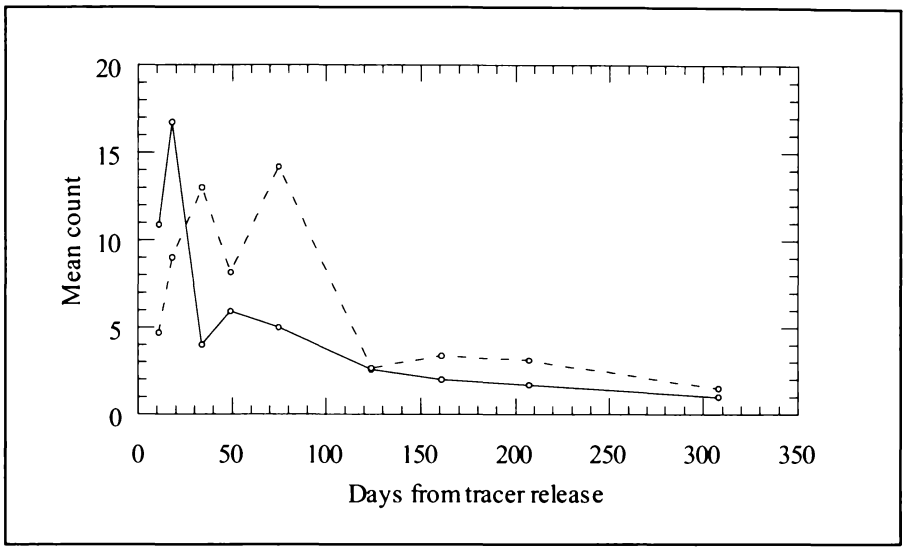

Figure 8.14: Time-series plot of the mean number of grains of red tracer (solid line) and yellow tracer (dashed line) from within a 500 m radius of the red and yellow release points. Data from visual inspection of the sediment samples under UV irradiation

8.10 Correlation of current and tracer data

The recorded currents from sites S1 and L2 provide a point source of information from within several hundred meters of the two tracer release transects, which may be usefully applied to consider how the currents at the release location are related to the observed tracer movements. The red release area has a well-defined current that flows parallel with the port breakwater, which is evident in the model output (Fig. 8.9) as well as the weighted current meter data (Fig. 8.8). This is also shown in Figure 8.15 with the data from site S1 over the period up to survey #5 (34 days) in terms of the current vectors. Individual tracer data from survey #5 are also given on this plot, expressed as a distance weighted by the concentration (Eqn. 8-1). The red tracer has a clear longshore vector to the east, which is similar to the S1 currents that run toward 071°. Comparison of the yellow tracer data and currents measured at site L2 (at the offshore limit of the yellow release transect) do not show similar vectors (Fig. 8.15). The westerly migration of the

centre of mass of tracer is not represented in the current meter data at all, even when those data are weighted to the wave height (Fig. 8.8).

Table 8.4: Position of the red and yellow tracer centroid relative to the release point (Y) over the first 34 days.

Survey	Y - yellow (m east)	Y - yellow (m north)	Y - red (m east)	Y - red (m north)
#2/3	19	-52.2	446.6	-25.3
#4	2.3	-8.4	515	11.8
#5	-214	-18.3	429.7	-42.1

Table 8.5: K_h spreading coefficients (Eqn. 4) for red and yellow tracer

Survey	K_h red (m^2s^{-1})	K_h yellow (m^2s^{-1})
0 - #4	0.288	0.095
#4 - #5	0.110	0.129
0 - #5	0.204	0.111

Table 8.6: Time series of the averaged tracer concentrations (ppb) for a 500 m radius surrounding the centre of the yellow (GY) and red (GR) tracer release transects

Survey	Days	GY zone (ppb)		GR zone (ppb)	
		red	yellow	red	yellow
#1	4	70.16	750.79	1422.35	3.19
#2/3	13	127.40	453.05	369.52	19.82
#4	18	100.76	890.48	128.53	21.8
#5	34	17.840	553.64	45.707	51.32
#6	49	7.82	322.64		

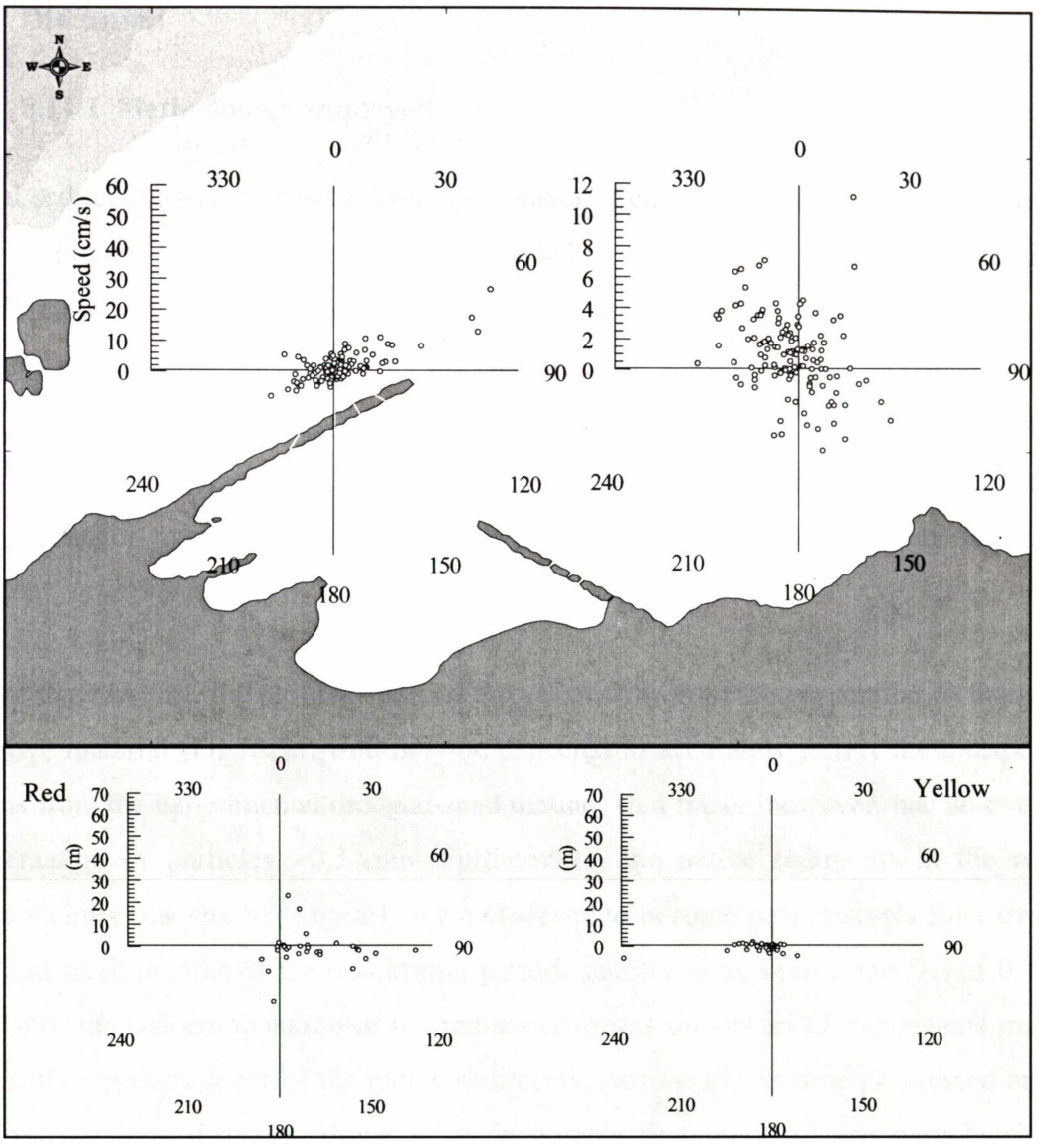

Figure 8.15: Currents and tracer movements over the first 34 days. Upper panel shows the directional current run from sites S1 and L2 (adjacent to the red and yellow release points, respectively). Lower panel shows the weighted tracer vector (derived using Eqn. 8-1) for data from survey #5.

8.11 Discussion

8.11.1 Methodology employed

Littoral sediment transport results from the transfer of energy from moving water to the sediment grains - whereby entrainment is related to the grain roughness skin-friction Shield's parameter ($\theta_{2.5}$). Several factors are important in this process, including the sediment particle size, shape and density, cohesion, bedforms and the near-bed fluid velocities (van Rijn, 1993; Nielsen, 1992). Grain-size dependency within the $\theta_{2.5}$ term means that small changes in grain size will affect whether a grain is "entrained" or "at rest". Thus for tracer particles, grain size matching to the native sediment is very important.

In these experiments, the particle sizes of the yellow tracer were very similar to that of the native material (Fig. 8.3a), and may be expected to accurately reflect the transport patterns from the experimental dredged-sand mound. Red tracer, however, had an over-representation of particles >0.3 mm. Furthermore, the native sediments in the red release vicinity (i.e. site S1; Fig. 8.1) were observed to become progressively finer over the initial three months of the monitoring period, stabilising at an average D_{50} of 0.18 mm. Thus, the size composition of the red tracer means the observed movements may not exactly represent those of the native sediments, particularly as time progressed and the finer fractions disperse. However, it is notable that much of the particle size distribution <0.3 mm is very similar (Fig. 8.3b), so that over the initial period (i.e. the first 34 days) the tracer movements would be very similar to the native sediments.

Of equal importance is the analysis methodology. While providing a very sensitive detection system, dissolution and spectrofluorimetric analysis does not include grain size information. Concentrations are related to both the number of tracer grains in a sample, and their volume. For example, one large grain (0.3 mm) would yield an equivalent concentration to 8 grains of 0.15 mm diameter. Combined with image analysis, enumeration is possible, although the small sample volumes used in that method both increase the sampling errors, and reduce the detection limits.

8.11.2 Advection, diffusion and dispersal

The observed tracer movements are the sum of horizontal advection and diffusion, and vertical mixing. The latter (vertical mixing of tracer within the transport thickness; Hanes, 1988) is not reported in this paper as it is assumed that surficial sampling provides a uniform representation of the tracer concentrations (with the exception of the sedimentary zones within the harbour). Furthermore, we are not applying mass balance calculations to the tracer data to estimate transport rates, which do require an understanding of dispersion (e.g. White, 1998). Such analyses are possible for studies with a regular sandy seabed, but at New Plymouth it was not possible to widely sample the interstitial sediments in the rocky areas, even without considering the energetic conditions and highly-mobile bed.

The advective process is characteristically Lagrangian, which is difficult to resolve with point-source data (e.g. from current meters or model outputs), especially with the spatial and temporal variability in circulation as found at New Plymouth. Nonetheless, the spatial distribution of red tracer was very similar to the measured current run data at the release site (Fig. 8.15), indicating the predominantly easterly-directed flows aligned with the breakwater are causing a net advection of those sediments to the east. The exponential decrease in the average red tracer concentration near the release site over time (Table 8.6; Fig. 8.14) is also indicative of the steady net transport of tracer from the release site. While a systematic centroid migration of the red tracer was not resolved (possibly due to strong advection gradients caused by the breakwater), the *TIM* data in Table 8.6 shows a maximum concentration of red tracer in the yellow release area 13 days after injection. This suggests an averaged longshore velocity of red tracer over the intervening distance of the order 0.15 cms^{-1}.

Yellow tracer did not show the steady exponential decrease in concentration over the initial 34 days as did the red tracer. The dumped sediments unbalance the local sedimentary equilibrium (McComb & Black, 2001), and it is likely that the action of "smoothing" of the mound isobaths following dumping resulted in a degree of tracer burial. Subsequent exposure of the tracer as the mound eroded is the probable cause of the variable averaged yellow concentrations (Table 8.6). In terms of advection, the current data from site L2 bears little resemblance to the yellow tracer movements (Fig.

8.15), which is an expected outcome for a region with considerable spatial and temporal variability in flow. Also, site L2 is at the offshore extremity of the dump mound, and does not necessarily represent the currents in the shallower regions. Indeed, the modelled currents near the dumpsite are more parabathic at 6 m than at 10 m (Black & McComb, 2000).

One clear result from the tracer is that sediments are frequently transported in both longshore directions. The reversals in direction are more apparent in the yellow tracer data than the red, possibly due to: i) the longshore extent of the sampling regime (i.e. fewer samples were collected west of the red release area), and ii) the headland morphology immediately west of the red release area and the associated salient to the offshore island (Fig. 8.1).

The rates of tracer spreading (Table 8.5) are estimated under the assumption that the sampling regime was sufficiently broad to define the extent of the tracer movement, and do not account for shoreline features such as the breakwater and harbour. These values represent the combined effect of spreading from diffusion and advection. Miller & Komar (1979) found that spreading rates under wave-orbital motion were proportional to the entrainment rate of the tracer, indicating that the wave-orbital excursion approximates the mixing length for horizontal turbulent diffusion (Madsen, 1987). Black & Gorman (submitted) suggest that such wave-induced horizontal diffusivities are likely to range between 0.1 to 10 m^2s^{-1} near the wave breakpoint, while Miller & Komar (1979) measured averaged values of 6.35 x 10^{-5} m^2s^{-1} in 16-18 m water depth. Indeed, the review of Riddle & Lewis (2000) notes that horizontal diffusivity coefficients for water bodies (not sediment) in a variety of coastal and estuarine sites were found to range from 0.003 to 0.42 m^2s^{-1} (median 0.05 m^2s^{-1}).

The diffusion of tracer (and sediment) is a function of the particle settling velocity, as well as the length and time scales of horizontal motion. Thus, on the wave-dominated coast at New Plymouth, it will occur at scales ranging from wave orbital excursions (i.e. metres), and perhaps extending to the spatial perturbations in longshore current flow due to the irregular bathymetry (i.e. 100s of metres). Accordingly, the cross-shore spreading rates for each tracer cannot be solely attributed to diffusion under wave

orbital motion. Furthermore, it is not possible to isolate the effects of cross-shore advection by currents in this consideration of diffusion.

8.11.3 Sediment transport along rocky coasts

Sampling for tracer was mostly limited to sites with sandy beds - including the small sandy pockets (e.g. 50 m in radius) within the rocky reef. A limited number of samples were also collected by SCUBA divers from rocky regions immediately east of the nearshore dumpsite (Surveys #5, #7, #9). Samples were also obtained from the rocky intertidal regions on each survey. It is interesting that the rocky reef areas often contained appreciable amounts of sand within the crannies and interstitial spaces. The presence of tracer within those samples, as well as on the beaches up to 4.5 km distant from the release point, shows that littoral sediments are able to cross the reefs and continue along the coast. Multiple side-scan surveys (McComb *et al.*, 1999b) have shown that these reefs have an enduring rocky character, while the tracer movements confirm the reefs are subject to a sediment flux, although they have low residency volumes. The irregular seabed topography does not appear to obstruct the longshore movement of littoral sediments, which are suspended by wave action and transported by coastal currents. This contrasts with the conclusions of Storlazzi & Field (2000) for nearshore transport on the Monterey Peninsula (California, U.S.A). In that high-energy wave climate, Storlazzi & Field consider that only the larger storms are capable of inducing longshore transport across bathymetric highs, which are of similar magnitude to those at New Plymouth (although the Monterey coastline is more indented). Here we have shown that a longshore flux occurs across the reefs even under moderate wave conditions, and our wider studies on this rocky coast (McComb *et al.*, 1999a, 1999b) confirm that the bedload transport of sediments is not significant, and the suspended form predominates. In a wave-dominated environment (e.g. Niedoroda *et al.*, 1984) it is perhaps of greater importance to consider the effect of shore-normal reefs and coastal indentations on the circulation patterns, rather than their direct potential for obstructing the longshore flux of sediments.

8.11.4 Sediment trapping/bypassing of the harbour

The ongoing accretion of littoral sediments in the Port Taranaki harbour (and associated offshore dumping operations) have undoubtedly influenced the "downdrift" nearshore sediment budgets. However, the red tracer data suggests that very little of the sediments from depths of greater than 6 m are trapped by the harbour. In a study of accretion on and around the Port Taranaki breakwater, McComb *et al.*, (1999a) identified wave refraction and wave penetration (into the harbour) as the dominant processes causing the characteristic sedimentation patterns on the tip-shoal. The manner of accretion is top-down deposition, in which shallow sediments "spill" into the harbour at the breakwater tip, and are then distributed along the inside of the breakwater by the refracting waves. This manner of accretion is similar to that observed at Caldera Port (Costa Rica) as reported by Rodoriguez & Katoh (1994). Red tracer released along the 6-10 m depth transect did not become trapped in the harbour, instead it showed a well-defined transport pathway past the harbour entrance to the east. While the high rates of sedimentation on the tip-shoal region (averaging 390 m^3 per day) will undoubtedly cause appreciable burial of any tracer deposited there, the sensitive detection methods we employed did find appreciable quantities of yellow tracer on the tip-shoal and in the harbour (e.g. Survey #5; Fig. 8.12).

Tip-shoal sedimentation accounts for approximately 75% of the maintenance dredging in the harbour, and it is likely that only the sediments from within ~100 m of the breakwater (i.e. depths of <6 m) are trapped on this shoal. Under most conditions, waves arrive obliquely to the breakwater (11° average), and the strong easterly flows measured at site S1 (particularly under large waves) are in agreement with the numerical simulations of currents near coastal structures given by Baquerizo & Losada (1998). Baquerizo & Losada also predict that the maximum sediment transport potential will be immediately adjacent to a breakwater under oblique wave attack. Given the strong flows along the breakwater, it is further likely that the volumes of sediment that accumulate at the tip of the breakwater are only a fraction of the flux within that <6 m depth range. This may be confirmed by the observation that sediments in the depositional areas of the tip-shoal are coarser than those immediately offshore of the breakwater (McComb *et al.*, 1999a), indicating that the sediments with lower settling velocities are less efficiently trapped on the tip-shoal.

Surveys #4 and #6 (18 and 49 days after release), show red tracer grains of > 0.3 mm at sites the east of the harbour entrance, up to 1200 m from the release point. This confirms that both the coarse and fine sediment fractions are able to bypass the harbour and cross the entrance channel. The mechanism for this bypassing is readily identified in the strong easterly flows along the breakwater (Figs. 8.8 and 8.9) and beyond. Inshore, and to the east of the harbour entrance (near site S2, Fig. 8.1), very little red tracer was found, which contrasts with the well-defined yellow tracer movements to that area. This is consistent with the deflection of sediments away from the "downdrift" lee of the harbour by the main breakwater orientation.

8.11.5 Nearshore sand dumping

The experimental nearshore dump mound introduced 47,000 m^3 of sand to a predominantly rocky environment (McComb & Black, in press), with the joint aim of testing the suitability of that area as a long-term placement ground, and understanding how a nearshore dump mound behaves under high-energy, rocky conditions. Douglass (1995) discusses a prediction methodology for nearshore dump mounds, based on the orbital velocity asymmetry of shoaling waves, with net flux derived using Bagnold's (1963) bed-load transport expressions. That model predicts the shoreward migration that is typically observed with nearshore dump mounds. However, previous studies on mound behaviour have only considered sandy environments with relatively uniform bathymetry.

The yellow tracer data indicates that spreading rates of the order 0.1 m^2s^{-1} were occurring. This is consistent with hydrographic monitoring the mound shape over 18 months (McComb & Black, in press), which shows a non-directional "smoothing" of the mound isobaths over time, and erosion of the dumped sediments in the suspended form. Coupled with the findings of yellow tracer on the distant eastern beaches within 13 days of release, the experiment indicates that diffusion and advection of suspended sediments is the primary mechanism of sediment transport from the mound.

The yellow tracer shows that while the dumped sediments exhibit a net easterly transport vector over the long-term (e.g. Fig. 8.13), the results from the first 34 days show a re-circulation mechanism in the region of the dumpsite - potentially trapping

sediments in the relatively quiescent lee of the harbour, and to a degree re-distributing them back into the harbour entrance (e.g. Fig. 8.12). The latter is represented in the slight westward migration of the centre-of-mass over the first 34 days from tracer release. This has the potential to cause sedimentation on the ecologically-sensitive rocky intertidal adjacent (east) of the harbour, as well as reducing the net longshore movement of the dumped sediments. Both these observations render this region as unsuitable for long-term dumping of dredged sediments.

8.12 Conclusions

A two-colour fluorescent tracing experiment was conducted over a 305-day period in a high-energy coastal environment, with complex seabed topography featuring both sandy and rocky beds. The experimental aims were twofold: i) to investigate sediment entrapment/bypassing of a harbour entrance, and ii) to investigate sediment transport from a 47,000 m^3 experimental nearshore dredged-sand mound "downstream" of that harbour. The two tracer release sites (one for each colour) were located on either side of the harbour entrance, 1400 m apart and along a 6-10 m depth transect. Tracer material was composed of a chromophore incorporated within polyamide resin, and manufactured with a particle size distribution based on the equivalent settling velocity of the *in-situ* sediment.

Monitoring of the tracer has clearly demonstrated that a net longshore sediment flux occurs over rocky, shore-normal reefs in water depths less than 15 m. The data suggest that the raised reefs do not present a significant impediment to longshore flux, but rather that the nearshore circulation patterns are the predominant influence on the transport vectors. Tracer was found on beaches 4.5 km distant from the release point within 13 days of injection. The experiment indicates that diffusion and advection of suspended sediments is the primary mechanism of sediment transport in this environment. Rates of tracer spreading were found to range from 0.095 to 0.288 m^2s^{-1}, which is consistent with a high-energy coastal environment.

A sediment pathway bypassing the harbour entrance channel was identified, and the tracer shows that only sediments very close to the harbour breakwater (i.e. within 100 m) are trapped at the harbour entrance. From the nearshore dump mound, the qualitative

long-term tracer results suggest a net longshore transport vector away from the port to the northeast, although the shorter-term centre-of-mass results indicate an opposing flux directed to and transgressing the harbour entrance.

8.13 Acknowledgements

Thanks to Jon Marsh from Environmental Tracing Systems (UK) for supplying the artificial tracer, as well as assisting in the experimental design and field operations for the tracer injection. Stuart Forsyth conducted the image and spectrofluorimetric analyses of sediment samples.

9 PREDICTING TIME-AVERAGED SUSPENDED SEDIMENT AND REFERENCE CONCENTRATIONS IN A HIGH-ENERGY, WAVE-DOMINATED ENVIRONMENT

9.1 Context of the paper within the thesis

Littoral transport on a wave-dominated coast is crucially dependent on the entrainment and suspension of the sediments. Similarly, the ability to quantify and predict the outcome of these processes is a vital component to understanding the dynamics of a littoral system. This paper addresses the knowledge shortfall regarding the entrainment and suspension of "black" volcanic sediments under high-energy wave conditions. Using coincident data from sediment traps and bottom-mounted wave/current meters (Chapter 2), the time-averaged near-bed reference concentration (C_o) is related to the wave-orbital induced stress on the seabed, and a methodology is established for predicting the suspended sediment reference concentration and profile. This paper has been submitted to Marine Geology (July, 2001) as:

McComb, P.J. and Black, K.P., (submitted). Predicting time-averaged suspended sediment and reference concentrations in a high-energy, wave-dominated environment.

9.2 Abstract

Multi-site field data from a high-energy environment were used in two commonly adopted expressions for predicting time-averaged near-bed sediment reference concentrations (C_o). These models relate C_o to the grain-roughness skin-friction ($\theta_{2.5}$), raised to the power of 3 (Nielsen, 1986) or 1.5 (van Rijn, 1984). Data were collected at an open-coast site over rocky and sandy beds, in a range of wave-orbital velocities including oscillatory sheet-flow conditions. Surficial sediments were of relatively dense andesitic volcanic origin, with wide range of median particle sizes. Time-averaged suspended sediment concentrations (SSC) were measured with calibrated sediment traps while wave-orbital velocities were recorded with bottom-mounted current meters.

The data show that C_o is best related to the excess skin friction raised to the power of 1.5 (van Rijn, 1984), and that the 3rd power in the Nielsen (1986) expression is likely to cause an over-prediction of C_o in high-energy conditions. Predictions using the van Rijn expression were further improved when the mean grain size was used in the sediment mobility term (Ψ) and the median grain size in the friction factor (f_w). Using this formulation, the van Rijn expression was found to be linearly correlated with the time-averaged SSC measured with sediment traps (R^2 = 0.91). The data also suggest that an asymptotic relationship between $\theta_{2.5}$ and C_o is likely under high-energy, sheet-flow conditions.

The scale of turbulent mixing (l_s) was found to increase linearly with elevation above the bed, with a gradient of 0.46. While close to the predicted clear water value of 0.4 (i.e. von Karman's constant, κ), the slightly steeper concentration profile is consistent with a vertical variation in mean grain size, as the suspended sediment data show a linear reduction in mean grain size with increasing elevation above bed.

The resolved suspended sediment concentration profile was applied to a pure-diffusion concentration model to reconcile C_o values (derived from current meter data) with SSC data (from sediment traps). A constant diffusivity/mixing length regime was employed in the near-bed region. The best agreement between measured and predicted SSC was found using a constant l_s of 0.1 m over the lower 0.2 m of the water column, above which l_s increased linearly with elevation above bed (at a gradient of 0.46). The

measured and predicted SSC were found to be highly correlated (R^2 =0.93, slope of 1.06) over a wide range of wave events.

9.3 Introduction

In quantifying the time-averaged suspended sediment loads under wave-dominated flow, it is usual to consider the amount of sediment in suspension, and the distribution of that material throughout the water column, as two separate, but linked processes. The near-bed reference concentration (C_o) relates to the first, describing the intensity of sediment suspension due to local entrainment, while the second is the product of advective/diffusive processes that characterise the vertical suspended sediment concentration (SSC) profile. Both are required for sediment transport modelling.

This paper examines expressions for predicting the time-averaged C_o from the wave-orbital induced stress on the seabed, and compares the findings with SSC profiles measured with sediment traps in a high-energy open-coast environment. The field measurements were made over both rocky and sandy seabeds, and feature sediments of relatively dense andesitic volcanic origin, with a range of median particle sizes.

9.3.1 Sediment entrainment

The initiation of motion of a sediment particle is influenced by many parameters including the particle size and shape, cohesion, bedforms and the near-bed fluid velocities (Nielsen, 1992; van Rijn, 1993). Under wave-orbital motion, the ratio of the stirring and stabilising forces acting on a sediment particle may be expressed as the grain-roughness dimensionless skin-friction Shield's parameter ($\theta_{2.5}$),

$$\theta_{2.5} = \frac{f_w U_w^{\,2}}{2 \quad sgD} = \frac{1}{2} f_w \Psi \qquad \text{Eqn. 9-1}$$

where $s = (\rho_s - \rho)/\rho$, ρ_s and ρ are the sediment and water densities respectively, g is the gravitational acceleration, D is the D_{50} median sediment grain size, U_w is the wave-orbital speed at the near-bed (free-stream) level and f_w the friction factor, calculated using Swart's (1974) explicit formula of Jonsson's (1966) implicit relationship:

$$f_w = \exp[5.213(k_s / a_s)^{0.194} - 5.977] \qquad \text{Eqn. 9-2}$$

where a_s is the orbital radius and k_s is the bed roughness, given by $k_s = 2.5D$ for flat beds. The sediment mobility number (Ψ) in Eqn. 9-1, is defined as

$$\Psi = \frac{U_w^{\,2}}{sgD} \qquad \text{Eqn. 9-3}$$

A correction factor may be applied to $\theta_{2.5}$ to account for enhanced stress due to bed ripples of wavelength λ, and height η (Du Toit and Sleath,1981). θ_r has the form;

$$\theta_r = \frac{\theta_{2.5}}{(1 - \pi\eta / \lambda)^2} \qquad \text{Eqn. 9-4}$$

For irregular waves over flat and rippled beds, Nielsen (1986) found that the near-bed reference concentration was related to the skin-friction by:

$$C_o = 0.005\rho_s\theta_r^{\,3} \qquad \text{Eqn. 9-5}$$

where $\theta_{2.5}$ may be used for flat beds. This relationship has been found to be robust in a wide range of studies (e.g. Black & Rosenberg, 1991; Green & Black, 1999). In applying this expression in non-breaking waves under time-averaged conditions, Black & Rosenberg (1991) found that the third moment of velocity (U_3) best represented the variability of U_w in this relationship, where:

$$U_3 = 1.4\left[\sum_{t=1}^{N} |U_t|^3 \,/\, N\right]^{\frac{1}{3}}. \qquad \text{Eqn. 9-6}$$

and U_t is the instantaneous wave-orbital velocity at time t. Further to the 1986 findings, Nielsen (1992) suggests that under oscillatory sheet flows, the time-averaged form of van Rijn's (1984) steady-flow pickup function may relate C_o to the excess skin-friction as:

$$C_o = 0.007\rho_s(\theta_{2.5} - \theta_c)^{1.5} \qquad \text{Eqn. 9-7}$$

where θ_c is the threshold stress for particle motion (usually taken to be 0.05, Fredsoe & Deigaard, 1992). It is notable that the oscillatory sheet flow data of Horikawa *et al.* (1982) and Staub *et al.* (1984) show reasonable agreement using both expressions (Nielsen, 1992).

The power relationships in Eqns. 9-5 and 9-7 mean that derived concentrations are critically dependent on variables within $\theta_{2.5}$, specifically the statistical representation of grain size and wave orbital velocity. Natural sand beds are comprised of a range of particle sizes, and the median diameter (D_{50}) is an often-used value for calculating reference concentrations (Nielsen, 1992). Grain size is used to describe two separate processes in the Shields parameter: within the Swart formulation (Eqn. 9-2) it is used to parameterise the intrusion of sediment particles into the flow, and as a D^{-1} dependence in the sediment mobility function (Eqn. 9-3) for the behaviour of the particle within that fluid. The use of the same particle size statistic for both terms is common, despite numerous observations that entrained sediments have very different particle size distributions to the bed sediments (e.g. Nishi *et al.*, 1992; van Rijn, 1993; Black, 1994; Whitehouse, 1995). An integrated model that applies the full grain size distribution in the entrainment calculation may partly address this issue, but still does not resolve the complex inter-granular reactions at the near-bed level, nor adequately define a particle size fraction as entrained or at rest.

In this paper we investigate C_o predictions based on the widely-accepted Nielsen (1986) formula (Eqn. 9-5), and further examine the alternative power as suggested by van Rijn in Eqn. 9-7. The findings are discussed in terms of the most suitable time-averaging expression for use in high-energy environments, where sheet flow predominates. While not specifically dealt with in this paper, this also leads to a consideration of upper limits to the $\theta_{2.5}$ - C_o relationship. A case is also presented for considering a different particle size statistic for the f_w and Ψ terms within $\theta_{2.5}$, and we illustrate the value of such an approach for predicting C_o over regions with spatially variable grain sizes. However, in order to validate predictions of C_o with field observations, it is necessary to extrapolate observations from higher elevations, down to the reference level. To achieve this requires an understanding of the SSC profile.

9.3.2 Suspended sediment concentration profiles

An exponential relationship for the vertical distribution of time-averaged suspended sediment concentration has been shown to exist in many studies (Nielsen, 1986; Antsyferov & Kos'yan, 1990; Black & Rosenberg, 1991; Greenwood *et al.*, 1990; Osborne & Greenwood, 1992a,b; Mocke & Smith, 1992; Black, 1994; Black *et al.*, 1995; Flint, 1998, among others). This concentration profile results from the balance of advective motion, turbulent diffusion, and acceleration from gravity, acting on the suspended particles, and may be obtained from:

$$\frac{\partial C}{\partial t} = \frac{\partial}{\partial z}\left[w(1-C) + \varepsilon_s \frac{\partial C}{\partial z} \right] \qquad \text{Eqn. 9-8}$$

where

t = time

z = height above the bed

C = volume concentration of sediment

w = settling velocity

ε_s = sediment diffusivity

Sediment diffusivity (ε_s) is a measure of the rate of diffusion of suspended sediment particles within the water column (with units $m^2.s^{-1}$). Empirical models have been developed to describe the suspended sediment concentration profile based on either the changes in sediment diffusivity with elevation above bed, or the mixing length (l_s). Mixing length is the distance over which fluid is transported by turbulent fluctuations across the flow (Fredsoe & Deigaard, 1992) and is related to the settling velocity of the suspended sediments through the relationship:

$$l_s = \varepsilon_s / w \qquad \text{Eqn. 9-9}$$

When mixing lengths are small (relative to the overall scale of suspension), the suspension mechanism is primarily diffusive (Nielsen, 1992), allowing Eqn. 9-8 to be expressed in the time-averaged form as:

$$C_z = C_o \exp^{(-z/ls)} \qquad \text{Eqn. 9-10}$$

Where C_z is the SSC at elevation z. This assumes a vertically-uniform mixing length (and sediment diffusivity) throughout the water column. Such a profile is often observed over vortex ripples (e.g. Nielsen, 1984). Alternatively, a common expression for l_s prescribes a linear variation with elevation above bed (Fredsoe and Deigaard, 1992), i.e.

$$l_s = \kappa z \qquad \text{Eqn. 9-11}$$

where κ = von Karman's constant (0.4) for water without sediment. This profile is derived from the full parabolic form which is:

$$l_s = \kappa z\,(1-z/h) \qquad \text{Eqn. 9-12}$$

where h is the water depth (m). This function reduces to Eqn. 9-11 in the lower water column when $z/h << 1$. If mixing lengths are considered to be uniform over small vertical increments, then Eqn. 9-10 may be expressed as;

$$l_s = -(z_2-z_1) / \ln(C_2/C_1) \qquad \text{Eqn. 9-13}$$

where z is the elevation above bed and C is the concentration at successive levels z_1 and z_2. This SSC profile description assumes that the size of the turbulent eddies increases linearly with elevation, with corresponding increases in the sediment diffusivity (i.e. from Eqn. 9-9). The pure-diffusion model cannot provide resolution at scales of less than the mixing length and a minimum amount of turbulent diffusion must apply in the near-bed region to maintain the process. Accordingly, this model requires a constant (or at least minimum) diffusivity in the lower, near-bed regions. Under non-broken waves, Deigaard *et al.*, (1986); Black & Rosenberg (1991); and Black *et a.l*, (1995), Green & Black (1999) suggest mixing lengths of the order 0.07 m (range 0.04-0.09 m) in the lower 0.1-0.3 m of the water column. This is also consistent with the flat bed oscillatory

flow data of Nielsen (1984) (Tests 40-42) where the profile steepens at around 0.2 m above bed under non-breaking waves.

Glenn & Grant (1987) also describe a two-layer model where a different sediment diffusivity distribution is applied above and below the wave boundary layer. This layer exists between the bed and the elevation at which the peak free-stream wave-orbital velocity occurs (van Rijn, 1993), having a thickness that ranges from millimetres (over smooth flat beds) to tens of centimetres over bedforms (Fredsoe & Deigaard, 1992). A variety of ε_s distributions have been suggested, such as those described by Sistermans & van de Graff (1999) and Green & Black (1999), for example.

9.4 Data collection

Measurements of SSC and wave-orbital motion were available from a large-scale field measurement programme conducted at New Plymouth, New Zealand (Fig. 9.1), as described by McComb *et al.*, (1999b). The study location is characterised by a high-energy wave climate and coastal sediments of (local) andesitic volcanic origin. Data were collected at 24 nearshore sites over a two-month period in March/April 1998, featuring both rocky and sandy seabed substrates. The present work considers data collected at 10 sandy sites, the positions of which are illustrated in Figure 9.1, and are further described in Table 9.1. The measurements were made at depths ranging from 5.9 to 11.7 m (below mean sea level).

Table 9.1: Water depth (mean sea level) and surficial sediment sizes for the sandy measurement sites shown in Figure 9-1.

Site	Depth msl (m)	D_{50} (um)	D_{mean} (um)
D1	7.1	146	216
D2	7.4	424	276
D6	5.9	296	258
L2	11.3	238	196
S1	8.1	152	185
T2	11.5	407	273
T6	11.7	226	247
T8	9.9	144	178
T9	9.9	277	212
T11	8.3	490	211

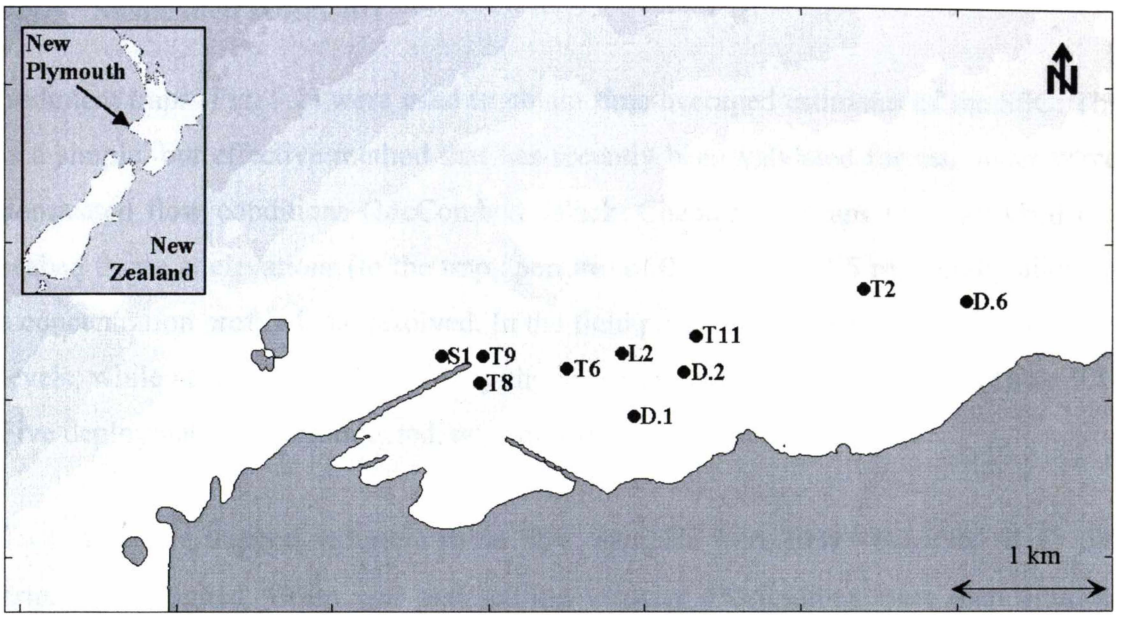

Figure 9.1: Field study site (New Plymouth, New Zealand) showing the location of the SSC measurement sites (sandy beds).

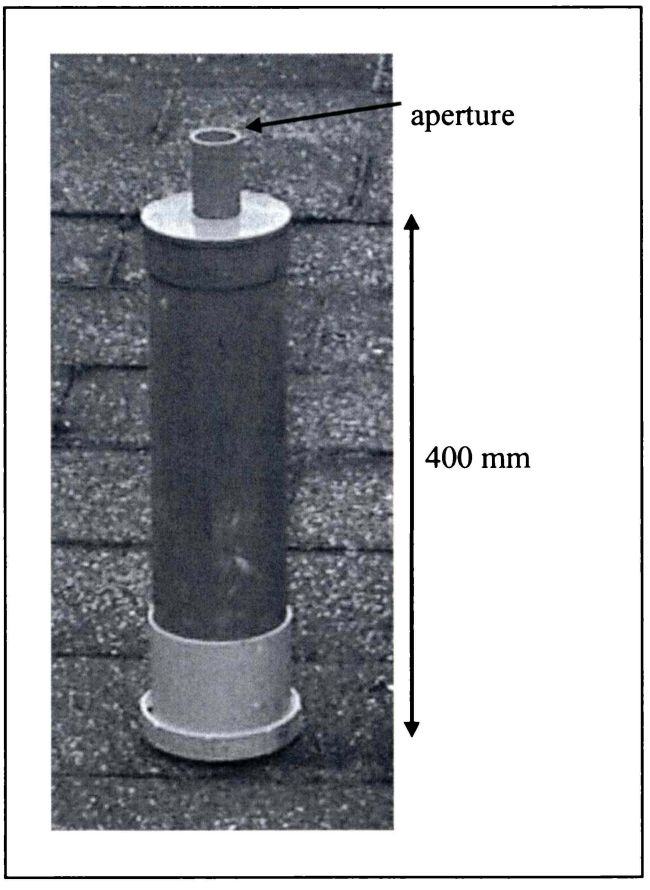

Figure 9.2: Photograph of a type S1 sediment trap

9.5 Suspended sediments

Sediment traps (Fig. 9.2) were used to obtain time-averaged estimates of the SSC. This is a simple, but effective method that has recently been validated for use under wave-dominated flow conditions (McComb & Black, Chapter 4). Traps were attached to a seabed frame at elevations (to the trap aperture) of 0.5, 1.0 and 1.5 m, thereby allowing a concentration profile to be resolved. In the field programme, six sites had all three trap levels, while at the other 18 sites only the lower two elevations were used (Table 9.1). Five deployments were conducted, ranging from 8-14 days in duration.

To convert the trapped sediment to an SSC, samples were first wet-sieved at 45 μm, dried and weighed. Grain size and settling velocity distributions were then obtained using a 1.9 m fall-tube. The masses (M) collected in the traps were converted to an average downward flux (f_d) with the units $kg.m^{-2}s^{-1}$ as follows:

$$f_d = M/At \qquad \text{Eqn. 9-14}$$

where A is the area of the aperture of the trap and t is the time of the sampling. The downward sediment flux was converted to a time-average suspended sediment concentration (C) using the full settling velocity distribution of the trapped sediment (Armanini & Ruol, 1988; Nishi *et al.*, 1992). Concentration distributions were calculated as:

$$C = \frac{M_i}{w_i A \Delta t}, \qquad \text{Eqn. 9-15}$$

where M_i is the mass trapped, A is the area of the collection orifice of the trap, w_i is the settling velocity of the sediment particles of the i^{th} sediment fraction in the distribution and Δt is the deployment time. These were then summed to provide concentrations for the whole sample as:

$$C = \frac{1}{\Delta t} \sum_{i=1} \frac{M_i}{w_i A}. \qquad \text{Eqn. 9-16}$$

McComb & Black (Chapter 4) report that the traps used in this study (type *S1*) have a 75% trapping efficiency, and the SSC values herein are adjusted accordingly.

A sequence of surficial sediment samples were collected over the experiment, from which fall velocity distributions were also obtained. These were converted to an equivalent particle size distribution (e.g. Greilach *et al.*, 1995) using the equations given by Gibbs *et al.* (1971). Particle size distributions were also measured with laser sizing equipment (Malvern Mastersizer). A sediment density of 2850 $kg.m^{-3}$ was used, in accordance with the survey data of Bartholomeusz (1985).

9.5.1 Wave-orbital velocities

Three different types of instruments were used to record data at 2 Hz in 9-minute bursts at intervals of 373 minutes. At sites D1 and D2, DOBIE wave meters recorded pressure at 0.2 m above bed level. At site S1 an InterOcean S4 current meter was positioned with the velocity sensors 1 m above bed level, while at site L2 an FSI 3D-ACM WAVE was also arranged with velocity sensors 1 m above bed.

Measured velocity data were transformed to bed level using linear wave theory, while the DOBIE pressure data were converted to horizontal velocities using linear theory, and then transformed to the bed level. The third moment of velocity (U_3) was obtained (Eqn. 9-6), while the orbital radius (a_s) was calculated as;

$$a_s = \frac{U_3 T_p}{2\pi} \qquad \text{Eqn. 9-17}$$

Standard spectral estimates of significant wave height (H_s) and peak spectral wave period (T_p) were also obtained from the pressure data (see Chapter 5 for methods). Mean currents from the velocity meters were also obtained.

9.6 Results

The five trapping deployments made over the two-month period field experiment are shown in Figure 9.3 as a time-series with the recorded wave statistics (i.e. H_s and T_p) from site L2. Significant wave heights were as high as 3.1 m, and the peak periods ranged from 4 to 16 seconds. The measured wave orbital velocities (U_3) ranged from 0.15 ms^{-1} to as high as 1.9 ms^{-1}. Appendix 5 provides time-series plots of U_3 as well as tables of the sediment trap and SSC values. Processed parameters for waves, winds, tides and currents are included on the CD with the thesis.

The SSC obtained are given in Table 9.2, with z = 0.5 m concentrations ranging from 0.003-0.173 $kg.m^{-3}$. The site-specific grain size data (Table 9.1) shows D_{50} values for the bed sediments of between 152 to 424 μm. At site L2, the mean currents were as high as 12 cms^{-1}, although the average value was 2.6 cms^{-1}.

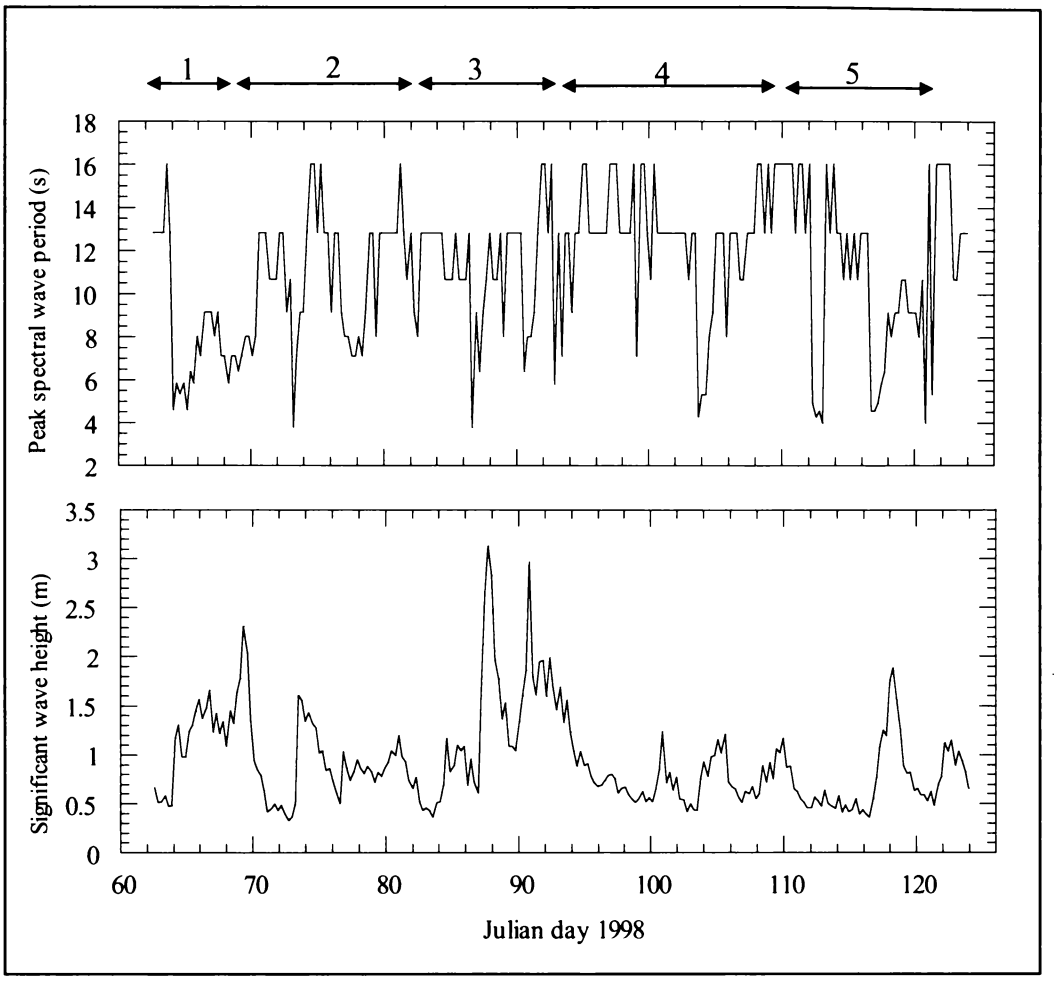

Figure 9.3: Time-series of significant wave heights and peak spectral wave periods recorded at site L2 (Fig. 9-1) showing the five trap-set periods (1-5).

Table 9.2: Time-averaged SSC results ($kg.m^{-3}$), with * indicating periods with coincident *U* data.

Site	Set	*U* data	Cz 0.5 m	Cz 1.0 m	Cz 1.5m
D1	1		0.00936		
D1	3	*	0.1732	0.03439	
D1	2	*	0.01416		
D1	4	*	0.00936		
D2	1	*	0.01368	0.00746	
D2	3	*	0.1417	0.05170	
D2	2	*	0.04445	0.00812	
D2	4	*	0.01368	0.00746	
D2	5		0.00454	0.00614	
D6	1		0.04650	0.01237	
D6	4		0.04650	0.01237	
D6	5			0.01572	
L2	3	*	0.11670	0.01615	0.00699
L2	5	*	0.00950		
S1	1		0.01820		
S1	3		0.07376	0.01394	0.01136
S1	2	*	0.01439		
S1	4	*	0.01820		
S1	5		0.01308	0.00408	
T1	3		0.02120	0.00482	
T11	1		0.00337		
T11	3		0.06580	0.01347	0.00974
T11	5		0.02698	0.00762	0.00132
T11	2		0.01033		
T11	4		0.00337		
T13	1		0.04090		
T13	3		0.14030	0.00954	
T13	2		0.02008		
T13	4		0.04090		
T1	5		0.00782		
T2	1		0.00734		
T2	3		0.11659	0.01177	
T2	4		0.00734		
T6	1		0.00719		
T6	3		0.06387	0.02600	
T6	4		0.00719		
T6	5		0.00706		
T9	1		0.08379	0.00613	
T9	3		0.20392	0.02153	
T9	2		0.02890	0.00766	
T9	4		0.08379	0.00613	
T9	5		0.08410	0.00778	

9.6.1 SSC profiles above 0.5 m

The variability of SSC with elevation was first examined on a regional level to define any broad-scale trends. Using data from both sandy and rocky sites, fifteen profiles were available with SSC data at three elevations (i.e. 0.5, 1.0 and 1.5 m), and, by first approximation, these data exhibited a vertical distribution that was reasonably well described by the uniform sediment diffusivity model. Eqn. 9-10 may be expressed as:

$$lnC_z = -z/l_s + lnC_o \qquad \text{Eqn. 9-18}$$

which allows a mixing length to be derived from the gradient of the best-fit linear function. By comparing mixing lengths resolved over the minimum possible increments of z, systematic variations of l_s with z may be identified. Thus, mixing lengths were calculated using concentrations at adjacent levels (i.e. between 0.5 and 1.0 m, 0.5 and 1.5 m, and 1.0 and 1.5 m), by assuming that the mixing length remains uniform over these increments (Eqn. 9-13). Using all data from the field experiment, an average mixing length was obtained for the mid-point elevations (i.e. z = 0.75, 1.0 and 1.25 m; Table 9.3), with the relationship

$$l_s = 0.46\, z \qquad (R^2 = 0.97), \qquad \text{Eqn. 9-19}$$

indicating that for the regions $z > 0.5$ m the mixing length is linearly increasing with elevation above bed. This is consistent with Eqn. 9-11.

Table 9.3: Averaged mixing lengths (l_s) calculated for mid-point elevations.

z range (m)	z mid-point (m)	l_s (m)
0.5-1.0	0.75	0.313
0.5-1.5	1.0	0.465
1.0-1.5	1.25	0.590

The profile data also show a decrease in the mean settling velocity with increasing height above the bed. From the 0.5, 1.0 and 1.5 m traps, overall mean values 0.0259, 0.0235 and 0.0220 ms^{-1} where obtained, respectively. Linear regression of these data were highly correlated (R^2 = 0.982), and extrapolation to the bed level gives a settling velocity of 0.0277 ms^{-1} (with an equivalent particle size of 235 μm).

9.6.2 Near-bed reference concentrations

Eleven measurement periods were available with coincident SSC data at the 0.5 m level as well as time-series orbital velocities (Table 9.2). For each 9-minute data burst, $\theta_{2.5}$ was calculated with three different grain sizes;

a) using the bed D_{50} values in f_w and in Ψ

b) using the bed D_{50} values in f_w , and the bed D_{mean} in Ψ

c) using the bed D_{50} values in f_w , and the $D_{near\text{-}bed}$ in Ψ

where the $D_{near\text{-}bed}$ is the value obtained through regression of the mean settling velocities obtained in the traps (in this case 235 μm). The latter provides a regional mean value that smoothes the spatial variation in bed grain size. Burst-averaged C_o values were calculated from these $\theta_{2.5}$ values using Eqns. 9-5 and 9-7, and a time-averaged C_o derived from the overall mean.

The results (Table 9.4) show that for these data, the power in the Nielsen (1986) equation is too high, and the lower value of 1.5 (van Rijn) is more appropriate, providing a near-linear relationship between SSC (0.5 m) and C_o (Fig. 9.4). Eqn 9-7 predictions are further improved when the D_{mean} and $D_{near\text{-}bed}$ grain size are used in the Ψ term, with the former giving the best result (with an R^2 correlation of the linear regression of 0.91, Figure 9.4)

Plot of the measured C_z (0.5m) vs C_o predicted using Eqn. 9-5a (Table 9.4). $R^2 = 0.99$ for the best-fit curve.

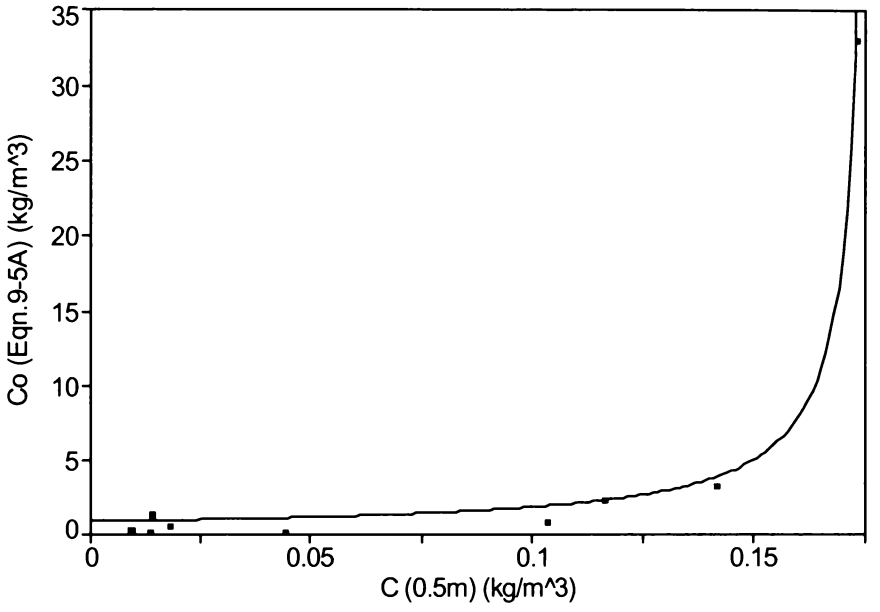

Plot of the measured C_z (0.5m) vs C_o predicted using Eqn. 9-5b (Table 9.4). $R^2 = 0.88$ for the best-fit curve.

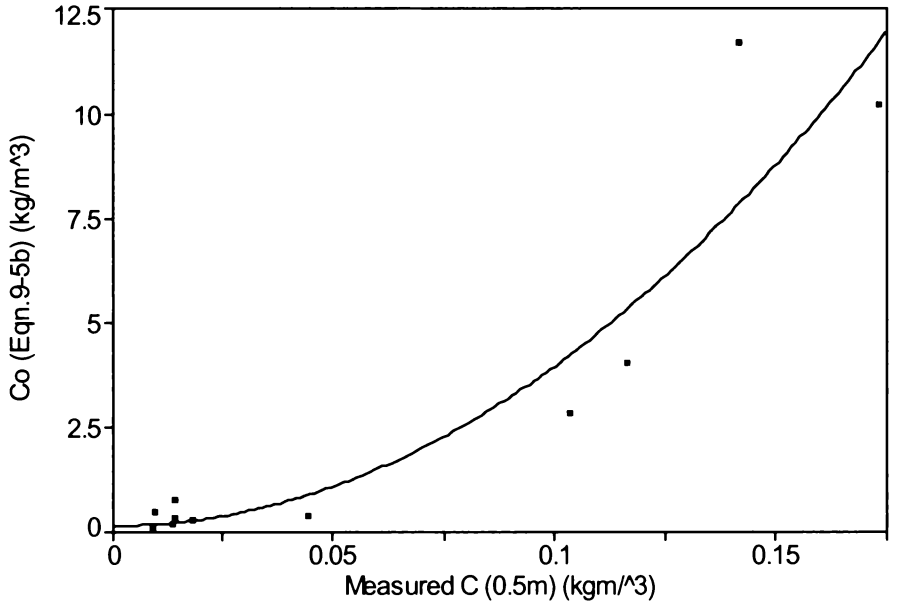

Plot of the measured C_z (0.5m) vs C_o predicted using Eqn. 9-5c (Table 9.4). $R^2 = 0.59$ for the best-fit curve.

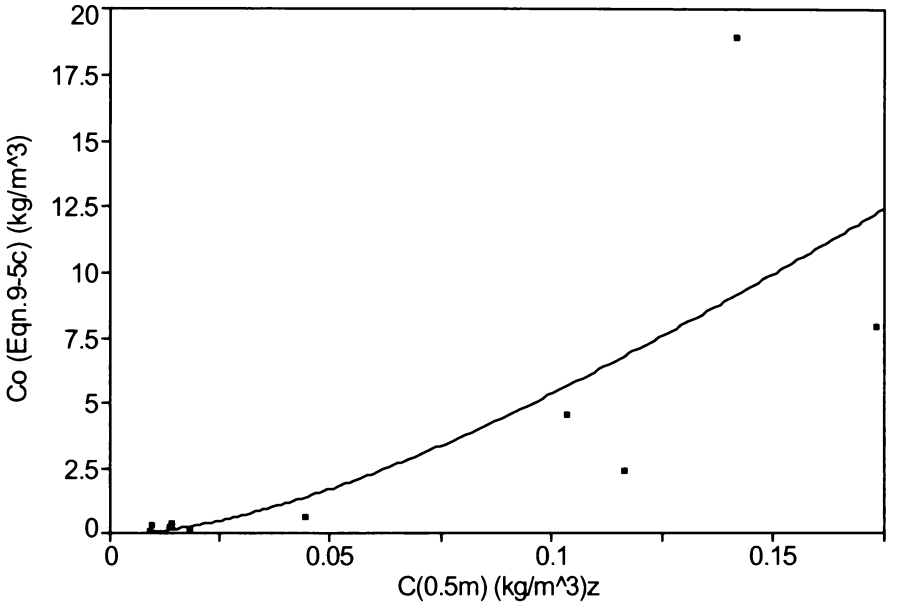

Plot of the measured C_z (0.5m) vs C_o predicted using Eqn. 9-7a (Table 9.4). $R^2 = 0.90$ for the best-fit curve.

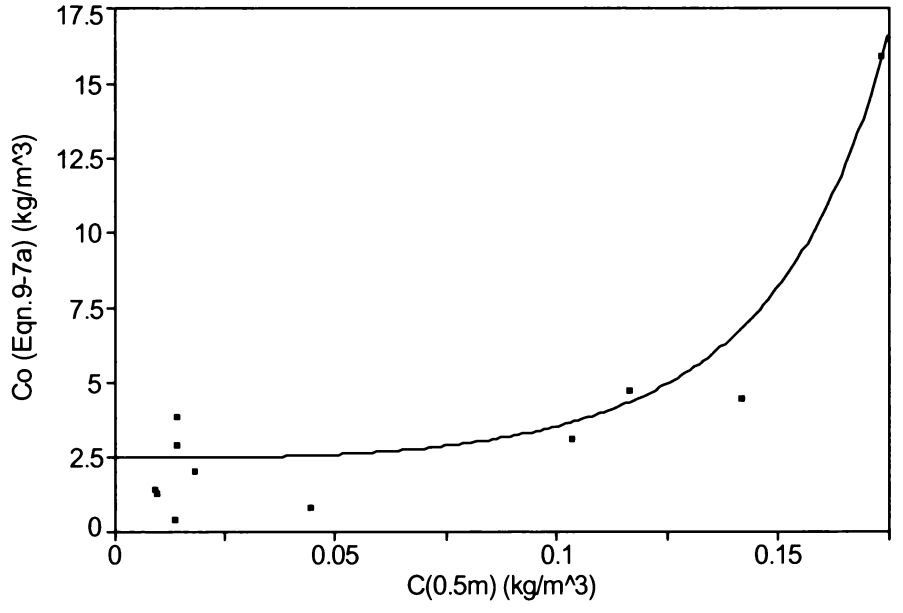

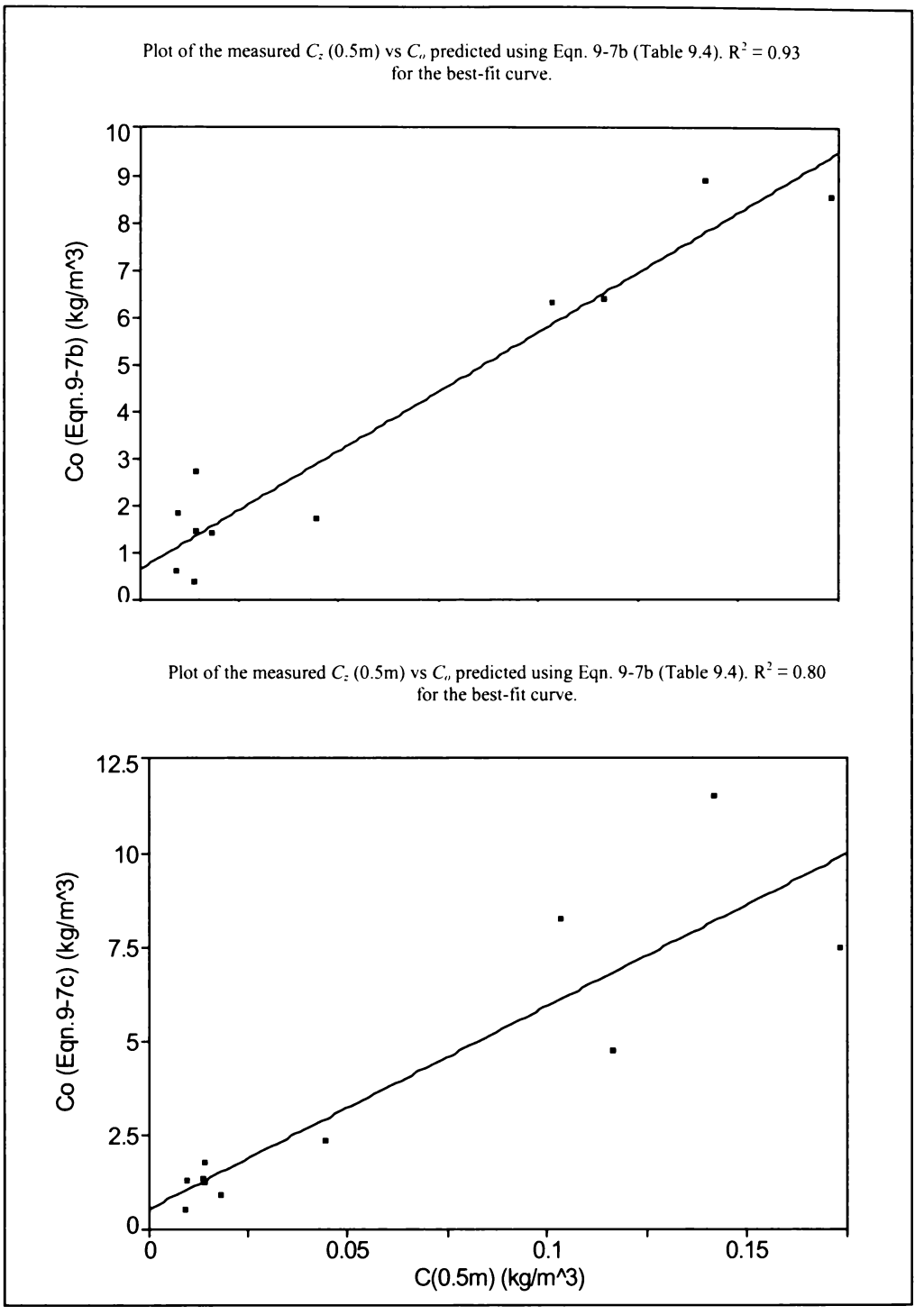

Figure 9.4: A series of plots showing the data in Table 9.4. Concentration ($kg.m^{-3}$) as measured by the traps at 0.5 m elevation ($C_{0.5\,m}$) and C_o is predicted using Eqns. 9-5 and 9-7. The Eqn. suffix indicates; (a) bed D_{50} values in f_w and in Ψ, (b) bed D_{50} values in f_w and the bed D_{mean} in Ψ and (c) bed D_{50} values in f_w and the $D_{near\text{-}bed}$ in Ψ.

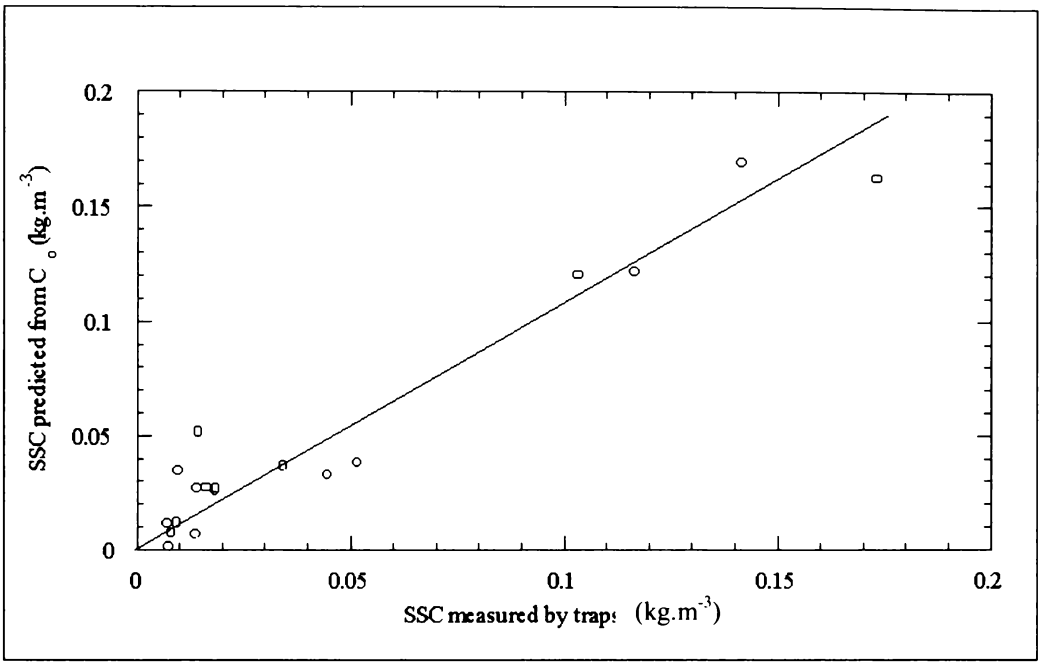

Figure 9.5: Plot of concentrations (kg.m^{-3}) measured by the traps vs calculated values using Eqn 9-7 (with bed D_{50} values in f_w and the bed D_{mean} in Ψ), extrapolated to levels 0.5, 1.0 and 1.5 m using Eqn. 9-18 (with $l_s = 0.46z$ and a lower l_s limit of 0.1 m). The linear regression line is shown, having a gradient of 1.06 and R^2 correlation of 0.93.

Table 9.4: Calculated C_o values (kg.m^{-3}) from Eqns. 9-5 and 9-7, with (a) bed D_{50} values in f_w and in Ψ, (b) bed D_{50} values in f_w and the bed D_{mean} in Ψ and (c) bed D_{50} values in f_w and the $D_{near\text{-}bed}$ in Ψ

Site	Set	C_z 0.5m (kg.m^{-3})	C_o (kg.m^{-3}) Eqn. 9-5(a)	C_o (kg.m^{-3}) Eqn. 9-5(b)	C_o (kg.m^{-3}) Eqn. 9-5(c)	C_o (kg.m^{-3}) Eqn. 9-7(a)	C_o (kg.m^{-3}) Eqn. 9-7(b)	C_o (kg.m^{-3}) Eqn. 9-7(c)
D1	3	0.1732	32.9085	10.1626	7.8916	15.8385	8.5145	7.4360
D1	2	0.1167	2.2409	4.0122	2.3278	4.6301	6.3815	4.7290
D1	4	0.1034	0.7671	2.7812	4.5056	3.0567	6.3033	8.1983
D2	1	0.0445	0.0941	0.3412	0.5528	0.7474	1.7217	2.3046
D2	2	0.1417	3.2167	11.6624	18.8934	4.4040	8.8655	11.4588
D2	3	0.0137	0.0325	0.1906	0.1906	0.3668	0.3525	1.3019
D2	4	0.0142	1.0195	0.3148	0.2445	2.8609	1.4192	1.2118
L2	3	0.0094	0.2267	0.0700	0.0544	1.3476	0.6121	0.5093
L2	5	0.0095	0.2496	0.4469	0.2593	1.2618	1.8047	1.2922
S1	2	0.0144	1.3171	0.7305	0.3564	3.7790	2.6942	1.7592
S1	4	0.0182	0.4544	0.2520	0.1230	1.9908	1.3837	0.8672

9.6.3 SSC profiles below 0.5 m

For the region below 0.5 m, an iterative approach was used to define the level at which a constant mixing length should apply, with consideration that previous studies indicate an l_s of 0.07 is common in unbroken waves. This approach involved the correlation of reference concentrations inferred by extrapolation of the SSC profile (C_{op}), with those obtained by calculation. Accordingly, predicted C_o values from the van Rijn Eqn. 9-7 (with the bed D_{50} values in f_w , and the bed D_{mean} in Ψ) were compared with C_{op} values, testing a range of minimum l_s values. The best agreement was found with using a minimum l_s of 0.1 m, which equates to a constant value over the lower 0.2 m in the water column. Thus,

$l_s = 0.46\,z$ for $z > 0.2$ m, and $l_s = 0.1$ for $z < 0.2$. Eqn. 9-20

9.6.4 SSC predictions

Measured SSC values (Table 9.2) were compared with concentrations derived from estimates of C_o (predicted using Eqn. 9-7 with D_{mean} in the Ψ term) and extrapolated to levels 0.5, 1.0 and 1.5 m using Eqns. 9-18 and 9-20. Figure 9.5 shows very good agreement between the measured and predicted concentrations, with an R^2 linear regression of 0.93, and a gradient of 1.06.

9.7 Discussion

This work relates time-averaged measurements of SSC with the $\theta_{2.5}$ grain-size skin friction, similarly averaged, with a view to confirming a prediction formula for use under high-energy, non-broken wave conditions. We note that the two measurement techniques herein employed are not entirely coincident, with the sediment traps providing a continuous time-average, while the wave/current data is from short bursts every 373 minutes. Furthermore, the trapping periods did not feature uniform wave conditions throughout; for example, in the third collection period (Fig. 9.3), U_3 values at site D1 ranged from 0.17 to 1.65 m s^{-1}. Such conditions are far-removed from controlled experimental situations, and present a rigorous test for prediction methodologies.

We firstly consider the assumption that sheet flow (i.e. flat bed) conditions were predominant during the experiments. Vortex ripples will exist up to a $\theta_{2.5}$ washout criteria, which has reported values of between 0.14 (Green & Black, 1999) and 0.8 (Soulsby, 1997). SCUBA diver observations of the bed at the beginning and end of each trap deployment indicated ripples were often present, although diving operations were necessarily conducted in the calmer periods. During the deployments however, the $\theta_{2.5}$ often exceeded 0.8, during which time sheet flow conditions would likely exist. To test the likely effect of ripple-enhanced skin friction on the time-averaged data, we applied Eqn.9-4 (with a $\theta_{2.5}$ = 0.8 washout criteria), after estimating the integral ripple dimensions with the method of Grant & Madsen (1982), as well as that of Wikramanayake (1993) (as applied by Black & Oldman, 1999). The results showed no significant difference in the calculated C_o values using Eqn. 9-5 or 9-7, thereby illustrating how the more vigorous events dominate the time-average - particularly with $\theta_{2.5}$ raised to the power 1.5 or 3.

The field measurements have validated the van Rijn (1984) expression (Eqn 9-7) as a predictive tool for high-energy conditions, but also raise the issue of an upper limit to the $\theta_{2.5}$ - C_o relationship. Both Eqns. 9-5 and 9-7 assume that C_o has no upper value, although from Bagnold's (1954) expression on the transfer of shear stress to the bed in constant flow, Engelund & Fredsoe (1976) show that the maximum volumetric concentration at the reference level is ~0.3, which Fredsoe (1993) suggests is close to the highest possible concentration for sediment in motion. Under waves a similarly asymptotic relationship is likely to exist between $\theta_{2.5}$ and C_o, with grain-grain interactions important at high concentrations. Moreover, the maximum C_o value will also be dependent on the sorting of the grain sizes. This occurs because the volumetric concentration is directly related to the ratio between interstitial spaces to the volume occupied by the sediment grains (Soulsby, 1997).

In our time-averaged application, Eqn 9-7 was found to be a good predictor over the range of events. It is possible that the less energetic sites / periods may be better predicted with the Nielsen Eqn. 9-5 (including flow contraction over ripples). However, to apply a different formulae for each time period on the basis of the wave energy would necessarily invoke an expression that relates C_o - $\theta_{2.5}$ with a power that varies according

to the magnitude of $\theta_{2.5}$. Such an expression, while beyond the scope of our data, remains consistent with Nielsen's (1986, 1992) observations including the oscillatory sheet flow data of Horikawa *et al.* (1982) and Staub *et al.* (1984). Furthermore, Zyserman & Fredsoe (1994) report an asymptotic expression for constant flow conditions as:

$$C_a = \frac{0.331(\theta_{2.5} - 0.045)^{1.75}}{1 + 0.720(\theta_{2.5} - 0.045)^{1.75}} \qquad \text{Eqn. 9-21}$$

which Soulsby (1999) notes is applicable to oscillatory sheet flow under waves. Here, C_a is the reference concentration at the level z_a=2D_{50}. However, for Eqn 9-21, the relationship between reference concentration and the grain-roughness skin-friction Shields parameter is markedly different to that of Eqns. 9-5 and 9-7. Figure 9.6 shows the relationship between $\theta_{2.5}$ and C (vol/vol) for the three expressions. In order to derive an appropriate semi-empirical expression that would cover the range from rippled beds through to flat-bed sheet-flow conditions, more data is required to provide a better insight to the processes that are occurring over this $\theta_{2.5}$ range.

Sediments become entrained when the particles are no longer supported by intergranular forces, and thresholds for entrainment are very much grain-size dependent. For this reason entrainment predictions often integrate over the entire grain size distribution. In the present case we have sought to test the use of a single statistic, and found that predictions were significantly improved when the mean grain size was used in the sediment mobility term (Ψ) and the median in the friction factor (f_w). When grain size has a Gaussian distribution, the median value will equal the arithmetic mean, but when the distribution is skewed the values will differ.

While the local bed is generally considered the source for entrainment (Fredsoe, 1993), this study has demonstrated that the particle sizes of the suspended sediments are characteristically different from those at the bed. Figure 9.7 shows how the median suspended grain size varies at a range of sites (with a range of bed D_{50}) by considering the ratio of the 0.5 m D_{50} / seabed D_{50} vs the seabed D_{50}. The data exhibit a "smoothing" effect, whereby the suspended sediments are coarser than the local bed in regions of fine bed sediments, with the reverse situation occurring in regions with coarse bed

sediments. This is a very important finding, which suggests that the particle size distribution of the suspended sediments at the 0.5 m elevation reflect a "regional" average, rather than solely the local bed constituents. It is noteworthy that the high-energy conditions on this coast provide ample horizontal advection to facilitate such a distribution. The particle size data also show that the ratio between suspended and bed D_{50} is equivalent to the ratio between the mean and D_{50} values for the surficial seabed sediments. Consistent with this, our findings indicate that using the D_{mean} in the Ψ term more appropriately represents the fraction of mobile particles in the surficial sediment layer.

The SSC profiles indicate that for regions >0.5 m above the seabed, the scale of turbulent mixing (l_s) increases linearly with elevation, with an apparent gradient of 0.46. This is slightly greater than the value of 0.4 for κ. Mixing length and diffusivity are linked by settling velocity (Eqn. 9-9), with the former being properties of the fluid, while the latter is due to the sediment and the fluid. When using a representative grain size to characterise the suspended sediments, a decrease in the mean suspended sediment grain size with increasing elevation (e.g. Nishi *et al.,* 1992) has the effect of increasing the gradient in Eqn. 9-11. Furthermore, the pure diffusivity model (i.e. Eqn. 9-10) assumes that the sediment diffusivity is equal to the eddy diffusivity i.e. the sediment particles diffuse in the same way as the fluid "particles". The ratio of sediment to eddy diffusivity (β) is inversely proportional to the settling velocity (Fredsoe and Deigaard, 1992), and the linear fining of the mean settling velocity with height above bed will result in an apparent increase in β, thereby further steepening this gradient. Thus, a steeper l_s profile is apparent when a single statistic (e.g. the mean) is used to characterise the range of settling velocities (and particle sizes) for the suspended sediments.

9.8 Conclusion

Expressions for predicting time-averaged near-bed sediment reference concentrations (C_o) were tested for a range of conditions, including high-energy oscillatory sheet-flow conditions. Field data were collected from a high-energy open-coast site with both rocky and sandy beds, with surficial sediments of relatively dense andesitic volcanic origin, and a wide range of median particle sizes. Suspended sediment concentrations

(SSC) were measured with sediment traps while wave-orbital velocities were recorded with bottom-mounted current meters.

The study has validated a methodology to predict the entrainment of the sediments, showing that the 3rd power in the Nielsen (1986) expression causes an over-prediction in the near-bed concentrations under high-energy conditions, while the lower-powered van Rijn (1984) expression provides a good agreement. Predictions using the van Rijn expression were further improved when the mean grain size was used in the sediment mobility term (Ψ) and the median grain size in the friction factor (f_w), which we relate to the characteristic grain-size distribution of the bed sediments. Using this formulation, the time-averaged grain-size Shields parameter ($\theta_{2.5}$) was found to be linearly related to time-averaged suspended sediment concentrations (from sediment traps) with an R^2 correlation of 0.91. The data also suggest that an asymptotic relationship between $\theta_{2.5}$ and C_o is likely under high-energy, sheet-flow conditions.

The scale of turbulent mixing (l_s) was found to increase linearly with elevation above the bed, with a gradient of 0.46. While close to the predicted value of 0.4 (i.e. von Karman's constant, κ), the slightly steeper measured profile is consistent with an observed reduction in suspended sediment grain size with increasing elevation above the bed.

The resolved suspended sediment concentration profile was applied to a pure-diffusion concentration model, in order to reconcile C_o values (derived from current meter data) with SSC data (measured from sediment traps), employing a constant diffusivity/mixing length was employed in the near-bed region. The best agreement between measured and predicted SSC was found using a minimum l_s of 0.1 m over the lower 0.2 m of the water column, above which the diffusivity/mixing length linearly increased with elevation above bed (at a gradient of 0.46). The measured and predicted SSC were highly correlated (R^2 = 0.93, slope of 1.06) over a wide range of wave events.

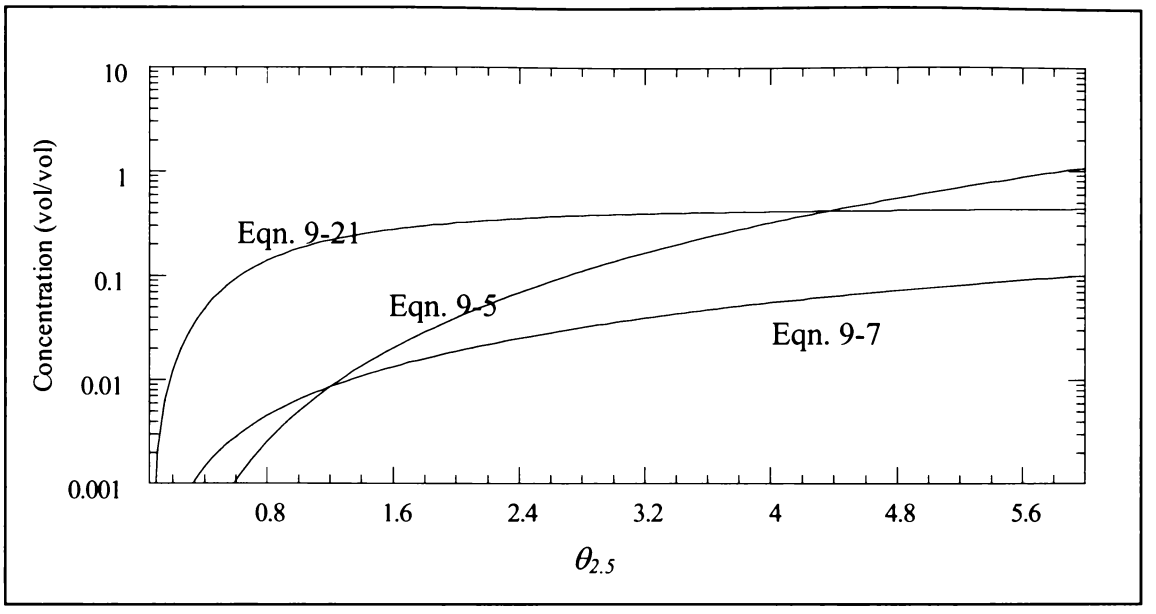

Figure 9. 6: Plot of the volumetric concentration derived from three expressions (Eqns. 9-5, 9-7 and 9-21) with increasing $\theta_{2.5}$ (grain-size skin-friction Shields parameter).

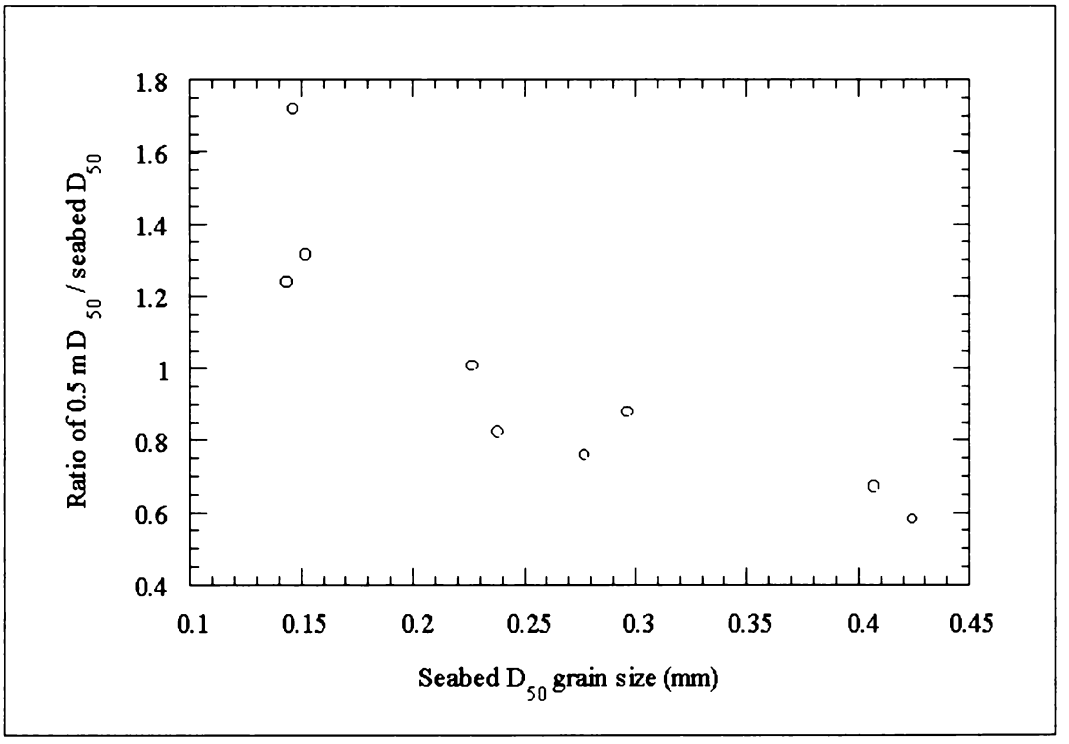

Figure 9.7: The ratio of suspended sediment (0.5 m) D_{50} / bed sediment D_{50} is related to the median seabed grain size.

10 SUMMARY AND DISCUSSION

10.1 Introduction

The key sediment transport processes are entrainment, suspension and advection. Sediment entrainment requires the transfer of sufficient energy from the fluid to the grains in order for them to overcome gravity and inter-granular forces (Fredsoe & Deigaard, 1992), and this process is influenced by the substrate, sediment characteristics (i.e. size, shape and density; Nielsen, 1992), and the magnitude of wave-orbital motions at the bed level (e.g. Green, 1999). The suspension process distributes the entrained sediments by turbulent diffusion and convective mechanisms, both horizontally (e.g. Black & Gorman, submitted) and vertically (e.g. Black & Rosenberg, 1991) through the water column. Suspension is influenced by elements of the seabed morphology (e.g. bedforms; Osbourne & Vincent, 1996), the turbulent structure of the water column (e.g. Fredsoe, 1993), and the sediment fall velocity (e.g. Nishi *et al.*, 1992). Advection is the net sediment transport resulting from currents acting on suspended particles, and ultimately the flux of those particles is crucially dependent on the circulation patterns (e.g. Lakhan, 1989).

The papers presented in this thesis have examined various aspects of these processes on a rocky, high-energy coast, using empirical observations and often overlapping experimental outcomes. This discussion chapter aims to consolidate those findings, and provide a systematic description of coastal and sediment dynamics at New Plymouth, in addition to considering the site-specific issues of dredging and dumping of sediments from Port Taranaki. Drawing on the results of the previous chapters as well as supporting data not included in those papers (but reported in the project studies detailed in Appendix 1), the study environment is described in terms of forcing functions (i.e. waves, currents and seabed topography) and responsive functions (i.e. suspended sediments, sediment flux and sedimentary equilibrium). This leads to an examination of the study findings in terms of the knowledge shortfalls outlined in the introduction section, and ultimately a discussion on the sediment dynamics of a rocky coast.

10.2 Data collection

Collecting oceanographic data in a high-energy coastal environment is challenging, and the field experiments conducted at New Plymouth have required the instrument mooring systems be refined to ensure security, as well as efficiency for SCUBA diver intervention. As a result, some 2124 wave/current meter days were successfully deployed without the loss of a single instrument. In terms of data collection methodologies, two significant advances have been made in the course of the research.

The first is the use of sediment traps to measure the downward flux of suspended sediments under wave-orbital motion. Calibration experiments (Chapter 4) have provided the first published evidence that sediment traps may be effectively applied to derive a time-averaged suspended sediment concentration in a wave-dominated coastal environment. Because traps are simple and inexpensive devices, they may be deployed in spatially-intensive arrays, thereby facilitating data collection on a scale not possible with other instrumented systems (e.g. water samplers or optical backscatter devices). This significantly extends the ability of researchers to collect suspended sediment data in the coastal environment.

The second advance involves the use of taut-wire mooring systems to measure directional wave spectra (Chapter 3). Measuring waves and currents at sites with water depths of 20-50 m is common in coastal studies; providing an "offshore" wave climate as well as a boundary condition for nearshore numerical modelling. Taut-wire moorings provide a useful platform to collect such data, allowing the *p, u, v* meter to be appropriately positioned in the water column. However, previous investigations on the effect of mooring motion on recorded current data have not considered effects at orbital-velocity scales, nor the concomitant effects on resolving directional wave spectra. The study in Chapter 3 describes how wave-induced mooring motion can corrupt the directional wave spectra, and offers an analysis method to minimise this effect. This is a field that would benefit from further research, as the data strongly suggest that a taut-wire mooring system could be designed for a specific site (i.e. water depth, wave climate) in order to minimise motion effects.

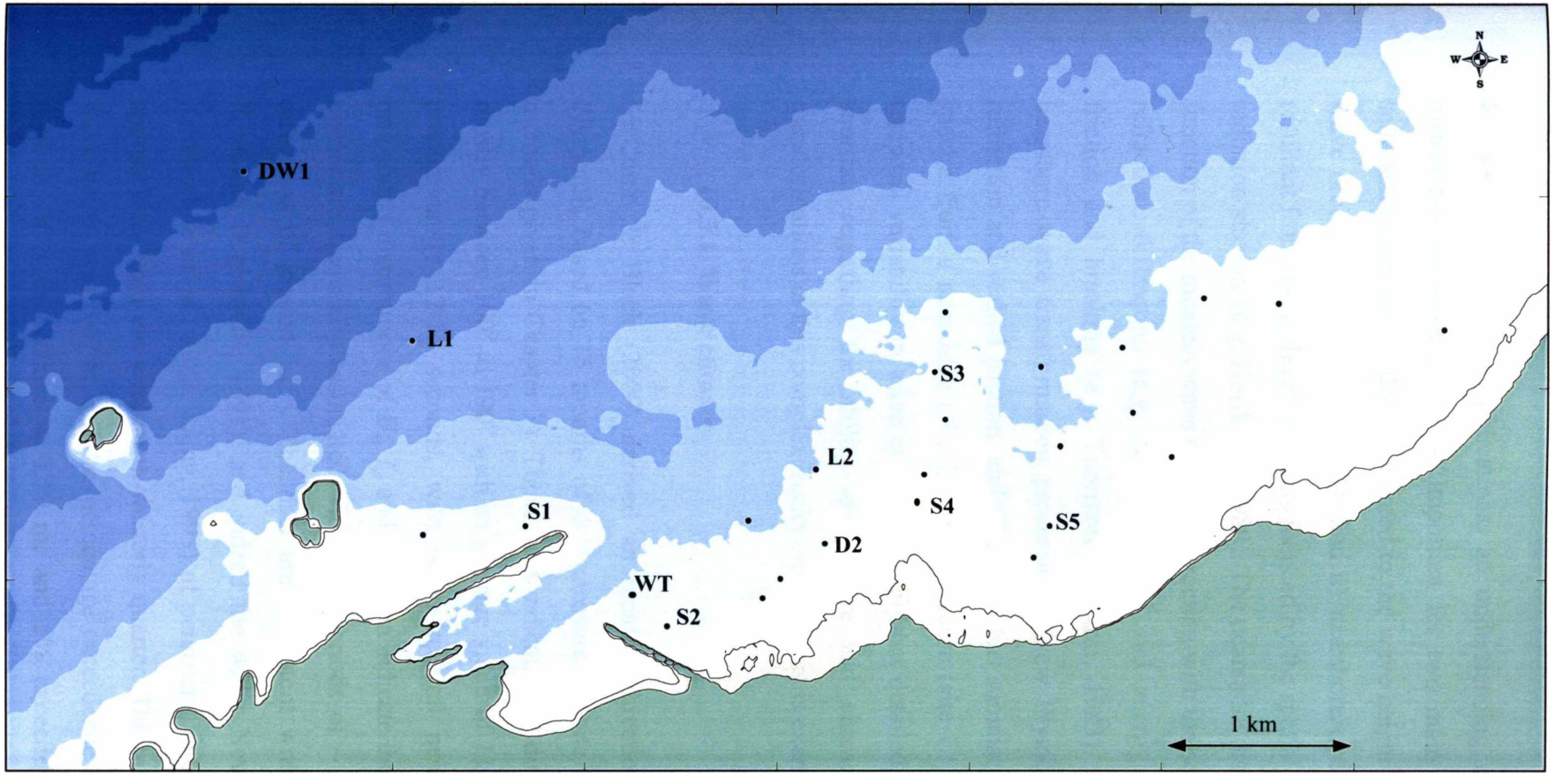

Figure 10.1: Map showing the location of measurement sites (e.g. Chapters 2 & 5), with selected sites named for reference within the text.

10.3 Waves

For sediment transport applications, an understanding of the spatial and temporal distribution in wave energy is important for two main reasons; i) the intensity of sediment suspension is directly related to the wave height and period (i.e. the near-bed wave orbital velocities; Chapter 9) and ii) nearshore circulation patterns are, in part, resultant from the sealevel gradients induced by the spatial variation in wave height and radiation stresses (e.g. Horikawa, 1989). The nearshore distribution of wave energy is a function of the incident wave energy interacting with the seabed through wave shoaling, refraction, diffraction (e.g. Nielsen, 1983) and energy dissipation through seabed friction and breaking (e.g. Thornton & Guza, 1983). Chapter 5 has defined the nearshore wave transformation processes at New Plymouth as being dominated by refraction and seabed friction, and Chapter 3 has summarised the averaged directional spectra from a nearshore (site L2) and offshore (site L1) area. Here, the spatial and temporal variability in wave conditions is further detailed, and the specific knowledge shortfall regarding the ability to measure and characterise the nearshore wave transformations in this complex, rocky environment is examined.

10.3.1 Wave climate

McComb & Black (2000) derived an incident directional wave climate for New Plymouth, based on 16 months of data measured at site L1 (and analysed as per the methods given in Chapter 3). Those data indicate that directions of wave advance lie mostly between 100° to 190° with an average value of 115°. Peak spectral periods are predominantly 12-14 seconds, with mean spectral periods of 6-7 seconds. Joint probability distributions of H_s, T_p and direction indicate that larger (i.e. H_s > 2 m) wave events are frequently associated with peak periods of ~ 10 seconds, and with wave directions of around 125°. The data are consistent with previous findings at New Plymouth (e.g. MOR, 1991), and indeed the wider New Zealand West Coast (e.g. Kibblewhite *et. al.*, 1982; Laing, 1993) of persistent long-period (>12 seconds) swell approaching from the west-north-westerly quarter. The maximum recorded significant wave height was 6.67 m, and the percentage exceedence for H_s is 95% exceedence at 0.49 m, 50% exceedence at 1.19 m, and 5% exceedence at 2.97 m. Cumulative frequency extrapolation of the data (McComb, 2000a) gives a 5-year extreme H_s value

of 7.69 m and a 10-year extreme of 7.98 m. These values are similar to the reported statistics for other high-energy wave climates, such as Southwestern Australia (Lemm, 1999) and the Northwest Coast of U.S.A. (Tillotson & Komar, 1997).

The coastal orientation at New Plymouth (i.e. approximately northeast-southwest) provides topographical sheltering from waves approaching from quarters south of southwest, and it is generally held that a wave energy gradient exists between New Plymouth and regions immediately south of Cape Egmont (e.g. Matthews, 1977). McComb (2000c) made coincident wave measurements at Opunake and at the offshore Maui oilfield (Fig. 1.1), finding that the coastal low-frequency (<0.1 Hz) swell heights were approximately 86% of the offshore deepwater values. A similar comparison between significant wave heights at the Maui B Platform (McComb, 1999a) and coincident measurements from site L1, suggests that New Plymouth H_s values are ~50% of the incident deepwater values, although the low-frequency swell components remain similar to Opunake (at 87% of the deepwater values). This comparison does not consider the effect of the incident deepwater wave direction (which strongly effects the Maui-New Plymouth relationship), nor wave shoaling. Nonetheless, it does show that significant amounts of the incident deepwater long-period swells do penetrate the North Taranaki continental shelf to the New Plymouth coast. It is of further interest that the New Plymouth coastal shelf is steep (the 30 m depth contour is approximately 1700 m offshore of Port Taranaki) and of an equivalent gradient that found on the Sydney-Jervis Bay coast (New South Wales, Australia). Wright (1976) investigated the frictional dissipation of wave energy in that region, and found that relatively little energy loss (i.e. ~3.4%) between the deepwater and inshore regions. This is very low compared with Wright's estimate of 29-84% for lesser gradient sites in North and South America. Similarly, Young & Gorman (1995) note that nearshore wave energy in the South Australian Bight is significantly attenuated by frictional effects of a wide continental shelf. McComb (2000b) suggests that nearshore wave heights in the North Taranaki Bight (i.e. east of Waitara; Fig. 1.1) are strongly attenuated by the low seabed gradients that extend out to the 40 m isobath.

10.3.2 Monochromatic wave transformations

While waves approach the New Plymouth coast from a wide range of directions, the nearshore spread of incident wave directions is not as broad as the offshore conditions (e.g. Fig. 3.3). This is due to topographical sheltering and refraction effects tending to align the wave crests with the isobaths. The averaged wave direction and monochromatic wave height ratio (i.e. nearshore H_s / offshore H_s) (Fig. 8.7) shows wave heights that attenuate with decreasing water depth, and a topographical wave-sheltering zone that includes the Port and extends eastward to approximately the landward tip of the Kawaroa Reef (Fig. 1.2). This sheltering is strongly dependent on the direction of the incident offshore waves, with the more oblique waves (i.e. where the directions of wave advance are <120°) having low penetration to that zone. The ratios also show the strong influence of seabed friction - smaller wave height ratios are associated with larger offshore wave heights, and lower tide levels. One notable exception is site WT (adjacent to the harbour entrance channel) where the opposite is true (due to heightened wave refraction around the main breakwater tip-shoal at low tide). Low-frequency swell is more effectively concentrated (refracted) on the protruding reefs than the short-period sea waves (e.g. wave periods of <8 seconds), a finding that was also made by Hutt (1997) at Raglan, New Zealand. This creates considerable longshore variability in wave energy, with areas of strong wave-height reinforcement and adjacent shadow zones. Such refractive effects have been noted at other rocky sites, such as the Monterey Peninsula, U.S.A. (Storlazzi & Field, 2000) and Opunake, N.Z. (McComb *et al.*, 2001).

10.3.3 Effects of wind vector on wave transformations

The effects of wind on nearshore wave transformations has been little studied (Carter *et al.*, 1998), and the new findings of Chapter 5 indicate that the wind vector does influence the distribution of wave energy in the nearshore regions, particularly where there is strong wave refraction. Whitecapping is a dissipative process (Hasselmann, 1973) which causes wave crests to partially break based on the steepness of the wave field (i.e. not depth-dependent). In a coastal setting, this will occur when strong winds (i.e. >6 ms^{-1}) are approximately colinear with the direction of wave advance (i.e. onshore-directed winds). Winds opposing the direction of wave advance (i.e. offshore-directed winds) will also cause an attenuation of the energy flux, although this is

considerably less than whitecapping and very frequency dependent (Young & Sobey, 1985). From an analysis of the data collected at New Plymouth, it is theorised that the partial breaking of wave crests under strong onshore wind causes a reduction in the longshore variation of wave energy. This occurs through a process of localised diffraction along the wave crests. Hence, there is an opposite effect to the wave height concentration caused by wave refraction, whereby the localised diffraction causes a longshore "smoothing" of the wave energy. Characteristic wave transformations under onshore and offshore winds were also measured by Vincent & Jensen (1997). Their data show an equivalent shoreward energy transfer in both wind cases, but a spectral shift to high frequencies in the strong (up to 25 ms^{-1}) onshore winds, and a converse low-frequency shift in offshore (8-20 ms^{-1}) winds. While those data were measured over uniform bathymetry without any strong refracting bed structures, the wind-derived spectral shifts were similar to those observed at New Plymouth (e.g. Fig. 5.3).

More work is required to further quantify the effects of wind on the nearshore wave transformations, and it was hoped that data from the second field measurement programme (Chapter 2) would provide a confirmation of the empirical findings in the first measurement period (Chapter 5). Unfortunately, however, there were insufficient onshore/offshore wind events in that period for detailed analysis. Future work on this topic would include a whitecapping dissipation term in the WBEND refraction model (as employed in the 2GWAVE model of Young, in Pang *et al.*, 1999) with testing and validation against the New Plymouth field data.

10.3.4 Frictional attenuation of nearshore wave heights

The dissipation of wave energy by frictional attenuation energy occurs through the interaction of wave-orbital motions with elements of the seabed. A widely used expression to define wave friction (f_w) is the Swart (1974) term (Eqn. 9-2), which is based on the relative roughness of the bed and the orbital radius. Over a rocky bed, the roughness may be characterised by the Nikuradse effective roughness (k_s). This parameter is often taken as representing the physical height of the bed roughness elements, and under the combined action of waves and currents is given as 30 times the roughness length z_o (where z_o is defined as the elevation above bed at which the free-stream velocities go to zero; Fredsoe & Deigaard, 1992). Accordingly, the amount of

frictional attenuation of wave energy will depend on the bed elements (i.e. fixed or varying in geometry) as well as the local wave height, wave period and water depth.

A comparison of the nearshore and offshore wave spectra show a trend for spectral shifts to longer periods as the waves progress shoreward. This is consistent with a frequency dependent attenuation; as waves advance into shallow water the effect of vertical attenuation of orbital motion becomes less pronounced, and frequency dependence dominates. Similarly, the effect of tide level on the monochromatic wave height ratios confirms that bed friction is an important influence. For example, wave heights at site D2 increase by approximately 10% over the average tidal range.

The initial WBEND wave refraction model studies (Chapter 5) applied a monochromatic and spectral calibration using a constant friction coefficient over both sandy and rocky beds alike. This model was refined, using the newly acquired side-scan data (Chapter 2) to characterise sandy and rocky beds within the model grid, and calibrated with monochromatic data from 63 individual events (see Appendix 2 for full details of the WBEND model calibration). A range of friction values and wave input types were tested, and ultimately the best simulation was found using a constant friction coefficient over sandy beds (C_f = 0.09), a Nikuradse effective roughness over rocky beds (10 m), and periodicity represented by the mean spectral wave period (T_m). The use of a constant roughness over the sandy beds, despite expected changes in bedform geometry with changing wave conditions, is consistent with the findings of Houwman & van Rijn (1999). A k_s value of 10 m is equivalent to a physical bed roughness of 0.33 m.

Model validation against a 13-day time-series of wave records shows a high-correlation between the measured and predicted significant wave heights (R^2 linear regression coefficient of 0.83). This model was used in the sediment transport studies of Black & McComb (2000) as well as in the investigations of Cole *et al.*, (submitted), which is presented in Appendix 4 to this thesis.

The good correlation of the model results with measured wave data indicates that the spatial wave transformations can be effectively resolved over complex bathymetry using a high-resolution grid (25-50 m spacing). Furthermore, the studies have shown that in

this case, a monochromatic representation of the sea-state provides an adequate simulation of the wave transformations.

10.4 Circulation patterns

In a wave-dominated environment, the coastal circulation patterns are responsible for the net advection of the sediments entrained by wave-orbital motion (e.g. Soulsby, 1999). On an open coast, the nearshore circulation may be driven by radiation stresses (Feddersen *et al.*, 1998) and have wind-driven components (Matsunaga *et al.*, 1996). The adjacent "continental shelf" currents (e.g. Webb, 1996) will also induce nearshore current flows (e.g. Holloway *et al.*, 1992), which are in turn influenced by the seabed topography through bathymetric steering (e.g. Slinn *et al.*, 2000; Storlazzi & Field, 2000) and bed friction (Houwman & van Rijn, 1999). Here, the field measurements are used to provide a quantitative description of the flow patterns at New Plymouth.

10.4.1 Shelf currents

The currents offshore of New Plymouth in intermediate water depths (i.e. >20 m) have characteristically different flow patterns to the nearshore currents - an observation also made by TCC (1981, 1985) at other North Taranaki sites. Mid-water data from site DW1 (in 35 m water depth; Chapter 5) has current directions that are strongly bimodal, with up-coast currents grouped about a heading of 060°, and down-coast currents centred around 250°. These orientations are approximately contiguous with the isobaths, which run at 050°-230° at that site. The deviation of +20° from the contour for the down-coast flow is suggestive that the slightly concave North Taranaki coastal shape (e.g. Fig. 1.1) influences the current direction. Site L1 is closer to shore (i.e. 23 m water depth) and exhibits directional peaks at 070° and 260°, albeit with more directional variability than DW1.

Over a 16-month period, mid-water current speeds at site L1 were most commonly of the order 7-10 cms^{-1}, with the 95% exceedence level at 2.1 cms^{-1}, 50% exceedence at 12.8 cms^{-1}, and 5% exceedence at 52.1 cms^{-1} (the maximum recorded velocity was 65 cms^{-1}). Up-coast currents (with directions 330°–120°) occurred 45.9% of the time, with a mean speed of 12.8 cms^{-1} at heading 055.9°. Down-coast current (with directions

121°–330°) occurred 54.1% of the time, with a mean speed of 9.8 cms^{-1} and heading of 252°.

The reversing shelf currents occur as low-frequency oscillations within the New Zealand weather-band ($0.033 < f < 0.6$ cpd) frequencies. Such flows are usually associated with coastal trapped waves, which are generated by regional wind stresses and barometric fluctuations (Stanton, 1995). McComb & Black (2000) analysed a 316-day record of currents at site L1 to determine the dependence of low-frequency current oscillations on the coincident wind vector. Those findings indicate that currents typically have a 0.5 day lag behind the wind forcing, and some 26% of the total longshore current variance can be related to the north-south orthogonal wind stress. This differs from Black & Sokolov (1993), who explain some 53% of the variance in longshore current from the east-west wind vector (V_e). However, Black & Sokolov used data from shallow water (9 m depth) offshore of the main breakwater (and in the lee of Moturoa Island). Current vectors in this region are strongly influenced by the main port breakwater (e.g. Chapter 8) and do not well represent the regional shelf flows.

10.4.2 Nearshore currents

The nearshore currents have been numerically modelled for a representative 13-day period (Black & McComb, 2000). The time and depth-averaged numerical output (Fig. 8.9) shows the broad circulation trends, which are resultant from wave-driven, wind-driven, and shelf-driven forces, as well as bathymetric steering. Key features of the model output are: i) strong easterly flows along the main port breakwater (directed across the harbour entrance), ii) strong eastward flows across the axis of the subtidal Kawaroa Reef, and iii) weak and reversing flows in the region between the port and Kawaroa, suggestive of a gyre in the lee of the port. Those features are generally represented in the averaged near-bed current meter data (e.g. Fig. 8.8), although vector averaging of time-series current data does not always represent the true circulation trends, particularly when the directions are bimodal. Accordingly, the measured currents (1 m above bed level) are here described for the different nearshore oceanographic regions, as well as for the wave-, wind- and shelf-current conditions that likely cause such flows. The large set of data from a wide range of sea conditions (Chapter 2) allows specific conditions to be isolated and examined as follows.

1) Current velocities

Offshore and adjacent to the main port breakwater (i.e. site S1) the currents are typically low (< 10 cms^{-1}), with both eastward and westward directions that are approximately aligned with the breakwater. When the wave energy is high (regardless of the incident wave direction), the current speeds are usually strong (>30 cms^{-1}) and directed toward 060°. In the sheltered corner adjacent to the port's lee breakwater (i.e. site S2), currents are weak (<8 cms^{-1}) with variable directions (ranging from 060° through to 340°), although showing a general alignment to the lee breakwater (i.e. SE-NW). On the axis of the subtidal Kawaroa Reef, current speeds are typically less than 10 cms^{-1}. In the deeper regions (8.8 m; site S3) velocities reach 21 cms^{-1} and show a broad bimodal directional distribution, with a predominant flow toward 030°–120°, and a secondary mode toward 250 – 350°. In the shallower regions (3.8 m; site S4) very strong currents (~37 cms^{-1}) periodically occur with high waves, with directions of around 100°. However, usually the flows are northerly-directed, ranging from 300° through to 040°. In the centre of the bathymetric channel adjacent (and east) of the Kawaroa Reef (i.e. site S5) the currents are generally of very low velocity (<3 cms^{-1}) and are uniformly directed offshore along the channel axis. The highest flows (~23 cms^{-1}) are associated with energetic wave conditions (i.e. H_s >2 m at site S5). Mean current velocities on the main axis of the Kawaroa Reef (sites S3 and S4) are approximately twice that of sites in the slightly deeper water on either side (sites L2 and S5).

2) Local wind-driven nearshore currents

The effect of local winds on the nearshore current regime can be identified during periods of low waves and shelf currents (i.e. site L1 H_s <1.5 m, current <10 cms^{-1}). Only two nearshore sites (S3 and S4 on the axis of the Kawaroa Reef) exhibit a systematic correlation between wind and current vector, although this was weak (i.e. R^2 ~0.18 for the linear regression of the easterly vectors of wind and current). The data suggest the local wind-driven currents provide only a minimal input to the overall nearshore circulation system.

3) Wave-driven nearshore currents

Wave-driven circulation can be identified when the offshore shelf currents are low (i.e. <10 cms^{-1} at site L1). Current velocities at all the nearshore measurement sites exhibit a systematic influence from the wave height, showing higher velocities under larger waves. Sites S1 and S4 (offshore of the main breakwater and on the shallow part of the Kawaroa Reef, respectively) are the most responsive, while much less influence is found in the quiescent lee of the port (site S2) and in the deeper regions of the Kawaroa Reef (site S3). Only sites S1 and S3 have a distinct relationship between wave height and current direction, whereby larger waves are associated with easterly-directed currents. In large wave conditions, the circulation patterns appear to be very complex, which was also found in the numerical studies of Black & McComb (2000).

4) Shelf-driven nearshore currents

The influence of shelf currents on the nearshore circulation can be investigated when the offshore wave heights are low. Linear regression analysis of the offshore and nearshore current vectors show that the sheltered inshore positions (i.e. sites S2 and S5) receive little or no influence from the offshore currents. Conversely, the most exposed sites (S3 and S4) are reasonably well linked to the shelf flows (R^2 ~0.4), while sites S1 and L2 are only weakly linked (R^2 ~0.2). The shelf currents have up- and down-coast directional modes, each of which has a different effect on the nearshore flow patterns, and these are illustrated in Figure 10.2. Flow reversals are evident at sites S1, S3 and S4, while sites S2, S5 and L2 remain similar for each shelf current directional mode.

10.4.3 Summary

The circulation regime may be reduced to three regions (Fig. 10.3). In the offshore regions beyond the influence of coastal indentations and irregular bathymetry (i.e. >20 m depth), currents are frequently strong (i.e. exceeding 50 cms^{-1}), externally forced, parabathic and typically feature reversals in direction at 2-5 day intervals. In the close nearshore regions (i.e. <5-10 m depths), currents are considerably weaker and are often sheltered by the coastal indentations. Flows here are predominantly wave-driven and are periodically strong (i.e. >30 cms^{-1}) near the breakwater (site S1) and on the ridge of the

Kawaroa Reef (site S4) during high waves. In between these two regions is a zone of intermediate flows that are derived from both the wave-driven and shelf-driven currents, and to a lesser extent from local wind-forcing.

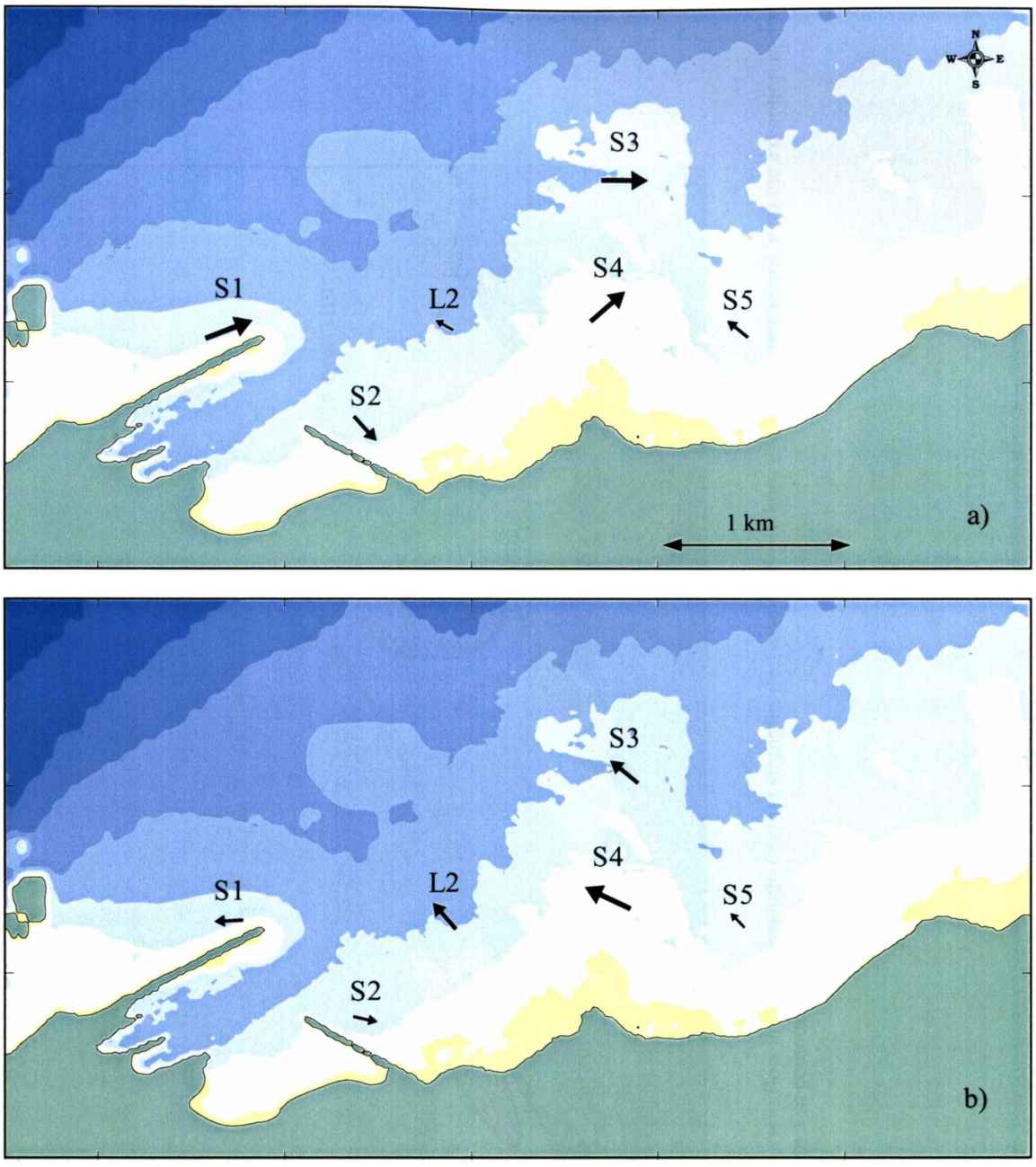

Figure 10.2: Nearshore circulation patterns under conditions of low incident wave height (H_s <1.5 m) when shelf currents exceed 10 cm^{-1} for: a) up-coast flows and, b) down-coast flows.

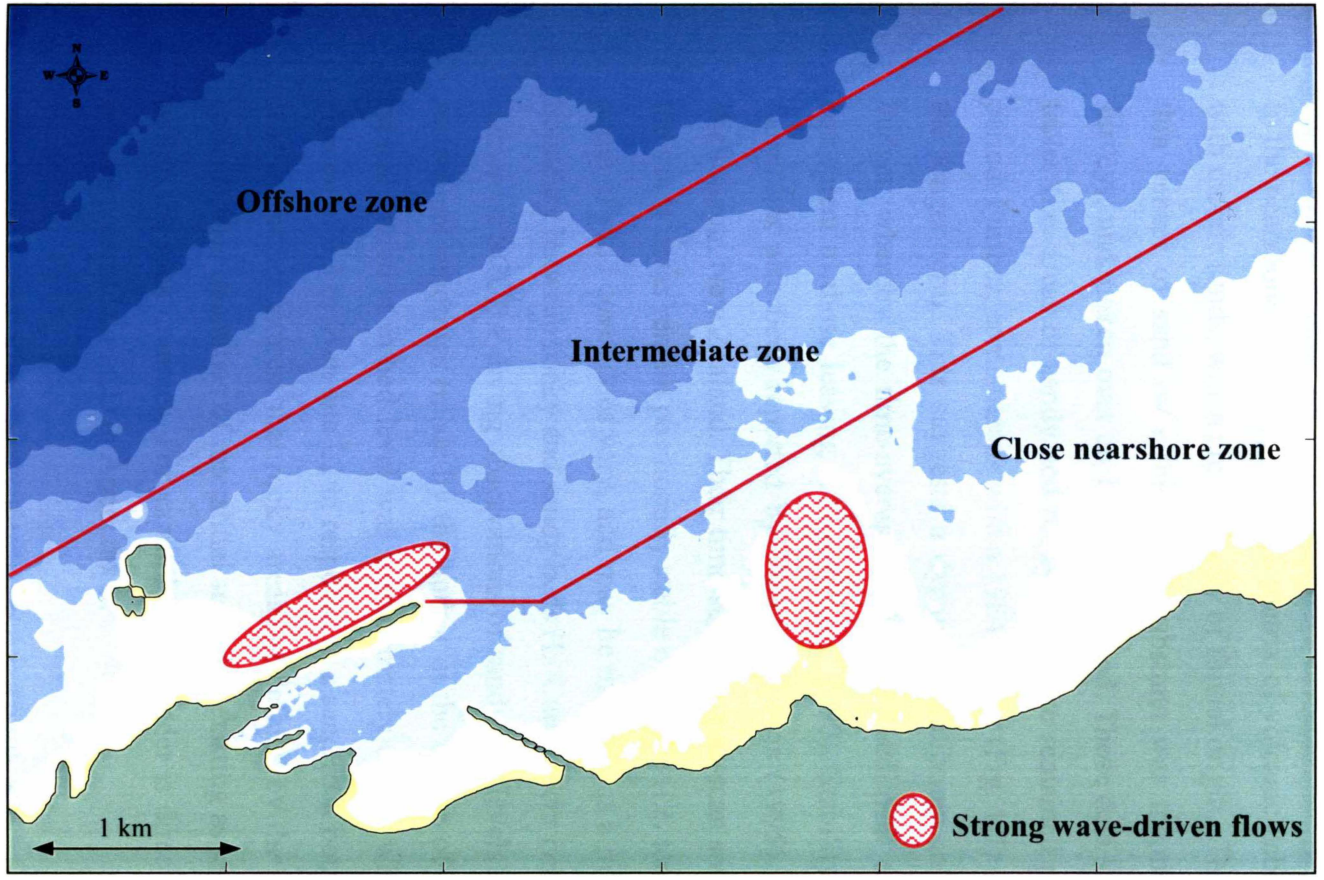

Figure 10.3: Schematic map showing zones of current flow at New Plymouth. Current strengths decrease from offshore to the close nearshore, with the exception in zones of strong wave-driven flow. Bathymetry is shaded in 5 m contours.

10.5 A description of the sedimentary environment

The Holocene marine transgression resulted in the progressive incision of lahar agglomerates of the Taranaki volcanic ring-plain, forming the rocky wave-cut platform that is evident in the intertidal regions today and extending to depths in excess of 50 m. In the nearshore coastal regions, this matrix of volcanic debris is intermittently overlain with mobile sands, which are primarily of fluvial origin. The distribution of a relatively thin veneer of sand over this rocky substrata was mapped in four side-scan sonar surveys, undertaken over an 18-month period. Those data show that the main sediment facies (i.e. areas of sandy and rocky bed) have remained positionally stable over that period. Further, comparisons with a 1984 survey (Fig. 1.7) suggest very little change in the longer term. This suggests a dynamic equilibrium in the nearshore sedimentary budget, whereby the time-average volumes of sediment entering the littoral cell are equivalent to those leaving it (e.g. Griggs, 1990). Stability in the nearshore sediment facies has also been reported by Carter & Lewis (1995) for an energetic coast near Wellington, New Zealand. Their time-series of side-scan sonar data indicates that while the sandy areas remain positionally stable over time (i.e. tens of years), the volume and depth of sand cover does vary, and may be manifest as a minor migration/retreat of the boundary between rocky and sandy beds (L. Carter, *pers comm*). This is consistent with numerous SCUBA diving observations of sandy bed levels next to reference points and instrument moorings (made by the author in the course of the field experiments). The typical variation in bed level was approximately 0.1 m, while the largest involved the erosion of 0.3 m from site L2 in response to a sand/rock boundary adjustment of ~50 m. It is of further interest that rocky areas (as defined by the side-scan sonar) often have considerable quantities of interstitial sediment existing as small patches (e.g. 0.5 m^2) or within the rock crannies. For examples, the reader is directed to the underwater video images presented on CD in Appendix 3.

The presence of a predominantly rocky bed with thin, intermittent sand cover is a ubiquitous feature of the nearshore Taranaki coast. This morphology is readily observed in the side-scan sonar records of the nearshore (i.e. <50 m depth) Maui gas pipeline route (*pers obs*), the TCC (1985) seabed maps from near Waitara (Fig. 1.1), as well as from a recent (December, 2000) nearshore side-scan sonar survey along a 20 km stretch of the northern Taranaki coast (unpublished data collected by the author). From these

observations, it may be considered that the presence of a large sandy area offshore and adjacent to the port entrance is unusual. Beamsley (2001) extended the side-scan sonar survey data presented in this thesis (e.g. Fig. 2.6) in a map of the Sugarloaf Islands Marine Protected Area (SLIMPA) (e.g. Fig. 1.2). He confirmed that the contiguous sandy bed continues around the Paritutu Headland to the west of the port, extending out to the survey limit (~30 m water depth), blending into the sandy beach on the western flank of the headland.

The distribution of mean grain sizes of the sediments (Fig. 10.4) shows that the sediments are fine on the offshore side of the main breakwater, but become coarser adjacent to the wall and toward the tip-shoal. The coarsest material is found along the main growth axis of the tip-shoal (Chapter 6), and the sediments become progressively finer with distance into the harbour. A wide range of sediment sizes is found in the lee of the harbour (i.e. between the lee breakwater and the Kawaroa Reef). Further to the east, the sediments show a well-defined fining trend with increasing depth.

Diving observations by the author indicate the rocky reefs are highly variable in terms of the geometry of the bed elements - ranging from cobble pavements with very low relief, to boulders and cemented scarps that exceed 1 m in height. This variability was mapped from the standard deviations in the side-scan sonar return signal[3] (Fig. 10.5), providing a relative measure of the bed roughness. The sandy facies are well matched to regions of low signal variance, while a considerable range is evident over the rocky beds.

[3] Data analysis by J. Kruger, Earth Science Department, University of Waikato

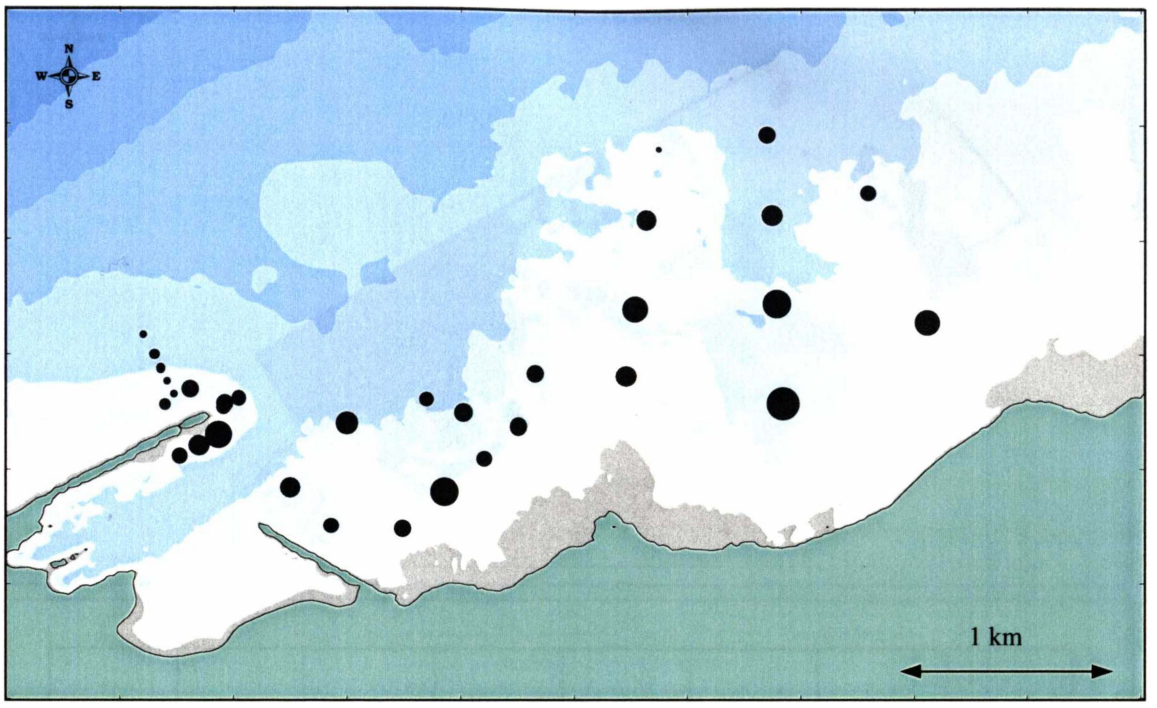

Figure 10.4: Mean grain sizes for surficial seabed samples represented by closed circles. Where the bed is rocky, interstitial sediments were collected by SCUBA divers. Grain size is linearly scaled from 0.151 mm to 0.301mm.

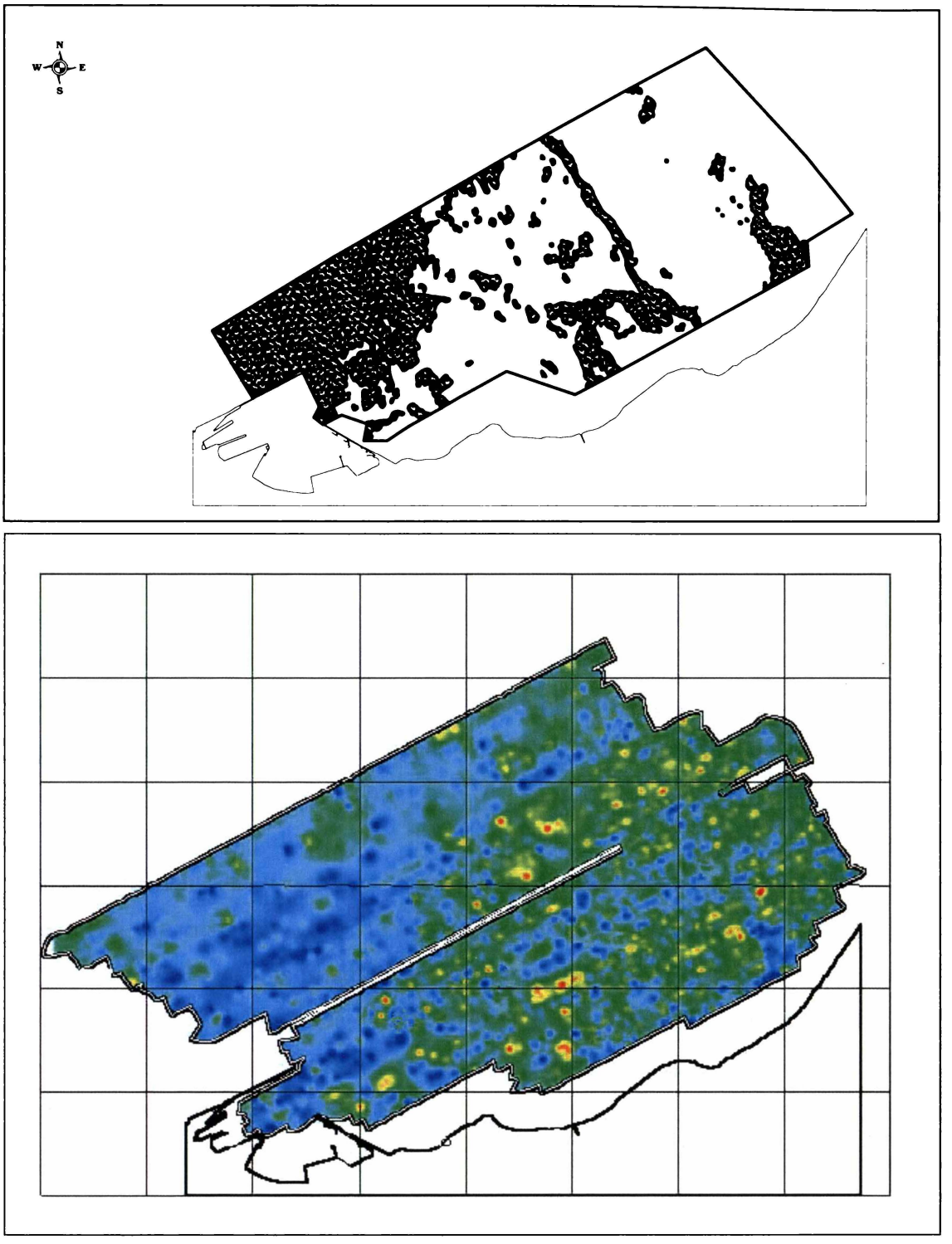

Figure 10.5: Upper panel shows areas of rocky and sandy bed (shaded) from 1997 side-scan sonar, lower panel shows the standard deviation in side-scan sonar signal return (where blue is low, red is high).

10.6 Sediment entrainment and suspended sediment concentrations

The findings of Chapter 9 have confirmed a methodology for predicting the time-averaged near-bed reference concentration (C_o) of relatively dense volcanic sediments under high-energy, wave-dominated conditions. Thus, C_o values may be effectively derived from wave and surficial sediment information. Additionally, multi-level SSC measurements have been fitted to a vertical concentration profile, thereby allowing C_o values to be related to the concentration of sediment suspended throughout the water column. This methodology is applicable to areas with sandy beds.

A rocky bed will affect the entrainment process through a limitation in the supply of sediments, and an alteration of the near-bed orbital velocity regime and greater generation of turbulence. The latter is a balance of increased velocities due to convergence of flow streamlines around the rocks (Nielsen, 1992), and near-bed quiescent zones that may exist because of those elements (Green *et al.*, 1998). The vertical distribution of entrained sediments may also be influenced by a rough rocky bed, potentially increasing the length scales of turbulent motion and inducing convective effects (e.g. Nielsen, 1992),

SSC measurements show comparatively lower concentrations over the rocky beds, with values that are inversely proportional to the distance from contiguous sandy beds. Figure 10.6 illustrates this trend, using SSC measurements from 0.5 m above the bed over a 13-day period (Julian days 82-95, 1998). Rocky bed SSCs are of the order 0.37 times the values measured on sandy beds. The trend is also apparent at 1.0 m above bed, although less marked (i.e. 0.76). More specifically, sites D2 (sandy) and S4 (on the rocky Kawaroa Reef axis) are in similar water depths and approximately 600 m apart. Site S4 measured only 0.27 times the SSC of D2 (0.5 m level), and 0.69 times the SSC of D2 at 1.0 m level (Fig. 10.1). These data indicate that; i) suspended sediments at a given location have a source not necessarily limited to the local bed (i.e. a "regional" source), and ii) the SSC profile over rocky beds is supply-limited. The scale at which the "regional" source occurs will depend on wave energy and current flows, for example under very stormy conditions the "regional" sense may have a spatial scale of hundreds of metres, while in less energetic periods that may be considerably lower.

The presence of fine sandy sediments within the rocky matrix even in the very shallow, high-energy sites (e.g. site S4) may be due to quiescent zones within the bed roughness, but may also represent an equilibrium response from the suspended sediment flux. The SSCs over rocky areas are still significant values, despite those beds having low residence volumes of sand. Furthermore, the data indicate a steeper SSC profile exists over the rocky beds (Table 2.2). This is consistent with both a local entrainment supply-limitation, and a "regional" source for the upper level (i.e. >0.5 m above bed) suspended sediments.

The influence of bed roughness on turbulence within the water column has been investigated by numerous researchers (e.g. Nielsen, 1992). The attenuation of wave heights due to bed friction is essentially a transfer of energy from oscillatory motion to turbulent motion - thereby influencing the sediment diffusivities. Large-scale eddies caused by the bed morphology may also cause strong, localised convection of sediment-laden water to higher levels. In shallow water these are observed on the surface as "boils", and are often associated with plumes of suspended sediments. Such turbulence effects from a rocky bed have been postulated as the reason why rocky areas appear to be resilient to sediment inundation (e.g. Curray, 1965; Arron & Mitchell, 1984). The results from monitoring of the nearshore dump mound lend credence to that theory, as the mound eroded without the adjacent rocky regions becoming inundated with sand.

In addition to the issues of sediment supply and bed roughness, entrainment is directly related to the magnitude of the wave-orbital velocities. This means that the near-bed velocities will be greatest in shallow water (prior to wave breaking), which is also evident in the trends in the SSC data of Figure 10.6. A simple conceptual model of the nearshore suspended sediment regime would therefore consider two main parameters; the sediment supply (i.e. proximity to a sandy bed), and the near-bed orbital velocities. The highest SSCs are expected in wave-exposed, shallow water (i.e. < 5 m depth) over sandy beds.

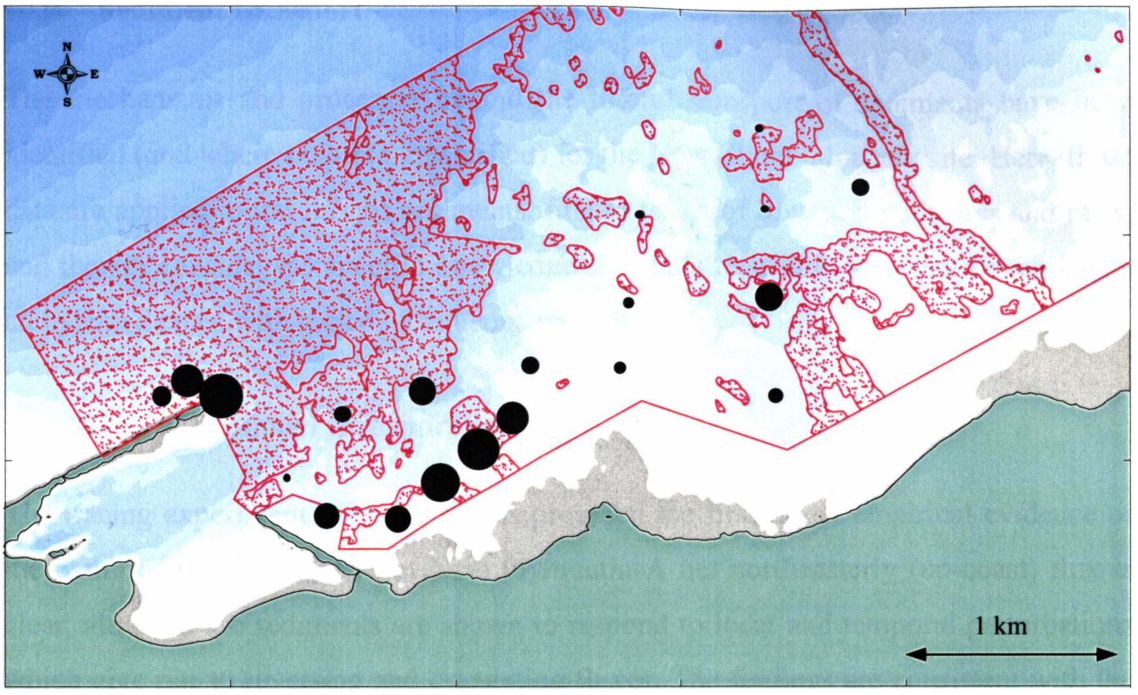

Figure 10.6: Time-average SSC measured with sediment traps over a 13-day period (Julian days 82-95, 1998). Closed circles are linearly scaled from 0.015 - 0.2 kgm^{-3}. Areas of sandy bed are shaded in red.

10.7 Sediment transport

The mechanisms and processes behind the littoral transport of sediments have been identified (and where possible, quantified) for the New Plymouth study site. Here, those data are applied to the flux of sediments, first in terms of transport pathways and rates, and then to consider the specific knowledge shortfalls regarding sediment dynamics on an indented coast with rocky subaqueous reefs.

10.7.1 Sediment transport pathways

The tracing experiment (Chapter 8) has provided the first direct empirical evidence of the path of littoral sediments at New Plymouth. A net northeasterly (up-coast) flux is clear, although the sediments are shown to respond to local and temporal perturbations which give rise to reversing and circulating fluxes. The findings are consistent with the estimates by HRS (1963) of a 3:1 ratio of up-coast and down-coast fluxes. The alignment of beaches and the accumulation of sediments on the western sides of groynes is also evidence of the net northeasterly transport (Hicks & Gibb, 1987), as well as the characteristic accretion at the western side of the port entrance (Chapter 6), and the growth of the salient tombolo shoreward of Moturoa Island concomitant with lengthening of the breakwater (McLennan, 1982). On a larger scale, north of New Plymouth and along the entire West Coast to North Cape are littoral sediments derived from Taranaki volcanic andesites (Gibb, 1979).

Patterns of sedimentation and grain size also provide evidence of littoral transport pathways. For example, there is a well-defined sorting of sediments within the harbour. Medium-coarse grained sands are found on the inside of the main breakwater (Fig. 10.4), decreasing in mean grain size with increasing distance from the tip-shoal (Chapter 6). These tip-shoal sediments have a very low silt content (< 10% of the particles are smaller than 63 μm; Black & McComb, 2000) and accrete at a rate of between 124,000 m^3 per year (Atkinson & McComb, 1997) and 142,000 m^3 per year (Chapter 6). In the shipping channel, the sediments are considerably finer (up to 80% silts) even at sites immediately adjacent to the tip-shoal. Water depth and wave energy influence the grain size distribution in the rest of the harbour, with only silty material found at the berths, and fine sand/silts on the sheltered Ngamotu Beach (Fig. 1.2).

Accretion at the tip-shoal is principally due to material being entrained along the outside of the breakwater, and then essentially spilling into the harbour (Fig. 10.7). Refracting waves then redistribute those sediments along the inside of the breakwater. The shipping channel outside of the harbour (and beyond the shelter of the breakwater) does not experience excessive accretion (Fig. 10.7), and the settlement rates there are similar to inner harbour rates. There is no significant long-term accretion on the lee breakwater side, despite this region having considerable wave-shelter from the main breakwater. These data depict the harbour as a classic sediment trap - providing a quiescent zone that allows the sediments to be fractionated on the basis of their particle settling velocity.

Tracer injected "upstream" of the port entrance has shown that most of sediments in water depths 6-10 m bypass the harbour, while the "top-down" pattern of accretion at the tip-shoal is consistent with a shallow sediment source. Thus, only sediments within a narrow zone close to the breakwater (i.e. <100 m) are trapped on the tip-shoal. A strong northeasterly sediment flux is shown for this region by the measured and modelled currents, which exhibit enhanced wave-driven flows parallel with the main breakwater.

Immediately east of the port (in the sheltered lee along the Kawaroa coast), the sediment transport vectors are less well defined, as are the circulation patterns. This is manifest in the rates of erosion of the experimental dump mound, which were low despite the very high SSCs measured in this region (e.g. Fig. 10.6). Thus, while the sediments are actively being entrained and suspended in this region, the net flux of sediments is low (compared with the site S1 region). Tracer injected at the experimental nearshore dumpsite shows a net northeasterly alongshore vector although an opposing flux was also observed, directed to and transgressing the harbour entrance.

The dominant spreading patterns of the tracer were alongshore, with cross-shore spreading accounting for approximately 5% of the total horizontal diffusivity. Sediments from "upstream" of the port, as well as from the sheltered lee have demonstrated a pathway to the eastern city beaches. However, from the "upstream" location, there is comparatively little sediment flux into the zone inshore and west of the experimental dumpsite (i.e. the western Kawaroa coast). This is likely to be due to the

deflection of sediments from this zone by the breakwater orientation, as well as trapping of the shallow sediments on the breakwater tip-shoal.

Further offshore (i.e. >20 m) where the isobaths are regular and there are no large impediments to the current flow, the parabathic currents flow up- and down-coast for an approximately equivalent percentage of the time. The northeasterly-directed up-coast flows are associated with slightly larger waves (4% larger on average) and have a higher average velocity (12% higher on average), thereby inferring a net sediment transport vector to the northeast. Sediment trapping experiments were conducted for a 3-month period (November 1998 to January 1999) at the shoreward limit of the offshore dumping ground (Fig. 1.5), measuring time-averaged SSCs of between 0.008 and 0.0187 $kg.m^{-3}$ (for the 0.5 m level above bed). These concentrations are approximately 10% of values obtained at the nearshore sites, indicating these offshore sediments are actively being entrained and suspended.

10.7.2 Nearshore sediment flux rates

Sediment flux occurs when suspended sediments are advected by the net current, and the maximum rates are likely to be experienced in regions of high SSC and high current flow. Accordingly, the shallow region along the main Port breakwater (i.e. near site S1) may be expected to have the highest flux rates, due to consistently high SSCs (Fig. 10.6) and the well defined longshore currents (particularly the wave-driven flows, Fig. 10.3). Transport rates in this region may be considered from the rates of accretion on the tip-shoal (e.g. Dean, 1989), and from measured wave and current data from site S1.

The monthly accretion rates at the breakwater tip-shoal are a reasonably constant value that equates to 390 m^3 per day (Chapter 6). This is approximately 75% of the volumes trapped in the harbour, with the remaining quantity being mostly fine silty material. If it is assumed that the tip-shoal sediments are sourced from within 100 m of the breakwater wall, this equates to a minimum longshore flux of 1420 m^3 per metre of seabed per annum. However, not all the sediments within 100 m are trapped, and the trapping efficiency will decrease with distance from the breakwater wall. Correlation of the accretion patterns (Fig. 10.7) with the bathymetric contours along the offshore side of the breakwater suggest that most of the tip-shoal sediments are from within 50 m of

the wall, where the depth grades from 2-4 m. Indeed, this shallow region next to the wall may often be considered as a surf zone.

Flux rates from site S1 data have been estimated for the 6 m depth range (which is 100 m from the breakwater wall). Using two-months of data from site S1, SSC profiles were derived (from the methods in Chapter 9), and a net longshore flux obtained by integrating the profiles with the current velocities (also integrated through the water column). The net northeasterly (longshore) flux along the 6 m contour was found to be 572 m^3 per metre of seabed per annum.

The longshore surfzone sediment transport rates were also calculated for the zone near the breakwater tip using the site S1 data. The model GENIUS was used to derive an annualised longshore transport rate based on 45 days of measurements. GENIUS uses the commonly-adopted CERC equations for longshore surfzone sand transport, and is similar to the GENESIS model of Hanson (1989). The model results indicate some 239,000 m^3 of sand is transported in a northeasterly direction along the breakwater wall per year.

Comparing these two measurements provides an indication of the quantities of sediment that bypass the harbour entrance and are not trapped on the tip-shoal. For example, if the annual tip-shoal accretion was assumed to represent the entire sediment flux from the 50 m cross-shore transect adjacent to the wall, and 572 m^3 per metre per annum of bypassing sediments was occurring in the 100 m zone beyond that, then bypassing volumes would be 40% of the trapped volumes. This simple analysis only considers the zone within 150 m of the breakwater wall, while active sediment transport will be occurring right across the inner continental shelf. Notably, McComb *et al.* (2000) report that regionally, the sediments may be considered as mobile at depths of up to 90 m. While the sediments trapped in the harbour are only a fraction of the total longshore littoral drift (i.e. a value that will be less than 70%), what is significant is the proximity of those trapped sediments to shore and the "downstream" impacts of dumping those sediments in deeper water.

10.7.3 Effects of coastal indentations and rocky reefs

On a sandy coast, the nearshore seabed morphology is dominated by the local wave and current regime (Niedoroda, *et al.,* 1984), and is responsive to changing sea conditions. Beach and intertidal sediments exist in a dynamic equilibrium with the subtidal sediments, balanced by the coastal morphology, sediment size and supply and energy gradients (Komar, 1998). Diabathic exchange of sediments is well noted for sandy coasts (e.g. Osborne & Greenwood, 1992), but on a rocky coast such as New Plymouth, the limited supply of mobile sediments does not allow the same response.

Firstly, it is worthy to consider the effects of the large-scale coastal morphology on the sediment dynamics. Small headlands such as Paritutu (Fig. 10.8) present "fixed partial" barriers to sediment flux (e.g. Bray *et al.*, 1995), which have an effect analogous to that of a shore-normal groyne on a beach. Sediments accumulate on the "up-stream" flank of such structures until equilibrium is established, after which they "leak" past. Accordingly, a small headland such as Paritutu does not interrupt the littoral drift, but may influence the conditions under which transport occurs (Hume *et al.*, 2000). Another important consequence of the Paritutu Headland is that it causes a local reduction in the continental shelf width. The headland protrudes by some 1.8 km from the regional coastal orientation (Fig. 10.8), yet this protrusion is not manifest as a continental shelf feature, thereby concentrating the zone of littoral flux closer to the shore. This is likely to be the reason why most of the seabed in that area is sandy (i.e. 74% of the seabed is sandy; Beamsley, 2001). Indeed, the effect of the headland may be likened to reducing a four-lane motorway by two lanes for a short distance, effectively increasing the density of traffic in that two-lane zone. Accordingly, when accounting for the sediment budgets on either side of the port, the width of the littoral transport zone needs to be considered, as well as the impacts from harbour dredging and dumping. It is notable that the 0-20 m littoral zone is 2500 m wide offshore of Fitzroy Beach, while near the port/Paritutu this distance is only 1100 m. The subaqueous concentration of sediments on the headland near the port entrance is likely to increase the trapping efficiency of the harbour.

The smaller scale subtidal morphologies, such as the shore-normal reefs, do not appear to present a significant obstacle to longshore sediment transport. This is evidenced in the tracer observations (i.e. the longshore pathway across the reefs to the eastern city

beaches) and also in the SSC measurements on the reefs. Rather, the main effect of the reefs arises from their influence on the circulation patterns. The variability in depth along the pathway from the port to Fitzroy Beach is given in Figure 10.9, showing values that are similar to those quoted by Storlazzi and Field (2000) for sites in Santa Cruz (California, U.S.A.). There, the nearshore reefs are thought to cause significant barriers to the longshore sediment flux, and Storlazzi and Field suggest that diabathic transport or storm conditions are necessary to circumvent these structures. However, the data from New Plymouth indicates that most sediment transport is due to suspended sediments (not bedload), which are able to cross the bathymetric highs. Furthermore, the data show that this occurs even under moderate wave conditions. Bathymetric highs may also encourage sedimentation on the "upstream" side (similar to the headland effect). This does not necessarily mean they impede the sediment transport, but rather indicates they have a localised effect on the sedimentary regime.

An observation that is in accordance with Storlazzi & Field (2000) is the enduring presence of sediments within bathymetric depressions. These occur throughout the rocky matrix at New Plymouth, and the most notable is the in-filled relict Te Henui fluvial channel, which has recently been used to bring a telecommunications cable ashore (McComb & Beamsley, 2000). These zones exist as an equilibrium response to the suspended sediments, as wave-orbital velocities decrease with increasing water depth (e.g. Chapter 7), allowing preferential settlement in the deeper environments.

Together, the tracer and the sediment trapping experiments have confirmed that suspended sediments traverse the large rocky reefs, and the side-scan sonar surveys have shown that the rocky nature of those beds under ongoing sediment flux is enduring. Indeed, the monitoring of the experimental nearshore sand mound clearly showed that adjacent regions maintained their rocky character and did not become inundated with sand, despite the erosion of the placed sands and tracer movements across the reef platform. Chapter 2 speculates that the hydraulic roughness of the reefs is an integral factor that precludes the settlement of sediments on those beds. Nelson (1996) studied the hydraulic roughness of a low-energy coral reef platform and concluded that the wave friction factor (f_w; Eqn. 9-2) was equivalent to movable beds of very coarse sand (i.e. 600 μm). While the roughness of the mobile beds at New Plymouth will vary with the bedform geometry (e.g. Black & Oldman, 1999) it will also

reduce under high-energy sheet-flow conditions. However, this is not the case on the immovable rocky beds, where the pressure gradients between the individual roughness elements will increase with the wave-orbital velocities (Nielsen, 1992). Very little experimental data exists to quantify the effects of this roughness, particularly in terms of sediment dynamics. The intertidal work of Howse (2000) and Gaylord (1999) both confirm that the roughness elements of rocky platforms do influence the velocity and turbulence structure under oscillatory wave motion, although to assess the effects on sediment entrainment and suspension remains a subject for ongoing research.

Coastal orientation plays an important role in determining the stability of beaches, even on sandy shorelines (e.g. Komar, 1998). On rocky coasts where the quantities of mobile sediments are limited, stable sandy beaches are usually only found in coastal embayments (forming pocket beaches protected by rocky headlands; Storlazzi & Field, 2000) or where the coastal orientation is such that the beach face is aligned with the incoming wave crests (Black & Rosenberg, 1992a). Rocky headlands also often feature characteristic zeta shaped bays in their lee in response to patterns of nearshore wave refraction (Silvester, 1985). Where the coastal alignment is oblique to the incoming wave crests, longshore currents generated within the surf zone provide a strong sediment transport mechanism that may preclude beach formation (e.g. Black & Rosenberg, 1992a). These features are also observed on the Taranaki coast, but with the addition of a sandy upper beach face and dune system often found co-existing with a rocky intertidal platform.

From Figure 10.8 it is evident that the alignment of the main port breakwater is coincident with the regional coastal orientation (i.e. 060°), which is approximately 10° oblique to the incoming wave crests (as measured at site S1). A considerable amount of sedimentation has occurred on the seaward side of the wall since the breakwater was constructed (estimated to be 1.7 million m^3; Hicks & Gibb, 1984), to the degree that water depths along the seaward edge of the wall are only 1-2 m at low tide. A comparison between hydrographic surveys of this region undertaken in 1984 and 1997 shows no volume change over that time, indicating an equilibrium state has been reached. This sedimentation is a response to both the wave-sheltering effect of Moturoa Island (causing a sedimentary salient shoreward of the island; Fig. 1.5), and the low angle of incidence between the breakwater and the wave crests. Indeed, it could be

surmised that if this angle was less (e.g. the breakwater was constructed at 050°), then the wave-driven flows along the structure would be reduced as an equilibrium beach orientation was approached. Conversely, if the angle between the breakwater and the wave crests were greater (e.g. the breakwater was constructed at 070°), then a very different sediment transport regime would exist, with the potential for higher wave-driven currents along the breakwater wall. Both scenarios have implications for sediment trapping at the harbour tip-shoal and wave impact/scouring forces on the wall.

The natural beaches in the New Plymouth region have orientations that range from 025° to 055° (Table 10.1), which is the combined response to headland effects (e.g. Oakura Beach) and the local incident wave angles (Fitzroy Beach; McLennan, 1981). Within New Plymouth City, only at Fitzroy is there a stable sandy beach, despite other locations having similar coastal alignments, and indeed exhibiting a sandy beach in pre-port times (e.g. Fig. 1.7). This shows that in addition to the coastal orientation, the supply of nearshore and surf-zone sediments is important in maintaining a sandy beach. Paritutu Beach, on the western flank of the Paritutu Headland also has a sandy character, but has a mean beach orientation of 025 degrees True, and this alignment would perhaps suggest a net longshore flux to the west, not eastward and feeding sediment toward the harbour entrance. However, the waves reaching this beach are refracted by the seabed contours, and modified by the presence of the offshore islands - thereby allowing sedimentary salients to form in the lee of the islands. These features permit a sandy beach to exist at this orientation.

The port breakwaters have been shown to influence the circulation patterns immediately east of the harbour. This effect is two-fold; creating a sheltering zone in the lee that is characterised by weak and reversing currents, and an intensification of the flow along the breakwater with deflection away from the Kawaroa coast. Thus, even without considering the impacts of harbour dredging and offshore dumping on the nearshore littoral sediment budgets, the flow deflection caused by the physical presence of the main port breakwater has a significant effect on the adjacent sedimentary environment.

It should also be noted that while the region between the port and the Kawaroa Reef has been termed here as quiescent, this is only a relative description as in very stormy

periods the entire nearshore environment is heavily impacted by waves. Indeed, this region receives no wave shelter in storms from the northerly quarter.

Table 10.1: Orientations of beaches in the New Plymouth area, where the coastline is aligned 060°

Beach	Distance from Port Taranaki	Mean orientation (degrees True)
Fitzroy	5 km (NE)	032
Rewarewa	7 km (NE)	046
Paritutu	1.5 km (SW)	025
Oakura	10 km (SW)	055
Komene	24 km (SW)	031

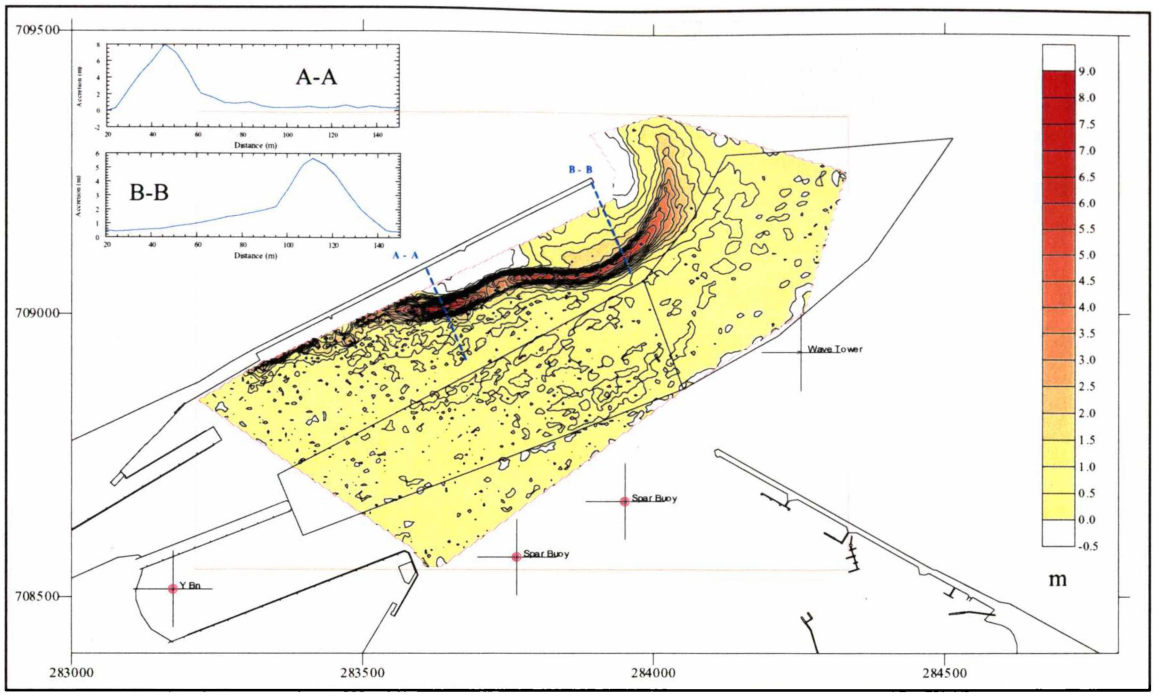

Figure 10.7: Surface difference map between post-dredge (1996) and pre-dredge (1998) survey data form Port Taranaki, showing areas and depths of sedimentation (m).

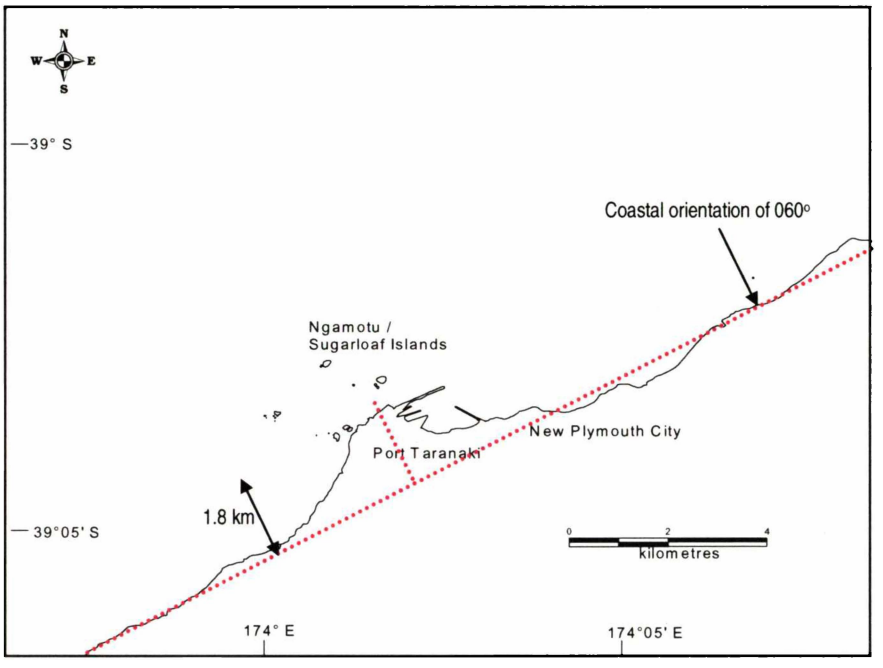

Figure 10.8: Map showing how the headland at Port Taranaki protrudes some 1.8 km from New Plymouth regional coastal orientation.

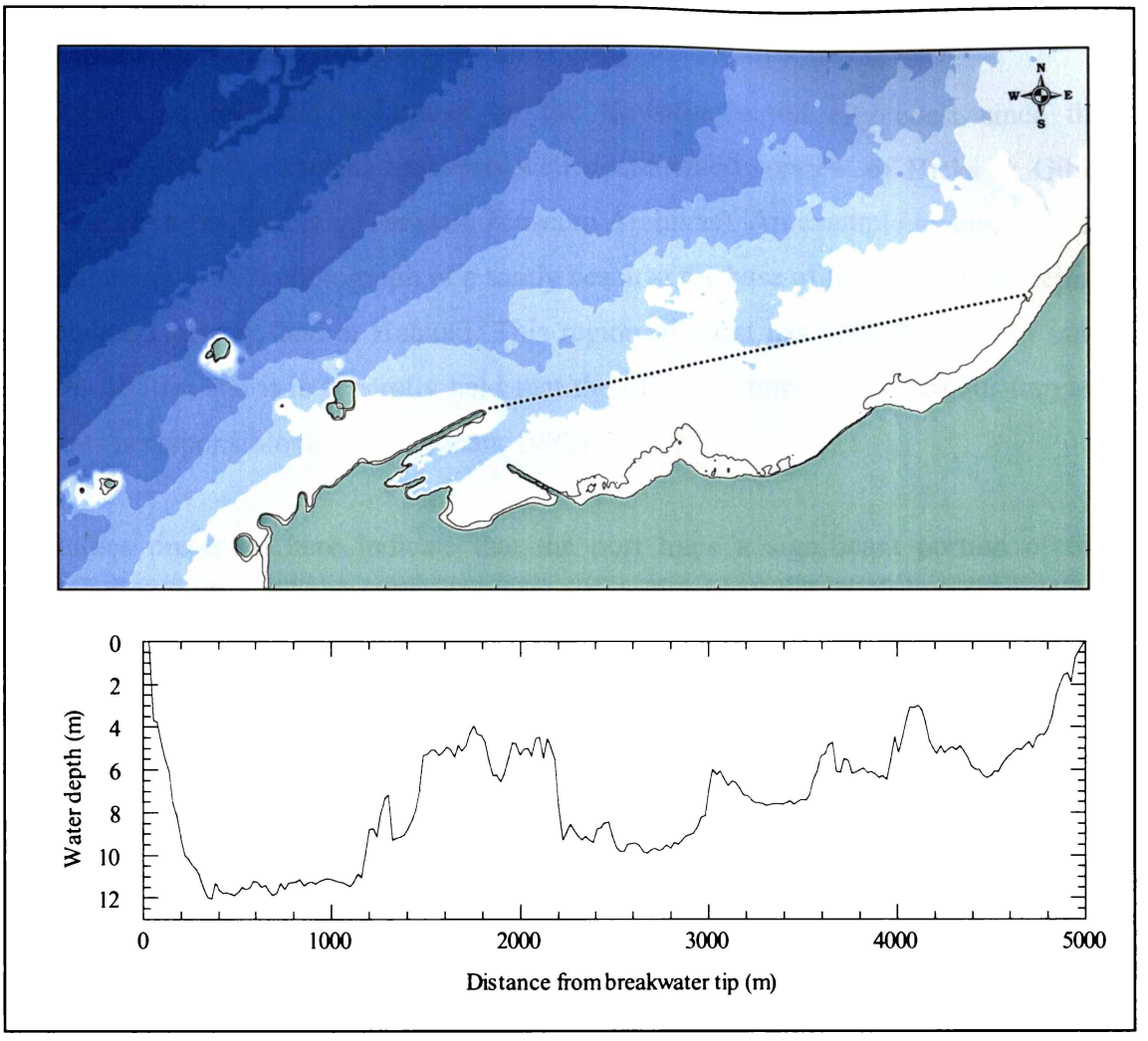

Figure 10.9: Depth transect across the New Plymouth coast from the tip of the main port breakwater to Fitzroy Beach.

10.8 Coastal erosion and the historical impacts of Port Taranaki

The erosion of intertidal sediments on the Kawaroa/central city coast since the construction of Port Taranaki has been well documented (review of Hicks & Gibb, 1987) and photographed (e.g. Taranaki Museum Archives). An example given is Figure 10.10, showing a 1926 photograph of a sandy beach at the base of the seawall protecting the reclaimed railway land at Huatoki. This region of coast has been denuded of sand since the 1950's, and it is generally held that the offshore dumping of harbour-trapped sediments is responsible (e.g. McLennan, 1982).

The studies presented here indicate that the port traps a significant portion of the northeasterly-moving shallow (< 6 m depth) littoral sediments. These trapped sediments are regularly dredged (biennially) and dumped offshore, and are thereby removed from the local nearshore littoral budget. Sediments in water depths of >6 m depth bypass the harbour, although the breakwater orientation deflects this flux away from the Kawaroa coast. Sediment tracing has demonstrated that a sediment transport pathway exists from the port region to Fitzroy Beach, indicating that the bypassing sediments are actively providing sediments to the city's eastern beaches. Under these reduced nearshore sediment fluxes, Fitzroy Beach has maintained its sandy character by virtue of the shoreline orientation (i.e. 032°) under the input of harbour-bypassing sediments.

The tracer experiments show that cross-shore diffusion of the sediments occurs at approximately 5% the rate of longshore values. Dumping of the harbour sediments in the deep water of the offshore site (Fig 1.5) causes a local discontinuity in the cross-shore sedimentary regime, which would presumably re-establish the sedimentary equilibrium at some distance "downstream" (i.e. to the northeast) as a result of diffusive and advective processes. Indeed, it is likely the characteristic shore-normal reef morphology that exists on this coast would aid the process of cross-shore sediment transport. Ultimately, the impacts of offshore sand dumping on the coastal beaches may be expected to decrease with distance from the port, and the enduring sandy nature of Fitzroy Beach, particularly at the eastern end near the Waiwakaiho River, would suggest that the impacts are limited to within approximately 7 km of the port entrance.

Within the New Plymouth City coastal region, the port impacts are likely to be exacerbated by the "headland effect", whereby the offshore deflection of the nearshore sediments, coupled with a broadening of the littoral zone, means that northeasterly-directed sediments are dispersed across a wider region. This may influence the diabathic exchange of sediments, and the response of beaches to changing sea conditions (e.g. Komar, 1998).

Prior to port construction in 1881, it is probable that the volumes presently trapped on the tip-shoal (i.e. 142,000 m^3yr^{-1}) would have continued along the coast, transported as surf-zone or intertidal sediments. The presence of such sediments is evident in an 1855 illustration of the central New Plymouth coast at the Huatoki River (Fig. 10.11), showing broad sandy beaches backed by dunes. It is also notable that this sandy shoreline featured extensive rocky intertidal reefs at Kawaroa (e.g. Fig. 1.8), demonstrating the resilience of these reefs to sediment inundation.

In addition to the impact of the port dredging operations, reclamation and coastal re-alignment at the Huatoki River (in 1908) have significantly changed the central city foreshore in New Plymouth. A steep rock wall (e.g. Fig. 10.10) now exists at an orientation that is approximately 20° oblique to the incident wave crests, which effectively precludes the accumulation of sandy sediments in front of the wall. However, recent studies by Black *et al.* (1999) have suggested specific coastal engineering may increase the public amenity value of this region. That proposal provides a coastal re-orientation of the Huatoki region, incorporating a pocket beach and artificial surfing reef.

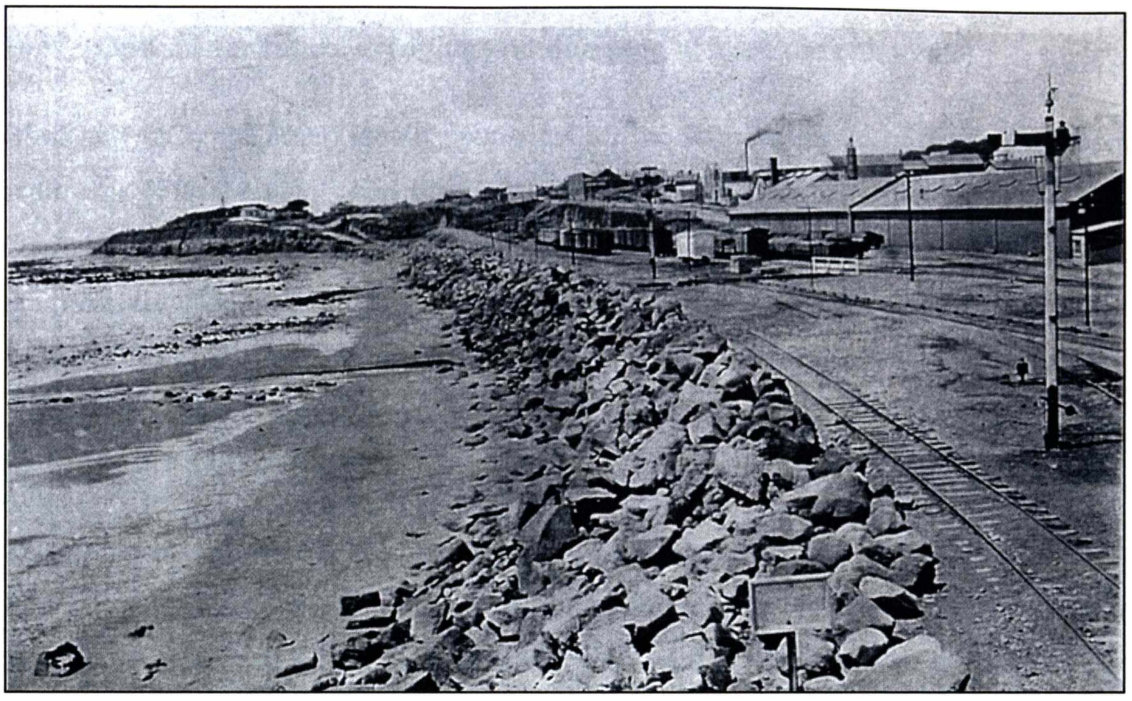

Figure 10.10: A 1926 low-tide photograph looking east along the Huatoki region, with a sandy beach below the rock wall that was constructed in 1908 to reclaim land for railway yards. This section of foreshore has been denuded of sand since the 1950's, and the rock wall is now 7-9 m high.

Figure 10.11: The Huatoki foreshore and river estuary as painted by William Strutt in 1855.

10.9 Options for future dredging and dumping of harbour sediments

Black & McComb (2000) identify two sites for the future disposal of dredged harbour sediments (Fig. 10.12), based on the constraints given in Chapter 1 (section 1.2.8). These are a nearshore site for the clean sandy sediments from the tip-shoal region, and the presently used offshore dumping ground for the silty sediments from the rest of the harbour. The rationale behind the site selection for each is summarised as follows.

10.9.1 Offshore dumping

The nature of sedimentation in the harbour results in the sorting of the particles, with fine silty sediments predominating in most areas apart from the tip-shoal. It is undesirable to deposit large quantities of such material in the nearshore environment, as these sediments would negatively impact the adjacent benthic ecology (e.g. Appendix 3). Furthermore, such sediments are not suitable beach sands and have little or no amenity value.

The parabathic currents at the presently used offshore dump ground mean that the periodic (biennial) placement of around 110,000 m^3 of silty sediments is not likely to impact the nearshore ecology at New Plymouth (Cole & McComb, 2000). Black & McComb (2000) note that the offshore dump ground is hydrodynamically isolated from the New Plymouth nearshore coastal and beach system. It is noteworthy, however, that the capacity of the offshore ground to disperse the dumped sediments is less than the volumes that have historically been placed there. Repetitive bathymetric surveys of the ground show that some 1,275,838 m^3 dredged material has been dumped there over the period 1989 - 1998, yet only 53% of that volume has been dispersed (Y.T. Lim, *pers comm.*). As the silty harbour sediments comprise only 25-30% of the previous volumes dumped at the offshore site, the proposed quantities are well within the capacity of the site for dispersal.

10.9.2 Nearshore dumping

Selection of the nearshore dumping site employed three numerical models: i) the WBEND wave refraction and longshore sediment transport model (Black & Rosenberg, 1992b); ii) the hydrodynamic and advection/dispersion model 3DD (Black, 1995), and

iii) the dispersal and sediment transport model POL3DD (Black, 1996). The models were calibrated with data from the field measurement programme, and validated against data from a 13-day period (Julian days 82-95, 1998) as well as tracer movements (Chapter 8). The reader is directed to Black & McComb (2000) for more details on the model calibration/validation.

The key requirements in selecting a nearshore dumping site were to place the dredged sediments on a transport pathway that would feed the central foreshore and eastern beaches (i.e. East End/Fitzroy Beach), while ensuring the rocky intertidal habitats on the Kawaroa coast were not inundated with sand. A long-term dumping ground also needs to have sufficient capacity to disperse the sediments placed in it over the period between dumping cycles. The selected site (Fig. 10.12) meets those criteria, but is the only suitable site on the New Plymouth coast that is able to do so. The ground straddles the axis of the Kawaroa Reef in water depths of 6-15 m and covers 661,225 m^2 in area, of which 75% is presently rocky bed. The site is positioned to maximise the wave exposure, and take advantage of the strong currents that flow over the reef platform top. The net flows from the site (as indicated in Fig. 10.13) are easterly and shoreward directed, providing a flux longshore toward the Huatoki and East End Beaches. The site is constrained from being positioned further offshore by the circulation patterns (which would cause the dumped sediments to be deflected away from the offshore, while an inshore limit is imposed by the dredging vessels' navigational requirements. The experimental sand dumping showed that a site positioned closer to the port experiences only slow dispersal, with significant potential for re-circulation back into the port, and accumulation near or on the *kaimoana* reefs along the Kawaroa shore adjacent to the port.

The boundaries of the nearshore site were adjusted to avoid vegetated areas of reef (Appendix 3). Reasonably dense stands of the laminarian *Ecklonia radiata* and the fucalean *Carpophyllum maschalocarpum* were found along the shoreward limit of the dump site and along the reef axis toward the shore (Appendices 3 & 4). This boundary adjustment allowed for a 150 m margin to exist between the seaweeds and the dump site, consistent with SCUBA observations that seaweed stands are generally at least 100 m from contiguous sand bodies. Based on the monitoring results of the experimental nearshore sand dumping (Chapter 7), sediments placed in the proposed new site will

disperse via suspension, and not migrate across the seabed as a mound or lens of sand. Thus, the seaweed habitat "downstream" of the dumped sediments is not expected to be negatively impacted.

This (biennial) contribution of approximately 142,000 m^3yr^{-1} of sand to the nearshore region of the central and eastern New Plymouth coast will alter the sedimentary regime. The areas of presently sandy bed within the subaqueous rocky matrix are likely to increase in dimension, and the volumes of sediment transported to the shallow subtidal and intertidal regions of the central city will rise. Beaches are not expected to re-establish along the Huatoki foreshore, due to the coastal re-alignment of that region, although the rocky coast immediately east of that (locally known as Bog Works) is of a similar angle to Fitzroy Beach and may experience sedimentation and beach formation. Similarly, East End and Fitzroy Beaches will have increased longshore sediment supply, which will benefit the coastal dunes and possibly reduce erosional trends.

A qualitative summary of the nearshore sediment pathways at New Plymouth is illustrated in Figure 10.14. Two cases are presented; the flux under the present dredging/dumping regime, and the situation if the proposed nearshore dump ground is utilised. It should be noted that no dumping has yet occurred in the proposed new ground, and this is presently a subject of a resource consent application by the Port company. Confirmation of the patterns of sediment transport from the new dumping ground, and indeed any positive or negative effects on the New Plymouth City coast, will be monitored as part of the conditions of the resource consent.

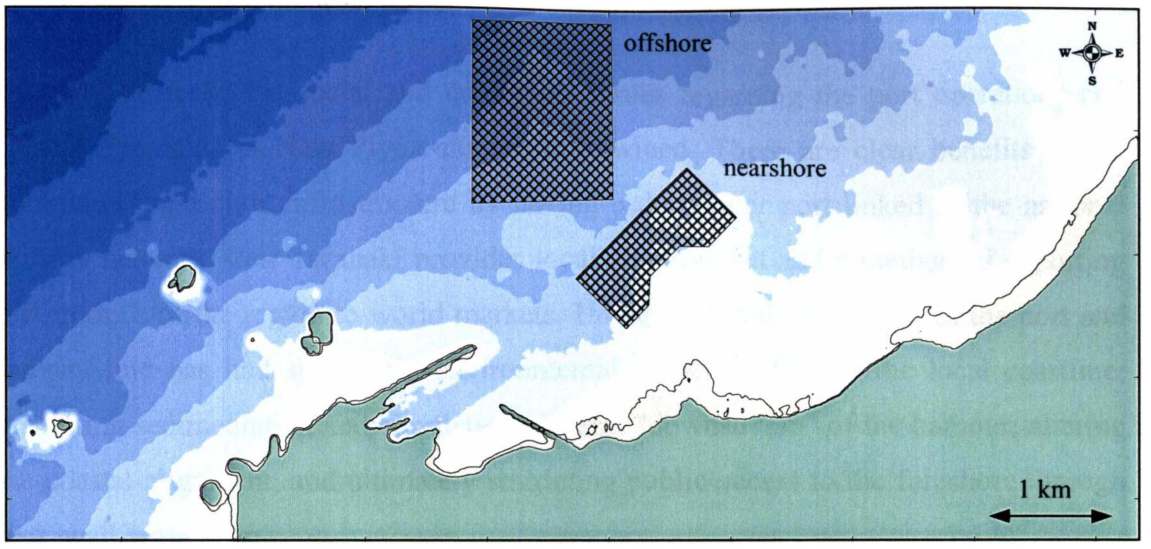

Figure 10.12: Map of New Plymouth showing the existing offshore dumping ground and the proposed nearshore ground. A section of the shoreward edge of the nearshore ground has been excluded to avoid vegetated areas of the reef.

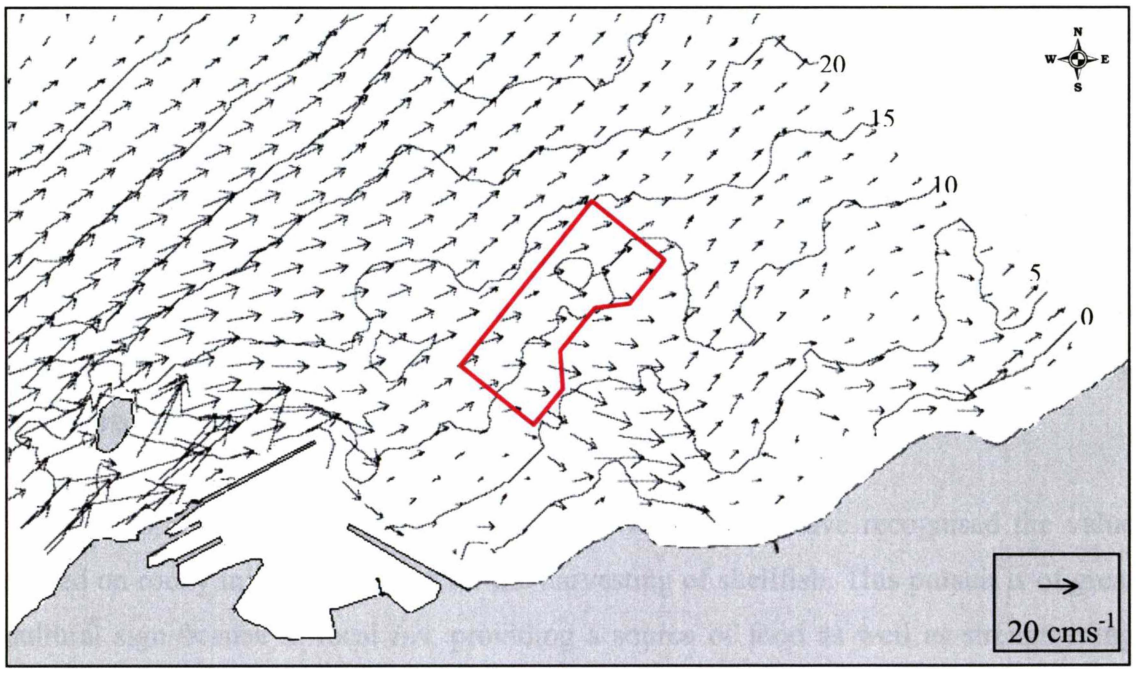

Figure 10.13: Position of the proposed nearshore dumping ground with respect to the vertically averaged circulation patterns (from Fig. 8.9).

10.10 Social and ecological issues

In many respects, the social and ecological issues regarding the port operations and coastal dynamics at New Plymouth are intertwined. There are clear benefits to the community and civic infrastructure by having a deepwater port linked to the national railway network. Port Taranaki provides local employment and a method of exporting the produce of the region to world markets. However, the development of the port and railway line has had significant environmental consequences for the local coastline; disrupting sedimentation and circulation patterns "downstream" of the harbour, altering the coastal alignment, and ultimately restricting public access to the foreshore through rock-wall armouring.

To many in the community, the loss of intertidal beaches is considered to be a deleterious effect, as it is concomitant with a reduction in the coastal amenity value to them. The re-direction of the railway line in 1908 has also had a significant impact on the coastal amenity at New Plymouth (e.g. Tullett, 1981), effectively cutting off public access to the central city foreshore. Indeed, the original vision to develop New Plymouth as a coastal resort town (Tullett, 1981) was truncated by routing the railway line along the foreshore. It may be hoped that recent plans (e.g. Black *et al.*, 1999) may come to fruition and allow the public amenity of this region to be optimised. Aside from an aesthetic perception of the beach, the loss of mobile sediments has allowed coastal erosion rates to increase, thereby necessitating rock wall armouring of the entire foreshore from the port to East End Beach.

Within this context, the present studies at New Plymouth have recognised the value placed on rocky intertidal regions for the harvesting of shellfish. This pursuit is of great cultural significance to local *iwi*, providing a source of food as well as strengthening familial bonds and instilling a sense of spiritual continuity with the local environment (R. Kipa, *pers comm.*). The potential inundation of key harvesting areas by the experimental sand dumping (particularly along the Kawaroa shoreline) was viewed by some members of the local Maori community as an act of cultural and ecological vandalism. Indeed, the permit to proceed with the experimental dumping (Chapter 7) was only granted after an Environmental Court hearing on the subject. Accordingly, the focus of Black & McComb (2000) was to seek a long-term dumping site that would

satisfy both concerns; avoiding sedimentation on the Kawaroa shoreline immediately east of the port, while returning the dredged sands to the longshore littoral drift feeding the city's central and eastern foreshore.

In assessing the likely ecological effects of dumping harbour sediments on the axis of the subaqueous Kawaroa Reef, the presence of the adjacent seaweed stands was rated as ecologically important on a local scale (Cole & McComb, 2000). While such seaweed habitats are common on the Taranaki coast (e.g. Willan, 1980), this was the only one observed at New Plymouth. The dumping of sand at the nearshore site is not predicted to cause significant negative impacts on the seaweed habitats. Cole *et al.* (submitted; Appendix 4) considers the presence of that habitat in terms of the ecology and physical oceanographic conditions on the reef. Those results indicate that sedimentation in the form of fine particulate matter (e.g. silts), is a major limiting factor on seaweed habitat. It is probable that silts of terrestrial origin cause the high turbidity (reducing the maximum water depth at which the seaweeds can adequately photosynthesize) and periodically smother regions of the substrate (apart from the reef axis), rendering them unsuitable for colonisation by juvenile plants.

10.11 Future research

Amid the knowledge gains of sediment dynamics within a high-energy, rocky reef environment, are several areas that remain the subject for future research, namely:

1. **Reef "roughness" effects on sediment entrainment and suspension:** Experimentation on rocky reefs to resolve the sediment "source" of the suspension profile, and the influence of bed geometry on the rates of entrainment (relative to supply) and the length scales of turbulent motion. Application of the findings to sediment transport modelling, using a spatial descriptor of bed roughness (e.g. Fig. 10.5).

2. **Wind effects on nearshore wave transformations:** Including a whitecapping dissipation term in the WBEND refraction model and attempting to simulate the wave transformation processes under strong onshore and offshore winds.

3. **Methods of reducing harbour sedimentation:** The numerical studies of wave refraction on the breakwater tip (Chapter 6) suggest there is potential for reducing wave penetration and sedimentation by adopting a selective dredging procedure. The bulbous seabed shape at the breakwater terminus is very effective at refracting the incident low-frequency (<0.1 Hz) swell into the harbour, thereby providing a mechanism to transport the sediments along the inside of the breakwater. By changing the shape of the tip-shoal (i.e. by specific dredging), the amount of wave energy refracting into the harbour may be reduced. This has the potential to lessen the tip-shoal sedimentation (and thereby enhance natural sediment bypassing the harbour entrance). However, careful studies would be required to ensure that changing sedimentation patterns were not detrimental or indeed financially disadvantageous. Specifically, causing sedimentation to occur in the dredged shipping channel rather than on the tip-shoal would be a negative outcome. Another potential method for reducing tip-shoal sedimentation is by enhancing the wave-driven flows along the breakwater. Essentially, this would entail a re-orientation near the terminus of the breakwater in order to optimise the angle between the incident wave crests and the wall, thereby increasing the wave-driven sediment flux.

4. **Taut-wire mooring motion:** To further investigate the response of a *p, u, v* meter on a taut-wire mooring, with a specific focus of identifying the optimum mooring configuration for a given wave climate and water depth.

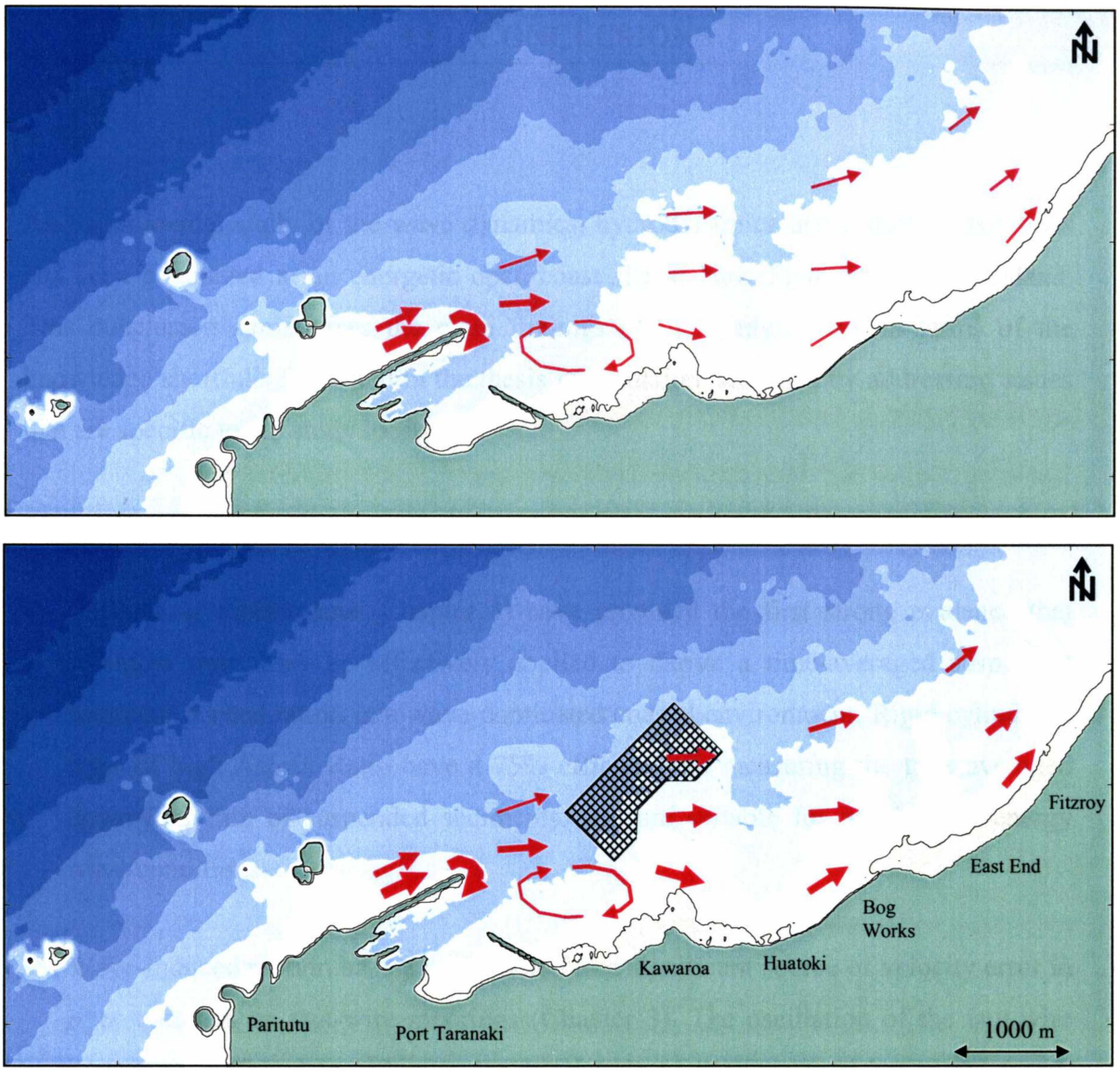

Figure 10.14: Qualitative nearshore sediment transport patterns at New Plymouth. Upper map shows the present situation, while the lower map shows an increased nearshore sediment flux from the proposed new dump ground for clean tip-shoal sediments (the proposed dump ground shown as hatched).

11 CONCLUSIONS

An experimental study of the wave dynamics, hydrodynamics and sediment dynamics has been conducted at an energetic open-coast site at New Plymouth, New Zealand. This conclusion summarises the main findings of the study; firstly in terms of the knowledge shortfalls identified in the thesis introduction, and then by addressing issues that are specific to the study location.

11.1 Knowledge gains

- Calibration experiments (Chapter 4) have provided the first strong evidence that sediment traps may be effectively applied to derive a time-averaged suspended sediment concentration in a wave-dominated coastal environment. Rigid cylindrical traps of high Aspect Ratio have a 75% efficiency in measuring the time-averaged downward flux of suspended sediments, and are suitable for use in high-energy wave conditions.

- Wave-induced motion has been identified as a significant source of velocity error in *p, u, v* meters on taut-wire moorings (Chapter 3). The oscillation of the taut-wire mooring was found to influence the magnitude of the measured horizontal wave-orbital velocities and induce a phase lag between velocity and sea-surface elevation. Comparison of data from a range of moorings shows a systematic relationship between the length of the mooring cable and the measured phase lag, consistent with the behaviour of the mooring system considered as a forced, linearly-damped oscillator. Directions resolved from the cross-spectra of pressure and velocity are likely to have frequency dependent errors due to the phase difference between the data. On these moorings, the spectra of wave direction should be resolved solely from velocity data.

- The transformation of waves over a complex nearshore bathymetry may be effectively simulated using the WBEND wave refraction model, applying a constant friction coefficient for mobile sandy beds, and a Nikuradse roughness for areas of

rocky reef. The wave transformation processes in the irregular reef environment are dominated by refraction and seabed friction, with the spatial distribution of wave energy additionally influenced by the wind vector. Strong, onshore-directed winds cause whitecapping which is thought to induce a longshore "smoothing" in the wave energy by a process of localised diffraction along the wave crests. This acts in opposition to the effect of wave refraction.

- Sediment tracing using an artificial fluorescent material offers an effective method for observing the transport of littoral sediments over sandy and rocky beds. Tracer shows that the coastal sediments exhibit a horizontal diffusivity of the order 0.1 m^2s^{-1}, of which approximately 5% is expressed in the cross-shore direction.

- In a wave-dominated environment, sediments are principally transported in the suspended form, and a system of irregular shore-normal reefs does not significantly obstruct the longshore flux of littoral sediments. Rather, the reefs influence the circulation patterns through the interaction of wave-driven forces and topographic steering.

- Rough, rocky seabeds appear to be resilient to sediment inundation, and the sediment facies remain positionally stable over time. The dumping of sand in a rocky reef environment does not necessarily result in adjacent beds becoming inundated with sand. In this environment, a nearshore dump mound did not migrate shoreward, but slowly dispersed as suspended sediments.

- The time-averaged near-bed reference concentration (C_o) of "black" volcanic sands under high-energy conditions may be effectively predicted using the excess skin friction ($\theta_{2.5}$) raised to the power of 1.5 (van Rijn, 1984). Predictions were further improved when the mean grain size was used in the sediment mobility term (Ψ) and the median grain size in the friction factor (f_w). The data suggest that an asymptotic relationship between $\theta_{2.5}$ and C_o is likely under high-energy, sheet-flow conditions.

- From measurements of SSC at 0.5, 1.0 and 1.5 m above the bed, the scale of turbulent mixing (l_s) was found to increase linearly with elevation, with a gradient of 0.46. While close to the predicted value of 0.4 (i.e. von Karman's constant, κ), the

slightly steeper concentration profile is consistent with a vertical variation in mean grain size. Suspended sediments show a systematic (and linear) reduction in mean grain size with increasing elevation above bed over the range 0.5-1.5 m..

- Rocky beds affect the entrainment process through a limitation in the supply of sediments, and an alteration of the near-bed orbital velocity regime. At 0.5 m above bed, SSCs are consistently lower over rocky beds than sandy beds, with values that are inversely proportional to the distance from contiguous sandy areas. This trend is less apparent at 1.0 m above the bed, suggesting that suspended sediments at a given location have a source not necessarily limited to the local bed (i.e. a "regional" source).

11.2 New Plymouth coastal dynamics, dredging and dumping of harbour sediments

- Regionally, the coastline is rocky, although beaches exist in response to sediment supply and coastal orientation relative to the incident wave angles. The subaqueous seabed is predominantly rocky reef, and mobile sediments (i.e. sands) exist in patches within the rocky matrix. These patches are often associated with seabed depressions or raised topographic features.

- Net sediment transport at New Plymouth is directed alongshore to the northeast, although the sediments respond to local and temporal perturbations, which give rise to reversing and circulating fluxes.

- The Paritutu Headland protrudes approximately 1.8 km from the regional coastal alignment, causing a significant local reduction in the continental shelf width. It is likely that this constriction of the nearshore littoral zone is the cause of the predominantly sandy bed in the headland region. This concentration of sediments near the port entrance is likely to increase the trapping efficiency of the harbour.

- Port Taranaki traps 174,000 m^3 of coastal sediments per year. Of this value, approximately 142,000 m^3 accumulates on the tip-shoal of the main port breakwater, and these sediments are derived from the seaward shallow zone close to

the breakwater (i.e. within ~50 m of the wall). Sediments in water depths of greater than 6 m (i.e. > 100 m from the breakwater wall) bypass the harbour, and traverse the rocky reefs toward the eastern beaches.

- Sediments dredged at the port and dumped offshore in the presently used dumping ground are removed from the nearshore littoral budget at New Plymouth. A consequence of this procedure over the last 120 years has been the reduction of intertidal sediments along the Kawaroa and Huatoki foreshore ("downstream" of the port).

- The orientation of the main port breakwater causes the longshore sediment flux to be directed away from the Kawaroa coast, further reducing the supply of littoral sediments to that region. Also, this region has a weak and reversing circulation pattern as a result of the shelter provided by the port breakwaters. Thus, dredged sediments dumped in this zone experience a relatively slow rate of dispersal.

- A new dumping ground has been identified for the tip-shoal sediments. This new site is projected to retain the dredged sediments within the nearshore littoral system, feeding sand to the central and eastern city foreshore. Sedimentation of the Kawaroa coast is not expected to result from the long-term use of this ground.

12 REFERENCES

Aagaard, T. and Greenwood, G., 1994. Suspended sediment transport and the role of infragravity waves in a barred surf zone, *Marine Geology*, **118,** 23-48.

Abramowitz, M. and Stegun, I.A., 1970. *Handbook of Mathematical Functions*. Dover, New York, 1046 p.

Agnew, R., 1973. New Plymouth beach erosion; Preliminary report. Unpublished report to the New Plymouth City Council by Smith, McNaught and Company. 25 p.

Agnew, R., 1976. Fitzroy sediment report: Beach investigation for New Plymouth City Council. Unpublished report to the New Plymouth City Council by Smith, McNaught and Company. 27 p.

Andrassey, C.J., 1991. Monitoring of a Nearshore Disposal Mound at Silver Strand State Park. *Coastal Sediments '91 Conference,* ASCE, Seattle, WA, pp. 1970-1984.

Antsyferov, S. and Kos'yan, R.D., 1990. Study of suspended sediment distribution in the coastal zone, *Coastal Engineering*, **14**, 147-172.

Armanini, A. and Ruol, P., 1988. Non-uniform suspended sediments under waves. *Coastal Engineering "88 Conference*, pp. 1129-1139

Arron, E.S. and Mitchell, J.S., 1984.Distribution and depth of nearshore sediments, Port Taranaki to Waiwakaiho River. N.Z. Oceanographic Institute, Wellington.

Atkinson, P.N. and McComb, P.J. (WTL), 1997. Environmental effects assessment of a trial of an inshore disposal site for maintenance dredgings from Port Taranaki. Westgate Transport Ltd. 35 p.

Bagnold, R.A., 1954. Experiments on a gravity-free dispersion of large solid spheres in a Newtonian fluid under shear. *Proc. R. Soc. London* (A), **225,** 49-63.

Bagnold, R.A., 1963. Mechanics of marine sedimentation. In: *The Sea*, M.N. Hill (Ed). New York: Interscience. pp. 507-528.

Bale, A.J., 1998. Sediment trap performance in tidal watres: comparison of cylindrical and conical collectors. *Continental Shelf Research*, **18**, 1401-1418.

Baquerizo A. and Losada M.A., 1998. Longitudinal current induced by oblique waves along coastal structures. *Coastal Engineering,* **35**(3), 211-230.

Bartholomeusz, W.G., 1985. Beach and nearshore sediment data for the New Plymouth beach restoration study. Central Laboratories Report 2-85/11. MWD, Lower Hutt. 59 p.

Bascom, W.N., 1951. The relationship between sand-size and beach-face slope. *Transactions American Geophysical Union*, **32**, 866-874.

Beamsley, B.J., 2001. Sediment facies map of the Sugarloaf (Nga Motu) Islands Marine Protected Area. Produced for the Department of Conservation by the University of Waikato.

Black, K.P. and Rosenberg, M.A., 1991. Suspended sediment load at three time scales. *Coastal Sediments '91 Conference,* ASCE, Seattle, WA, pp. 313-327.

Black, K.P. and Rosenberg, M.A., 1992a. Natural stability of beaches around a large bay. *Journal of Coastal Research*, **8**(2), 385-397.

Black, K.P. and Rosenberg, M.A., 1992b. Semi-emperical treatment of wave transformation outside and inside the breaker line. *Coastal Engineering,* **16**, 313-345.

Black, K. and Sokolov, S., 1993. New Plymouth Power Station consent renewal thermal plume studies. A report to ElectroCorp NZ Ltd. by Victorian Institute of Marine Sciences, 35 p.

Black, K.P. and Rosenberg, M.A., 1994. Suspended sand measurements in a turbulent environment: field comparison of optical and pump sampling techniques. *Coastal Engineering,* **24**, 137-150.

Black, K.P., 1994. Suspended sediment load during an asymmetric wave cycle over a plane bed. *Coastal Engineering*, **23**, 95-114.

Black, K.P., 1995. The hydrodynamic model 3DD and support software. Occasional Report No. 19. Department of Earth Sciences, University of Waikato, 53 p.

Black, K.P.; Gorman, R.M. and Symonds, G., 1995. Sediment transport near the break point associated with cross-shore gradients in vertical eddy diffusivity. *Coastal Engineering*, **26**, 153-175.

Black, K.P., 1996. Lagrangian dispersal and sediment transport model POL3DD. Occasional Report No. 21. Department of Earth Sciences, University of Waikato.

Black, K.P., 1997. Wave refraction model WBEND. Department of Earth Sciences, University of Waikato. New Zealand.

Black, K.P., Osborne, K.P., Green, M.O. and Villard, P., 1997. Intra-wave suspended sediment concentrations over bedforms. *Pacific Coasts and Ports '97 Conference*. Christchurch, New Zealand, pp. 365-370.

Black, K.P., Mead, S., McComb, P. J., Jackson, A. and Armstrong, K., 1999. New Plymouth Foreshore Redevelopment: Reef and Beach feasibility Study. A report to the New Plymouth District Council by the Department of Earth Sciences, University of Waikato, 57 p.

Black, K. P., and Oldman, J.W., 1999. Wave mechanisms responsible for grain sorting and non-uniform ripple distribution across two moderate-energy, sandy continental shelves. *Marine Geology*, **162**, 121-132.

Black, K., Green, M., Healy, T., Bell, R., Oldman, J. and Hume, T., 1999. Lagrangian Modelling Techniques Simulating Wave and Sediment Dynamics Determining Sand-Body Equilibria. Chapter 1 In: *Computerized Modeling of Sedimentary Systems*, Harff, J., Lemke, W. and Stattegger, K. (Ed.), pp. 321-242.

Black, K. P. and McComb, P.J., 2000. Port Taranaki maintenance dredging consent renewal studies. Report 2: Site selection and effects. Department of Earth Sciences, University of Waikato, 116 p.

Black, K.P. and Gorman, R. (submitted). Diffusion bars formed by orbital motion acting on horizontal suspended sediment concentration gradients. *Coastal Engineering.*

Bloesch, J. and Burns, N.M. 1980. A critical review of sedimentation trap technique. *Schweizerische Zeitschrift für Hydrologie*, **42**, 15-55.

Blomquist, S. and Håkanson, L., 1981. A review on sediment traps in aquatic environments. *Archiv für Hydrobiologie*, **91**, 101-132.

Bodge, K.R., 1994. Performance of nearshore berm disposal at Port Canaveral, Florida. *Dredging '94 Conference*, ASCE, pp. 1182-1191.

Bosman, J., Van Der Velden, E. and Hulsbergen, C. 1987. Sediment concentration measurements by transverse suction. *Coastal Engineering,* **11**, 353-370.

Bray, M.J.; Cater, D.J., and Hooke, J.M. 1995. Littoral cell definition and budgets for central southern England. *Journal of Coastal Research,* **11**, 381-400.

Brown, N.L.A., 1992. Simple Low Cost Acoustic Current Meter. *Oceanology International '92 Conference*, Brighton, United Kingdom.

Butman, C.A., 1986. Sediment trap biases in turbulent flows: results from a laboratory flume study. *Journal of Marine Research*, **44**, 645-693.

Butman, C.A., Grant, W.D. and Stolzenbach, K.D., 1986. Predictions of sediment trap biases in turbulent flows: a theoretical analysis based on observations from the literature. *Journal of Marine Research*, **44**, 601-644.

Cacchione, D.A. and Drake, D.E. 1990. Shelf sediment transport: An overview with application to the Northern California continental shelf., In *The Sea, Ocean Engineering Research.* LeMehaute, B. and Hanes, D. (Ed.), Wiley-Interscience, New York, pp. 729-773.

Carter, J., Hobensack, W., Kennedy, D. and Cox, D., 1998. Wind Effects on Wave Transformation and Undertow. *Proceedings of Ocean Wave Kinematics '98 Conference - Dynamics and Loads on Structures,* pp. 439-445

Carter, L. and Lewis, K., 1995. Variability of the modern sand cover on a tide and storm driven inner shelf, South Wellington, New Zealand. *New Zealand Journal of Geology and Geophysics,* **38**, 451-470.

Cartwright, D.E. and Longuet-Higgins, M.S., 1956. The statistical distribution of the maxima of a random function. *Proc. Roy. Soc.*, **A237**, 212-232.

Chawla, A., Ozkan-Haller, H.T. and Kirby, J.T., 1998. Spectral model for wave transformation and breaking over irregular bathymetry. *Journal of Waterway, Port, Coastal and Ocean Engineering*, **124**(4), 189-198.

Cheong H.F., Shankar N.J., Radhakrishnan R. and Toh A.C., 1993. Estimation of sand transport by use of tracers along a reclaimed shoreline at Changi Airport. *Coastal Engineering,* **19**(3-4), 311-325.

Cheong, H.F., Shankar, N.J., Radhakrishnan, R., 1992. The dispersion of radioactive tracers along the east coast of Singapore. *Coastal Engineering,* **17**, 71-92.

Chhabra, N.K., 1985. Computation of errors in current meters attached to near-surface moorings. *Journal of Geophysical Research,* **90** (C3), 4995-4999.

Ciavola, P., Taborda, R., Ferreira, O. and Dias, J.A., 1997. Field measurements of longshore sand transport and control processes on a steep meso-tidal beach in Portugal. *Journal of Coastal Research,* **13**, 1119-1129.

Cole, R., McComb, P. and Sait, J., 1999. Effect of nearshore sand disposal on subtidal and intertidal organisms at New Plymouth, New Zealand. *Pacific Coasts and Ports '99 Conference*, Perth, Australia, pp 129-134.

Cole, R.G. & McComb, P.J., 2000. Port Taranaki Maintenance Dredging Consent Renewal Studies. Report 4: Biological description and assessment. NIWA Client Report WTL00403/1. 83 p.

Corson, W.D., Rhee, J.P., Welp, T.L. and Mckinney, J.P., 1997. Wave Measurement in Upper Galveston Bay, TX (USA). MTS/IEEE *Oceans '97 Conference*, Halifax, Nova Scotia, pp. 1099-1103.

Cowper, N.T. and Nankervis, L., 1997.Innovative sand shifter technology for maintaining clear ocean entrances year round. Sands bypassing at Port of Portland, Victoria, Australia. *Pacific Coasts and Ports '97 Conference*, Christchurch, New Zealand, pp. 871-875.

Curray, J.R., 1965. Late quaternary history, continental shelves of the United States, pp. 723-736, In: *The Quaternary of the United States*, Wright, H.E. and Frey, D.G. (Ed.), Princeton University Press, 922 p.

Davies, A.G. and Li, Z., 1997. Modelling sediment transport beneath regular symmetrical and asymmetrical waves above a plane bed. *Continental Shelf Research*, **17**(5), 555-582.

Davis, R.A. (Jr.), 1971. Beach and nearshore zone. In: *Coastal Sedimentary Environments*, R.A. (Jr.) Davis (Ed), pp. 379-438, Springer-Verlag Press.

Dean, R.G. and Dalrymple, R.A. 1991. *Water wave mechanics for engineers and scientists.* Advanced Series on Ocean Engineering - Volume 2. World Scientific, 353 p.

Dean, R.G., 1973. Heuristic models of sand transport in the surf zone. *1ST Australian Conference on Coastal Engineering*, Sydney, Australia, pp. 209-214.

Dean, R.G., 1983. Principles of Beach Nourishment. In: *Handbook of Coastal Processes and Erosion*, P.D. Komar (Ed), pp. 217-231, Baco Ration, FL, CRC Press.

Dean, R.G., 1989. Measuring longshore transport with traps. In: *Nearshore Sediment Transport*, J. Seymour (Ed), pp. 313-336. Plenum, New York, 418 p.

De Lange, W.P and Healy, T.R., 1994. Assessing the stability of inner shelf dredge spoil mounds using spreadsheet applications on personal computers. *Journal of Coastal Research*, **10**(4), 946-958.

Dewey, R.K., 1999. Mooring Design and Dynamics - a Matlab package for designing and analyzing oceanographic moorings. *Marine Models* **1**, 103-157.

Dickey, T., Plueddemann, A.J. and Weller, R., 1998. Current and Water Property Measurements in the Coastal Ocean. In: *The Global Coastal Ocean,* K. H. Brink and A. R. Robinson, (Eds.), John Wiley and Sons, Inc., pp. 367-398.

Douglass S.L., 1995. Estimating the landward migration of nearshore constructed sand mounds. *Journal of Waterway Port Coastal and Ocean Engineering*, **121**(5), 247-250.

Douglass, S.L., 1996. Nearshore placement of sand. *Coastal Engineering '96 Conference,* ASCE, pp. 3708-3721.

Du Toit, C.G. and Sleath, J.F.A., 1981. Velocity measurements close to rippled beds in oscillatory flow. *Journal of Fluid Mechanics*, **112**, 71-96.

Duane, D.B. and James, W.R., 1980. Littoral transport in the surf zone elucidated by an Eulerian sediment tracer experiment. *Journal of Sedimentary Petrology*, **50** (3), 929-942.

Dubois, R.N., 1972. Inverse relation between foreshore slope and mean grain size as a function of the heavy mineral content. *Geological Society of America Bulletin*, **83**, 871-875.

Earle, M.D. and Bishop, J.M. 1984. A Practical Guide to Ocean Wave Measurement and Analysis. Endeco Inc., Marion, MA.

Engelund, F. and Fredsoe, J., 1976. A sediment transport model for straight alluvial channel. *Nordic Hydrology*, **7**, 293-306.

Ewans, K.C. and Kibblewhite, A.C., 1992. Spectral features of the New Zealand deep-water ocean wave climate. *New Zealand Journal of Marine and Freshwater Research*, **26**, 323-338.

Falmouth Scientific Inc. 1998, *3D-ACM WAVE Operating Manual,* 159 p.

Feddersen, F., Guza, R.T., Elgar, S. and Herbers, T.H.C., 1998. Alongshore momentum balances in the nearshore. *Journal of Geophysical Research-Oceans,* **103**(C8): 15667-15676.

Flint, S. 1998. Sediment trapping in the nearshore coastal environment. Unpublished M.Sc. thesis, University of Waikato, New Zealand, 196 p.

Forsyth, S.H., 2000. New developments in artificial fluorescent tracer counting techniques applied to sand transport studies. Unpublished M.Sc. thesis, University of Waikato, New Zealand, 210 p.

Foster, G.A., Healy, T.R., and DeLange, W.P., 1996. Presaging beach renourishment from a nearshore dredge dump mound, Mt. Maunganui beach, New Zealand. *Journal of Coastal Research*, **12**(2), 395-405.

Fredsoe, J., 1993. Modelling of non-cohesive sediment transport in the marine environment. *Coastal Engineering*, **21**, 71-103.

Fredsoe, J. and Deigaard, R., 1992. *Mechanics of coastal sediment transport.* Advanced Series on Ocean Engineering - Volume 3, World Scientific, 369 p.

Fredsoe, J., Anderson, O.H., and Silberg, S., 1986. Distribution of suspended sediment in large waves. *Journal of Waterway, Port, Coastal and Ocean Engineering*, **111**(6), 1041-1059.

Gardner, W.D., 1980a. Sediment trap dynamics and calibration. A laboratory evaluation. *Journal of Marine Research.* **38,** 17-39.

Gardner, W.D., 1980b. Field assessment of sediment traps. *Journal of Marine Research.* **38,** 41-52.

Gardner, W.D., Hinga, K.R. and Marra, J., 1983. Observations on the degradation of biogenic material in the deep ocean with implications on the accuracy of sediment trap fluxes. *Journal of Marine Research*, **41**, 195-214.

Gardner, W.D., 2000. Sediment trap sampling in surface waters. In*: The Changing Ocean Carbon Cycle - A midterm synthesis of the Joint Global Ocean Flux Study.* Cambridge University Press, pp. 240 -281.

Gaylord, B., 1999. Detailing agents of physical disturbance: wave-induced velocities and accelerations on a rocky shore. *Journal of Experimental Biology and Ecology,* **239**, 85-124.

Gibb, J., 1979. Late quaternary shoreline movements in New Zealand. PhD thesis, Victoria University, New Zealand, 217 p.

Gibb, J., 1983. Report on coastal processes, port development and beach restoration at New Plymouth, Taranaki region. National Water and Soil Conservation Organisation, 41 p.

Gibbs, R., Matthews, M. and Link, D. 1971. The relationship between sphere size and settling velocity. *Journal of Sedimentary Petrology*, **41**(1), 7-18.

Glenn, A.H., 1972. Meteorological and oceanographic investigations at offshore buoy site, New Plymouth. Report to Taranaki Harbours Board. Glenn Associates, New Orleans. 18 p.

Glenn, S.M. and Grant, W.D., 1987. A suspended sediment stratification correction for combined wave and current flows. *Journal of Geophysical Research*, **92**, 8244-8264.

Gobat, J. and Grosenbaugh, M., 1998. WHOI Cable: Time domain numerical modelling of moored and towed oceanographic systems. *Ocean '98 Conference*, IEEE, pp. 1681-1685.

Gomez-Pina, G. and Raminez, J.L., 1994. The complementary interaction between beach nourishment and harbour management: four cases in Spain. *Coastal Engineering '94 Conference*, pp. 3507-3521.

Gorman, R. and Black, K., 1997. Harbour wave studies with a hybrid explicit-implicit hydrodynamics model. *Pacific Coasts and Ports '97 Conference*, Christchurch, New Zealand, pp. 631-636.

Gorman, R., Black, K. and Sokolov, S., 1995. Physical processes and sediment transport study for the proposed modifications to the Port of Taranaki Victorian Institute of Marine Sciences, 146 p.

Gorman, R.G., 1997. TSERIES – A Matlab system for time-series analysis. Operating Manual, National Institute of Water and Atmospheric Research, New Zealand.

Grant, W.D. and Madsen, O.S., 1982. Movable bed roughness in unsteady oscillatory flow. *Journal of Geophysical Research,* **87**(C1), 469-481.

Green, M.O., 1999. Test of sediment initial-motion theories using irregular-wave field data. *Sedimentology,* **46** (3) 427-441.

Green, M.O. and Black, K.P., 1999. Suspended-sediment reference concentration under waves: Field observations and critical analysis of two predictive models. *Coastal Engineering*, **38**, 115-141.

Green, M.O. and Vincent, C.E., 1990. Wave entrainment of sand from a rippled bed. *Coastal Engineering '90 Conference,* pp. 2200-2212.

Green, M.O., Hewitt, J.E. and Thrush, S.F., 1998. Seabed drag coefficient over natural beds of horse mussels (*Atrina zelandica*). *Journal of Marine Research,* **13**(1), 111-133.

Greenwood, B., Osborne, P.D., Bowen, A.J. and Hazen, D.G., 1990. Nearshore sediment flux and bottom boundary dynamics: The Canadian Sediment Transport Programme (C-Coast). *Coastal Engineering '90 Conference*, pp. 2227-2240.

Greilach, P.R., Black, K.P., Parry, G.D; and Forsyth, M., 1995. Scallop dredging and sedimentation in Port Phillip Bay. Victorian Institute of Marine Sciences, Working Paper No. 29.

Griggs, G.B., 1990. Littoral drift impoundment and beach nourishment in Northern Monterey Bay, California. *Journal of Coastal Research*, **6**, 115-126.

Gunther, H., Hasselmann, S. and Janssen, P.A.E.M., 1992. WAM model Cycle 4 (revised version). DKRZ Report No 4., p. 5, Eqn. 2.1.12.

Gust G., Bowles W., Giordano S., and Huttel, M., 1996. Particle accumulation in a cylindrical sediment trap under laminar and turbulent steady flow – an experimental approach. *Aquatic Sciences,* **58** (4), 297-326.

Halpern, D. and Pillsbury, R.D., 1976. Influence of surface waves on sub-surface current measurements in shallow water. *Liminology and Oceanography*, **21,** 611-616.

Hamilton J., Fowler, G. and Belliveau, D., 1997. Mooring vibration as a source of current meter error and its correction. *Journal of Atmospheric and Oceanic Technology*, **14**(3/2), 644-655.

Hamilton, J. and Fowler, G., 1997. Quiet mooring systems for accurate oceanographic measurements. *Sea Technology*, **38** (3), 70-74.

Hands, E.B. and Allison, M.C., 1991. Mound migration in deeper water and methods of categorising active and stable depths. *Coastal Sediments '91 Conference,* ASCE, pp. 1985-1999.

Hanes, D.M., 1988. Intermittent sediment suspension and its implications to sand tracer dispersal in wave-dominated environments. *Marine Geology*, **81**, 175-183.

Hanson, H., 1989. GENESIS – A generalised shoreline change numerical model., *Journal of Coastal Research*, Vol 5(1), 1-27.

Hargrave, B.T. and Burns, N.M., 1979. Assessment of sediment trap efficiency. *Liminology and Oceanography*, **24** (6). 1124-1137.

Harris, T.F., 1990. Greater Cook Strait: form and flow. DSIR Marine and Freshwater, Wellington, 212 p.

Haskins, G.L., 1957. NZ 4432 Taranaki Roads 1:24000 and Port Taranaki 1:6000. Hydrographic Branch, Navy Department, Wellington.

Hasselmann, K. 1973. On the spectral dissipation of ocean waves due to whitecapping. *Boundary-layer Meteorology*, **6**, 107-127.

Heath R. A., 1982. What drives the mean circulation on the New Zealand west coast continental shelf. *New Zealand Journal of Marine and Freshwater Research*, **16**, 215-226.

Healy, T.R., Kirk, R.M. and De Lange W.P., 1990. Beach renourishment in New Zealand. *Journal of Coastal Research*, **6**, 77-90.

Healy, T.R., Stephens, S.A., Black, K.P., Gorman, R.G. and Beamsley, B.J., 1998. Numerical and physical process studies for Port of Gisborne redesign for the 21st century. *Journal of Coastal Research,* **26**, 1304-311.

Hicks, D.M. and Gibb, J.G., 1987. Background and design information for a restored beach at New Plymouth. Report to the New Plymouth Sand By-pass Committee. 67 p.

Hoekstra, P., Houwman, K.T., Kroon, A., van Vessem, P. and Ruessink, B.G., 1997. The Nourtec experiment of Terschelling: process-oriented monitoring of a shoreface nourishment (1993-1996). *Coastal Dynamics '97 Conference,* pp. 402-416.

Holloway, P.E., Symonds, G., and Nunes Vaz, R., 1992. Observations of circulation and exchange processes in Jervis Bay, New South Wales. *Australian Journal of Marine and Freshwater Research,* **43**, 1487-1515.

Honjo, S., Connell, J.F. and Sachs, P.L., 1980. Deep-ocean sediment trap; design and function of PARFLUX Mark II. *Deep-Sea Research*, **27**, 745-753.

Horikawa, K., Watanabe, A. and Katori, S., 1982. Sediment transport under sheet flow condition. *Coastal Engineering '82 Conference, Capetown,* pp. 1335-1352.

Horikawa, K., 1989. *Nearshore dynamics and coastal processes: Theory, measurement and predictive models.* University of Tokyo Press, Tokyo, 522 p.

Houwman, K.Y. and van Rijn, L.C., 1999. Flow resistance in the coastal zone. *Coastal Engineering,* **38**, 261-273.

Howse, B., 2000. Bed roughness of reefs and the relationship of sediment flux to benthic reef ecology. Unpublished M.Sc. thesis, University of Waikato, New Zealand, 184 p.

HRS, 1963. Taranaki Harbour model investigations. Report No. 220. Hydraulics Research Station, Wallingford and DSIR, Wellington.

Huang, M. and Chen, J., 1998. Wave Direction Analysis from Data Buoys. *Ocean Engineering,* **25** (8), 621-637.

Hume, T.M., Oldman, J.W. and Black K.P., 2000. Sediment facies and pathways of sand transport about a large deep water headland, Cape Rodney, New Zealand. *New Zealand Journal of Marine and Freshwater Research*, **34**, 695-717.

Hutt, J.A. 1997. Bathymetry and wave parameters defining the surfing quality of 5 adjacent reefs. Unpublished M.Sc. thesis, University of Waikato, New Zealand, 170 p.

Hutt, J.A. and Black, K.P., 1997. Vertical attenuation of wave-induced pressure. *Pacific Coasts and Ports '97 Conference*, Christchurch, New Zealand, pp. 965-970.

Jackson, L.A. and Tomlinson, R.B., 1990. Nearshore nourishment implementation, monitoring and model studies of $1.5m^3$ at Kirra Beach. *Coastal Engineering '90 Conference* ASCE, pp. 2241- 2254.

Jones, B., 2000. A numerical study of wave refraction in shallow tidal waters. *Estuarine, Coastal and Shelf Science*, **51**, 331-347.

Jonsson, I.G., 1966. Wave boundary layers and friction factors. *Coastal Engineering '66 Conference* ASCE, pp. 127-148.

Kibblewhite, A.C., Bergquist, P.R. and Gregory, M.R., 1982. Maui Development Environmental Study. Report on Phase II 1977-1981. The University of Auckland, 169 p.

Kingsford, M. J. and Battershill, C. N., 1998 Subtidal habitats and benthic organisms. In: *Studying temperate marine environments. A handbook for ecologists.* Kingsford, M. J. and Battershill, C. N., (Eds). Canterbury University Press, Christchurch, pp. 84-114.

Kirk, R.M., 1980. Coastal erosion at New Plymouth: sand transport past the port and options for beach re-nourishment. Unpublished report to the New Plymouth City Council Foreshore Erosion committee, 66 p.

Komar, P.D. and Inman, D.L., 1970. Longshore sand transport on beaches. *Journal of Geophysical Research*, **75**, 5914-5927.

Komar. P.D., 1989. Physical processes of waves and currents and the formation of marine placers. *Aquatic Sciences,* **1** (3), 393-423.

Komar, P.D., 1998. *Beach Processes and Sedimentation.* Prentice Hall Press, New Jersey, 544 p.

Komen, G.J., Cavaleri, M., Donelan, K., Hasselmann, K., Hasselmann, S., and Janssen, P.A.E.M., 1994. *Dynamics and modelling of ocean waves.* Cambridge University Press, pp. 143-155.

Krause, N.C., 1987. Application of portable traps for obtaining point measurements of sediment transport rates in the surf zone. *Journal of Coastal Research*, **3**, 139-152.

Kruger, J., 1999. Sedimentation at the entrance channel of Tauranga Harbour, New Zealand. Unpublished M.Sc. thesis, University of Waikato, New Zealand, 244 p.

Kun, A.L., Fougere, A., McComb, P., 1999. A New Wave Directional Spectrum Measurement Instrument. *IEEE Sixth Working Conference on Current Measurement*, San Diego, CA. pp. 49-53.

Laing, A. K., 1993. Estimates of wave height data for New Zealand waters by numerical modelling. *New Zealand Journal of Marine and Freshwater Research*, **27**,157-175.

Lakhan, V.C. 1989, Modelling and simulation of the coastal system. In: *Applications in coastal modelling*, Elsevier Oceanography Series, 49.

Lemm, A., 1999. Offshore wave climate, Perth (Western Australia), 1994-98. *Pacific Coasts and Ports '99 Conference*, Perth, Australia, pp. 352-359.

Li, Z.H. and Komar. P., 1992. Selective entrainment and transport of mixed size and density sands: Flume experiments simulating the formation of black-sand placers. *Journal of Sedimentary Petrology,* **62** (4), 584-590.

Longuet-Higgins, M.S., 1983. On the joint distribution of wave periods and amplitudes in a random wave field. *Proc. Roy. Soc.*, A389: 241-258

Longuet-Higgins, M.S., Cartwright, D.E. and Smith, N.D., 1963. Observations of the directional spectrum of sea waves using the motions of a floating buoy. In: *Ocean wave spectra.* Englewood Cliffs, New York, pp. 111-136.

Lou, J. and Ridd, P.V., 1997. Modelling of suspended sediment transport in coastal areas under waves and currents. *Estuarine, Coastal and Shelf Sciences*, **45**, 1-16.

Madsen, O.S., 1987. Use of tracers in sediment transport studies. *Coastal Sediments '87 Conference* (ASCE). New York, USA, pp. 424-435.

Marsh, J.K., Pillsworth, M.W. and Kenny, A.J., 1997. Application of innovative fluorescent artificial sand and silt tracers for maintenance dredging optimisation, beneficial use and environmental dredging. *Proceedings of 2nd Asian and Australasian Ports and Harbours Conference* 1997, Ho Chi Minh City, Vietnam, pp. 173-188.

Massel, S.R., 1996. Ocean surface waves: their physics and prediction. In: *Advanced Series on Coastal Engineering*, 11, World Scientific, Singapore.

Matsunaga, N., Hashida, M. and Kawakami, H., 1996. Wind-induced waves and currents in a nearshore zone. *Coastal Engineering '96 Conference,* pp. 3363-3377.

Matthews, E., 1977. Movement of sand on some western Taranaki beaches. Unpublished M.Sc. thesis, University of Auckland, New Zealand, 135 p.

Maunder, W., 1970. The climate of New Zealand – physical and dynamic features. In: *World survey of climatology*, H. E. Landsberg (Ed.), Elsevier, London.

McComb, P., Black, K., Atkinson, P., Bell, R. and Healy, T., 1997. High-resolution wave transformations on a coast with complex bathymetry. *Pacific Coasts and Ports '97 Conference*, Christchurch, New Zealand, pp. 995-1000.

McComb, P., Black, K., Atkinson, P., Lim, Y. and Healy, T. 1999a. The accretion of a breakwater-tip shoal following dredging. *Pacific Coasts and Ports '99*, Perth, Australia, pp. 420-425.

McComb, P., Black, K., Healy, T. and Atkinson, P 1999b. Coastal and sediment dynamics at Port Taranaki, New Zealand: a large, multi-faceted, field experiment. *Coastal Structures '99 Conference*, Santander, Spain, pp. 823-832.

McComb, P.J., 2000a. A review of the sedimentary and oceanographic conditions for a Single Point Mooring Buoy and pipeline at Port Taranaki. A report to Westgate Transport Ltd. by ASR Ltd, 32 p.

McComb, P.J., 2000b. A review of the sedimentary and oceanographic conditions at Pohokura. A report to TransField Worley Ltd by ASR Ltd, 19 p.

McComb, P.J. and Black, K.P., 2000. Port Taranaki maintenance dredging consent renewal studies. Report 1: Field measurements. A report to Westgate Transport Ltd. Department of Earth Sciences, University of Waikato, New Zealand, 102 p.

McComb, P.J. and Beamsley, B., 2000. Telstra Saturn Aqualink Project: An evaluation of the Te Henui Landing Site. A report to Telstra Saturn Communications Ltd and the Taranaki Regional Council by ASR Ltd, 38 p.

McComb, P.J., Beamsley, B. and Mead, S., 2000. Telstra Saturn Aqualink Project: An evaluation of the route survey data and fishing activities. A report to Telstra Saturn Communications Ltd by ASR Ltd, 118 p.

McComb, P., Gorman, R., Black, K. and Kun, A., 2001. Measuring directional wave spectra with the 3D-ACM WAVE. *Journal of Oceanic Engineering* **26**, (2), 171-180.

McComb, P.J., Black, K.P., Mead, S., and Hutt, J. 2001. Opunake surfing reef feasibility studies. A report to the South Taranaki District Council by ASR Ltd, 111 p.

McComb, P.J. and Black K.P. (2001). Dynamics of a nearshore dredged-sand mound on a rocky, high-energy coast. *Journal of Coastal Research*, ICS 2000 Proceedings, 550-563.

McLennan, N.R., 1982. Fitzroy beach processes and quantitative estimation of littoral drift. Unpublished M.Sc. thesis, University of Waikato, New Zealand, 200 p.

Mesa, C., 1996. Nearshore Berm Performance at Newport Beach, California, USA. *Coastal Engineering '96 Conference,* ASCE, pp. 4636-4649.

Miller, M.C. and Komar, P.D., 1979. Measurements of sand spreading rates under near-bottom wave orbital motions. *Journal of Geology* **87**(6), 593-608.

Mocke, G.P. and Smith, G.G., 1992. Wave breaker turbulence as a mechanism for sediment suspension. *Coastal Engineering*, **2**, 2279-2292.

Moon, V., De Lange, W., Warren, S. and Healy T., 1994. Post-disposal behaviour of sandy dredged material at an open-water, inner shelf disposal site. *Journal of Coastal Research*, **10**(3), 651-662.

MOR., 1991. Analysis and climatological statistics of the ocean wave data recorded outside the entrance to Port Taranaki. A report to Westgate Transport Ltd by Metocean Research Ltd.

Morang, A., Larson, R. and Gorman, L. 1997. Monitoring the coastal environment. 1. Waves and currents. *Journal of Coastal Research,* **13**(1),111-133.

Neall, V. E., 1979. Geological map of New Zealand, Sheets P19 – P21 and Notes. DSIR, Wellington, 36 p.

Nelson, R.C., 1996. Hydraulic roughness of coral reef platforms. *Applied Ocean Research*, **18**, 265-274.

Niedoroda, A.W., Swift, D.J., Hopkins, T.S. and Ma, C., 1984. Shoreface dynamics on a wave-dominated coasts. *Marine Geology*, **60**, 331-354.

Nielsen, P., 1983. An analytical determination of nearshore wave height variation due to refraction, shoaling and friction. *Coastal Engineering*, **7**, 233-251.

Nielsen, P., 1984. Suspended sediment concentrations under waves. *Coastal Engineering*, **10**, 23-31.

Nielsen, P., 1986. Field measurements of time-averaged suspended sediment concentrations under waves. *Coastal Engineering*, **8**, 51-72.

Nielsen, P., 1992. Coastal bottom boundary layers and sediment transport. *Advanced Series on Ocean Engineering. Vol. 4*. World Scientific, 324 p.

Nishi, R., Sato, M., and Nakamura, K., 1992. Grain-size distribution of suspended sediments. *Coastal Engineering*, **2**, 2293-2306.

Nodder, S.D. and Alexander, B.L., 1999. The effects of multiple trap spacing, baffles and brine volume on sediment trap collection efficiency. *Journal of Marine Research*, **57**, 537-559.

Osbourne, P.D. and Greenwood, B., 1992a. Frequency dependent cross-shore suspended sediment transport. 1. A non-barred shoreface. *Marine Geology*, **106**, 1-24.

Osbourne, P.D. and Greenwood, B., 1992b. Frequency dependent cross-shore suspended sediment transport. 2. A barred shoreface. *Marine Geology*, **106**, 25-51.

Osbourne, P.D. & Vincent, C.E. 1996. Vertical and horizontal structure in suspended sand concentrations and wave-induced fluxes over bedforms. *Marine Geology,* **131**, 195-208.

OSL, 1989. Physical Oceanography of the Waitara Outfall. A report to Waitaki International Ltd. Oceanographic Services Ltd, 53 p.

Otay, E., 1995. Monitoring results of a nearshore disposal berm. *Coastal Dynamics '95 Conference* (ASCE), pp. 547-558.

Pang, D.T.K., Rodgers, M.P. and Young, I.R., 1999. Directional wave conditions at Fremantle, Western Australia. *Pacific Coasts and Ports '99 Conference,* Perth, Australia, pp. 473-478.

Panicker, N.N. and Borgman, L.E., 1970. Directional Spectra from Wave-Gauge Arrays. *Coastal Engineering 1970 Conference*, Washington, DC, pp. 117-136.

Phillips, D., Black, K., Hume, T. and Healy, T., 1999. Sediment dynamics along a surfing headland. *Pacific Coasts and Ports '99 Conference*, Perth, Australia, pp. 513-518.

Pickrill, R. A., and Mitchell, J. S., 1979. Ocean Waves Characteristics Around New Zealand. *New Zealand Journal of Marine and Freshwater Research*, **13**(4), 501-520.

Pilkey, O.H., Young, R.S., Bush, D.M. and Thieler, E.R., 1994. Predicting the behaviour of beaches: alternatives to models. *Littoral '94 Conference*, Lisbon, Portugal, pp. 53-60.

Pizzuto, J.E., 1987. Dispersion of dyed sand tracers in an oscillatory flow field. *Journal of Geophysical Research,* **92**(C2), 1923-1933.

Ribberink, J.S. and Al-Salem, A.A., 1995. Sheet flow and suspension of sand in oscillatory boundary layers. *Coastal Engineering*, **25**, 205-225.

Riddle, A.M. and Lewis, R.E., 2000. Dispersion experiments in U.K. coastal waters. *Estuarine, Coastal and Shelf Science*, **51**, 243-254.

Rodoriguez, J.G. and Katoh, K., 1994. Control of littoral drift in Caldera Port, Cost Rica. *Hydro-port '94 Conference,* pp. 1019-1040.

Scheffner, N.W., 1996. Systematic analysis of long-term fate of disposed dredged material. *Journal of Waterway Port Coastal and Ocean Engineering*, **122** (3), 127-133.

Schiel, D. R. and Foster, M. S., 1986. The structure of subtidal algal stands in temperate waters. *Oceanography and Marine Biology Annual Review* **24**, 265-307.

Schwartz, R.K. and Musialowski, F.R., 1977. Nearshore disposal: onshore sediment transport. *Coastal Sediments '77 Conference,* ASCE, pp. 85-101.

Seymour, R.J., 1986. Results of Cross-Shore Transport Experiments. *Journal of Waterway, Port, Coastal and Ocean Engineering*, **112**(1), 168-173.

Sherman, D.J., Bauer, B.O., Nordstrom, K.F., Allen, J.R., 1990. A tracer study of sediment transport in the vicinity of a groin: New York, USA. *Journal of Coastal Research,* **6**(2), 427-438.

Shih, S.M. and Komar, P.D., 1994. Sediments, beach morphology and sea cliff erosion within an Oregon coast littoral cell. *Journal of Coastal Research*, **10**, 144-157.

Sistermans, P.G. and van de Graff, J., 1999. The effect of grading on the vertical distribution of suspended sediment. *Coastal sediments '99 Conference, New York,* pp. 48-63.

Silvester, R., 1985. Natural headland control of beaches. *Continental Shelf Research,* **4**(5), 581-596.

Slinn D.N., Allen J.S. and Holman, R.A., 2000. Alongshore currents over variable beach topography. *Journal of Geophysical Research-Oceans.* **105**(C7), 16971-16998.

Soulsby, R., 1999. *Dynamics of marine sands.* Thomas Telford, 249 p.

Stanton, B. R., 1995. Sea level variability on the west coast of New Zealand. *Journal of Physical Oceanography*, **25** (6), 1265-1272.

Staub, C., Jonsson, I.G. and Svendsen, I.A., 1984. Variation of sediment suspension under oscillatory flow. *Coastal Engineering '84 Conference,* Houston, pp. 2310-2321.

Storlazzi, C.D. and Field, M.E., 2000. Sediment distribution and transport along a rocky, embayed coast: Monterey Peninsula and Carmel Bay, California. *Marine Geology,* **170**(3-4), 289-316.

Swart, D.H., 1974. Offshore sediment transport and equilibrium beach profiles. Pub. No. 131. Delft Hydraulics Laboratory.

Tait, J.F. and Revenaugh, J., 1998. Source-transport inversion - an application of geophysical inverse theory to sediment transport in Monterey Bay, California. *Journal of Geophysical Research-Oceans,* **103**(C1), 1275-1283.

TCC, 1980a. Maritime recreational park proposal for the Sugar Loaf Islands area of North Taranaki. Taranaki Catchment Commission, Stratford.

TCC, 1980b. Preliminary investigations of oceanographic conditions in the Waitara Embayment. Taranaki Catchment Commission, Stratford.

TCC, 1981. Oceanography – Synthetic petrol plant – Motunui. Taranaki Catchment Commission, Stratford.

TCC, 1985. Oceanographic studies, Part 3, Waitara Regional Wastewater Disposal Study. Taranaki Catchment Commission, Stratford.

Terray, E., Brumley, B. and Strong, B., 1999. Measuring Waves and Currents with an Upward-Looking ADCP. *Proceedings of the IEEE Sixth Working Conference on Current Measurement,* San Diego, CA, pp. 66-71.

Thornton, E.B. and Guza, R.T., 1983. Transformation of wave height distribution. *Journal of Geophysical Research*, **88**, 5925-5938.

Tillotson, K. and Komar, P.D., 1997. The wave climate of the Pacific Northwest (Oregon & Washington): A comparison of data sources. *Journal of Coastal Research*, **13,** 440-452.

Timoshenko, S. and Young, D.H., 1948. *Advanced Dynamics*. McGraw-Hill, New York, 400 p.

Tullett, J.S., 1981. *The industrious heart: a history of New Plymouth*. New Plymouth District Council, New Plymouth, New Zealand, 350 p.

Uda, T., Naito, K. and Kanda, Y., 1991. Field experiment on sand bypass of the Iioka Coast. *Coastal Engineering in Japan*. **34** (2), 205-220.

van Rijn, L.C., 1984. Sediment pickup functions. *Journal of Hydraulic Engineering,* **110** (12), 1733-1754.

van Rijn, L.C., 1993. *Principles of sediment transport in rivers, estuaries and coastal seas*. Aqua Publications, Amsterdam, pp. 13-86.

Vera-Cruz, D., 1972. Artificial nourishment of Copacabana Beach. *Coastal Engineering '72 Conference*, ASCE, pp. 1451-1463.

Vincent, C.L. and Jensen, R.E., 1997. Observations of wave transformations near breaking. *Journal of Waterway Port Coastal and Ocean Engineering,* **123**(5), 249-251.

Webb, T.W., 1996. Steady coastal circulation on a narrow irregular shelf. *Journal of Physical Oceanography*, **26**(9), 1673-1689.

Weber, N., 1991. Bottom friction for wind, sea and swell in extreme depth-limited situations. *Journal of Physical Oceanography*, **21**, 149-172.

White, J., 1990. The use of sediment traps in high-energy environments. *Marine Geophysical Researches*, **12,** 145-152.

White, T.E. and Inman, D.L., 1989. Measuring longshore transport with tracers. In: *Nearshore Sediment Transport*. Seymour, R.J. (Ed.), Chap. 13, Plenum, New York, pp. 287-312.

White, T.E., 1998. Status of measurement techniques for coastal sediment transport *Coastal Engineering,* **35**(1-2), 17-45.

Whitehouse, R.J.S., 1995. Observations of the boundary layer characteristics and the suspension of sand at a tidal site. *Continental Shelf Research,* **15**(13), 1549-1567.

Wikramanayake, P.N. 1993. Velocity profiles and suspended sediment transport in wave-current flows. PhD Thesis, Massachusetts Institute of Technology, 285 p.

Willan, R. C. 1980. Report on the subtidal marine biological surveys in inshore waters of the Taranaki coast. Maui development environmental study Phase II. Subtidal monitoring study. Report 79-18.

Wright, L.D., 1976. Nearshore wave-power dissipation and the coastal energy regime of the Sydney-Jervis Bay region, New South Wales: A comparison. *Australian Journal of Marine and Freshwater Research,* **27**, 633-640.

Wright, L.D., 1987. Shelf-surfzone coupling: diabathic shoreface transport. *Coastal Sediments '87 Conference,* ASCE, pp. 25-40.

Wright, L.D. and Short, A.D., 1983. Morphodynamics of beaches and surf zones in Australia. In: *Handbook of Coastal Processes and Erosion*, P.D. Komar (Ed.), CRC Press, Boca Raton, FL, pp. 35-64.

Young, I.R. and Gorman, R.M., 1995. Measurements of the evolution of ocean wave spectra due to bottom wave friction. *Journal of Geophysical Research*, **100**, 987-11,004.

Young, I.R. and Sobey, R.J., 1985. Measurements of the wind-wave energy flux in an opposing wind. *Journal of Fluid Mechanics*, **151**, 427-442.

Zenk, Halpern, and Kase, D., 1980. Influence of mooring configuration and surface waves upon deep-sea near-surface current measurements. *Deep-Sea Research*, **27**, 217-224.

Zyserman, J.A. and Fredsoe, J., 1994. Data analysis of bed concentration of sediment. *Journal of Hydraulic Engineering,* **120**(9), 1021-42.

APPENDIX 1

LIST OF ADDITIONAL REPORTS AND SCIENCE PAPERS

Atkinson, P. & McComb, P., 1997. Environmental effects assessment of a trial of an inshore disposal site for maintenance dredgings from Port Taranaki. Westgate Transport Ltd. 35 p.

Black, K.P., Mead, S., McComb, P. J., Jackson, A. & Armstrong, K., 1999. New Plymouth Foreshore Redevelopment: Reef and Beach feasibility Study. A report to the New Plymouth District Council. 57 p.

Black, K.P. & McComb, P.J., 2000. Port Taranaki Maintenance Dredging Consent Renewal Studies. Report 2: Site selection, effects and outcomes. Department of Earth Sciences, University of Waikato. 142 p.

Cole, R.; McComb, P., & Sait, J., 1999 Effects of nearshore sand disposal on subtidal and intertidal organisms at New Plymouth, New Zealand. *Proceedings of the 1999 Pacific Coasts and Ports Conference*, Perth, Australia. pp. 129-134.

Cole, R.G. & McComb, P.J., 2000. Port Taranaki Maintenance Dredging Consent Renewal Studies. Report 4: Biological description and assessment. NIWA Client Report WTL00403/1. 83 p.

Atkinson, P.N., Black, K.P., Dunlop, R., McComb P.J. & Cole, R.G., 2001. Port Taranaki Maintenance Dredging Consent Renewal Applications. Report 5: Assessment of environmental effects.

Howse, B.S., Black, K.P., Cole, R.G. & McComb, P.J., 2000. Port Taranaki Maintenance Dredging Consent Renewal Studies. Report 3: The relationship of sediment flux to abundance and sizes of paua and kina on New Plymouth reefs. Department of Earth Sciences, University of Waikato. 49 p.

Kun, A., Fougere, A., & McComb, P., 1999. A new wave direction spectrum measurement instrument. *Proceedings of the IEEE 6th Working Conference on current Measurement*, San Diego. pp 49-53.

McComb, P.J., 1999a. FPSO motions study: data collection and analysis report. A report to Shell Todd Oil Services Ltd. 11 p.

McComb, P.J., 1999b. An evaluation of the directional wave climate at the Port Taranaki harbour entrance. A report to Westgate Transport Ltd by ASR Ltd. 19 p.

McComb, P.J. & Black, K.P., 2000. Port Taranaki Maintenance Dredging Consent Renewal Studies. Report 1: Field measurements. Department of Earth Sciences, University of Waikato. 102 p.

McComb, P.J., 2000a. A review of the sedimentary and oceanographic conditions for a Single Point Mooring Buoy and pipeline at Port Taranaki. A report to Westgate Transport Ltd. by ASR Ltd. 32 p.

McComb, P.J., 2000b. A review of the sedimentary and oceanographic conditions at Pohokura. A report to TransField Worley Ltd by ASR Ltd. 19 p.

McComb, P.J. & Beamsley, B., 2000. Telstra Saturn Aqualink Project: An evaluation of the Te Henui Landing Site. A report to Telstra Saturn Communications Ltd and the Taranaki Regional Council by ASR Ltd. 38 p.

McComb, P. J., Black, K.P. Mead, S.T & Hutt, J., 2001. Opunake surfing reef feasibility studies. A report to the South Taranaki District Council by ASR Ltd. 111 p.

McComb, P.J., 2001a. A metocean summary of the Awakino site for rig specification purposes. A report to Pacific Tiger Energy Ltd by ASR Ltd. 25 p.

McComb, P.J., 2001b. South Taranaki wave climate summary. A report to the Taranaki Regional Council by ASR Ltd. 25 p.

McComb, P.J., 2001c. Metocean conditions at Patea: a review for operational survey purposes. A report to Shell Todd Oil Services Ltd by ASR Ltd. 15 p.

APPENDIX 2

WBEND MODEL CALIBRATION

A2.1 Background

The initial wave refraction studies at New Plymouth (Chapter 5) did not include a variable seabed substrate, and applied a constant friction coefficient throughout the model grid. However, in later work the WBEND model (Black and Rosenberg, 1992a) was refined to include a spatially variable bed roughness according to the newly acquired side-scan sonar data (Black & McComb, 2000). This appendix presents the results of the WBEND model calibration for the variable substrate.

A2.2 Calibration requirements

WBEND calibration involves setting the friction coefficient as well as a smoothing algorithm that simulates wave diffraction. The latter increases the model accuracy, particularly in regions of strong wave height and angle convergence or divergence. This diffraction smoothing is based on a horizontal eddy viscosity term given by

$$\psi = \varepsilon\left(\frac{\partial^2 \varphi}{\partial y^2}\right) \qquad \textbf{(A2.1)}$$

where ε is the eddy viscosity coefficient and φ is either wave height or angle. Wave-energy frictional dissipation in WBEND is defined by,

$$F_f = \frac{\rho C_f}{6\pi}\left(\frac{H\omega}{\sinh(kd)}\right)^3 \qquad \textbf{(A2.2)}$$

where ω is the radian frequency, H is the wave height, d is the water depth and k is the wave number. C_f is the friction coefficient, which is taken to be $C_f = 0.5 f_w$, where f_w is form given by of Swart (1974) as

$$f_w = \exp\left[5.213\left(\frac{k_b}{a_s}\right)^{0.194} - 5.977\right]. \qquad \textbf{(A2.3)}$$

Here, the bed roughness is given by k_b, and a_s is the semi-orbital excursion. For sandy beds, k_b can reflect a range of range of roughness values based on the bedform dimensions (e.g. Wikramanayake, 1993). From wave and sediment data, WBEND is able to predict the bedform dimensions (e.g. Black and Oldman, 1999), and thereby adjust the friction coefficients according to the bed roughness. Alternatively, a constant friction may be applied. Over rocky beds, the effective roughness is very different to sandy beds, essentially unchanging over time but being highly variable in scale. WBEND uses k_s, the Nikuradse equivalent roughness, which is taken to represent the physical height of the roughness elements and is 30 times the roughness length z_o (Nielsen, 1992).

A2.3 WBEND model calibration

The model requires a boundary wave reference condition that describes the input wave height, period and direction. WBEND may utilise either a directional spectral input or monochromatic input, and in this application the latter was employed. This approach was based on the results of previous WBEND modelling (Chapter 5) and a consideration for the increase in computational time required for the spectral wave input. Site L1 (Fig. A2.1) provided the model boundary wave reference condition in terms of significant wave height (H_s), mean spectral wave period (T_m), peak spectral wave period (T_p) and mean wave direction (θ). The input wave directions were rotated according to the orientation of the model bathymetry grid (i.e. 45°).

A set of 63 calibration events was extracted from the intensive two-month period of wave measurements at site L1. These data represent the "ideal" conditions for modelling the transformation of waves from the model boundary to the nearshore zones; being approximately monochromatic, unidirectional and non-breaking at the nearshore measurement sites. A wind speed criteria of <6 ms^{-1} was also applied, following the finding that wave transformations were influenced by the wind vector. These cases were chosen to isolate the height attenuation effects due to bed friction and thereby best calibrate the friction coefficients. Regions of sandy and rocky seabed substrate were

represented in the model as a grid with equivalent dimensions and orientation as the bathymetry. Grids were constructed by digitising the side-scan images to define the seabed substrate within a grid cell as either rocky (0) or sandy (1). The model was coded to recognise these values and apply the specified bed friction coefficients to these cells. Thus, separate friction terms for each substrate type could be tested.

In excess of 140 model runs were conducted using the 63 calibration events over a range of friction coefficients (for sandy and rocky areas) and eddy viscosity coefficients (for wave height and wave angle). Tests were also performed to determine the most appropriate representation of wave period for the boundary input (i.e. the peak or mean spectral wave period), the sediment particle fall velocity (for bedform generation on sand) and the use of a variable or constant friction term for the two seabed substrate types. The results of each test were evaluated by comparing the numerical output of wave height at the nearshore measurement sites (e.g. Fig. A2.1) with the actual field data. This comparison was achieved by calculating an error as;

$$E_r = \sum (H_p - H_m)^2 / \sum (H_m)^2 \qquad \textbf{(A2.4)}$$

where H_p is the predicted wave height and H_m is the measured wave height. A wave height difference (measured – predicted) and ratio (predicted / measured) were also calculated.

A2.3.1 Calibration results

The best model simulation was found using the mean spectral wave period (T_m) for the boundary-input condition, a constant friction term for sandy beds (C_f = 0.09), and a Nikuradse equivalent roughness of 10 m for the rocky beds (Table A2.1).

The performance of the model was validated by simulating a 13-day data time-series (Julian days 82 - 95, 1998). While the frictional resistance has been obtained using pre-selected cases, no pre-selection of wave conditions was undertaken for the validation. The period includes a broad range of wave conditions (up to 4.5 m wave height) and a wide range of wave and wind direction conditions (McComb & Black, 2000). Results are reported in Table A2.2 and presented in time-series (Fig. A2.1). Linear regression

analysis of the measured and predicted wave heights over this period show a high-correlation, with an overall average R^2 value of 0.83.

Table A2.1: Final WBEND calibration coefficients where C_f is the friction coefficient for sandy beds, k_s is the Nikuradse equivalent roughness and φ is the eddy viscosity term (for wave height and wave angle).

C_f (sandy beds)	K_s (rocky beds)	φ (wave height)	φ (wave angle)
0.09	10 m	0.1	0.2

Table A2.2: Comparison of the measured and predicted significant wave heights (m) using the calibration coefficients in Table A2.1. Site-averaged values are presented from the 63 calibration events. E_r is the error (Eqn. A2.5), *Difference* is the measured – predicted wave height and *Ratio* is the predicted / measured wave height.

Site	E_r	Difference (m)	Ratio
L2	0.038	-0.055	1.084
S1	0.074	0.049	0.972
S3	0.019	0.034	0.982
S4	0.066	-0.084	1.105
D1	0.066	0.018	0.982
D2	0.037	0.007	0.997
D3	0.028	0.136	0.909
D4	0.068	-0.032	1.051
D5	0.077	0.301	0.812
D6	0.103	0.244	0.766
AVE	0.055	0.062	0.966

Table A2.3: Comparison of the measured and predicted significant wave heights (m) using the calibration coefficients in Table A2.1. Site-averaged values are presented from the TRAP3 period (day 82.5-95.5, 1998). E_r is the error (Eqn. A2.4), *Difference* is the measured – predicted wave height, *Ratio* is the predicted / measured wave height and R^2 is the correlation of the linear regression between measured and predicted wave heights.

Site	E_r	Difference (m)	Ratio	R^2
L2	0.037	-0.088	1.080	0.879
S1	0.080	-0.255	1.161	0.818
S3	0.018	0.011	0.988	0.864
S4	0.035	-0.034	1.047	0.838
D1	0.041	-0.002	0.994	0.889
D2	0.028	-0.055	1.037	0.884
D3	0.039	0.227	0.887	0.823
D4	0.081	-0.170	1.134	0.733
D5	0.051	0.195	0.901	0.702
AVE	0.046	-0.019	1.025	0.826

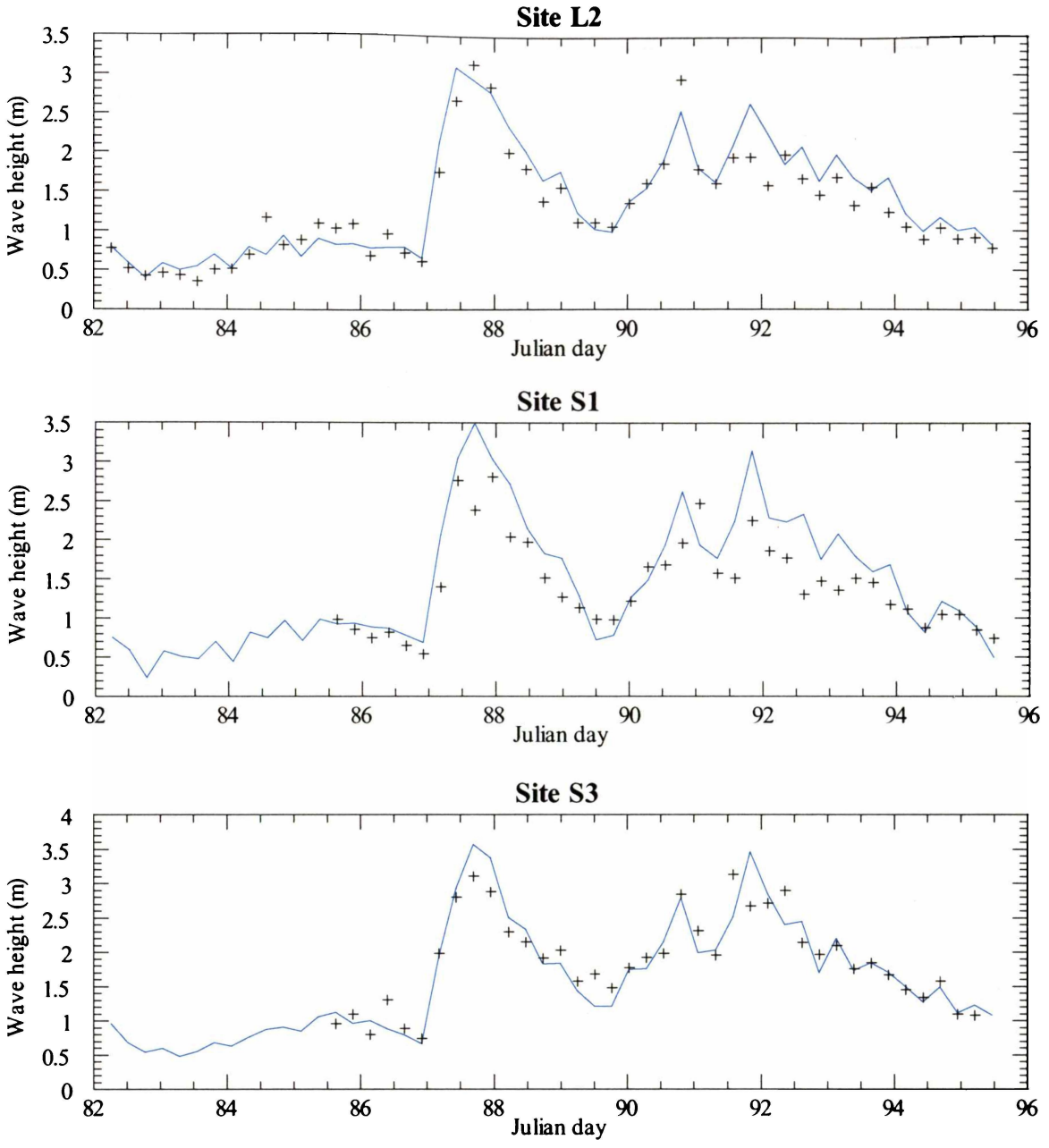

Figure A2.1. Comparison of the significant wave heights (H_s) of the model (solid blue line) and the nearshore measurements (black stars) made over a 13-day period (Julian days 82-95, 1998).

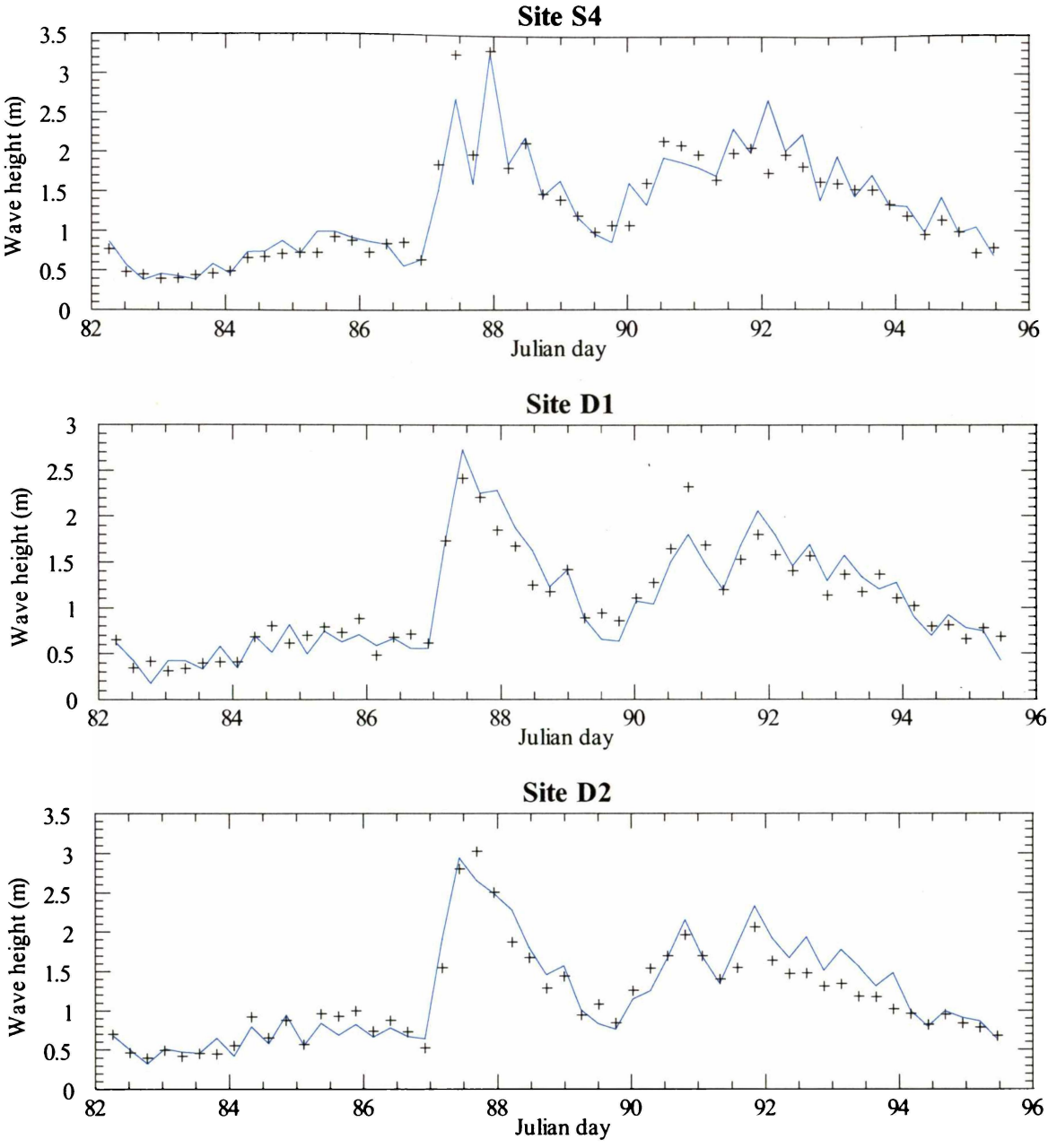

Figure A2.1 (cont.). Comparison of the significant wave heights (H_s) of the model (solid blue line) and the nearshore measurements (black stars) made over a 13-day period (Julian days 82-95, 1998)

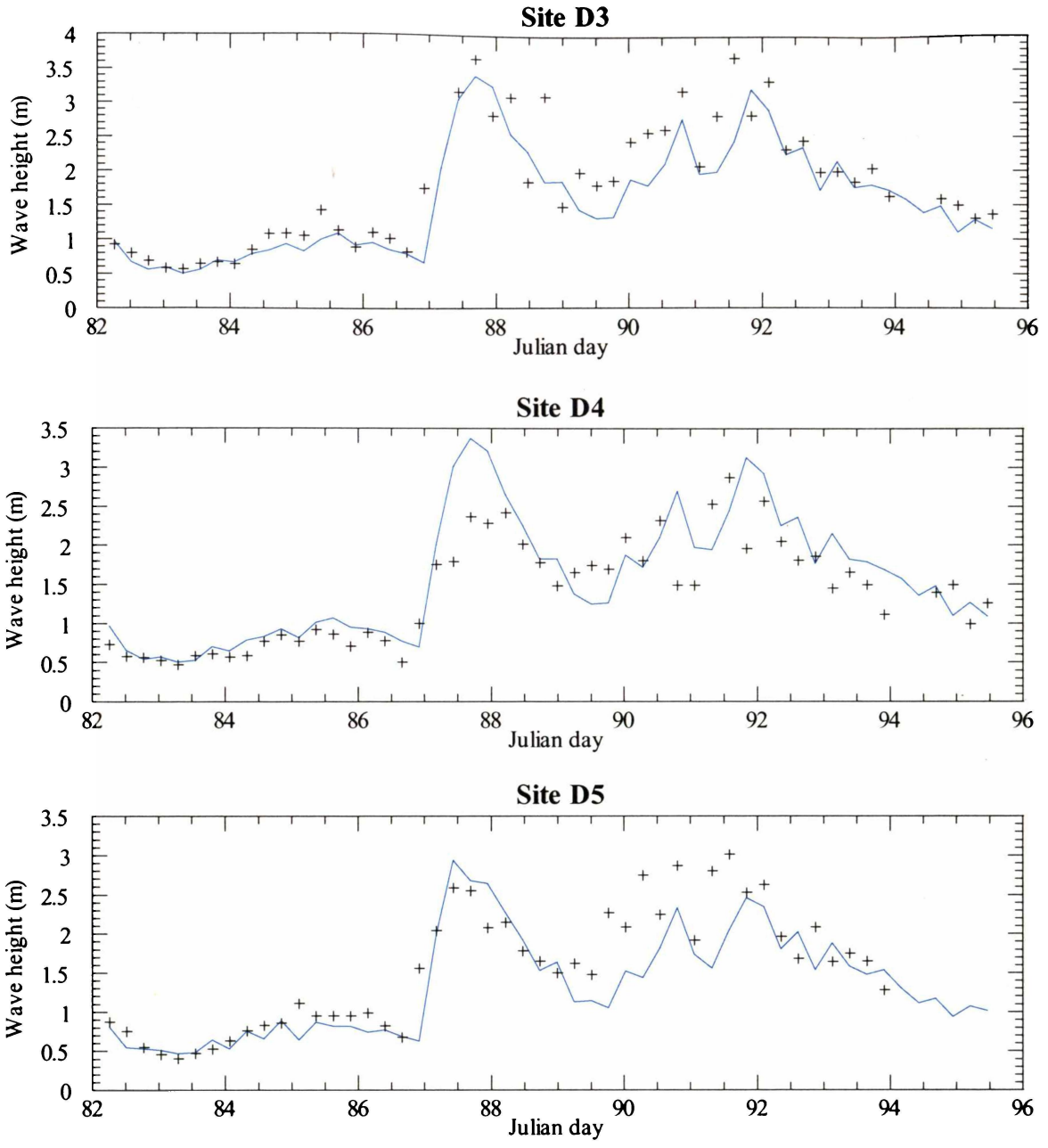

Figure A2.1 (cont.). Comparison of the significant wave heights (H_s) of the model (solid blue line) and the nearshore measurements (black stars) made over a 13-day period (Julian days 82-95, 1998).

APPENDIX 3

USE OF DROP VIDEO TO MAP HABITATS IN A HIGH ENERGY SHALLOW REEF ENVIRONMENT

Cole, R., McComb, P., & Sait, J. 2000. Use of drop video to map habitats in a high-energy shallow reef environment. Presented at: *Direct sensing of the size and abundance of target and non-target fauna in Australian fisheries*: National Workshop FRDC 2000/187, Rottnest Island, Western Australia, September 2000.

A CD is included with this abstract.

A3.1 Introduction

As part of a study to optimise the placement of clean dredged sands from Port Taranaki (Fig. A3.1), we undertook an investigation of benthic habitats near New Plymouth, New Zealand (174° 11'E 41° 03'S) (Fig. A3.1). Until recently, there had been few in situ ecological investigations of this coast, in no small part due to the harsh physical environment; dominated by long-period (12 - 16 second) swell with wave heights of up to 6 m (McComb *et al.*, 1999a,b). Underwater visibility is frequently very poor. It is therefore imperative that when suitable conditions occur, ecological information is gathered quickly and efficiently.

A four-year study has recently gathered much information regarding the physical oceanographic and sedimentary environment at New Plymouth (McComb *et al.*, 1997; McComb *et al.*, 1999a,b; McComb & Black, 2000). That study used an intensive field data collection program (including sidescan sonar, wave and current meters, sediment trapping, sediment tracing) and numerical modelling to identify a nearshore (6-10 m water depth) placement ground for clean sand dredged from the harbour (Fig. A3.1). Instead of offshore placement, the use of a nearshore ground retains the harbour-trapped littoral sediments within the nearshore littoral cell – thereby mitigating downstream erosion / depletion effects.

The key aim of this work was to optimise the benefits of nearshore placement (i.e. renourishing city beaches) while at the same time minimising the biological impacts (i.e. inundating important ecological habitats). To identify the habitats that may be affected by the proposed nearshore sand placement, we needed to map a relatively large area. Furthermore, as we were faced with adverse conditions for much of the time, we required a technique that allowed us to map biological habitats across a broad area in a short period.

In areas of shallow water and good water clarity remote sensing techniques (e.g. aerial photography) can be used effectively to map underwater habitats and variations in substratum type (e.g. Andrew & O'Neill, 2000, and review of Kingsford & Battershill, 1998). However, many temperate systems have murky water and therefore do not lend themselves readily to aerial photographic techniques. Sonar-based techniques have not

been found to be suitable for distinguishing biological habitats either, as they cannot distinguish between presence and absence of seaweed beds, for example. The most common alternative to these remote sensing techniques is to use SCUBA divers. However, the resulting data are often spatially inaccurate, and are very time-consuming and expensive to collect if the study site covers a large area. An alternative to using SCUBA divers is to use drop video. We have found that the drop video technique can be used to map habitats rapidly and accurately when combined with modern navigation techniques. To this end we employed a vessel-mounted drop video to record the benthic habitat over a grid pattern. Subsequently, quantitative sample sites for SCUBA divers were allocated on the basis of the area occupied by the different habitats.

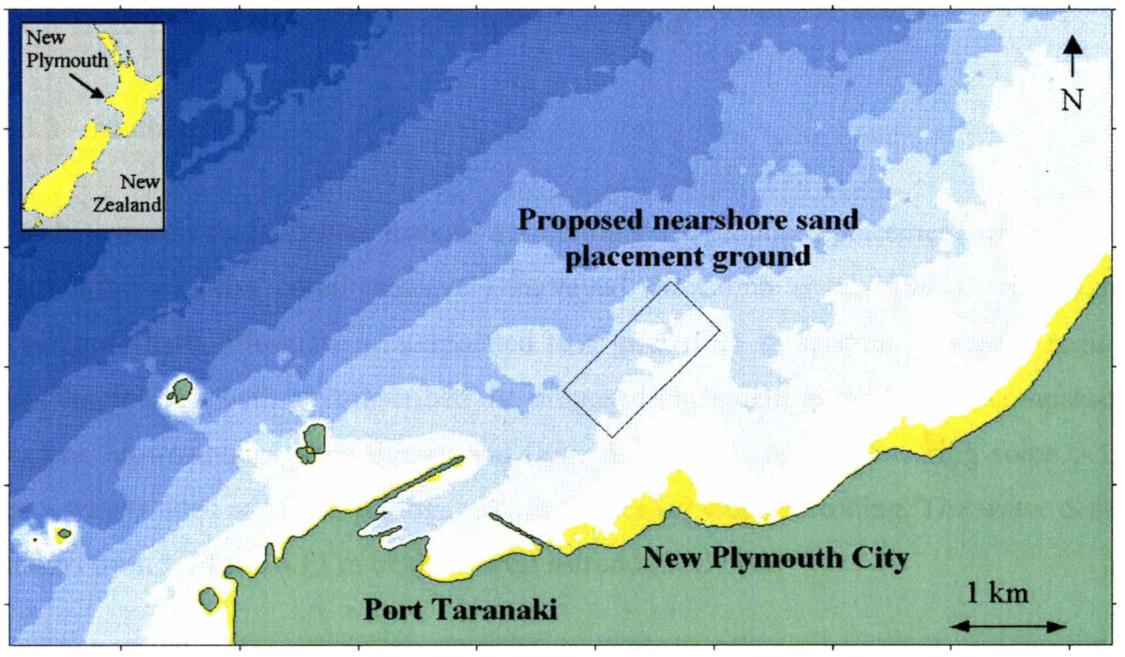

Figure A3.1. Location map showing the New Plymouth coast with land coloured green, intertidal in yellow, and 5m depth contours in shades of blue. The proposed placement area is outlined in black. Location of New Plymouth on the west coast of North Island, New Zealand given in inset.

A3.1.1 Presentation of Results

It is important for the future of coastal management that the results of habitat surveys can be effectively communicated to a non-technical audience. In our experience aerial-photographs, maps, graphs and tables often fail to convey to the audience the presence of crucial variations in habitat (such as those examples demonstrated in Choat & Schiel, 1982, & Taylor, 1998). Recent technological developments have made it possible to present raw qualitative data, such as video recordings (e.g. Fabricius & Wolanski, 2000), which have potential for much higher audience impact. To this end, an important part of our study is the production of an interactive CD to present the findings of our study to the public. The CD contains excerpts of video footage from some 217 sites. Each video excerpt is linked to a site on a locality map.

A3.2 Methods

The bathymetry and physical features surrounding the proposed placement area at New Plymouth had been comprehensively surveyed (McComb *et al.*, 1997), with high-resolution depth information interpolated to a grid of 25 m spacing. A survey region was defined that both circumscribed the proposed placement ground and encompassed regions 'downstream' from the ground (Fig. A3.2). This region, covering some 3.15 km^2, was gridded at 150m spacings to extract sites for video recording. The water depth ranged from 1.54 to 16.15 m below lowest astronomical tide.

Benthic habitats at each site were observed using a dropped video camera. This consists of an underwater lens and lights on a 100m cable attached to a handheld Hi-8 video recorder on the boat. In an 11-hour period over two days in February 2000, we surveyed 217 sites in that area with the drop video from a survey vessel with differential GPS. At each site, around 30 seconds of data was recorded along with real-time observational notes and a habitat classification. We ascribed four generic habitats; sand, coralline pavement, mixed macro-algae, or kelp (*Ecklonia radiata*) forest. These data were subsequently mapped and quantitative sample sites allocated on the basis of the area occupied by reef. They were sampled with divers by use of $1m^2$ quadrats (n=5).

The video data formed the basis of the interactive CD. Between 10 and 30 seconds of analogue video footage was converted to digital images and saved as *.mpg files. The site name and depth information was edited onto the video images. An interactive HTML structure was written to allow the digital video from each site to be accessed by clicking positions on a map. Further, habitat and location maps were included, along with an explanation of the methodology. The HTML file structure was then burned to CD.

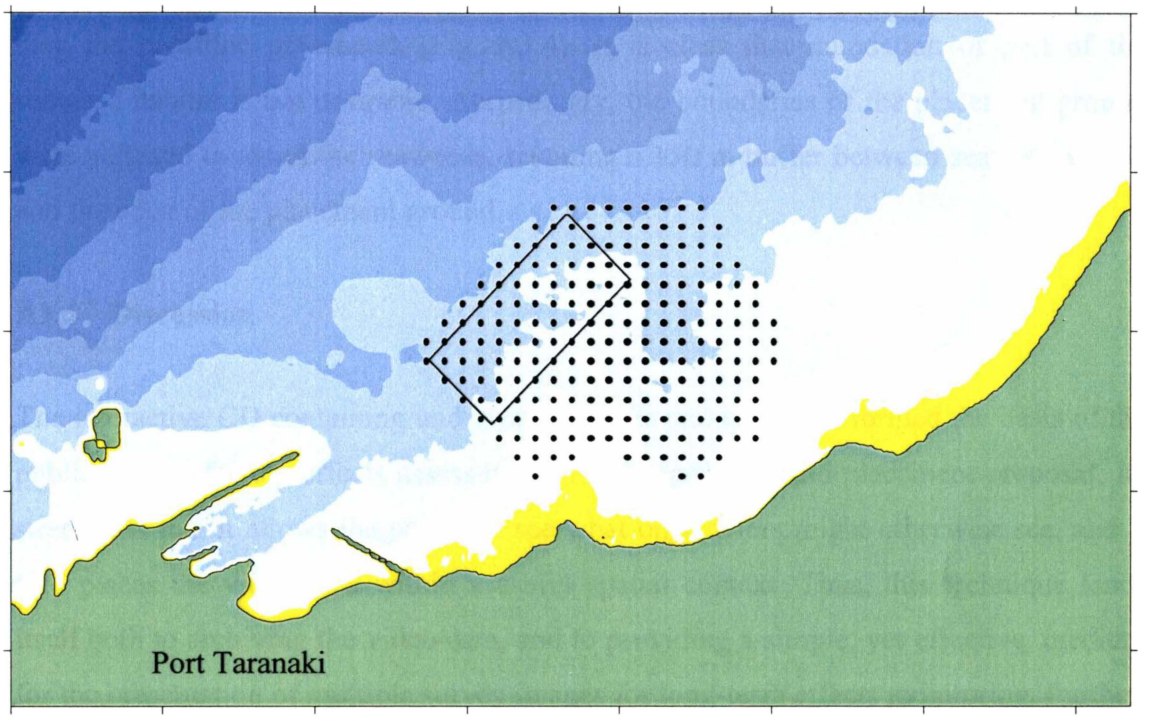

Figure A3.2. Location map showing the New Plymouth coast as for Fig. A3.1, and including map of sampling sites over 3.15 km^2.

A3.3 Results

The video survey was carried out during a period of calm weather with exceptional water clarity. The video data revealed the rocky substratum comprised coralline pavements, with an area of seaweed habitat on a raised topographical feature

immediately shoreward of the proposed placement region. Indeed, it was found that the shoreward boundary of the ground transgressed the seaweed habitat (Fig. A3.3).

On the basis of the observed habitats, nine quantitative sampling sites were allocated to coralline pavements, and two quantitative sampling sites were allocated to each of mixed macroalgae and kelp forest, for a total of 13 quantitative sample sites. That sampling was conducted over a 10-hour period. Overall, the fauna was found to be generally depauperate, with low abundances of all organisms. However, the results show that seaweed habitats had greater numbers of species and individuals within them than the coralline pavements (Fig. A3.4). It is clear that inundation of part of the seaweed habitat is not desirable. Accordingly, the boundaries of the placement ground were adjusted to avoid the seaweeds, retaining a 150 m buffer between seaweed stands and the edge of the placement ground.

A3.4 Discussion

The interactive CD containing underwater images and maps has formed the basis of the public liaison for the effects assessment of the nearshore sand placement proposal. Its strength is that it allows the public to see what only divers might otherwise see, and it also places the video data within a useful spatial context. Thus, this technique lends itself both to archiving the video data, and to providing a simple, yet effective, medium for the presentation of multiple survey images for long-term effects monitoring. Further, the justification for adjusting the boundaries of the proposed placement ground (to avoid inundating seaweed stands) is readily apparent. Fieldwork, data reduction and analysis, and CD production were both time- and cost-effective. Further, the mapping exercise has also formed the basis of further investigations into the reasons for the localisation of stands of seaweed in one small area of reef (Appendix 4). While in the present study the technique was applied in excellent weather and underwater visibility, we believe that it may also be effective in less than ideal conditions. Some difficulties may be encountered including the possibility of snagging the camera lens in rugose rocky areas, in kelp forests with surface canopies, or among corals. However, for most situations on rocky reefs or sand flats the approach we have used is straightforward, very efficient, and has good positional accuracy.

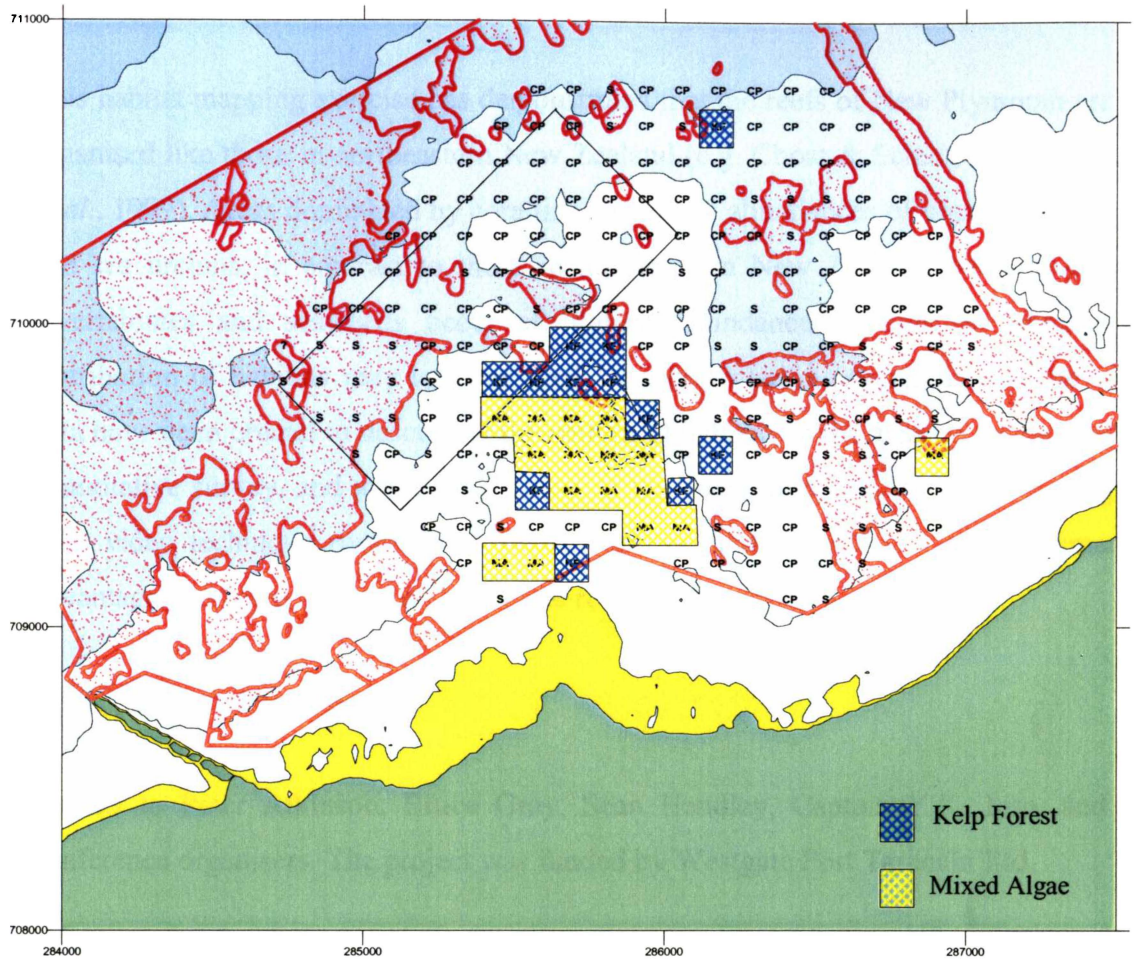

Figure A3.3. Map of habitats derived from video survey. CP = coralline pavement; S = sand, kelp forest (*Ecklonia radiata* only) is cross-hatched blue, and mixed algae (*Ecklonia radiata* and *Carpophyllum maschalocarpum*) is cross-hatched yellow. Sand – rock borders are indicated by the red line.

Aerial imagery presents an alternative to this technique. Differences in costs are probably small, but aerial photography cannot readily distinguish among different species of seaweeds (unless they have surface canopies), and cannot operate to depths more than 10 m unless water clarity is very high. The drop video is capable of being used in very low underwater visibility, and in our experience Hi-8 images are often clearer than divers' observations. It would be possible to carry out the mapping at night, by attaching suitable lights to the video lens. While we were able to compile a species

list of fishes off the video footage, the addition of bait would permit an index of abundance to be derived (e.g. Willis *et al.*, 2000) that is independent of diver-negative reactions.

This habitat mapping exercise has demonstrated that the reefs of New Plymouth are not organised like those in northeastern New Zealand (e.g. Choat & Schiel, 1982, Babcock *et al.*, 1999). Areas dominated by corallines have low abundances of grazing gastropods and sea urchins, in contrast to those in northeastern New Zealand. Most species of invertebrates and seaweeds occur at highest abundances in shallow water. The distribution of habitats may be controlled by sedimentation (Appendix 4). The video data have been crucial to describing the pattern of habitats in the area, to structuring our quantitative survey, and to the preparation of the interactive CD. We will be using the drop video technique routinely in future surveys, and suggest that it has numerous advantages for many studies on temperate reefs.

A3.5 Acknowledgements

Thanks to Peter Atkinson, Bruce Gray, Sean Handley, Captain Y.K. Lim, and the conference organisers. The project was funded by Westgate Port Taranaki Ltd.

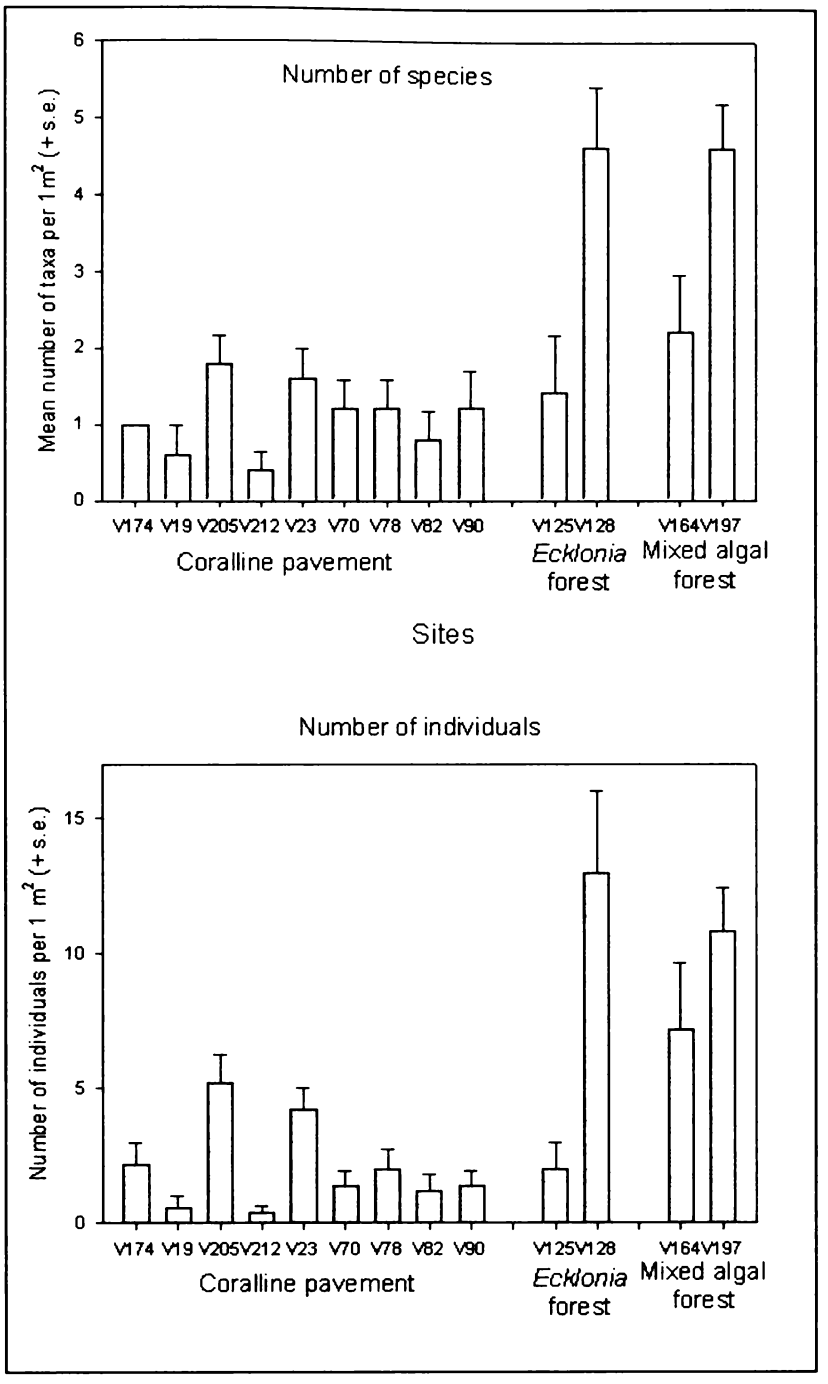

Figure A3.4. Species richness and number of individuals for each site, with seaweeds excluded. Data are means + 1 s.e. from $1m^2$ quadrats (n=5) from sites allocated randomly to each habitat. X-axis labels represent the individual sites; they are not indicated on Figure A3.1.

A3.6 References

Andrew, N. L. & O'Neill, A. L. O. 2000. Large-scale patterns in habitat structure on subtidal rocky reefs in New South Wales. *Marine and Freshwater Research,* **51**, 255-263.

Babcock, R. C., Kelly, S., Shears, N. T., Walker, J. W., & Willis, T.J., 1999. Changes in community structure in temperate marine reserves. *Marine Ecology Progress Series,* **189**, 125-134.

Cole, R. Choat, J. H. & Schiel, D. R., 1982. Patterns of distribution and abundance of large brown algae and invertebrate herbivores in subtidal regions of northern New Zealand. *Journal of Experimental Marine Biology and Ecology,* **60**, 129-162.

Choat, J. H. & Schiel, D. R. 1982. Patterns of distribution and abundance of large brown algae and invertebrate herbivores in subtidal regions of northern New Zealand. *Journal of Experimental Marine Biology and Ecology* 60, 129-162.

Fabricius, K. E. & Wolanski, E. 2000. Rapid smothering of coral reef organisms by muddy marine snow. *Estuarine Coastal and Shelf Science,* **50**, 115-120.

Kingsford, M. J. & Battershill, C. N. 1998. Subtidal habitats and benthic organisms of rocky reefs. In 'Studying Temperate Marine Environments. A Handbook for Ecologists'. (Eds M. J. Kingsford and C. N. Battershill.) pp. 84-114. Canterbury University Press: Christchurch.

McComb, P. J., Black, K. P., Atkinson, P. N., Bell, R. G. & Healy, T. R. 1997. High-resolution wave transformation on a coast with complex bathymetry. *Proceedings of the Pacific Coasts & Ports '97 Conference,* Christchurch, New Zealand, pp. 995-1000.

McComb, P. J., Black, K. P., Atkinson, P. N., Lim, Y. T., & Healy, T. R. 1999a. The accretion of a breakwater-tip shoal following dredging. *Proceedings of the Pacific Coasts & Ports '99 Conference,* Perth, Australia. pp. 420-425.

McComb, P., Black K., Healy, T. & Atkinson, P. 1999b. Coastal and sediment dynamics at Port Taranaki, New Zealand: a large, multi-faceted, field experiment. *Proceedings of Coastal Structures '99 Conference,* Santander, Spain, 2, 823-832.

McComb, P. J. & Black, K. P. (in press). Dynamics of a nearshore dredged-sand mound on a rocky, high-energy coast. *Journal of Coastal Research.*

Taylor, R. B., 1998. Density, biomass and productivity of animals in four subtidal rocky reef habitats: the importance of small mobile invertebrates. *Marine Ecology Progress Series,* **172**, 37-51.

Willis, T. J., Miller, R. B. & Babcock, R. C., 2000. Detection of spatial variability in relative density of fishes: comparison of visual census, angling, and baited underwater video. *Marine Ecology Progress Series,* **198**, 249-260.

APPENDIX 4

RELATING HABITAT DISTRIBUTION AND BIOLOGICAL ABUNDANCE TO PHYSICAL OCEANOGRAPHIC DYNAMICS IN A HIGH ENERGY, ROCKY SUBTIDAL ENVIRONMENT

Cole, R.G., McComb, P.J., & Black, K.P., (in prep.). Relating habitat distribution and biological abundance to physical oceanographic dynamics in a high energy, rocky subtidal environment. Prepared for submission to Liminology and Oceanography.

ABSTRACT

Biologically-defined habitats were intensively surveyed using a drop video system over a 3.15 km^2 nearshore area on the wave-swept, rocky coast at New Plymouth, New Zealand. Four habitats were identified and mapped between 1.5 and 16 m depth; sand, coralline pavement, *Ecklonia radiata* forest and mixed-algal stands. The habitat map was used to randomly select habitat-stratified sites lying on reef for quantitative survey by SCUBA divers. Abundances of mobile invertebrates on the reef were low, and seaweed stands of moderate density were found almost exclusively in shallow water (<8 m depth) on the axis of the reef. Habitat distributions were compared with oceanographic data, including substratum characteristics, currents, suspended sediment concentrations, subsurface light penetration, and wave patterns derived from a high-resolution wave refraction model.

Seaweed stands occurred almost exclusively in areas with high wave energy, although the seaweed species present occur in relatively sheltered conditions elsewhere in New Zealand. Physical variables alone explained almost one-third of the variation in the occurrence of habitats, and when combined with spatial information, more than half of the variability in habitats was accounted for. The data suggest that the characteristic depth distribution of seaweeds is imposed by the highly-turbid water, as well as occasional deposition of silty fluvial sediments and the wave-orbital and mean current regimes. Seaweed stands at New Plymouth are tolerant of high suspended sand flux rates, but may require strong wave action to persist.

A4.1 Introduction

The role of physical processes in determining the distributions of temperate seaweeds is becoming increasingly well-documented (e.g. Denny, 1995; reviews of Koehl, 1999; Hurd, 2000). Although descriptions of the distributions of organisms along gradients of depth (e.g. Choat & Schiel, 1982) and wave exposure (e.g. Graham *et al.*, 1997), are common, oceanographic data from nearshore rocky reefs are rare. That paucity of data may reflect difficulties with oceanographic instrumentation in environments where damage or loss of expensive equipment is likely (Denny, 1995). The complexity of nearshore flows is such that obtaining measurements would require hundreds of

instruments, and modelling approaches are frequently adopted. Several previous studies have integrated numerical models of oceanographic processes with biological information in order to understand or predict dispersal of passive particles such as eggs or larvae (e.g. Black & Moran, 1991; Jenkins *et al.*, 1999). However, combining the use of high-resolution biological data with physical oceanographic data (including numerical model outputs) to understand benthic ecology is uncommon (see Kawamata, 2001; Stevens *et al.*, 2001), despite a recently expanded appreciation of the physics of wave action as applied to organisms in the shallow subtidal (e.g. Koehl & Alberte, 1988; Denny *et al.*, 1997).

Denny (1993) argued that the maxima of wave action are important in determining the survival of organisms in wave-swept environments (see also Gaines & Denny, 1993). While those arguments focus on wave action being an agent of mortality, wave action is known to have other consequences for organisms on reefs (review for seaweeds in Hurd, 2000). For example, waves may agitate seaweeds and thus repel grazers (Vasquez & McPeak, 1998), alter the light environment (Wing & Patterson, 1993), provide food (Paine & Vadas, 1969; Harrold & Reed, 1985), and modify sedimentation patterns (Airoldi, 1998). Since most of those agents just listed may directly modify the survivorship of the organism, wave action clearly may have important roles other than simply removing organisms from reefs. Information regarding the spatial and temporal dynamics of wave action in nearshore environments is thus important to ecologists, and under-described.

Seaweeds are biologically important components of temperate reef systems (Schiel & Foster, 1986), providing food for invertebrates and vertebrates, both while they are attached to the seabed (e.g. Choat & Clements, 1992) and as drifting detritus (e.g. Harrold & Reed, 1985). Further, small mobile invertebrates that contribute much of the secondary productivity on reefs shelter on seaweeds (e.g. Edgar & Moore, 1986; Taylor, 1998), and the fronds may also modify the distribution of fishes, by acting as habitat for recruits and for adults (e.g. Jones, 1984; Syms & Jones, 1999). The presence or absence of a seaweed stand may not only alter the abundances of other organisms, but may also modify wave action itself (Eckman *et al.*, 1989; Elwany *et al.*, 1995), and have impacts that extend to terrestrial environments (e.g. Duggins *et al.*, 1989; Bradley & Bradley,

1993). Hence understanding controls on the distribution and abundance of seaweeds has been a focus of subtidal ecological research.

Most investigations of wave forces on seaweeds have been done in the intertidal regions (e.g. Gaylord *et al.*, 1994; Blanchette, 1997; Gaylord & Denny, 1997; Denny *et al.*, 1997; Utter & Denny, 1996). The majority of studies that consider the influence of wave action on seaweeds have focussed on individual thalli and the levels of stresses on tissues (Gaylord *et al.*, 1994; Johnson & Koehl, 1994; Friedland & Denny, 1995; Utter & Denny, 1996). Kawamata (2001) examined differences in holdfast attachment strength between sheltered and exposed sites for subtidal *Laminaria japonica*, but provided little other information regarding the physical environment. We are aware of no studies that have examined the distribution of seaweed stands in relation to physical oceanography in the shallow subtidal, which may in part relate to the relatively sparse literature describing spatial patterns of waves and currents on and around rocky reefs.

Although there have been numerous qualitative descriptions of wave exposure gradients (e.g. Ballantine, 1961), some cartographic methodologies for assessing overall wave climate (e.g. Keddy, 1984), and some simple instrumentation to compare relative magnitudes of maximal wave action (Denny, 1983; Bell & Denny, 1994), none of those approaches is altogether satisfactory. The formulation of wave exposure scales is tautological and non-predictive, wave climate varies with bathymetry as well as wind fetch, and whereas extremes of wave action may cause mortality of organisms, other biological processes may be influenced by the more pervasive average conditions (arguments above). Numerical simulation is an effective method to resolve spatial distribution of wave energy, provided suitable field measurements are available for model calibration and validation (Lakhan, 1989). This is particularly true over irregular bathymetry or heterogeneous substrates, although it is noteworthy that very few applications of wave transformation models over topographically complex rocky reefs have been published (but see McComb *et al.*, 1997).

Here, we consider the relationship between the physical oceanography of a rocky, temperate reef system and the distribution of benthic habitat types, including seaweeds, over that reef. Reef structures are physically heterogeneous, which presents challenges in resolving the spatial patterns of both the oceanographic and biological parameters. To

address this variability, we adopted a high-resolution approach; supplementing eulerian measurements of the waves, currents and suspended sediments with numerical wave refraction modeling and dropped-video mapping of habitats. Through direct comparison, and statistical analysis, this paper illustrates the strong link between habitat and physical oceanographic processes, and presents a comprehensive physical and ecological description of this predominantly rocky, but sediment-influenced, high-energy environment.

A4.2 Background

New Plymouth, Taranaki lies in the western central North Island, New Zealand (39°02.5'S 174°04'E; Fig. A4.1). Taranaki is largely pasture surrounding a 2516 m volcanic cone, and the province is relatively wet and windy. Annual Taranaki rainfall averaged between about 1100 and 2000 mm per year between 1948 and 1998 (NIWA Climate Archives) and monthly averages of the mean daily windrun at New Plymouth varied between 380 and 516 km between 1992 and 1998. Winds from the westerly quarter (i.e. onshore-directed) predominate, and the area has an exposed aspect; open to swells generated in the Tasman Sea, as well as those from the Southern Ocean (McComb *et al.*, 2001).

The present study considers a reef system on the New Plymouth coast, at a site approximately 1 km east of Port Taranaki (Fig. A4.1). Subtidal habitats and ecology in this region (and that of Taranaki in general) have been relatively little-described (Willan, 1980; Cole *et al.*, 1999), due, in no small part, to a high-energy wave climate and frequently turbid waters—conditions that hinder *in situ* observations. The subtidal environment off New Plymouth is predominantly rocky, featuring a heterogeneous assemblage of pyroclastic materials, both cemented within a lahar matrix and as loose boulders and cobbles. The relatively small areas of sandy bed within this nearshore environment are persistent in space and time, suggesting the sedimentary environment is in a dynamic equilibrium (McComb *et al.*, 1999). The complex bathymetry, with approximately shore-normal reef/channel structures, gives rise to strong wave-height gradients (McComb *et al.*, 1997). Wave conditions can vary from short storm-swell (1-5 m high and 4-8 s period), to long ground swell generated in the Southern Oceans, with inshore heights of 6-7 m and spectral peak periods of up 16-18 s. Tides at New

Plymouth are mixed semi-diurnal, with a spring range of 3.1 m and a neap range of 1.7 m.

Port Taranaki is an artificial harbour, and its breakwaters and channel interrupt the alongshore littoral sediment flux. This necessitates a regular maintenance dredging and offshore dumping programme and causes "downstream" (northward-flowing) coastal erosional effects. A large-scale experimental field programme has been conducted at New Plymouth (McComb *et al.*, 1999), investigating the coastal and sediment dynamics in order to evaluate options to mitigate this effect. Black & McComb (2000) report on those findings, having identified a nearshore dumpsite (in 6-15 m depth adjacent to the port) that retains the harbour-dredged sediments within the nearshore littoral zone and feeds the city beaches. The present work derives from biological studies that were required to assess the likely environmental effects of sand dumping in this area, locally known as Kawaroa Reef (Fig. A4.1).

Previous subtidal ecological studies at New Plymouth (Cole *et al.*, 1999) suggested that coralline pavements and seaweed stands would be the dominant habitats, with some large mobile invertebrates (e.g. sea urchins and gastropods) and sessile invertebrates (e.g. sponges) being common. Nationally, those organisms are characteristic of a range of habitats, with seaweeds generally being most abundant in the shallow subtidal and sponges being most often found in deeper areas (e.g. Ayling *et al.*, 1981). Willan (1980) described two seaweed species as dominating; the fucalean *Carpophyllum maschalocarpum* in the shallow regions (0-5 m depth), and the laminarian *Ecklonia radiata* (5-20 m depth). Given the complex environment at New Plymouth, an accurate representation of the benthic habitats across the region was necessary to stratify sites for subsequent quantitative sampling investigating the effects of sand placement on the biota.

A habitat mapping study of the Kawaroa Reef system (Fig. A4.1) found that seaweed stands were localised and occurred mainly in shallow water on the raised shore-normal reef platform (Cole *et al.*, 2000). The limitation of seaweed stands within these zones was surprising, as we had anticipated that severe wave action might prevent seaweeds from inhabiting these shallow parts of the reef. Indeed, we predicted that seaweeds would be more prolific in the channels and slight seabed depressions adjacent to the

raised reef, finding refuge from wave action in the slightly deeper water. Given public concern that seaweed beds should not be damaged by sand dumping, we sought to investigate possible controls on this characteristic distribution, through a comparison of the ecological attributes with the physical oceanography of the reef (e.g. waves, currents, bathymetry, seabed type, suspended sediments, and light penetration of the seawater). A calibrated high-resolution numerical wave refraction model was employed to predict the near-bed wave orbital regime at sampled sites throughout the reef system.

A4.3 Methods

A subtidal region of 3.15 km^2 was defined for study (Fig. A4.2), ranging in depth from 1.54 to 16.15 m (below lowest astronomical tide). The extent of the study region was established through interpretation of numerical model studies of sediment transport (described in Black & McComb, 2000), with an inshore limit consonant with the boundaries of prior side-scan sonar surveys. The study region is approximately centered about the New Plymouth City foreshore. High-resolution bathymetric data were available for this coast, with hydrographic survey lines undertaken at spacings between 10 and 25 m. Side-scan sonar data had been digitised to provide a sedimentary facies map, with the substratum classified as either sandy or rocky bed, and numerous SCUBA observations of the seabed provided verification of substratum represented in the sonographs.

A4.3.1 Benthic Ecology

The distribution of habitats at 217 sites within the 3.15 km^2 study area was mapped with a dropped-video by Cole *et al.* (2000) (http://www.aims.gov.au/pages/research/video-sensing/papers/cole/dc/DC-START.htm). Three habitat types occurred on reefs (coralline pavement, *Ecklonia* kelp forest, mixed algal stands). Those habitats correspond—in kind but not distribution pattern—to the coralline flats, kelp forest, and shallow broken rock habitats respectively of Choat & Schiel (1982). The habitat map was used to allocate sites for quantitative sampling by SCUBA, with nine sites allocated to areas of coralline pavement, and two each to kelp forest and mixed algal stands on the basis of areal coverage (Fig. A4.3). The coralline pavement sites were allocated

throughout the depth range. Five 1-m^2 quadrats were sampled at each site, with distances between consecutive samples being determined by random number tables.

For each of the 167 sites that had reefs, the video footage was viewed and a haphazard videoframe chosen, and freeze-framed. On that frame the percent cover of brown seaweed covering 80 systematic points was assessed, and converted to numeric percentage for analysis.

A4.3.2 Oceanographic data

Oceanographic data (including waves, currents, suspended sediment concentrations, sub-surface light levels) were available from 26 sites along the New Plymouth coast, derived from the two intensive field studies described by McComb *et al.* (1997, 1999). Of those sites, 13 are within, or adjacent to, the region described here (Fig. A4.2). Time-averaged suspended sediment concentrations were measured using bottom-mounted sediment traps positioned at 0.5, 1.0 and 1.5 m above bed level (McComb & Black, submitted). Sub-surface light levels were measured at a single location (site L2, Fig. A4.2) with meters attached at 1, 4 and 9 m below surface, as well as a surface reference meter placed on a wave-measuring tower nearby (site WT, Fig. A4.2). Light data were collected over a 55-day period (March/April, 1998), and were converted to a percentage transmission (T_x) after normalisation to the surface reference meter. We assumed that turbidity measurements from site L2 are representative of the study region, used curvilinear regression to describe the light-depth relationship, and then predicted seabed light on the basis of depth below low tide.

A4.3.3 Numerical wave modeling

The WBEND wave transformation model (Black & Rosenberg, 1992) was used to resolve the spatial distribution of wave energy over the study region. WBEND is a 2-dimensional numerical wave refraction model for monochromatic waves or a wave spectrum over variable topography. The model applies a fast, iterative, finite-difference solution of the wave action equations to solve for wave height, wave period, breakpoint location, longshore sediment transport and bottom orbital currents. The model simulates wave transformations (shoaling, refraction and dissipation) and incorporates a range of

options for dissipation, bed friction, breaking and diffusion. WBEND has been previously applied in numerous coastal studies (e.g. Black *et al.*, 1995, 1997, Hutt, 1997). For the New Plymouth coast, the model was calibrated to numerically replicate the wave transformation processes, adjusting the bed friction (for sandy and rocky beds) and eddy viscosity coefficients (to simulate wave diffraction). The reader is directed to McComb (2001) for full model calibration / validation details.

WBEND model simulations were run for the 240 recorded events from a two-month data collection period, covering a wide range of incident wave conditions, including offshore H_s up to 4.5 m. For each non-sandy dropped-video site (i.e. 167 out of 217 sites, Fig. A4.3), near-bed wave-orbital velocities (U) were output from the model, where the third moment of the velocity distribution (as described by Black & Rosenberg, 1991) was used to define U. A range of U statistics were derived to represent each site; the mean (U_{mean}), maximum (U_{max}), average highest tenth ($U_{1/10}$), and the average highest third wave-orbital velocities ($U_{1/3}$).

A4.3.4 Statistical analysis

Partial canonical correspondence analysis (ter Braak 1995) was used to partition the effects of space and physical oceanographic variables (physics) on benthic habitat variables over the study region. By calculating the simple relationships between each of habitat and space and habitat and physics, followed by the partial forms (habitat*space|physics, habitat*physics|space), we were able to assess the variation due to physical variables, space, and spatial physics (e.g. Borcard *et al.* 1992). Habitats (mixed algae, coralline pavement, kelp forest) were coded as three binary variables and used as the target variables. All of the physical variables (water depth, U_{mean}, U_{max}, U_{median}, $U_{1/10}$, $U_{1/3}$) were highly inter-correlated, violating assumptions of multivariate analysis. We therefore ran a principal component analysis beforehand, to obtain orthogonal variables. The first three principal components in the analysis together accounted for more than 99.5% of the variation, and individually accounted for 91%, 4.7%, and 3.5% of the variation. The analysis in CANOCO (ter Braak 1997) used scores from those three principal components at each site for detailed analysis. Space was treated by analysing 3 simple variables x, y, and xy, where x was the easting, y the northing, and xy their product. The final Canoco analysis was then run with the three

habitat variables, three explanatory physical variables, and three selected spatial variables. The calculation of habitat variability among sources (non-spatial physics, spatial physics, simple space, and unexplained) followed Borcard *et al.* (1992:1048).

A4.4 Results

A4.4.1 Benthic Ecology

Approximately 23% of the survey area is sandy although the main reef axis is predominantly rocky. A large contiguous sandy region exists to the west of the reef, and sandy patches to the east occur on the western flank of raised bathymetric features, or in seabed depressions (e.g. Fig. A4.3). Most of the rocky reef was occupied by coralline pavements, with seaweed forests occupying 17% of the surveyed area. The respective proportions of total area, and reef area occupied by each habitat were: coralline pavement 64%, 83%; kelp forest 6%, 7%; and mixed seaweed 7%, 10%.

There are clear trends for total number of individuals and species to be greatest in the vegetated habitats. Numbers of individuals in coralline pavement habitat were about one-sixth those in other habitats: coralline pavements mean number of individuals = 7.2 (sd=9.6), in kelp forest 41.9 (sd=28.8), and in mixed algae 45.4 (sd=23.8). For numbers of species the relevant numbers were: coralline pavement - 1.5 (sd=1.0), kelp forest - 5.4 (sd=2.8), and mixed algae - 5.9 (sd=2.0). The number of species varied greatly between sites in each of the seaweed habitats, though that difference was less pronounced in mixed algal forest. For number of individuals, the variance component among sites was greater in coralline pavements, kelp forest, and mixed algae, whereas for number of species, no consistent pattern emerged; the components were roughly equal in coralline pavement, higher between sites in kelp forest, and higher among replicates in mixed algae.

Mobile invertebrates occurred at low abundances in all habitats. The densities of grazing gastropods and the sea urchin *Evechinus* averaged <1 m^{-2} in the coralline pavement habitat, and of those grazers, only *Evechinus* reached densities >1 m^{-2} in the vegetated habitats (mixed algae: mean=1.0, sd=1.9; kelp forest: mean=1.4, sd=2.3). Although site V128 was classified as kelp forest in the video survey, the fucalean

Carpophyllum maschalocarpum was abundant in quadrats at that site, indicating habitat patchiness at the scale of metres. High abundances of golfball sponges *Tethya* sp. occurred in kelp forest and mixed algae, whereas they were relatively uncommon elsewhere.

The dominant percentage covers were turfing red seaweeds (overall mean cover = 40.7%, sd=31%) and coralline paint (overall mean cover = 36.5%, sd=25%). Those encrusting growth forms showed contrasting patterns with depth; covers of turfing red seaweeds generally increased with depth (Spearman's rank correlation coefficient ρ = 0.72), whereas those of coralline paint decreased (Spearman's rank correlation coefficient ρ = -0.68). Other percent cover variables had weaker relationships with depth: percent sand ρ = -0.23, percent gravel ρ = 0.33, and percent encrusting organisms ρ = -0.34. Mud only occurred in coralline pavement habitat. There was a clear pattern of increasing covers of turfing red seaweeds from mixed algae (mean=14.5, sd=15.9), to kelp forest (mean=30, sd=29), to coralline pavements (mean = 48.9, sd = 30.5), whereas for coralline paints the opposite trend occurred (mixed algae: mean = 60, sd = 23.6; kelp forest: mean = 49.5, sd = 26.8; coralline pavements: mean = 28.4, sd = 20.6). Low abundances of *Ecklonia* recruits occurred in coralline pavement habitat (mean = 1.3, sd = 3.7).

Most species were more abundant in shallower water, including sponges, seaweeds, and starfish. Rank correlations between mean density and depth were strongly negative for *Patiriella regularis* (ρ = -0.76) and moderately negative for *Stichaster australis* (ρ = -0.51), and generally negative for seaweeds; adult *Ecklonia radiata* (ρ = -0.50), juvenile *Ecklonia radiata* (ρ = -0.66), adult *Carpophyllum maschalocarpum* (ρ = -0.70), and juvenile *Carpophyllum maschalocarpum* (ρ = -0.23). Two molluscan grazers had positive relationships of abundance with depth: *Cantharidus purpureus* ρ = 0.57, *Trochus viridis* ρ = 0.36, whereas *Cookia sulcata* ρ = -0.28, and the echinoid *Evechinus chloroticus* ρ = -0.24 had weaker negative relationships of abundance with depth. The habitat types also showed a clear relationship with depth; average depths were 4.6 m for mixed algae, 5.4 m for kelp forest, and 9.8 m for coralline pavements. Stands of seaweeds were confined to sites less than 8 m depth.

A4.4.2 Oceanographic data

The average currents are significantly higher on the main reef axis (4.3 and 5.1 cms^{-1} for sites S3 and S4, respectively), compared with sites in the slightly deeper water on either side (1.5 and 2.7 cms^{-1} for sites S5 and L2, respectively) (Fig. A4.2). The nearshore circulation primarily responds to wave-driven forces, although the shelf currents, wind forcing and bathymetric / topographic steering are influential. Periodically strong flows (>30 cms^{-1}) are observed on the raised reef platform in high wave events. SSCs are dependent on the intensity of wave-orbital motion at the bed and the sediment supply. The main reef axis (where the seaweeds stands are present) is in a high-energy zone for waves, but has lower SSCs due to the supply limitation for entrainment, and the distance from sandy beds (McComb *et al.* 1999). SSCs in the rocky, vegetated areas of the Kawaroa Reef are approximately one third that of the adjacent sandy regions. The sub-surface light data from site L2 (Fig. A4.2) indicate a turbid environment, with mean percentage light transmissions of 26.3%, 7.75% and 2.11% for the depths 1, 4 and 9 m, respectively. A log-linear regression of the mean percentage light transmission and water depth was fitted as;

$$T_x = \exp[(d/3.13283) - 1.1402] \qquad (R^2 = 0.98) \qquad \textbf{(Eqn. A4.1)}$$

where d is the water depth. Thus at depths of 10-11 m, on average only ~1% of the incident surface light intensity is present.

A4.4.3 Near-bed wave orbital velocities

In general, U_{mean} values were highest in the mixed algae (MA) habitat (0.52 ms^{-1}), intermediate in the *Ecklonia* kelp forest (KF) habitat (0.47 ms^{-1}), and lowest in the coralline pavement (CP) habitat (0.34 ms^{-1}). However, those trends primarily relate to water depth, and the MA and KF habitats were not found in depths greater than 8 m (Fig. A4.4). If only sites < 8 m depth are considered, the average depth for CP habitat is 5.78 m and U_{mean} = 0.43 ms^{-1}, still illustrating that the seaweed-dominated areas coincide with higher mean orbital velocity. The greatest U_{mean} values occurred inshore in the central part of the video survey grid (Fig. A4.5). However, intermingled among those algal stands there also occurred sites with coralline pavements. The magnitude of

wave-orbital velocity at the seabed depends on the wave height, wave period and water depth. For non-breaking waves, orbital velocities at the bed increase as the water depth decreases. However, the spatial patterns of wave-height reinforcement (due to refraction) will result in wave-height gradients, and regions of equivalent depth may thus experience different wave heights (and near-bed orbital currents).

The U_{mean} data from coralline (CP) and seaweed (MA and KF) habitats suggest that seaweed habitats experience a slightly more energetic wave climate, although the differences are not large, and we note that all habitat types are represented throughout the U_{mean} range. A summary of the various physical parameters based on habitat type is given in Table A4.1a.

We limited subsequent analysis to 66 sites (40 CP, 10 KF, 16 MA) where depth was less than 8 m. When the descriptors of U were plotted for those sites, U_{mean} and U_{median} clearly increased from CP, to KF, to MA (the reverse of the relationship with actual depth), whereas U_{max} differed little among habitats (Fig. A4.6). Thus U_{max} offered poor discrimination among habitats, whereas the two measures of central tendency, U_{mean} and U_{med}, discriminated among the habitats clearly. A similar trend was evident when residuals from regressions of the three estimators of U on depth were plotted for each habitat (data not shown).

All the U descriptors were strongly negatively correlated with depth, and positively correlated with each other (Table A4.1b). The relationships between light and U was generally weak (all $R^2 < 0.8$), and U_{max} was less well correlated to the other wave variables than U_{mean}, U_{median}, $U_{1/3}$, or $U_{1/10}$.

The plots of percentage algal cover vs physical variables (Fig. 7) indicate a sharp step function in the relationship between percent algal cover and U_{ave}, U_{med}, depth, but not with U_{max}. The step occurred at values of about 0.4 $m.s^{-1}$ for U_{ave}, 0.35 $m.s^{-1}$ for U_{med}, and 8 m depth. Although the step occurred distinctly, a large number of sites in the acceptable ranges had no seaweed cover (Fig. A4.7). The relationship between percentage algal cover and U_{max} was somewhat trapezoid, with a broad plateau of high algal covers between 1.2 and 1.8 $m.s^{-1}$. Again, a number of sites within that range had no seaweed cover.

A4.4.4 Statistical analysis

The canonical correspondence analysis accounted for 24% of the variation, and attributed 14% of the variation in habitat to non-spatial physics, 7% to spatial physics, and almost 3% to space alone (Fig. A4.8). A high proportion of the variation is unexplained. The ordination plot (Fig. A4.8) indicates a strong association between the KF habitat and the first physical principal component, which was a contrast of depth with all measures of wave action. MA habitat also lay close to the vector of wave action, whereas the point for CP habitat lay isolated. Prin2 and Prin3, which explained almost 5% and 3.5% of the variation respectively, were not strongly related to any habitat.

A4.5 Discussion

Vegetated regions of Kawaroa Reef are confined to a relatively small contiguous area where wave energy is very high. Seaweed forests exist >100 m from persistent sand bodies, and the mixed seaweed and kelp forest habitats were also weakly separated by physical variables. These features combine to provide a very different pattern of habitat organisation compared to other New Zealand sites (e.g. Schiel, 1988, 1990). Globally, occurrences of seaweeds in wave extremes often relate to limitations on grazers (e.g. Velimirov & Griffith, 1979), whereas the abundances of invertebrate grazers at New Plymouth are very low, and they are unlikely to control the abundances of large brown seaweeds. The only herbivorous fishes we observed at New Plymouth were marblefish *Aplodactylus arctidens*, which consume mainly red seaweeds (Choat & Clements, 1992), and they were uncommon, both during this survey and during 2 years of diving prior to this survey (P. McComb, *pers. obs.*).

The multivariate analysis accounted for only 24% of the total variation. Given the severe environmental conditions at New Plymouth, and the relatively clear pattern of seaweed distribution in relation to wave orbital motions (e.g. Fig. A4.5), that proportion of variability seems surprisingly small. However, there are several sites inshore with no seaweed and high U_{mean} values (Fig. A4.7). Environmental heterogeneity (e.g. proximity to sand bodies), patchy colonisation and mortality, the influence of freshwater from the Huatoki Stream, and historical effects (e.g. grazing) doubtless contribute some of that

variability. The small total variation explained may also reflect that the first principal component of the physical variables accounted for 91% of the variability, and thus the remaining physical variables are of lesser importance. There are also possible statistical reasons for that effect (http://www.okstate.edu/artsci/botany/ordinate/varpar.html), which we intend to explore further.

Elsewhere in New Zealand, seaweed habitats support higher numbers of benthic individuals and more species than coralline-dominated areas (e.g. Taylor, 1998). Either the physical structure of the seaweed forests modifies near-bed oceanography in ways that are important to larval or adult benthic invertebrates (e.g. Eckman *et al.*, 1989), or their biological attributes (e.g. fragments of drift thalli) afford shelter and food to many organisms. Furthermore, Taylor (1998) has demonstrated that the greatest proportion of secondary productivity on shallow reefs in northeastern New Zealand stems from small mobile invertebrates associated with seaweed fronds. Accordingly, such macroalgal habitats likely have a greater ecological importance (than coralline pavements), and human impacts on such areas should be minimised where possible. Indeed, we note that it may be possible to increase reefal productivity by establishing such stands.

Within our study region, the seaweed-dominated habitats are concentrated on the reef axis in depths of less than 8 m. The statistical analysis suggests that approximately one quarter of the spatial variance in habitat may be explained by the physical parameters tested (i.e. percent light transmitted and near-bed wave-orbital velocity). Ultimately however, the habitat distribution is the summation of the physical (e.g. substratum, waves and currents, sedimentation and light levels) and biological (e.g. grazing, recruitment, loss to wave action) factors, which influence the colonisation / mortality rates of individuals. The likely importance of these various factors on Kawaroa Reef are discussed below.

5.1 Wave action

Wave action is well-known as an agent of seaweed mortality (e.g. Seymour *et al.*, 1989; reviews of Schiel & Foster, 1986; Chapman, 1995), with the oscillating wave-orbital motion causing stipes to break or holdfasts to fail. The calibrated / validated WBEND

model of near-bed wave-orbital velocities provides a good indication of the relative magnitudes of such forces likely to impact on seaweeds in the study region.

Wave-orbital velocities at the bed are strongly dependent on water depth, consistent with linear wave theory. Seaweeds mainly inhabit the shallower sites, where the average velocities are strongest—suggesting that such an environment does not limit their growth and maintenance. Novaczek (1984) and Haggitt & Babcock (unpubl. data) found that individuals in populations of *Ecklonia radiata* in shallow areas at Goat Island turned over (i.e. died and were replaced) much more rapidly than those in deeper water. As noted above, neither *Ecklonia radiata*, nor *Carpophyllum maschalocarpum*, however, are characteristic of the immediate subtidal elsewhere in New Zealand (e.g. Choat & Schiel, 1982; Schiel, 1988).

Gaines & Denny (1993) discuss the importance of extremes in determining the survival of organisms, suggesting that the maxima often determine the survivorship of a species within a given environment. Obviously, maximal wave-orbital velocities are most likely to cause mortality, as well as limit the size of the seaweeds (e.g. Denny *et al.*, 1998). On a reef system such as Kawaroa, nearshore wave heights do not linearly increase with the offshore incident wave height, because the frictional attenuation of wave energy is nonlinear, and energy may be dissipated by prior—full or partial—wave breaking. That trend is apparent in the coincident wave data measure at an offshore site and on the reef axis. (Fig. A4.9). Thus, while the shallower parts of the reef may show higher U_{mean} values, depth-limited wave breaking will effectively reduce the maximum orbital motion in those regions, meaning that the deeper regions of the reef may actually experience greater maximum orbital velocities in large storms.

That distinction between broken and unbroken waves may be important to the relative importance of U_{max} vs U_{median} vs U_{mean} values in discriminating seaweed habitats from coralline pavement. Most discussions of wave action and seaweeds centre on it being an agent of mortality. Off New Plymouth, the distribution patterns indicate that seaweeds are found mainly in areas where wave action is consistently strong, although the extreme events do cause mortality (e.g. Denny *et al.*, 1998), as evidenced by abundant kelp stranded on the shore after storms. In the next sections we consider possible causal agents.

5.2 Substrate and mobile sediments

Both SCUBA diving and dropped-video observations have confirmed the sediment facies map (Fig. 3), and further indicate that interstitial sandy sediments are common in rocky areas. The rocky bed appears suitable for seaweed colonisation throughout the study area, with the cobbles and boulders being well-cemented and showing little evidence of mobility, and coralline seaweeds are ubiquitous in the area.

The SSC and current data indicate that a sediment flux occurs across the vegetated regions, and the multiple side-scan surveys indicate the sediment facies are stable (McComb *et al.*, 1999), thereby suggesting a dynamic equilibrium within that littoral sediment flux. Howse (2000) and McComb *et al.* (1999) discuss the resilience of the rocky reef to sand inundation, even under high SSC loads, considering that the hydraulic roughness of the reefs may preclude sand settlement and thereby maintain the rocky character (see also Curray, 1965; Nelson, 1996). The coexistence of dense algal stands with reasonably high levels of suspended sandy sediments suggests that these plants are tolerant of it.

Periodic inundation of a rocky bed by sand to depths of a few cm is not likely to affect adult seaweeds, but may negatively impact on the germling / gametophyte and juvenile stages. We have observed storm-induced sand influxes that appeared to have killed *Ecklonia radiata* sporophytes up to an estimated 50 cm stipe length on reefs in northeastern New Zealand. The presence of fine sediments (i.e. < 63 μm), rather than sand, may also influence habitat distributions. Indeed, DeVinny & Volse (1978) describe the gametophytes of laminarians as being susceptible to fine sedimentation. The New Plymouth hinterland receives a high rainfall, and the fluvial discharges into the sea often have high loads of suspended silty material. This both increases the turbidity of the water and provides fine sedimentary material that may inundate the seabed.

Fine fluvial sediments have been noted settling on the reef in the study area (P. McComb, *pers. obs.*), consistent with the regional observations of Willan (1980). Our SCUBA diving observations over several years confirm that the substratum off New Plymouth is occasionally overlain with up to 10 cm of silty sediment, usually following

periods of persistent heavy rain. However, such temporary depositions were not observed among the seaweeds on the raised reef platform or in the very shallow subtidal zones, but rather in the regions adjacent (such as sites L2 and S5, Fig. A4.2). We interpret this as due to the more active wave / current regime along the reef axis precluding settlement of the silts. It is likely that juvenile or microscopic seaweeds would be subjected to the most severe effects from this inundation.

The presence of fine, silty material in the water column also contributes to the turbidity of the water. At the 8 m depth contour (i.e. approximately the observed limit of the seaweed habitats in our study), the average light level is of the order of 1.3% of surface levels (calculated using a mean sea level). The effects of suspended fine material on the spectral transmission of incident light was not investigated, but we noted that this may be of importance to small seaweeds. Microscopic seaweeds have been shown to be sensitive to light composition (Deysher & Dean, 1984), and also are much less mobile. Large seaweeds are agitated by waves, which may remove sediment from the surface of the plant, whereas microscopic seaweeds are relatively immobile near the seabed, where sediments may settle on them.

5.3 Recruitment

Laminarians have complex life cycles involving a macroscopic adult kelp, which produces spores that develop into a microscopic gametophyte phase, which then reproduce and give rise to kelp sporelings. Fucaleans have a simpler life history, in which fertilisation occurs on the adult, and microscopic germlings fall to the substratum, attach, and grow. Dispersal distances of the microscopic stages of both groups are thought to be small (4-8 m – e.g. Schiel, 1988). As there are few offshore forests, but also few echinoid and gastropodan grazers, longshore dispersal of detached kelp sporophytes and large fucaleans bearing spores may be important in establishing kelp forests at New Plymouth. It is noteworthy that *Ecklonia radiata* produces benthic drift, and thus may disperse within the reef environment, whereas fucaleans are more buoyant and often disperse at the surface (e.g. Kingsford, 1992). The fates of detached seaweeds in nearshore regions are not well-known (though readily amenable to experimentation). Seaweeds may seldom occur in deeper water because (a) they do not disperse there, (b) the gametophytes or spores cannot survive there because of occasional sedimentation, or

(c) the gametophytes or spores cannot survive there because of low light levels. We cannot exclude mesograzers as agents of mortality, having no data regarding their abundances at New Plymouth. The presence of coralline pavement in some shallow areas may also relate to freshwater input from the adjacent Huatoki stream.

Further experimentation is required to distinguish among the explanations identified above. Having identified the wave climate over the entire area, we are now in a position to carry out experimental analyses stratified by levels of wave action. We can choose sites that have different levels of wave action, and perturb canopies, attempt to establish canopies, and manipulate light, sediment, and grazers. A proposed sand dumping at the site may allow the underlying sedimentary processes to be tested in more detail.

6 Conclusion

This study analysed a comprehensive database of physical oceanographic parameters to explain a characteristic habitat distribution on a high-energy, rocky reef. The statistical analysis suggested that physical oceanography may account for nearly quarter of the variability of habitat distribution. We note, however, that physical forcing may occur via a biological or a sedimentary mechanism. Manipulative experiments with grazers and sediments have been used elsewhere (e.g. Airoldi *et al.*, 1996; Airoldi, 1998) to address similar questions, and such experiments would be required to disentangle those effects. The subtidal ecology of high energy, temperate environments has only rarely been studied, and the present work is unique in providing coincident high-resolution physical and ecological data.

Carpophyllum maschalocarpum and *Ecklonia radiata* inhabit regions of high wave energy on the axis of a shore-normal reef system at New Plymouth, whereas those species are characteristic of areas outside wave energy maxima elsewhere in New Zealand. We hypothesise that the distribution pattern is linked to the prevailing oceanographic and sedimentary conditions. Specifically we suggest that nearshore turbidity imposes a depth limitation for photosynthesis and the spatial distribution of seaweeds is further influenced by the occasional deposition of fluvial silts. The higher wave / current regime of the reef axis precludes sediment deposition, and thus seaweeds are able to grow in such regions. It remains likely that extreme wave events cause

mortality, and / or limit the size of the plants on the reef. Ecological experimentation will be required to further distinguish the degree to which fluvial sedimentation, light levels and wave-orbital motion act as agents that influence the recruitment and mortality of these temperate seaweeds.

7 Acknowledgements

The authors thank Mr. Bruce Gray of Westgate Transport Ltd. (WTL) for survey vessel operation, Mr. Jason Sait for field assistance, and Mr. Peter Atkinson (WTL), Dr. Ken Grange and Ms. Jenny McLean (NIWA) for project support, and C. Stevens and R. Taylor for comments on the manuscript.

8 References

Airoldi, L., Fabiano, M. & Cinelli, F. 1996 Sediment deposition and movement over a turf assemblage in a shallow rocky coastal area of the Ligurian Sea. *Marine Ecology Progress Series,* **133**, 241-251

Airoldi, L. 1998 Roles of disturbance, sediment stress, and substratum retention on spatial dominance in algal turf. *Ecology,* **79**, 2759-2770

Ayling, A. M., Cumming, A. & Ballantine, W. J. 1981 Map of shore and sub-tidal habitats of the Cape Rodney - Okakari Point Marine Reserve, North Island, New Zealand in 3 sheets, scale 1:2000. New Zealand Department of Lands and Survey, Wellington

Ballantine, W. J. 1961 A biologically-defined exposure scale for the comparative description of rocky shores. *Field Studies,* **1**, 1-19

Bell, E. C., Denny, M. W. 1994. Quantifying "wave exposure': a simple device for recording maximum velocity and results of its use at several field sites. *Journal of Experimental Marine Biology and Ecology,* **181**, 9-29

Black, K. P. & Moran, P. J. 1991 Influence of hydrodynamics on the passive dispersal and initial recruitment of larvae of *Acanthaster planci* (Echinodermata: Asteroidea) on the Great Barrier Reef. *Marine Ecology Progress Series,* **69**, 55-65

Black, K.P. and Rosenburg, M.A. 1992. Semi-empirical treatment of wave transformation outside and inside the breaker line. *Coastal Engineering*, **16**, 313-345.

Black, K., Rosenberg, M., Symonds, G., Simons, R., Pattiaratchi, C. & Nielsen, P. 1995 *Measurements of wave, current and sea level dynamics of an exposed coastal site.* Chapter 2 in "Mixing Processes in estuaries and coastal seas". C. Pattiaratchi (ed.). American Geophysical Union. pp.29-58.

Black, K., Andrews, C., Green, M.O., Gorman, R.M., Healy, T.R., Hume, T.M., Hutt, J., Mead, S., Sayce, A. 1997. Wave dynamics and shoreline response on and around surfing reefs. *1st International Surfing Reef Symposium*, Sydney, March 1997.

Black, K. P. & McComb, P.J. 2000. Port Taranaki maintenance dredging consent renewal studies. Report 2: Site selection and effects. Department of Earth Sciences, University of Waikato. 142 p.

Blanchette, C. A. 1997. Size and survival of intertidal plants in response to wave action: a case study with *Fucus gardneri*. *Ecology,* **78**: 1563-1578

Borcard, D., Legendre, P. & Drapeau, P. 1992 Partialling out the spatial component of ecological variation. *Ecology,* **73**, 1045-1055

Bradley, R. A. & Bradley, D. W. 1993 Wintering shorebirds increase after kelp (*Macrocystis*) recovery. *The Condor,* **95**, 372-376

Chapman, A. R. O. 1995. Functional ecology of fucoid algae: twenty-three years of progress. *Phycologia,* **34**, 1-32

Choat, J. H., Clements, K. D. 1992 Diet in odacid and aplodactylid fishes from Australia and New Zealand. *Australian Journal of Marine and Freshwater Research,* **43**, 1451-1459

Choat, J. H. & Schiel, D. R. 1982 Patterns of distribution and abundance of large brown algae and invertebrate herbivores in subtidal regions of northern New Zealand. *Journal of Experimental Marine Biology and Ecology,* **60**, 129-162.

Cole, R. G., McComb, P. & Sait, J. 1999 Effects of nearshore sand disposal on subtidal and intertidal organisms at New Plymouth, New Zealand. Coasts & Ports '99 Challenges and directions for the new century. *Proceedings of the 14th Australasian Coastal and Ocean Engineering Conference and the 7th Australasian Port and Harbour Conference* **1**, 128-134

Cole, R.; M^{c}Comb, P., & Sait, J. 2000. Use of drop video to map habitats in a high-energy shallow reef environment. Presented at: *Direct sensing of the size and abundance of target and non-target fauna in Australian fisheries*: National Workshop FRDC 2000/187, Rottnest Island, Western Australia, September 2000. See extended abstract at http://www.aims.gov.au/pages/research/video-sensing/report/report_frames.html

Curray, J.R., 1965. Late quaternary history, continental shelves of the United States, p. 723-736, In Wright, H.E. and Frey, D.G. (Eds.), *The Quaternary of the United States*, Princeton University Press, 922 p.

Denny, M. W. 1983 A simple device for recording the maximum force exerted on intertidal organisms. *Limnology and Oceanography,* **28**, 1269-1274

Denny M. W. 1993 Disturbance, natural selection, and the prediction of maximal wave-induced forces. *Contemporary Mathematics*, **141**, 65-90

Denny, M. W. 1995 Predicting physical disturbance: mechanistic approaches to the study of survivorship on wave-swept shores. *Ecological Monographs,* **65**, 371-418

Denny, M.W., Gaylord, B.P., Cowen, E.A. 1997. Flow and flexibility II. The roles of size and shape in determining wave forces on the bull kelp *Nereocystis luetkeana. Journal of Experimental Biology*, 200: 3165-3183

Denny, M.W., Gaylord, B., Helmuth, B., Daniel, T. 1998. The menace of momentum: dynamic forces on flexible organisms. *Limnology and Oceanography.* **43**: 955-968

DeVinny, J. S. & Volse, L. A. 1978 Effects of sediments on the development of *Macrocystis pyrifera* gametophytes. *Marine Biolog,y* **48**, 343-348

Deysher, L. E. & Dean, T. A. 1984 Critical irradiance levels and the interactive effects of quantum irradiance and dose on gametogenesis in the giant kelp, *Macrocystis pyrifera. Journal of Phycology*, **20**, 520-524

Duggins, D. O., Simenstad, C. A., & Estes, J. A. 1989 Magnification of secondary production by kelp detritus in coastal marine ecosystems. *Science,* **245**, 170-173

Eckman, J. E., Duggins, D. O., & Sewell, A. T. 1989 Ecology of understory kelp environments. I. Effects of kelps on flow and particle transport near the bottom. *Journal of Experimental Marine Biology and Ecology,* **129**, 173-187

Edgar, G. J., Moore, P. G. 1986 Macro-algae as habitats for motile macrofauna. *Monografias Biologia,* **4**, 255-277

Elwany, M.H.S., O'Reilly, W.C., Guza, R.T., Flick, R.E. 1995. Effects of southern California kelp beds on waves. *Journal of Waterway Port Coastal & Ocean Engineering,* **121**: 143-150

Gaines, S. D. & Denny, M. W. 1993 The largest, smallest, highest, lowest, longest, and shortest: extremes in ecology. *Ecology,* **74**, 1677-1692

Gaylord, B.; Blanchette, C.A. & Denny, M.W. 1994 Mechanical consequences of size in wave-swept algae. *Ecological Monographs,* **63**, 287-313

Gaylord, B., Denny, M.W. 1997. Flow and flexibility. I. Effects of size, shape and stiffness in determining wave forces on the stipitate kelps *Eisenia arborea* and *Pterygophora californica. Journal of Experimental Biology,*. **200**: 3141-3164

Graham, M. H., Harrold, C., Lisin, S., Light, K., Watanabe, J. M. & Foster, M. S. 1997 Population dynamics of giant kelp *Macrocystis pyrifera* along a wave exposure gradient. *Marine Ecology Progress Series,* **148**, 269-279.

Haggitt, T. R. & Babcock, R.C. submitted ms. Relationship between the stipe-boring lysianassid amphipod *Orchomenella aahu* and dieback in the kelp *Ecklonia radiata.*

Harrold, C. & Reed, D. C. 1985 Food availability, sea urchin grazing, and kelp forest community structure. *Ecology,* **66**, 1160-1169

Howse, B. 2000. Bed roughness of reefs and the relationship of sediment flux to benthic reef ecology. Unpublished M.Sc. thesis, Earth Science Department, University of Waikato, New Zealand. 184 p.

Hurd, C.L. 2000. Water motion, marine macroalgal physiology, and production. *Journal of Phycology,* **36**: 453-472

Hutt, J.A. (1997) Bathymetry and wave parameters defining the surfing quality of 5 adjacent reefs. Unpublished M.Sc. thesis, Earth Sciences Department, University of Waikato, New Zealand. 170 pp.

Jenkins, G. P., Black, K. P. & Keough, M. J. 1999 The role of passive transport and the influence of vertical migration on the pre-settlement distribution of a temperate, demersal fish: numerical model predictions compared with field sampling. *Marine Ecology Progress Series,* **184**, 259-271.

Jones, G. P. 1984 Population ecology of the temperate reef fish *Pseudolabrus celidotus* Bloch & Schneider (Pisces: Labridae). I. Factors influencing recruitment. *Journal of Experimental Marine Biology and Ecology,* **75**:257-276

Kawamata. S. 2001. Adaptive mechanical tolerance and dislodgement velocity of the kelp *Laminaria japonica* in wave-induced water motion. *Marine Ecology Progress Series,*. **211**: 89-104

Keddy, P. A. 1984 Quantifying a within-lake gradient of wave energy in Gillfillan Lake, Nova Scotia. *Canadian Journal of Botany* **62**, 301-309

Kingsford, M. J. 1992. Drift algae and small fish in coastal waters of northeastern New Zealand. *Mar. Ecol. Prog. Ser.* **80**: 41-55

Koehl, M. A. R., Alberte, R. S. 1988. Flow, flapping, and photosynthesis of *Nereocystis luetkeana*: a functional comparison of undulate and flat blade morphologies. *Marine Biology*, **99**:435-444

Koehl, M.A.R. 1999. Ecological biomechanics of benthic organisms: life history, mechanical design and temporal patterns of mechanical stress. *Journal of Experimental Biology,* **202**: 3469-3476

Lakhan, V.C. 1989, Modelling and simulation of the coastal system. In: *Applications in coastal modelling*, Elsevier Oceanography Series, 49.

M^{c}Comb, P.; Black K.; Atkinson, P.; Bell, R. & Healy, T. 1997. High-resolution Wave Transformations on a Coast with Complex Bathymetry. *Proceedings of the 1996 Pacific Coasts and Ports Conference*, Christchurch, NZ, Vol 2: 995-1000.

M^{c}Comb, P.; Black K.; Healy, T. & Atkinson, P. 1999. Coastal and sediment dynamics at Port Taranaki, New Zealand: a large, multi-faceted, field experiment. *Proceedings of Coastal Structures '99 Conference*, Santander, Spain. Vol. 2: 823-832.

M^{c}Comb, P., Gorman, R., Black K. and Kun, A., 2001. Measuring directional wave spectra using the 3D-ACM WAVE on fixed and taut-wire moorings. *Journal of Oceanic Engineering*, **26** (2), 171-180.

McComb, P. J. 2001. Coastal and sediment dynamics in a high-energy, rocky environment. PhD Thesis, Department of Earth Sciences, University of Waikato, New Zealand.

M^{c}Comb, P.J. and Black, K.P., (submitted to *Marine Geology*). Measuring time-averaged suspended sediment concentrations by sediment trap and automated water sampler: a comparative study under wave-dominated flow.

M^{c}Comb, P.J. and Black, K.P., (submitted to *Marine Geology*). Predicting time-averaged suspended sediment and reference concentrations in a high-energy, wave-dominated environment.

Nelson R.C. 1996. Hydraulic roughness of coral reef platforms. *Applied Ocean Research*, **18**: 265-274.

Novaczek, I. 1984 Development and phenology of *Ecklonia radiata* at two depths in Goat Island Bay, New Zealand. *Marine Biology* **81**, 189-197

Paine, R. T. & Vadas, R. L. 1969 The effects of grazing by sea urchins, *Strongylocentrotus* spp., on benthic algal populations. *Limnology &Oceanography* **14**, 710-719

Schiel, D. R. 1988 Algal interactions on shallow subtidal reefs in northern New Zealand: a review. *New Zealand Journal of Marine & Freshwater Research* **22**, 481-489.

Schiel, D. R. 1990 Macroalgal assemblages in New Zealand: structure, interactions and demography. *Hydrobiologia* **192**, 59-76

Schiel, D. R. & Foster, M. S. 1986 The structure of subtidal algal stands in temperate waters. *Oceanography & Marine Biology Annual Review* **24**, 265-307.

Seymour, R. J., Tegner, M. J., Dayton, P. K. & Parnell, P. E. 1989 Storm wave induced mortality of giant kelp, *Macrocystis pyrifera*, in southern California. *Estuarine Coastal and Shelf Science* **28**, 277-292.

Stevens, C. L., Hurd, C.L., & Smith, M.J. 2001. Water motion relative to subtidal kelp fronds. *Limnology & Oceanography* 46: 668-678

Syms, C. & Jones, G. P. 1999 Scale of disturbance and the structure of a temperate fish guild. *Ecology* **80**, 921-940

Taylor, R. B. 1998 Density, biomass and productivity of animals in four subtidal rocky reef habitats: the importance of small mobile invertebrates. *Marine Ecology Progress Series* **172**, 37-51.

ter Braak, C.J.F. 1995. Ordination. Chapter 5 in: Data analysis in community and landscape ecology. Jongman, RGH, ter Braak, CJF, van Tongeren, OFR, eds. Cambridge University Press, Cambridge, UK, pp.91-173

ter Braak, C.J.F. 1997. Program CANOCO Version 4.0. Centre for Biometry Wageningen, CPRO-DLO Box 100, 6700 AC Wageningen, the Netherlands.

Utter, B.D., and Denny, M.W. 1996 Wave-induced forces on the giant kelp *Macrocystis Pyrifera* (Agardh) : Field test of a computer model. *Journal of Experimental Biology* **199**, 2645-2654.

Vasquez, J. A., & McPeak, R. H. 1998 A new tool for kelp restoration. *California Fish & Game* **84**, 149-158

Velimirov, B., Griffiths, C. L. 1979 Wave-induced kelp movement and its importance for community structure. *Botanica Marina* **22**, 169-172

Willan, R. C. 1980. Report on the subtidal marine biological surveys in inshore waters of the Taranaki coast. Maui development environmental study Phase II. Subtidal monitoring study. Report 79-18, University of Auckland.

Wing, S.R. & Patterson, M.R. 1993 Effects of wave-induced lightflecks in the intertidal zone on photosynthesis in the macroalgae *Postelsia palmaeformis* and *Hedophyllum sessile* (Phaeophyceae). *Marine Biology* **116**, 519-525

Table A4.1a Physical data for coralline pavement (CP, n=141), kelp forest (KF, n=10), and mixed algal (MA, n=16) habitats. Values presented are average (standard deviation).

Habitat type	Water depth (m)	Seabed light levels (% transmitted from surface)	Average wave-orbital velocity (ms^{-1})	Maximum wave-orbital velocity (ms^{-1})	Median wave-orbital velocity (ms^{-1})	Top third of wave-orbital velocities (ms^{-1})	Top tenth wave-orbital velocities (ms^{-1})
CP	9.77 (3.27)	1.27 (1.44)	0.34 (0.08)	1.29 (0.28)	0.31 (0.07)	0.55 (0.12)	0.74 (0.15)
KF	5.45 (1.85)	3.58 (2.64)	0.47 (0.09)	1.54 (0.24)	0.43 (0.08)	0.73 (0.14)	0.96 (0.17)
MA	4.64 (1.02)	4.07 (1.32)	0.52 (0.07)	1.60 (0.26)	0.46 (0.06)	0.82 (0.12)	1.07 (0.15)

Table A4.1b Correlation matrix among physical variables generated from model WBEND, based on 167 sites over reef at Kawaroa Reef, New Plymouth. Table entries are Pearson correlation coefficients.

	Depth	Light at seabed	Top 1/3 U	Top 1/10 U	Average U	Maximum U
Light at seabed	-0.86					
Top 1/3 U	-0.83	0.77				
Top 1/10 U	-0.80	0.72	0.99			
Average U	-0.86	0.80	1.00	0.98		
Maximum U	-0.74	0.58	0.86	0.89	0.85	
Median U	-0.85	0.80	0.99	0.96	1.00	0.82

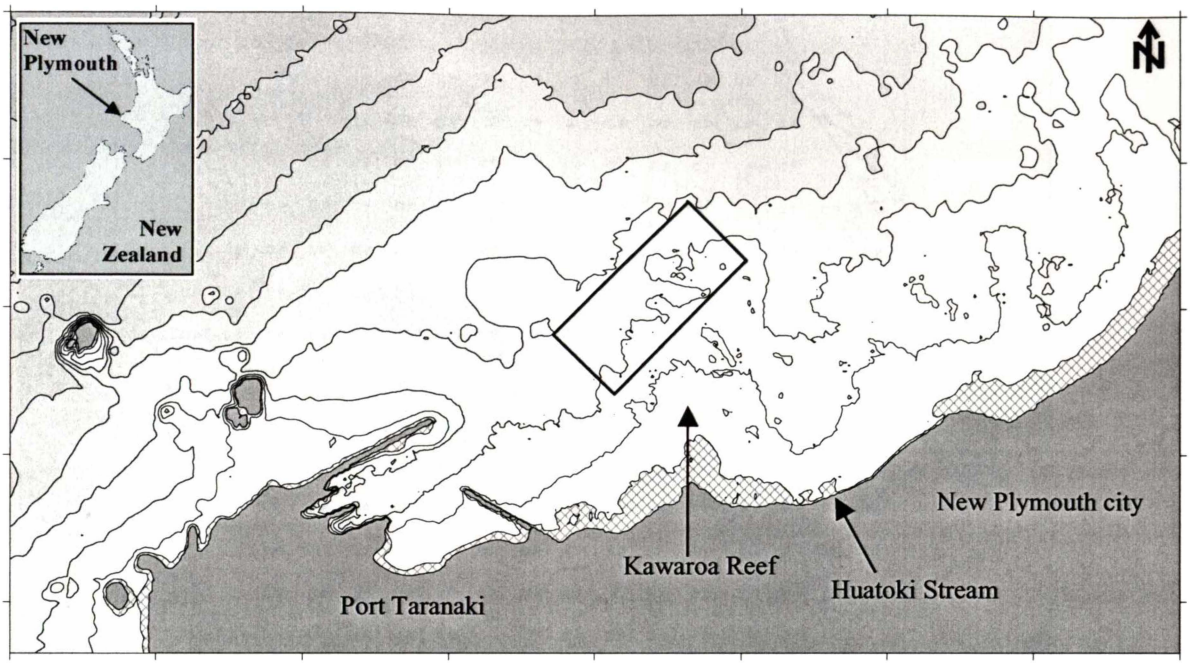

Figure A4.1. Location map of New Plymouth, New Zealand (39°02.5'S 174°04'E) with bathymetry (5 m isobaths). The proposed nearshore sand-dumping site is indicated by the square box, and intertidal regions are crosshatched.

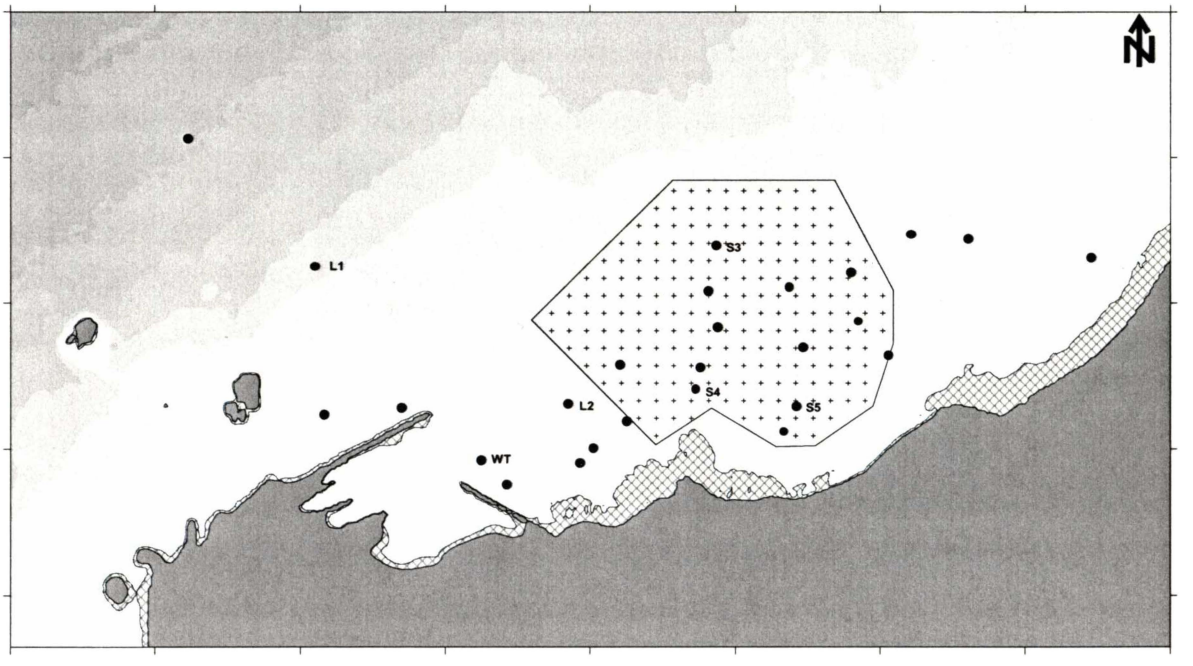

Figure A4.2. Map, showing sites at which oceanographic instruments were deployed (dots), and dropped-video survey sites (crosses).

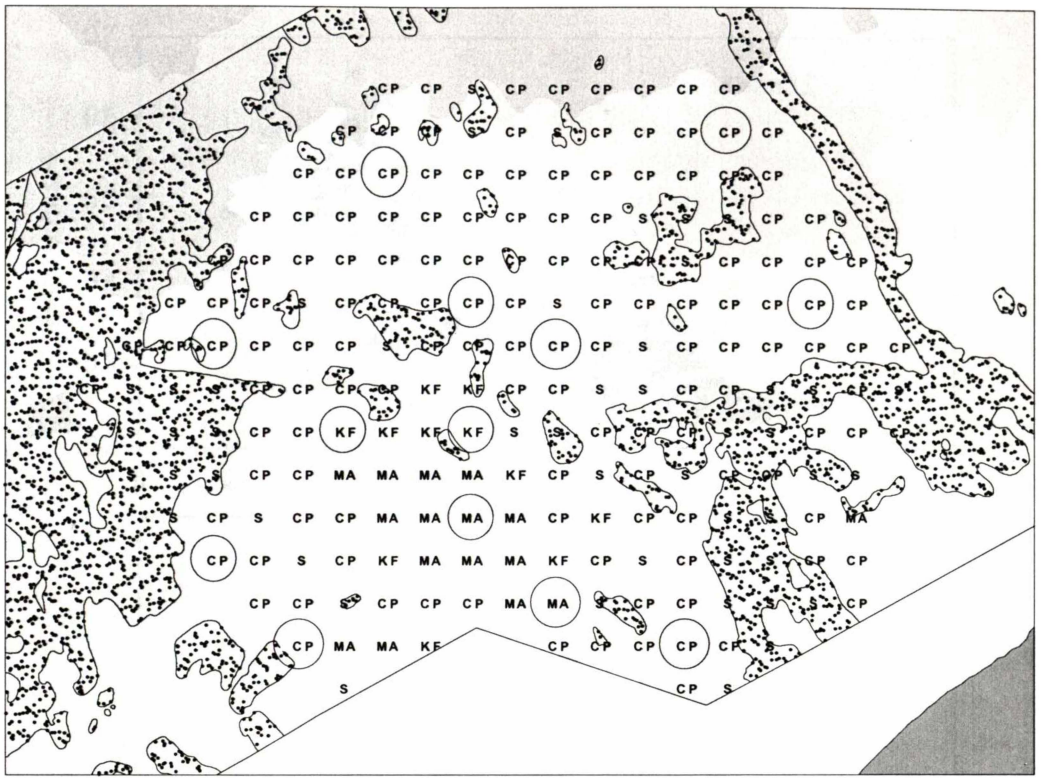

Figure A4.3. Map showing the rock and sand facies from side-scan sonar (sandy areas are shaded) and the habitat codes from the drop video survey of Cole *et al.* (2000). Quantitative survey sites are circled.

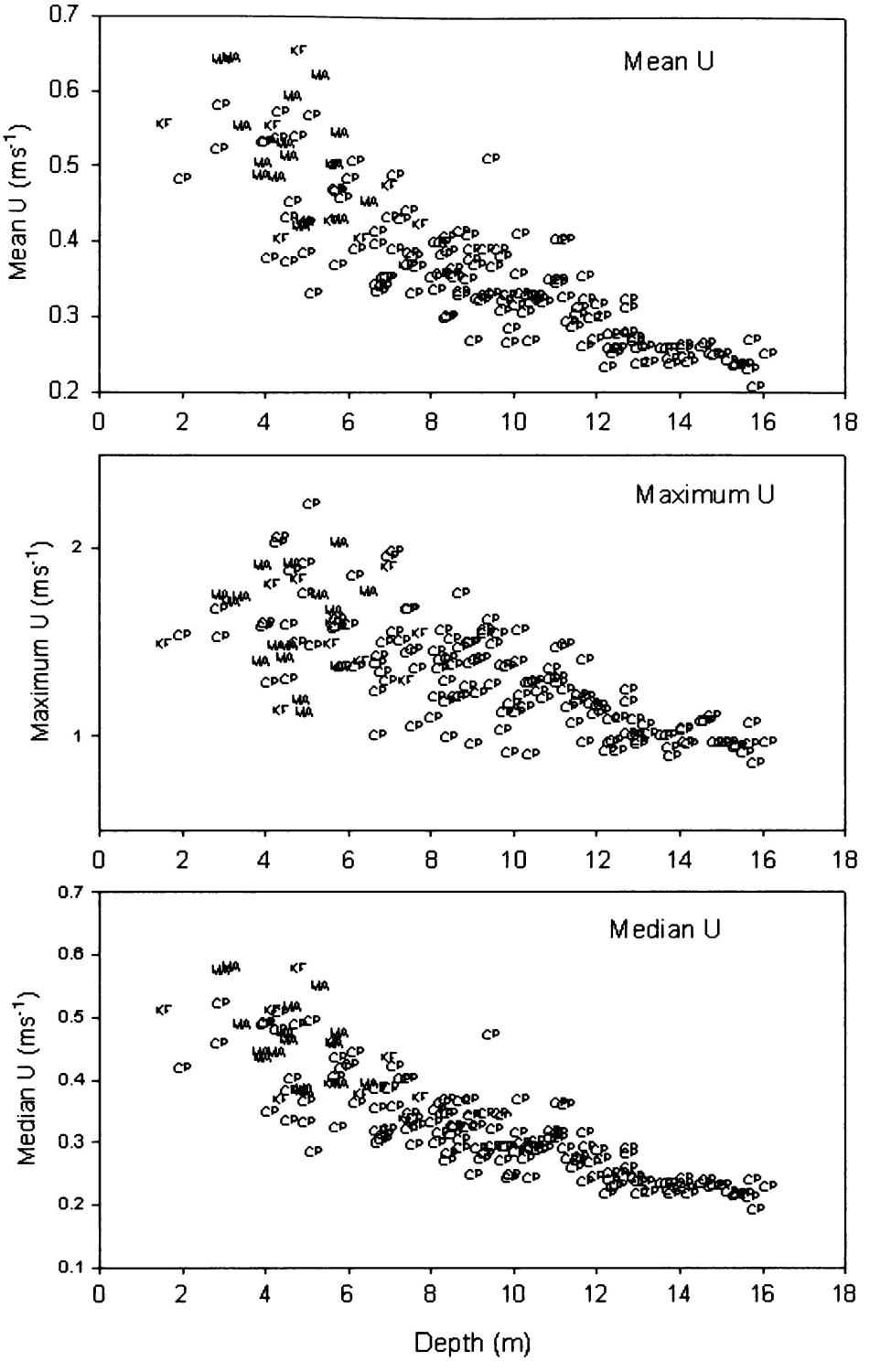

Figure A4.4: Plot of model output for various parameters of *U* vs depth for 167 sites at which reef occurred. Symbols indicate habitat at site: CP = coralline pavement; KF = kelp forest; MA = mixed algae.

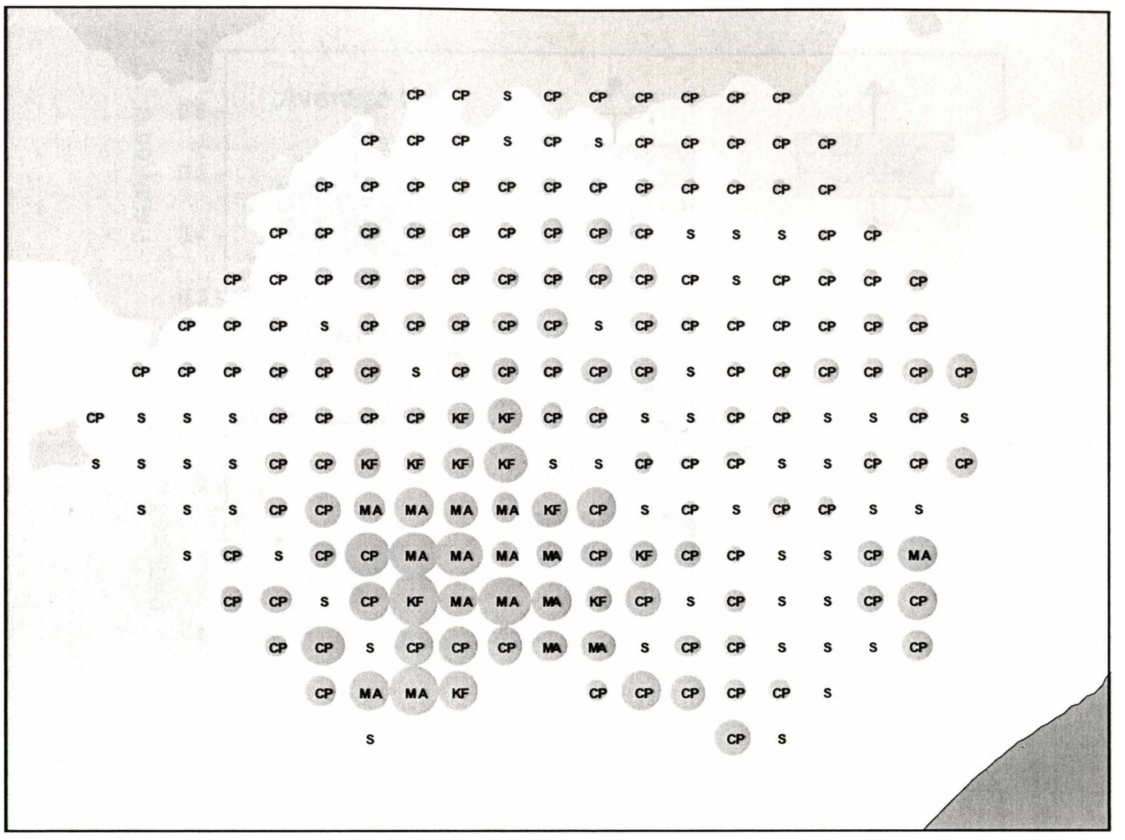

Figure A4.5: Map showing the habitat codes (CP = coralline pavement; KF = kelp forest; MA = mixed algae; S = sand) and relative intensity of wave orbital motion at the seabed for the rocky sites (derived from the WBEND model from a two-month simulation). The symbol size is scaled to U_{mean}.

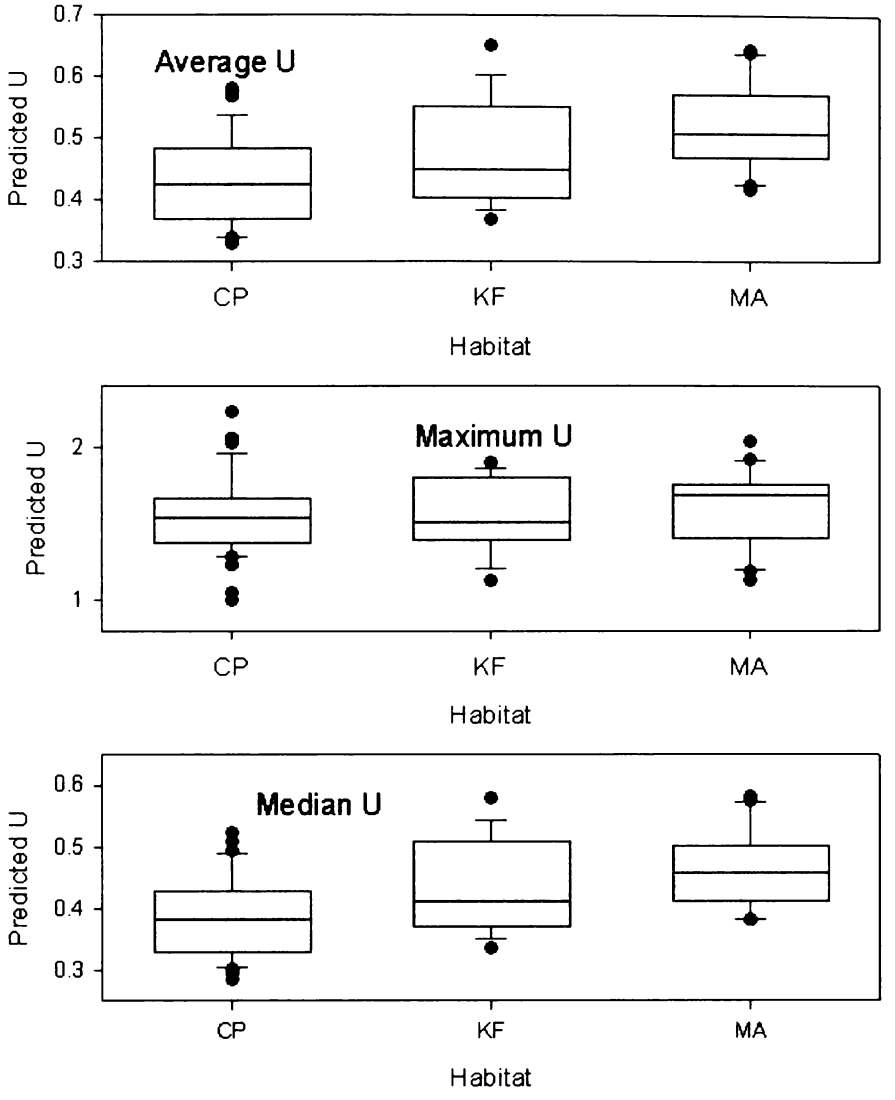

Figure A4.6 Boxplots of mean, median and maximum *U* for each habitat category .

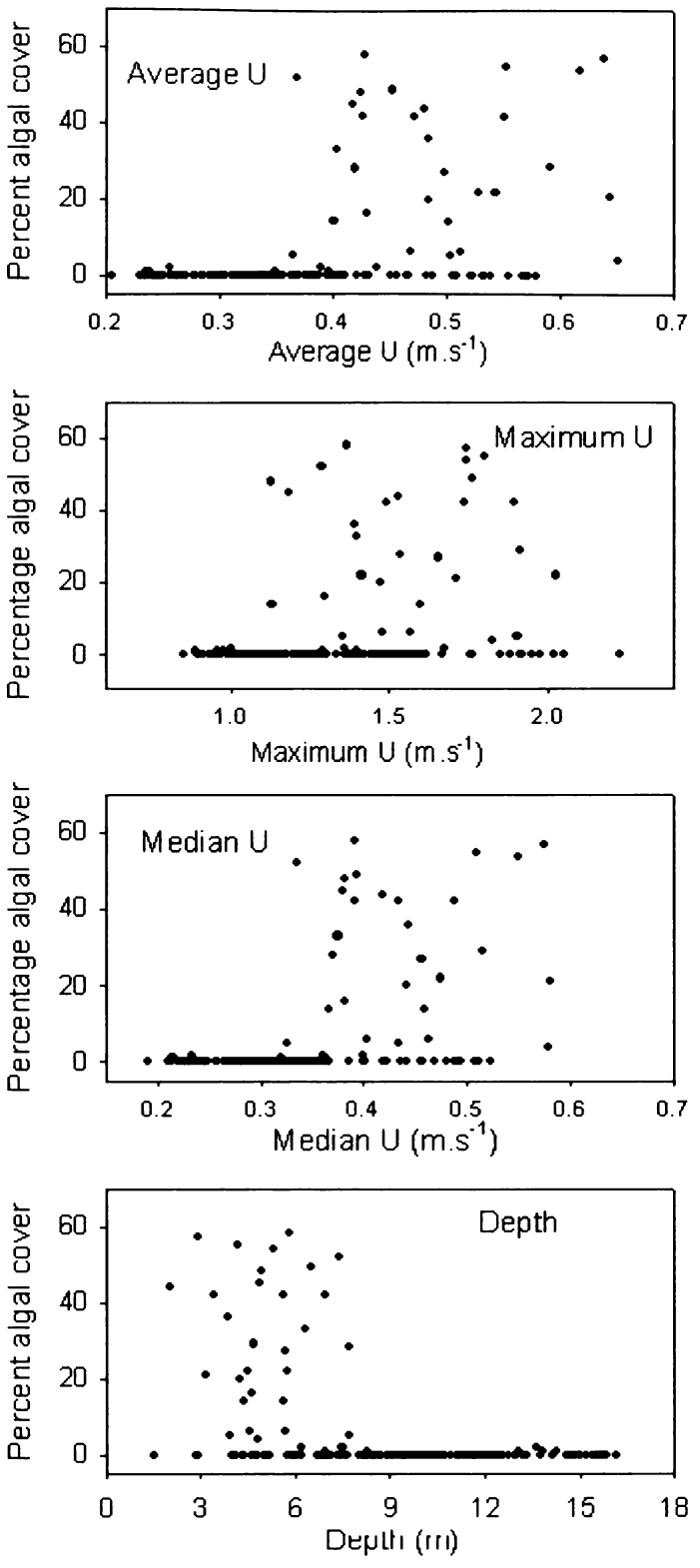

Figure A4.7. Plots of percentage algal cover from video survey vs wave model outputs (U_{mean}, U_{med}, U_{max}), and depth (m) at mean tidal level.

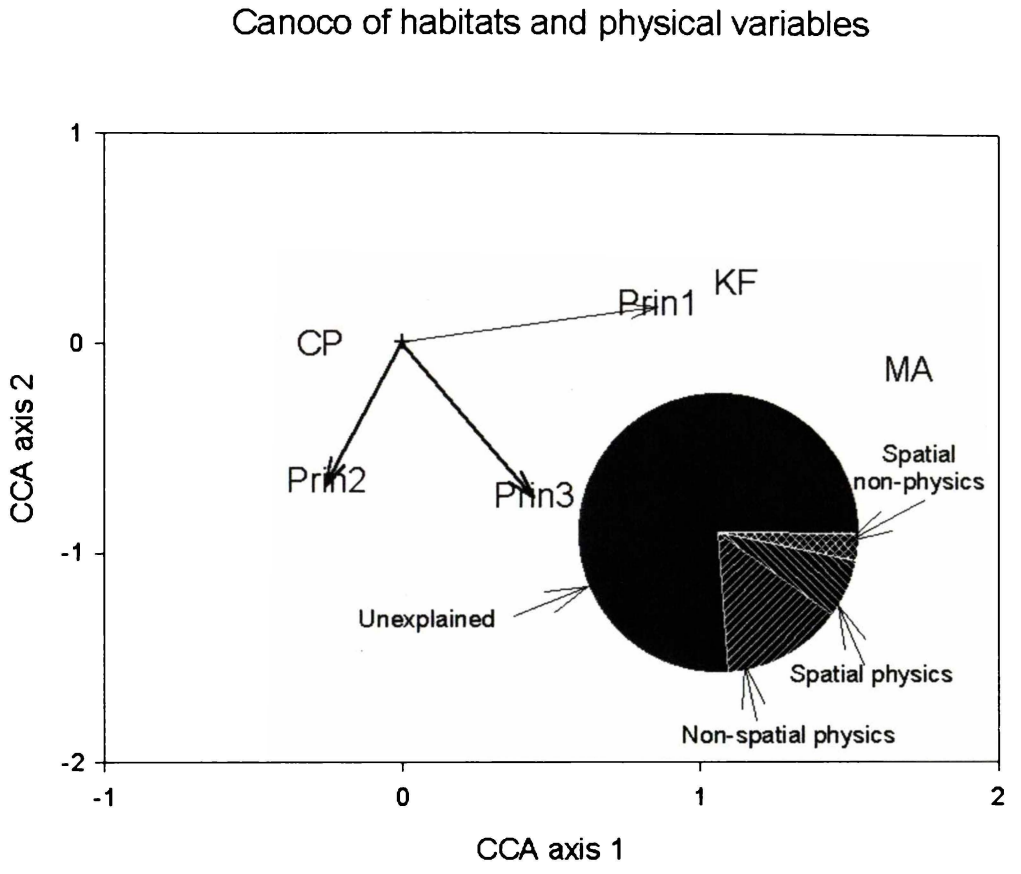

Figure A4.8: Canonical correspondence analysis of biological habitats in relation to physical variables. Habitats are kelp forest (KF); mixed algae (MA), and CP (coralline pavement). Physical variables are the first 3 principal components of the physical dataset. See Results text for details.

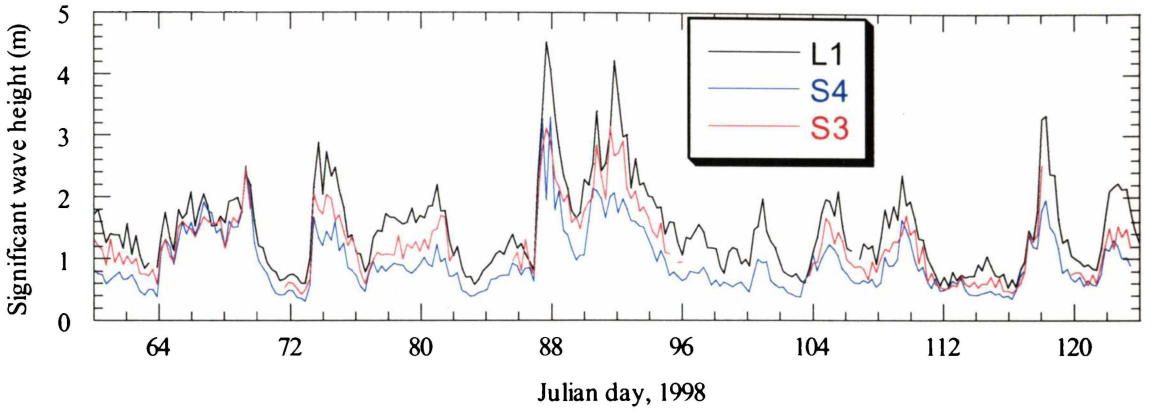

Figure A4.9: Significant wave heights measured at an offshore location (site L1; Fig. A4.2) and on the Kawaroa Reef (S4 and S3; Fig. A4.2) over a 60-day period in 1998.

APPENDIX 5

ADDITIONAL DATA

- Trapped sediments (Tabled data)
- Time-series plots of wave orbital current velocities (U_3) for the sediment trapping periods
- Time-series plots of wave orbital current velocities (U_3) for the sediment trap calibration experiments
- Maps showing tracer movements (Figures 1-43)
- CD with wave, wind, current and tide data from 1996 and 1998 field programmes

SUSPENDED SEDIMENT TRAP DATA

Suspended Sediment Trap Data - Deployment Averaged Values

Deployment Number	1	2	3	4	5
Mean settling velocity 0.5m trap (m/s)	0.027	0.031	0.029	0.025	0.022
Mean settling velocity 1.0m trap (m/s)	0.025	0.028	0.025	0.025	0.021
Mean settling velocity 1.5m trap (m/s)			0.023	0.021	0.020
Mass collected 0.5m trap (kg)	0.468	0.181	0.814	0.211	0.160
Mass collected 1.0m trap (kg)	0.156	0.028	0.191	0.038	0.041
Mass collected 1.5m trap (kg)	0.009	0.005	0.059	0.067	0.024
***Cz(i)* 0.5m trap (kg/m^3)**	0.052	0.022	0.073	0.022	0.022
***Cz(i)* 1.0m trap (kg/m^3)**	0.026	0.009	0.019	0.007	0.006
***Cz(i)* 1.5m trap (kg/m^3)**			0.007	0.001	0.001

Suspended Sediment Trap Data - Site Averaged Values

Site	Depth	Mean settling velocity (m/s)			Mass collected (kg)			Cz(i) (kg/m^3)		
	(m)	0.5m	1.0m	1.5m	0.5m	1.0m	1.5m	0.5m	1.0m	1.5m
L2	9.4	0.020	0.017	0.022	0.1437	0.0310	0.0297	0.0474	0.0121	0.0052
S1	6.2	0.019	0.018	0.020	0.1576	0.0270	0.0276	0.0199	0.0068	0.0085
S2	6.4	0.020	0.023	0.026	0.1837	0.0622	0.0310	0.0291	0.0114	0.0066
S3	8.8	0.027	0.022	0.021	0.0739	0.0235	0.0457	0.0089	0.0034	0.0005
S4	3.8	0.035	0.024	0.024	0.1362	0.0908	0.0536	0.0149	0.0161	0.0008
S5	7.6	0.021	0.021	0.020	0.4179	0.0881	0.0495	0.1041	0.0164	0.0085
D1	5.2	0.019	0.022		0.2702	0.0494		0.0408	0.0258	
D2	5.5	0.033	0.029		0.6033	0.1709		0.0569	0.0138	
D3	9.1	0.019	0.031		0.0216	0.0278		0.0034	0.0113	
D4	13.5	0.020	0.018		0.0458	0.0156		0.0088	0.0035	
D5	9.1	0.028	0.018		0.1738	0.0411		0.0161	0.0108	
D6	4.0	0.039	0.028		0.6921	0.1094		0.0349	0.0105	
T1	12.8	0.021	0.022		0.0538	0.0151		0.0109	0.0036	
T2	9.6	0.035	0.032		0.6604	0.0358	0.0138	0.0465	0.0088	
T3	5.8	0.035	0.029		0.1829	0.0363		0.0118	0.0044	
T4	5.8	0.028	0.023		0.7189	0.2028		0.0730	0.0224	
T5	3.0	0.032	0.035		0.5502	0.2298		0.0384	0.0200	
T6	9.8	0.019	0.021		0.1833	0.0553		0.0195	0.0195	
T8	8.0	0.023			0.6667	0.0059		0.0941		
T9	8.0	0.027	0.023		0.6874	0.0601		0.0752	0.0081	
T11	6.4	0.034	0.024	0.021	0.2762	0.0406	0.0251	0.0200	0.0079	
T12	0.5	0.026			0.8048			0.0981		
T13	8.0	0.025	0.018		0.3979	0.0155		0.0391	0.0072	
WT	8.0	0.020	0.019		0.0280	0.0162			0.0120	

Suspended Sediment Trap Data
Deployment 1: 4/03/98 - 12/03/98 (691200 seconds)

Site	Trap	Mass (kg)	Settling flux (kg/m^2/s)	w mean (m/s)	Cz(i) (kg/m^3)
L2	L2T-L	0.00142	2.90638E-06		
S1	S1T-H	0.03288	6.72970E-05		
	S1T-L	0.04249	8.69663E-05	0.019	0.00986
S2	S2T-H	0.00348	7.12268E-06		
	S2T-M	0.01087	2.22481E-05		
	S2T-L	0.02979	6.09726E-05	0.023	0.00599
S3	S3T-H	0.00083	1.69880E-06		
	S3T-M	0.00232	4.74845E-06		
	S3T-L	0.00830	1.69880E-05		
S4	S4T-H	0.00555	1.13594E-05		
	S4T-M	0.01144	2.34148E-05		
	S4T-L	0.04460	9.12849E-05	0.034	0.00567
S5	S5T-H	0.00298	6.09931E-06		
	S5T-L	0.04460	9.12849E-05		
D1	D1T-M	0.01219	2.49498E-05		
	D1T-L	0.06668	1.36477E-04	0.020	0.01565
D2	D2T-M	0.09049	1.85210E-04	0.023	0.01394
	D2T-L	0.45030	9.21650E-04	0.031	0.07762
D3	D3T-M	0.00218	4.46191E-06		
	D3T-L	0.00524	1.07250E-05		
D4	D4T-L	0.00037	7.57296E-07		
T3	T3T-M	0.00500	1.02337E-05		
	T3T-L	0.11547	2.36338E-04		
T4	T4T-M	0.12784	2.61656E-04	0.021	0.02697
	T4T-L	0.45870	9.38843E-04	0.031	0.08880
T5	T5T-M	0.24830	5.08207E-04	0.032	0.03690
	T5T-L	0.25360	5.19055E-04	0.029	0.03780
T8	T8T-M	0.00590	1.20758E-05		
	T8T-L	0.66670	1.36457E-03	0.023	0.09410
T9	T9T-M	0.00588	1.20349E-05		
	T9T-L	0.03527	7.21888E-05		
T12	T12T-L	1.35246	2.76814E-03	0.030	0.17590
T13	T13T-M	0.00496	1.01519E-05		
	T13T-L	0.02559	5.23762E-05	0.026	0.00523
WT	WTT-M	0.01182	2.41925E-05		
	WTT-L	0.01602	3.27889E-05		

Note: Trap suffix refers to the elevation i.e. L=0.5 m, M=1.0 m and H=1.5 m

Suspended Sediment Trap Data
Deployment 2: 12/03/98 - 24/03/98 (1036800 seconds)

Site	Trap	Mass (kg)	Settling flux (kg/m^3/s)	w mean (m/s)	Cz(i) (kg/m^3)
L2	L2T-L	0.00729	9.947189E-06		
S1	S1T-H	0.00783	1.068402E-05		
	S1T-M	0.01369	1.867997E-05		
	S1T-L	0.07806	1.065127E-04	0.023	0.01080
S2	S2T-H	0.00014	1.910297E-07		
	S2T-M	0.00241	3.288440E-06		
	S2T-L	0.00445	6.072015E-06		
S3	S3T-M	0.00468	6.385850E-06		
	S3T-L	0.03526	4.811219E-05		
S4	S4T-H	0.00777	1.060215E-05		
	S4T-M	0.01202	1.640126E-05		
	S4T-L	0.03920	5.348831E-05		
S5	S5T-M	0.00050	6.822489E-07		
	S5T-L	0.01508	2.057663E-05		
D1	D1T-M	0.02145	2.926848E-05		
	D1T-L	0.07337	1.001132E-04	0.018	0.01063
D2	D2T-M	0.06155	8.398484E-05	0.024	0.00610
	D2T-L	0.38130	5.202830E-04	0.034	0.03337
D3	D3T-M	0.00459	6.263045E-06		
	D3T-L	0.01241	1.693342E-05		
D5	D5T-L	0.05145	7.020341E-05	0.028	0.00479
D6	D6T-M	0.05493	7.495186E-05		
	D6T-L	0.86532	1.180727E-03	0.048	
T1	T1T-M	0.00003	4.093493E-08		
	T1T-L	0.00507	6.918004E-06		
T2	T2T-M	0.00026	3.547694E-07		
T3	T3T-M	0.00731	9.974479E-06		
	T3T-L	0.14841	2.025051E-04	0.041	0.00819
T4	T4T-M	0.07314	9.979937E-05	0.019	0.01011
	T4T-L	0.29880	4.077119E-04	0.027	0.03415
T5	T5T-M	0.18560	2.532508E-04	0.039	0.01420
	T5T-L	0.54949	7.497779E-04	0.033	0.03711
T9	T9T-M	0.04600	6.276690E-05	0.031	0.00575
	T9T-L	0.18613	2.539740E-04	0.026	0.02169
T11	T11T-H	0.00514	7.013519E-06		
	T11T-M	0.01033	1.409526E-05		
	T11T-L	0.12015	1.639444E-04	0.043	0.00775
T12	T12T-L	0.61820	8.435325E-04	0.031	0.05828
T13	T13T-M	0.01040	1.419078E-05		
	T13T-L	0.11842	1.615838E-04	0.022	0.01507
WT	WTT-M	0.00223	3.042830E-06		
	WTT-L	0.00540	7.368288E-06		

Note: Trap suffix refers to the elevation i.e. L=0.5 m, M=1.0 m and H=1.5 m

Suspended Sediment Trap Data
Deployment 3: 24/03/98 - 6/04/98 (1123200 seconds)

Site	Trap	Mass (kg)	Settling flux (kg/m^3/s)	w mean (m/s)	Cz(i) (kg/m^3)
L2	L2T-H	0.03640	4.584713E-05	0.019	0.00524
	L2T-M	0.07371	9.284043E-05	0.017	0.01213
	L2T-L	0.65124	8.202605E-04	0.022	0.08761
S1	S1T-H	0.05525	6.958939E-05	0.018	0.00853
	S1T-M	0.06734	8.481718E-05	0.021	0.01046
	S1T-L	0.49380	6.219591E-04	0.020	0.05537
S2	S2T-H	0.08936	1.125522E-04	0.023	0.01244
	S2T-M	0.17900	2.254570E-04	0.022	0.02304
	S2T-L	0.65262	8.219987E-04	0.019	0.07835
S3	S3T-M	0.05668	7.139052E-05	0.027	0.00544
	S3T-L	0.21107	2.658504E-04	0.030	0.01694
S4	S4T-H	0.05975	7.525730E-05	0.038	0.00042
	S4T-M	0.30900	3.891968E-04	0.030	0.02694
	S4T-L	0.33610	4.233302E-04	0.043	0.02938
S5	S5T-H	0.05592	7.043328E-05	0.019	0.00849
	S5T-M	0.16052	2.021808E-04	0.021	0.02365
	S5T-L	0.43186	5.439434E-04	0.030	0.03921
D1	D1T-M	0.20059	2.526504E-04	0.022	0.02581
	D1T-L	1.10294	1.389193E-03	0.021	0.13002
D2	D2T-M	0.55240	6.957679E-04	0.037	0.03881
	D2T-L	1.77440	2.234921E-03	0.038	0.10639
D3	D3T-M	0.05333	6.717108E-05	0.020	0.01127
	D3T-L	0.11213	1.412318E-04	0.031	
D4	D4T-L	0.07818	9.847056E-05	0.020	0.01146
D5	D5T-M	0.07255	9.137937E-05	0.018	0.01084
	D5T-L	0.51710	6.513063E-04	0.029	0.04798
T1	T1T-M	0.03245	4.087196E-05	0.022	0.00362
	T1T-L	0.12539	1.579333E-04	0.023	0.01592
T2	T2T-M	0.09585	1.207266E-04	0.032	0.00883
	T2T-L	1.20644	1.519555E-03	0.032	0.08753
T3	T3T-M	0.09245	1.164441E-04	0.032	0.00639
	T3T-L	0.42883	5.401270E-04	0.041	0.02289
T4	T4T-M	0.68388	8.613718E-04	0.029	0.06133
	T4T-L	1.89120	2.382035E-03	0.031	0.14369
T5	T5T-M	0.55660	7.010580E-04	0.040	0.03689
	T5T-L	1.51912	1.913387E-03	0.043	0.08168
T6	T6T-M	0.15784	1.988052E-04	0.021	0.01951
	T6T-L	0.46538	5.861631E-04	0.025	0.04795
T9	T9T-M	0.15107	1.902782E-04	0.025	0.01616
	T9T-L	1.68234	2.118968E-03	0.027	0.15308
T11	T11T-H	0.05578	7.025694E-05	0.022	0.00731
	T11T-M	0.09948	1.252987E-04	0.029	0.01011
	T11T-L	0.78742	9.917842E-04	0.040	0.04940
T12	T12T-L	1.58284	1.993645E-03	0.027	0.14685
T13	T13T-M	0.04446	5.599899E-05	0.018	0.00716
	T13T-L	1.08386	1.365161E-03	0.027	0.10533
WT	WTT-M	0.04512	5.683028E-05	0.019	0.00727
	WTT-L	0.08143	1.025641E-04	0.020	0.01197

Note: Trap suffix refers to the elevation i.e. L=0.5 m, M=1.0 m and H=1.5 m

Suspended Sediment Trap Data
Deployment 4: 6/04/98 - 22/04/98 (1382400 seconds)

Site	Trap	Mass (kg)	Settling flux (kg/m^3/s)	w mean (m/s)	Cz(i) (kg/m^3)
L2	L2T-L	0.04344	1.424345E-05	0.024	
S1	S1T-H	0.01044	1.068402E-05		
	S1T-M	0.02451	8.036531E-06	0.020	
	S1T-L	0.11775	1.205022E-04	0.014	0.01366
S2	S2T-M	0.05153	5.273443E-05	0.018	0.00669
	S2T-L	0.08139	8.329236E-05	0.018	0.01038
S3	S3T-H	0.02003	2.049817E-05		
	S3T-M	0.05959	6.098282E-05	0.024	
	S3T-L	0.12265	4.021545E-05	0.026	0.00458
S4	S4T-H	0.04523	1.483037E-05	0.022	0.00121
	S4T-M	0.17460	1.786810E-04	0.030	0.01112
	S4T-L	0.16591	1.697879E-04	0.023	0.01495
S5	S5T-H	0.07512	2.463094E-05	0.021	
	S5T-M	0.10108	1.034426E-04	0.019	0.01348
	S5T-L	0.96464	9.871869E-04	0.018	0.15236
D1	D1T-M	0.00496	5.075932E-06		
	D1T-L	0.04754	4.865117E-05	0.015	0.00702
D2	D2T-M	0.08051	8.239179E-05	0.028	0.00560
	D2T-L	0.14587	1.492795E-04	0.028	0.01027
D3	D3T-M	0.00669	6.846368E-06		
	D3T-L	0.01262	1.291497E-05		
D4	D4T-M	0.01244	1.273076E-05		
	D4T-L	0.04104	4.199924E-05	0.022	0.00412
D5	D5T-M	0.00957	9.793683E-06		
	D5T-L	0.04514	4.619507E-05	0.028	0.00341
D6	D6T-M	0.17290	1.769412E-04	0.033	0.00929
	D6T-L	0.51890	5.310284E-04	0.030	0.03491
T1	T1T-M	0.01433	1.466494E-05		
T2	T2T-H	0.01541	5.052752E-06		
	T2T-M	0.01120	1.146178E-05		
	T2T-L	0.11434	1.170125E-04	0.038	0.00551
T3	T3T-M	0.03922	4.013670E-05	0.028	0.00304
	T3T-L	0.11014	1.127143E-04	0.029	0.00655
T4	T4T-M	0.04825	4.937776E-05	0.022	0.00429
T5	T5T-M	0.07274	7.444018E-05	0.034	0.00404
	T5T-L	0.21545	2.204858E-04	0.033	0.01277
T6	T6T-M	0.00313	3.203159E-06		
	T6T-L	0.05157	5.277536E-05	0.019	0.00540
T9	T9T-M	0.06080	6.222110E-05	0.026	0.00460
	T9T-L	0.91079	9.320782E-04	0.028	0.06290
T11	T11T-H	0.02173	7.125003E-06		
	T11T-M	0.00952	9.742514E-06		
	T11T-L	0.06230	6.375616E-05	0.036	0.00253
T12	T12T-L	0.16614	1.700232E-04	0.022	0.01143
T13	T13T-M	0.00886	9.067088E-06		
	T13T-L	0.36366	3.721599E-04	0.025	0.03070
WT	WTT-M	0.00618	6.324447E-06		
	WTT-L	0.00893	9.138724E-06		

Note: Trap suffix refers to the elevation i.e. L=0.5 m, M=1.0 m and H=1.5 m

Suspended Sediment Trap Data
Deployment 5: 22/04/98 - 4/05/98 (1036800 seconds)

Site	Trap	Mass (kg)	Settling flux (kg/m^3/s)	w mean (m/s)	Cz(i) (kg/m^3)
L2	L2T-H	0.00917	4.00898E-06		
	L2T-M	0.01427	1.94714E-05		
	L2T-L	0.04349	5.93420E-05	0.017	0.00713
S1	S1T-H	0.01750	7.65072E-06	0.023	
	S1T-M	0.01645	2.24460E-05	0.015	0.00306
	S1T-L	0.05570	7.60025E-05	0.017	0.00982
S2	S2T-H	0.03085	1.34871E-05	0.029	0.00075
	S2T-M	0.06739	9.19535E-05	0.029	0.00454
	S2T-L	0.15007	2.04770E-04	0.020	0.02166
S3	S3T-H	0.01355	5.92384E-06	0.016	0.00046
	S3T-M	0.03369	4.59699E-05	0.016	0.00138
	S3T-L	0.05510	7.51838E-05	0.026	0.00519
S4	S4T-H	0.02914	1.27395E-05	0.011	
	S4T-M	0.07632	1.04138E-04	0.021	0.01014
	S4T-L	0.08645	1.17961E-04	0.034	0.00981
S5	S5T-H	0.06399	2.79754E-05		
	S5T-M	0.09030	1.23214E-04	0.022	0.01200
	S5T-L	0.63330	8.64136E-04	0.016	0.12058
D1	D1T-M	0.00804	1.09706E-05		
	D1T-L	0.06042	8.24430E-05		
D2	D2T-M	0.06968	9.50782E-05	0.035	0.00461
	D2T-L	0.26447	3.60869E-04		
D3	D3T-M	0.01332	1.81751E-05		
	D3T-L	0.02438	3.32665E-05	0.017	0.00341
D4	D4T-M	0.01872	2.55434E-05	0.018	0.00348
	D4T-L	0.06353	8.66865E-05	0.017	0.01072
D5	D5T-L	0.08157	1.11302E-04	0.025	0.00833
D6	D6T-M	0.10051	1.37146E-04	0.023	0.01180
T1	T1T-M	0.01340	1.82843E-05		
	T1T-L	0.03105	4.23677E-05	0.018	0.00587
T2	T2T-H	0.01217	1.66059E-05		
T3	T3T-M	0.03761	5.13188E-05	0.027	0.00384
	T3T-L	0.11186	1.52633E-04	0.029	0.00943
T4	T4T-M	0.08070	1.10115E-04	0.023	0.00909
	T4T-L	0.22674	3.09386E-04	0.024	0.02530
T5	T5T-M	0.08563	1.16842E-04	0.030	0.00816
	T5T-L	0.21330	2.91047E-04	0.022	0.02248
T6	T6T-M	0.00500	6.82249E-06		
	T6T-L	0.03304	4.50830E-05	0.012	0.00530
T9	T9T-M	0.03663	4.99816E-05	0.009	0.00584
	T9T-L	0.62235	8.49195E-04	0.027	0.06313
T11	T11T-H	0.01771	7.74253E-06	0.020	0.00099
	T11T-M	0.04290	5.85370E-05	0.019	0.00572
	T11T-L	0.13495	1.84139E-04	0.017	0.02025
T12	T12T-L	0.30424	4.15135E-04	0.019	
T13	T13T-M	0.00881	1.20212E-05		
WT	WTT-M	0.00580	7.91409E-06		
	WTT-L	0.00922	1.25807E-05		

Note: Trap suffix refers to the elevation i.e. L=0.5 m, M=1.0 m and H=1.5 m

Suspended Sediment Trap Data
Offshore Dump Ground (OD) Deployments

Dates	Trap	Trap Elevation (m)	Mass (kg)	Settling flux (kg/m^2)	w mean (m/s)	Cz(i) (kg/m^3
OD1	OD1-H	1.31	0.0523	3.79253E-06	0.00929	0.00061
20-Nov-98 to	OD1-M	0.9	0.1318	9.56393E-06	0.01250	0.00115
16-Dec-98	OD1-L	0.5	2.9800	2.16150E-04	0.02916	0.01403
OD2	OD2-H	1.37	0.0172	1.57583E-06	0.01269	0.00020
16-Dec-98 to	OD2-M	0.78	0.0752	6.87424E-06	0.01734	0.00064
5-Jan-99	OD2-L	0.41	1.5820	1.44513E-04	0.02916	0.00794
OD3	OD3-H	1.34	0.0376	2.27962E-06	0.02200	0.00018
5-Jan-99 to	OD3-M	0.77	0.1400	8.49155E-06	0.02628	0.00057
4-Feb-99	OD3-L	0.49	2.1312	1.29244E-04	0.03235	0.00620
OD4	OD4-H	1.32	0.0387	2.51587E-06	0.01250	0.00030
4-Feb-99 to	OD4-M	0.7	0.1394	9.06111E-06	0.02134	0.00073
4-Mar-99	OD4-L	0.4	0.6264	1.17376E-04	0.02800	0.00730

TIME-SERIES PLOTS OF THE WAVE ORBITAL CURRENTS (U_3) MEASURED OVER THE FIVE SEDIMENT TRAPPING PERIODS

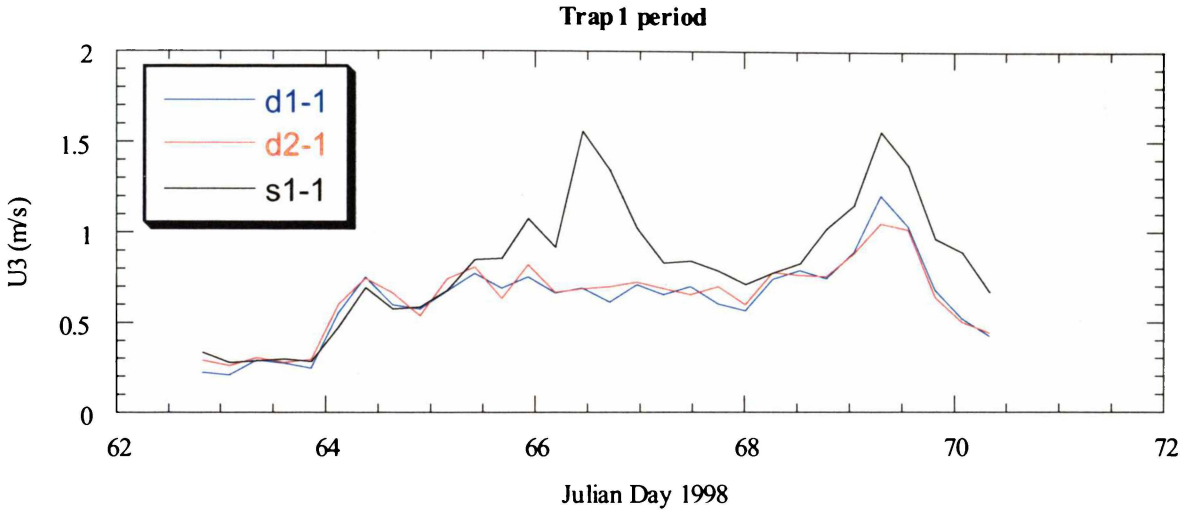

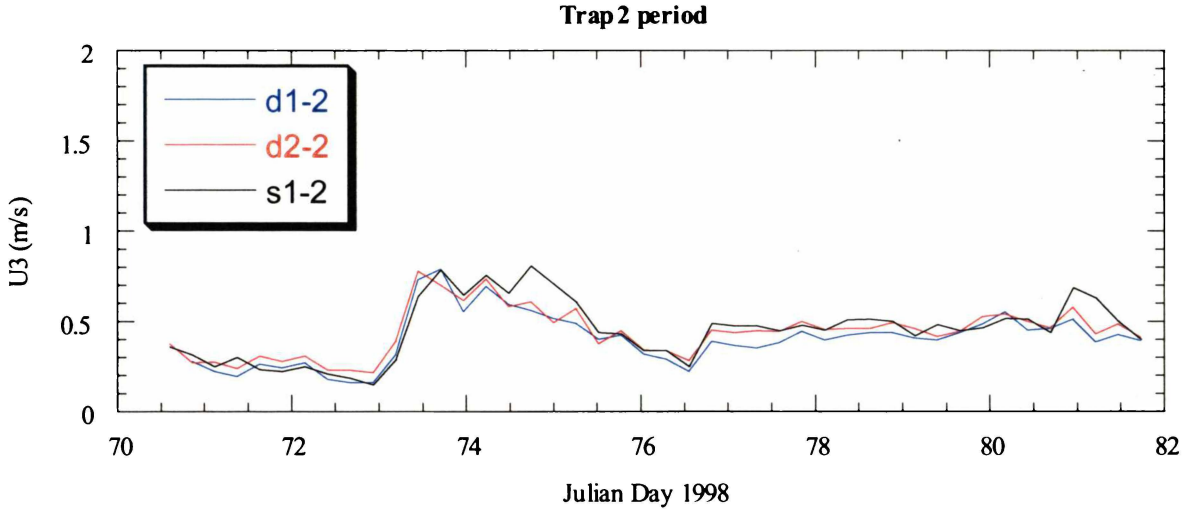

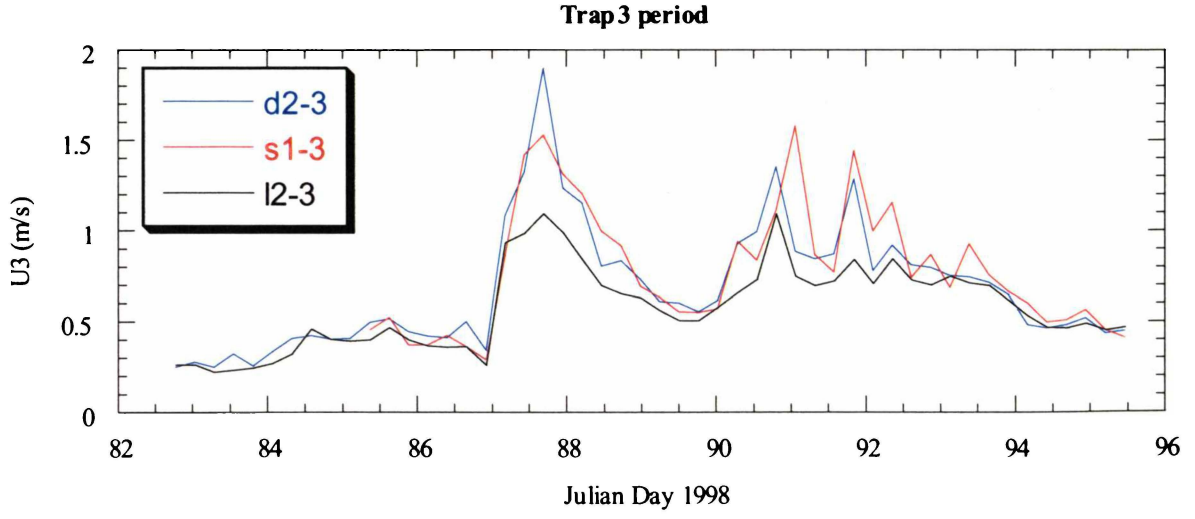

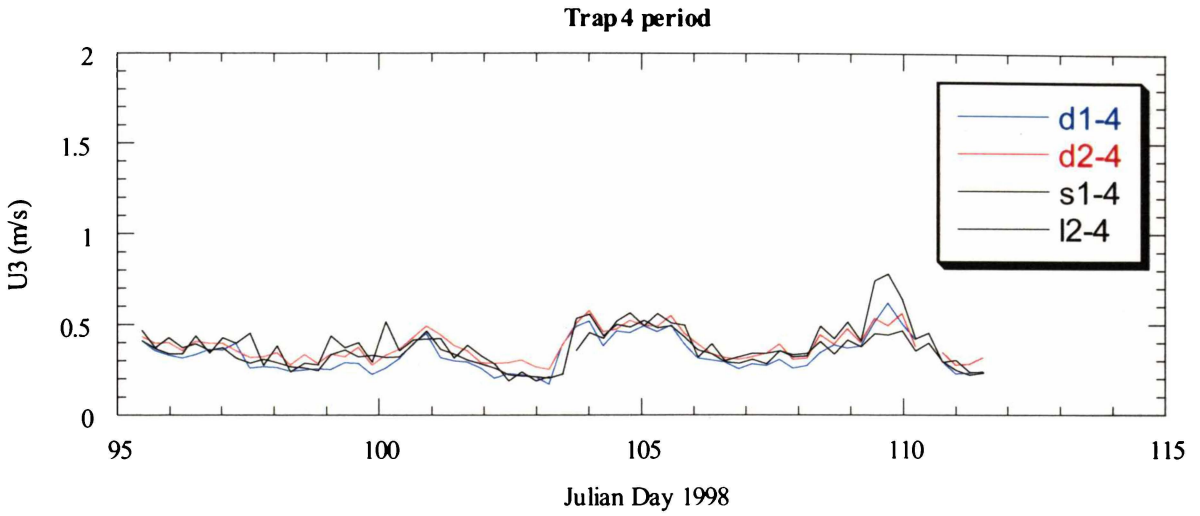
Trap 4 period
U3 (m/s)
2
1.5
1
0.5
0
95
100
105
110
115
Julian Day 1998
d1-4
d2-4
s1-4
l2-4

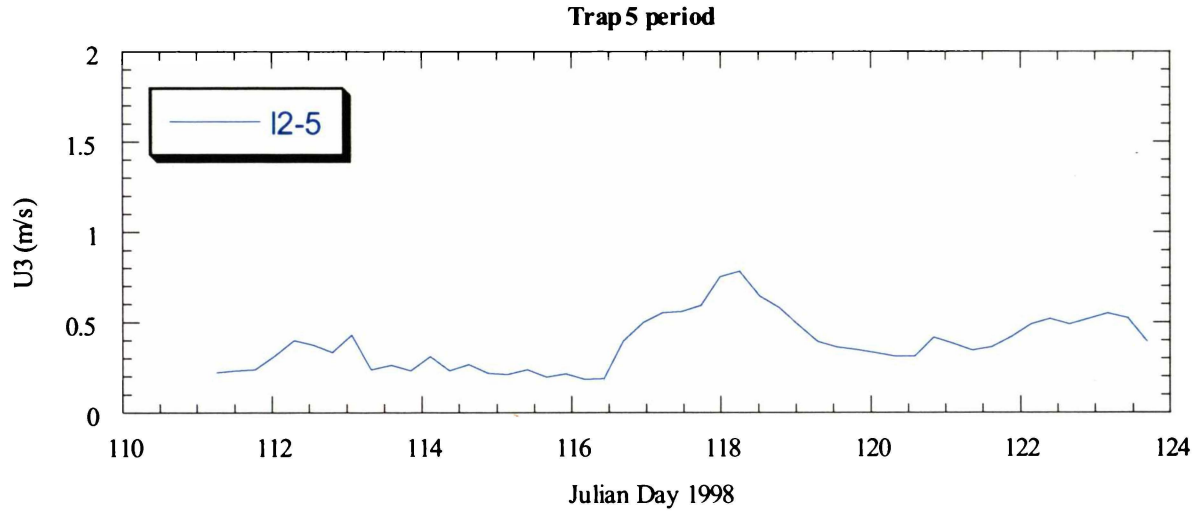
Trap 5 period
U3 (m/s)
2
1.5
1
0.5
0
110
112
114
116
118
120
122
124
Julian Day 1998
l2-5

TIME-SERIES PLOTS OF THE WAVE ORBITAL CURRENTS (U_3) MEASURED OVER THE SIX SEDIMENT TRAP CALIBRATION EXPERIEMNTS. U_3 DATA HAVE BEEN COMPUTED FOR THE TRAP ELEVATION USING LINEAR WAVE THEORY

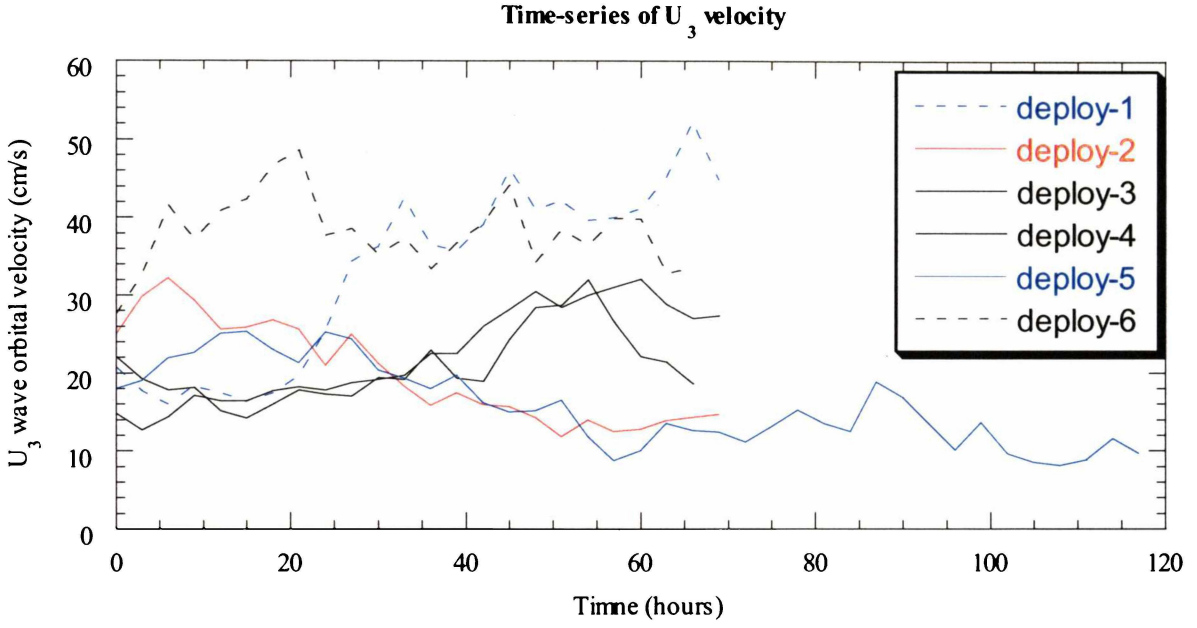

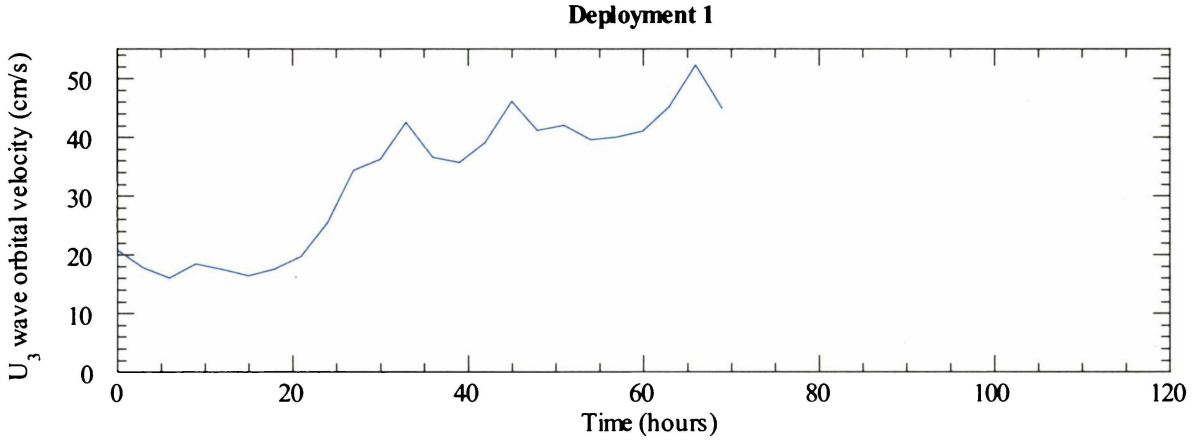

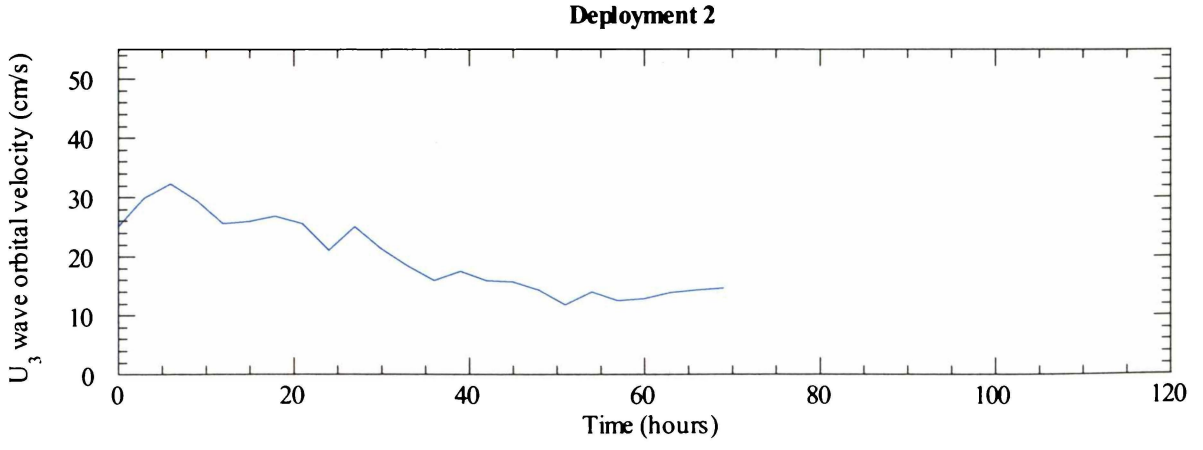

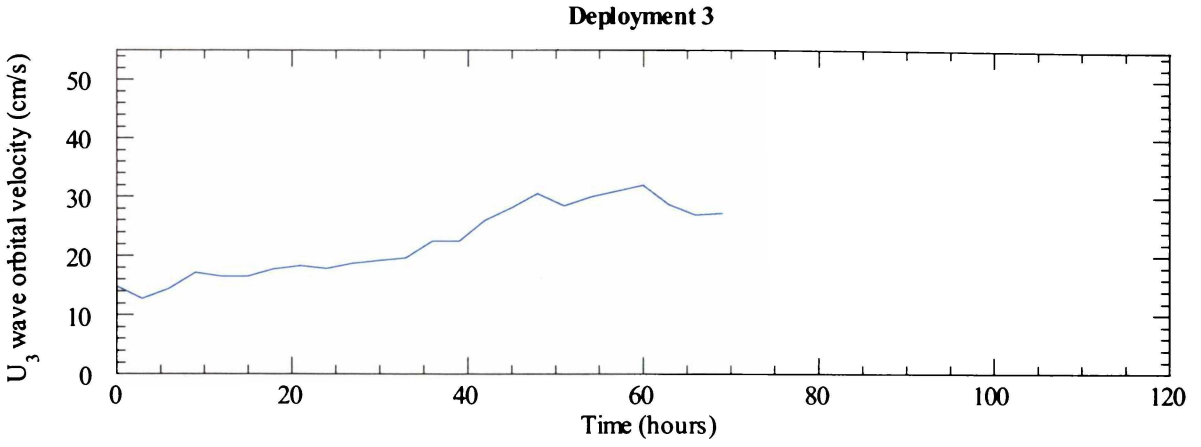
Deployment 3
U_3 wave orbital velocity (cm/s)
0
10
20
30
40
50
0
20
40
60
80
100
120
Time (hours)

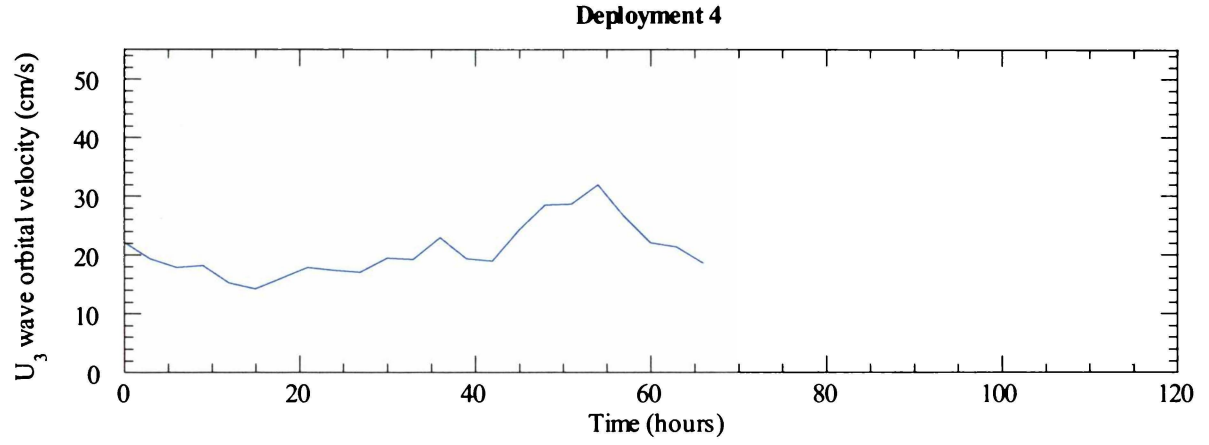
Deployment 4
U_3 wave orbital velocity (cm/s)
0
10
20
30
40
50
0
20
40
60
80
100
120
Time (hours)

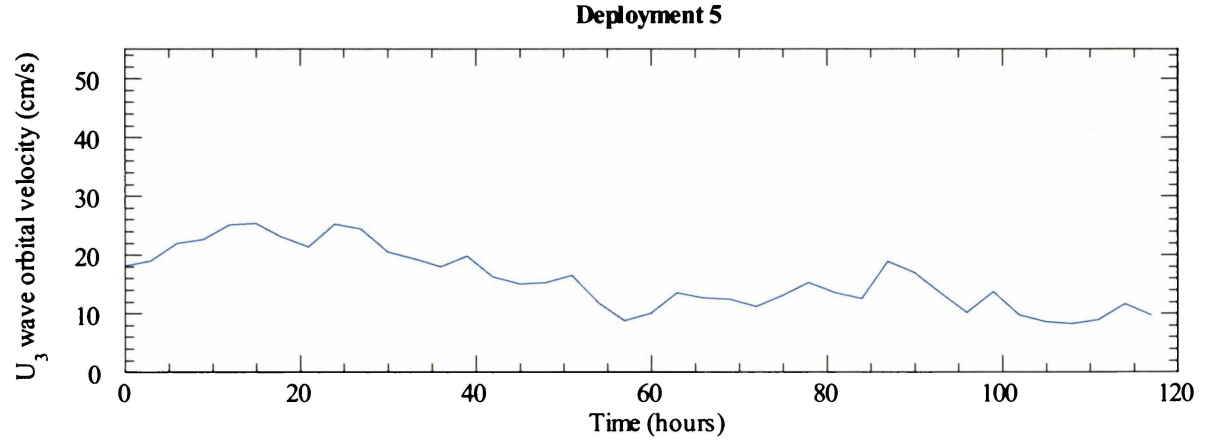
Deployment 5
U_3 wave orbital velocity (cm/s)
0
10
20
30
40
50
0
20
40
60
80
100
120
Time (hours)

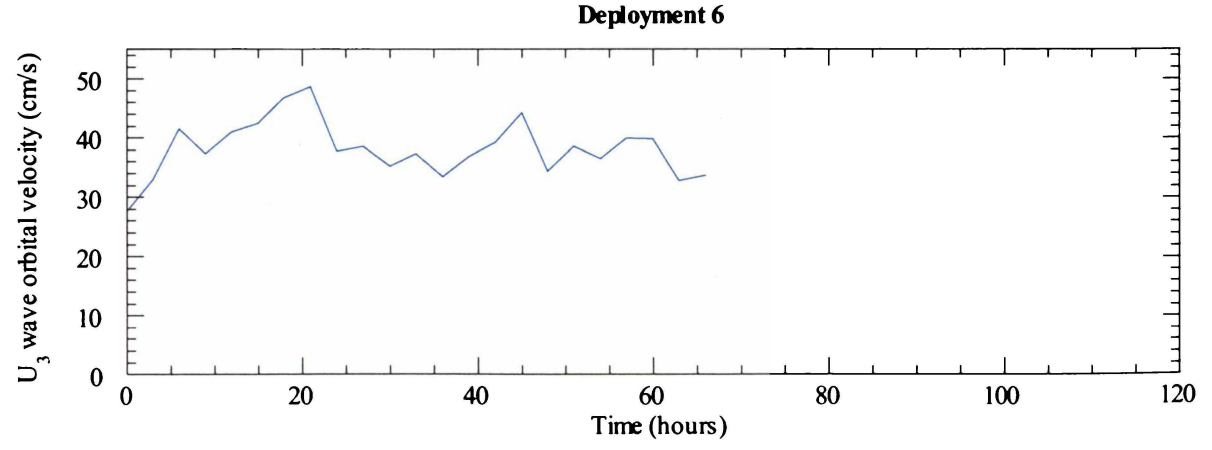
Deployment 6
U_3 wave orbital velocity (cm/s)
0
10
20
30
40
50
0
20
40
60
80
100
120
Time (hours)

MAPS OF TRACER MOVEMENT

Figure 1 Results of visual analysis of tracer samples collected in sample period 1 (Day 4). Red tracer is represented by red numerals, yellow tracer is represented by black numerals and orange zeros indicate locations where no tracer was found.

Figure 2 Results of visual analysis of tracer samples collected in sample periods 2 & 3 (Days 10 & 13). Red tracer is represented by red numerals, yellow tracer is represented by black numerals and orange zeros indicate locations where no tracer was found.

Figure 3 Results of visual analysis of tracer samples collected in sample period 4 (Day 18). Red tracer is represented by red numerals, yellow tracer is represented by black numerals and orange zeros indicate locations where no tracer was found.

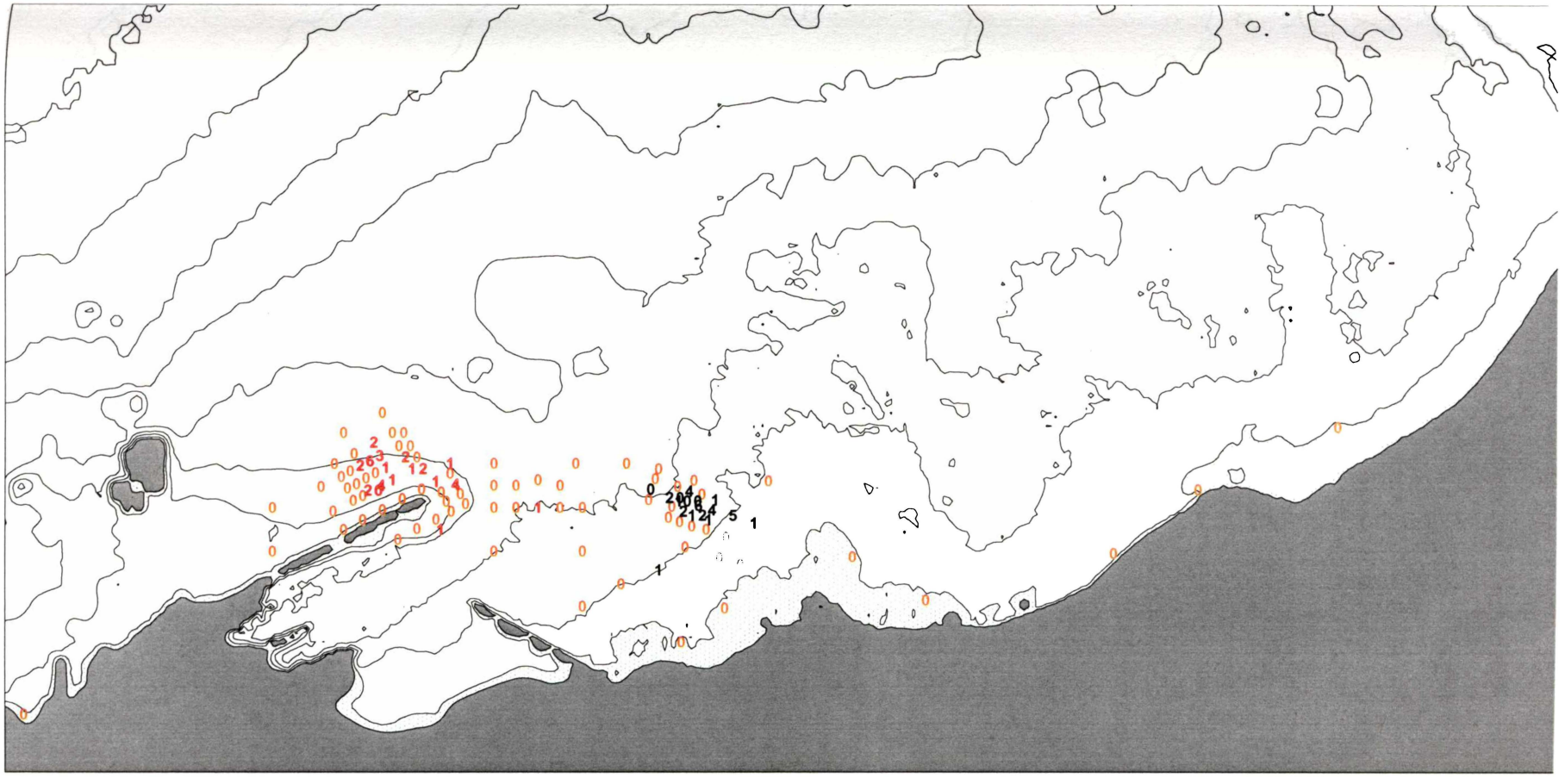

Figure 4 Results of visual analysis of tracer samples collected in sample period 5 (Day 34). Red tracer is represented by red numerals, yellow tracer is represented by black numerals and orange zeros indicate locations where no tracer was found.

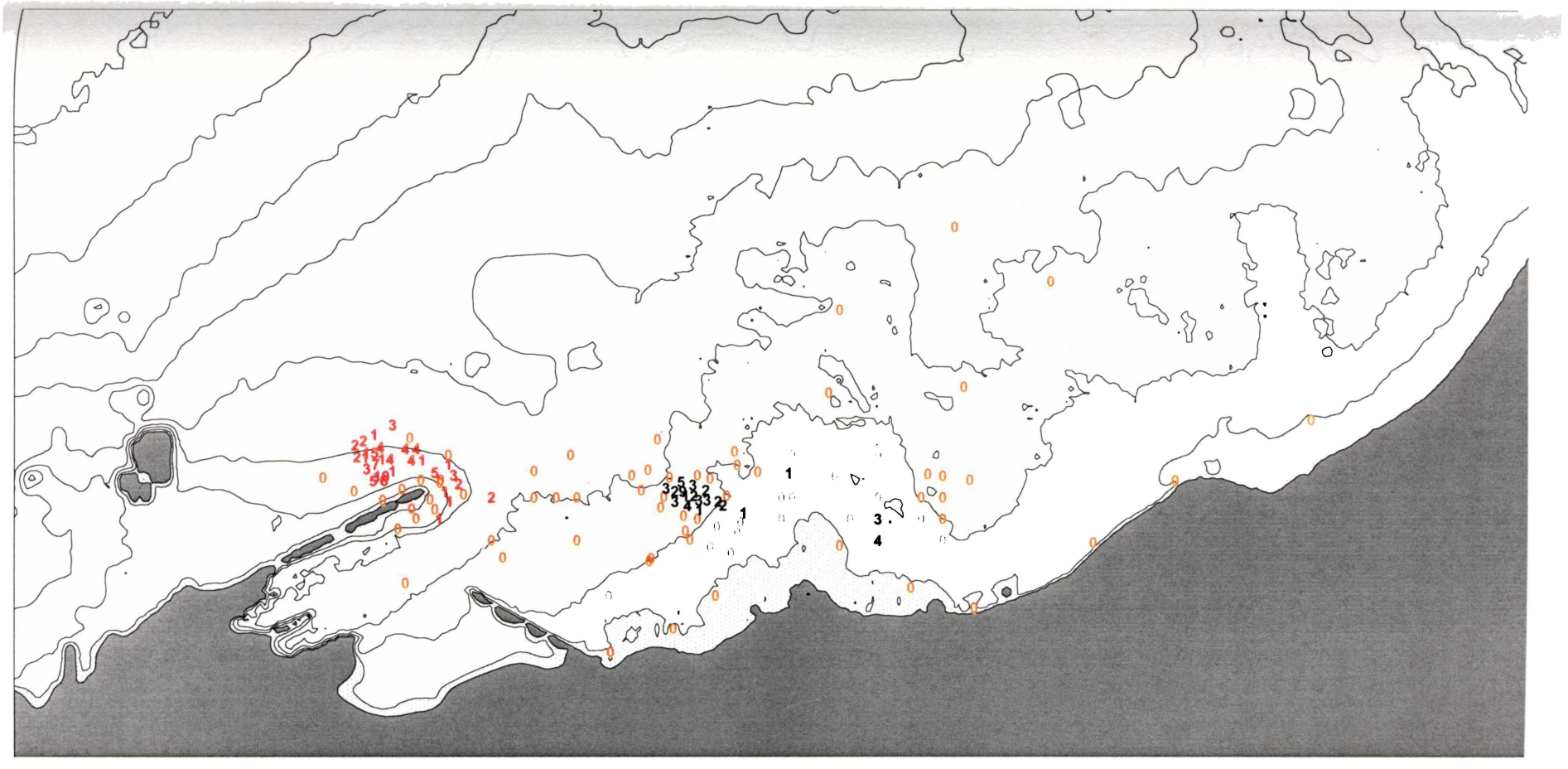

Figure 5 Results of visual analysis of tracer samples collected in sample period 6 (Day 49). Red tracer is represented by red numerals, yellow tracer is represented by black numerals and orange zeros indicate locations where no tracer was found.

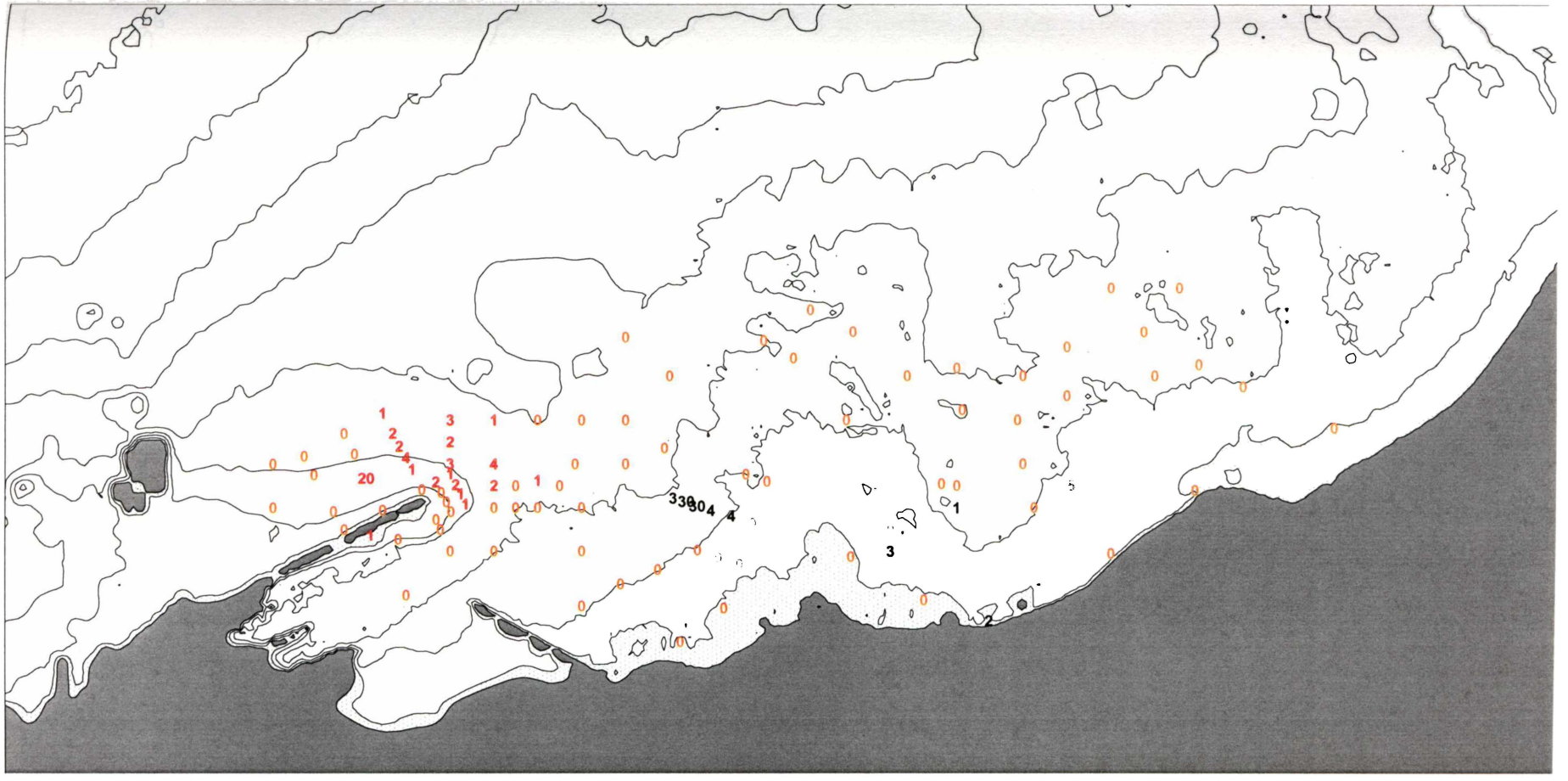

Figure 6 Results of visual analysis of tracer samples collected in sample period 7 (Day 75). Red tracer is represented by red numerals, yellow tracer is represented by black numerals and orange zeros indicate locations where no tracer was found.

Figure 7 Results of visual analysis of tracer samples collected in sample period 8 (Day 124). Red tracer is represented by red numerals, yellow tracer is represented by black numerals and orange zeros indicate locations where no tracer was found.

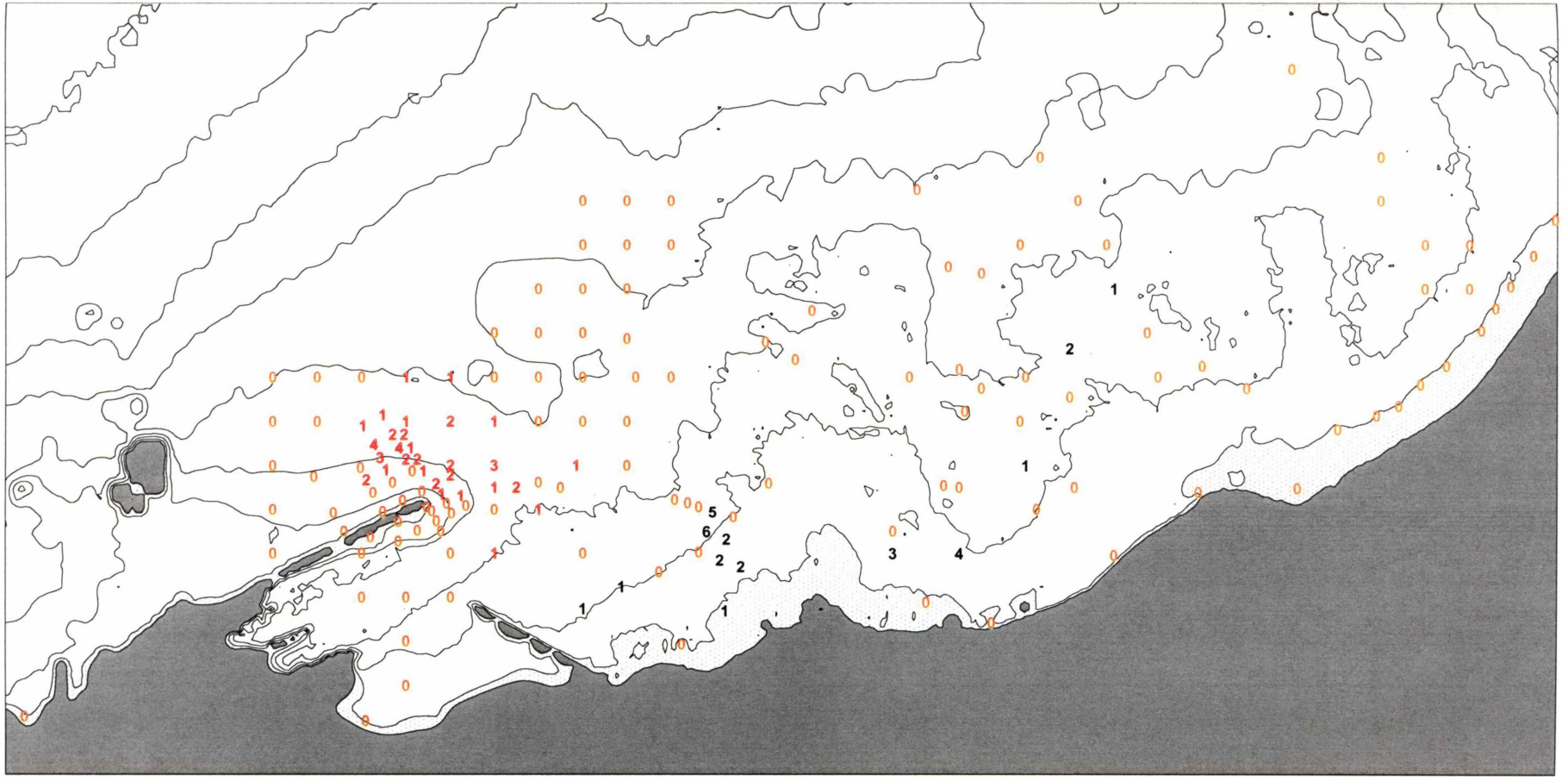

Figure 8 Results of visual analysis of tracer samples collected in sample period 9 (Day 161). Red tracer is represented by red numerals, yellow tracer is represented by black numerals and orange zeros indicate locations where no tracer was found

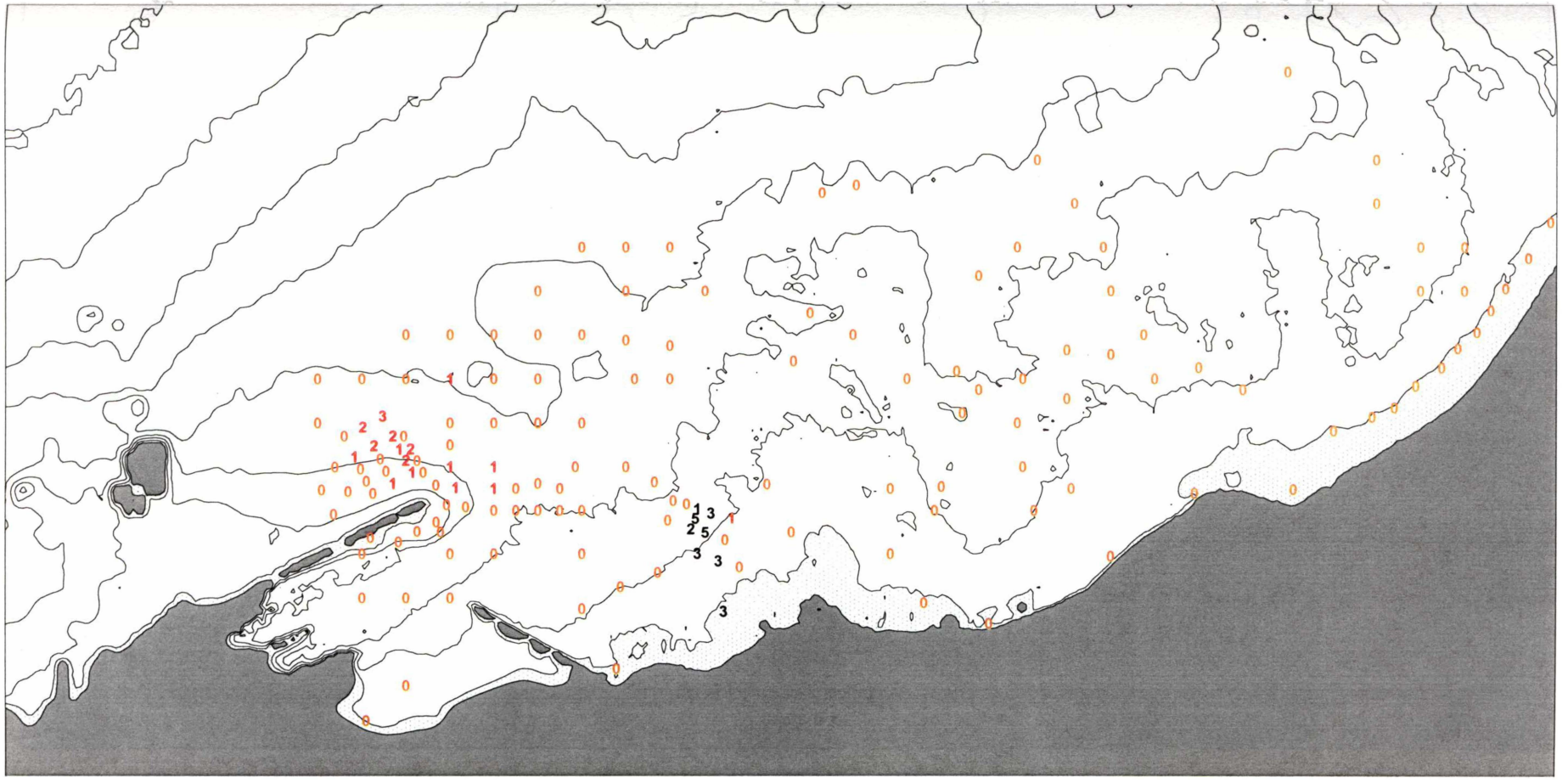

Figure 9 Results of visual analysis of tracer samples collected in sample period 10 (Day 207). Red tracer is represented by red numerals, yellow tracer is represented by black numerals and orange zeros indicate locations where no tracer was found.

Figure 10 Results of visual analysis of tracer samples collected in sample period 11 (Day 308). Red tracer is represented by red numerals, yellow tracer is represented by black numerals and orange zeros indicate locations where no tracer was found.

Figure 11 Results of video analysis of tracer samples collected in sample period 1 (Day 4) with grain size <120μm. Red tracer is represented by red numerals, yellow tracer is represented by black numerals.

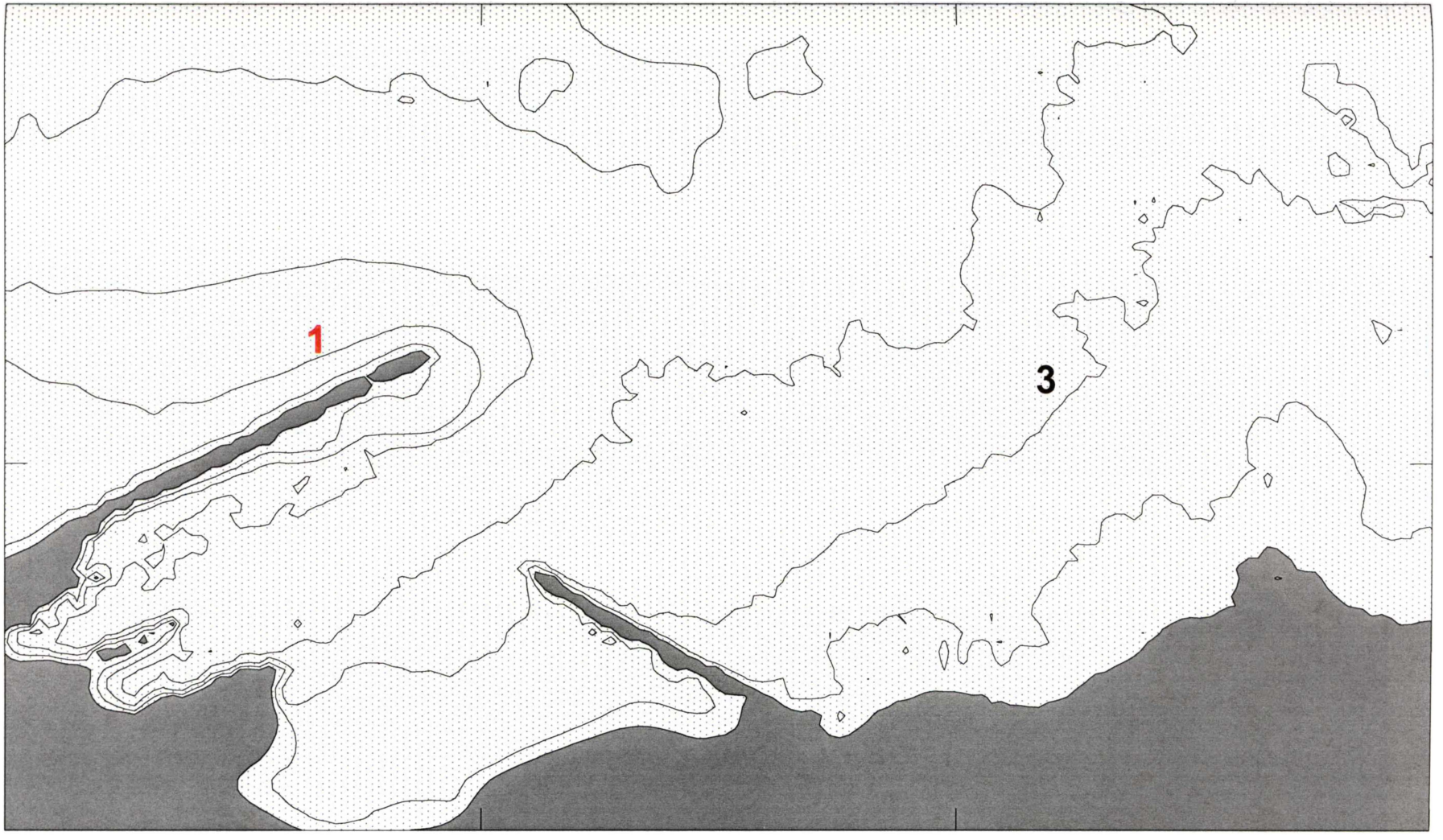

Figure 12 Results of video analysis of tracer samples collected in sample period 1 (Day 4) with grain size <200 - >120μm. Red tracer is represented by red numerals, yellow tracer is represented by black numerals.

Figure 13 Results of video analysis of tracer samples collected in sample period 1 (Day 4) with grain size <300 - >200μm. Red tracer is represented by red numerals, yellow tracer is represented by black numerals.

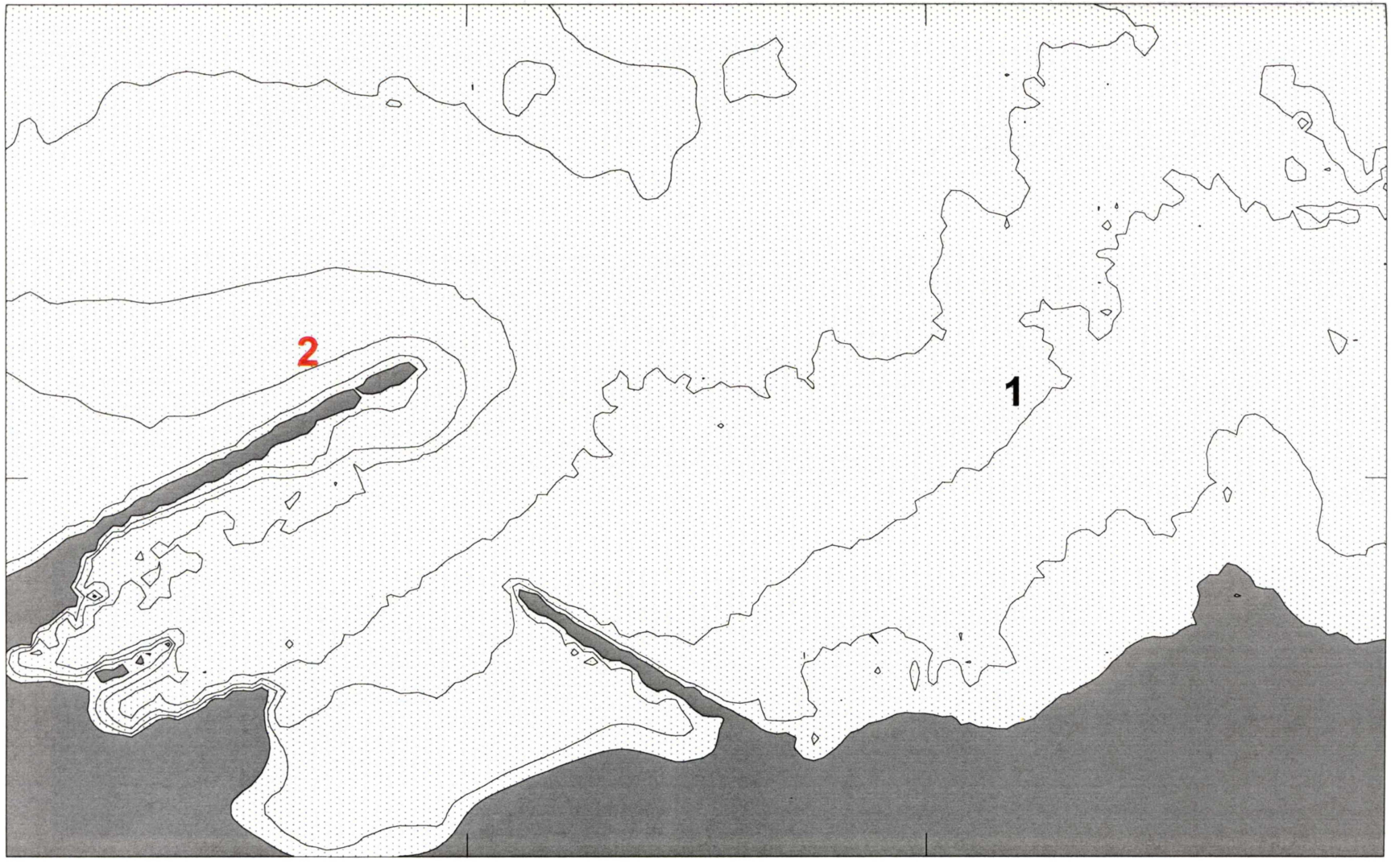

Figure 14 Results of video analysis of tracer samples collected in sample period 1 (Day 4) with grain size >400μm. Red tracer is represented by red numerals, yellow tracer is represented by black numerals.

Figure 15 Results of video analysis of tracer samples collected in sample periods 2 & 3 (Days 10 & 13) with grain size <120μm. Red tracer is represented by red numerals, yellow tracer is represented by black numerals.

Figure 16 Results of video analysis of tracer samples collected in sample periods 2 & 3 (Days 10 & 13) with grain size <200 - >120µm. Red tracer is represented by red numerals, yellow tracer is represented by black numerals.

Figure 17 Results of video analysis of tracer samples collected in sample periods 2 & 3 (Days 10 & 13) with grain size <300 - >200μm. Red tracer is represented by red numerals, yellow tracer is represented by black numerals.

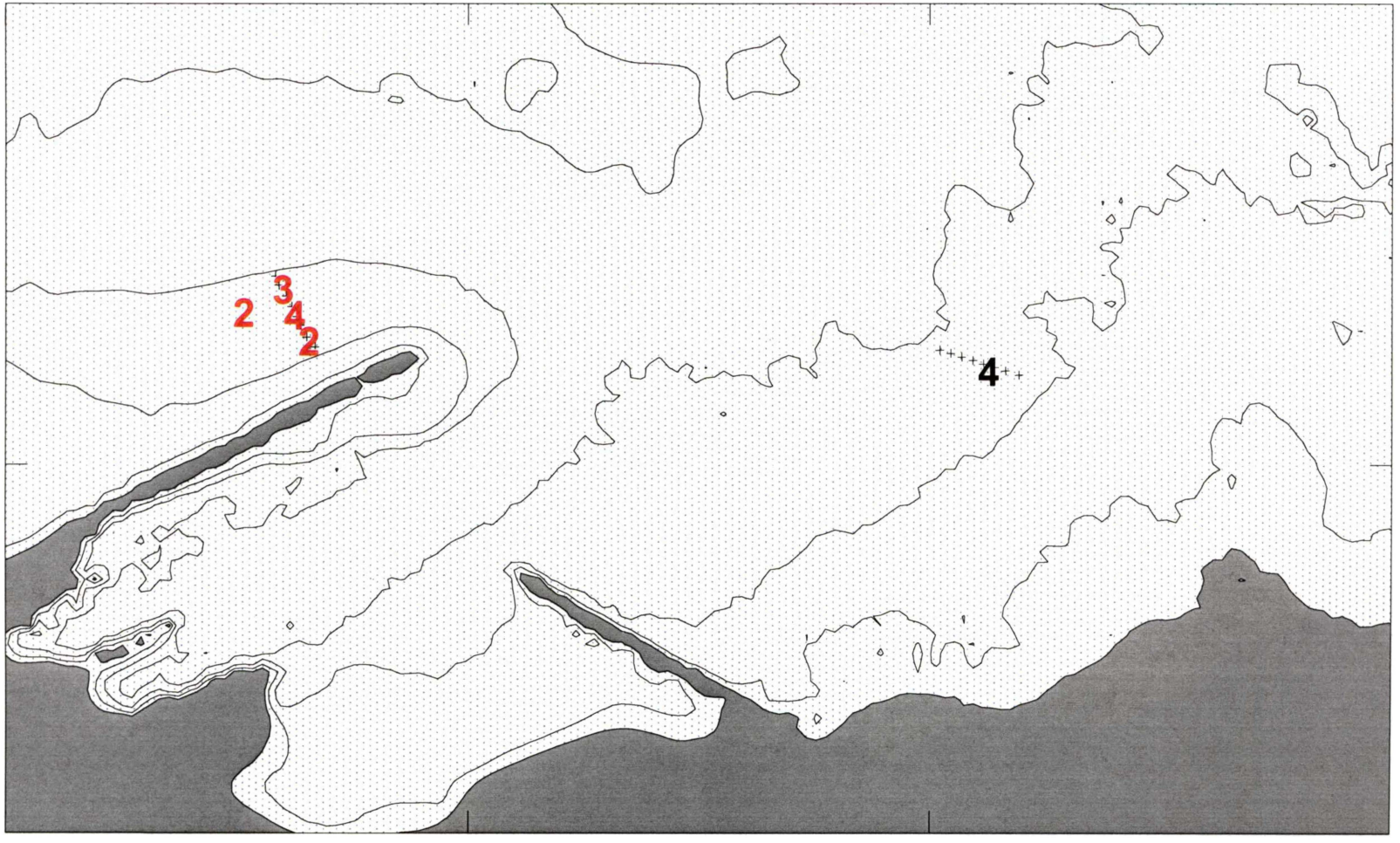

Figure 18Results of video analysis of tracer samples collected in sample period 4 (Day 18) with grain size <120μm. Red tracer is represented by red numerals, yellow tracer is represented by black numerals.

Figure 19 Results of video analysis of tracer samples collected in sample period 4 (Day 18) with grain size <200 - >120μm. Red tracer is represented by red numerals, yellow tracer is represented by black numerals.

Figure 20 Results of video analysis of tracer samples collected in sample period 4 (Day 18) with grain size <300 - >200μm. Red tracer is represented by red numerals, yellow tracer is represented by black numerals.

Figure 21Results of video analysis of tracer samples collected in sample period 4 (Day 18) with grain size >400μm. Red tracer is represented by red numerals, yellow tracer is represented by black numerals.

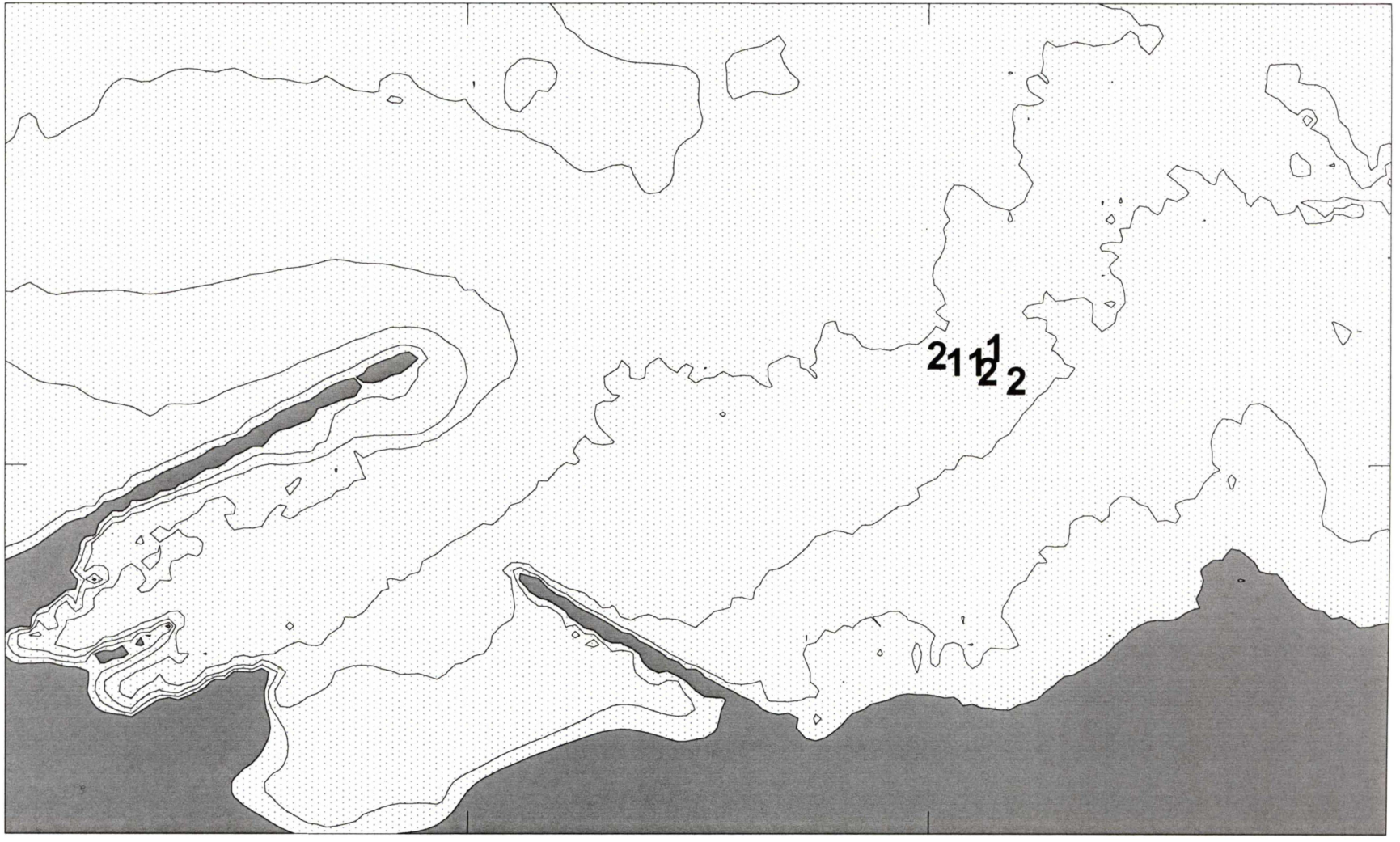

Figure 22Results of video analysis of tracer samples collected in sample period 5 (Day 34) with grain size <120μm. Red tracer is represented by red numerals, yellow tracer is represented by black numerals

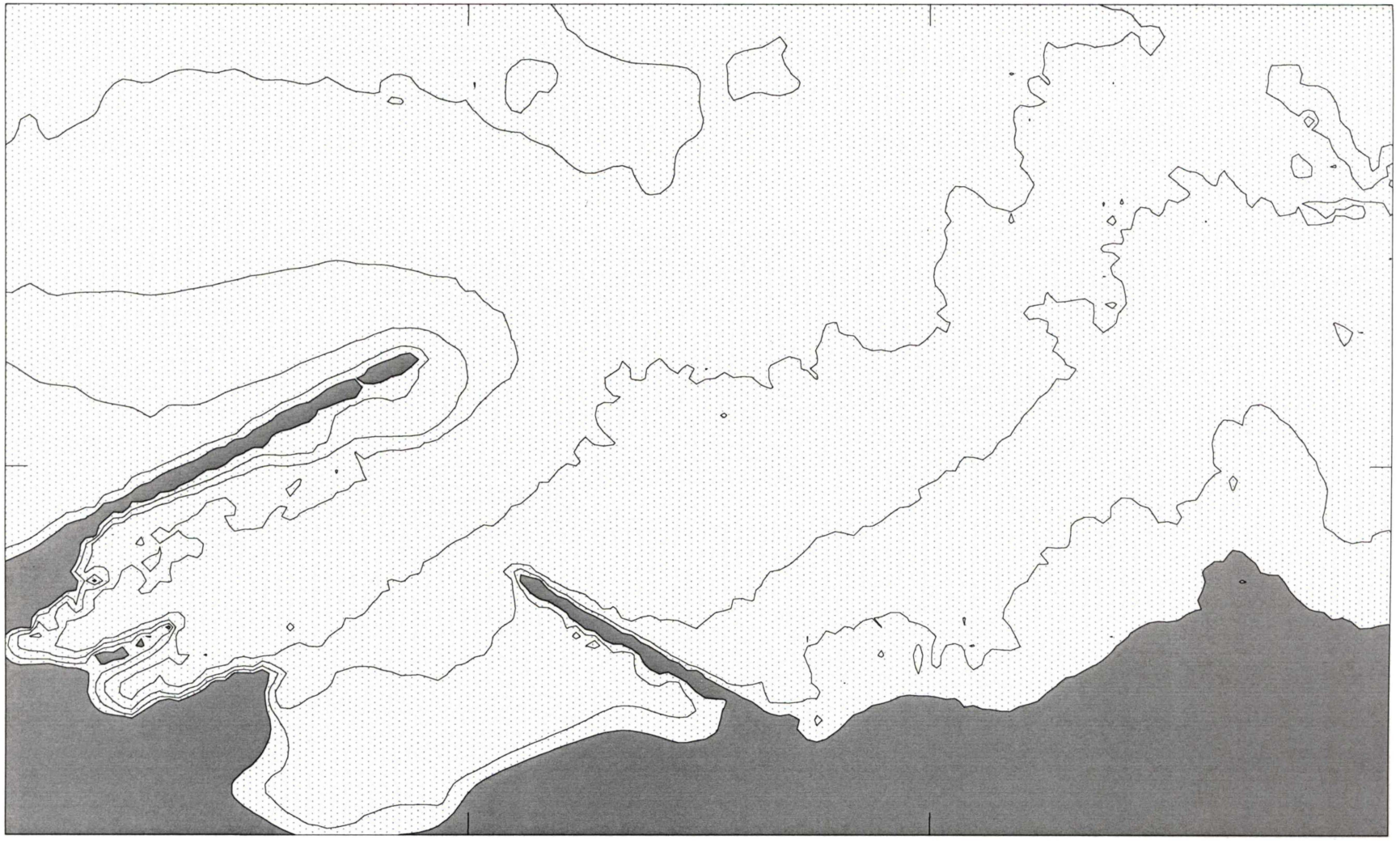

Figure 23Results of video analysis of tracer samples collected in sample period 5 (Day 34) with grain size <200 - >120μm. Red tracer is represented by red numerals, yellow tracer is represented by black numerals

Figure 24Results of video analysis of tracer samples collected in sample period 5 (Day 34) with grain size <300 - >200μm. Red tracer is represented by red numerals, yellow tracer is represented by black numerals.

Figure 25 Results of video analysis of tracer samples collected in sample period 5 (Day 34) with grain size >400μm. Red tracer is represented by red numerals, yellow tracer is represented by black numerals

Figure 26 Results of video analysis of tracer samples collected in sample period 6 (Day 49) with grain size <120μm. Red tracer is represented by red numerals, yellow tracer is represented by black numerals

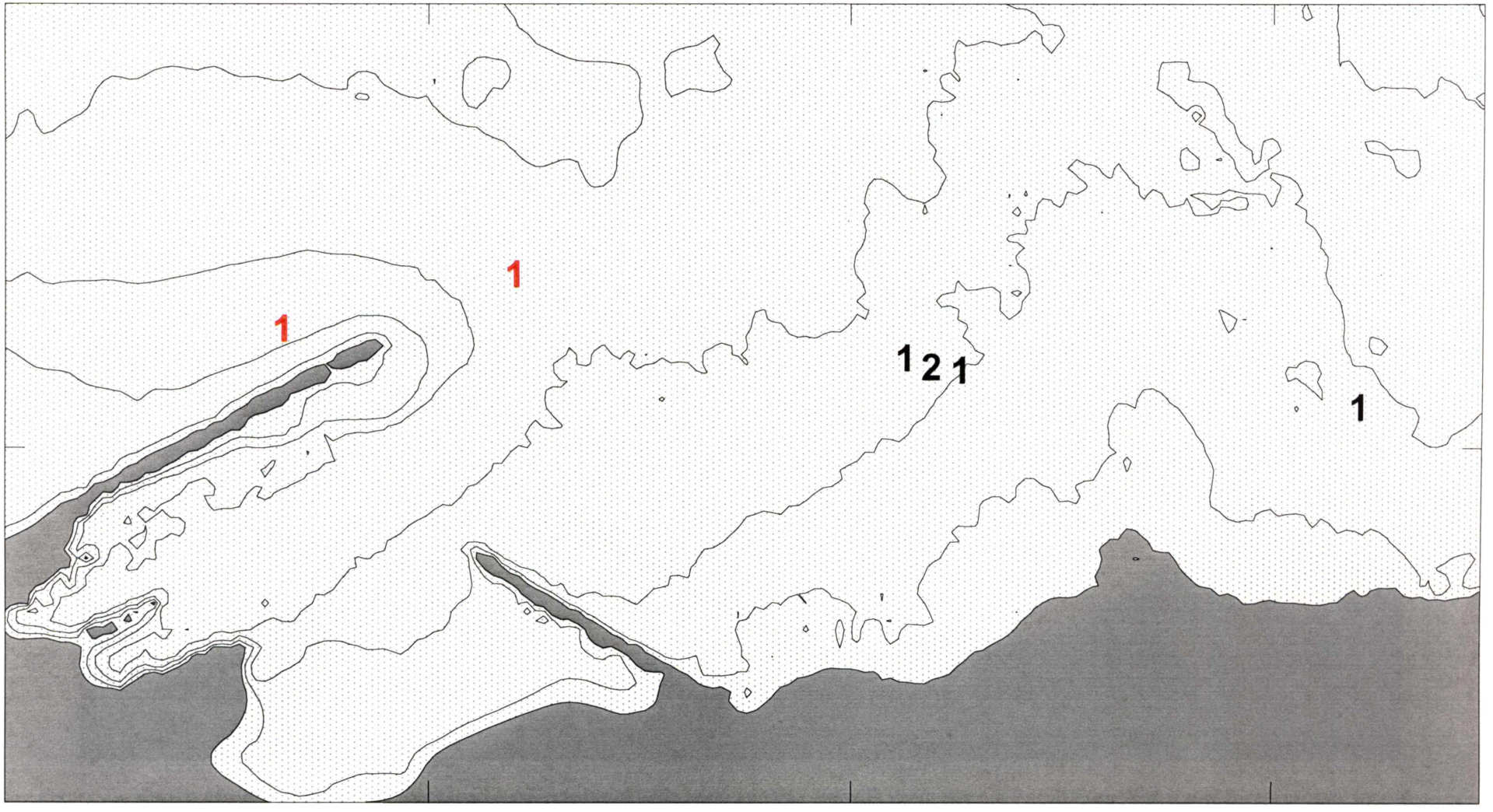

Figure 27 Results of video analysis of tracer samples collected in sample period 6 (Day 49) with grain size <200 - >120μm. Red tracer is represented by red numerals, yellow tracer is represented by black numerals.

Figure 28 Results of video analysis of tracer samples collected in sample period 6 (Day 49) with grain size <300 - >200μm. Red tracer is represented by red numerals, yellow tracer is represented by black numerals

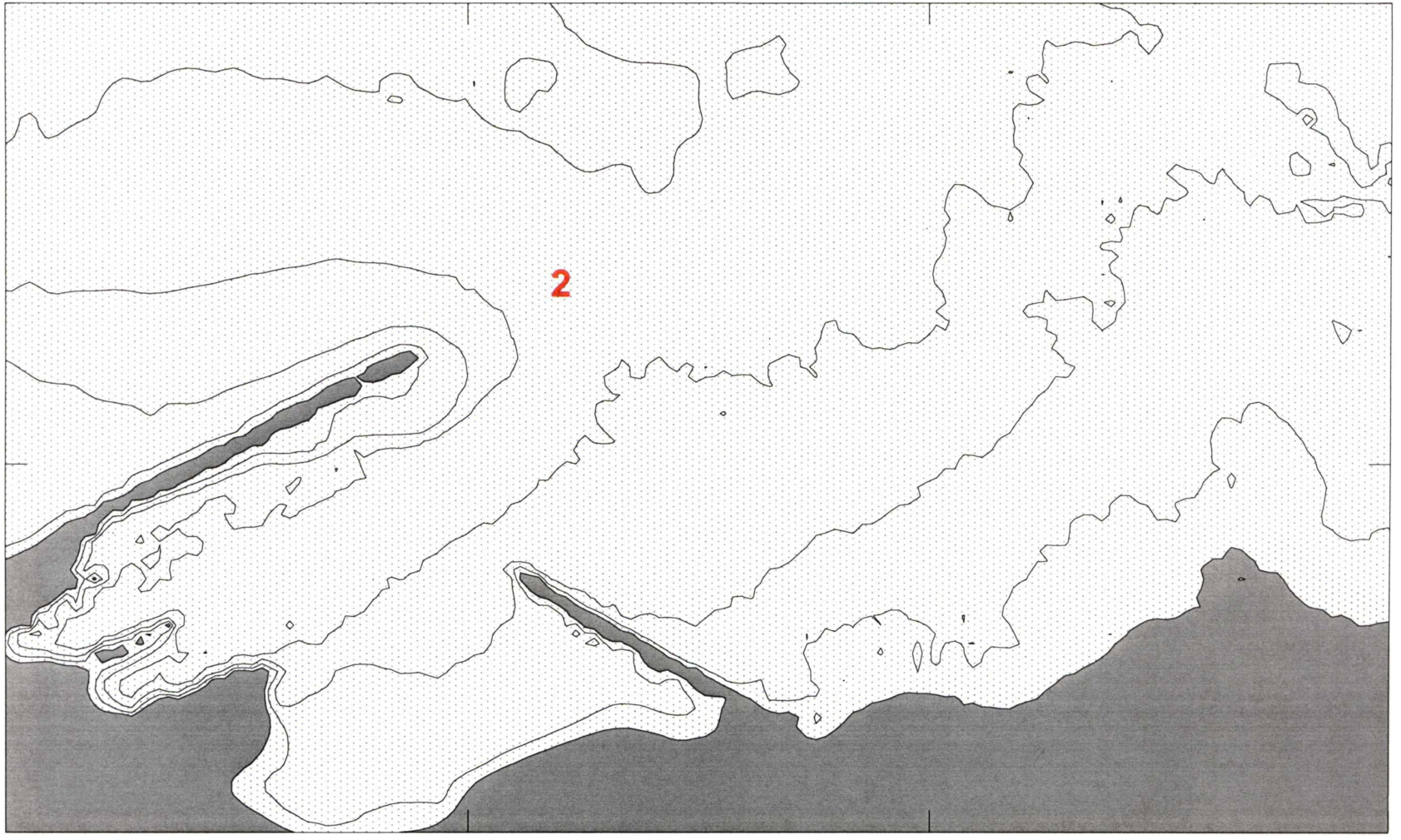

Figure 29 Results of video analysis of tracer samples collected in sample period 6 (Day 49) with grain size >400μm. Red tracer is represented by red numerals, yellow tracer is represented by black numerals

Figure 30 Results of video analysis of tracer samples collected in sample period 7 (Day 75) with grain size <120μm. Red tracer is represented by red numerals, yellow tracer is represented by black numerals.

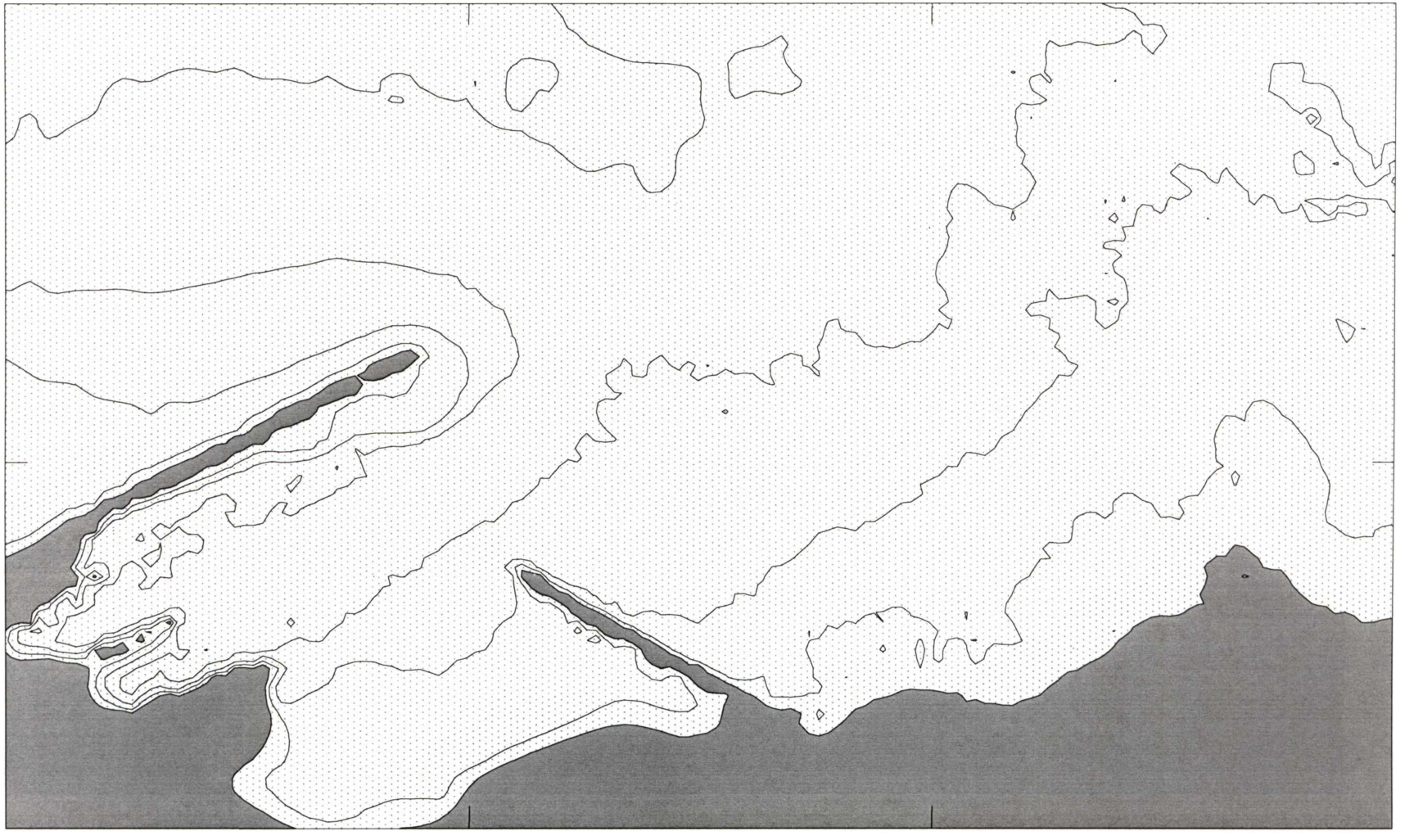

Figure 31 Results of video analysis of tracer samples collected in sample period 7 (Day 75) with grain size <200 - >120μm. Red tracer is represented by red numerals, yellow tracer is represented by black numerals.

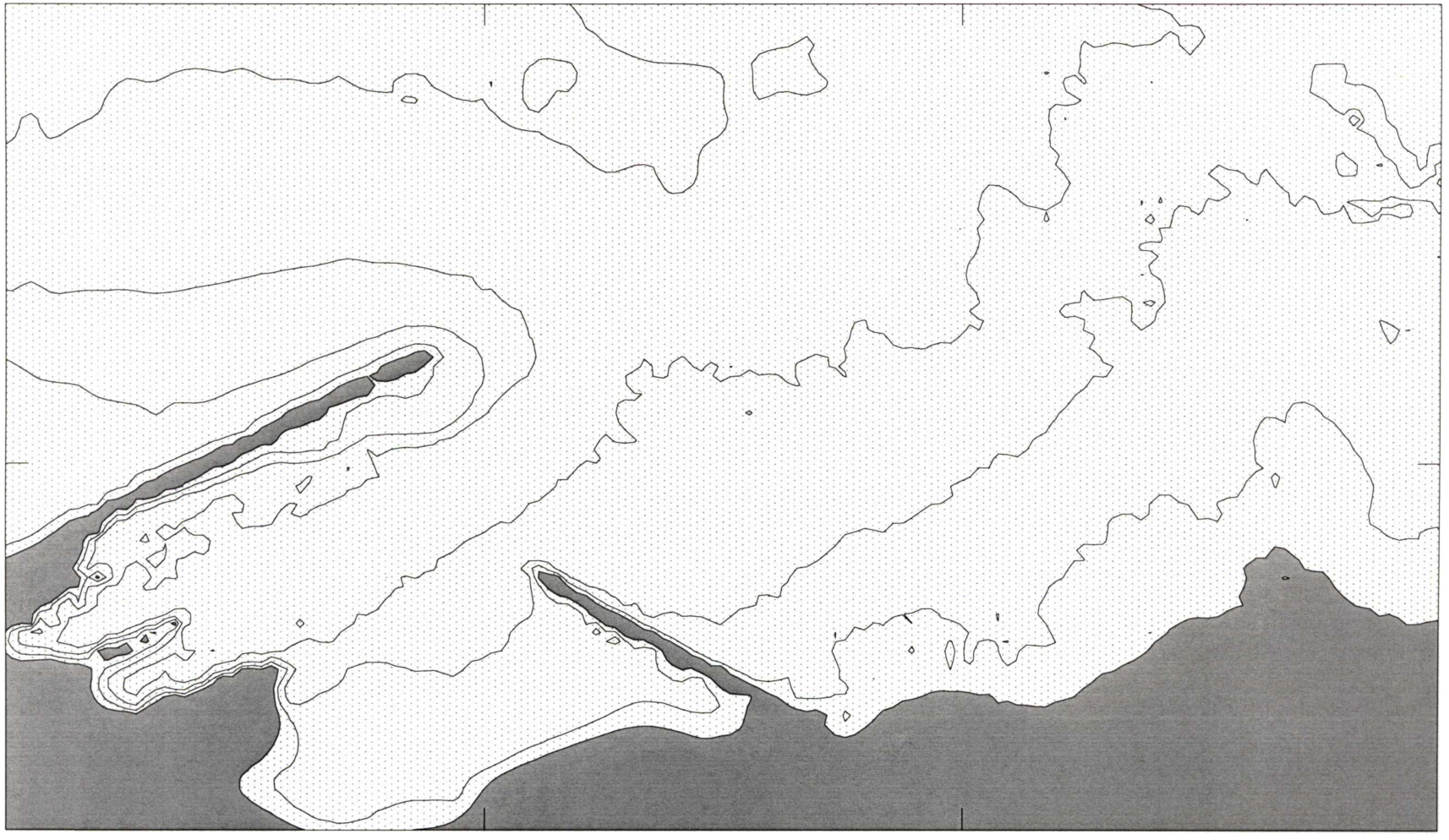

Figure 32 Results of video analysis of tracer samples collected in sample period 7 (Day 75) with grain size <300 - >200μm. Red tracer is represented by red numerals, yellow tracer is represented by black numerals.

Figure 33 Results of video analysis of tracer samples collected in sample period 7 (Day 75) with grain size >400μm. Red tracer is represented by red numerals, yellow tracer is represented by black numerals.

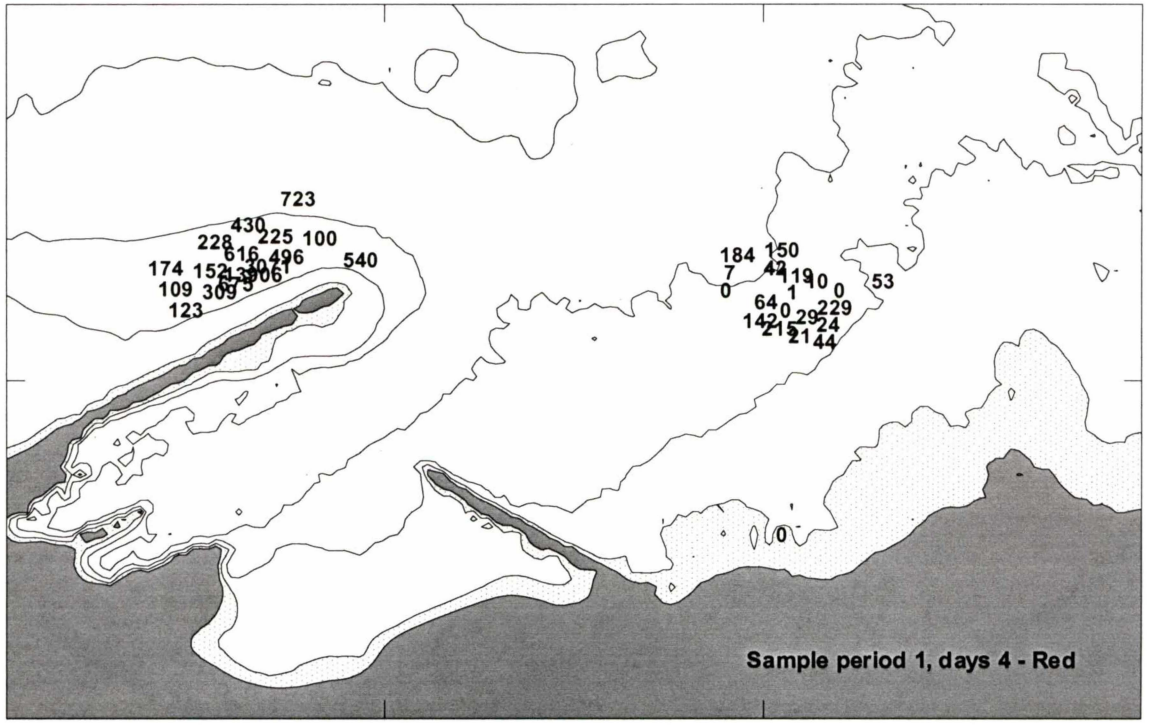

Figure 34 Results (ppb) of spectrofluorometric analysis of red tracer in samples collected in sample period 1 (Day 4).

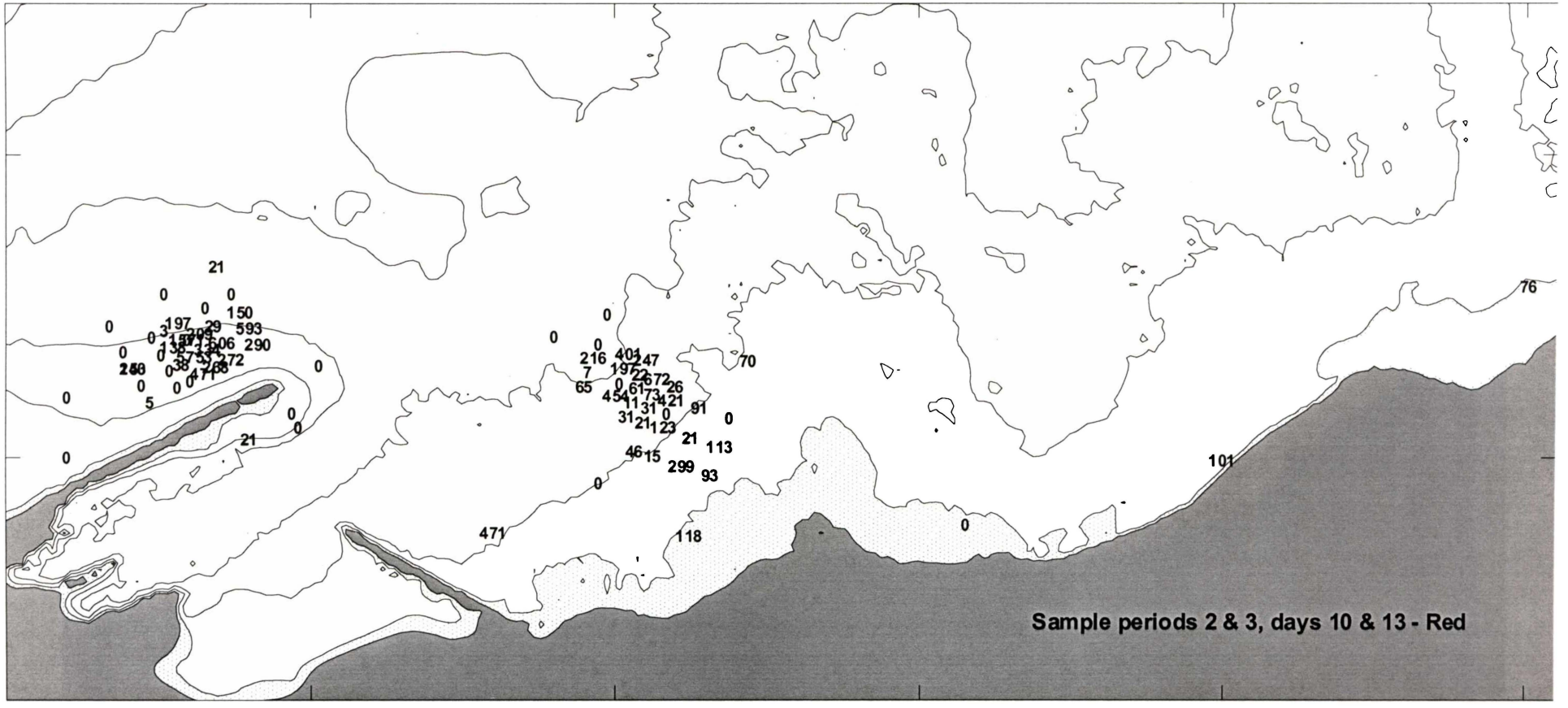

Figure 35 Results (ppb) of spectrofluorometric analysis of red tracer samples collected in sample periods 2 & 3 (Days 10 & 13).

Figure 36 Results (ppb) of spectrofluorometric analysis of red tracer in samples collected in sample period 4 (Day 18).

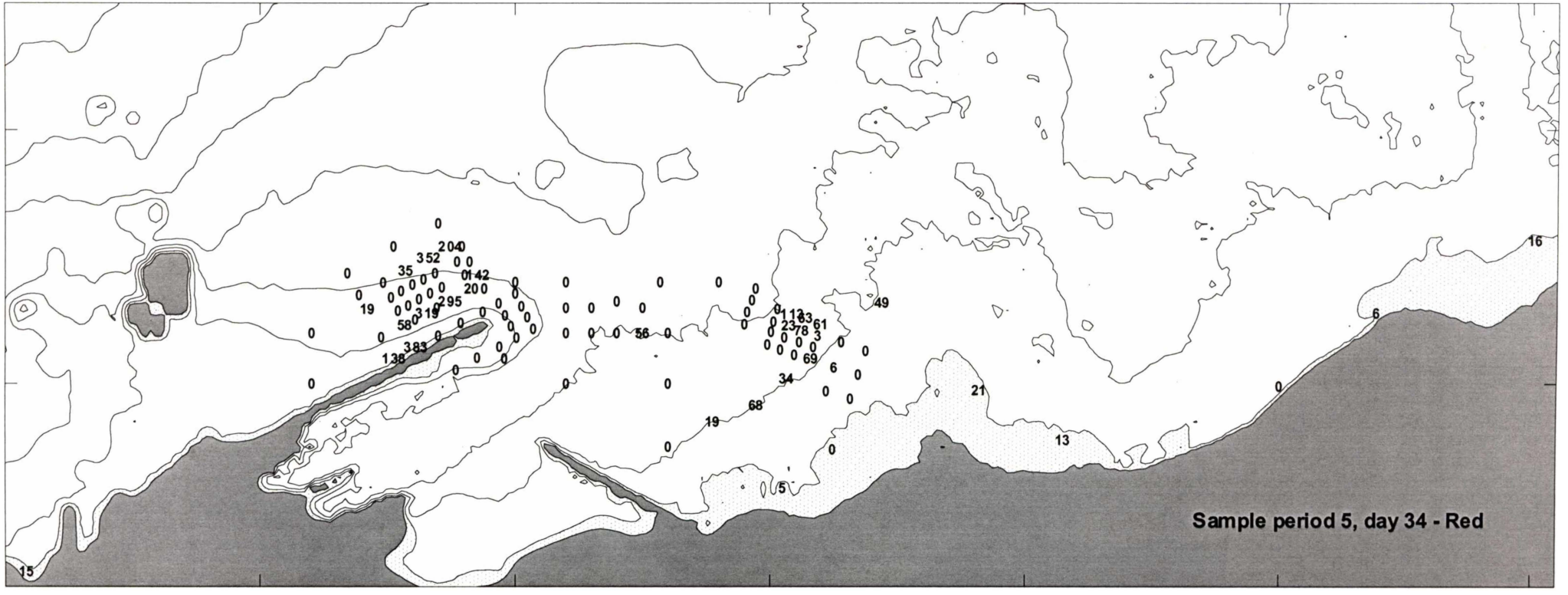

Figure 37 Results (ppb) of spectrofluorometric analysis of red tracer in samples collected in sample period 5 (Day 34).

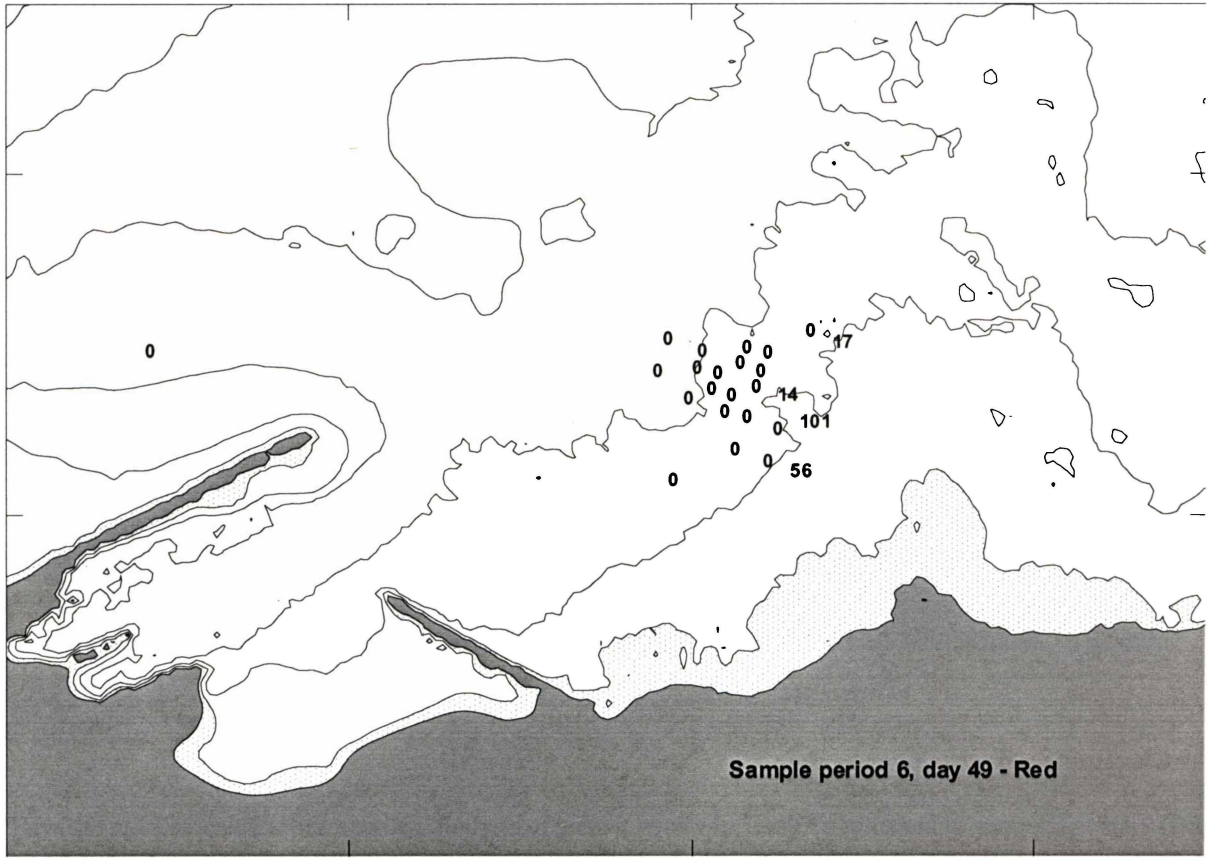

Figure 38 Results (ppb) of spectrofluorometric analysis of red tracer in samples collected in sample period 6 (Day 49).

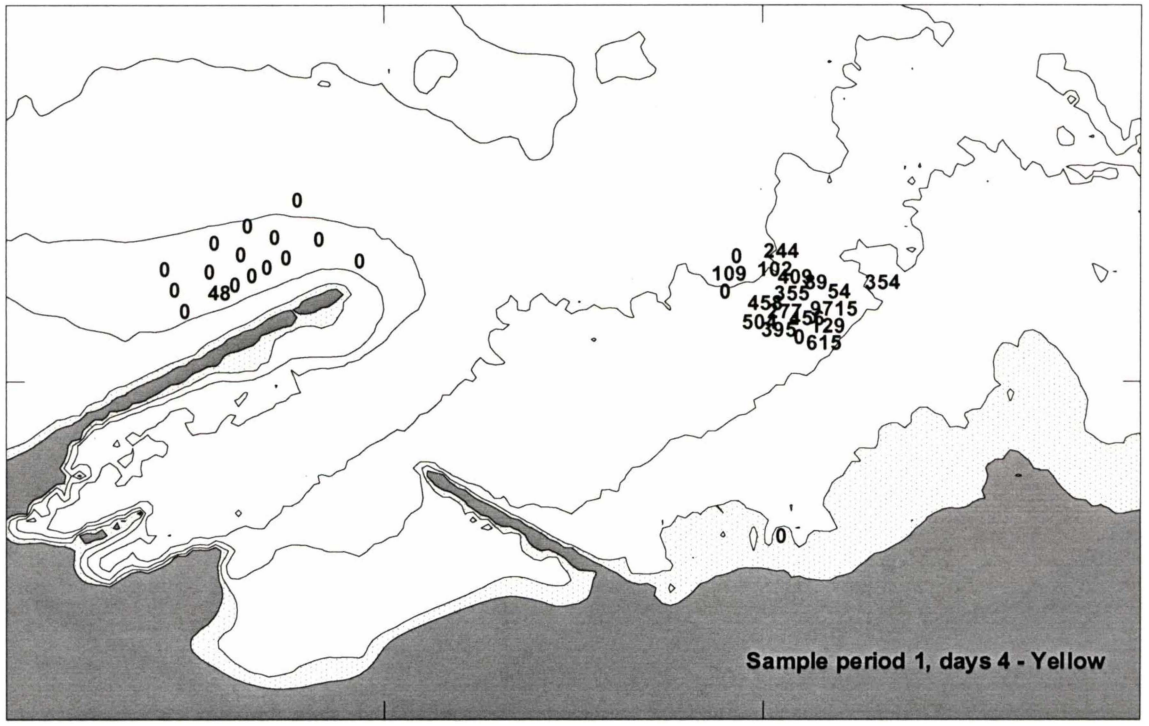

Figure 39 Results (ppb) of spectrofluorometric analysis of yellow tracer in samples collected in sample period 1 (Day 4).

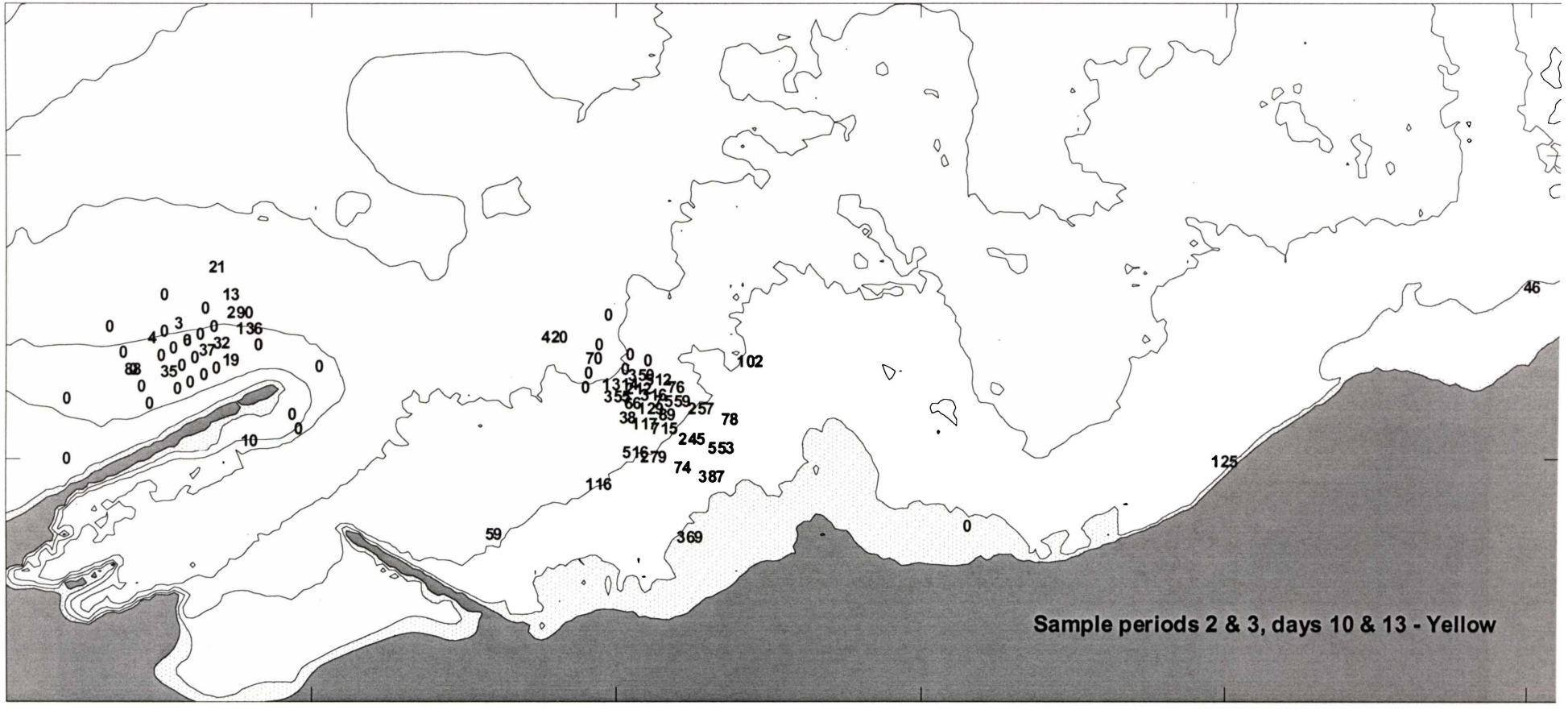

Figure 40 Results (ppb) of spectrofluorometric analysis of yellow tracer in samples collected in sample periods 2 & 3 (Days 10 & 13).

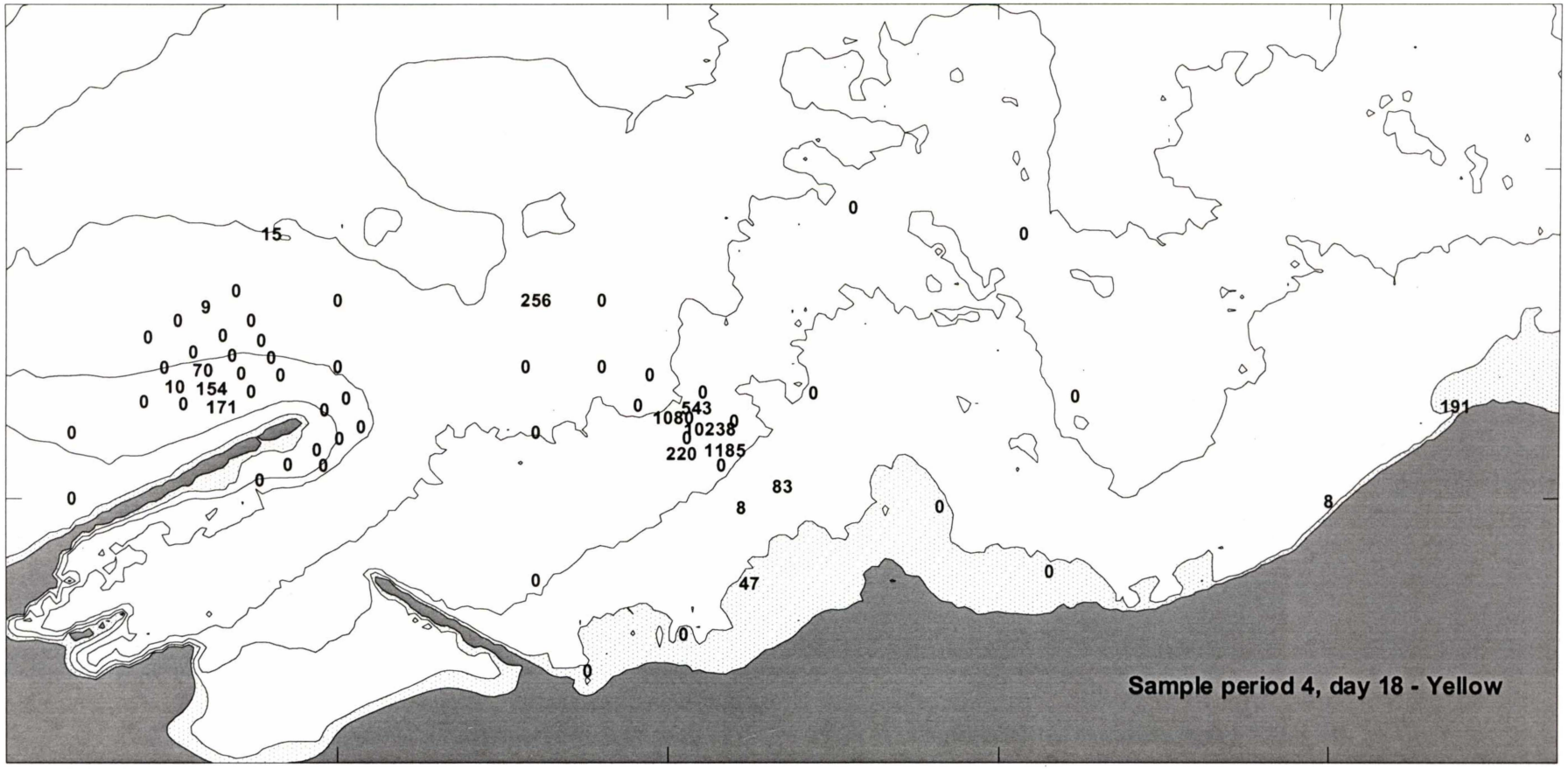

Figure 41 Results (ppb) of spectrofluorometric analysis of yellow tracer in samples collected in sample period 4 (Day 18).

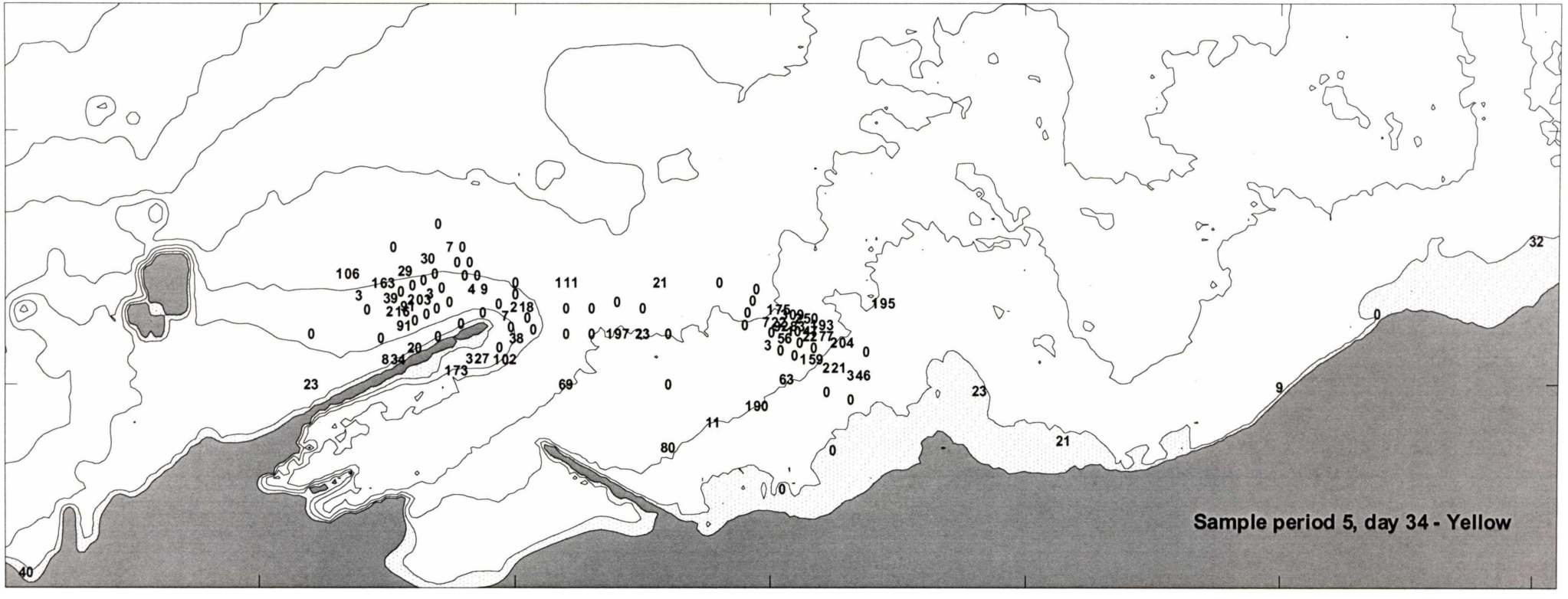

Figure 42 Results (ppb) of spectrofluorometric analysis of yellow tracer in samples collected in sample period 5 (Day 34).

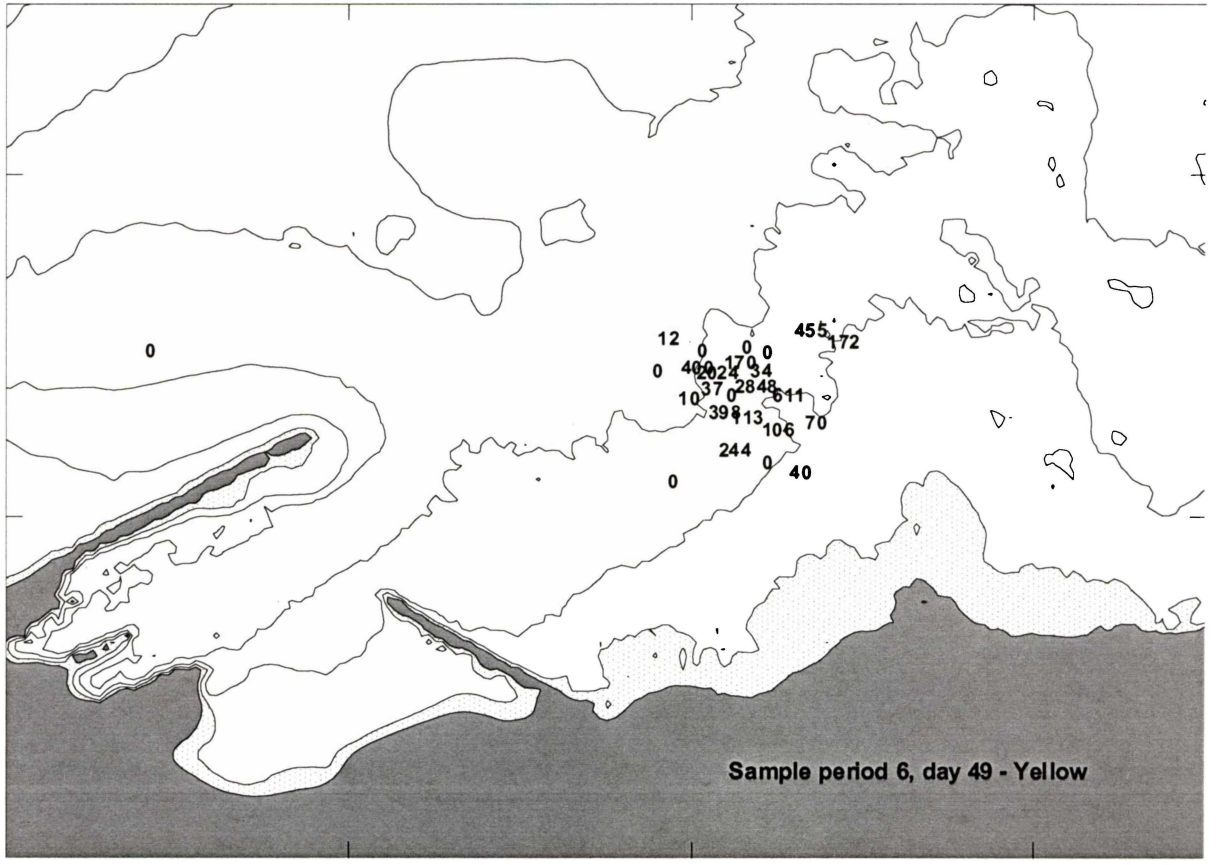

Figure 43 Results of spectrofluorometric analysis of yellow tracer in samples collected in sample period 6 (Day 49).